FLECHT SEASET Program
NRC/EPRI/Westinghouse Report No. 7
NUREG/CR-1532
EPRI NP-1459
WCAP-9699

PWR FLECHT SEASET UNBLOCKED BUNDLE, FORCED AND GRAVITY REFLOOD TASK DATA REPORT

Volume 1

JUNE 1980

Program Jointly Sponsored by USNRC, EPRI and

Westinghouse Under Contract Number

NRC-04-77-127

FLECHT SEASET Program
NRC/EPRI/Westinghouse Report No. 7
NUREG/CR - 1532
EPRI NP-1459
WCAP-9699

PWR FLECHT SEASET UNBLOCKED BUNDLE, FORCED AND GRAVITY REFLOOD TASK DATA REPORT

Volume I

June 1980

M. J. Loftus
L. E. Hochreiter
C. E. Conway
C. E. Dodge
A. Tong
E. R. Rosal
M. M. Valkovic
S. Wong

prepared for

United States Nuclear Regulatory Commission
Washington, D. C. 20555

Electric Power Research Institute
3412 Hillview Avenue
Palo Alto, California 94303

and

Westinghouse Electric Corporation
Nuclear Energy Systems
P.O. Box 355
Pittsburgh, Pennsylvania 15230

by

Westinghouse Electric Corporation

under

Contract No. NRC-04-77-127, EPRI Project No. RP959-1

Program Management Group

NRC - L. H. Sullivan
EPRI - K. H. Sun
Westinghouse - L. Chajson

NOTICE

This report was prepared as an account of work sponsored by the U. S. Nuclear Regulatory Commission, the Electric Power Research Institute, Inc., and the Westinghouse Electric Corporation. Neither the United States government nor any agency thereof, nor the Institute or members thereof, nor the Westinghouse Electric Corporation, nor any of their employes, makes any warranty, express or implied, or assumes any legal liability or responsibility for any third party's use or the results of such use of any information, apparatus, product, or process disclosed in this report or represents that its use by such third party would not infringe privately owned rights.

ABSTRACT

This report presents data from the Unblocked Bundle, Forced and Gravity Reflood Task of the Full-Length Emergency Core Heat Transfer Separate Effects and Systems Effects Tests (FLECHT SEASET) program. The tests consisted of forced and gravity reflood experiments and steam cooling tests, using electrical heater rods to simulate current nuclear fuel arrays (similar to Westinghouse 17 x 17 assemblies) of PWR and PWR fuel vendors. Data obtained include rod clad temperatures, turnaround and quench times, heat transfer coefficients, inlet flooding rates, overall mass balance, differential pressures and calculated void fractions in the test section, thimble wall and steam temperatures, and exhaust steam and liquid carryover rates.

ACKNOWLEDGMENTS

The work of the following Westinghouse Nuclear Energy Systems contributors is hereby acknowledged:

NTD STRATEGIC PROJECTS
L. Chajson
H. W. Massie, Jr.

SAFEGUARDS DEVELOPMENT
R. P. Vijuk
N. Lee
K. Beatty
D. H. Dixon
M. A. Emery
D. P. Kitzmiller
K. F. McNamee
D. P. Remlinger
D. W. Sklarsky

MATHEMATICS AND PROGRAMMING
R. W. Steer

FACILITIES ENGINEERING
L. R. Katz
B. R. Sinwell
P. M. Brumbaugh

TEST OPERATIONS
C. E. Fuchs
P. F. Orangio
F. L. Lilly
J. T. Martin
N. Washington
J. Kalo
M. Mulligan
J. Tomasic
J. Latta

NFD METALLOGRAPHY
P. Heasley

PUBLICATION PROGRAMS
J. G. Nagle

The work of the following members of the Program Management Group, their colleagues, and their consultants is hereby acknowledged:

EPRI - K. H. Sun, R. B. Duffey
NRC-RSR - L. B. Thompson
NRC-NRR - W. Hodges
EG&G - G. Wilson
NUS Corporation - D. A. Prelewicz

GLOSSARY

This glossary explains definitions, acronyms, and symbols included in the text which follows.

Analysis -- the examination of data to determine, if possible, the basic physical processes that occur and the interrelation of the processes. Where possible, physical processes will be identified from the data and will be related to first principles.

Average fluid conditions -- average thermodynamic properties (for example, enthalpy, quality, temperature, pressure) and average thermal-hydraulic parameters (for example, void fraction, mass flow rate) which are derived from appropriately reduced data for a specified volume or a specified cross-sectional area

Axial peaking factor -- ratio of the peak-to-average power for a given power profile

Blocked -- a situation in which the flow area in the rod bundle or single tube is purposely obstructed at selected locations so as to restrict the flow

Bottom of core recovery (BOCR) -- a condition at the end of the refill period in which the lower plenum is filled with injected ECC water as the water is about to flood the core

Bundle -- a number of heater rods, including spares, which are assembled into a matrix with CRG-type rods, using necessary support hardware to meet the Task Plan design requirements

Carryout -- same as carryover

Carryout rate fraction -- the fraction of the inlet flooding flow rate which flows out the rod bundle exit by upflowing steam

Carryover -- the process in which the liquid is carried in a two-phase mixture out of a control volume, that is, the test bundle

Computational methods -- the procedure of reducing, analyzing, and evaluating data or mathematical expressions, either by hand calculations or by digital computer codes

Computer code -- a set of specific instructions in computer language to perform the desired mathematical operations utilizing appropriate models and correlations

Computer data acquisition system (CDAS) -- the system which controls the test and records data for later reduction and analysis

Computer tape -- magnetic tapes that store FLECHT SEASET data

Core rod geometry (CRG) -- a nominal rod-to-rod pitch of 12.6 mm (0.496 inch) and outside nominal diameter of 9.50 mm (0.374 inch) representative of various nuclear fuel vendors' new fuel assembly geometries (commonly referred to as the 17 x 17 or 16 x 16 assemblies)

Correlation -- a set of mathematical expressions, based on physical principles and experimental data but resting primarily on experimental data, which describes the thermal-hydraulic behavior of a system

Cosine axial power profile -- the axial power distribution of the heater rods in the CRG bundle that contains the maximum (peak) linear power at the midplane of the active heated rod length. This axial power profile will be used on all FLECHT SEASET tests as a fixed parameter.

Data -- recorded information, regardless of form or characteristic, of a scientific or technical nature. It may, for example, document research, experimental, developmental, or engineering work, or be usable or used to define a design or process or to procure, produce, support, maintain, or operate material. The data may be graphic or pictorial delineations in media such as drawings or photographs, text in specifications or related performance or design type documents, or computer printouts. Examples of data include research and engineering data, engineering drawings and associated lists, specifications, standards, process sheets, manuals, technical reports, catalog item identifications and related information, computer programs, computer codes,

computer data bases, and computer software documentation. The term data does not include financial, administrative, cost and pricing, and management information or other information incidental to contract administration.

Data validation -- a procedure used to ensure that the data generated from a test meet the specified test conditions, and that the instrumentation was functioning properly during the test

Design and procurement -- the design of the system, including the specification (consistent with the appropriate Task Plan) of the material, component, and/or system of interest; and the necessary purchasing function to receive the material, component, and/or system on the test site. This does not preclude Contractor from constructing components and systems on the test site to meet requirements of the Task Plan.

ECC -- emergency core cooling

Entrainment -- the process by which liquid, typically in droplet form, is carried in a flowing stream of gas or two-phase mixture

Evaluation -- the process of comparing the data with similar data, other data sets, existing models and correlations, or computer codes to arrive at general trends, consistency, and other qualitative descriptions of the results

Fallback -- the process whereby the liquid in a two-phase mixture flows countercurrent to the gas phase

FLECHT -- Full-Length Emergency Core Heat Transfer test program

FLECHT SEASET -- Full-Length Emergency Core Heat Transfer - Systems Effects and Separate Effects Tests

FLECHT SET -- Full-Length Emergency Core Heat Transfer - Systems Effects Tests

Heat transfer mechanisms -- the process of conduction, convection, radiation, or phase changes (for example, vaporization, condensation, boiling) in a control volume or a system

Hypothetical -- conjectured or supposed. It is understood that this program is concerned with study of physical phenomena associated with reactor accidents that have an extremely low probability and are therefore termed hypothetical.

Loss-of-coolant accident -- a break in the pressure boundary integrity resulting in loss of core cooling water

Model -- a set of mathematical expressions generated from physical laws to represent the thermal-hydraulic behavior of a system. A model rests mainly on physical principles.

PMG -- Program Management Group

Pressurized water reactor (PWR) -- a nuclear reactor type in which the system pressure exceeds saturation pressure, thus preventing gross vapor formation under normal operating conditions

Reduce data -- convert data from the measured signals to engineering units. In some cases the data are manipulated in a simple fashion to calculate quantities such as flows.

Separation -- the process whereby the liquid in a two-phase mixture is separated and detached from the gas phase

Silicon-controlled rectifier (SCR) -- a rectifier control system used to supply dc current to the bundle heater rods

Spacer grids -- the metal matrix assembly (egg crate design) used to support and space the heater rods in a bundle array

Test section -- lower plenum, bundle, and upper plenum

Test site -- the location of the test facilities where tests will be conducted

Transducer -- the devices used in experimental systems that sense the physical quantities, such as temperature, pressure, pressure difference, or power, and transform them into electrical outputs, such as volts

Unblocked -- the situation in which the flow area in the rod bundle or a single tube is not purposely obstructed

TABLE OF CONTENTS

Section	Title	Page
1	SUMMARY	1-1
2	INTRODUCTION	2-1
	2-1. General	2-1
	2-2. Task Objectives	2-4
	2-3. Test Facility	2-4
	2-4. Reference Conditions and Test Parameters	2-5
	2-5. Test Matrix	2-7
3	SYSTEM DESCRIPTION	3-1
	3-1. As-Built Facility Description	3-1
	3-2. Gravity Reflood Tests	3-2
	3-3. Steam Cooling Tests	3-6
	3-4. Heater Rod Bundle	3-6
	3-5. System Design Features	3-6
	3-6. Low Mass Housing	3-19
	3-7. Bundle Differential Pressure Cells	3-19
	3-8. Heater Rod Seals	3-21
	3-9. Steam Probes	3-21
	3-10. Pressure Control	3-22
	3-11. Facility and Bundle Operation	3-22
	3-12. Power Measurement	3-22
	3-13. Coolant Injection System	3-23
	3-14. Data Acquisition Systems	3-23
	3-15. Computer Data Acquisition System (CDAS)	3-23
	3-16. Fluke Data Logger	3-24

TABLE OF CONTENTS (cont)

Section	Title	Page
	3-17. Multiple-Pen Strip Chart Recorders	3-25
	3-18. Instrumentation	3-25
	3-19. Heater Rod Bundle Instrumentation	3-26
	3-20. Test Section Instrumentation	3-26
	3-21. Carryover Tank Instrumentation	3-26
	3-22. Steam Separator Instrumentation	3-29
	3-23. Exhaust Pipe Instrumentation	3-29
	3-24. Accumulator Tank Instrumentation	3-29
	3-25. Injection Line Instrumentation	3-29
	3-26. Gravity Reflood Test Instrumentation	3-29
	3-27. Test Procedure	3-30
	3-28. Gravity Reflood Test Procedure	3-31
	3-29. Steam Cooling Test Procedure	3-32
	3-30. Boiloff Test Procedure	3-32
	3-31. Heater Rod Replacement	3-32
	3-32. Photographic Studies	3-35
4	TEST RESULTS	4-1
	4-1. Summary of Run Conditions and Test Results	4-1
	4-2. Data Reduction Methods	4-2
	4-3. Mass Balance Data	4-2
	4-4. Quench Criteria	4-2
	4-5. Heat Transfer Coefficients	4-20
	4-6. Failed Rods	4-22
	4-7. Steam Cooling Tests	4-24
	4-8. Rod Bundle Distortion	4-25
	4-9. Summary and Conclusions	4-26

TABLE OF CONTENTS (cont)

Section	Title	Page
APPENDIX A	DETAILED FACILITY DESCRIPTION	A-1
APPENDIX B	PHOTOGRAPHIC STUDIES	B-1
APPENDIX C	DATA TABLES AND PLOTS	C-1
APPENDIX D	ERROR ANALYSIS	D-1
APPENDIX E	CALCULATION TECHNIQUES	E-1
APPENDIX F	FAILED ROD ANAYSIS	F-1
APPENDIX G	ROD BUNDLE DISTORTION	G-1

LIST OF ILLUSTRATIONS

Figure	Title	Page
2-1	Decay Power Curve (ANS + 20%) 30 Seconds After Initiation of a Loss-of-Coolant Accident	2-6
2-2	Cosine Axial Power Profile	2-8
3-1	FLECHT SEASET Unblocked Bundle Flow Diagram, Forced Reflood Configuration	3-3
3-2	FLECHT SEASET Upper Plenum Baffle	3-5
3-3	Bundle Cross Section	3-7
3-4	FLECHT SEASET Unblocked Bundle Test Section Housing Differential Pressure Cell Hookup	3-20
3-5	FLECHT SEASET Computer Hardware Interface (Unblocked Bundle Task)	3-27
3-6	Upper and Lower Plenum Thermocouple Location	3-28
4-1	FLECHT SEASET Data Reduction Flow Chart	4-17
4-2	Mass Balance Versus Time (Reference Run)	4-18
4-3	FLECHT SEASET Unblocked Bundle Mass Balance Results	4-19
4-4	Temperature History of Hottest Rod Thermocouple (Reference Run)	4-21
4-5	Smoothed Versus Average Heat Transfer Data	4-23

LIST OF TABLES

Table	Title	Page
2-1	Comparison of PWR Vendors' Fuel Rod Geometries (Old and New)	2-2
2-2	Reference Test Conditions for Unblocked Bundle Task	2-9
2-3	Range of Initial Test Conditions for Unblocked Bundle Task	2-11
2-4	Original Forced Reflood, Gravity Reflood, and Steam Cooling Test Matrix	2-13
3-1	Initial Data Acquisition System Channel Assignments	3-8
4-1	FLECHT SEASET Unblocked Bundle Reflood Test Data Summary	4-3
4-2	FLECHT SEASET Unblocked Bundle Steam Cooling Test Data Summary	4-15

SECTION 1
SUMMARY

As part of the NRC/EPRI/Westinghouse Full-Length Emergency Core Heat Transfer Separate Effects and Systems Effects Tests (FLECHT SEASET) reflood heat transfer and hydraulic program,[1] a series of forced flow and gravity feed bundle reflooding tests and steam cooling tests were conducted on a heater rod bundle whose dimensions are typical of current PWR fuel rod arrays. The purpose of these tests was to provide a reflooding data base which can be used to help develop or verify reflood prediction methods, to serve as a comparison to the existing FLECHT reflood data on previous fuel rod array sizes,[2-5] and to provide a baseline to evaluate the effects of flow blockage in a 161-rod FLECHT bundle during reflood. The purpose of the steam cooling tests was to provide a data base from which a correlation for steam flow heat transfer in a rod bundle array could be developed.

In this test program, the existing FLECHT facility[6,7] was modified to accept a new heater rod bundle whose dimensions are typical of the newer PWR fuel rod array sizes currently in use by PWR and PWR fuel vendors. Sufficient instrumentation was installed in the test facility that mass and energy balances could be computed from the data.

These tests examined the effects of initial clad temperature, variable stepped flooding rates, rod peak power, constant low flooding rates, coolant subcooling, and system

---

1. Conway, C. E., et al., "PWR FLECHT Separate Effects and Systems Effects Test (SEASET) Program Plan," NRC/EPRI/Westinghouse-1, December 1977.
2. Cadek, F. F., et al., "PWR FLECHT (Full Length Emergency Cooling Heat Transfer) Final Report," WCAP-7665, April 1971.
3. Cadek, F. F., et al., "PWR FLECHT Final Report Supplement," WCAP-7931, October 1972.
4. Lilly, G. P., et al., "PWR FLECHT Cosine Low Flooding Rate Test Series Evaluation Report," WCAP-8838, March 1977.
5. Lilly, G. P., et al., "PWR FLECHT Skewed Profile Low Flooding Rate Test Series Evaluation Report," WCAP-9183, November 1977.
6. Rosal, E. R., et al., "FLECHT Low Flooding Rate Skewed Test Series Data Report," WCAP-9108, May 1977.
7. Hochreiter, L. E., et al., "PWR FLECHT SEASET Unblocked Bundle, Forced and Gravity Reflood Task: Task Plan Report," NRC/EPRI/Westinghouse-3, March 1978.

pressure. Data obtained in runs which met the test specifications are reported here; they include rod clad temperatures, turnaround and quench times, heat transfer coefficients, inlet flooding rates, overall mass balance, differential pressures and calculated void fractions in the test section, thimble wall and steam temperatures, and exhaust steam and liquid carryover rates.

During this test program, rod distortion in the outer rows of rods was observed through the housing windows. At the conclusion of the test program, the rod bundle was removed and subsequently examined. It was found that severe rod distortion had occurred at the 1.83 m (72 in.) elevation even in the center of the bundle. The test data were examined to ascertain the point in the test program at which the extent of the rod distortion negated the use of the data for hot rod reflood heat transfer correlation development. Analysis of the data indicated that there was no rod distortion in the center region of the bundle (two rod rows away from the housing) up through test 31805. Between tests 31922 and 33749, some distortion of the center rods was possible, but it is believed to have been a second-order effect. Beyond test 34610, the distortion cannot be ignored; data above the 1.52 m (60 in.) elevation should not be used for heat transfer development.

A complete set of data for all valid tests performed in the unblocked bundle test program will be available in the NRC Data Bank.

SECTION 2
INTRODUCTION

2-1. GENERAL

The present nonproprietary data base for reflood heat transfer in a simulated pressurized water reactor (PWR) is limited to heater rod bundles that are typified by the Westinghouse 15 x 15 design and resulted from FLECHT tests.[1-4] These tests utilized Westinghouse 15 x 15 (or 14 x 14) dimensions and were representative of all the PWR vendors' dimensions (table 2-1). PWR reactor and fuel vendors are currently using fuel assemblies with smaller fuel rod diameter and pitch (table 2-1); there is therefore a need for testing assemblies with the new dimensions.

Models which predict the dependence of reflood heat transfer and mass carryout rate fractions (CRF) as a function of fuel bundle geometry (particularly rod diameter and pitch) have not been fully established in either phenomenological or correlational form. Carryout rate fraction models have been developed utilizing an energy balance method by Sun and Duffey[5] and similarly by Yeh and Hochreiter.[6] However, these models could benefit from experimental verification relative to fuel rod geometries other than the 15 x 15 type rod geometry.

---

1. Cadek, F. F., et al., "PWR FLECHT (Full Length Emergency Cooling Heat Transfer) Final Report," WCAP-7665, April 1971.

2. Cadek, F. F., et al., "PWR FLECHT Final Report Supplement," WCAP-7931, October 1972.

3. Lilly, G. P., et al., "PWR FLECHT Cosine Low Flooding Rate Test Series Evaluation Report," WCAP-8838, March 1977.

4. Lilly, G. P., et al., "PWR FLECHT Skewed Profile Low Flooding Rate Test Series Evaluation Report," WCAP-9183, November 1977.

5. Sun, K. H., and Duffy, R. B., "A Generalized Model for Predicting Mass Effluences During Reflooding," Nucl. Tech. 43, 22-27 (1979).

6. Yeh, H. C., and Hochreiter, L. E., "Mass Effluence During FLECHT Forced Reflood Experiments," Trans. Amer. Nucl. Soc. 24, 301-302 (1976).

The tests planned under the Unblocked Bundle, Forced and Gravity Reflood Task utilized a new core rod geometry (CRG)[1] that is typified by the Westinghouse 17 x 17 fuel rod design (table 2-1). This CRG is representative of all current vendors' PWR fuel assembly geometries.

TABLE 2-1

COMPARISON OF PWR VENDORS' FUEL ROD GEOMETRIES (OLD AND NEW)

Vendor	Dimension	
	Rod Diameter [mm (in.)]	Rod Pitch [mm (in.)]
NEW FUEL ASSEMBLIES (CRG)		
Westinghouse	9.5 (0.374)	12.6 (0.496)
Babcock & Wilcox	9.63 (0.379)	12.8 (0.502)
Combustion Engineering	9.7 (0.382)	12.9 (0.506)
OLD FUEL ASSEMBLIES		
Westinghouse	10.7 (0.422)	14.3 (0.563)
Babcock & Wilcox	10.9 (0.430)	14.4 (0.568)
Combustion Engineering	11.2 (0.440)	14.7 (0.580)

The tests performed in this task are classified as separate effects tests. In this case the bundle is isolated from the system and the thermal-hydraulic conditions are prescribed at the bundle entrance and exit. Within the bundle, the dimensions are full scale, compared to a PWR, with the exception of overall radial dimension. The low mass housing used in these test series was designed to minimize the wall effects such that the rods one row or more away from the housing in the FLECHT bundle are representative of any region in a PWR core. Examination of the housing performance for the skewed axial profile FLECHT tests indicates that it does simulate this radial boundary condition and that only the rods immediately adjacent to the housing are affected by the housing presence. To preserve proper thermal scaling of the

1. The CRG is defined in this program as a nominal rod-to-rod pitch of 12.6 mm (0.496 in.) and outside nominal diameter of 9.5 mm (0.374 in.), representative of various nuclear fuel vendors' new fuel assembly geometries and commonly referred to as the 17 x 17 or 16 x 16 assemblies.

FLECHT facility with respect to a PWR, the power to flow area ratio is nearly the same as that of a PWR fuel assembly. In this fashion, the steam vapor superheat, entrainment, and fluid flow behavior should be similar to that expected in a PWR for the same boundary conditions.

In addition to examination of fuel assembly geometry effects on reflood heat transfer and carryout rate fraction behavior, the data resulting from this task will be utilized as a baseline in assessing the effects of flow blockage. At present the Appendix K rule requires a conservative steam cooling heat transfer calculation when the core flooding rate is below 25 mm/sec (1 in./sec).[1] This restriction is a result of having only a limited amount of flow blockage data. The test results of the limited data base (22 forced flooding tests) indicated heat transfer improvement at flooding rates of 25 mm/sec (1 in./sec) or more. Since the existing data base is sparse and only one test exists at flooding rates of less than 25 mm/sec (1 in./sec), the observed improved reflood heat transfer was disallowed in the Appendix K rule for flooding rates above 25 mm/sec (1 in./sec), and a steam cooling calculation was imposed when the flooding rate during reflood is below 25 mm/sec (1 in./sec). This steam cooling calculation results in an increase in calculated peak cladding temperature for flow blockage cases. Currently, flow blockage tests utilizing the new CRG are planned as part of the FLECHT SEASET program[2] and are described in the 21-rod bundle flow blockage task plan[3] and the 161-rod blocked bundle task plan.[4]

The data in this task will be utilized as a baseline or reference point for no flow blockage in a CRG bundle. To this extent, the data from this task will be used as an aid in addressing Appendix K flow blockage/steam cooling requirements.

---

1. "Acceptance Criteria for Emergency Core Cooling Systems for Light-Water Cooled Nuclear Power Reactors," 10CFR50.46 and Appendix K of 10CFR50, Federal Register, Vol. 39, No. 3, January 4, 1974.

2. Conway, C. E., et al., "PWR FLECHT Separate Effects and Systems Effects Test (SEASET) Program Plan," NRC/EPRI/Westinghouse-1, December 1977.

3. Hochreiter, L. E., et al., "PWR FLECHT SEASET 21-Rod Flow Blockage Task: Task Plan Report," NRC/EPRI/Westinghouse-5, March 1980.

4. Hochreiter, L. E., et al., "PWR FLECHT SEASET 161-Rod Blocked Bundle Task: Task Plan Report," NRC/EPRI/Westinghouse Report No. 6, July 1980.

The data generated from this task will also aid in the development or verification of phenomenological reflood models which attempt to mechanistically describe the reflood process. The additional instrumentation within the bundle and the separate effects nature of these experiments make the resulting data useful for this purpose. The data will also be analyzed with the express purpose of providing the basis for reflood code comparison and verification.

2-2. TASK OBJECTIVES

The objectives of the unblocked bundle cosine axial power profile task are to develop a data base which meets the following objectives:

- To aid in the development or verification of computational methods used by others to predict the reflood thermal-hydraulic behavior of CRG rod arrays

- To establish a baseline for comparison with the flow blockage task data to determine the effect of blockage

- To evaluate the effects of bundle geometry on reflood heat transfer in comparison with previous FLECHT 15 x 15 unblocked tests

- To provide and evaluate data for single-phase steam cooling heat transfer correlation development

2-3. TEST FACILITY

The existing FLECHT facility in which the low flooding rate test series[1] was conducted was utilized as the basic configuration for this task. Design features of the facility include the following:

- A cylindrical low mass bundle housing to minimize housing heat release

1. Rosal, E. R., et al., "FLECHT Low Flooding Rate Skewed Test Series Data Report," WCAP-9108, May 1977.

-- Housing differential pressure cells every 0.30 m (12 in.) to obtain void fraction measurements along the heated length of the bundle

-- Steam probes in each of 11 thimble tubes to measure steam superheat radially and axially across the bundle

-- 177 heater rod thermcouple computer channels

-- Housing windows at the 0.91, 1.83, and 2.74 m (36, 72, and 108 in.) elevations

2-4. REFERENCE CONDITIONS AND TEST PARAMETERS

The reflood phase of the PWR design basis LOCA transient is calculated to start approximately 30 seconds after initiation of a hypothetical break. At this time the lower plenum, which had emptied during the postulated blowdown, has refilled to the bottom of the core. The applicable reference assumptions for the reflood transient for a worst-case analysis of a hypothetical LOCA typical of a standard Westinghouse 17 x 17 four-loop[1] or other PWR vendor plant are as follows:

-- The core hot assembly is simulated in terms of peak power (kw/m) and initial temperatures at the time of core recovery.

-- Decay power is ANS plus 20 percent (figure 2-1).

-- The initial rod clad temperature is primarily dependent on the full-power linear heating rate at the time of core recovery. For the period from 30 seconds to core recovery, typical results yield an initial clad temperature in the hot assembly of 871°C (1600°F).

-- Coolant temperatures are selected to maintain a constant subcooling to facilitate the determination of parametric effects.

---

1. Johnson, W. J., et al., "Westinghouse ECCS - Four-Loop Plant (17x17) Sensitivity Studies," WCAP-8566, July 1975.

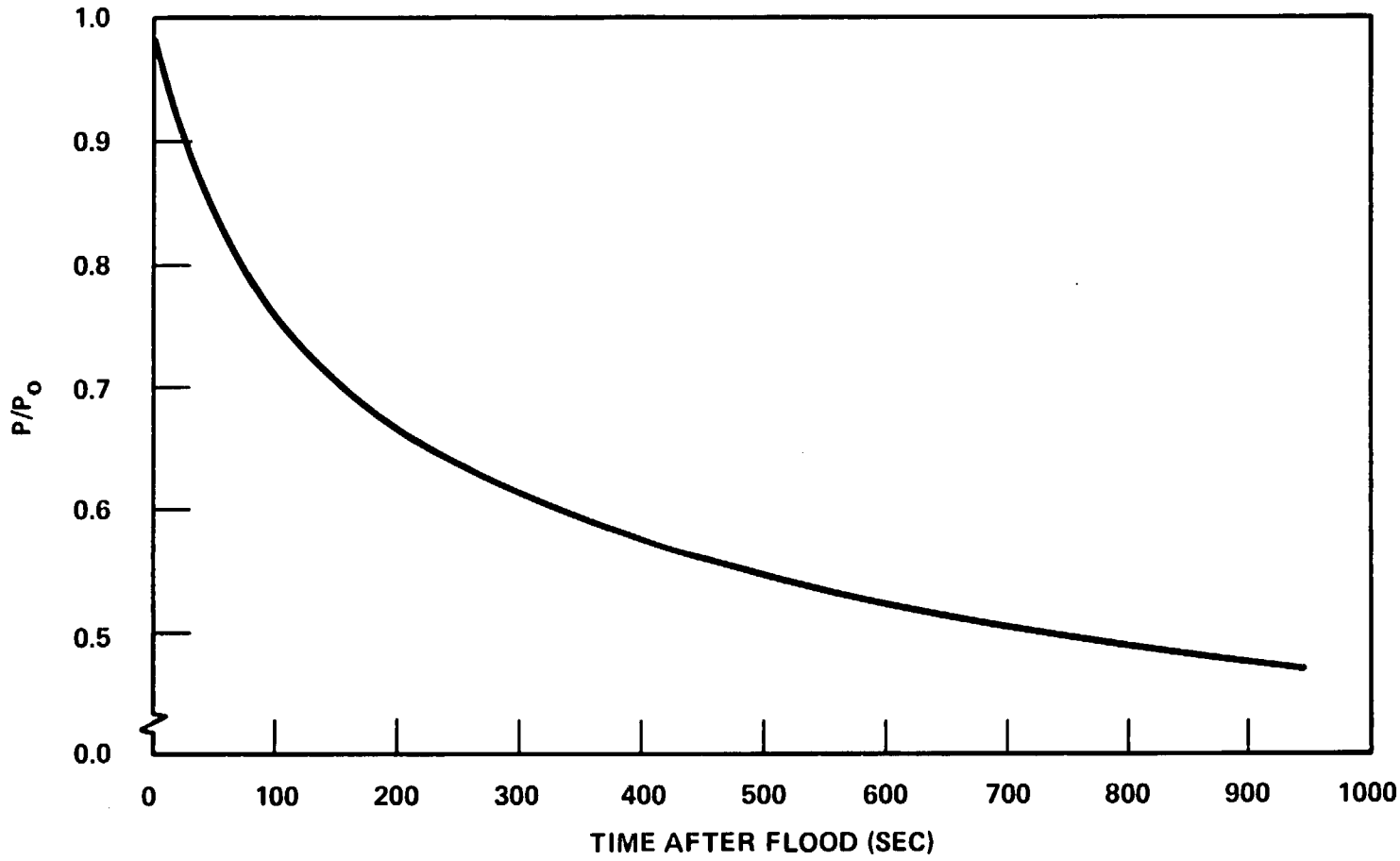

Figure 2-1. Decay Power Curve (ANS + 20%) 30 Seconds After Initiation of a Loss-of-Coolant Accident

16539-7

-- Coolant is injected directly into the test section lower plenum for the forced flooding rate tests, and into the bottom of the downcomer for the gravity reflood scoping tests. Injection into the bottom of the downcomer is used for better test facility pressure control.

-- Upper plenum pressure at the end of blowdown is approximately 0.14 MPa (20 psia) for an ice condenser plant, and about 0.28 MPa (40 psia) for a dry containment plant.

-- The axial power shape built in the heater rod is the modified cosine with a power peak-to-average ratio of 1.66 (figure 2-2).

The majority of tests were performed with a uniform radial power profile, but some tests were performed with radial power distribution which assumes a 1.05 peak-to-average ratio based on simulating a quarter section of a 17 x 17 PWR fuel assembly. The use of the 1.66 axial power profile will allow easier comparisons with the earlier 15 x 15 FLECHT tests, since only rod array dimensions are different between the two test series. The effect of different axial power shapes has been studied in the FLECHT program and data are available to the code developer on different power shapes. In addition, although the 1.66 axial power profile is more peaked than current LOCA analysis (which indicates an axial peaking factor at 1.5), these differences are relatively small, typically 15 percent variation over a given axial increment.

The reference initial conditions are listed in table 2-2, based on the above reference assumptions.

2-5. TEST MATRIX

To meet the objectives of the test program, a test matrix was designed to provide experimental data on the following effects:

-- Constant flooding rate

-- Pressure at constant rate

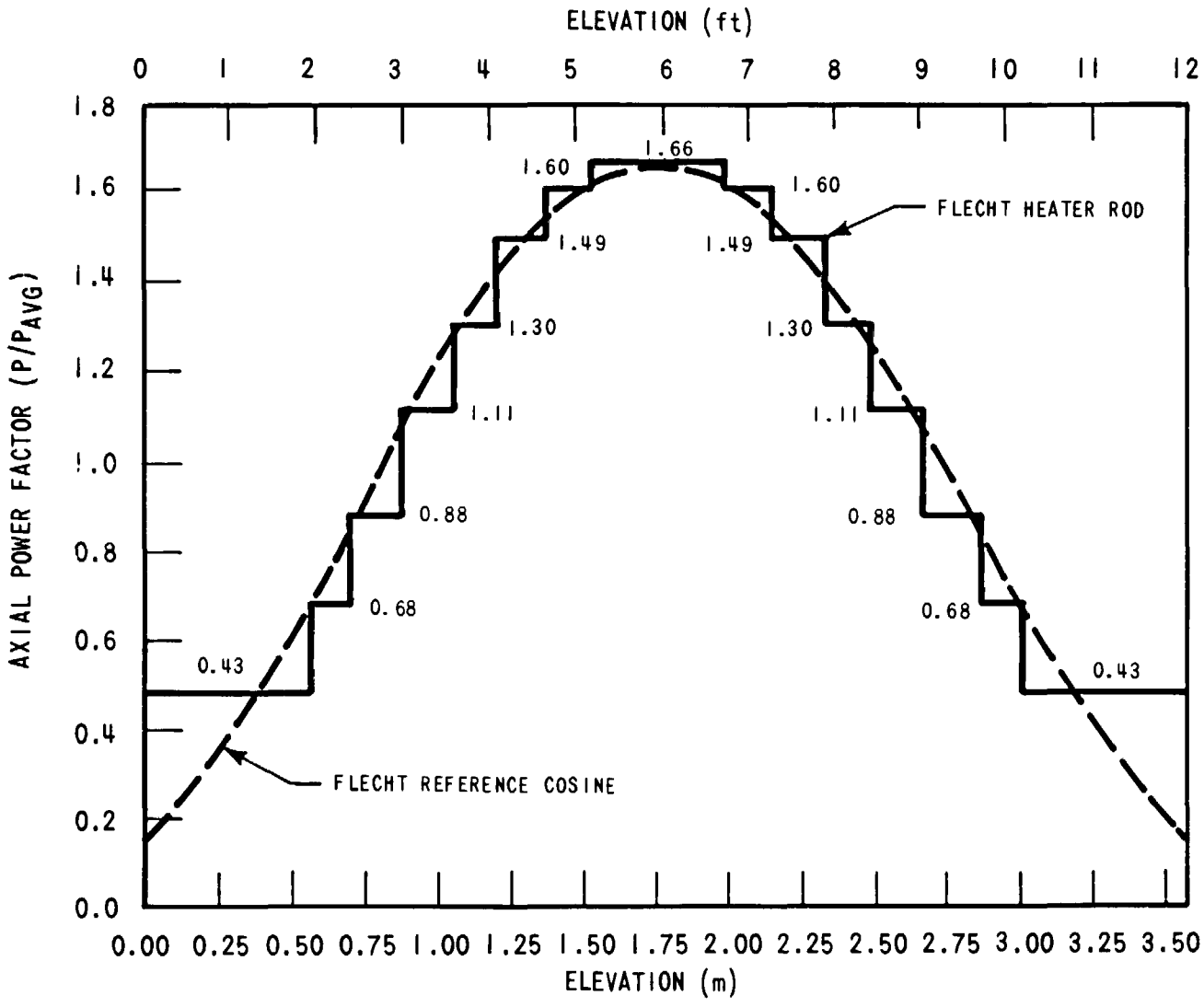

Figure 2-2. Cosine Axial Power Profile

TABLE 2-2

REFERENCE TEST CONDITIONS FOR UNBLOCKED BUNDLE TASK

Parameter	Initial Condition
Initial clad temperature	871°C (1600°F)
Peak power	2.3 kw/m (0.7 kw/ft)
Upper plenum pressure	0.28 MPa (40 psia)
Injection rate with lower plenum initially full	25 mm/sec (1.0 in./sec)
Coolant ΔT subcooling	78°C (140°F)
Radial power distribution	Uniform
Axial power shape	Cosine
Initial downcomer head	0.0 m (0.0 ft)

-- Coolant subcooling

-- Initial clad temperature

-- Rod peak power

-- Radial power

-- Variable stepped flow

-- Data repeatability within the test matrix

-- Gravity reflood

-- Coolant subcooling transient

-- Steam cooling and boiloff

The range of test conditions and parameters studied during the test program is shown in table 2-3.

The approved test matrix consisted originally of 51 tests grouped into the first 15 series (table 2-4). However, during the course of the test program, modifications and/or additions were made to the test matrix to obtain the most relevant data for heat transfer correlation development, within bundle life limitations. The two steam cooling tests, tests 45 and 46, could not be conducted because of the 204°C (400°F) temperature limit of the upper heater rod seals. These two steam cooling tests were replaced with a series of low-temperature [$\leq$ 204°C (400°F) steam temperature] steam cooling tests, tests 52 through 70.

Three tests (57, 58, and 59) were also conducted in which the bundle was prefilled with saturated water to the 3.05 m (120 in.) elevation and subsequently allowed to boil off.

The tests actually conducted in this test program are listed in section 4.

TABLE 2-3

RANGE OF INITIAL TEST CONDITIONS FOR UNBLOCKED BUNDLE TASK

Initial clad temperature	135°C-1079°C (300°F-2000°F)
Peak power	0.87-3.1 kw/m (0.27-0.95 kw/ft)
Upper plenum pressure	0.14-0.41 MPa (20-60 psia)
Flooding rates:	
Constant	10-152 mm/sec (0.4 - 6 in./sec)
Variable in steps	152 → 15 mm/sec (6.0 → 0.6 in./sec)[a]
Injection rates (gravity reflood tests):	
Variable in steps	6.49 → 0.77 kg/sec (14.3 → 1.7 lb/sec)[a]
Coolant subcooling	3°C-78°C (5°F-140°F)

a. For specific variable flooding rate, see section 6.

TABLE 2-4

ORIGINAL FORCED REFLOOD, GRAVITY REFLOOD, AND STEAM COOLING TEST MATRIX

Test No.	Upper Plenum Pressure [MPa (psia)]	Rod Initial T_{clad} [°C (°F)]	Rod Peak Power [kw/m (kw/ft)]	Flooding Rate [mm/sec (in./sec)]	Inlet Subcooling [°C (°F)]	Radial Power Distribution	Movies/ Pictures	Test Series	Comments
1	0.28 (40)	871 (1600)	2.3 (0.7)	152 (6.0)	78 (140)	Uniform	X	1	Radial power distribution[a]
2	0.28 (40)	871 (1600)	2.3 (0.7)	76 (3.0)	78 (140)	Uniform		Constant	
3	0.28 (40)	871 (1600)	2.3 (0.7)	38 (1.5)	78 (140)	Uniform		flooding rate	Overlap test - low flooding
4	0.28 (40)	871 (1600)	2.3 (0.7)	25 (1.0)	78 (140)	Uniform	X		rate cosine run 03113
5	0.28 (40)	871 (1600)	2.3 (0.7)	20 (0.8)	78 (140)	Uniform	X		
6	0.28 (40)	871 (1600)	1.3 (0.4)	15 (0.6)	78 (140)	Uniform			Overlap test - low flooding
7	0.28 (40)	871 (1600)	1.3 (0.4)	10 (0.4)	78 (140)	Uniform	X		rate cosine run 02414
8	0.14 (20)	871 (1600)	2.3 (0.7)	76 (3.0)	78 (140)	Uniform		2	
9	0.14 (20)	871 (1600)	2.3 (0.7)	25 (1.0)	78 (140)	Uniform	X	Pressure	
10	0.14 (20)	871 (1600)	1.3 (0.4)	20 (0.8)	78 (140)	Uniform			
11	0.14 (20)	871 (1600)	1.3 (0.4)	15 (0.6)	78 (140)	Uniform			
12	0.14 (20)	871 (1600)	1.3 (0.4)	10 (0.4)	78 (140)	Uniform	X		
13	0.41 (60)	871 (1600)	2.3 (0.7)	25 (1.0)	78 (140)	Uniform			
14	0.28 (40)	871 (1600)	2.3 (0.7)	25 (1.0)	2.8 (5)	Uniform	X	3	
15	0.14 (20)	871 (1600)	2.3 (0.7)	25 (1.0)	2.8 (5)	Uniform		ΔT sub-	
16	0.28 (40)	871 (1600)	2.3 (0.7)	25 (1.0)	78-2.8 (140-5) linear over 500 sec	Uniform		cooling	
17	0.28 (40)	538 (1000)	2.3 (0.7)	38 (1.5)	78 (140)	Uniform		4	
18	0.28 (40)	260 (500)	2.3 (0.7)	38 (1.5)	78 (140)	Uniform		Initial	
19	0.14 (20)	260 (500)	2.3 (0.7)	38 (1.5)	78 (140)	Uniform		T_{clad}	
20	0.28 (40)	1093 (2000)	2.3 (0.7)	38 (1.5)	78 (140)	Uniform			
21	0.28 (40)	871 (1600)	1.3 (0.4)	38 (1.5)	78 (140)	Uniform		5	
22	0.14 (20)	871 (1600	1.3 (0.4)	25 (1.0)	78 (140)	Uniform		Rod peak power	
23	0.28 (40)	260 (500)	1.3 (0.4)	38 (1.5)	78 (140)	Uniform			
24	0.28 (40)	871 (1600)	3.1 (0.95)	38 (1.5)	78 (140)	Uniform	X		
25	0.28 (40)	871 (1600)	2.3 (0.7)	25 (1.0)	78 (140)	FLECHT (15x15)		6	Overlap test - low flooding
								Radial power	rate cosine run 05132
									Radial power distribution[b]
26	0.28 (40)	871 (1600)	2.3 (0.7)	25 (1.0)	78 (140)	FLECHT (17x17)			Radial power distribution[c]
27	0.28 (40)	871 (1600)	2.3 (0.7)	20 (0.8)	78 (140)	FLECHT (17x17)			Radial power distribution[c]
28	0.14 (20)	871 (1600)	2.3 (0.7)	25 (1.0)	78 (140)	FLECHT (17x17)	Still		Radial power distribution[c]

a. Figure 6-2, NRC/EPRI/Westinghouse-3
b. Figure 6-4, NRC/EPRI/Westinghouse-3
c. Figure 6-3, NRC/EPRI/Westinghouse-3

TABLE 2-4 (cont)

ORIGINAL FORCED REFLOOD, GRAVITY REFLOOD, AND STEAM COOLING TEST MATRIX

Test No.	Upper Plenum Pressure [MPa (psia)]	Rod Initial T_{clad} [°C (°F)]	Rod Peak Power [kw/m (kw/ft)]	Flooding Rate [mm/sec (in./sec)]	Inlet Subcooling [°C (°F)]	Radial Power Distribution	Movies/ Pictures	Test Series	Comments
29	0.28 (40)	871 (1600)	2.3 (0.7)	25 (1.0)	78 (140)	Uniform	Still	7 Repeat test	
30	0.28 (40)	871 (1600)	2.3 (0.7)	25 (1.0)	78 (140)	Uniform	Still		
31	0.28 (40)	871 (1600)	2.3 (0.7)	0-483-32 (0-19-1.25) 5 sec 32-13 (1.25-0.5) onward	78 (140)	Uniform		8 Variable flooding rate	Continuously variable flow - dry containment plant[d]
32	0.14 (20)	871 (1600)	1.6 (0.5)	0-102-38 (0-4-1.5) 5 sec 38-13 (1.5-0.5) onward	2.8 (5)	Uniform			Continuously variable flow - UHI plant[e]
33	0.28 (40)	871 (1600)	2.3 (0.7)	152 (6) 5 sec 20 (0.8) onward	78 (140)	Uniform	X		Variable stepped flow - dry containment plant[f]
34	0.14 (20)	871 (1600)	2.3 (0.7)	152 (6) 5 sec 20 (0.8) onward	78 (140)	Uniform	X		Variable stepped flow - dry containment plant[f]
35	0.28 (40)	871 (1600)	2.3 (0.7)	152 (6) 5 sec 25 (1.0) 200 sec 15 (0.6) onward	78 (140)	Uniform	X		Variable stepped flow - dry containment plant[g]
				Injection Rate [kg/sec (lbm/sec)]					
36	0.28 (40)	871 (1600)	2.3 (0.7)	6.5 (14.3) 14 sec 0.77 (1.7) onward	78 (140)	Uniform	X	9 Simulated gravity reflood	
37	0.14 (20)	871 (1600)	2.3 (0.7)	6.5 (14.3) 14 sec 0.77 (1.7) onward	78 (140)	Uniform	X		
38	0.28 (40)	871/260 (1600/500)	2.3/1.3 (0.7/0.4)	6.5 (14.3) 14 sec 0.77 (1.7) onward	78 (140)	Hot and cold channels			Radial power distribution[h]
39	0.14 (20)	871/260 (1600/500)	2.3/1.3 (0.7/0.4)	6.5 (14.3) 14 sec 0.77 (1.7) onward	78 (140)	Hot and cold channels			Radial power distribution[a]

a. Figure 6-2, NRC/EPRI/Westinghouse-3
d. Figure 6-6, NRC/EPRI/Westinghouse-3
e. Figure 6-7, NRC/EPRI/Westinghouse-3
f. Figure 6-9, NRC/EPRI/Westinghouse-3
g. Figure 6-10, NRC/EPRI/Westinghouse-3
h. Figure 6-5, NRC/EPRI/Westinghouse-3

TABLE 2-4 (cont)

ORIGINAL FORCED REFLOOD, GRAVITY REFLOOD, AND STEAM COOLING TEST MATRIX

Test No.	Upper Plenum Pressure [MPa (psia)]	Rod Initial T_{clad} [°C (°F)]	Rod Peak Power [kw/m (kw/ft)]	Flooding Rate [mm/sec (in/sec)]	Inlet Subcooling [°C (°F)]	Radial Power Distribution	Movies/ Pictures	Test Series	Comments
40	0.28 (40)	871/260 (1600/500)	2.3/1.3 (0.7/0.4)	38 (1.5)	78 (140)	Hot and cold channels		10 Hot and cold channels	Radial power distribution[a]
41	0.14 (20)	871/260 (1600/500)	2.3/1.3 (0.7/0.4)	38 (1.5)	78 (140)	Hot and cold channels			Radial power distribution[a]
42	0.28 (40)	871/260 (1600/500)	2.3/1.3 (0.7/0.4)	38 (1.5)	78 (140)	Half bundle			Radial power distribution[h]
43	0.28 (40)	871/260 (1600/500)	2.3/1.3 (0.7/0.4)	20 (0.8)	78 (140)	Hot and cold channels			
				Injection Rate [kg/sec (lbm/sec)]					
44	0.14 (20)	0-0.9 m-149°C (0-3 ft-300°F) 1.8 m-871°C (6 ft-1600°F)	2.3 (0.7)	6.5 (14.3) 14 sec 0.77 (1.74) onward	78 (140)	Uniform	X	11 Axial temperature distribution simulated gravity reflood	
45	0.28 (40)	871 (1600)	2.3 (0.7)	0.36 (0.81) steam at 131°C (267°F)	0 (0)	Uniform		12 Steam cooling	
46	0.14 (20)	871 (1600)	2.3 (0.7)	0.37 (0.82) steam at 108°C (228°F)	0 (0)	Uniform			
47	0.27 (39)	845 (1554)	2.5 (0.75)	2.7 (6) 5 sec 0.36 (0.8) onward	75 (135)	FLECHT (15x15)		13 Overlap test	Overlap test low flooding cosine run 04516, radial power distribution[b]
48	0.14 (20)	844 (1552)	2.5 (0.75)	0.46 (1.0)	77 (139)	FLECHT (15x15)			Overlap test low flooding rate cosine run 04641, radial power distribution[b]

a. Figure 6-2, NRC/EPRI/Westinghouse-3
b. Figure 6-4, NRC/EPRI/Westinghouse-3
h. Figure 6-5, NRC/EPRI/Westinghouse-3

TABLE 2-4 (cont)

ORIGINAL FORCED REFLOOD, GRAVITY REFLOOD, AND STEAM COOLING TEST MATRIX

Test No.	Upper Plenum Pressure [MPa (psia)]	Rod Initial T_{clad} [°C (°F)]	Rod Peak Power [kw/m (kw/ft)]	Flooding Rate [mm/sec (in/sec)]	Inlet Subcooling [°C (°F)]	Radial Power Distribution	Movies/ Pictures	Test Series	Comments
49	0.28 (40)	732 (1350)	1.9 (0.57)	25 (1.0)	67 (120)	Uniform		14 Comparison with Westinghouse proprietary reflood data	
50	0.14 (20)	732 (1350)	1.5 (0.46)	25 (1.0)	67 (120)	Uniform			
51	0.28 (40)	871 (1600)	2.3 (0.7)	25 (1.0)	78 (140)	Uniform		15 Power decay	Power decay based on 40 sec after initiation of LOCA
				Flow Rate [kg/sec (kw/ft)]					
52	0.28 (40)	131 (267)	0.02 (0.006)	0.045 (0.10)	0 (0)	Uniform		16 Steam cooling	
53	0.28 (40)	131 (267)	0.16 (0.05)	0.36 (0.80)	0 (0)	Uniform			
54	0.28 (40)	131 (267)	0.059 (0.018)	0.14 (0.30)	0 (0)	Uniform			
55	0.28 (40)	131 (267)	0.1 (0.03)	0.23 (0.50)	0 (0)	Uniform			
56	0.28 (40)	131 (267)	1.3 (0.40)	0.36 (0.80)	0 (0)	Uniform			
57	0.41 (60)	145 (293)	1.38 (0.421)	0 (0)	0 (0)	Uniform		17 Boiloff	
58	0.14 (20)	108 (228)	1.38 (0.421)	0 (0)	0 (0)	Uniform			
59	0.28 (40)	131 (267)	1.38 (0.421)	0 (0)	0 (0)	Uniform			
60	0.28 (40)	131 (267)	0.16 (0.048)	0.36 (0.80)	0 (0)	Uniform		16 Steam cooling	
61	0.28 (40)	131 (267)	0.13 (0.039)	0.29 (0.65)	0 (0)	Uniform			
62	0.28 (40)	131 (267)	0.079 (0.024)	0.18 (0.40)	0 (0)	Uniform			
63	0.28 (40)	131 (267)	0.0472 (0.0144)	0.11 (0.24)	0 (0)	Uniform			
64	0.28 (40)	131 (267)	0.0374 (0.0114)	0.086 (0.19)	0 (0)	Uniform			
65	0.28 (40)	131 (267)	0.03 (0.009)	0.068 (0.15)	0 (0)	Uniform			
66	0.28 (40)	131 (267)	0.024 (0.0072)	0.054 (0.12)	0 (0)	Uniform			
67	0.28 (40)	131 (267)	0.02 (0.006)	0.045 (0.10)	0 (0)	Uniform			
68	0.28 (40)	131 (267)	0.01 (0.003)	0.02 (0.05)	0 (0)	Uniform			
69	0.28 (40)	131 (267)	0.059 (0.018)	0.1 (0.3)	0 (0)	Uniform			
70	0.28 (40)	131 (267)	0.098 (0.030)	0.2 (0.5)	0 (0)	Uniform			

SECTION 3
SYSTEM DESCRIPTION

3-1. AS-BUILT FACILITY DESCRIPTON

The FLECHT low flooding rate skewed test facility[1] was modified to conduct the unblocked bundle, forced and gravity reflood tests as shown in figure 3-1.

The facility with modifications consisted of the following:

-- A new low mass housing test section and upper and lower plenums

-- An upper plenum baffle (figure 3-2) to improve liquid carryover separation

-- The 161-rod bundle and related instrumentation

-- The existing pressurized water supply accumulator and injection line with three rotameters and a turbine meter to measure injection rates from 10 mm/sec (0.4 in./sec) in forced flooding tests to 6.49 kg/sec (14.3 lb/sec) in gravity reflood tests

-- A close-coupled carryover tank connected to the test section upper plenum with a storage capacity of 65.8 kg (145 lb)

-- A commercially available steam separator with a capacity of 0.315 kg/sec (2500 lb/hr) and a liquid collection tank with a volume of 9.5 kg (21 lb) to collect liquid entrained in the exhaust line. The steam separator had a storage capacity of approximately 193 kg (425 lb).

-- Exhaust piping with a system pressure control valve and an orifice plate flowmeter to measure exhaust steam flow rate

---

1. Rosal, E. R., et al., "FLECHT Low Flooding Rate Skewed Test Series Data Report," WCAP-9108, May 1977.

-- A commercially available electric steam boiler with a capacity of 0.016 kg/sec (125 lb/hr) to establish initial loop pressure and temperature

A detailed facility description and facilty drawings are presented in appendix A.

During operation, coolant flow from the 1.51 m^3 (400 gal) capacity water supply accumulator entered the test section housing through a manifold to assure proper flow distribution. The flow was regulated manually through a series of hand valves or automatically through a hydraulic control valve or series of solenoid valves.

Test section pressure was initially established by the electric steam boiler, which is connected to the upper plenum of the test section. During the experimental run, the boiler was valved out of the system and the pressure was maintained by a pneumatically operated control valve located in the exhaust line.

Liquid effluent leaving the test section was separated in the upper plenum and collected in a close-coupled carryover tank. A baffle assembly (figure 3-2) in the upper plenum was used to improve liquid carryout separation and minimize liquid entrainment into the exhaust vapor. An entrainment separator located in the exhaust line was used to separate any remaining entrained liquid carryout from the vapor. Dry steam flow leaving the separator was measured at an orifice section before exhausting to atmosphere. To help ensure single-phase flow measurement, the piping upstream of the orifice section was heated to a temperature well above the saturation temperature.

3-2. Gravity Reflood Tests

During the test series, the facility was modified to conduct gravity reflood tests. The modified test facility configuration is shown in figure A-4. The modifications consisted of connecting the downcomer to the lower plenum, moving the injection line from the lower plenum to the bottom of the downcomer, installing a resistance orifice plate to simulate the hot leg resistances between the test section outlet pipe and the inlet flange of the entrainment separator, venting the top of the downcomer to the entrainment separator, and installing additional differential pressure cells.

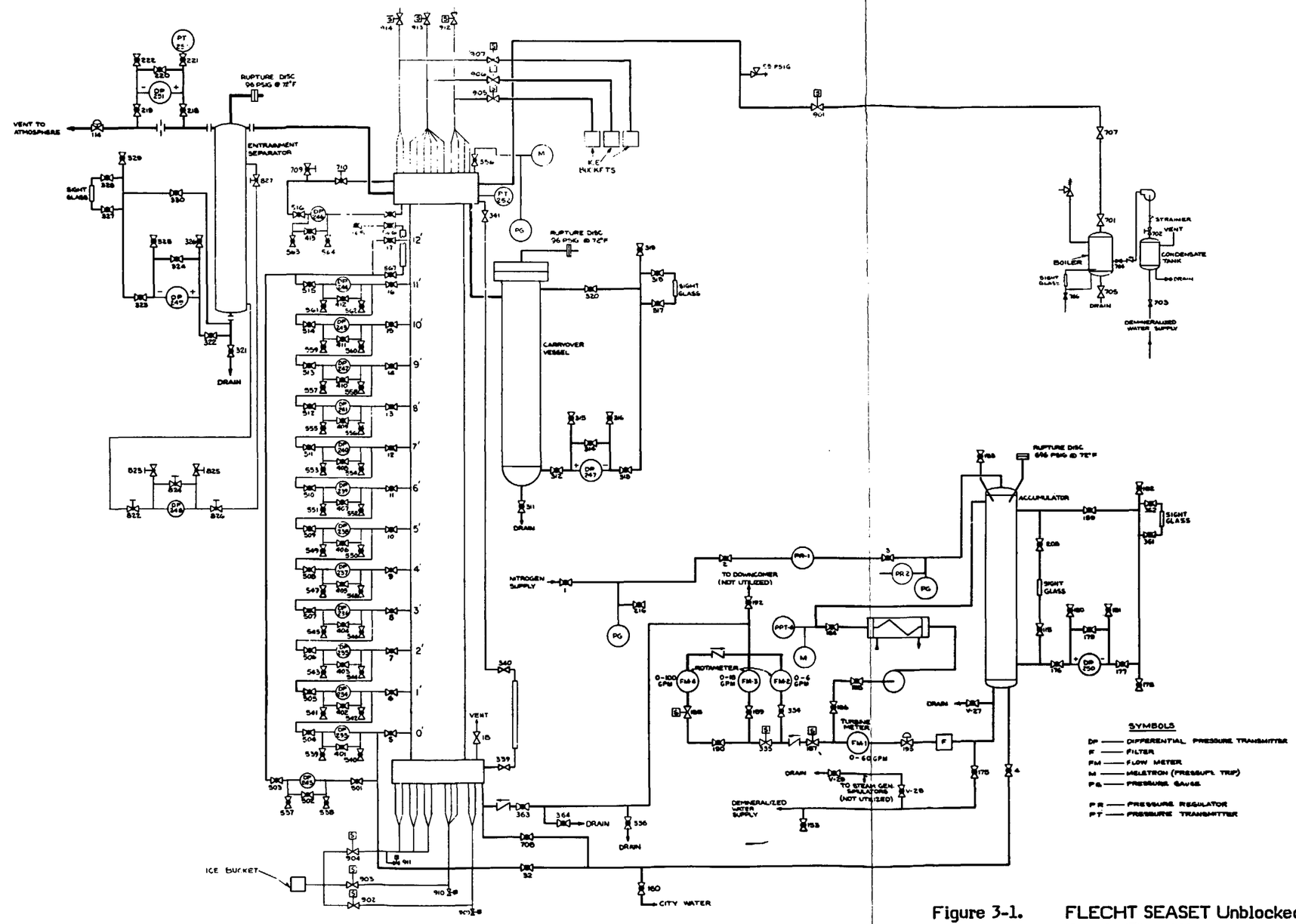

Figure 3-1. FLECHT SEASET Unblocked Bundle Flow Diagram, Forced Reflood Configuration

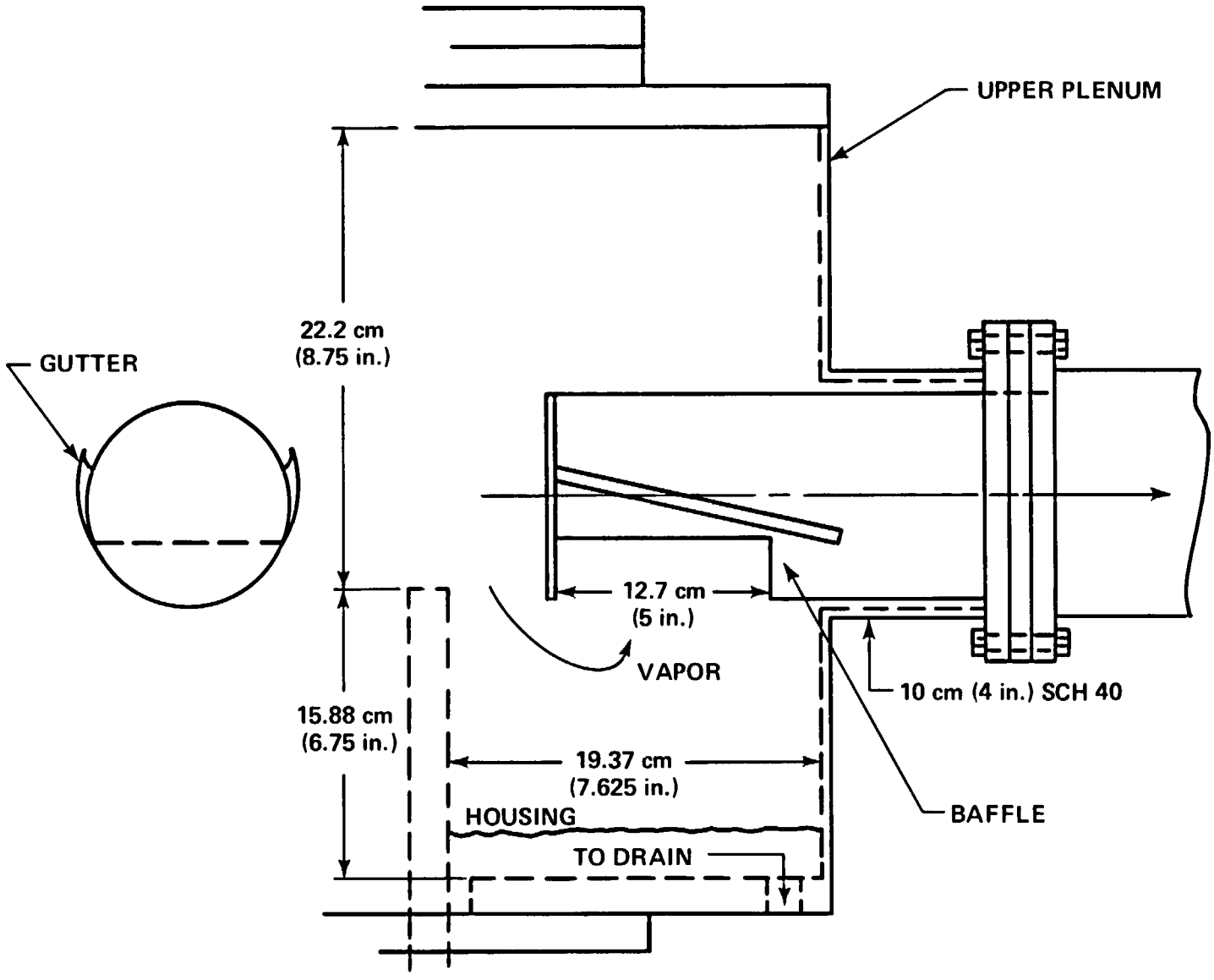

Figure 3-2. FLECHT SEASET Upper Plenum Baffle

3-3. Steam Cooling Tests

To obtain steam flow heat transfer data in the rod bundle geometry, a series of low-temperature steam cooling tests were conducted. For these tests, the facility was modified by running a 5.1 cm (2 in.) diameter steam flow line from the FLECHT SEASET steam generator facility boiler[1] to the lower plenum of the test section. The instrumentation and control valves utilized for the steam generator test were used to supply the proper steam flow rate.

3-4. HEATER ROD BUNDLE

During the test series, heater rods were replaced (see paragraph 3-30) and heater rod thermocouple and thimble wall thermocouple computer channel assignments were changed because of rod failures and thermocouple failures. The data for each run includes an updated thermocouple channel assignment list.

A cross section of the test bundle is shown in figure 3-3 in the original configuration with the corresponding heater rod instrumentation groups. Bundle assembly details are shown in figure A-9. The bundle comprised 161 heater rods (93 uninstrumented and 68 instrumented), 4 instrumented thimbles, 12 steam probes, 8 solid triangular fillers, and 8 grids. Details of the heater rods are shown in figure A-1; of the steam probes in figures A-10, A-11, and A-12; and of the grids in figures A-13 and A-14. The triangular fillers were welded to the grids to maintain the proper grid location. The fillers also reduced the amount of excess flow area from 9.3 to 4.7 percent.

Table 3-1 shows the original heater rod thermocouples that were monitored. The remaining thermocouples were used as spares when originally connected thermocouples failed.

3-5. SYSTEM DESIGN FEATURES

The following paragraphs describe the major design features utilized for the FLECHT SEASET unblocked bundle test series.

---

1. Howard, R. C., et al., PWR FLECHT SEASET Steam Generator Separate Effects Task Data Report," NRC/EPRI/Westinghouse-4, January 1980.

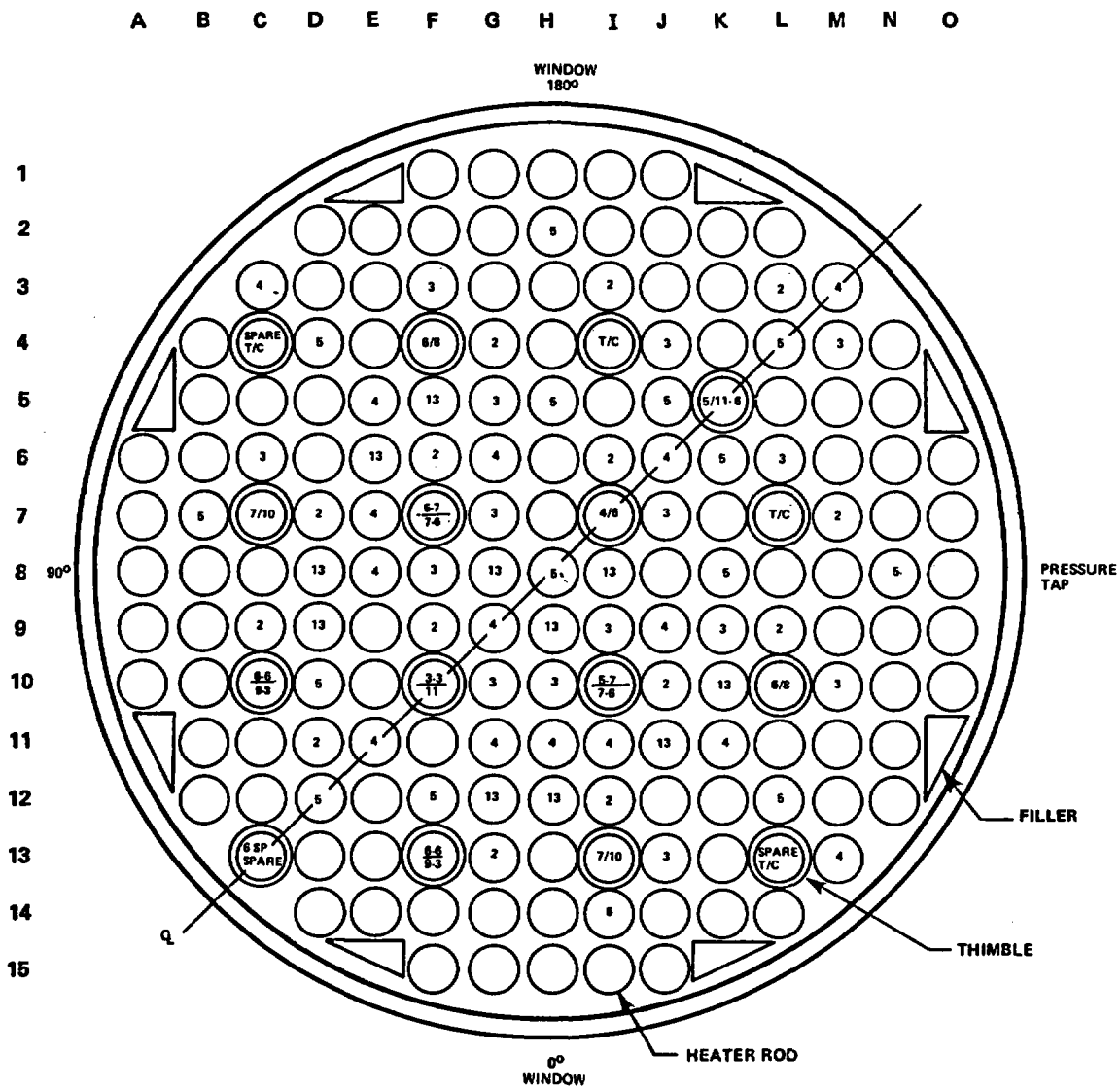

Figure 3-3. Bundle Cross Section

TABLE 3-1

INITIAL DATA ACQUISITION SYSTEM CHANNEL ASSIGNMENTS

Channel No.	Description	Location	Elevation [m (in.)]	Fluke Channel[a]	Strip Chart Recorder[b]
1	Heater rod T/C	7E	0.30 (12)		
2	Heater rod T/C	9G	0.30 (12)		
3	Heater rod T/C	11I	0.30 (12)		
4	Heater rod T/C	5H	0.61 (24)		
5	Heater rod T/C	8N	0.61 (24)		
6	Heater rod T/C	12F	0.61 (24)		
7	Heater rod T/C	7E	0.99 (39)		
8	Heater rod T/C	9G	0.99 (39)		
9	Heater rod T/C	11I	0.99 (39)		
10	Heater rod T/C	2H	1.22 (48)		
11	Heater rod T/C	5H	1.22 (48)		
12	Heater rod T/C	5J	1.22 (48)		
13	Heater rod T/C	8H	1.22 (48)		F - red pen
14	Heater rod T/C	8K	1.22 (48)		
15	Heater rod T/C	8N	1.22 (48)		
16	Heater rod T/C	12D	1.22 (48)		
17	Heater rod T/C	3C	1.52 (60)		
18	Heater rod T/C	3M	1.52 (60)		
19	Heater rod T/C	4J	1.52 (60)		
20	Heater rod T/C	5E	1.52 (60)		
21	Heater rod T/C	6L	1.52 (60)		
22	Heater rod T/C	7E	1.52 (60)		
23	Heater rod T/C	7G	1.52 (60)		
24	Heater rod T/C	9I	1.52 (60)		
25	Heater rod T/C	11I	1.52 (60)		

a. See paragraph 3-16
b. See paragraph 3-17

TABLE 3-1 (cont)

INITIAL DATA ACQUISITION SYSTEM CHANNEL ASSIGNMENTS

Channel No.	Description	Location	Elevation [m (in.)]	Fluke Channel[a]	Strip Chart Recorder[b]
26	Heater rod T/C	11K	1.52 (60)		
27	Heater rod T/C	13M	1.52 (60)		
28	Heater rod T/C	3C	1.70 (67)		
29	Heater rod T/C	3M	1.70 (67)		
30	Heater rod T/C	4J	1.70 (67)		
31	Heater rod T/C	6J	1.70 (67)		
32	Heater rod T/C	6L	1.70 (67)		
33	Heater rod T/C	8E	1.70 (67)		
34	Heater rod T/C	7G	1.70 (67)		
35	Heater rod T/C	9I	1.70 (67)		
36	Heater rod T/C	11I	1.70 (67)		
37	Heater rod T/C	11K	1.70 (67)		
38	Heater rod T/C	13M	1.70 (67)		
39	Heater rod T/C	3F	1.78 (70)		
40	Heater rod T/C	4J	1.78 (70)		
41	Heater rod T/C	4M	1.78 (70)		
42	Heater rod T/C	6C	1.78 (70)		
43	Heater rod T/C	6L	1.78 (70)		
44	Heater rod T/C	7G	1.78 (70)		
45	Heater rod T/C	7J	1.78 (70)		
46	Heater rod T/C	9I	1.78 (70)		
47	Heater rod T/C	10G	1.78 (70)		
48	Heater rod T/C	10M	1.78 (70)		
49	Heater rod T/C	13J	1.78 (70)		
50	Heater rod T/C	2H	1.83 (72)		
51	Heater rod T/C	3F	1.83 (72)		
52	Heater rod T/C	4D	1.83 (72)		

TABLE 3-1 (cont)

INITIAL DATA ACQUISITION SYSTEM CHANNEL ASSIGNMENTS

Channel No.	Description	Location	Elevation [m (in.)]	Fluke Channel[a]	Strip Chart Recorder[b]
53	Heater rod T/C	4G	1.83 (72)		
54	Heater rod T/C	4L	1.83 (72)		
55	Heater rod T/C	6F	1.83 (72)		
56	Heater rod T/C	6I	1.83 (72)		
57	Heater rod T/C	7B	1.83 (72)		
58	Heater rod T/C	7G	1.83 (72)		
59	Heater rod T/C	7J	1.83 (72)		
60	Heater rod T/C	8H	1.83 (72)		F - blue pen
61	Heater rod T/C	8N	1.83 (72)		
62	Heater rod T/C	9I	1.83 (72)		
63	Heater rod T/C	9L	1.83 (72)		
64	Heater rod T/C	10J	1.83 (72)		
65	Heater rod T/C	10M	1.83 (72)		
66	Heater rod T/C	12D	1.83 (72)		
67	Heater rod T/C	12L	1.83 (72)		
68	Heater rod T/C	14I	1.83 (72)		
69	Heater rod T/C	3I	1.88 (74)		
70	Heater rod T/C	3L	1.88 (74)		
71	Heater rod T/C	4G	1.88 (74)		
72	Heater rod T/C	6F	1.88 (74)		
73	Heater rod T/C	6I	1.88 (74)		
74	Heater rod T/C	7D	1.88 (74)		
75	Heater rod T/C	7M	1.88 (74)		
76	Heater rod T/C	9L	1.88 (74)		
77	Heater rod T/C	10J	1.88 (74)		
78	Heater rod T/C	12I	1.88 (74)		
79	Heater rod T/C	3I	1.83 (72)		

TABLE 3-1 (cont)

INITIAL DATA ACQUISITION SYSTEM CHANNEL ASSIGNMENTS

Channel No.	Description	Location	Elevation [m (in.)]	Fluke Channel[a]	Strip Chart Recorder[b]
80	Heater rod T/C	3L	1.93 (76)		
81	Heater rod T/C	4G	1.93 (76)		
82	Heater rod T/C	6F	1.93 (76)		
83	Heater rod T/C	6I	1.93 (76)		
84	Heater rod T/C	7D	1.93 (76)		
85	Heater rod T/C	7M	1.93 (76)		
86	Heater rod T/C	9L	1.93 (76)		
87	Heater rod T/C	10J	1.93 (76)		
88	Heater rod T/C	12I	1.93 (76)		
89	Heater rod T/C	2H	1.98 (78)		
90	Heater rod T/C	7B	1.98 (78)		
91	Heater rod T/C	4G	1.98 (78)		
92	Heater rod T/C	6F	1.98 (78)		
93	Heater rod T/C	10D	1.98 (78)		
94	Heater rod T/C	7D	1.98 (78)		
95	Heater rod T/C	14I	1.98 (78)		
96	Heater rod T/C	8H	1.98 (78)		
97	Heater rod T/C	8N	1.98 (78)		
98	Heater rod T/C	5H	1.98 (78)		
99	Heater rod T/C	8K	1.98 (78)		
100	Heater rod T/C	10J	1.98 (78)		
101	Heater rod T/C	12I	1.98 (78)		
102	Heater rod T/C	13G	1.98 (78)		
103	Heater rod T/C	3I	2.13 (84)		
104	Heater rod T/C	4G	2.13 (84)		
105	Heater rod T/C	6F	2.13 (84)		
106	Heater rod T/C	6I	2.13 (84)		

TABLE 3-1 (cont)

INITIAL DATA ACQUISITION SYSTEM CHANNEL ASSIGNMENTS

Channel No.	Description	Location	Elevation [m (in.)]	Fluke Channel[a]	Strip Chart Recorder[b]
107	Heater rod T/C	7D	2.13 (84)		
108	Heater rod T/C	7M	2.13 (84)		
109	Heater rod T/C	9C	2.13 (84)		
110	Heater rod T/C	9L	2.13 (84)		
111	Heater rod T/C	10J	2.13 (84)		
112	Heater rod T/C	11E	2.13 (84)		
113	Heater rod T/C	12I	2.13 (84)		
114	Heater rod T/C	13G	2.13 (84)		
115	Heater rod T/C	3I	2.29 (90)		
116	Heater rod T/C	4G	2.29 (90)		
117	Heater rod T/C	6F	2.29 (90)		
118	Heater rod T/C	6I	2.29 (90)		
119	Heater rod T/C	7D	2.29 (90)		
120	Heater rod T/C	7M	2.29 (90)		
121	Heater rod T/C	9C	2.29 (90)		
122	Heater rod T/C	9L	2.29 (90)		
123	Heater rod T/C	10J	2.29 (90)		
124	Heater rod T/C	11E	2.29 (90)		
125	Heater rod T/C	12I	2.29 (90)		
126	Heater rod T/C	6J	2.29 (90)		
127	Heater rod T/C	2H	2.44 (96)		
128	Heater rod T/C	4G	2.44 (96)		
129	Heater rod T/C	4L	2.44 (96)		
130	Heater rod T/C	6F	2.44 (96)		
131	Heater rod T/C	7D	2.44 (96)		
132	Heater rod T/C	7M	2.44 (96)		
133	Heater rod T/C	8H	2.44 (96)		F - black pen

TABLE 3-1 (cont)

INITIAL DATA ACQUISITION SYSTEM CHANNEL ASSIGNMENTS

Channel No.	Description	Location	Elevation [m (in.)]	Fluke Channel[a]	Strip Chart Recorder[b]
134	Heater rod T/C	9L	2.44 (96)		
135	Heater rod T/C	10J	2.44 (96)		
136	Heater rod T/C	12D	2.44 (96)		
137	Heater rod T/C	12I	2.44 (96)		
138	Heater rod T/C	5F	2.44 (96)		
139	Heater rod T/C	5H	2.44 (96)		
140	Heater rod T/C	8K	2.44 (96)		
141	Heater rod T/C	10K	2.44 (96)		
142	Heater rod T/C	7B	2.59 (102)		
143	Heater rod T/C	8H	2.59 (102)		
144	Heater rod T/C	8K	2.59 (102)		
145	Heater rod T/C	2H	2.59 (102)		
146	Heater rod T/C	5J	2.59 (102)		
147	Heater rod T/C	4L	2.59 (102)		
148	Heater rod T/C	3I	2.82 (111)		
149	Heater rod T/C	6F	2.82 (111)		
150	Heater rod T/C	6I	2.82 (111)		
151	Heater rod T/C	7D	2.82 (111)		
152	Heater rod T/C	7M	2.82 (111)		
153	Heater rod T/C	9C	2.82 (111)		
154	Heater rod T/C	10J	2.82 (111)		
155	Heater rod T/C	11E	2.82 (111)		
156	Heater rod T/C	12I	2.82 (111)		
157	Heater rod T/C	13G	2.82 (111)		
158	Heater rod T/C	2H	3.05 (120)		
159	Heater rod T/C	4D	3.05 (120)		
160	Heater rod T/C	5H	3.05 (120)		

TABLE 3-1 (cont)

INITIAL DATA ACQUISITION SYSTEM CHANNEL ASSIGNMENTS

Channel No.	Description	Location	Elevation [m (in.)]	Fluke Channel[a]	Strip Chart Recorder[b]
161	Heater rod T/C	5J	3.05 (120)		
162	Heater rod T/C	7B	3.05 (120)		
163	Heater rod T/C	8H	3.05 (120)		F - green pen
164	Heater rod T/C	8K	3.05 (120)		
165	Heater rod T/C	8N	3.05 (120)		
166	Heater rod T/C	12L	3.05 (120)		
167	Heater rod T/C	14I	3.05 (120)		
168	Heater rod T/C	5E	3.35 (132)		
169	Heater rod T/C	6J	3.35 (132)		
170	Heater rod T/C	7E	3.35 (132)		
171	Heater rod T/C	9G	3.35 (132)		
172	Heater rod T/C	11E	3.35 (132)		
173	Heater rod T/C	11I	3.35 (132)		
174	Heater rod T/C	11K	3.35 (132)		
175	Heater rod T/C	5I	3.51 (138)		
176	Heater rod T/C	7B	3.51 (138)		
177	Heater rod T/C	8H	3.51 (138)		
178	Thimble T/C	4I	2.13 (84)		C - blue pen
179	Steam probe T/C	10F	0.99 (39)		
180	Steam probe T/C	7I	1.22 (48)		
181	Steam probe T/C	5K	1.52 (60)		
182	Steam probe T/C	7F	1.70 (67)		
183	Steam probe T/C	10I	1.70 (67)		C - green pen
184	Steam probe T/C	4F	1.83 (72)		
185	Steam probe T/C	7I	1.83 (72)		
186	Steam probe T/C	10L	1.83 (72)		
187	Steam probe T/C	10C	1.98 (78)		

TABLE 3-1 (cont)

INITIAL DATA ACQUISITION SYSTEM CHANNEL ASSIGNMENTS

Channel No.	Description	Location	Elevation [m (in.)]	Fluke Channel[a]	Strip Chart Recorder[b]
188	Steam probe T/C	13F	1.98 (78)		
189	Steam probe T/C	7C	2.13 (84)		
190	Steam probe T/C	13I	2.13 (84)		C - red pen
191	Steam probe T/C	7F	2.29 (90)		
192	Steam probe T/C	10I	2.29 (90)		C - blue pen
193	Steam probe T/C	4F	2.44 (96)		
194	Steam probe T/C	10L	2.44 (96)		
195	Steam probe T/C	10C	2.82 (111)		
196	Steam probe T/C	13F	2.82 (111)		C - green pen
197	Steam probe T/C	7C	3.05 (120)		
198	Steam probe T/C	13I	3.05 (120)		
199	Steam probe T/C	10F	3.51 (138)		C - red pen
200	Steam probe T/C	5K	3.51 (138)		
201	Exhaust line steam probe T/C				
202	Thimble T/C	7L	1.22 (48)		
203	Thimble T/C	4I	1.83 (72)		
204	Out of service				
205	Thimble T/C	13L	2.44 (96)		
206	Thimble T/C	7L	2.82 (111)		
207	Thimble T/C	4I	3.05 (120)		
208	Upper plenum bundle out fluid T/C				
209	Upper plenum fluid T/C				
210	Upper plenum housing extension fluid T/C				
211	Lower plenum fluid T/C				

TABLE 3-1 (cont)

INITIAL DATA ACQUISITION SYSTEM CHANNEL ASSIGNMENTS

Channel No.	Description	Location	Elevation [m (in.)]	Fluke Channel[a]	Strip Chart Recorder[b]
212	Accumulator fluid T/C		0.18 (7.25)	10	
213	Carryover tank fluid T/C		0.0064 (2.5)	8	
214	Steam separator drain tank fluid T/C		0.076 (3)	9	
215	Exhaust orifice fluid T/C				
216	Carryover tank wall T/C		0.30 (12)	1	
217	Steam separator middle wall T/C				
218	Steam separator drain tank wall T/C		1.07 (42)	6	
219	Test section outlet pipe wall T/C			7	
220	Pipe upstream exhaust orifice wall T/C			15	
221	Lower plenum bundle in fluid T/C			11	
222	Primary power - zone A				E - red pen
223	Redundant power - zone A				
224	Primary power - zone B				E - blue pen
225	Redundant power - zone B				
226	Primary power - zone C				E - green pen
227	Redundant power - zone C				

TABLE 3-1 (cont)

INITIAL DATA ACQUISITION SYSTEM CHANNEL ASSIGNMENTS

Channel No.	Description	Location	Elevation [m (in.)]	Fluke Channel[a]	Strip Chart Recorder[b]
228	0-3.8 x 10^{-3} m^{-3}/sec (0-60 gal/min) turbine/meter or 0-9.5 x 10^{-3} m^{-3}/sec (0-150 gal/min) turbine/meter			59	A - red pen
229	Low-flow rotameter				A - blue pen
230	Medium-flow rotameter				A - black pen
231	High-flow rotameter				A - green pen
232	Bidirectional turbo-probe				D - black pen
233	Bundle 0-0.30 m (0-12 in.) D/P			45	
234	Bundle 0.30-0.61 m (12-24 in.) D/P			46	
235	Bundle 0.61-0.91 m (24-36 in.) D/P			47	
236	Bundle 0.91-1.22 m (36-48 in.) D/P			48	
237	Bundle 1.22-1.52 m (48-60 in.) D/P			49	
238	Bundle 1.52-1.83 m (60-72 in.) D/P			50	
239	Bundle 1.83-2.13 m (72-84 in.) D/P			51	
240	Bundle 2.13-2.44 m (84-96 in.) D/P			52	
241	Bundle 2.44-2.74 m (96-108 in.) D/P			53	
242	Bundle 2.74-3.05 m (108-120 in.) D/P			54	
243	Bundle 3.05-3.35 m (120-132 in.) D/P			55	

TABLE 3-1 (cont)

INITIAL DATA ACQUISITION SYSTEM CHANNEL ASSIGNMENTS

Channel No.	Description	Location	Elevation [m (in.)]	Fluke Channel[a]	Strip Chart Recorder[b]
244	Bundle 3.35-3.66 m (132-144 in.) D/P			56	
245	Bundle overall D/P			57	
246	Upper plenum level D/P			58	
247	Carryover tank level D/P				B - green pen
248	Steam separator tank level D/P				
249	Steam separator drain tank level D/P				D - blue pen
250	Accumulator level D/P				D - red pen
251	Exhaust orifice D/P				B - black pen
252	Upper plenum pressure PT				D - green pen
253	Exhaust orifice pressure PT				
254	Upper plenum to steam separator D/P				
255	Downcomer to steam separator D/P				
256	Downcomer level D/P				B - blue pen

3-6. Low Mass Housing

A low mass housing design was utilized in the previous FLECHT skewed test series to minimize the housing effects. The behavior of the skewed test low mass housing was studied by performing two tests with the same initial conditions except for the housing wall initial temperature. The effect of the cold and hot housing on the rod surface temperature and the corresponding heat transfer coefficient, excluding the peripheral rods, was found to be negligible. In addition, the hot and cold housing did not affect the quench front along the bundle. It was concluded that performing reflood tests with an unheated low mass housing is acceptable, since a cold housing does not significantly affect the reflood heat transfer and hydraulic behavior of the rod bundle.

A low mass housing design was utilized again for the unblocked bundle test series. The present design (figure A-15) is a low mass cylindrical housing with a 19.37 cm (7.625 in.) ID by 0.478 cm (0.188 in.) wall. The wall thickness, the minimum thickness allowed by the ASME Code, was chosen so that the housing would absorb and hence release the minimum amount of heat to the rod bundle.

The inside diameter of the housing was made as close to the diameter of the rod bundle as possible to minimize excess flow area. The excess flow area was further minimized by the solid fillers noted in paragraph 3-4. The housing was constructed of 304 stainless steel and is rated for 0.52 MPa (60 psig) at 816°C (1500°F). The design allowed for 1000 pressure and temperature cycles. The housing was provided with end flanges to mate with the upper and lower plenums used in the previous test series. Two commercial quartz sight glasses were located 180 degrees apart at the 0.91, 1.83, and 2.74 m (36, 72, and 108 in.) elevations for viewing and photographic study. The sight glass configuration allowed back lighting as well as front lighting for the purpose of photographic studies. The sight glasses had clamp-on heaters to raise the quartz temperature at the initiation of reflood to approximately 260°C (500°F). This eliminated the formation of a liquid film on the quartz during a run.

3-7. Bundle Differential Pressure Cells

The test section differential pressure cells provided data used in determining mass balance and bundle void fraction. Low-range [± 0.0069 MPa (± 1 psid)] pressure

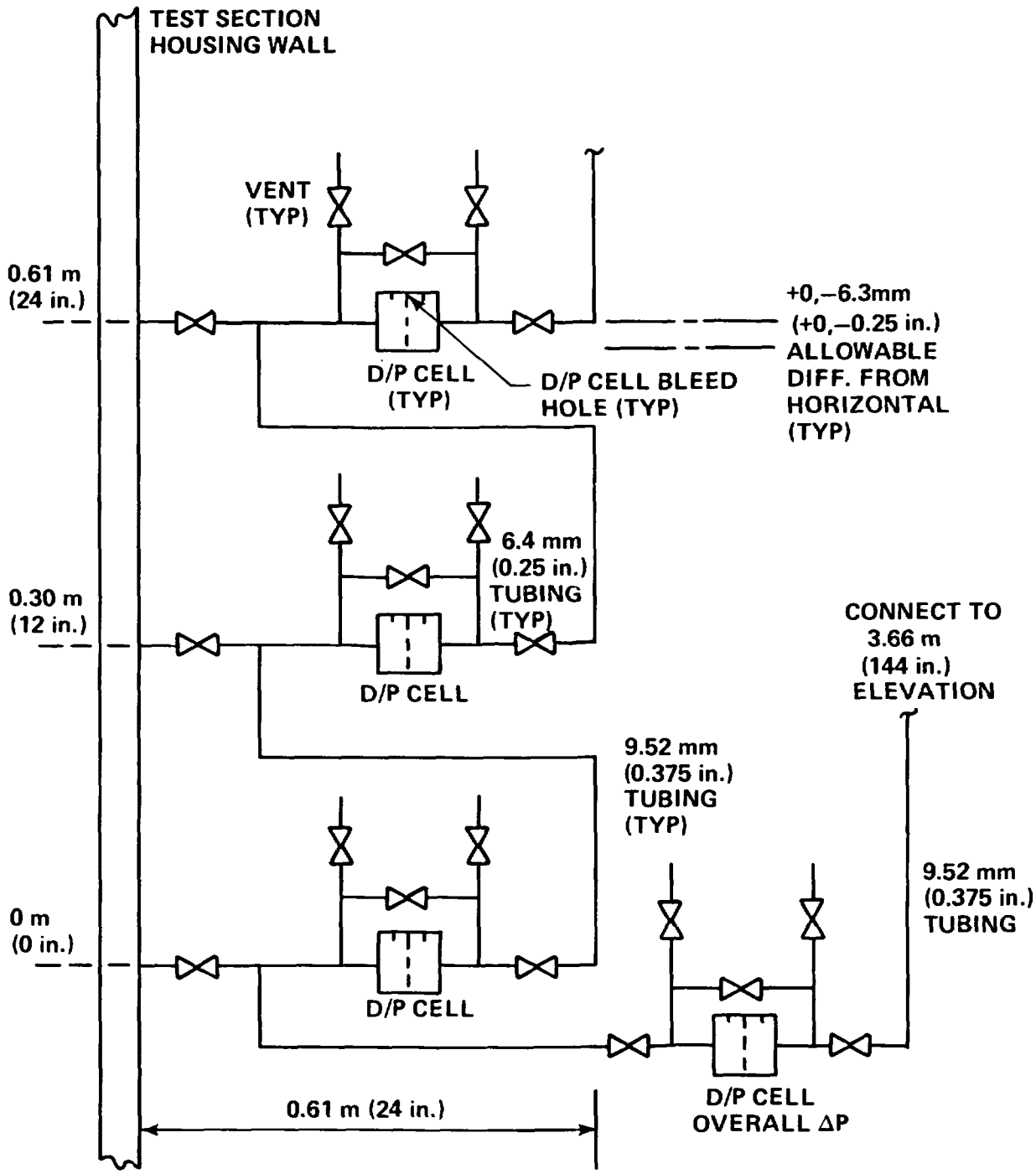

Figure 3-4. FLECHT SEASET Unblocked Bundle Test Section Housing Differential Pressure Cell Hookup

transducers were used to improve the accuracy of the data. The cells were located every 0.30 m (12 in.) along the test section, arranged as shown in figure 3-4. The differential pressure cell manifold was carefully bled to eliminate any trapped air and thus improve the repeatability of the readings.

3-8. Heater Rod Seals

The bundle heater rods passed through polyurethane O-ring seals in the upper and lower seal plates. This design was improved by sealing each rod individually with an O-ring sleeve. The O-rings were inserted into the sleeve (figure A-21). In the previous FLECHT tests, the O-ring was located in a groove in the seal plate. The new design allowed for the removal and replacement of individual O-rings, which was not possible in previous designs. This feature permitted the replacement of heater rods in the bundle without a total bundle disassembly.

3-9. Steam Probes

Steam probes were located in the bundle and in the test section outlet pipe. The bundle steam probes, which were located in the thimble tubes (figure A-10), were redesigned from the previous FLECHT test series. There were two probes per thimble as opposed to one in previous designs; this increased the number of steam measurement locations. The probe was designed to separate moisture from the high-temperature steam, and aspirate the steam across the thermocouple and into an ice bucket. Because of the larger number of probes, the probes were controlled to limit the amount of steam aspirated from the test section. This was accomplished by manifolding the aspiration lines for common elevations of steam probes together and closing the lines when the particular elevation had quenched.

The probe in the outlet pipe was installed in the elbow of the test section outlet pipe, as shown in figure A-26. This probe, which measured the temperature of the steam leaving the test section, was designed to measure steam temperature in the same manner as the bundle probes. The end of the thermocouple was formed so that it did not touch the walls of the 6.4 mm (0.25 in.) diameter tubing.

3-10. Pressure Control

Maintaining a constant upper plenum pressure had been a difficult problem in previous FLECHT test programs. In an effort to reduce the pressure oscillations, several modifications were made to the facility for the FLECHT skewed test series. These modifications were utilized in the FLECHT SEASET unblocked bundle test series. The first modification was to increase the volume of the steam separator to help reduce the magnitude of the oscillations. The second modification was to replace the air-operated globe exhaust control valve with an air-operated V-ball control valve. The V-ball valve had a larger flow loss coefficient and a more linear operating characteristic.

3-11. Facility and Bundle Operation

The test facility was designed for automatic operation whenever critical functions required a high degree of sophistication, safety, or repeatability. The Computer Data Acquisition System (CDAS) was the heart of the operation; it monitored, protected, and controlled the facility operation as well as collected data. Both contact and analog outputs were used to control pressure, power, and flow during the test. The CDAS software monitored critical safety parameters during the test and used corresponding outputs to run the test. These outputs included the safety interlock for proper operation of the bundle power control system.

3-12. Power Measurement

The technique of bundle power measurement was improved for the FLECHT low flooding rate skewed test series, and the improved technique was utilized again for the present unblocked bundle test series. The bundle power measurement systems were improved by the addition of a secondary independent power measurement system and the adoption of a system calibration.

A secondary power-measuring system consisting of wide-band Hall-effect watt transducers and stepdown current and potential transformers was installed in each power zone as a check on the primary. With the two data channels measuring the same parameter, any change in one system was detected by the other.

3-13. Coolant Injection System

The facility configuration provided for both forced and gravity reflood injection (figures A-3 and A-4). The injection system consisted of a hydraulic valve for programmed flow and a turbine meter in series with three rotameters. The flow out of the rotameters went either to the lower plenum of the test section for forced reflood or to the bottom elbow of the downcomer for gravity reflood. Solenoid valves were used to initiate flood and channel the flow through the desired rotameter. A bidirectional turbo-probe in the downcomer crossover pipe (figure A-30) measured the flow between the downcomer and the test section in the gravity reflood tests.

In the forced flooding configuration, the flooding rate into the test section lower plenum was measured directly by a turbine meter with a range of 3.78×10^{-5} to 3.78×10^{-3} m^3/sec (0.6 to 60 gal/min) or by one of three rotameters with ranges of 0 to 3.78×10^{-4}, 0 to 1.14×10^{-3}, and 0 to 6.31×10^{-3} m^3/sec (0 to 6, 0 to 18, and 0 to 100 gal/min). The desired flow through each rotameter was preset using the hand throttling valves located upstream of the rotameters.

In the gravity reflood configuration, the injection flow rate into the bottom elbow of the downcomer was measured by the 0 to 9.46×10^{-3} m^3/sec (0 to 150 gal/min) turbine meter, with the rotameters providing the backup measurement.

In the steam cooling configuration, the steam was supplied to the lower plenum from the boiler used for the FLECHT SEASET steam generator facility. The steam flow rate was measured by the vortex meter and related hardware used on the steam generator facility.

3-14. DATA ACQUISITION SYSTEMS

Data acquisition was accomplished by the following three systems.

3-15. Computer Data Acquisition System (CDAS)

The CDAS, the primary data collecting system used on the FLECHT SEASET unblocked bundle facility, consisted of a PDP-11 computer and associated equipment. The system could record 256 channels of analog input data representing bundle and system

temperatures, bundle power, flows, and absolute and differential pressures. The computer was capable of storing 1400 data scans for each of the 256 analog input channels.

Typically, each data channel was recorded once every second until flood, then once every 0.5 second for 200 seconds, and then back to once every second thereafter to a maximum of 1400 data points.

The computer software had the following features:

-- A calibration file to convert raw data into engineering units

-- A preliminary data reduction program which transferred the raw data stored on disk to a magnetic tape, in a format compatible for entry into a Control Data Corporation 7600 computer.

-- A program (FLOOK) which reduces raw data into engineering units

-- A program (F VALID) which prints out key data used in validating the FLECHT runs

-- A program (PLOT) which plots up to four data channels on a single graph

The last three programs were utilized to quickly understand and evaluate test runs.

In addition to its role as a data acquisition system, the computer also played a key role in the performance of an experimental run. Important control functions included initiation and control of reflood flow and power decay as well as termination of bundle power in the event of an overtemperature condition. Table 3-1 lists the instrumentation recorded on the CDAS.

3-16. Fluke Data Logger

The Fluke data logger had 60 channels of analog input for efficient monitoring of loop heatup and aiding in equipment troubleshooting. The Fluke recorded key facility vessel

and fluid temperatures, displaying temperature directly in degrees Fahrenheit. The Fluke also recorded millivolt data from the test section differential pressure cells, allowing the operator to keep a check on the operation and repeatability of the differential pressure cells. In addition, the Fluke was used to troubleshoot problems with the loop equipment in a quick and convenient manner. Table 3-1 lists channels monitored on the Fluke.

3-17. Multiple-Pen Strip Chart Recorders

Six Texas Instruments strip chart recorders were used to record bundle power, selected bundle thermocouple readings; reflood line rotameter and turbine meter flows; turbo-probe flows; accumulator, separator drain tank, housing, and carryover tank levels; exhaust orifice differential pressure; and selected bundle steam probe thermocouple readings. These recorders gave the loop operators and test directors immediate information on test progress and warning in the event of any system anomalies. The strip charts gave an analog recording of these critical data channels as a backup to the computer. These strip charts were also needed during the heatup phase of the facility, when the computer was not available. Readings from the strip chart recorder used for bundle steam probes were used to shut off groups of probes when that elevation quenched (paragraph 3-9). Table 3-1 lists the channels associated with the strip chart recorders.

3-18. INSTRUMENTATION

The instrumentation on the unblocked bundle facility was designed to measure temperature, pressure, flow, liquid level, and power. The temperature data were recorded by type K (chromel-alumel) thermocouples using 66°C (150°F) reference junctions. The liquid level data and pressure data, both static and differential, were measured by balanced bridge strain gage transducers. Power input to the bundle was measured by Hall-effect watt transducers, which produce a direct current electrical output proportional to the power input. The fluid flow measurements were made by a turbine meter and rotameters for coolant injection, an orifice with a differential pressure transducer for exhaust steam flow, and a bidirectional turbo-probe for downcomer crossover flow during gravity reflood.

Figure 3-5 is a schematic diagram of the computer hardware interface. Standard thermocouple calibration table entries and corresponding coefficients were used for the computer thermocouple channels. All other channel calibration files were straight-line interpolations of calibration data. The slope, intercept, and zero for the least-squares fit of a straight line to the equipment calibration data were computed for each channel and entered into its calibration file. The software used this straight-line formula to convert millivolts to engineering units. Table 3-1 shows the original channel assignment for all the recorded instrumentation, and figure A-5 shows the location of each channel on the facility.

3-19. Heater Rod Bundle Instrumentation

The bundle instrumentation is described in paragraph 3-4. Not all of the available instrumentation in the bundle was recorded because of the 256-channel limit of the CDAS. However, 205 thermocouples, including those pertaining to heater rods, thimbles, and steam probes, were recorded by the CDAS. Table 3-1 lists the original assigned channel for each thermocouple, including radial location and elevation in the bundle.

3-20. Test Section Instrumentation

The upper and lower plenums had fluid thermocouples (figure 3-6). The upper plenum had a differential pressure transducer to measure liquid collection rates, a static pressure transducer to measure the test section pressure, and a static pressure transducer (not recorded) to provide a control signal to the V-ball exhaust valve. The low mass housing had differential pressure transducers located every 0.30 m (12 in.) along the heated length of the bundle and one differential pressure transducer to obtain liquid level and average bundle void fraction over the entire heated length.

3-21. Carryover Tank Instrumentation

The carryover tank was instrumented with two wall thermocouples and one fluid thermocouple. A differential pressure transducer was used to measure the liquid collected in the tank as a function of time.

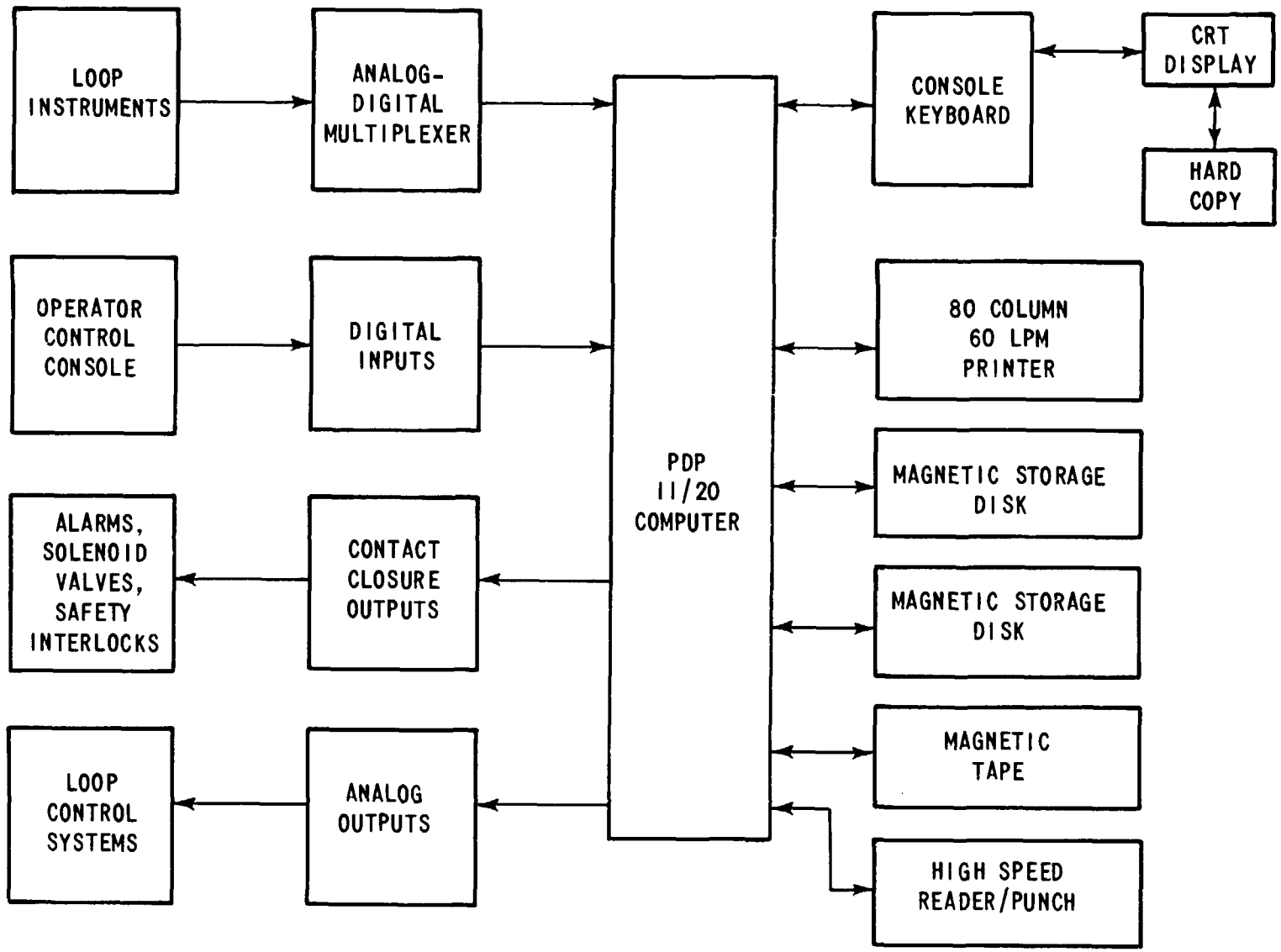

Figure 3-5. FLECHT SEASET Computer Hardware Interface (Unblocked Bundle Task)

12325-25

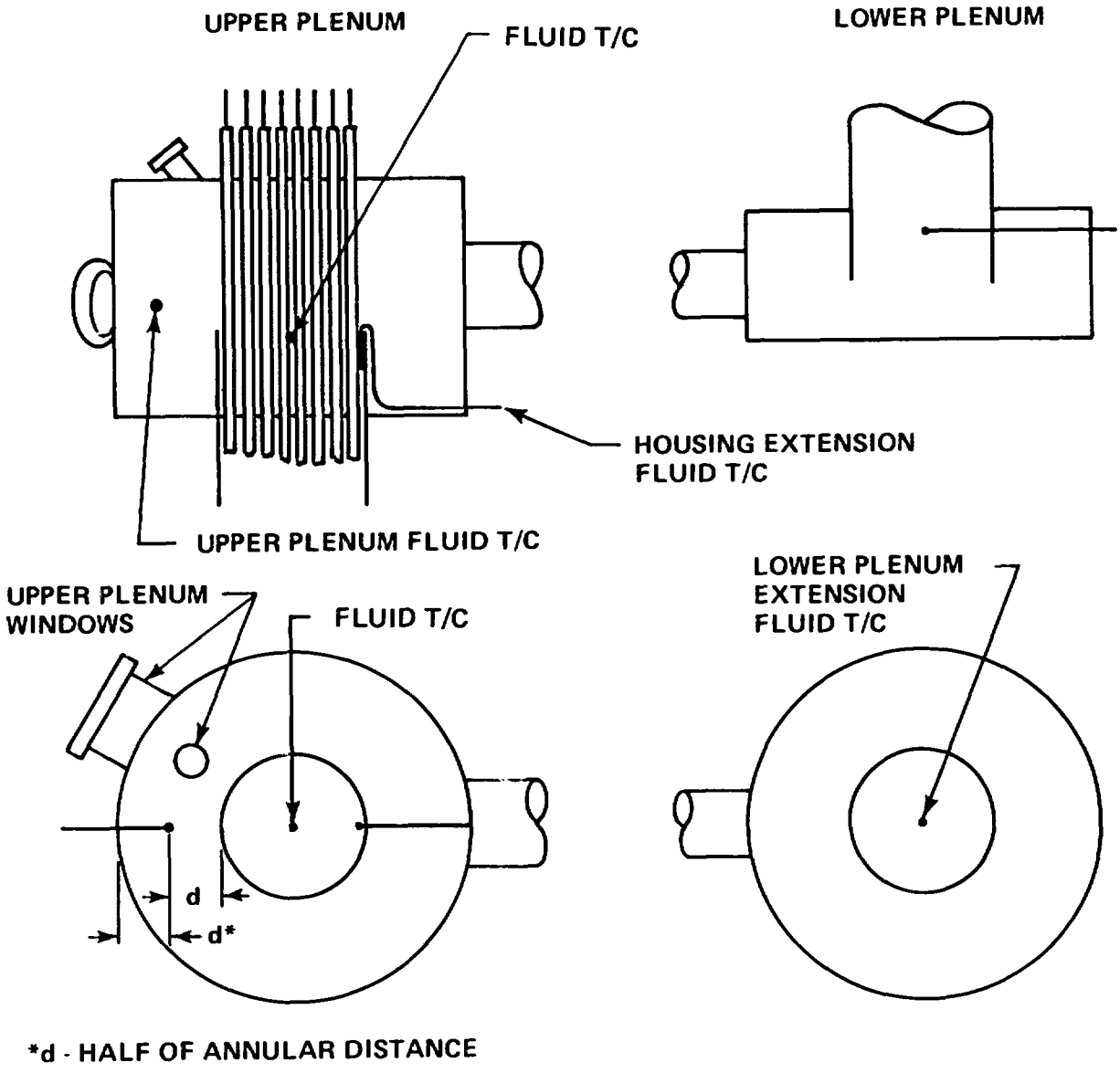

Figure 3-6. Upper and Lower Plenum Thermocouple Location

3-22. Steam Separator Instrumentation

The steam separator was instrumented with three wall thermocouples and a differential pressure transducer for measuring the entrained liquid carryout rate. The steam separator drain tank was instrumented with two wall thermocouples, one fluid thermocouple, and a differential pressure transducer for measuring the entrained liquid carryout rate.

3-23. Exhaust Pipe Instrumentation

The exhaust pipe was equipped with a differential pressure transducer connected across an orifice plate for measuring single-phase steam flow. A fluid thermocouple and static pressure transducer were used to determine exhaust steam thermodynamic conditions. Two wall thermocouples were used to record exhaust line temperatures during heatup and the experimental run. A steam probe located in the exhaust line measured the temperature of the steam leaving the upper plenum (figure A-26).

3-24. Accumulator Tank Instrumentation

Accumulator tank instrumentation included a fluid thermocouple and a differential pressure transducer for measurement of liquid level.

3-25. Injection Line Instrumentation

Injection line instrumentation consisted of a 3.78×10^{-5} to 3.78×10^{-3} m^3/sec (0.6 to 60 gal/min) turbine meter to measure coolant injection with three rotameters, 0 to 3.78×10^{-4}, 0 to 1.14×10^{-3}, and 0 to 6.31×10^{-3} m^3/sec (0 to 6, 0 to 18, and 0 to 100 gal/min), as a redundant measurement. Two fluid thermocouples were used to measure coolant injection temperatures.

3-26. Gravity Reflood Test Instrumentation

For the gravity reflood tests, two differential pressure transducers were installed to measure the pressure difference between the top of the downcomer and the steam separator and the pressure difference between the steam separator and the upper

plenum. A differential pressure transducer was installed to measure the liquid level in the downcomer. A bidirectional turbo-probe was installed in the crossover leg of the downcomer to measure liquid flow rates into and out of the test section. The two static pressure transducers previously located on the upper plenum were moved to the steam separator (see figure A-8).

The 3.78×10^{-5} to 3.78×10^{-3} m^3/sec (0.6 to 60 gal/min) turbine meter in the injection line was replaced with a 9.45×10^{-5} to 9.45×10^{-3} m^3/sec (1.5 to 150 gal/min) turbine meter.

3-27. TEST PROCEDURE

The following is a general procedure used to establish initial test conditions and perform a typical FLECHT SEASET unblocked bundle reflood test. (Figure A-3 shows the valves and components mentioned in the procedure.)

The accumulator is filled with water and heated to the desired coolant temperature of 53°C (127°F) nominal.

The boiler is turned on and brought up to nominal gage pressure of 0.62 MPa (75 psig).

The carryover vessel, entrainment separator, separator drain tank, test section upper plenum, and test section outlet piping (located before the entrainment separator) are heated while empty to slightly above the saturation temperature corresponding to the test run pressure. The exhaust line between the separator and exhaust orifice is heated to 260°C (500°F) nominal and the test section lower plenum is heated to the temperature of the coolant in the accumulator. The above component heating is accomplished by using clamp-on strip heaters.

The test section, carryover vessel, and exhaust line components are pressurized to the desired system pressure of 0.14 to 0.41 MPa (20 to 60 psia) by valving the boiler into the system and setting the exhaust line air-operated control valve V-114 to the desired pressure.

The coolant in the accumulator is pressurized to 2.76 MPa (400 psia). Water is then injected into the test section lower plenum until it reaches the beginning of the heated length of the bundle heater rods. Coolant is circulated and drained to assure that the water in the lower plenum and injection line are at the specified temperature prior to the run.

Power is then applied to the test bundle and the rods are allowed to heat up. When the temperature in any two designated bundle thermocouples reaches the preset value of 260°C to 871°C (500°F to 1600°F), the computer automatically initiates flood and controls power decay. Solenoid valves V-187, V-188, and V-335 in conjunction with hydraulic control valve V-193 control coolant injection into the test section. The exhaust control valve V-114 regulates the system pressure at the preset value by releasing steam to the atmosphere.

After all the designated heater rods have quenched, as indicated by the rod thermocouples, power to the heater rods is terminated, coolant injection is terminated, the entire system is depressurized by opening control valve V-114, and the CDAS is deactivated. Water stored in all components is drained and weighed.

After runs 30223 through 30817 had been conducted, a modification was made to the above test procedure. This modification consisted of power pulsing the bundle to approximately 260°C (500°F) prior to applying full power and subsequently venting the bundle steam probe lines before achieving the designated flood temperature. This procedure was followed to dry out the bundle thimbles and steam probes, in order to achieve faster response and higher reliability of the steam probes.

3-28. Gravity Reflood Test Procedure

During the test series the facility was modified to perform gravity reflood tests (figure A-4). The same procedure was used to perform the gravity reflood tests with the following exception: After flood was initiated, the flooding rate was adjusted if necessary to assure that the level in the downcomer did not go past the 4.88 m (192 in.) elevation.

3-29. Steam Cooling Test Procedure

The steam cooling tests were initiated by injecting steam at a high flow rate [approximately 0.3 kg/sec (0.6 lb/sec)] into the bundle from the FLECHT SEASET steam generator facility boiler (see paragraph 3-3). When the system had reached the saturation condition, the steam flow rate was adjusted to the specified condition. When the steam flow had stabilized, constant bundle power was applied and the CDAS was activated. The test was terminated when a steady-state condition was achieved. Both transient and steady-state data were recorded.

3-30. Boiloff Test Procedure

For the boiloff tests, the bundle was prefilled with saturated water to the 3.05 m (120 inch) elevation. The accumulator was isolated from the test section. Power was subsequently applied at a constant rate of 1.38 kw/m (0.42 kw/ft) to the heater rods. The bundle was allowed to essentially boil dry. Th bundle was protected from overtemperature by initiating reflood when the maximum rod temperature reached 1093°C (2000°F), at which time bundle power was terminated. The boiloff tests were conducted at three different system pressures.

3-31. HEATER ROD REPLACEMENT

During the test series, heater rods were removed from the bundle and replaced with new heater rods. This was done to replace rods with low isolation resistance and/or to recover the thermocouple coverage lost because of failed thermocouples. The replacement rods were either unblocked bundle uninstrumented spare rods or instrumented rods purchased for the FLECHT SEASET 21-rod bundle test program. (Figure A-2 shows the thermocouple locations for these rods.)

The original complement of heater rods described in paragraph 3-4 was used for runs 30123 through 31302. Following run 31302 the following heater rod replacements were made:

Location	Original Rod Serial Number	Replacement Rod Serial Number
6J	243	366 - heater rod group 4B[a]
6L	223	322 - heater rod group 2B[a]
7E	244	348 - heater rod group 13B[a]
8E	235	345 - heater rod group 13B[a]
8J	64	11 - unblocked bundle uninstrumented spare heater rod
11G	239	372 - heater rod group 4B[a]
14H	2	91 - unblocked bundle uninstrumented spare heater rod

These changes were in effect for runs 31404 through 31615. After run 31615 the following replacement was made:

Location	Original Rod Serial Number	Replacement Rod Serial Number
11K	267	335 - heater rod group 2C[a]

This change was in effect for runs 31701 through 33056. After run 33056 the following heater rod replacements were made:

a. See figure A-2.

Location	Original Rod Serial Number	Replacement Rod Serial Number
6D	26	356 - heater rod group 14[a]
7H	95	339 - heater rod group 2C[a]
7K	23	321 - heater rod group 2B[a]
8C	84	306 - heater rod group 2C[a]
8D	79	364 - heater rod group 14[a]
8J	11	314 - heater rod group 14[a]
9F	29	338 - heater rod group 2C[a]
9E	28	376 - heater rod group 2B[a]
9L	216	316 - heater rod group 14[a]
10J	203	307 - heater rod group 2C[a]

a. See figure A-2.

Data	C/T	
12+6	18	FSS
24+6	30	
39+6	45	
48+6	54	
60+6	66	
67+6	73	
72+6	78	
76+6	82	
78+6	84	
84+6	90	
90+6	96	
96+6	102	
111+6	117	
132+6	138	

Location	Original Rod Serial Number	Replacement Rod Serial Number
12H	41	318 - heater rod group 14[a]
5I	31	377 - heater rod group 2B[a]
12J	75	357 - heater rod group 14[a]
13H	89	332 - heater rod group 2C[a]
11F	58	302 - heater rod group 2C[a]

This change was in effect for runs 33238 through 37170.

3-31. PHOTOGRAPHIC STUDIES

Motion pictures taken during certain test runs are detailed in appendix B.

a. See figure A-2.

FSK4

Data	C/T
12+6	18 ✓
24+6	30 31.12
36+6	42 ✓
48+6	54 ✓
60+6	66 ✓
72+6	78 ✓
84+6	90 ✓
96+6	102 ✓
108+6	114 ✓
114+6	120 ✓
120+6	126 ✓
126+6	132 ✓
132+6	138 ✓
138+6	144 144.78

Data	C/T
0.5+6	6.5 ✓
1.5+6	7.5 ✓
24+6	30 ✓
36+6	42 ✓
48+6	54 ✓
72+6	78 ✓
78+6	84 ✓
84+6	90 ✓
96+6	102 ✓
108+6	114 ✓
120+6	126 ✓
132+6	138 ✓

F-COS

SECTION 4
TEST RESULTS

4-1. SUMMARY OF RUN CONDITIONS AND TEST RESULTS

Data from 63 reflood and steam cooling tests performed during the FLECHT SEASET unblocked bundle test program met the specified test conditions and are reported herein. The initial run conditions and summary results are listed in tables 4-1 and 4-2. The test numbers in table 4-1 comprise five digits each. The first digit, 3, refers to the unblocked bundle test program; the second and third refer to the sequential bundle cycle number; the fourth and fifth are the test matrix number (table 2-4). For example, run 31504 is matrix test number 4 of the 15th cycle of the unblocked bundle tests. The summary results for the reflood tests include the following information:

-- Location of the hottest temperature recorded during the test, which is characterized by the radial location of the rod in the bundle and the thermocouple nominal elevation with respect to the bottom of the heated length. This nomencla- ture is explained in appendix C.

-- Initial and maximum temperature of the hot rod

-- Turnaround time, which is the time after the start of flooding at which the hot rod maximum temperature was recorded

-- Hottest rod quench time, which is the time after the start of flooding at which the temperature of the hottest rod started to drop very rapidly

-- Bundle quench time, which is the time after the start of flooding at which all thermocouples in the bundle had quenched. On the average, the thermocouples located at the 3.35 m (132 in.) elevation quenched last.

-- Location of rods which were disconnected during testing (refer to figure 3-3)

-- Those tests in which the data above the 1.52 m (60 in.) elevation should not be utilized for heat transfer correlation development because of severe bundle distortion

Additional data for each test are reported in detail in appendix C.

4-2. DATA REDUCTION METHODS

Data collected for each run by the CDAS at the test site was compiled on a binary magnetic tape in engineering units. This tape was processed by a CDC-7600 computer utilizing a series of data reduction programs (figure 4-1).

The error analysis of the data is presented in appendix D.

The following paragraphs describe the reduced data obtained from these programs.

4-3. Mass Balance Data

An overall mass balance was performed for each test utilizing the FFLOWS code to verify the measured mass accumulation and the bundle exit flow. The total injected water mass was compared to the total mass accumulated in the test facility plus the total mass which exited the test facility. The mass difference was then determined at the end of each test as follows:

$$M_{diff} = M_{injected} - M_{accumulated} - M_{exited} \qquad (4\text{-}1)$$

M_{diff} was corrected by the mass measured in the steam probe collection tanks. A mass balance plot for the reference run (31504) is shown in figure 4-2. For the 43 valid reflood tests, the average mass difference at the end of the test was found to be approximately 5.3 percent, as shown in figure 4-3. The average mass difference at the end of injection was generally less than 5 percent, since some mass could have been lost through the exhaust orifice during depressurization. Details of these calculations are given in appendix E.

The mass balance plot for each reflood test shown in figure 4-3 is included in the data package summaries in appendix C.

4-4. Quench Criteria

The heater rod thermocouple data were reduced by the QUENCH code, which was designed to determine the key points on the temperature time histories. The functions

TABLE 4-1

FLECHT SEASET UNBLOCKED BUNDLE REFLOOD TEST DATA SUMMARY

Test No.	Run No.	Actual Test Conditions: Upper Plenum Pressure [MPa (psia)]	Rod Initial T_{clad} at 1.83m (72 in.) [°C(°F)]	Rod Peak Power [kw/m (kw/ft)]	Flooding Rate [mm/sec (in./sec)]	Coolant Temperature [°C(°F)]	Radial Power Distribution	Results: Hottest Rod T/C and Elevation [m(in.)	Initial Temperature [°C(°F)]	Maximum Temperature [°C(°F)]	Temperature Rise [°C(°F)]	Turn-around Time (sec)	Quench Time (sec)	Bundle Quench Time (sec)	Disconnected Rod Location
CONSTANT FLOODING RATE															
1	31701	0.28 (40)	872 (1601)	2.3 (0.70)	155 (6.1)	53 (127)	Uniform	9I-1.78(70)	893 (1640)	923 (1694)	30 (54)	5	55	114	4G, 5G
2	31302	0.28 (40)	869 (1597)	2.3 (0.69)	76.5 (3.01)	52 (126)	Uniform	8E-1.70(67)	889 (1631)	932 (1710)	43 (79)	8	124	262	4G, 5G, 6J, 11G
3	31203	0.28 (40)	872 (1601)	2.3 (0.70)	38.4 (1.51)	52 (126)	Uniform	9L-1.93(76)	870 (1597)	1037 (1898)	167 (301)	63	246	435	4G, 5G
	33903	0.28 (40)	881 (1619)	2.3 (0.70)	40.1 (1.58)	52 (125)	Uniform	7K-1.98(78)	868 (1594)	1048 (1919)	180 (325)	68	220	335	4G, 5G, 11I, 11J, 11K, 12IJK, 13JK
	34103	0.28 (40)	885 (1626)	2.4 (0.74)	38.1 (1.50)	51 (123)	Uniform	7K-1.98(78)	872 (1601)	1089 (1992)	217 (391)	71	241	381	4G, 5G, 11IJK, 12IJK, 13JK
4	31504	0.28 (40)	863 (1585)	2.3 (0.70)	24 (0.97)	51 (123)	Uniform	8K-1.98(78)	820 (1507)	1150 (2101)	330 (593)	130	325	594	4G, 5G
	35304[a]	0.28 (40)	915 (1679)	2.4 (0.74)	25.9 (1.02)	51 (124)	Uniform	9F-1.93(76)	797 (1467)	1230 (2246)	433 (779)	125	249	499	4G, 5G, 11IJK, 12IJK, 13JK,
5	31805	0.28 (40)	871 (1600)	2.3 (0.70)	21 (0.81)	51 (124)	Uniform	11K-1.98(78)	851 (1563)	1232 (2250)	381 (687)	134	419	691	4G, 5G
6	34006	0.27 (39)	882 (1620)	1.3 (0.40)	15 (0.59)	51 (124)	Uniform	7K-1.98(78)	864 (1587)	1163 (2126)	299 (539)	175	327	566	4G, 5G, 11IJK, 12IJK, 13JK
7	34907[a,b]	0.28 (40)	897 (1648)	1.4 (0.42)	11 (0.45) 76 (3.0)	51 (123)	Uniform	9F-1.98(78)	836 (1538)	1230 (2246)	394 (708)	203	326	385	4G, 5G, 11IJK, 12IJK, 13JK
	35807[a]	0.28 (40)	886 (1628)	0.89(0.27)	10 (0.41)	50 (121)	Uniform	9F-1.88(74)	849 (1560)	1182 (2160)	333 (600)	217	368	734	4G, 5G, 11IJK, 12IJK, 13JK
PRESSURE AT CONSTANT FLOODING RATE															
8	31108	0.13 (19)	871 (1600)	2.3 (0.70)	79.0 (3.11)	33 (91)	Uniform	9I-1.78(70)	884 (1624)	938 (1720)	54 (96)	10	156	364	4G, 5G
9	34209	0.14 (20)	889 (1636)	2.4 (0.72)	27.2 (1.07)	32 (90)	Uniform	7K-1.98(78)	854 (1570)	1161 (2121)	307 (551)	127	427	701	4G, 5G, 11IJK, 12IJK, 13JK

a. Significant rod bundle distortion occurred between 1.52 and 2.27 m (60 and 90 in.)

b. Scrammed at 279 seconds because of high rod temperature

TABLE 4-1 (cont)

FLECHT SEASET UNBLOCKED BUNDLE REFLOOD TEST DATA SUMMARY

Test No.	Run No.	As-Run Test Conditions						Results							Disconnected Rod Location
		Upper Plenum Pressure [MPa (psia)]	Rod Initial T_{clad} at 1.83m (72 in.) [°C(°F)]	Rod Peak Power [kw/m (kw/ft)]	Flooding Rate [mm/sec (in./sec)]	Coolant Temperature [°C(°F)]	Radial Power Distribution	Hottest Rod T/C and Elevation [m(in.)]	Initial Temperature [°C(°F)]	Maximum Temperature [°C(°F)]	Temperature Rise [°C(°F)]	Turn-around Time (sec)	Quench Time (sec)	Bundle Quench Time (sec)	
10	34610	0.14 (20)	892 (1637)	1.4 (0.42)	21 (0.82)	32 (90)	Uniform	6D-1.88 (74)	845 (1554)	1052 (1926)	207 (372)	137	310	507	4G, 5G, 11IJK, 12IJK, 13JK
11	34711[a]	0.13 (19)	888 (1630)	1.4 (0.42)	17 (0.67)	33 (91)	Uniform	9E-1.93 (76)	855 (1571)	1119 (2045)	264 (474)	135	361	600	4G, 5G, 11IJK, 12IJK, 13JK
12	35212[a,c]	0.14 (20)	879 (1613)	1.4 (0.42)	11 (0.43) 178 sec 79 (3.1)	32 (89)	Uniform	9E-1.83 (72)	830 (1526)	1231 (2247)	401 (721)	173	236	294	4G, 5G, 11IJK, 12IJK, 13JK
	35912[a]	0.14 (20)	889 (1632)	0.89 (0.27)	11 (0.42)	34 (93)	Uniform	9G-2.29 (90)	802 (1476)	1128 (2062)	326 (586)	289	558	789	4G, 5G, 11IJK, 12IJK, 13JK
13	32013	0.41 (60)	887 (1629)	2.3 (0.70)	26.4 (1.04)	66 (150)	Uniform	6L-1.93 (76)	846 (1555)	1171 (2139)	325 (584)	115	269	461	4G, 5G
SUBCOOLING															
14	32114	0.28 (40)	893 (1639)	2.3 (0.70)	25→31 (1.0→1.22)	125 (257)	Uniform	6L-1.88 (74)	840 (1544)	1189 (2172)	349 (628)	114	405	633	4G, 5G
	35114	0.28 (40)	892 (1638)	2.4 (0.74)	25 (0.98)	123 (253)	Uniform	9D-1.83 (72)	886 (1628)	1192 (2178)	306 (550)	123	394	651	4G, 5G, 11IJK, 12IJK, 13JK
15	31615	0.14 (20)	876 (1609)	2.3 (0.70)	0 (0)	-	Uniform	11H-1.70 (67)	881 (1617)	1220 (2228)	339 (611)	57	-	-	4G, 5G
	34815[a]	0.14 (20)	895 (1643)	2.4 (0.74)	25 (0.98)	94 (221)	Uniform	7J-1.83 (72)	870 (1597)	1178 (2152)	308 (555)	132	562	919	4G, 5G, 11IJK, 12IJK, 13JK
16	34316	0.28 (40)	889 (1631)	2.4 (0.74)	25 (0.97)	51→119 (124→246)	Uniform	6D-1.88 (74)	849 (1560)	1207 (2206)	358 (646)	107	349	592	4G, 5G, 11IJK, 12IJK, 13JK
INITIAL CLAD TEMPERATURE															
17	30817	0.27 (39)	531 (987)	2.3 (0.70)	38.6 (1.52)	53 (128)	Uniform	10J-1.98 (78)	519 (965)	832 (1530)	313 (565)	84	219	395	4G, 5G
18	30518	0.28 (40)	256 (494)	2.3 (0.70)	38.9 (1.53)	52 (126)	Uniform	8H-1.98 (78)	246 (475)	653 (1208)	407 (732)	96	187	344	4G, 5G
19	30619	0.134 (19.5)	256 (494)	2.3 (0.70)	38.9 (1.53)	36 (96)	Uniform	2H-1.98 (78)	243 (469)	727 (1340)	484 (871)	142	292	572	4G, 5G

c. Scrammed at 178 seconds because of high rod temperature

TABLE 4-1 (cont)

FLECHT SEASET UNBLOCKED BUNDLE REFLOOD TEST DATA SUMMARY

Test No.	Run No.	As-Run Test Conditions						Results							Disconnected Rod Location
		Upper Plenum Pressure [MPa (psia)]	Rod Initial T_{clad} at 1.83m (72 in.) [°C(°F)]	Rod Peak Power kw/m [(kw/ft)]	Flooding Rate mm/sec [(in./sec)]	Coolant Temperature [°C(°F)]	Radial Power Distribution	Hottest Rod T/C and Elevation [m(in.)]	Initial Temperature [°C(°F)]	Maximum Temperature [°C(°F)]	Temperature Rise [°C(°F)]	Turn-around Time (sec)	Quench Time (sec)	Bundle Quench Time (sec)	
20	34420	0.27 (39)	1119 (2045)	2.4 (0.74)	38.9 (1.53)	51 (124)	Uniform	7J-1.83 (72)	1102 (2016)	1207 (2205)	105 (189)	34	222	376	4G, 5G, 11IJK, 12IJK, 13JK
ROD PEAK POWER															
21	30921[d]	0.27 (39)	879 (1614)	1.3 (0.40)	38.9 (1.53)	52 (126)	Uniform	9I-1.78 (70)	887 (1629)	949 (1740)	62 (111)	17	152	158	4G, 5G
	31021	0.28 (40)	880 (1615)	1.3 (0.40)	38.6 (1.52)	52 (126)	Uniform	9H-1.78 (70)	891 (1635)	941 (1726)	50 (91)	14	158	271	4G, 5G
22	31922	0.14 (20)	883 (1621)	1.3 (0.40)	27.2 (1.07)	35 (95)	Uniform	6F-1.83 (72)	883 (1621)	975 (1787)	92 (166)	70	229	435	4G, 5G
23	30223	0.27 (39)	258 (497)	1.3 (0.40)	37.8 (1.49)	54 (129)	Uniform	6F-1.93 (76)	261 (501)	455 (852)	194 (351)	44	113	181	None
	30323	0.27 (39)	259 (499)	1.3 (0.40)	38.6 (1.52)	52 (126)	Uniform	6F-1.98 (78)	256 (494)	459 (859)	203 (365)	57	115	171	None
24	34524	0.28 (40)	878 (1612)	3.0 (1.0)	39.9 (1.57)	52 (125)	Uniform	7J-1.83 (72)	873 (1604)	1204 (2199)	331 (595)	89	266	520	4G, 5G, 11IJK, 12IJK, 13JK
RADIAL POWER DISTRIBUTION															
25	Not run														
26	35426[a]	0.28 (40)	886 (1627)	2.54 (0.773) 2.42 (0.737) 2.08 (0.633)	25.7 (1.01)	52 (126)	FLECHT	9F-1.93 (76)	814 (1497)	1229 (2243)	415 (746)	113	240	485	4G, 5G, 11IJK, 12IJK, 13JK
	36026[a]	0.28 (40)	900 (1651)	2.42 (0.737) 2.31 (0.703) 2.19 (0.667)	25 (1.0)	51 (124)	FLECHT	11F-1.88 (74)	862 (1583)	1174 (2145)	312 (562)	113	286	475	4G, 5G, 11IJK, 12IJK, 13JK
27	Not run														
28	Not run														
REPEAT TESTS															
29	35304														

d. Scrammed because of high-temperature thermocouple failure at 125 seconds

TABLE 4-1 (cont)

FLECHT SEASET UNBLOCKED BUNDLE REFLOOD TEST DATA SUMMARY

Test No.	Run No.	As-Run Test Conditions						Results							Disconnected Rod Location
		Upper Plenum Pressure [MPa (psia)]	Rod Initial T_{clad} at 1.83m (72 in.) [°C(°F)]	Rod Peak Power [kw/m (kw/ft)]	Flooding Rate [mm/sec (in./sec)]	Coolant Temperature [°C(°F)]	Radial Power Distribution	Hottest Rod T/C and Elevation [m(in.)]	Initial Temperature [°C(°F)]	Maximum Temperature [°C(°F)]	Temperature Rise [°C(°F)]	Turn-around Time (sec)	Quench Time (sec)	Bundle Quench Time (sec)	
30	Not run														
VARIABLE FLOODING RATE															
31	Not run														
32	Not run														
33	32333	0.28 (40)	889 (1631)	2.3 (0.70)	162 (6.36) 5 sec 21 (0.82) onward	52 (125)	Uniform	6L-1.93 (76)	843 (1550)	1148 (2099)	305 (549)	131	337	639	4G, 5G
34	Not run														
35	32235	0.14 (20)	888 (1630)	2.3 (0.70)	166 (6.53) 5 sec 25 (0.98) 200 sec 16 (0.62) onward	31 (88)	Uniform	6K-1.98 (78)	823 (1514)	1146 (2096)	323 (582)	142	546	964	4G, 5G
					Injection Rate [kg/sec (lbm/sec)]										
GRAVITY REFLOOD															
36	33436	0.27 (39)	878 (1611)	2.3 (0.70)	5.80 (12.8) 15 sec 0.785 (1.73) onward	52 (125)	Uniform	10H-1.78 (70)	891 (1636)	910 (1670)	19 (34)	4	121	174	4G, 5G
37	Not run														
38	33338	0.28 (40)	871 (1600)(e) 591 (1096)(f)	2.3 (0.70)(e) 1.3 (0.40(f)	5.9 (13) 15 sec 0.807 (1.78) onward	52 (125)	Hot/ cold channels	10H-1.78 (70)	906 (1664)	925 (1697)	19 (33)	6	76	181	4G, 5G

e. Hot channel
f. Cold channel

TABLE 4-1 (cont)

FLECHT SEASET UNBLOCKED BUNDLE REFLOOD TEST DATA SUMMARY

Test No.	Run No.	As-Run Test Conditions: Upper Plenum Pressure [MPa (psia)]	Rod Initial T_{clad} at 1.83m (72 in.) [°C(°F)]	Rod Peak Power [kw/m (kw/ft)]	Injection Rate [kg/sec (lbm/sec)]	Coolant Temperature [°C(°F)]	Radial Power Distribution	Results: Hottest Rod T/C and Elevation [m(in.)]	Initial Temperature [°C(°F)]	Maximum Temperature [°C(°F)]	Temperature Rise [°C(°F)]	Turn-around Time (sec)	Quench Time (sec)	Bundle Quench Time (sec)	Disconnected Rod Location
39	Not run														
HOT AND COLD CHANNELS															
40	Not run														
41	Not run														
42	Not run														
43	Not run														
AXIAL TEMPERATURE DISTRIBUTION															
44	33544	0.27 (39)	196 (385)(g) (0 to 3) 874 (1605)	2.3 (0.69)	5.85 (12.9) 15 sec 0.780 (1.72) onward	52 (125)	Uniform	11K-1.93 (76)	877 (1610)	908 (1668)	31 (58)	8	121	213	4G, 5G
	33644	0.27 (39)	182 (359)(g) (0 to 3) 877 (1610)	2.3 (0.70)	5.81 (12.8) 15 sec 0.789 (1.76) onward	52 (125)	Uniform	7D-1.93 (76)	884 (1623)	930 (1705)	46 (82)	9	104	250	4G, 5G
STEAM COOLING															
45, 46	32652 through 33056; 36160 through 37170														
OVERLAP COSINE TESTS															
47	Not run														
48	Not run														

9. Axial temperature distribution - simulated gravity reflood

TABLE 4-1 (cont)

FLECHT SEASET UNBLOCKED BUNDLE REFLOOD TEST DATA SUMMARY

Test No.	Run No.	As-Run Test Conditions: Upper Plenum Pressure [MPa (psia)]	Rod Initial T_{clad} at 1.83m (72 in.) [°C(°F)]	Rod Peak Power [kw/m (kw/ft)]	Flooding Rate [mm/sec (in./sec)]	Coolant Temperature [°C(°F)]	Radial Power Distribution	Results: Hottest Rod T/C and Elevation [m(in.)]	Initial Temperature [°C(°F)]	Maximum Temperature [°C(°F)]	Temperature Rise [°C(°F)]	Turn-around Time (sec)	Quench Time (sec)	Bundle Quench Time (sec)	Disconnected Rod Location
COMPARISON WITH WESTINGHOUSE PROPRIETARY REFLOOD DATA															
49	33749	0.27 (39)	745 (1374)	1.9 (0.57)	26.9 (1.06)	61 (142)	Uniform	11K-1.88 (74)	730 (1346)	1017 (1861)	287 (515)	103	250	430	4G, 5G
	33849[h]	0.28 (40)	745 (1374)	1.9 (0.57)	25.9 (1.02)	58 (138)	Uniform	8K-1.98 (78)	705 (1302)	1025 (1878)	320 (576)	105	254	437	4G, 5G
50	35050[a]	0.14 (20)	758 (1397)	1.6 (0.48)	25.9 (1.02)	43 (109)	Uniform	9D-1.83 (72)	758 (1397)	958 (1758)	200 (361)	98	243	433	4G, 5G, 11IJK, 12IJK, 13JK
POWER DECAY															
51	Not run														

h. Rod 12J failed during test.

TABLE 4-2

FLECHT SEASET UNBLOCKED BUNDLE STEAM COOLING TEST DATA SUMMARY

Test No.	Run No.	Actual Test Conditions							Disconnected Rod Location
		Upper Plenum Pressure [MPa (psia)]	Rod[a] Initial T_{clad} at 1.83m (72 in.) [°C(°F)]	Rod Peak Power kw/m [(kw/ft)]	Inlet Flow Rate kg/sec [(lbm/sec)]	Coolant Temperature [°C(°F)]	Inlet Bundle Reynolds Number	Bundle Radial Power Profile	
STEAM COOLING									
52	32452	0.27 (39)	131 (267)	0.018 (0.0054)	0.0472 (0.104)	131 (268)	2200	Uniform	4G, 5G
	32652	0.28 (40)	130 (266)	0.019 (0.0057)	0.0472 (0.104)	131 (268)	2200	Uniform	4G, 5G
53	32753	0.28 (40)	135 (275)	0.16 (0.050)	0.36 (0.80)	132 (269)	16720	Uniform	4G, 5G
54	32854	0.28 (40)	132 (269)	0.0587 (0.0179)	0.14 (0.30)	132 (269)	6330	Uniform	4G, 5G
55	32955	0.28 (40)	131 (268)	0.098 (0.030)	0.23 (0.50)	131 (268)	10550	Uniform	4G, 5G
56	33056	0.28 (40)	157 (316)	1.3 (0.40)	0.36 (0.80)	132 (269)	16720	Uniform	4G, 5G
60	36160[b]	0.27 (39)	143 (289)	0.16 (0.049)	0.37 (0.81)	144 (292)	16575	Uniform	4G, 5G, 11IJK, 12IJK, 13JK
61	36261[b]	0.27 (39)	139 (283)	0.13 (0.039)	0.297 (0.655)	142 (287)	13480	Uniform	4G, 5G, 11IJK, 12IJK, 13JK
62	36362[b]	0.27 (39)	142 (287)	0.079 (0.024)	0.18 (0.40)	138 (280)	8310	Uniform	4G, 5G, 11IJK, 12IJK, 13JK
63	36463[b]	0.28 (40)	131 (268)	0.0479 (0.0146)	0.110 (0.243)	134 (273)	5080	Uniform	4G, 5G, 11IJK, 12IJK, 13JK
64	36564[b]	0.28 (40)	147 (296)	0.039 (0.012)	0.0853 (0.188)	133 (271)	3950	Uniform	4G, 5G, 11IJK, 12IJK, 13JK
65	36665[b]	0.28 (40)	174 (345)	0.03 (0.009)	0.671 (0.148)	131 (267)	3130	Uniform	4G, 5G, 11IJK, 12IJK, 13JK

a. Rod location 7J, channel 59

b. Significant rod bundle distortion occurred between 1.52 and 2.27 m (60 and 90 in.)

TABLE 4-2 (cont)

FLECHT SEASET UNBLOCKED BUNDLE STEAM COOLING TEST DATA SUMMARY

Test No.	Run No.	Actual Test Conditions							Disconnected Rod Location
		Upper Plenum Pressure [MPa (psia)]	Rod[a] Initial T_{clad} at 1.83m (72 in.) [°C(°F)]	Rod Peak Power kw/m [(kw/ft)]	Inlet Flow Rate kg/sec [(lbm/sec)]	Coolant Temperature [°C(°F)]	Inlet Bundle Reynolds Number	Bundle Radial Power Profile	
66	36766[b]	0.28 (40)	180 (356)	0.02 (0.007)	0.054 (0.12)	131 (267)	2535	Uniform	4G, 5G, 11IJK, 12IJK, 13JK
67	36867[b]	0.27 (39)	174 (346)	0.02 (0.006)	0.0531 (0.117)	131 (267)	2470	Uniform	4G, 5G, 11IJK, 12IJK, 13JK
68	Invalid								
69	37069[b]	0.27 (39)	143 (289)	0.059 (0.018)	0.137 (0.303)	131 (267)	6400	Uniform	4G, 5G, 11IJK, 12IJK, 13JK
70	37170[b]	0.28 (40)	131 (268)	0.10 (0.030)	0.230 (0.508)	139 (282)	10520	Uniform	4G, 5G, 11IJK, 12IJK, 13JK
BOILOFF							Water Level [m(ft)]		
57	35557[b]	0.41 (60)	135 (275)	1.38 (0.422)	0 (0)	139 (281)[c]	3.054 (10.02)	Uniform	4G, 5G, 11IJK, 12IJK, 13JK
58	35658[b]	0.14 (20)	104 (220)	1.38 (0.422)	0 (0)	108 (227)[c]	3.063 (10.05)	Uniform	4G, 5G, 11IJK, 12IJK, 13JK
59	35759[b]	0.28 (40)	122 (251)	1.38 (0.422)	0 (0)	123 (254)[c]	3.002 (9.85)	Uniform	4G, 5G, 11IJK, 12IJK, 13JK

c. 1.83m (72 in.) steam probe temperature

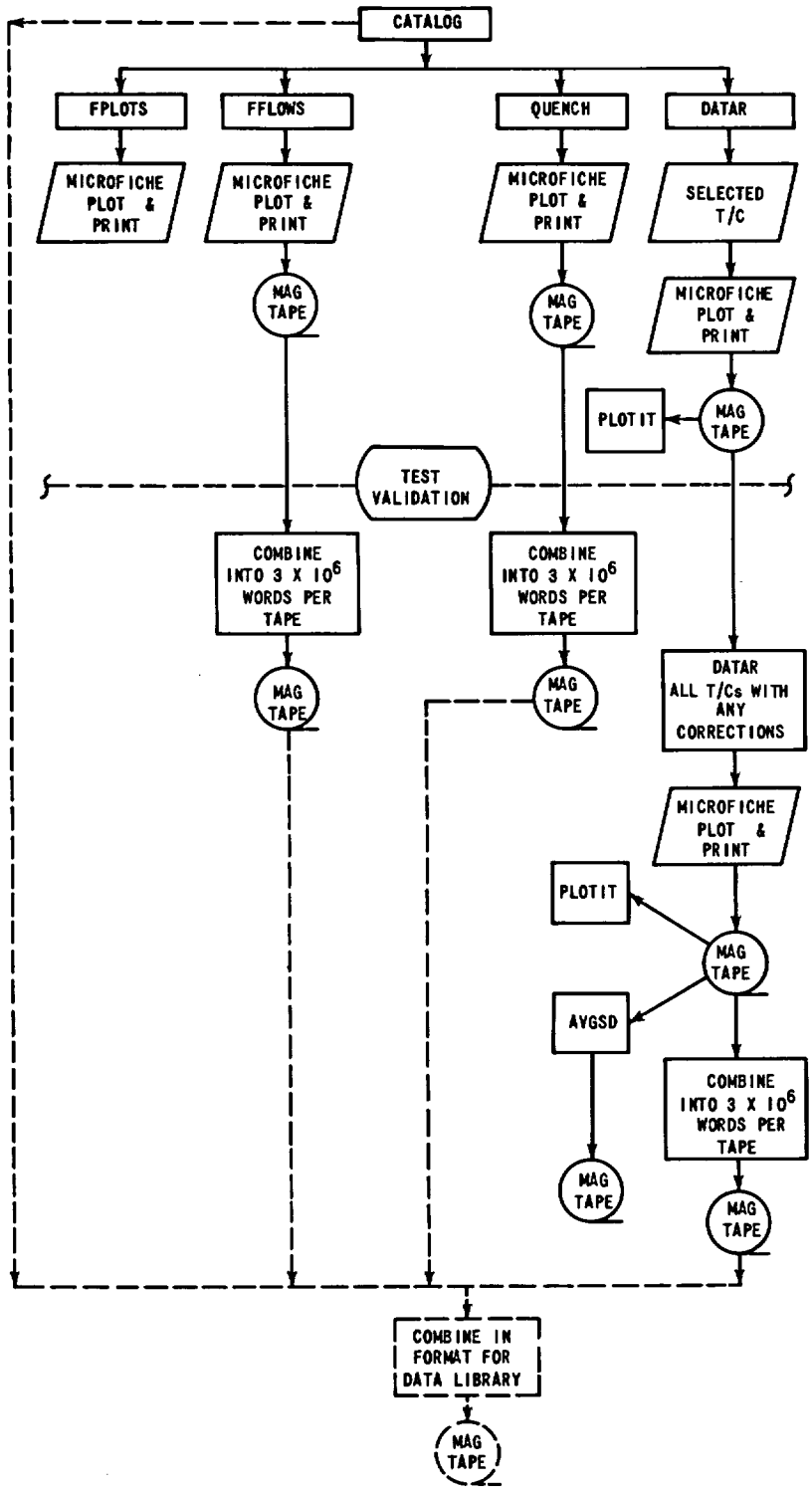

Figure 4-1. FLECHT SEASET Data Reduction Flow Chart

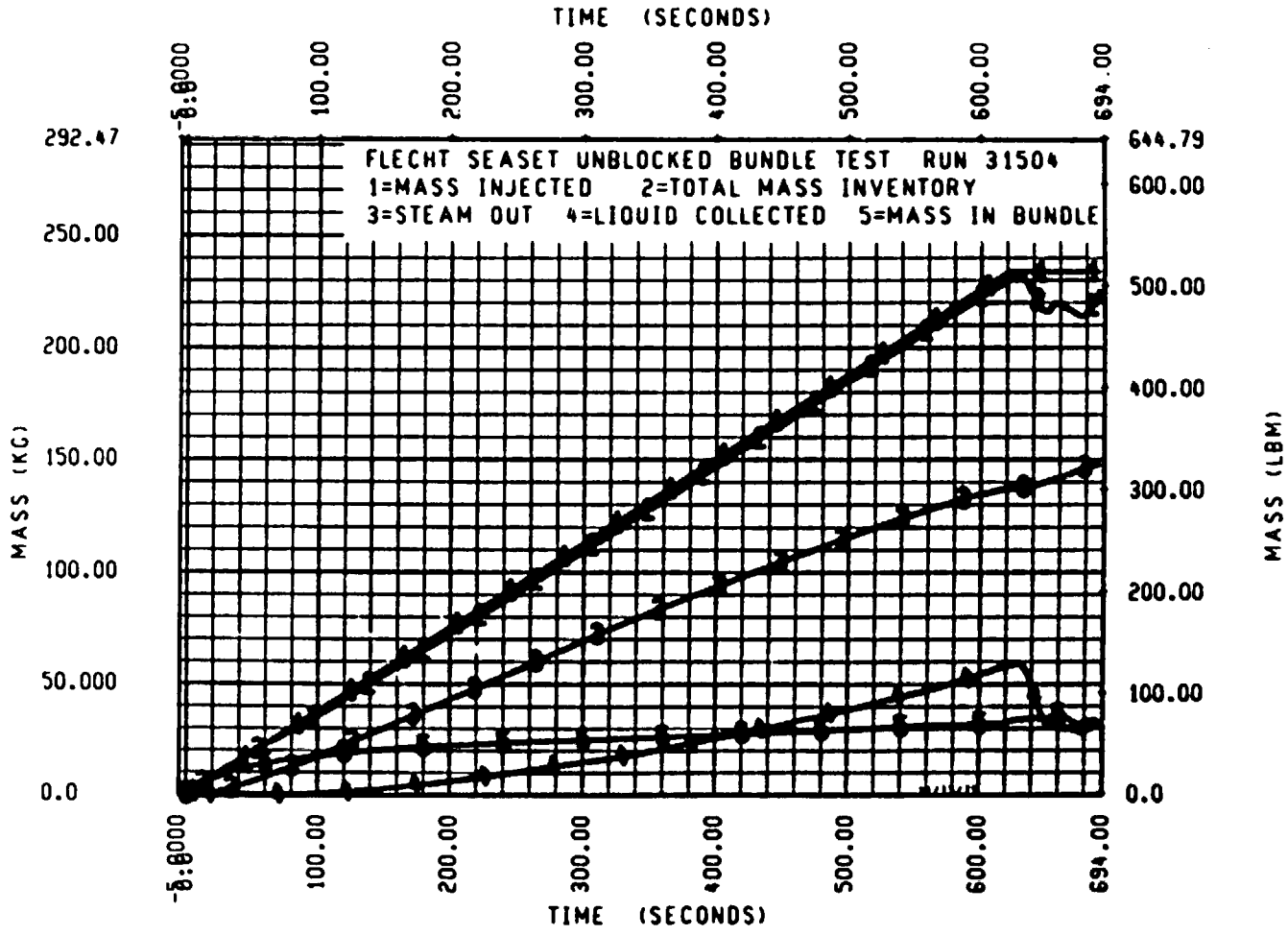

Figure 4-2. Mass Balance Versus Time (Reference Run)

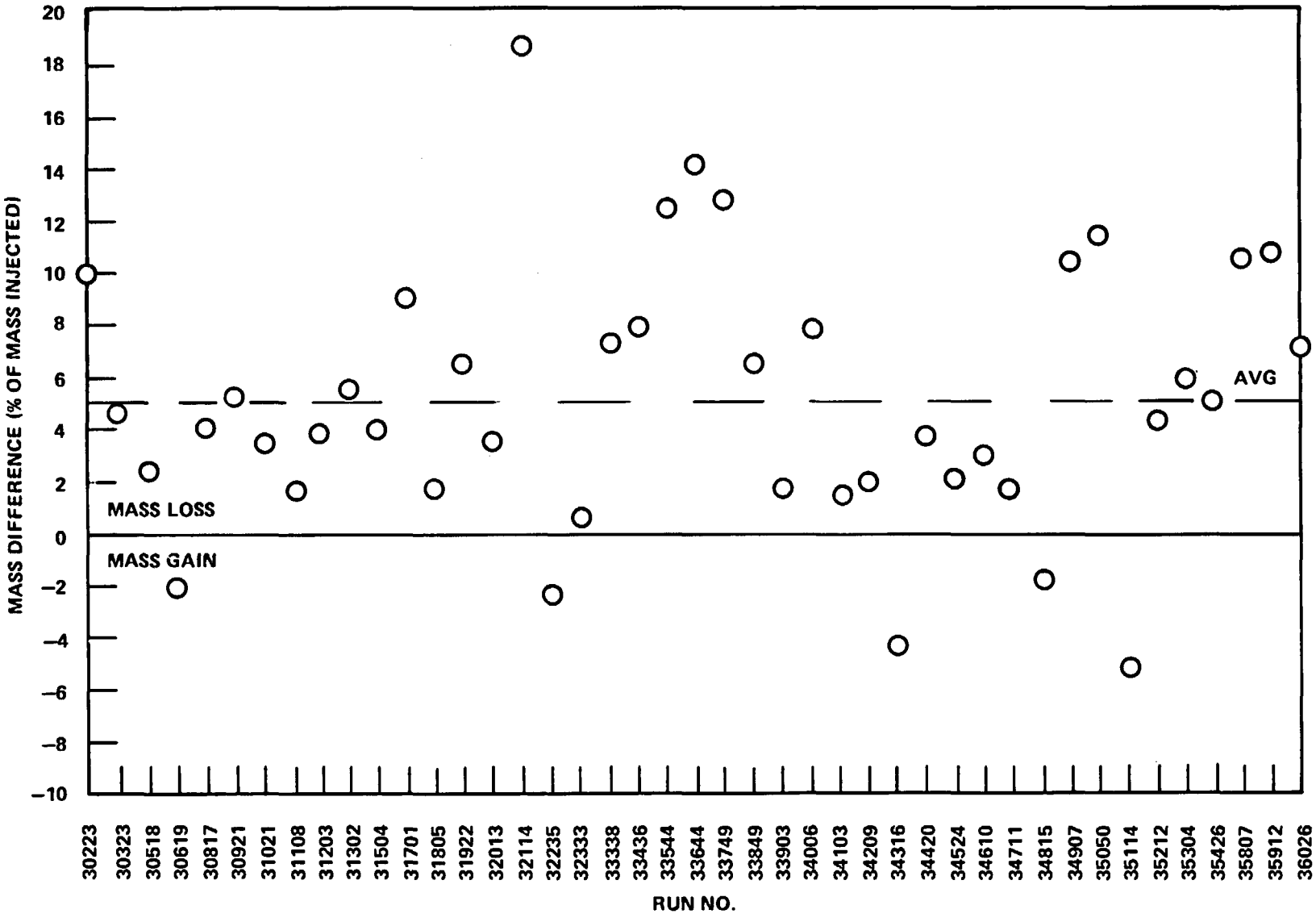

Figure 4-3. FLECHT SEASET Unblocked Bundle Mass Balance Results

of this code include rejection of data because of noise or shorting of the thermocouple and determination of the initial temperature, maximum temperature, and time at which maximum temperature occurs, and quench time and temperature. The temperature history of the hottest rod thermocouple for the reference run (31504) is shown in figure 4-4 with the actual data points and the quench time and temperature chosen by the data reduction code. The use of a standard procedure for determination of quench time and temperature reduces the number of possible errors and produces a consistent criterion independent of individual judgment. Details of the criteria used for choosing quench time and temperature are provided in appendix E.

The time-temperature data for heater rod thermocouples connected for the entire test program are included in the data package summary for each test in appendix C.

4-5. Heat Transfer Coefficients

The DATAR program was used to calculate the rod surface heat fluxes and heat transfer coefficients. The program employs a finite difference method to solve the inverse conduction problem, using such parameters as the material properties, rod dimensions, and measured rod power and temperature. This program is described in greater detail in appendix E.

The rod model used in DATAR accounts for the actual volume of Kanthal in the heater element region, similar to the DATARH program used to calculate heat transfer coefficients in the FLECHT skewed test series.[1] In the versions of DATARH code employed to calculate the heat transfer coefficient for the previous FLECHT and FLECHT-SET programs, it was assumed that the entire heater element coil consisted of Kanthal. This modification of the rod model in the DATAR code accounts for the average properties of the heater core region, reduces the overall heat capacity of the rod, and provides a more accurate representation of the rod. The results of this modification showed higher heat transfer coefficients than those previously calculated, particularly at early times in the tests, which should be considered when these data are compared to previous FLECHT data. Comparisons with clad temperatures calculated

---

1. Rosal, E. R., "FLECHT Low Flooding Rate Skewed Test Series Data Report," WCAP-9108, May 1977.

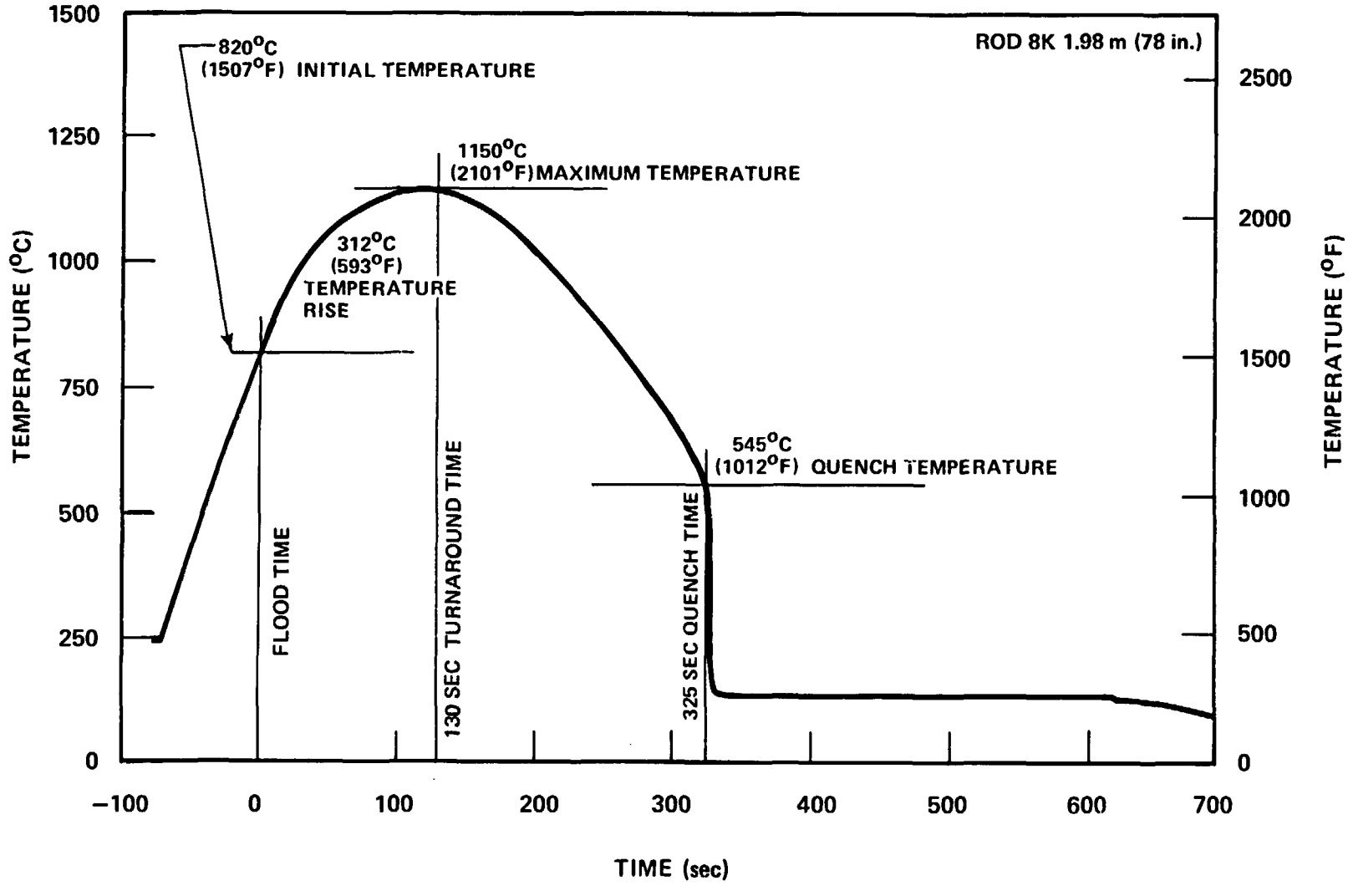

Figure 4-4. Temperature History of Hottest Rod Thermocouple (Reference Run)

16539-6

by a TAP-A[1] model of a FLECHT rod showed that the change of heat transfer coefficient due to the change of rod properties is correct and that the higher heat transfer coefficients obtained have a very small effect on the predicted rod temperatures.

It was desirable to obtain smoothed (or averaged) heat transfer data in order to produce data which were more meaningful and useful for graphic presentation.

To accomplish this, a data smoothing technique was applied which consisted of replacing each data point with an average value of the original data point and a specified number of points before and after the time of interest. Each point was weighed equally in obtaining the average, and a time interval of the "window" was chosen empirically to produce the best results for graphic presentation. The technique used is explained in appendix E. An example of the original data and the averaged data is shown in figure 4-5. This graph shows that, although the smoothed data significantly reduce the amplitude of the oscillations, the smoothed and original data are virtually equal. These data have been smoothed over a total time of 10 seconds, that is $2\Delta = 10$ seconds (or $\Delta = 5$ seconds), where Δ equals the time period before and after the original data point over which the data were averaged.

4-6. FAILED RODS

During the initial matrix tests, heater rod 4G failed because the heater coil shorted to ground. An adjacent heater rod, rod 5G, was found to have a low isolation resistance. The low isolation resistance was initially believed to be a result of damp boron nitride insulation. As a normal procedure, a low power supply was applied to rod 5G in order to dry out the insulation; however, this procedure resulted in shorting the heater coil to ground. To minimize damage to other rods, these rods were disconnected from the power supply and remained unpowered for the rest of the test series. These rods were located in the third and fourth rows of rods from the bundle center.

Later in the unblocked bundle test series, rod 12J failed because of the element shorting to ground. The isolation resistance of the adjacent seven rods was found to be low.

---

1. Pierce, B. L., and Stumpf, H. J., "TAP-A, A Program for Computer Transient or Steady-State Temperature Distributions," WANL-TME-1872, December 1969.

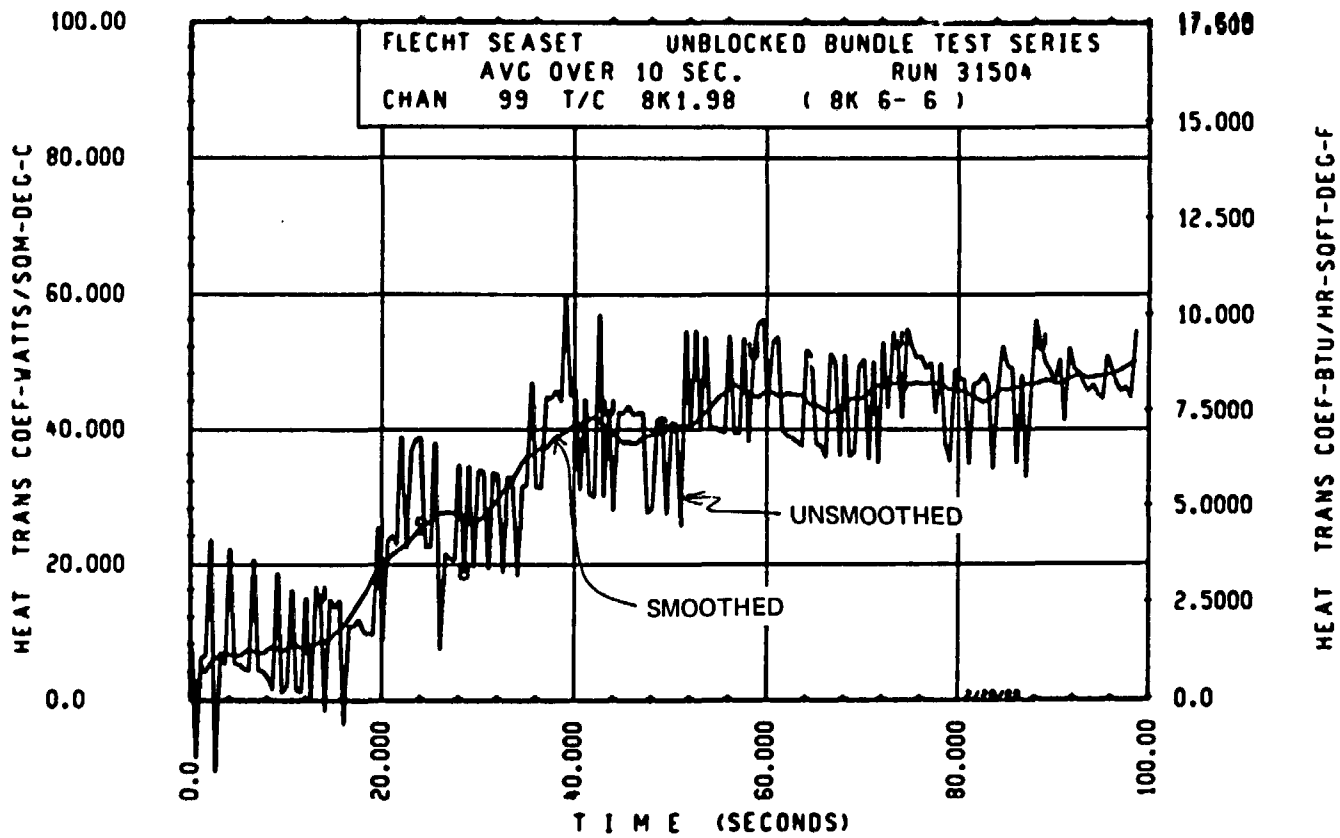

Figure 4-5. Smoothed Versus Average Heat Transfer Data

These eight rods were disconnected from the power supply for the remainder of the test series. These eight rods were located diagonally from the initial pair of failed rods. With the eight additional rods disconnected, the rod power was increased by 5.3 percent to maintain the same power to flow area ratio as in the tests conducted prior to disconnecting the eight rods. A comparison of repeat tests with and without the 5.3 percent increase in rod power is shown in appendix F. It was concluded that the rod power increase adequately compensated for the eight disconnected rods.

The effects of failed rods on the hot rods' heat transfer coefficients and the two-phase flow structure within the bundle were extensively analyzed in the FLECHT cosine and skewed test series.[1,2] Results from these analyses showed that only the rods in the first row surrounding a failed rod are affected. Similar analyses were performed for the unblocked bundle unpowered rods and the same results were obtained, as shown in appendix F.

4-7. STEAM COOLING TESTS

Steam cooling tests were conducted to provide data from which a heat transfer correlation for steam flow heat transfer in a rod bundle could be developed. These tests were conducted at low temperatures because of the 204°C (400°F) temperature limit of the upper heater rod O-ring seals. The tests were initiated from saturation conditions at 0.28 MPa (40 psia) and were allowed to attain steady-state conditions. The power and the steam flow were the only parameters varied in the tests. The inlet Reynolds number varied between 2200 and 17,000. Three boiloff tests were also conducted in which saturated water covered approximately 3 m (120 in.) of the bundle heated length. The saturated water was allowed to boil off, with no water injection, at system pressures of 0.14, 0.28, and 0.41 MPa (20, 40, and 60 psia). Data from the steam cooling tests are included in appendix C. A detailed evaluation of the steam cooling tests will be presented in the steam cooling data evaluation report.

---

1. Lilly, G. P., et al., "PWR FLECHT Cosine Low Flooding Rate Test Series Evaluation Report," WCAP-8838, March 1977.

2. Lilly, G. P., et al., "PWR FLECHT Skewed Profile Low Flooding Rate Test Series Evaluation Report," WCAP-9183, November 1977.

4-8. ROD BUNDLE DISTORTION

Rod bundle distortion was initially observed through the 1.83 m (72 in.) elevation housing window after test 31615. However, this rod distortion occurred in only one subchannel in the outer row of rods. Rod distortion was observed in all subchannels after test 31805 at the 1.83 m (72 in.) elevation window, and backlighting for movies could not penetrate the bundle during most of the test. During test 31922, four of the six subchannels were blocked at the 2.74 m (108 in.) window elevation. Filler distortion was initially observed through the 1.83 m (72 in.) window after test 32013. During test 32235, backlighting could not penetrate the bundle at the 1.83 m (72 in.) window elevation and through two of the six subchannels at the 2.74 m (108 in.) window elevation. During test 32333, backlighting could not penetrate through four of the six subchannels at the 2.74 m (108 in.) window elevation. There was no distortion observed through the 0.91 m (36 in.) window elevation. For the remainder of the test program, no rod or filler distortion was observed.

At the conclusion of the test program, the bundle was removed from the housing and thoroughly examined. It was observed that the fillers had severly distorted into the bundle at about the 1.83 m (72 in.) elevation. The bundle was disassembled by removing successive rows of rods, and photographs of each rod row were taken in 0.51 m (20 in.) increments. These photographs, shown in appendix G, indicate that the distortion occurred mostly between the 1.52 and 2.13 m (60 and 84 in.) elevations even in the center of the bundle. Although permanent heater rod bow does occur because of restraint on free expansion and after repeated high-temperature thermal cycling, the bowing of the eight fillers into the bundle caused the severe rod distortion in the center of the bundle.

Filler rod distortion was observed in the FLECHT skewed test series; however, the distortion was limited to the outer rows of heater rods and did not affect the hot rods utilized for heat transfer correlation development.

An analysis was performed to determine the point at which the center region of the bundle bowed such that the center rods could no longer be utilized for heat transfer correlation development. Several repeat tests were conducted throughout the test

program; comparisons of data from these tests show that the data had lost their repeatability by test 35304. Also, a statistical analysis of the heat transfer shows an increase in the standard deviation after test 34610. This analysis is presented in detail in appendix G. It has been concluded that data generated prior to test 34711 can be utilized for hot rod heat transfer correlation development.

4-9. SUMMARY AND CONCLUSIONS

This test series has extended the reflood data base to include the 17 x 17 rod design. The expanded data base will be useful for model development and verification.

The unblocked bundle test series was judged to be successful in spite of severe technical problems caused by a large number of heater rod thermocouple failures, heater rod failures, and rod bowing and distortion. The most severe problem was the heater rod bowing and distortion, which caused the test data to lose repeatability. A systematic analysis of the rod distortion effects on the rod-to-rod heat transfer was performed and is included as appendix G. It can be said that no center rod distortion occurred before test 31805. Some rod bowing may have occurred between tests 31922 and 33749, but its effect on the data was second-order and within the scatter caused by other rod-to-rod variables. The data obtained beyond test 34610 should not be used for heat transfer correlation or comparisons above the 1.52 m (60 in.) elevation because of bundle distortion.

Steam cooling tests were also successfully completed. The results represent the only steam cooling data at low Reynolds numbers in rod bundles. Bundle boiloff tests were also completed, but the heat transfer information from these experiments cannot be utilized because of bundle distortion. The hydraulic information, however, is valid and can be utilized to assess boiloff hydraulic methods.

APPENDIX A
DETAILED FACILITY DESCRIPTION

A-1. INTRODUCTION

This appendix supplements the general facility description given in section 3. Included is a more detailed description of the primary facility components, secondary systems of interest, and safety devices employed on the facility. Figures referenced in this appendix are located at its end.

All vessels in the FLECHT SEASET unblocked bundle facility were designed and built to comply with the ASME Boiler and Pressure Vessel Code, Section 1. Facility piping conformed to the USAS B31.1 - 1973 Code for Power Piping. Weld procedures and qualifications conformed to section IX of the ASME Boiler and Pressure Vessel Code.

Table A-1 summarizes component design and maximum operating conditions and the applicable design code.

A-2. FACILITY COMPONENTS

Components described in the following paragraphs may be located in figures A-5 and A-6, the facility piping layouts.

A-3. Test Section

The low mass housing together with the lower and upper plenums constituted the test section. The low mass housing was a cylindrical vessel, 19.37 cm (7.625 in.) inside diameter by 0.477 cm (0.188 in.) wall, constructed of SA-312, type 304 stainless steel. The actual average inside diameter of the housing was determined by filling the housing with water, then draining and weighing the water. The water was drained from each pressure tap starting at the top, so that an average diameter was obtained for each 0.30 m (12 in.) of the housing. The results of the measurements were as follows:

TABLE A-1

SUMMARY OF COMPONENT DESIGN AND MAXIMUM OPERATING CONDITIONS

Component	Material	Design		Maximum Operating		Design Code
		Pressure [MPa (psig)]	Temperature [°C (°F)]	Pressure [MPa (psig)]	Temperature [°C (°F)]	
Test section	SA-312, type 304	0.52 (60)	816 (1500)	0.45 (50)	816 (1500)	ASME Sect 1
Upper plenum	SA-106 Gr-B	0.52 (60)	371 (700)	0.45 (50)	371 (700)	ASME Sect 1
Lower plenum	SA-106 Gr-B	0.52 (60)	371 (700)	0.45 (50)	371 (700)	ASME Sect 1
Carryover vessel	SA-106 Gr-B	0.791 (100)	343 (650)	0.45 (50)	149 (300)	ASME Sect 1
Entrainment separator		1.34 (180)	204 (400)	0.45 (50)	149 (300)	ASME Sect 1
Exhaust piping	SA-106 Gr-B	0.791 (100)	343 (650)	0.45 (50)	260 (500)	ASME Sect 1
Loop pressure control valve	Type 316	0.69 (85)	343 (650)	0.45 (50)	260 (500)	USAS B 31.1.0
Boiler	Carbon steel	0.791 (100)	171 (340)	0.62 (75)	160 (320)	ASME Sect 1
Boiler piping	SA-106 Gr-B	10.4 (1500)	343 (650)	7.00 (1000)	285 (545)	USAS B 31.1.0
Pressurization line valves	Carbon steel	10.4 (1500)	538 (1000)	7.00 (1000)	285 (545)	USAS B 31.1.0
Nitrogen line	SA-312, type 304	41.5 (6000)	343 (650)	41.5 (6000)	38 (100)	USAS B 31.1.0
Nitrogen line valves	Carbon steel	41.5 (6000)	121 (250)	41.5 (6000)	38 (100)	USAS B 31.1.0
Accumulator	SA-106 Gr-B	4.93 (700)	343 (650)	2.86 (400)	149 (300)	ASME Sect 1
Coolant injection line	SA-53 Gr-B	4.23 (600)	288 (550)	2.17 (300)	149 (300)	USAS B 31.1.0
Coolant injection line valves	Carbon steel, bronze	2.17 (300)	260 (500)	2.17 (300)	149 (300)	USAS B 31.1.0
Rotameters	Carbon steel, glass	1.55 (210)	149 (300)	0.45 (50)	149 (300)	USAS B 31.1.0
Pressure transducer lines	SA-213, type 316	20.8 (3000)	343 (650)	7.00 (1000)	121 (250)	USAS B 31.1.0
Transducer valves	SS, type 316	20.8 (3000)	232 (450)	7.00 (1000)	121 (250)	USAS B 31.1.0
Housing level sight gage	Glass (borosilicate)	1.83 (250)	204 (400)	0.45 (50)	149 (300)	ASME Sect 1
Downcomer	SA-53 Gr-B	0.791 (100)	343 (650)	0.45 (50)	260 (500)	USAS B 31.1.0

Section of Housing	Average Diameter [cm (in.)]
1st to 2nd pressure tap	19.31 (7.604)
2nd to 3rd pressure tap	19.46 (7.664)
3rd to 4th pressure tap	19.15 (7.541)
4th to 5th pressure tap	19.32 (7.607)
5th to 6th pressure tap	19.46 (7.663)
6th to 7th pressure tap	19.31 (7.604)
7th to 8th pressure tap	19.36 (7.622)
8th to 9th pressure tap	19.40 (7.638)
9th to 10th pressure tap	19.41 (7.643)
10th to 11th pressure tap	19.38 (7.630)
11th to 12th pressure tap	19.38 (7.630)
12th to 13th pressure tap	19.39 (7.633)
Overall average diameter	19.36 (7.623)

When the bundle was inserted into the housing, the housing was again filled with water and the water was drained and weighed at each pressure tap to get incremental volumes. The results were as follows:

Section of Housing	Volume [m^3 ($in.^3$)]
Lower plenum to 1st pressure tap	0.04512 (2751)
1st to 2nd pressure tap	0.00499 (304)
2nd to 3rd pressure tap	0.00500 (305)
3rd to 4th pressure tap	0.00507 (309)
4th to 5th pressure tap	0.00502 (306)
5th to 6th pressure tap	0.00503 (307)
6th to 7th pressure tap	0.00503 (307)
7th to 8th pressure tap	0.00492 (300)
8th to 9th pressure tap	0.00499 (304)
9th to 10th pressure tap	0.00492 (300)
10th to 11th pressure tap	0.00499 (304)
11th to 12th pressure tap	0.00481 (293)
12th to 13th pressure tap	0.00341 (208)

Design and fabrication of the low mass housing complied with the ASME Boiler and Pressure Vessel Code. The vessel was rated for 0.52 MPa (60 psig) at 816°C (1500°F) and bore a Section I code stamp. Figure A-15 shows the details of construction of the vessel. The housing had two commercial quartz sight glass assemblies located at 180 degrees at the 0.9, 1.8, and 2.7 m (36, 72, and 96 in.) elevations. The housing also had pressure taps spaced every 0.30 m (12 in.) along the housing.

Flange connections joined the upper and lower plenums to the low mass housing. The upper and lower plenums (figures A-17 and A-18) were designed and fabricated to Section I of the ASME code and were rated for 0.52 MPa (60 psig) at 371°C (700°F). The upper plenum had two sight glasses which allowed photographic studies in the upper plenum. Figure A-16 shows the assembly of the low mass housing to the plenums. There were an upper and a lower extension in the upper and lower plenums, respectively. The upper extension prevented the entrained liquid collected in the upper plenum from falling back into the bundle. The lower extension helped to diffuse the injected coolant.

The test section was supported from the upper plenum to permit downward expansion of the housing due to thermal expansion.

A-4. Carryover Vessel

The carryover vessel was constructed of SA-106 Gr-B carbon steel pipe and SA-105 Gr-II and SA-234 WPB flange and fitting material. The vessel shell was 15.2 cm (6 in.) diameter standard weight pipe with 5.1 cm (2 in.) diameter and 2.5 cm (1 in.) diameter standard weight nozzle connection and nine 1.3 cm (0.5 in.) diameter extra-strong nozzle connections.

Design and fabrication of the vessel complied with the ASME Boiler and Pressure Vessel Code. The vessel was rated for 0.79 MPa (100 psig) at 343°C (650°F) and bore a Section I code stamp. Figure A-29 shows the details of construction of the vessel.

The function of the carryover vessel was to collect liquid overflow from the test section. The vessel was attached to the upper plenum by means of a stainless steel flexible hose rated for 3.89 MPa (550 psig) at 454°C (850°F).

A-5. Entrainment Separator

The entrainment separator was a standard, commercially available liquid-vapor separator designed and manufactured by Wright-Austin Company. Constructed of carbon steel, its design and fabrication complied with the ASME Boiler and Pressure Vessel Code. The vessel shell was 0.30 m (12 in.) diameter standard weight pipe. The separator was rated for 1.34 MPa (180 psig) at 204°C (400°F) and bore a Section I code stamp. The volume of the separator was increased by a factor of five over that in the past FLECHT low flooding rate skewed test series to help reduce the magnitude of the housing pressure oscillations. This was accomplished by welding in a longer center section (figure A-27). The volume of the separator was 0.22 m^3 (7.8 ft^3).

Located in the exhaust line, the separator was designed to remove any remaining water droplets exiting the test section, so that a meaningful single-phase flow measurement could be obtained by an orifice section positioned downstream of the separator.

The separator operated by utilizing centrifugal action to force the heavier moisture against the wall, where it drained to the bottom and through a 3.18 cm (1.25 in.) diameter outlet. Water was collected in a separator drain tank (figure A-28). The vessel shell was 10.2 cm (4 in.) diameter standard weight pipe. The drain tank was rated for 0.79 MPa (100 psig) at 343°C (650°F) and bore a Section I code stamp. The volume of the drain tank was 0.011 m^3 (0.4 ft^3).

The manufacturer rated the separator as capable of removing 99 percent of all liquid and solid entrainment where the particle size exceeds 10 microns (3.9×10^{-4} in.). Separator capacity varied with operating pressure. At 0.14 MPa (20 psia), the maximum recommended saturated steam flow rate is 0.315 kg/sec (2500 lb/hr); at 0.41 MPa (60 psia), the capacity is 0.592 kg/sec (4700 lb/hr).

A-6. Exhaust Piping

Test section effluent discharged to the atmosphere through the exhaust line piping. The existing flanged 12.7 cm (5 in.) diameter nozzle penetration on the upper plenum provided the attaching point for the exhaust line piping. Sandwiched between the two

mating flanges was a 1.3 cm (0.5 in.) plate which served as the structural attachment for an internal 7.6 cm (3 in.) baffle pipe assembly. The assembly, called the upper plenum baffle, served to improve liquid carryout separation and minimize liquid entrainment into the exhaust vapor. After passing through the upper plenum baffle pipe, the exhaust vapor passed through a 10.2 cm (4 in.) diameter 90-degree elbow and into a straight run of 10.2 cm (4 in.) diameter standard weight pipe. A steam probe was located in the 10.2 cm (4 in.) diameter elbow to measure the temperature of the exhaust steam. The straight run of 10.2 cm (4 in.) diameter pipe took the effluent into the entrainment separator. Dry steam leaving the separator passed through a 10.2 cm (4 in.) by 7.6 cm (3 in.) diameter 90-degree reducing elbow and along a straight run of 7.6 cm (3 in.) diameter standard weight pipe to a 2.07 MPa (300 lb) weld neck orifice flange assembly utilized to measure flow rate. Clamp-on strip heaters on the 7.6 cm (3 in.) pipe were used to heat the pipe to 260°C (500°F), to assure single-phase flow through the orifice section. Steam then entered the 2.07 MPa (300 lb) system pressure control valve and exhausted to the atmosphere by way of a 12.7 cm (5 in.) diameter standard weight pipe run.

A 5.113 mm (2.013 in.) diameter resistance orifice plate was installed before the inlet flange of the entrainment separator for the gravity reflood tests (figure A-6). The orifice plate was installed to simulate the hot leg resistances.

Design and fabrication of the exhaust line complied with Section I of the ASME Boiler and Pressure Vessel Code. The pipe complied with the specification SA-106 Gr-B. To provide for thermal expansion of the exhaust line, the piping was positioned on roller supports attached to spring stanchion hangers. Figures A-24 and A-25 show the details of construction of the exhaust line components. Each detail has an assembly number which locates its position on the facility piping layout (figure A-5).

A-7. Boiler

The boiler was a Reimers electric steam boiler, model RHC 45, with a steam capacity of 0.016 kg/sec (125 lb/hr) at 100°C (212°F).

The boiler was used to pressurize the facility and for pretest facility heatup. This was accomplished by valving the boiler into the upper plenum of the test section.

A-8. Coolant Injection System

The coolant injection system provided reflood water to quench the rod bundle during testing. In brief, coolant injection water was supplied by the 1.51 m^3 (400 gal) accumulator by a series of valves and flowmeters. Nitrogen overpressure on the accumulator provided the driving head necessary to attain the required flow rates of 0 to 6.62×10^{-3} m^3/sec (0 to 105 gal/min). The nitrogen gas was supplied by a liquid nitrogen pump vaporizer system maintained at 24.1 MPa (3500 psi). Gas overpressure on the accumulator was maintained at 2.07 MPa (300 psi) by a pressure-reducing regulator.

Constant or stepped injection flow was accomplished by the proper sequencing of solenoid valves located in a piping manifold arrangement. This is shown on the facility flow diagram (figure A-3).

The accumulator was the largest component of the facility. It was designed and built in accordance with the ASME Boiler and Pressure Vessel Code, Section I. The vessel was constructed of 0.61 m (24 in.) diameter seamless carbon steel pipe, SA-106 Gr-B, and was designed for 4.93 MPa (700 psig) at 343°C (650°F).

The coolant injection system piping was 2.5 cm (1 in.) diameter and 3.8 cm (1.5 in.) diameter schedule 40 (SA-53 Gr-B). The control valves and solenoid valves in the system were of at least the 2.07 MPa (300 lb) class.

The flowmeters included a 0 to 3.8×10^{-4}, 0 to 1.1×10^{-3}, and 0 to 6.3×10^{-3} m^3/sec (0 to 6, 0 to 18, and 0 to 100 gal/min) rotameter, a 3.8×10^{-5} to 3.8×10^{-3} m^3/sec (0.6 to 60 gal/min) turbine meter and a 0 to 9.5×10^{-3} m^3/sec (0-150 gpm) turbine meter. The rotameters were used in conjunction with the turbine meters to provide a redundant system of flow rate measurement.

A 1.1×10^{-2} m^3/sec (180 gal/min) bidirectional turbo-probe was installed in the downcomer spool piece (figure A-30) during the gravity reflood tests to measure flow into the test section and any reverse flow from the test section to the downcomer.

A-9. Downcomer

The downcomer was connected to the test section lower plenum for the gravity reflood tests (figure A-2). The downcomer was fabricated of a 12.7 cm (5 in.) outside diameter by 0.30 cm (0.12 in.) wall thickness carbon steel tubing, a 12.5 cm (5 in.) diameter 90-degree schedule 40 long radius elbow, 1.03 MPa (150 lb) flanges, a specially designed spool piece for a turbo-probe, and a 12.7 cm (5 in.) diameter flexible rubber pipe. The spool piece consisted of two 12.7 cm (5 in.) diameter 2.07 MPa (300 lb) weld neck flanges welded to a 7.6 cm (3 in.) diameter schedule 40 tee-section which housed the turbo-probe. The turbo-probe measured reflood flow to the test section and any reverse flow from the test section to the downcomer. Details of the spool piece and downcomer are shown in figure A-30. The flexible rubber pipe connected the downcomer to the lower plenum of the test section and allowed the housing to move downward because of thermal expansion.

The horizontal run of the downcomer was 2.29 m (90 in.) long, including the spool piece and rubber pipe. The vertical run was approximately 6.10 m (240 in.) high. A 1.3 cm (0.5 in.) diameter carbon steel pressure equalization line was run from the top of the downcomer to the top of the steam separator. A 3.8 cm (1.5 in.) diameter nozzle located in the downcomer elbow was used to inject the coolant water from the accumulator.

A-10. Nitrogen Purge System

The nitrogen purge system was used to minimize oxidation in the facility components between tests. With all vents closed, nitrogen gas was throttled into the system through a series of valves until the pressure reached approximately 0.17 MPa (10 psig). The nitrogen supply was then valved out and the facility allowed to sit overnight. The nitrogen purge line teed off the accumulator pressurization line and entered the system through the test section lower plenum.

A-11. Heater Rod Bundle Power Control

The method of power control for the heater rods is shown in figure A-32. Power was supplied by a 1500 kva transformer through a 1600 amp, 600 v circuit breaker. Power

was distributed to three phase-fired silicon-controlled rectifier (SCR) units through individual 1000 amp circuit breakers representing three power zones. Each of the power units was rated for 1200 amps at 600 v. The secondary of the supply transformer was star-connected with a neutral. Each heater zone was connected in series with an SCR unit; all three zones formed a delta connection. To simulate the calculated decay heat generated by a shutdown reactor, the three SCR power control units could be biased either with three manually adjustable potentiometers or automatically through a curve-following programmer. The programmer used for this purpose was the output from the minicomputer analog output section. An alternate method was a pen instrument that followed a decay heat curve drawn on electrostatic paper. The programmer then sent a control signal to each power control unit to produce the required power decay.

An undervoltage relay in the control circuit tripped the power to the heater rods if the voltage to the instrumentation and control circuits was lost. Each heater rod was protected against burnout on each side of the line by fast-acting fuses. If the coolant flow in the SCR unit fell below a specific value, a thermal switch tripped and power to the test rods was turned off immediately.

A-12. FACILITY HEATING

Facility heating was accomplished by strip heaters on the various loop components. The following is a listing of the heater capacities of the facility components:

Component	Heater Capacity (kw)
Carryover vessel	7.5
Entrainment separator and separator drain tank	6.3
Exhaust piping	3.9
Accumulator	66

All vessel and pipe wall temperatures were controlled by temperature controllers fed by thermocouples attached to the outside component surface.

Heater sheath temperatures were protected by temperature limits fed by thermocouples attached directly to the heater.

A-13. SAFETY DEVICES

The following safety devices were associated with the various facility components:

-- Accumulator

Rupture disk with burst pressure of 4.90 MPa (696 psig) at 22°C (72°F)

Letdown regulator with relief setting of 2.86 MPa (400 psig)

Pressure trip, set to turn off heaters and sound alarm at 4.93 MPa (700 psig)

-- Housing

Rupture disk with burst pressure of 0.48 MPa (55 psig) at 22°C (72°F)

Pressure trip, set to turn off bundle heater and sound alarm at 0.45 MPa (50 psig)

-- Carryover vessel

Rupture disk with burst pressure of 0.76 MPa (96 psig) at 22°C (72°F)

-- Entrainment separator

Rupture disk with burst pressure of 0.76 MPa (96 psig) at 22°C (72°F)

-- Boiler

Relief valve set at 0.79 MPa (100 psig)

In addition to the above safety devices, the computer had its own built-in safety features which turned off bundle power and continued flooding on rod thermo-

couple overtemperature, computer power failure, instrument failure (multiplexers), and software error.

A-14. FACILITY DRAWINGS

The drawings listed in table A-2 and reproduced on the following pages illustrate the test facility.

TABLE A-2

DRAWING LIST

Figure	Engineering Drawing Number	Title
A-1	1224E16	FLECHT SEASET Heater Rods
A-2	1460E39	FLECHT SEASET 21-Rod Bundle Heater Rods
3-1	1453E42	FLECHT SEASET Flow Diagram - Forced Reflood
A-3	1453E43	FLECHT SEASET Flow Diagram - Gravity Reflood
A-4	1453E40	FLECHT SEASET Piping Layout - Forced Reflood
A-5	1453E41	FLECHT SEASET Piping Layout - Gravity Reflood
A-6	1453E50	FLECHT SEASET Instrumentation Schematic Diagram - Forced Reflood
A-7	1453E51	FLECHT SEASET Instrumentation Schematic Diagram - Gravity Reflood
A-8	1447E30 (2 sheets)	FLECHT SEASET Unblocked Bundle Assembly
A-9	1453E21	FLECHT SEASET Steam Probe Detail Assembly
A-10	8764D47	FLECHT SEASET Instrumented Thimbles
A-11	8764D49	FLECHT SEASET Thimble Detail
A-12	8763D58	FLECHT SEASET Grid Strip Assembly
A-13	8763D57 (7 sheets)	FLECHT SEASET Grid Strap Details
A-14	1446E97	FLECHT SEASET Low Mass Housing
A-15	1453E32	FLECHT SEASET Low Mass Housing Assembly
A-16	1447E25	FLECHT SEASET Upper Plenum Detail Assembly
A-17	1447E29	FLECHT SEASET Lower Plenum Detail Assembly
A-18	1463F27	FLECHT SEASET Upper Seal Plate
A-19	1463F33	FLECHT SEASET Lower Seal Plate
A-20	1680C97	FLECHT SEASET O-Ring Sleeve

TABLE A-2 (cont)
DRAWING LIST

Figure	Engineering Drawing Number	Title
A-21	1680C98	FLECHT SEASET Thimble Sleeve
A-22	8763D64	FLECHT SEASET Filler Strip Detail
A-23	1188E88	Exhaust Line Details
A-24	8764D64	FLECHT SEASET Exhaust Line Details
A-25	1683C18	Exhaust Line Steam Probe
A-26	1683C19	Steam Separator
A-27	8757D25	Separator Drain Tank
A-28	1144E64	Carryover Tank
A-29	1683C20	Downcomer for Gravity Reflood Configuration
A-30	1453E47 (2 sheets)	Strong Back and Assembly Fixture
A-31	--	Bundle Power

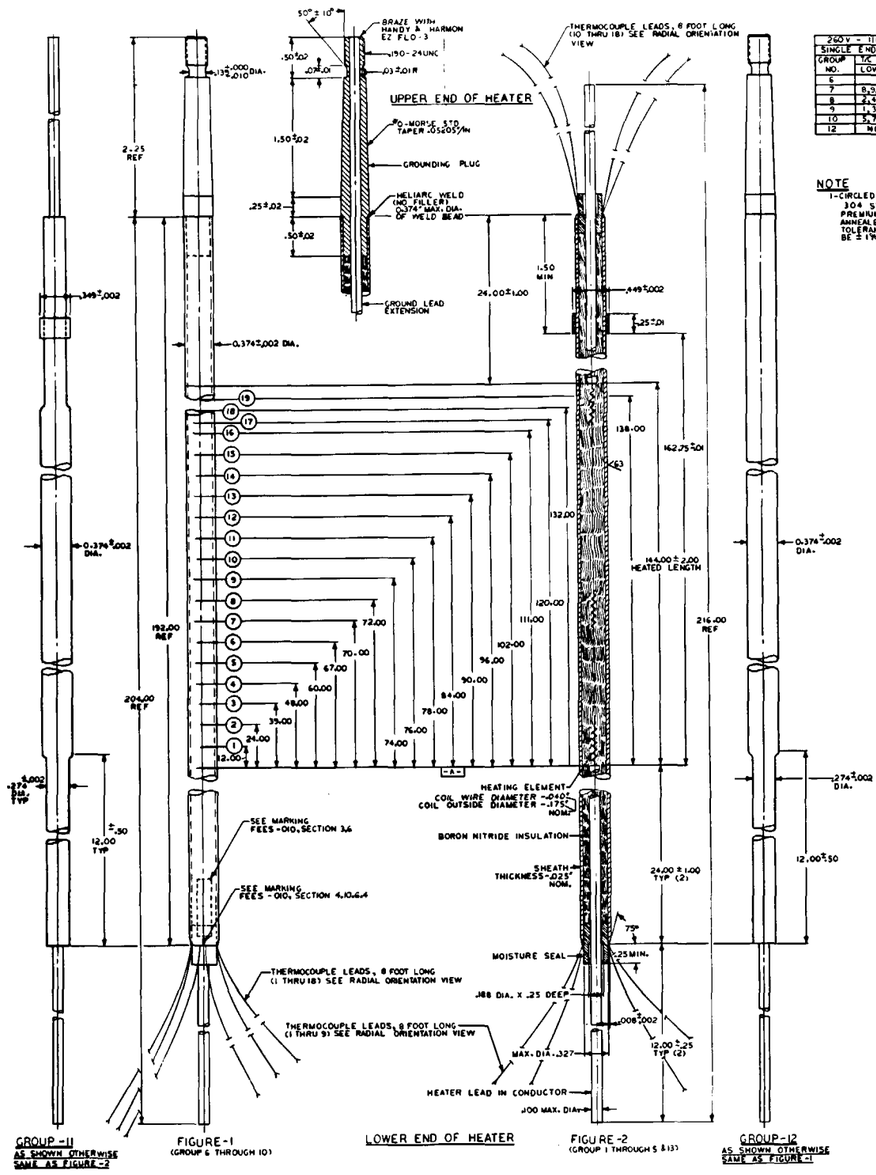

260V - 11KW SINGLE ENDED ROD	
GROUP NO.	T/C REQUIRED LOWER END
6	NONE
7	8,9,10,11,12,13
8	2,4,5,6,8,12,16
9	1,3,5,7,15,17
10	5,7,8,14,16,18
12	NONE

420V - 8KW DOUBLE ENDED ROD		
GROUP NO	T/C REQUIRED LOWER END	T/C REQUIRED UPPER END
1	NONE	NONE
2	8,9,10,11,12,13	12,13,14,16,
3	5,6,7,8,	—
4	1,3,5,7,	12,13,16,18,
5	2,4,8,	14,15,17,19,
11	NONE	NONE
13	9,12,	14,16,17,

NOTE

1-CIRCLED (1) THRU (18) ARE THERMOCOUPLES (.025 MIN. 304 STAINLESS STEEL SHEATH TYPE K PREMIUM GRADE INSULATED JUNCTIONS ANNEALED OVER ENTIRE LENGTH-) TOLERANCE ON ALL T/C DIMENSIONS TO BE ± 1% AS MEASURED FROM DATUM A.

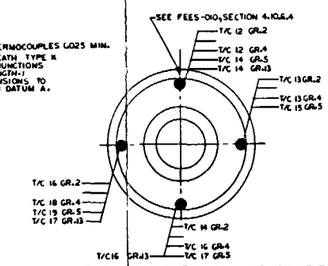

RADIAL ORIENTATION OF THERMOCOUPLES AS VIEWED FROM TOP END OF ROD FIG-2

NOTES

1-THIS DWG IS NOT INTENDED TO BE A COMPLETE FABRICATION DWG. THIS DWG IS TO BE USED IN CONJUNCTION WITH ORDERING DATA INCLUDED WITH (B) SPECIFICATION FEES-010.

2-REMOVE ALL BURRS AND SHARP EDGES.

3-SURFACE ROUGHNESS 63√ UNLESS OTHERWISE NOTED.

4-ULTRASONIC INSPECT PER ASME BOILER AND PRESSURE VESSEL CODE, SECTION III, CLASS 2 COMPONENTS. CALIBRATION STANDARDS AND DEFECT ACCEPTANCE CRITERIA ARE AS FOLLOWS:

(A) CALIBRATION DEFECT STANDARDS:
DEPTH-.0025 IN.
LENGTH-.050 IN.
WIDTH-.0025 IN.

(B) ACCEPTANCE CRITERIA:
DEFECT IN SHEATH MUST BE LESS THAN THE CALIBRATION DEFECT STANDARDS.

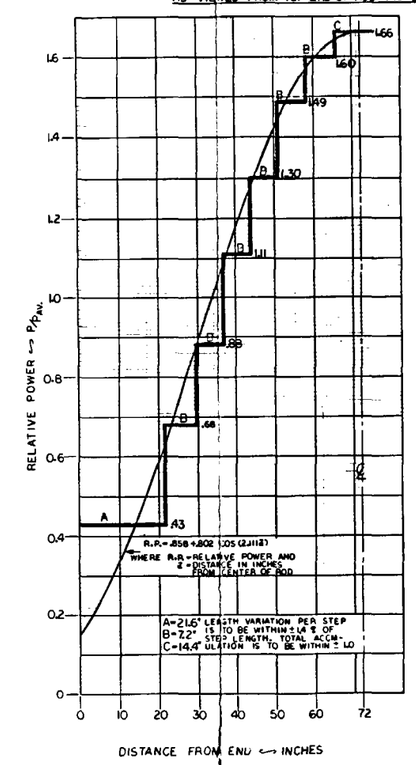

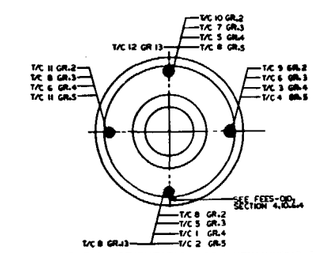

RADIAL ORIENTATION OF THERMOCOUPLES AS VIEWED FROM BOTTOM END OF ROD FIG-2

Figure A-1. FLECHT SEASET Heater Rods

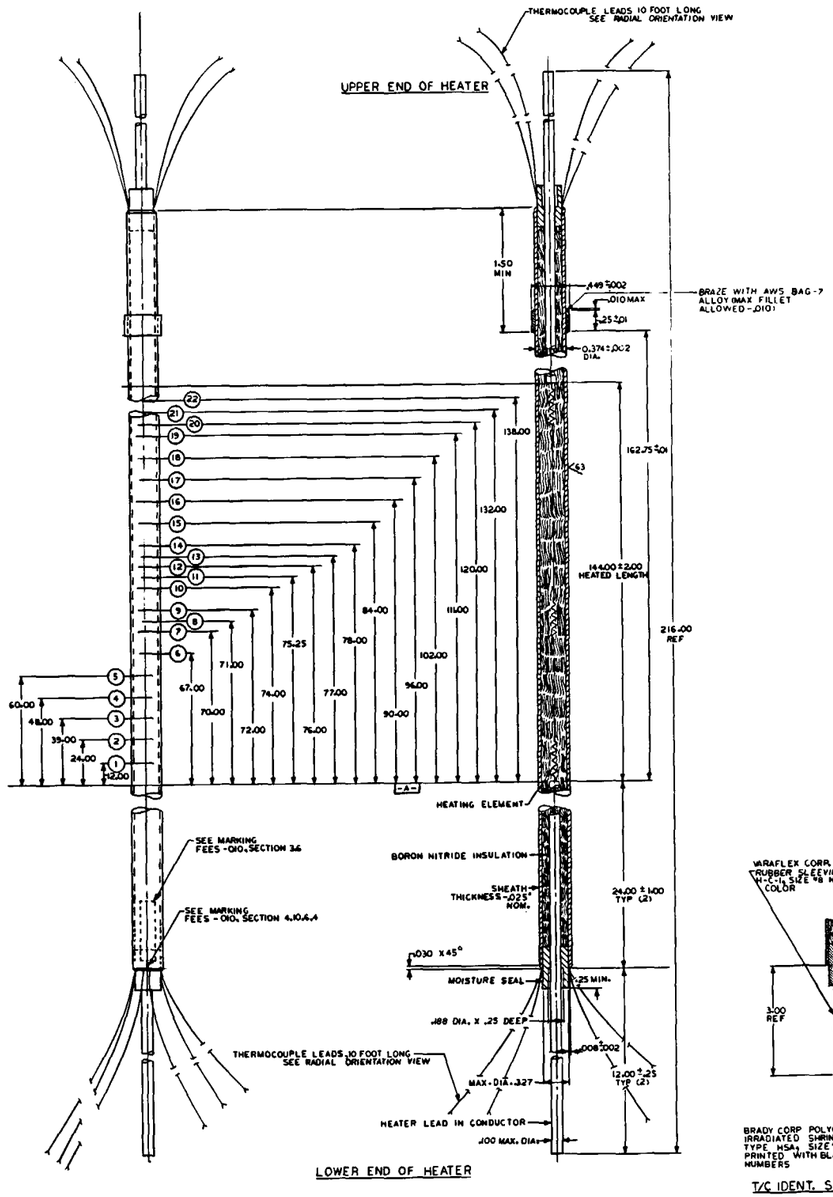

420 V - 8KW DOUBLE ENDED ROD		
GROUP NO	T/C REQUIRED	
	LOWER END	UPPER END
2 B	7,8,9,10,11,12,13,14,	
2 C	9,10,12,14,	15,16,17,19,
4 B	1,3,5,6,12,14,	19,21,
13 B	2,4,7,9	15,17,18,20,
14	8,10,11,13,	18,18,20,22,

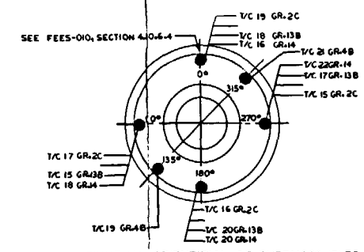

AZIMUTHAL ORIENTATION OF THERMOCOUPLES AS VIEWED FROM BOTTOM END OF ROD

NOTES

1-THIS DWG IS NOT INTENDED TO BE A COMPLETE FABRICATION DWG. THIS DWG IS TO BE USED IN CONJUNCTION WITH ORDERING DATA INCLUDED WITH (W) SPECIFICATION FEES-010.

2-REMOVE ALL BURRS AND SHARP EDGES.

3-SURFACE ROUGHNESS 63√ UNLESS OTHERWISE NOTED.

4-ULTRASONIC INSPECT PER ASME BOILER AND PRESSURE VESSEL CODE, SECTION III, CLASS 2 COMPONENTS. CALIBRATION STANDARDS AND DEFECT ACCEPTANCE CRITERIA ARE AS FOLLOWS:

(A) CALIBRATION DEFECT STANDARDS:
DEPTH -.0025 IN.
LENGTH-.050 IN.
WIDTH-.0025 IN.

(B) ACCEPTANCE CRITERIA:
DEFECT IN SHEATH MUST BE LESS THAN THE CALIBRATION DEFECT STANDARDS.

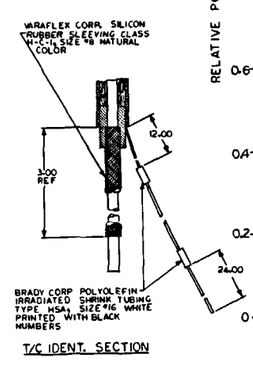

T/C IDENT. SECTION

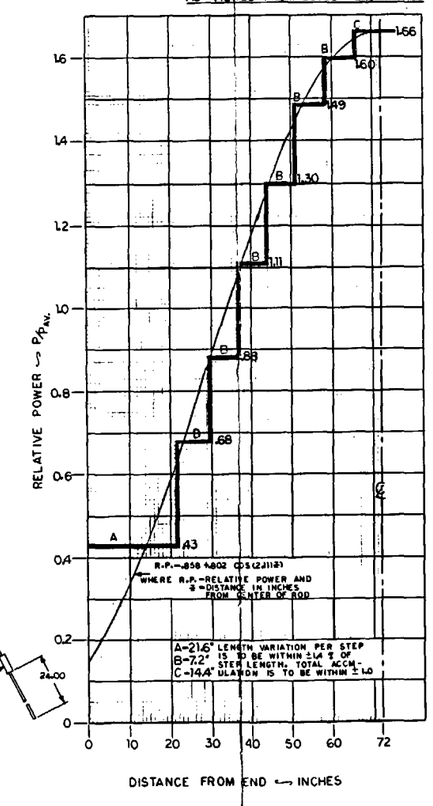

NOTE

1-CIRCLED (1) THRU (22) ARE THERMOCOUPLES (.040 DIA. 304 STAINLESS STEEL SHEATH TYPE K PREMIUM GRADE INSULATED JUNCTIONS ANNEALED OVER ENTIRE LENGTH.) TOLERANCE ON ALL T/C DIMENSIONS TO BE ±1% AS MEASURED FROM DATUM A.

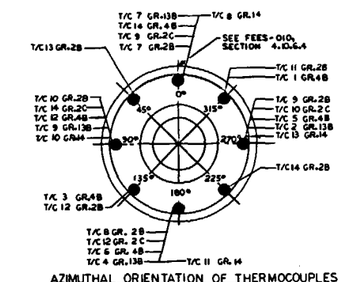

AZIMUTHAL ORIENTATION OF THERMOCOUPLES AS VIEWED FROM BOTTOM END OF ROD

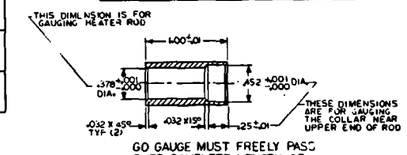

GO GAUGE MUST FREELY PASS OVER COMPLETE LENGTH OF ROD, INCLUDING END SEALS.

Figure A-2. FLECHT SEASET 21-Rod Bundle Heater Rods

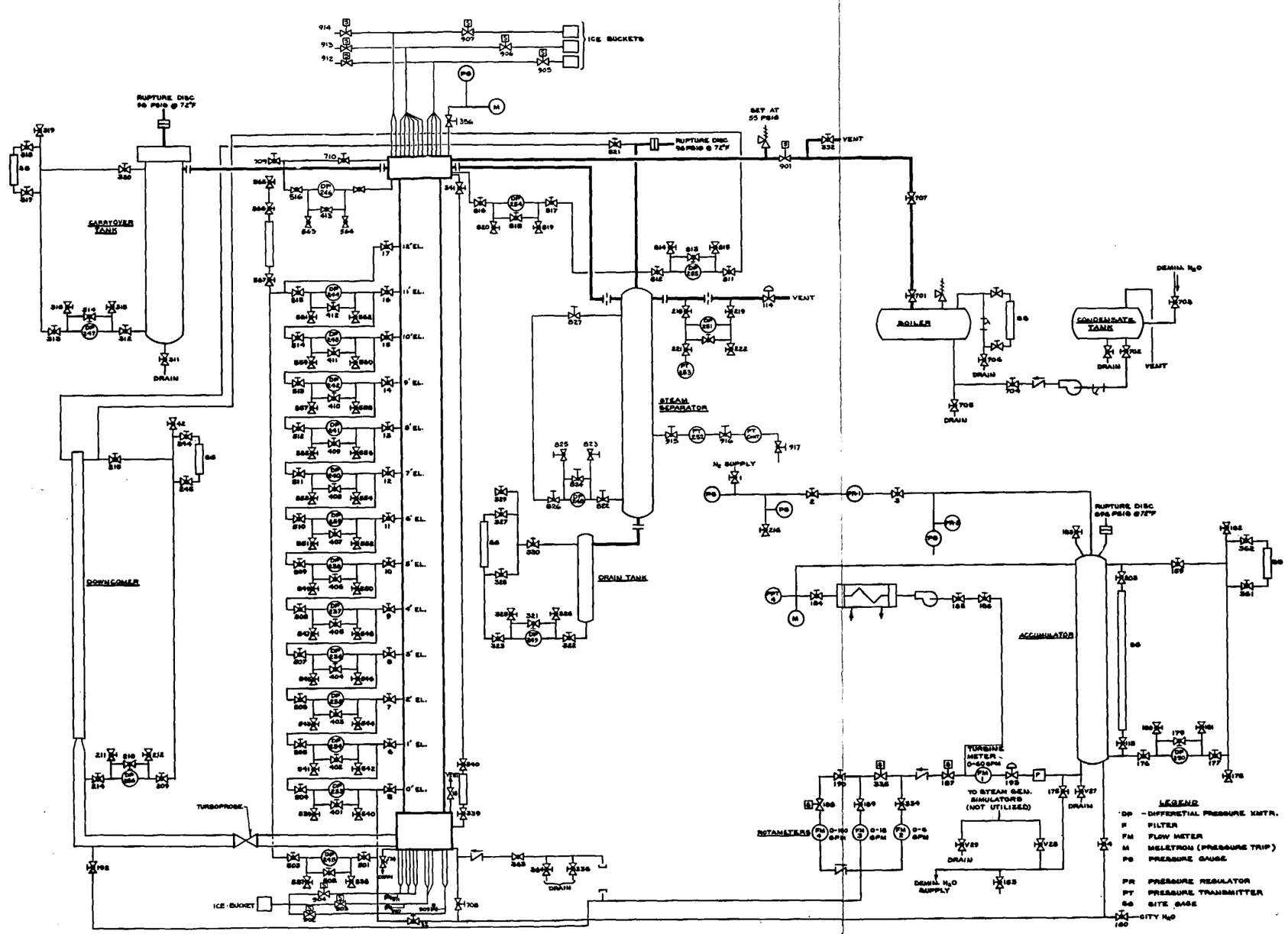

Figure A-3. FLECHT SEASET Flow Diagram - Gravity Reflood

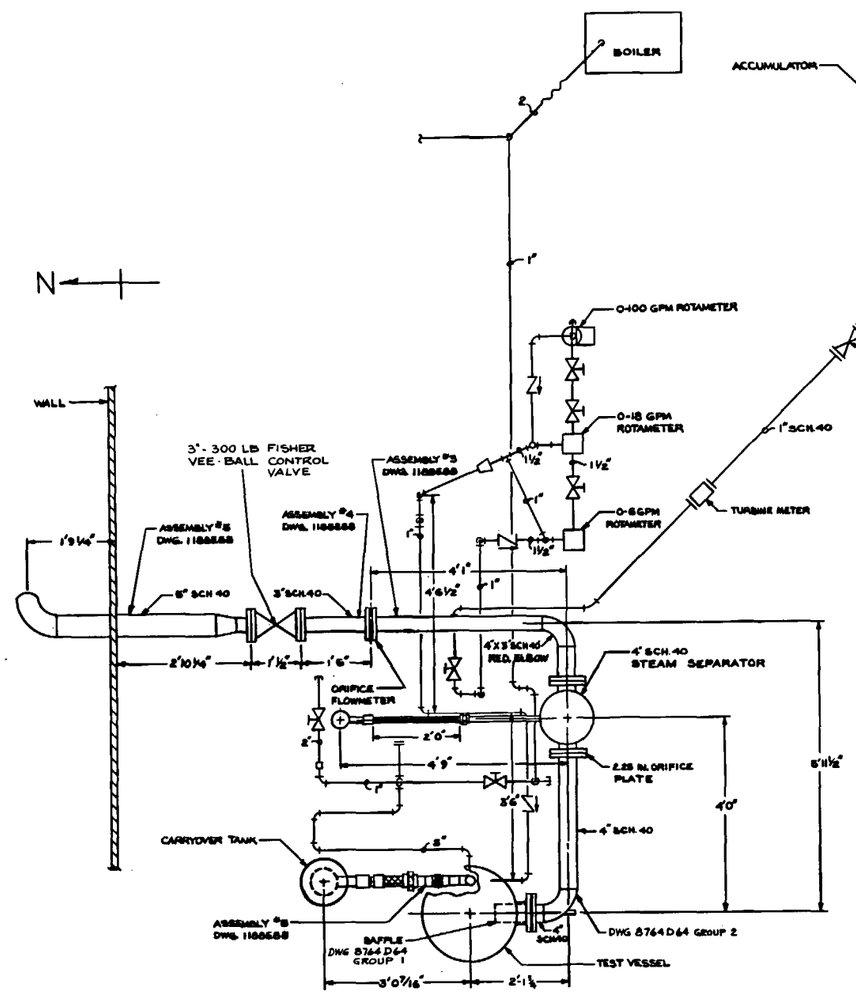

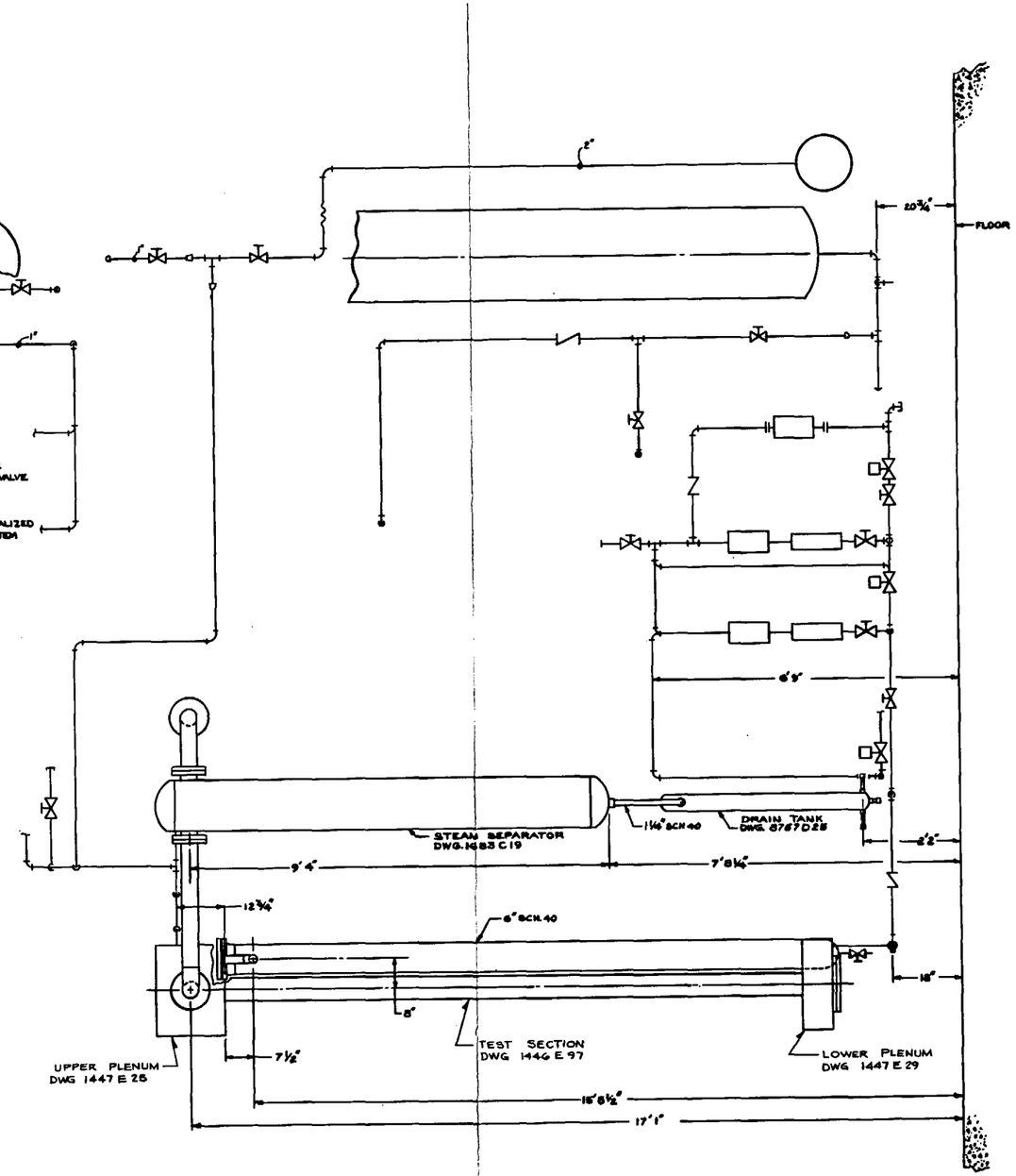

Figure A-4. FLECHT SEASET Piping Layout - Forced Reflood

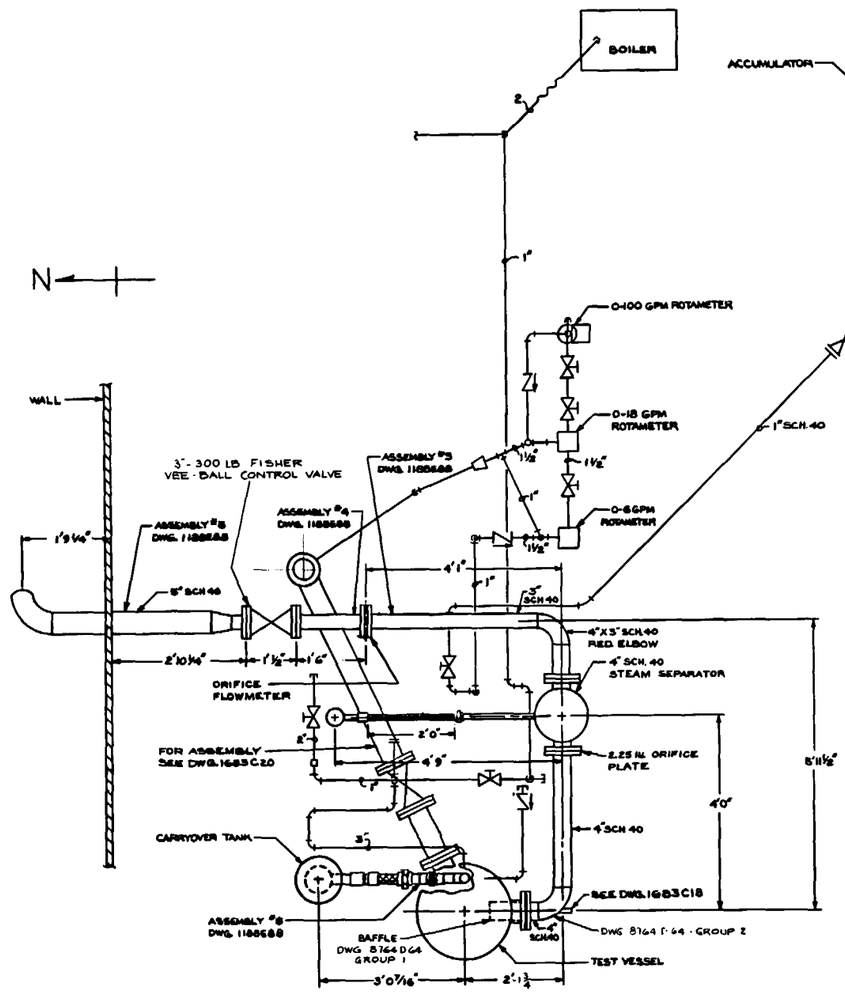

PLAN VIEW

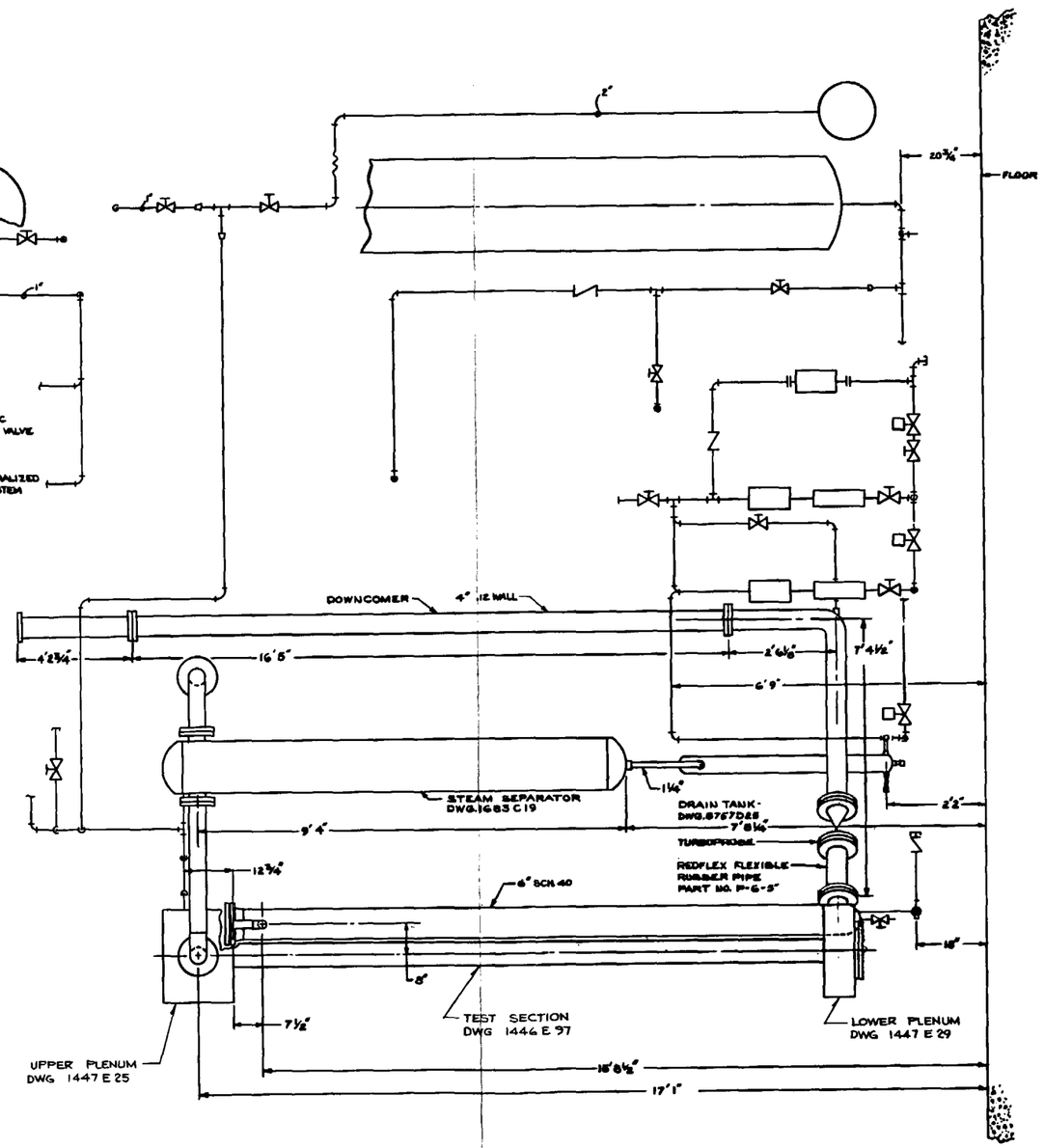

ELEVATION VIEW

Figure A-5. FLECHT SEASET Piping Layout - Gravity Reflood

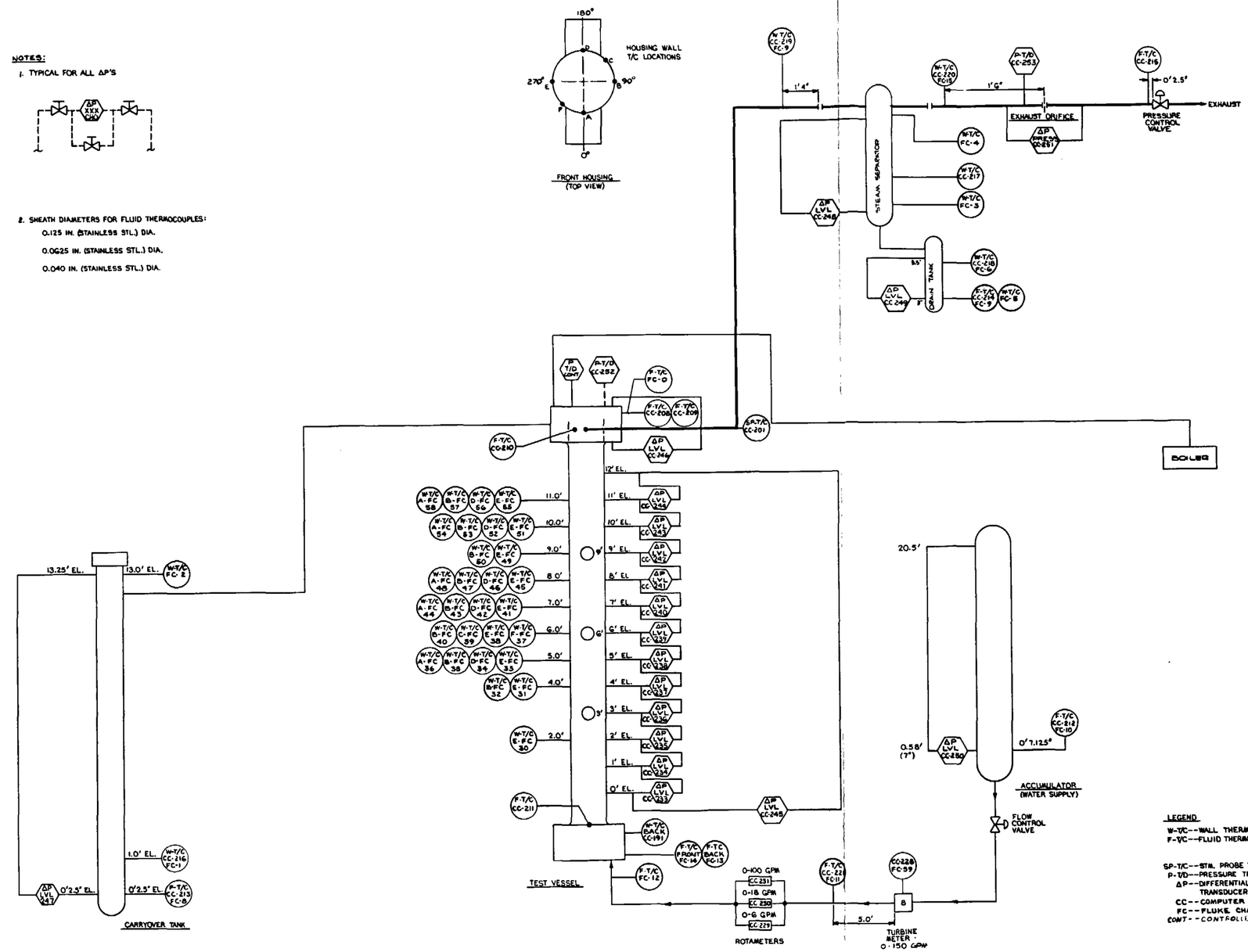

Figure A-6. FLECHT SEASET Instrumentation Schematic Diagram - Forced Reflood

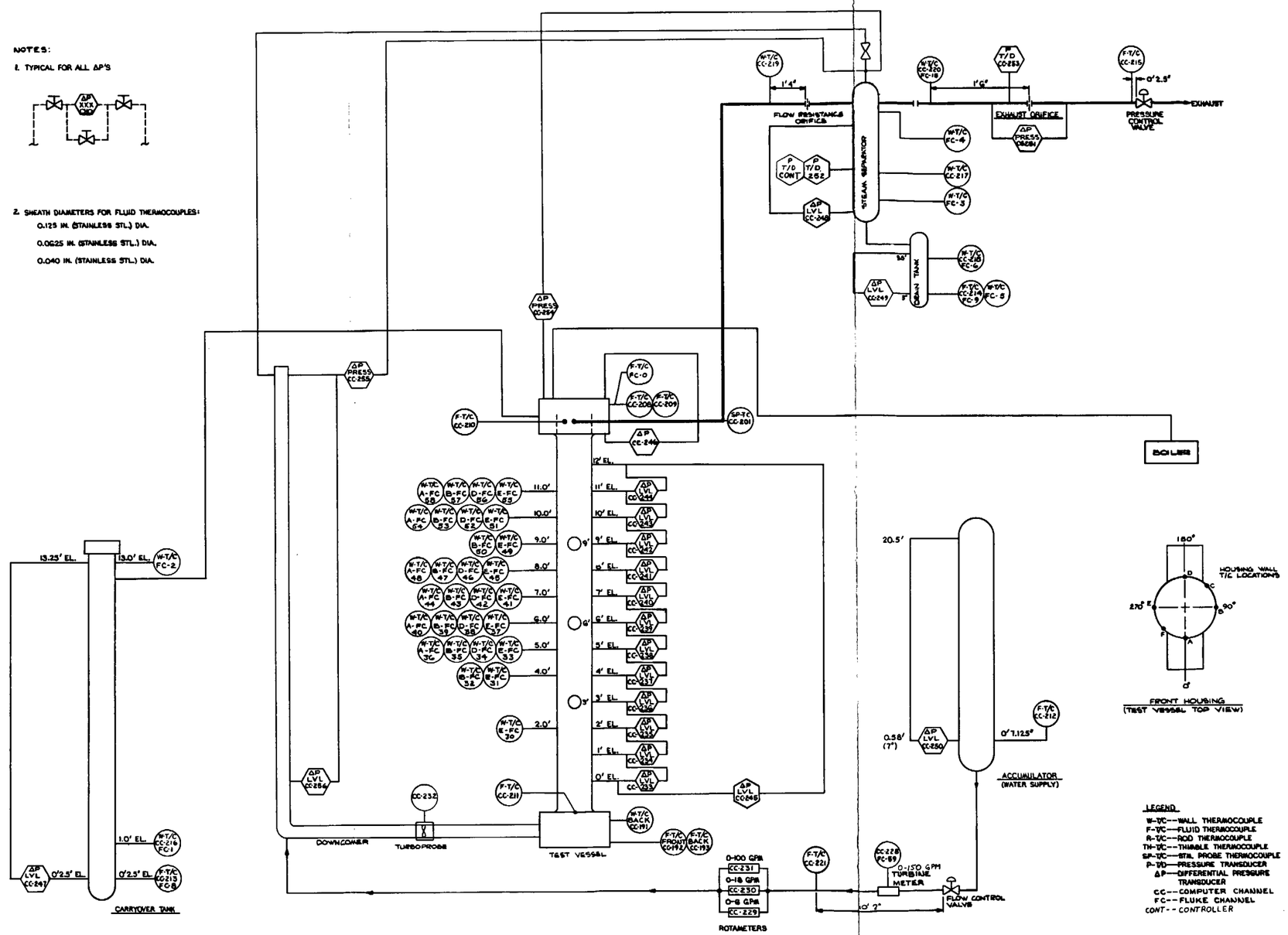

Figure A-7. FLECHT SEASET Instrumentation Schematic Diagram - Gravity Reflood

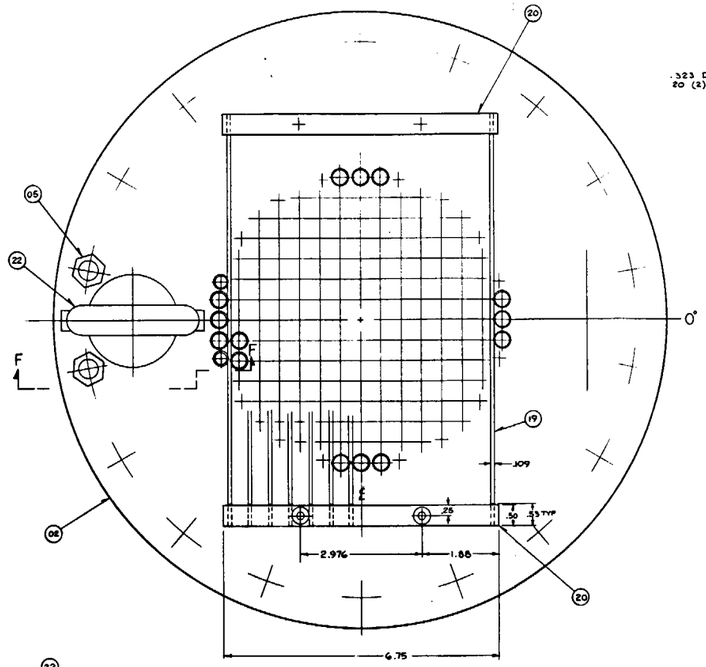

SECTION C-C (ROTATED)

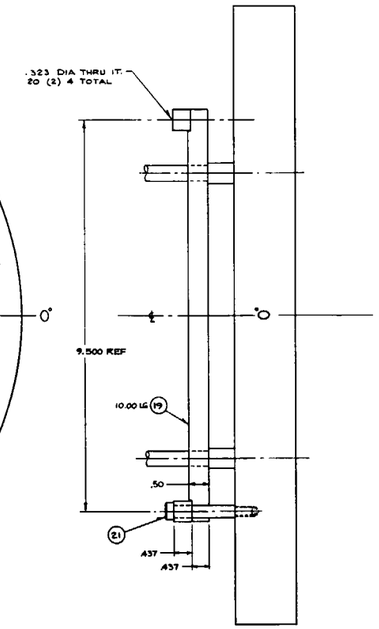

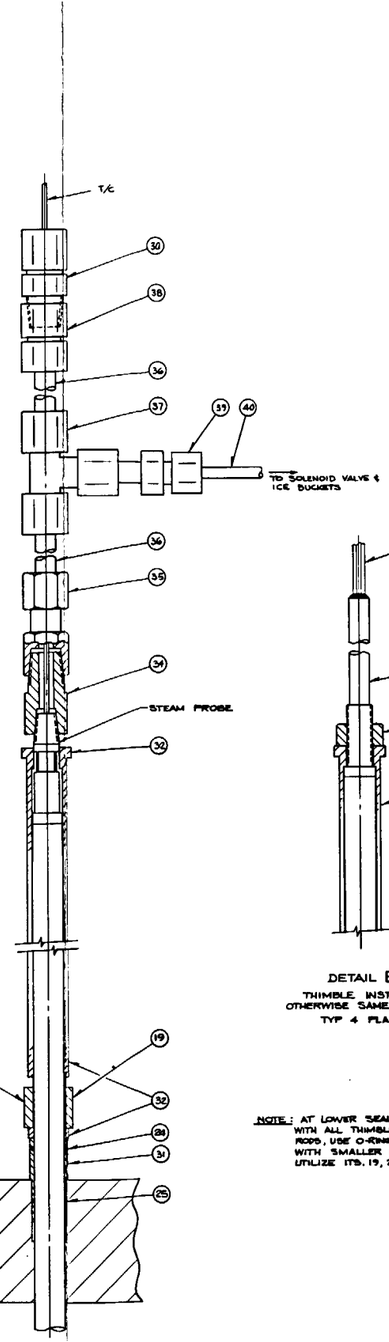

DETAIL "A"
STEAM PROBE
TYP 12 PLACES

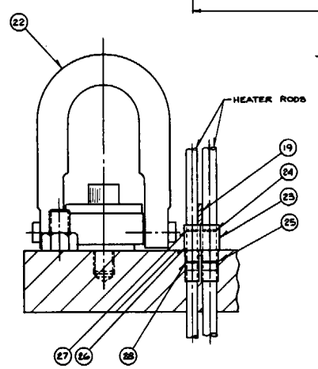

SECTION F-F

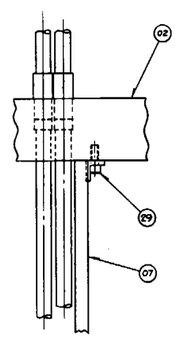

DETAIL "D"

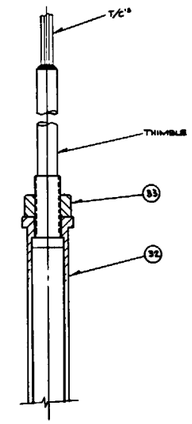

DETAIL B
THIMBLE INSTALLATION
OTHERWISE SAME AS DETAIL "A"
TYP 4 PLACES

NOTE: AT LOWER SEAL #, IT. 03, THE FOLLOWING IS REQ'D:
WITH ALL THIMBLES, STEAM PROBES, & STD. SIZE HEATER RODS, USE O-RING SLEEVE, IT. 23, & O-RINGS, IT. 24 & 25.
WITH SMALLER HEATER RODS USE ITS. 26, 27, 28. ALSO UTILIZE ITS. 19, 20 & 21 IN SAME MANNER AS ON UPPER SEAL #

Figure A-8. FLECHT SEASET Unblocked Bundle Assembly (Sheet 1 of 2)

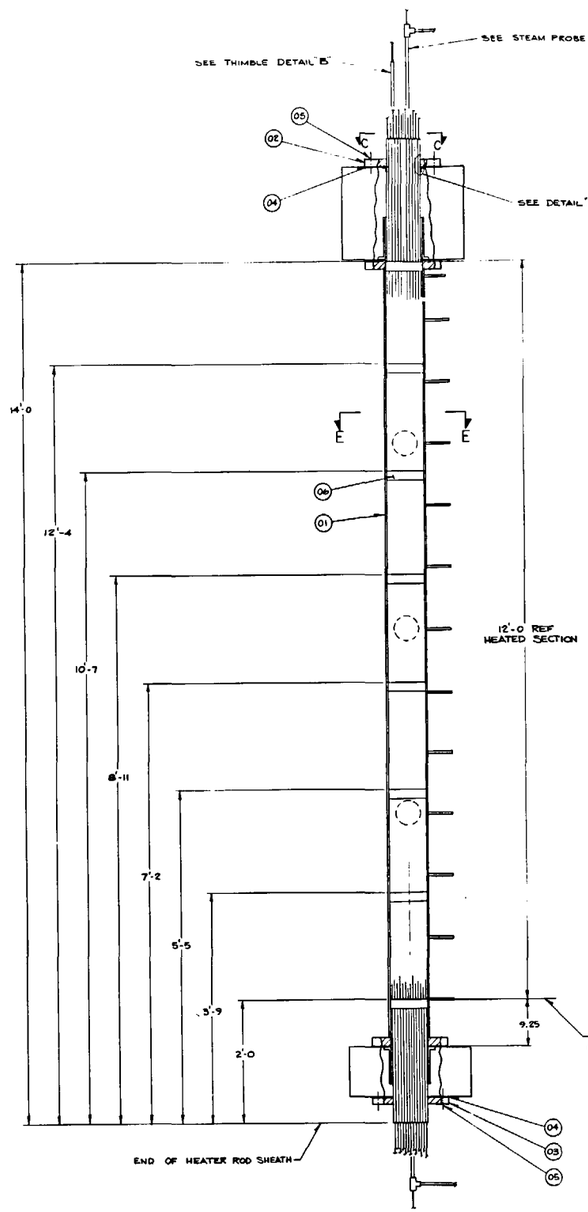

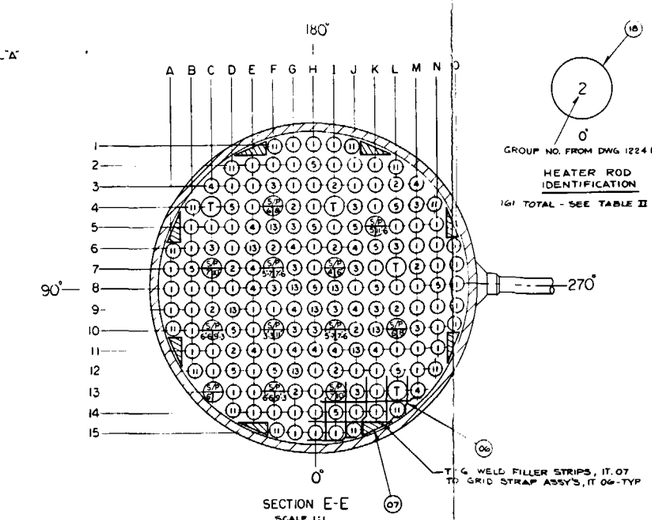

SECTION E-E
SCALE 1:1

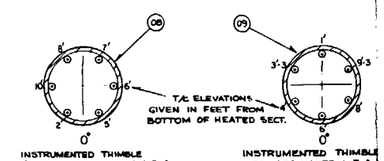

INSTRUMENTED THIMBLE @ CO-ORDINATES C-4 & I-4

INSTRUMENTED THIMBLE @ CO-ORDINATES L-7 & L-13

GROUP NO. FROM DWG 1224 E 16

HEATER ROD IDENTIFICATION

161 TOTAL - SEE TABLE II

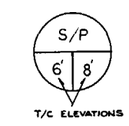

T/C ELEVATIONS

TYPICAL STEAM PROBE IDENTIFICATION

12 TOTAL - SEE TABLE I

A - PARKER SEALS, LEXINGTON, KENTUCKY
B - PGH VALVE & FITTING CO., PGH, PA.
C - CONAX CORP, PGH, PA.

BILL OF MATERIAL

ITEM	REV	PART NAME	DRAWING & GR OR IT	MATERIAL	REQ PER GROUP 01	02	03	04
01		HOUSING	1453 E 32 G01		1			
02		UPPER SEAL ✱	1463 F 27 H01		1			
03		LOWER SEAL ✱	1463 F 33 H01		1			
04		GASKET	8764 D 55 H02		2			
05		.500 13 UNC 2B HEX NUT			36			
06		GRID STRAP ASSY	8763 D 58 G01		8			
07		FILLER STRIP	8763 D 64 G01		8			
08		THIMBLE	8764 D 47 G01		2			
09		THIMBLE	8764 D 47 G02		2			
10		STEAM PROBE	1453 E 1 G03		1			
11		↑	G03		1			
12			G08		2			
13			G07		2			
14			G01		1			
15			G07		2			
16		↓	G04		1			
17		STEAM PROBE	1453 E 1 G04		1			
18		HEATER RODS	1224 E 16		161			
19		COMB		ASTM A569	14			
20		RETAINER		M 1020	2			
21		.25-20 UNC 2A SOC HD SHOULDER SCR.	(310 DIA x 1.50 LG)		4			
22		LIFTING LUG	IN-HOUSE		2			
23		O-RING SLEEVE	1680 C 97 H02		300			
24	A	O-RING .370 I.D. x .040	S-207	E652-90	322			
25	A	O-RING .404 I.D. x .031	SPECIAL	E652-90	322			
26		O-RING SLEEVE	1680 C 97 H03		32			
27	A	O-RING .2701.D. x .040	SPECIAL	E652-90	32			
28	A	O-RING .304 I.D. x .031	SPECIAL	E652-90	32			
29		.190-24 UNC-2A x .50 SOC. HD CAP SCR.		SST	8			
30	C	CONAX CONN.	MPG-040-TYPE A		23			
31		O-RING SLEEVE	1680 C 97 H01		16			
32		SLEEVE	1680 C 98 G01		16			
33		.312-18 UNC-2B HEX NUT		SST	4			
34	B	REDUCER 3/8 TO 1/16 NPT	SS-2-RB-1		23			
35	B	SWAGELOK CONN	SS-400-1-2		23			
36		.250 O.D. x .035 W. TUBING		304 SST	AR			
37	B	SWAGELOK TEE	SS-400-3		23			
38		SWAGELOK CONN	SS-400-7-2		23			
39		SWAGELOK REDUCER	SS-200-R-4		23			
40		.125 O.D. x .028 W TUBING		304 SST	AR			

TABLE I

STEAM PROBES	
ITEM	CO-ORDINATES
10	F-4, L-10
11	K-5
12	C-7, I-13
13	F-7, I-10
14	I-7
15	C-10, F-13
16	F-10
17	C-13

TABLE II

HEATER ROD SERIAL NO. BY CO-ORDINATES

	A	B	C	D	E	F	G	H	I	J	K	L	M	N	O
1	—	—	—	—	—	171	92	46	35	153	—	—	—	—	—
2	—	—	—	165	63	61	67	253	52	43	20	169	—	—	—
3	—	—	241	65	83	226	90	68	215	16	6	206	237	—	—
4	—	159	—	264	81	—	209	86	—	223	45	266	251	170	—
5	—	13	85	74	269	274	228	260	31	254	—	88	22	50	—
6	158	12	229	26	278	204	258	42	217	243	265	227	72	38	163
7	51	252	—	248	244	—	220	95	—	219	23	—	213	54	5
8	36	3	84	79	235	224	271	258	275	64	255	93	8	262	17
9	94	21	250	276	28	29	280	272	218	242	232	216	34	48	70
10	166	66	—	257	33	—	272	230	—	203	273	—	225	77	154
11	—	55	7	210	233	58	219	270	234	280	267	62	69	76	—
12	—	151	14	259	47	261	277	41	211	75	39	256	37	172	—
13	—	—	—	25	49	—	212	89	—	231	60	—	238	—	—
14	—	—	—	160	71	82	33	2	263	73	87	167	—	—	—
15	—	—	—	—	—	156	55	44	53	157	—	—	—	—	—

Figure A-8. FLECHT SEASET Unblocked Bundle Assembly (Sheet 2 of 2)

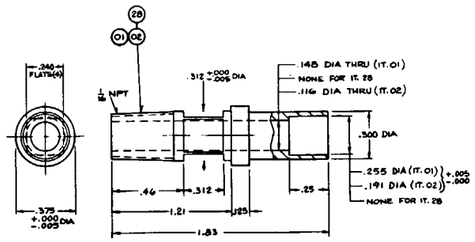

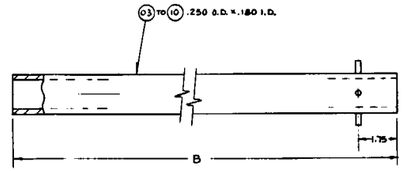

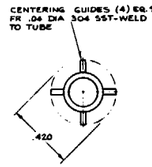

ITEM	DIM. B
03	9'-3.25
04	7'-9.25
05	3'-9.25
06	4'-3.25
07	7'-3.25
08	9'-3.25
09	6'-0.25
10	5'-3.25

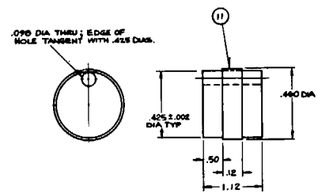

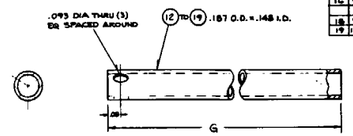

ITEM	DIM. G
12	7'-3.25
13	9'-0.25
14	8'-5.25
15	6'-9.25
16	9'-9.25
18	9'-11.25
19	10'-5.25

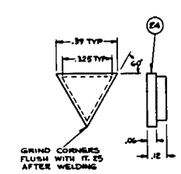

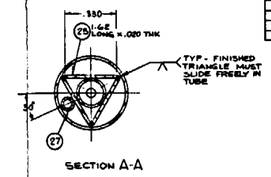

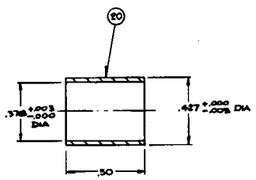

GROUP	C	D	E	F		
1	8'-5.88	5'-6	9'-0	7'-0		
2	6'-10.88	7'-1	6'-7	8'-6		
3	7'-5.88	6'-6	6'-0	12'-6		
4	9'-2.88	6'-9	6'-3	12'-0		
5	6'-5.88	7'-6	7'-0	9'-0		
6	—	—	—	7'-0		
7	8'-11.88	8'-0	7'-6	10'-3		
8	8'-5.88	8'-6	8'-0	11'-0		

BILL OF MATERIAL

ITEM	SIZE	PART NAME	DRAWING & SPEC OR ID.	MATERIAL	NO. PER GROUP 1	2	3	4	5	6	7	8
01		END PLUG		ASTM A213 TP304	1	1	1	1	1	1	1	1
02		END PLUG				1	1	1	1	—	1	1
03		T/C TUBE (UPPER)					1					
04								1				
05									1			
06										1		
07											1	
08												1
09												1
10		T/C TUBE (UPPER)										1
11		CONN. PLUG			1	1	1	1	1	1	1	1
12		T/C TUBE (LOWER)			1							
13						1						
14							1					
15								1				
16									1			
18										1		
19		T/C TUBE (LOWER)									1	1
20		SLEEVE			2	2	2	2	2	2	2	2
21		UPPER EXTEN. TUBE			1	1	1	1	1	1	1	1
22		BODY			2	2	2	2	2	1	2	2
23		LOWER EXTEN. TUBE			1	1	1	1	1	1	1	1
24		CAP			1	1	1	1	1	—	1	1
25		SHROUD (3 PIECE)		ASTM A213 TP304	1	1	1	1	1	1	1	1
26	A	T/C		SEE NOTE A	3	2	2	2	2	1	2	2
27		DRAIN TUBE		ASTM A213 TP304	1	1	1	1	1	—	1	1
28		END PLUG		ASTM A213 TP304	—	—	—	—	—	1	—	—

A - .040 O.D SST SHEATH, TYPE K, MAGNESIUM OXIDE INSULATION, UNGROUNDED JUNCTION, COLD END STRIPPED & SEALED.

NOTES:
1 - MAKE FR .50 O.D. x .430 I.D. SST TUBING, ASTM A213, TYPE 304. CENTERLESS GRIND O.D. TO .474 +.000 -.003.
E-WELD PER W P.S. 82127 x 4 & DYE PENETRANT CHECK PER W. P.S. RD-TE-70-612.
2 - T/C'S TO EXTEND AT LEAST 10 FT BEYOND END OF FRIGE
4 - GROUP 6 IS MADE UP OF 1 CONTINUOS LENGTH OF IT. 28, (14'-0 LG)

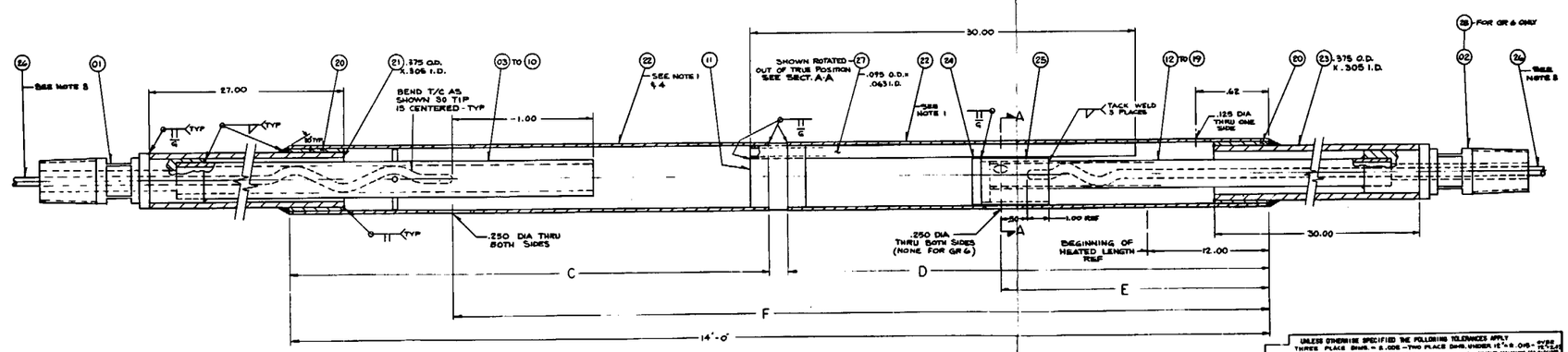

UNLESS OTHERWISE SPECIFIED THE FOLLOWING TOLERANCES APPLY
THREE PLACE DIMS. = ±.005 — TWO PLACE DIMS. UNDER 10" = ±.015 — OVER 10" = ±.015
[illegible]
SEE PROCESS SPECIFICATION NO CAP986128 FOR SUPPLEMENTARY MANUFACTURING INFORMATION

Figure A-9. FLECHT SEASET Steam Probe Detail Assembly

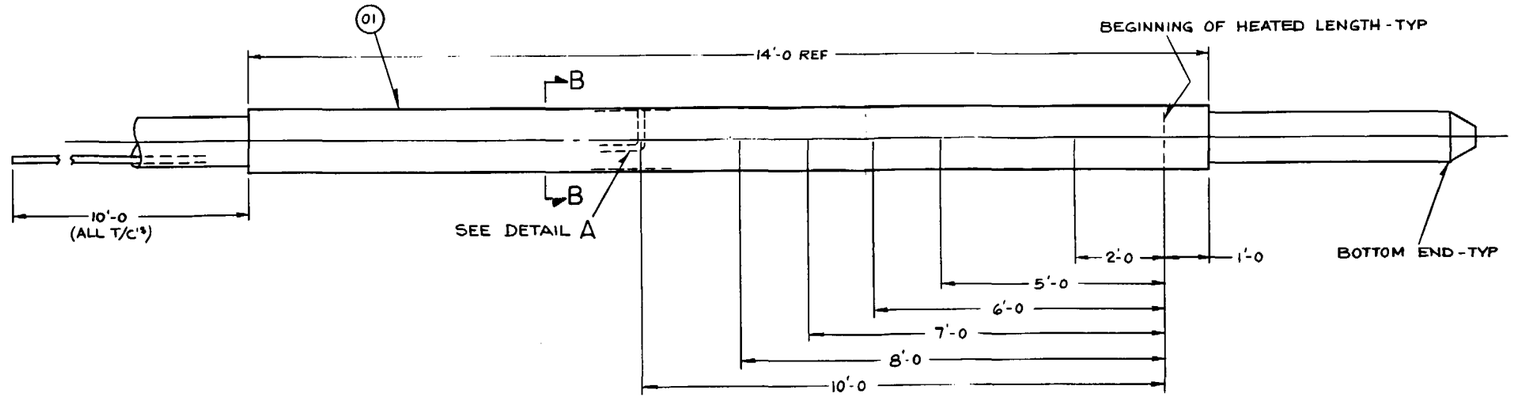

GROUP 1

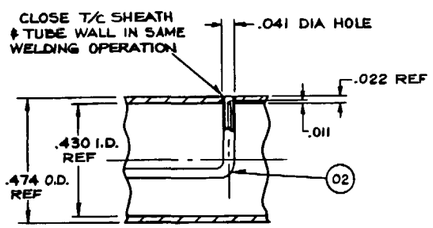

DETAIL A
SCALE 4:1
TYP 6 PLACES FOR GR.1 & 6 FOR GR.2

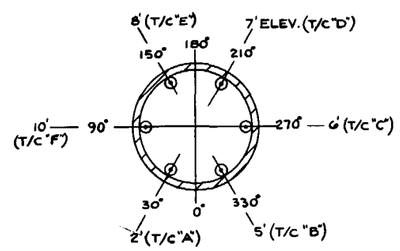

SECTION B-B
SCALE 4:1

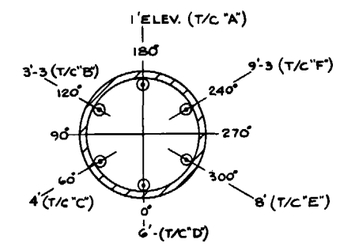

SECTION C-C
SCALE 4:1

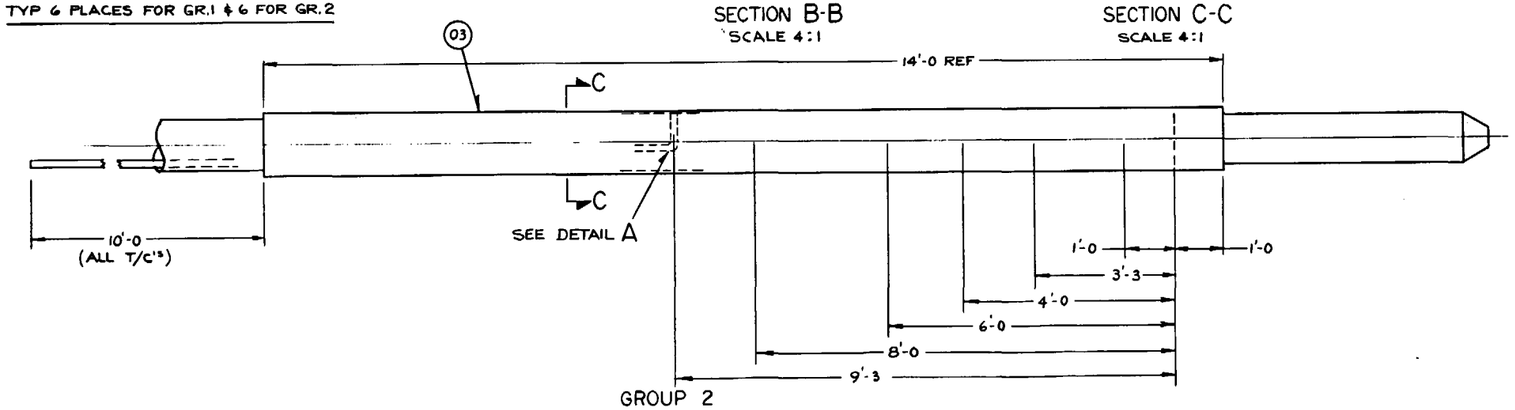

GROUP 2

BILL OF MATERIAL

ITEM	NOTE	PART NAME	DRAWING & GR OR IT.	MATERIAL	REQ. PER GROUP 01	02	03	04
01		THIMBLE	8764 D49-G01		1			
02	A	T/C			6	6		
03		THIMBLE	8764 D49-G01			1		

A - .040 O.D. SST SHEATH, TYPE K, MAGNESIUM OXIDE INSULATION, UNGROUNDED JUNCTION, COLD END STRIPPED & SEALED.

NOTES:
1 - WELD PER W P.S. 82127XG & DYE PENETRANT CHECK PER W P.S. RD-TE-70-612.
2 - ROUTE ALL T/C LEADS OUT SAME END OF TUBE AS SHOWN ALL T/C LEADS TO EXTEND 10 FT. BEYOND TUBE.
3 - POLISH TUBE SURFACE SMOOTH AFTER T/C INSTALLATION.
4 - LABEL ALL LEADS WITH APPROPRIATE IDENTIFICATION: (A - B - C - D - E - F)

Figure A-10. FLECHT SEASET Instrumented Thimbles

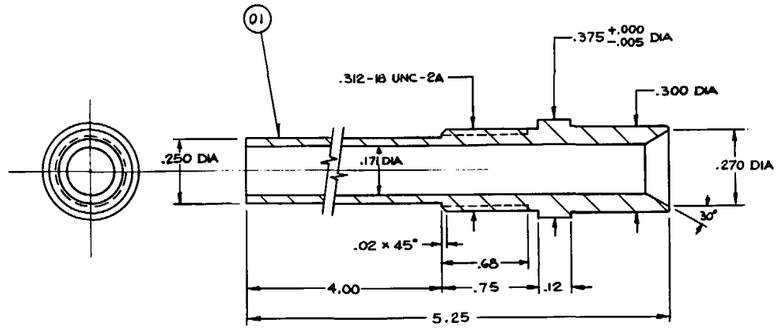

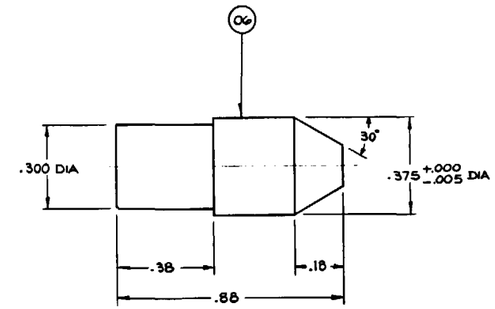

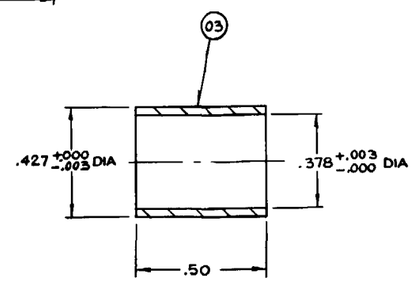

BILL OF MATERIAL								
ITEM	NOTE	PART NAME	DRAWING & GR OR IT.	MATERIAL	REQ. PER GROUP			
					01	02	03	04
01		END PLUG		ASTM A213 TYPE 304	1			
02		UPPER EXTEN. TUBE		↓	1			
03		SLEEVE			2			
04		BODY			1			
05		LOWER EXTEN. TUBE		↓	1			
06		END PLUG		ASTM A213 TYPE 304	1			

NOTES:

1- MAKE FR..50 O.D. x .430 I.D. SST TUBING. CENTERLESS GRIND O.D. TO .474 +.000 -.003

2- WELD PER W P.S. 82127 XG & DYE PENETRANT CHECK PER W P.S. RD-TE-70-612.

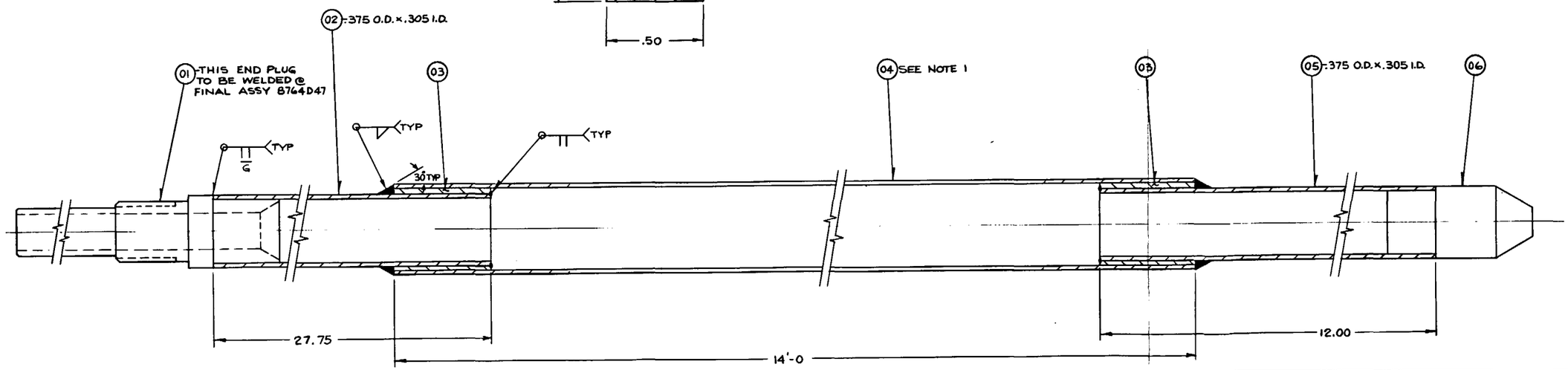

UNLESS OTHERWISE SPECIFIED THE FOLLOWING TOLERANCES APPLY

THREE PLACE DIMS = ±.005 TWO PLACE DIMS UNDER 12" = ±.015 OVER 12" = ±.03

STRAIGHTNESS, FLATNESS, PERPENDICULARITY, ROUNDNESS, PARALLELISM, SYMMETRY AND ANGULARITY VARIATIONS FOR MACHINED SURFACES ARE PERMITTED WITHIN THE PROFILE ESTABLISHED BY THE LIMITS OF SIZE. VARIATIONS IN FORM FOR UNMACHINED FEATURES ARE PERMITTED WITHIN ESTABLISHED COMMERCIAL STANDARDS. CONCENTRICITY MUST BE WITHIN THE SUM OF THE TOLERANCES OF THE DIAMETERS BEING COMPARED. SURFACE ROUGHNESS ON MILLED: 250√ MAX. ALL EDGES OR CORNERS .005 - .020 (APPROXIMATE RADIUS OR CHAMFER) - ALL FILLETS .005 - .020 (APPROXIMATE RADIUS). SCREW THREADS PER MS33161.1 - PIPE THREADS PER MS33162.1 - WELD DIMENSIONS ARE MINIMUM - ALL DIMENSIONS CORRECTED TO 68°F ± 2°.

SEE PROCESS SPECIFICATION NO. CAP595128 FOR SUPPLEMENTARY MANUFACTURING INFORMATION.

Figure A-11. FLECHT SEASET Thimble Detail

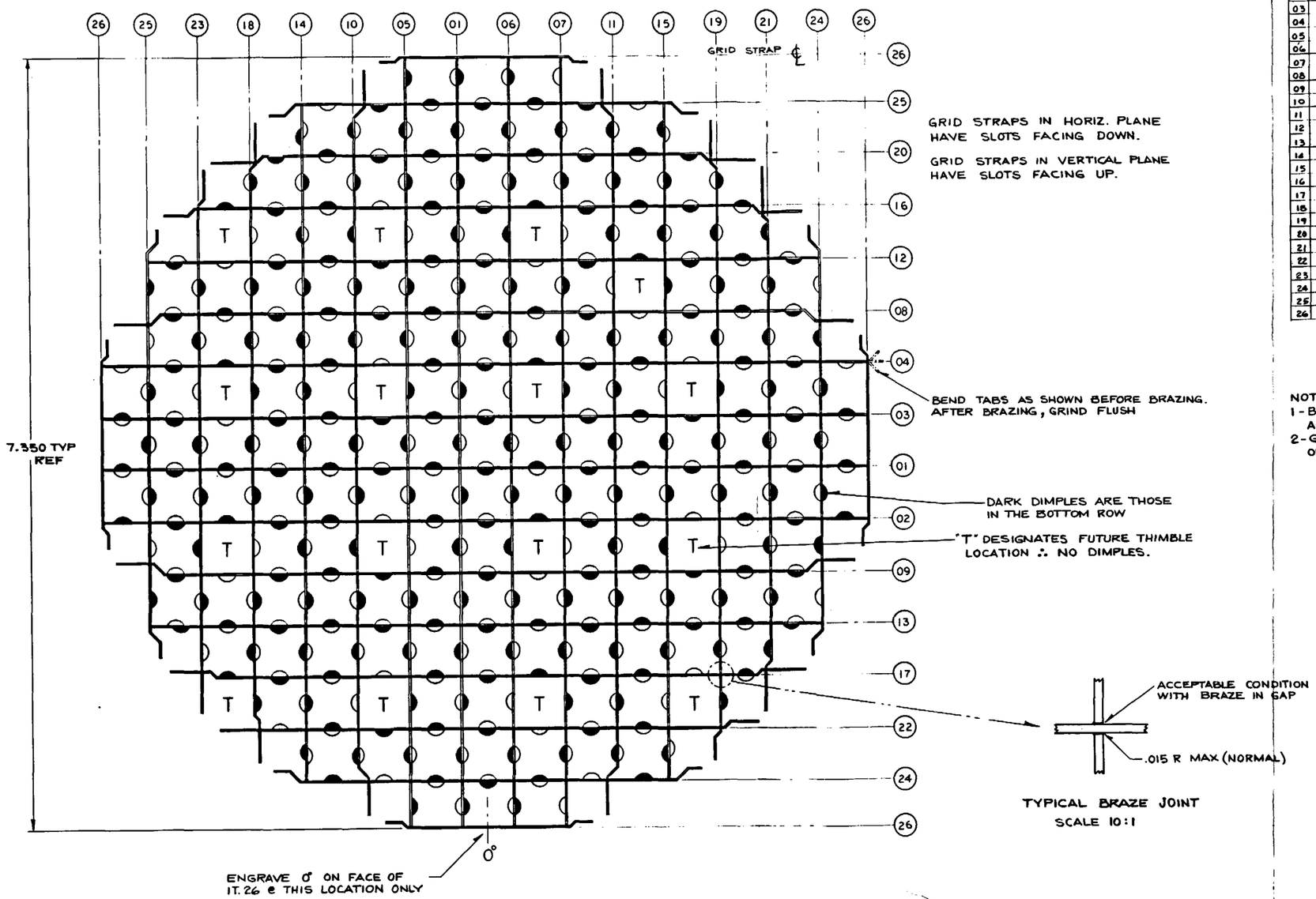

BILL OF MATERIAL								
ITEM		PART NAME	PART NO.	MATERIAL	REQ. PER GROUP			
					01	02	03	04
01		GRID STRAP	8763D57-IT.01		2			
02			02		1			
03			03		1			
04			04		1			
05			05		1			
06			06		1			
07			07		1			
08			08		1			
09			09		1			
10			10		1			
11			11		1			
12			12		1			
13			13		1			
14			14		1			
15			15		1			
16			16		1			
17			17		1			
18			18		1			
19			19		1			
20			20		1			
21			21		1			
22			22		1			
23			23		1			
24			24		2			
25			25		2			
26		GRID STRAP	8763D57-IT.26		4			

NOTES:
1 - BRAZE PER W PROC. SPEC. CAP 595151 - DELETE THE AGING CYCLE.
2 - GRID ASSY MUST PASS THRU AN INSPECTION ENVELOPE OF 7.525 DIA.

Figure A-12. FLECHT SEASET Grid Strap Assembly

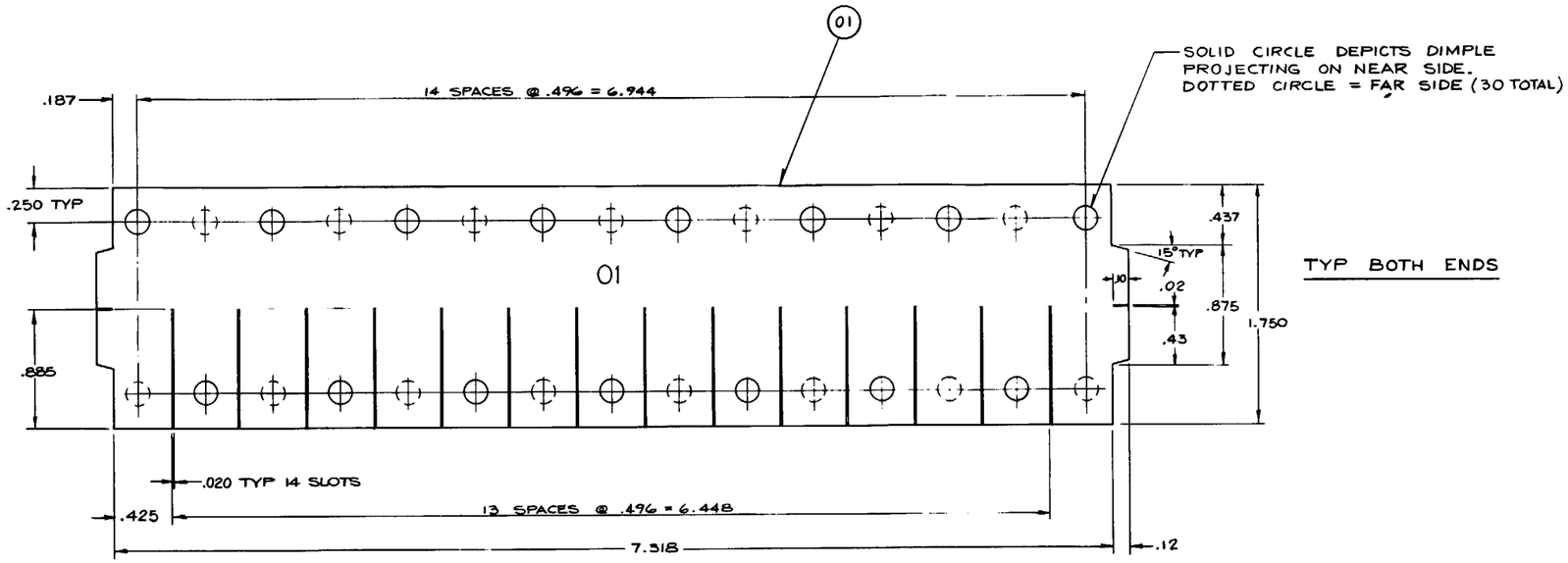

TYP BOTH ENDS

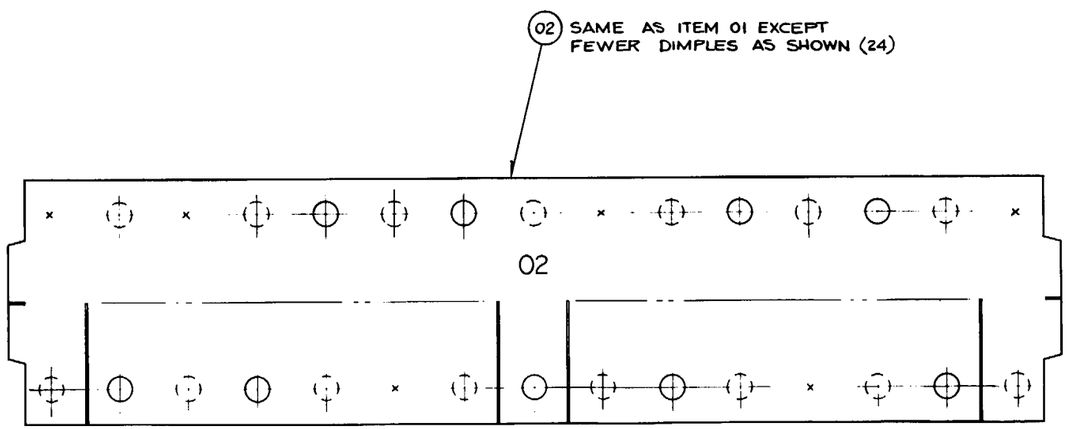

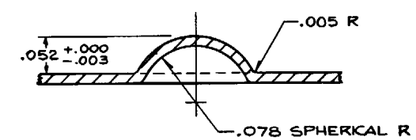

TYPICAL DIMPLE
SCALE 10:1

BILL OF MATERIAL

ITEM		PART NAME	PART NO.	MATERIAL	REQ. PER GROUP 01	02	03	04
01		GRID STRAP .015 THK		INCONEL 718				
02								
03								
04								
05								
06								
07								
08								
09								
10								
11								
12								
13								
14								
15								
16								
17								
18								
19								
20								
21								
22								
23								
24								
25								
26		GRID STRAP .015 THK		INCONEL 718				

NOTES:
1 - ALL GRID STRAPS ARE THE SAME HEIGHT, THICKNESS & HAVE THE SAME DIMPLE SIZE & SLOT SIZE. DIMPLE POSITIONS ARE AS SHOWN @ EACH VIEW.
2 - ENGRAVE .12 HIGH ITEM NO. AS SHOWN ON EACH STRAP.

Figure A-13. FLECHT SEASET Grid Strap Details (Sheet 1 of 7)

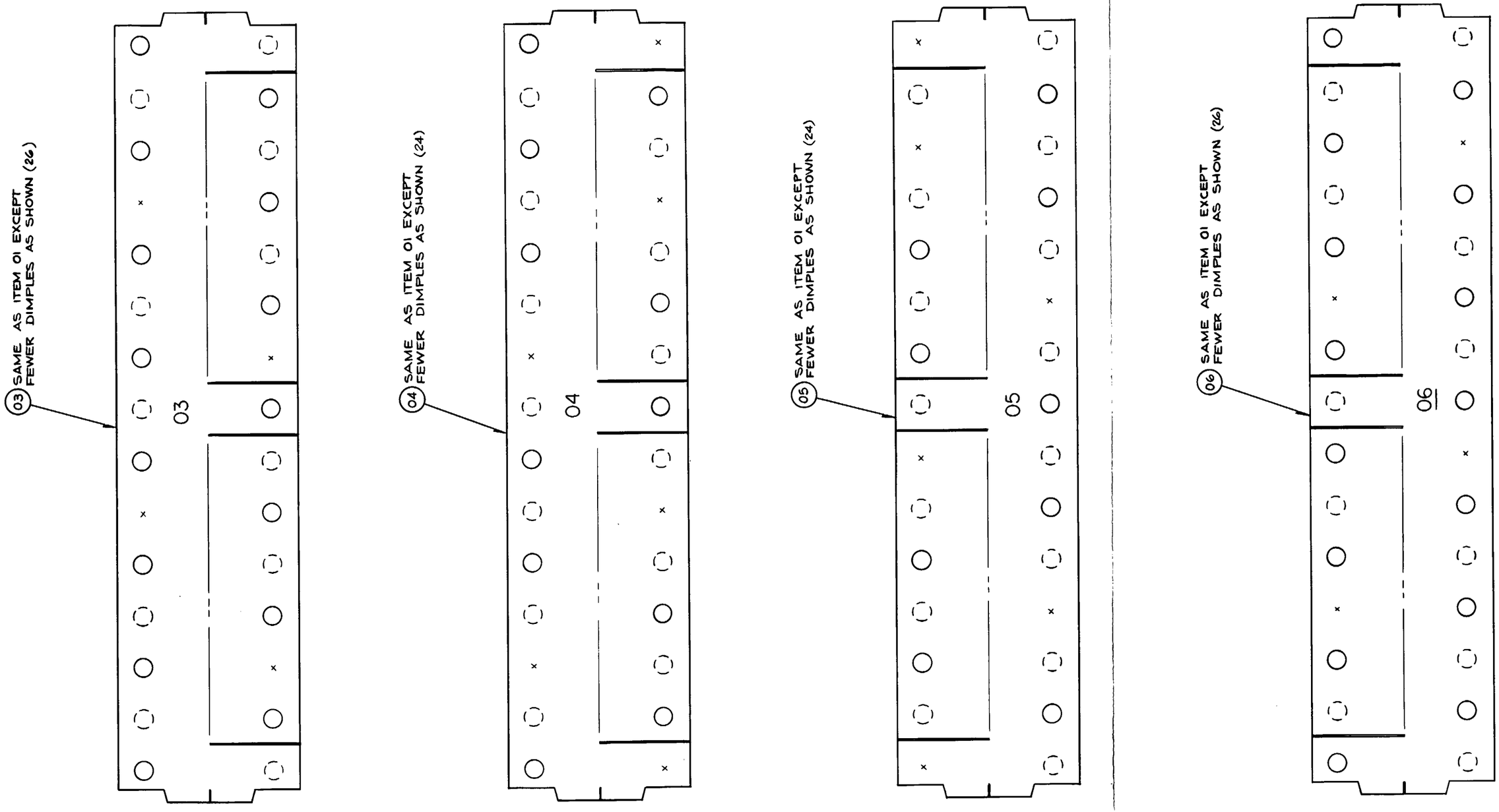

Figure A-13. FLECHT SEASET Grid Strap Details (Sheet 2 of 7)

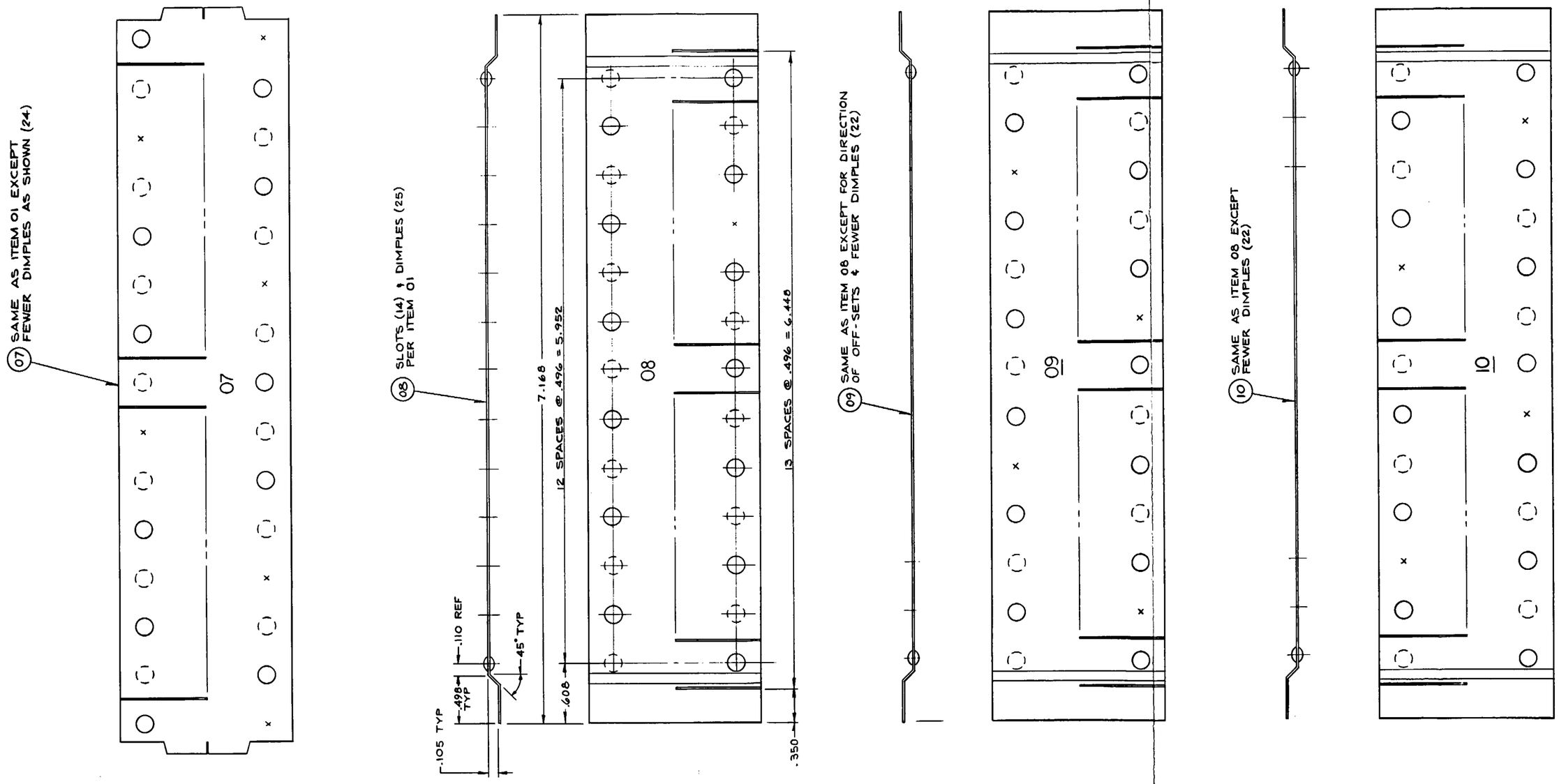

Figure A-13. FLECHT SEASET Grid Strap Details (Sheet 3 of 7)

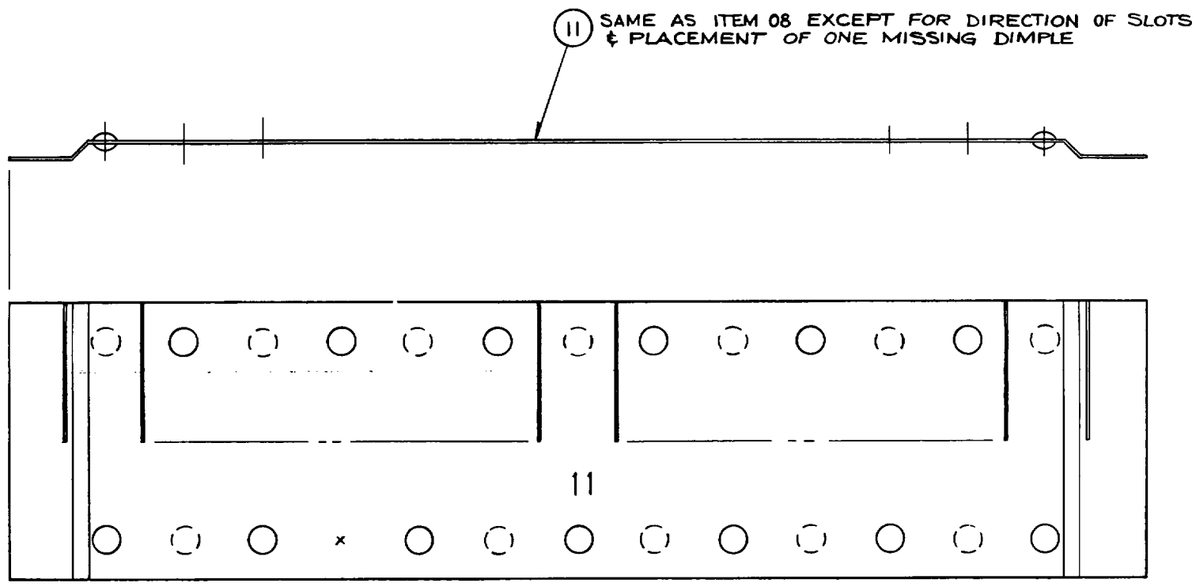

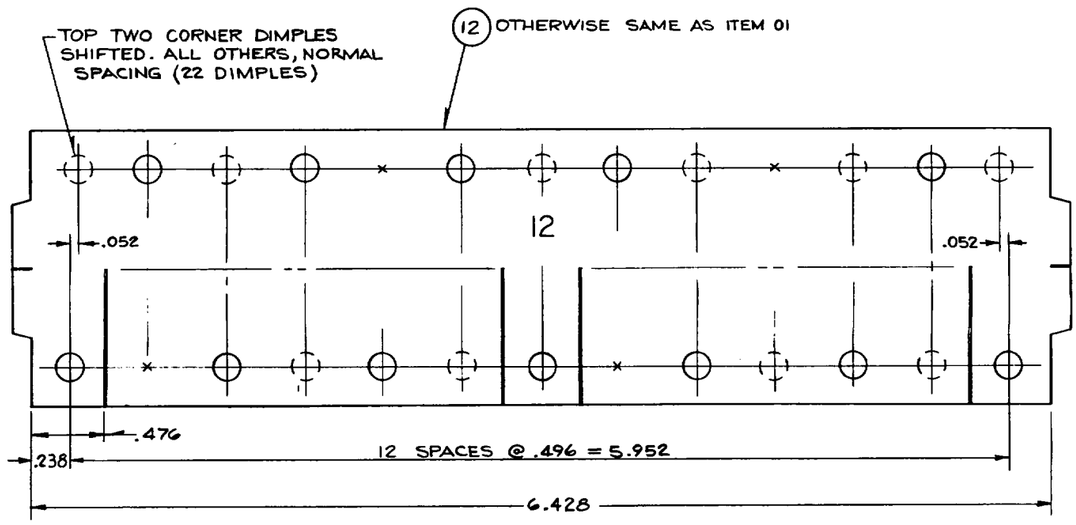

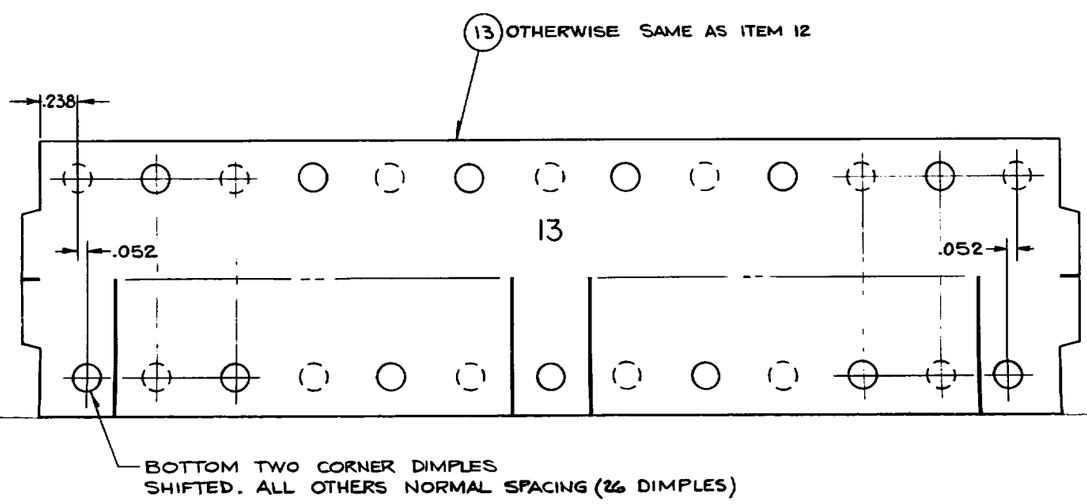

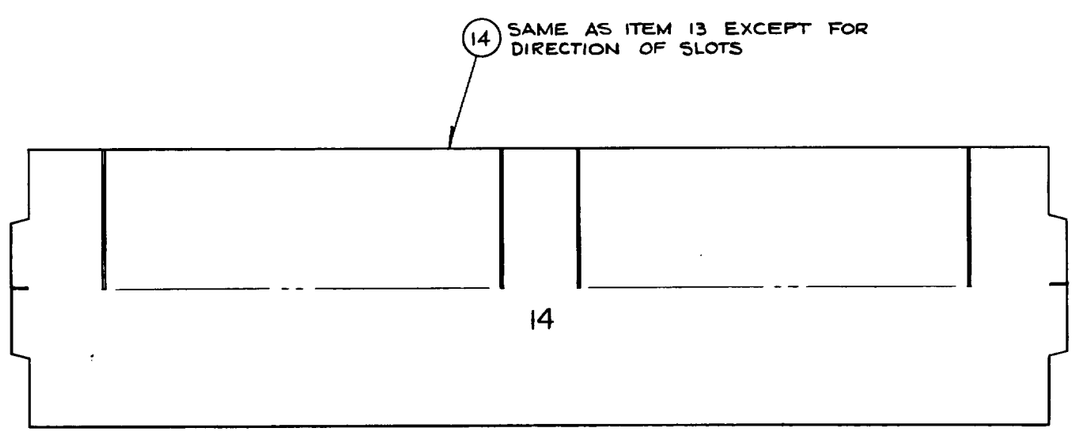

Figure A-13. FLECHT SEASET Grid Strap Details (Sheet 4 of 7)

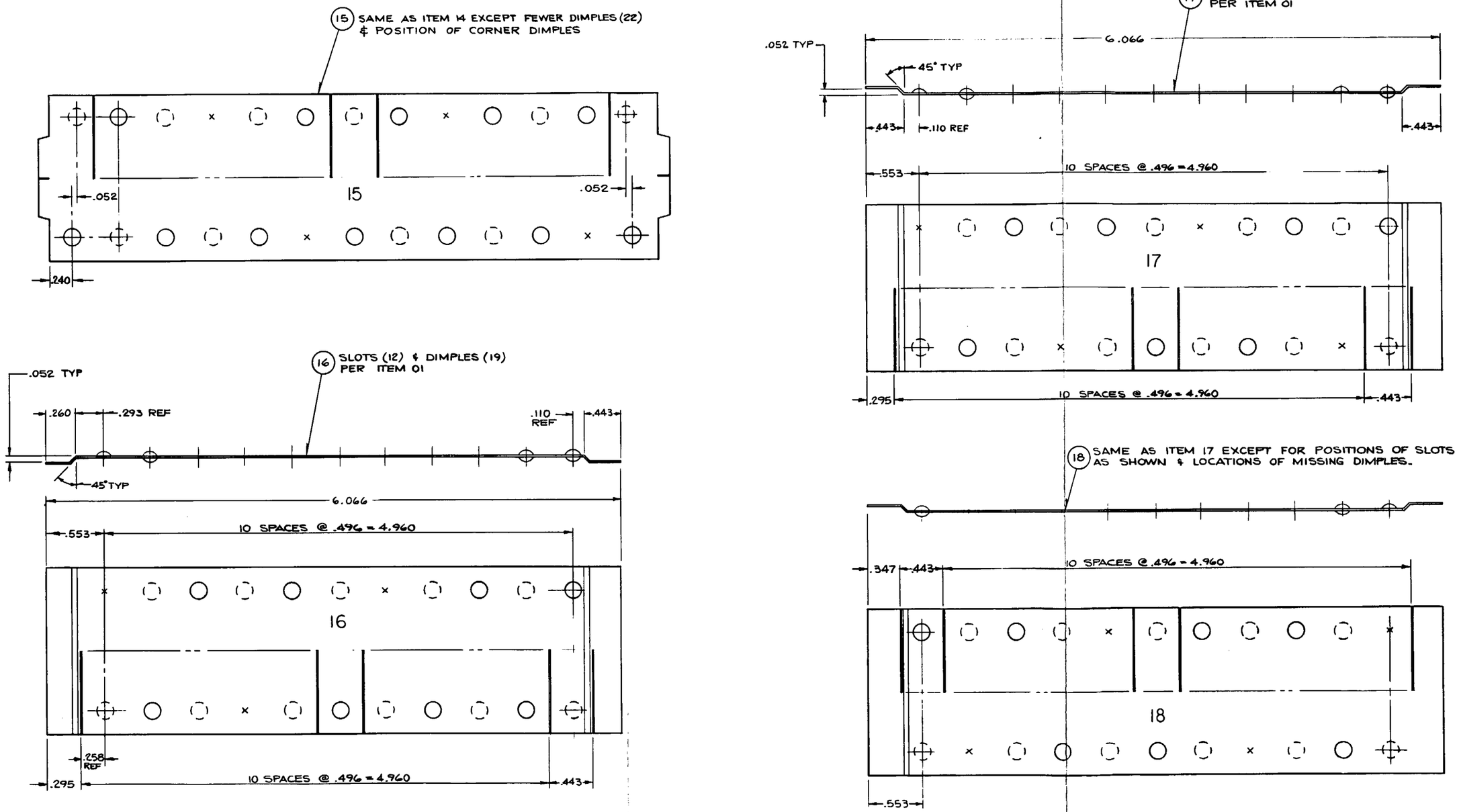

Figure A-13. FLECHT SEASET Grid Strap Details (Sheet 5 of 7)

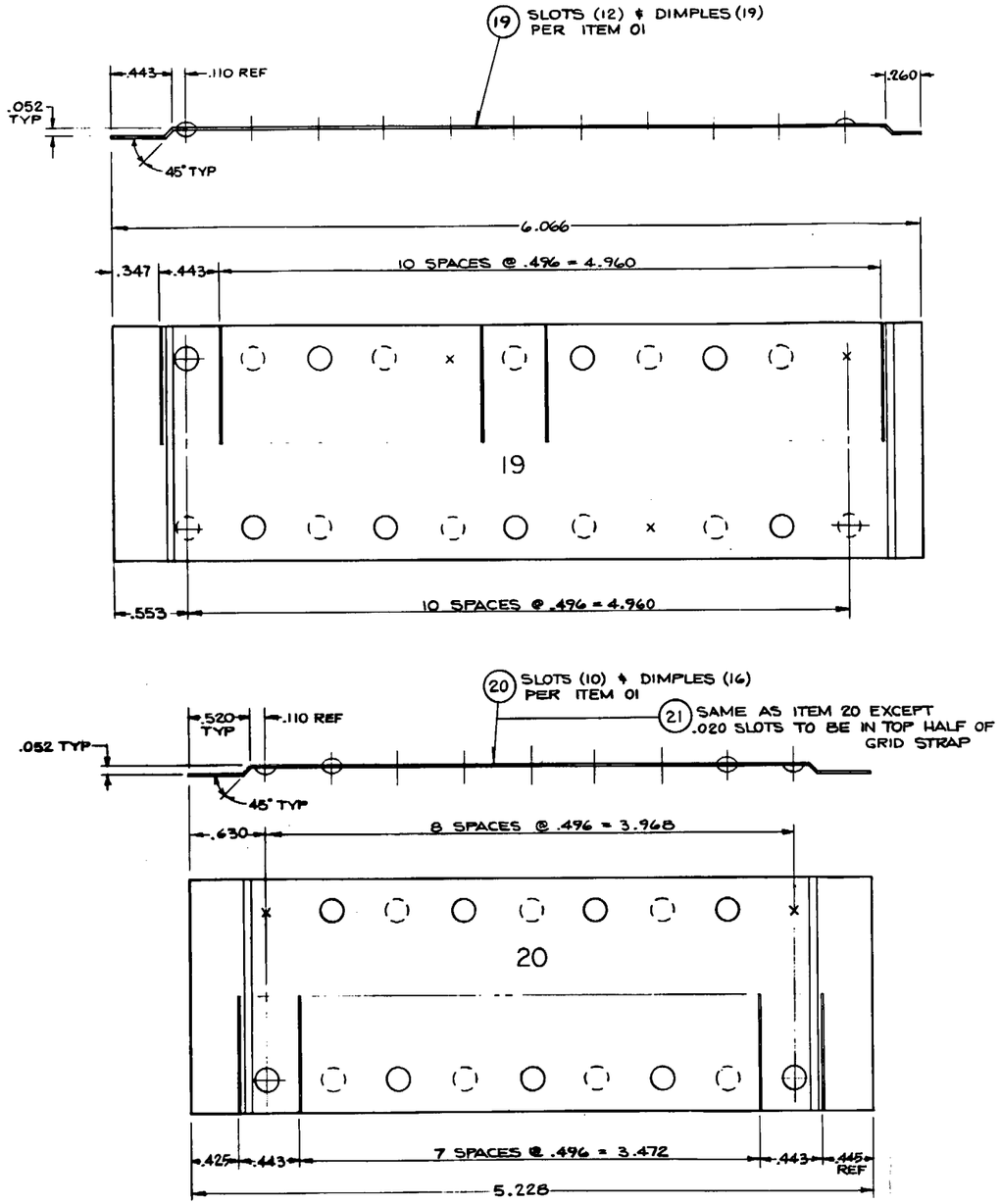

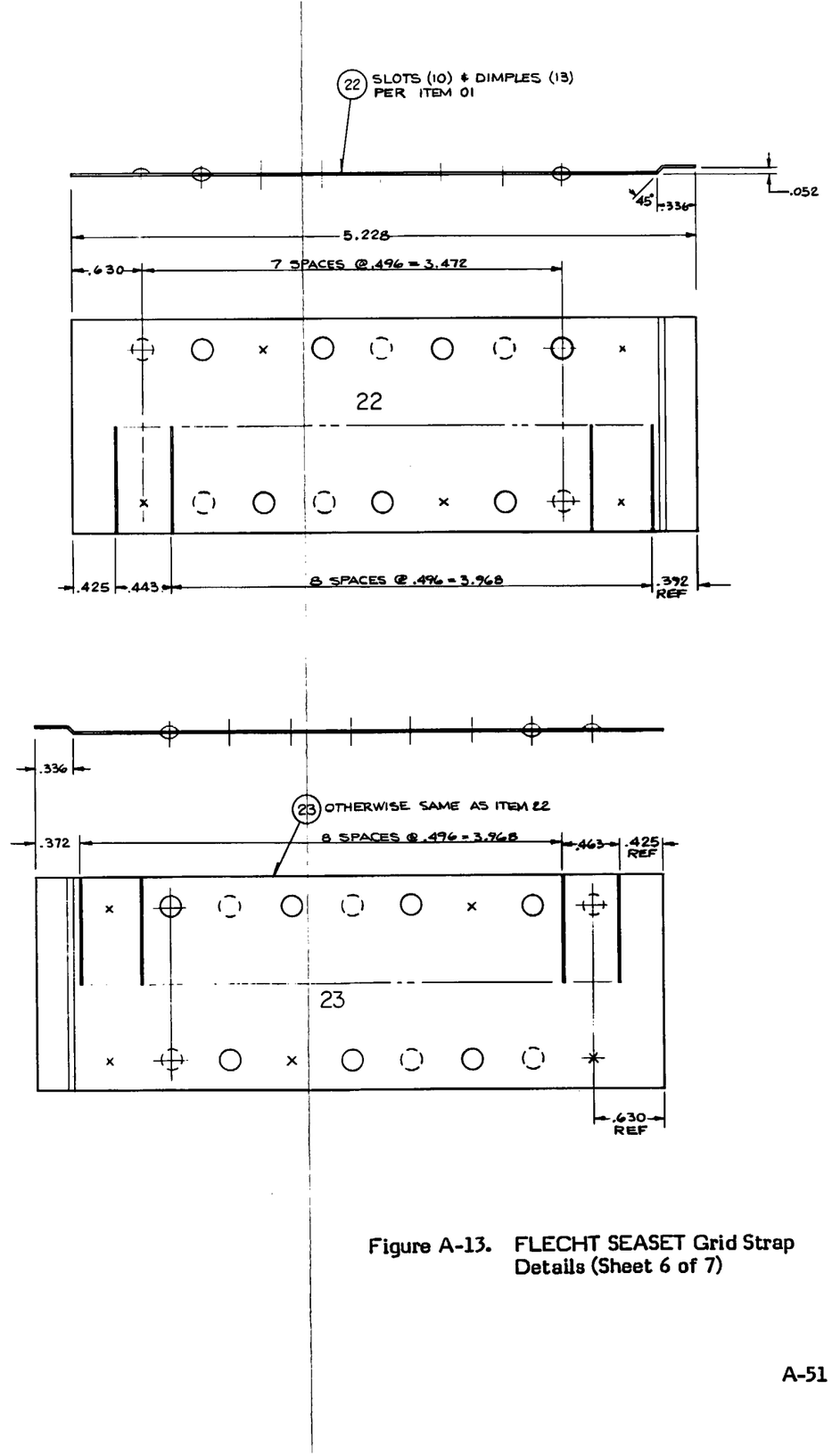

Figure A-13. FLECHT SEASET Grid Strap Details (Sheet 6 of 7)

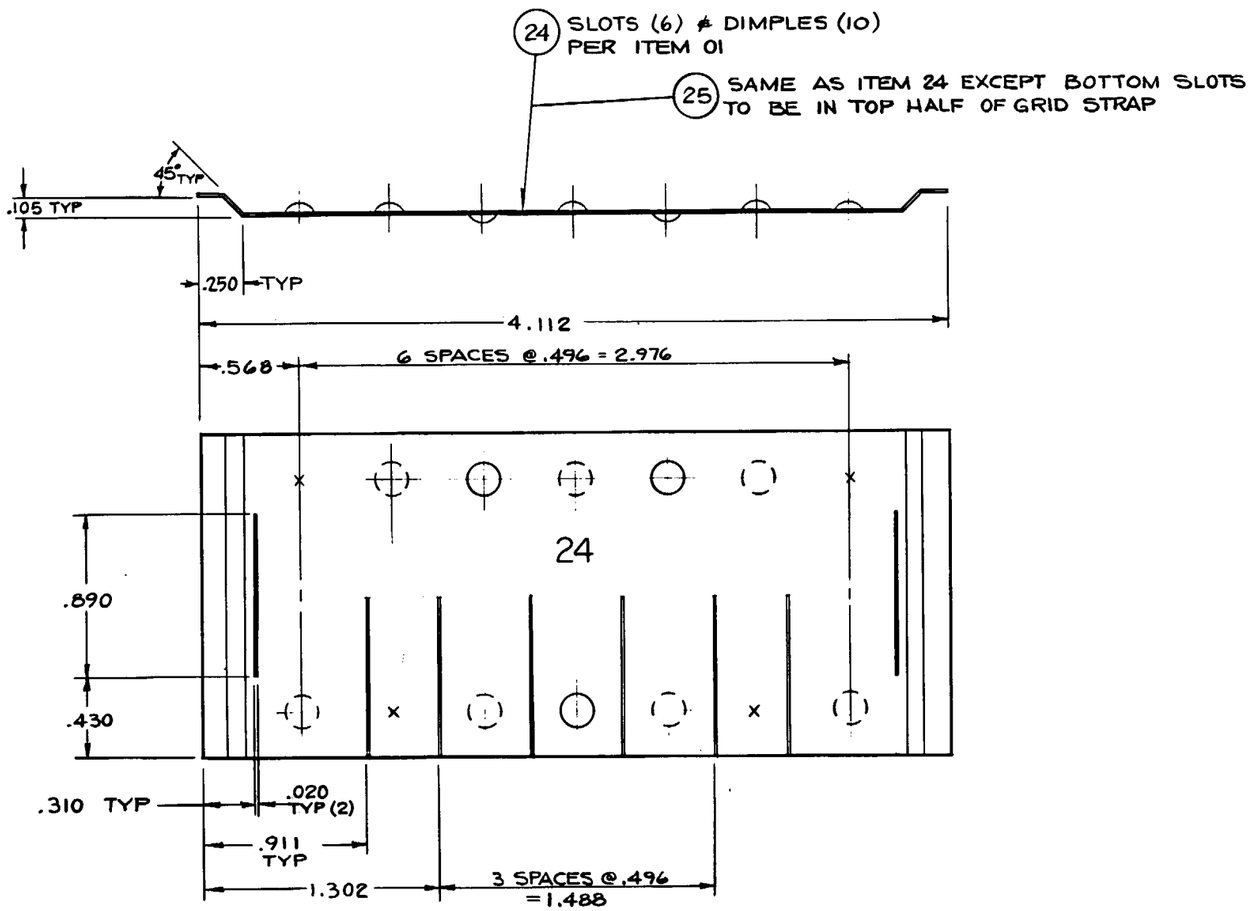

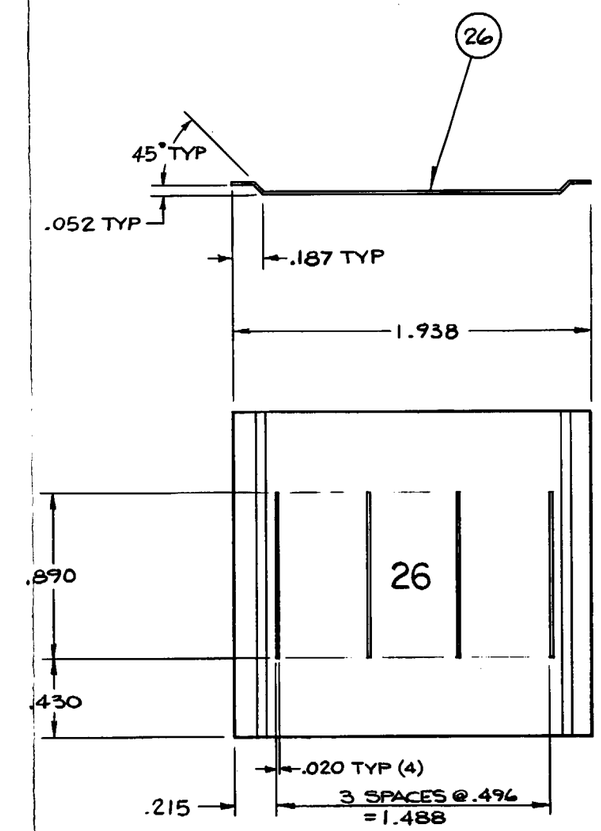

Figure A-13. FLECHT SEASET Grid Strap Details (Sheet 7 of 7)

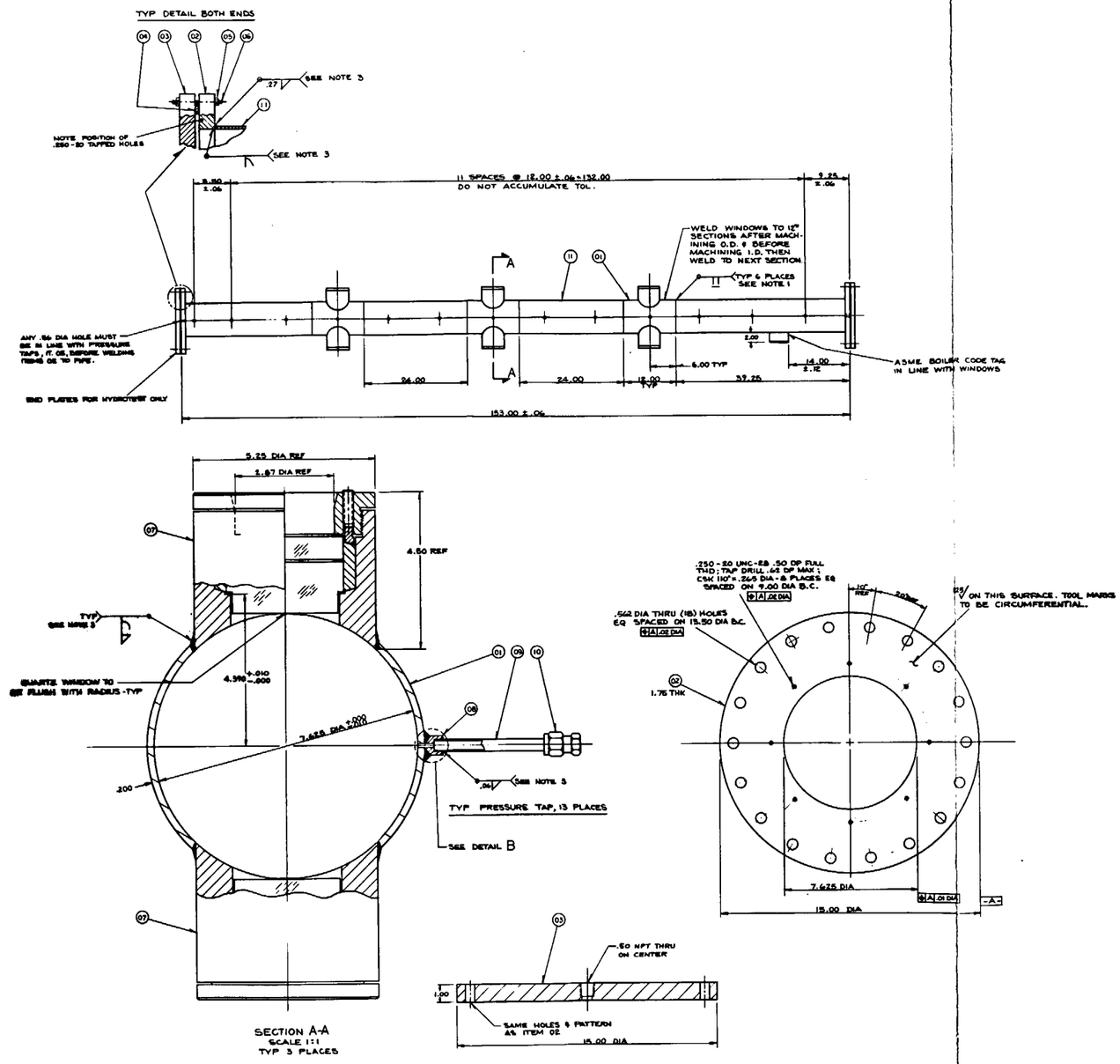

BILL OF MATERIAL								
ITEM	REV LTR	PART NAME	PART NO.	MATERIAL	NO. PER GROUP 01	02	03	04
01		BAR		SA 182 TYPE 304	2			
02		FLANGE		SA 240 TYPE 304	2			
03		BLIND FLANGE			2			
04	A	GASKET		CG-1HF	2			
05		.500-13 UNC HEX NUT		C.STL	72			
06		.500-13 UNC × 4 7/16 ALL THD		C.STL	36			
07	B	WINDOW ASSY: 2" 600 LB	MODEL B		6			
08		COUPLING		SA 479 GR 304	13			
09		TUBING .375 O.D. × .049W. × 6.00 LG		SA 213 TYPE 304	13			
10	C	SWAGELOK CAP		SS-600-C	13			
11		PIPE		SA 312 TYPE 304	6			

A - FLEXITALLIC GASKET CO, CAMDEN, N.J.
B - PRESSURE PRODUCTS CO, CHARLESTON, W.VA.
C - PGH VALVE & FITTING CO, PGH, PA.

NOTES:
1 - WELD PER W PWR PROC. SPEC. 292613-1.
2 - TO BE MADE PER ASME BOILER CODE SECTION I FOR 60 PSIG AT 1500°F. PEAK TEMP. @ END ELEVATION, 1000°F @ FLANGES, ITEM 08.
3 - WELD PER W PWR PROC. SPEC. 292613. LIQUID PENETRANT EXAM PER W P.S. 8481139, QUALITY LEVEL A.
4 - ITEMS 01 & 11 TO BE STRESS RELIEVED BEFORE FINAL MACHINING.
5 - HOUSING BODY TO BE STRAIGHT WITHIN .25 OVER ENTIRE LENGTH.

UNLESS OTHERWISE SPECIFIED THE FOLLOWING TOLERANCES APPLY
THREE PLACE DIMS. = ±.005 TWO PLACE DIMS. = ±.02
SEE PROCESS SPECIFICATION NO. CAF88126 FOR SUPPLEMENTARY MANUFACTURING INFORMATION.

Figure A-14. FLECHT SEASET Low Mass Housing

BILL OF MATERIAL								
ITEM	PART NAME	DRAWING & OR SPEC.	MATERIAL	REQ. PER GROUP				
01	HOUSING	1446E97601		1				
02	UPPER PLENUM	1447E29601		1				
03	LOWER PLENUM	1447E29601		1				
04	UPPER EXTENSION	8764D86601		1				
05	LOWER EXTENSION	8764D86602		1				
06	.75-20 UNC-2A X 1" SOC HD CAP SCR		321T	16				
07	GASKET	8764D86604		8				
08	.50-13 UNC-2B HEX NUT		321T	36				
09	GASKET	8764D86605		1				

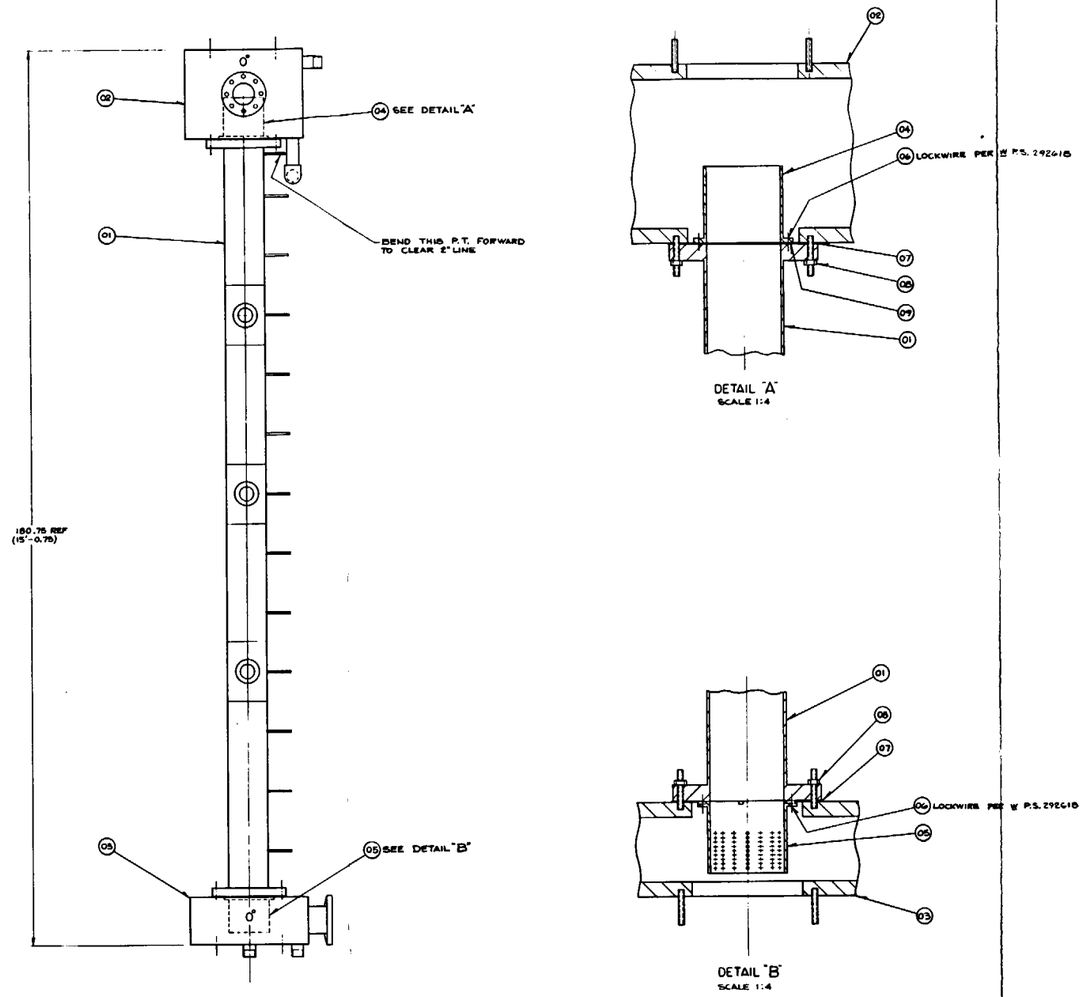

UNLESS OTHERWISE SPECIFIED THE FOLLOWING TOLERANCES APPLY

[redacted]

SEE PROCESS SPECIFICATION NO CAPS8128 FOR SUPPLEMENTARY MANUFACTURING INFORMATION

Figure A-15. FLECHT SEASET Low Mass Housing Assembly

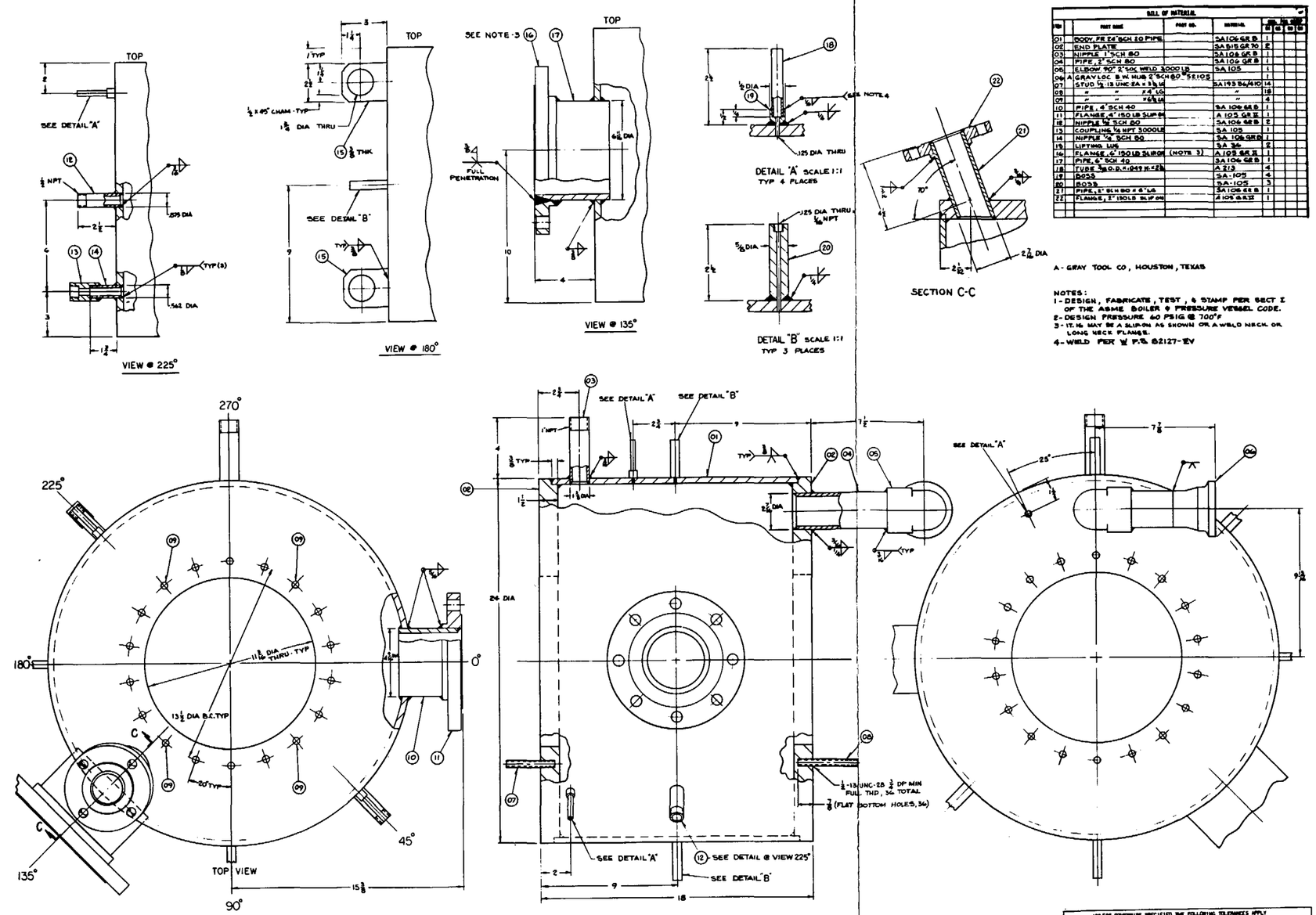

ITEM		PART NAME	PART NO.	MATERIAL	QTY. PER ASSEM.			
01		BODY, PR 24" SCH 20 PIPE		SA106 GR B	1			
02		END PLATE		SA 515 GR 70	2			
03		NIPPLE 1" SCH 80		SA106 GR B	1			
04		PIPE, 2" SCH 80		SA106 GR B	1			
05		ELBOW 90° 2" SOC WELD 3000 LB		SA 105	1			
06	A	GRAYLOC B.W. HUB 2" SCH 80	52105		1			
07		STUD ½-13 UNC-2A × 3¼ LG		SA193 B6/410	14			
08		" " ×4 LG		"	18			
09		" " ×6¾ LG		"	4			
10		PIPE, 4" SCH 40		SA 106 GR B	1			
11		FLANGE, 4" 150 LB SLIP ON		A 105 GR II	1			
12		NIPPLE ¾" SCH 80		SA 106 GR B	2			
13		COUPLING ¾ NPT 3000 LB		SA 105	1			
14		NIPPLE ¾" SCH 80		SA 106 GR B	1			
15		LIFTING LUG		SA 36	2			
16		FLANGE, 6" 150 LB SLIP ON	(NOTE 3)	A 105 GR II	1			
17		PIPE, 6" SCH 40		SA 106 GR B	1			
18		TUBE ⅜ O.D. × 0.049 W × 2¾		A 213	4			
19		BOSS		SA-105	4			
20		BOSS		SA-105	3			
21		PIPE, 1" SCH 80 × 6" LG		SA 106 GR B	1			
22		FLANGE, 2" 150 LB SLIP ON		A 105 GR II	1			

Figure A-16. FLECHT SEASET Upper Plenum Detail Assembly

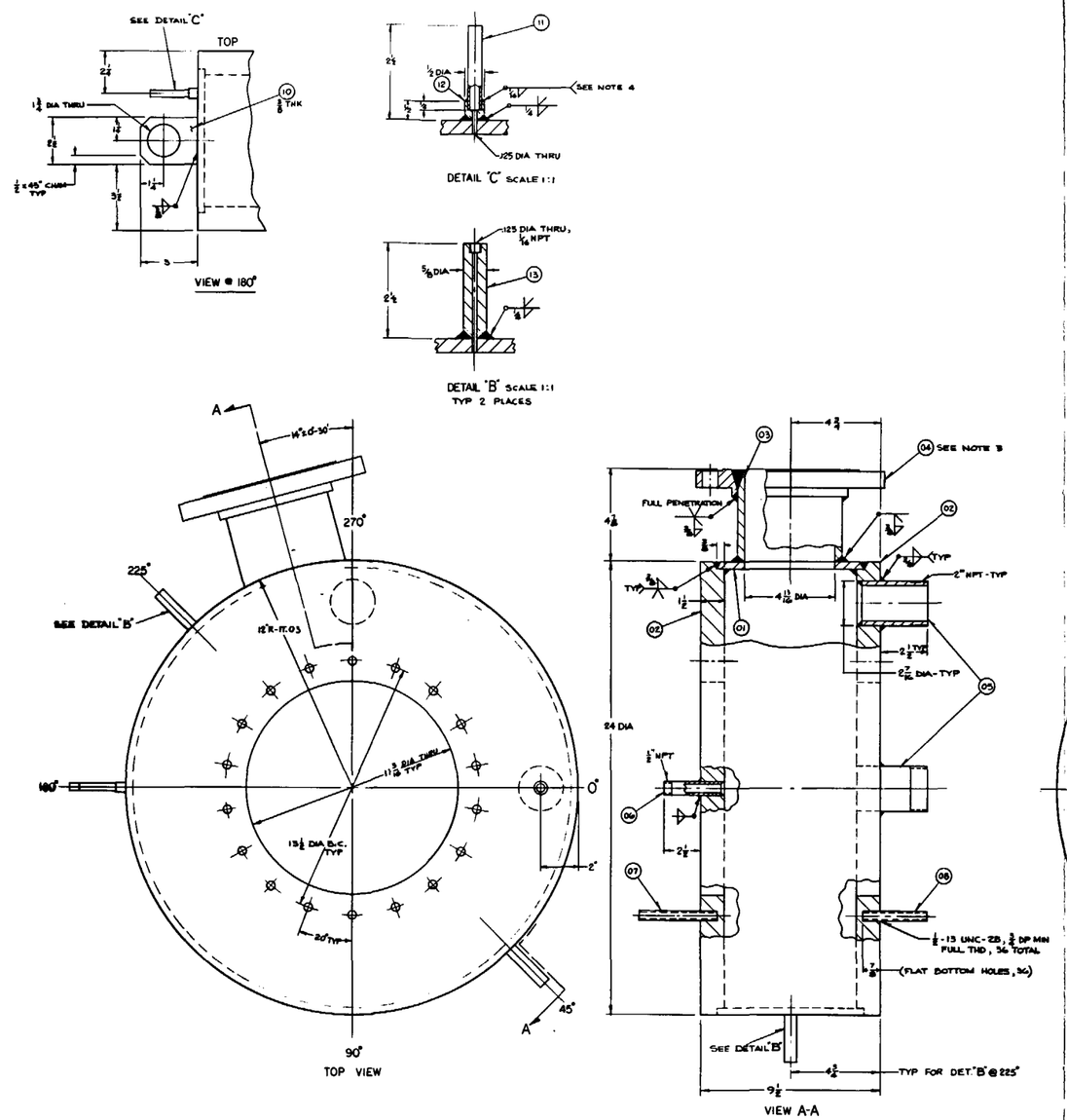

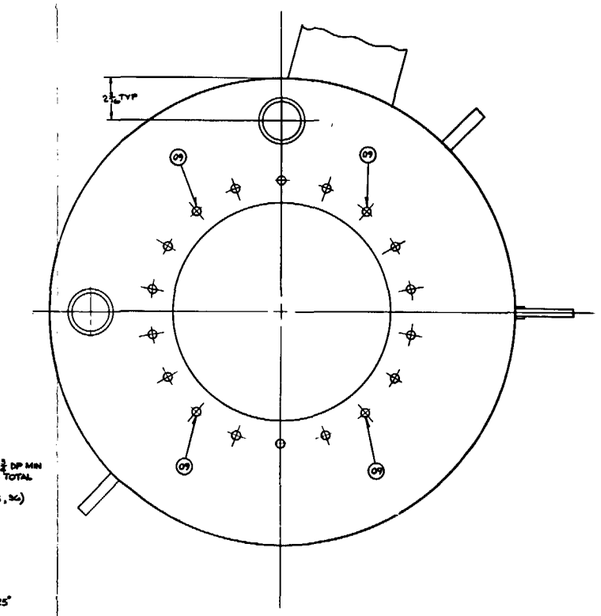

BILL OF MATERIAL								
ITEM	QTY	PART NAME	DRAWING & GR OR IT	MATERIAL	QUA PER GROUP			
					01	02	03	04
01		BODY FR 24" SCH 20 PIPE		SA106 GR B	1			
02		END PLATE		SA515 GR 70	2			
03		NOZZLE FR 3" SCH 80		SA106 GR B	1			
04		FLANGE 6"-150 LB SLIP-ON		A105 GR II	1			
05		NIPPLE 2" SCH 80		SA106 GR B	2			
06		NIPPLE 1/2" SCH 80		SA106 GR B	1			
07		STUD 1/2-13 UNC-2A X 4" LG		SA193 B6/B8C	18			
08		STUD 1/2-13 UNC-2A X 3 1/2" LG		" "	14			
09		STUD 1/2-13 UNC-2A X 5" LG		" "	4			
10		LIFTING LUG		SA 36	1			
11		TUBE 5/8 O.D. X .049 W X 2 1/4		A213	1			
12		BOSS		SA 105	1			
13		BOSS		SA 105	2			

NOTES:
1 - DESIGN, FABRICATE, TEST & STAMP PER SECT I OF THE ASME BOILER & PRESSURE VESSEL CODE.
2 - DESIGN PRESSURE 60 PSIG @ 700°F.
3 - IT. 04 MAY BE A SLIP-ON AS SHOWN, OR A WELD NECK OR A LONG NECK FLANGE.
4 - WELD PER W P.S. 8E127-2V

UNLESS OTHERWISE SPECIFIED THE FOLLOWING TOLERANCES APPLY
ALL DIMS ± 1/32
SEE PROCESS SPECIFICATION NO. CAPS86128-1 FOR SUPPLEMENTARY MANUFACTURING INFORMATION.

Figure A-17. FLECHT SEASET Lower Plenum Detail Assembly

BILL OF MATERIAL							
ITEM	PART NAME	PART NO.	MATERIAL	REQ. PER GROUP			
				01	02	03	04
01	SEAL PLATE		ASTM 240 TYPE 304	1			

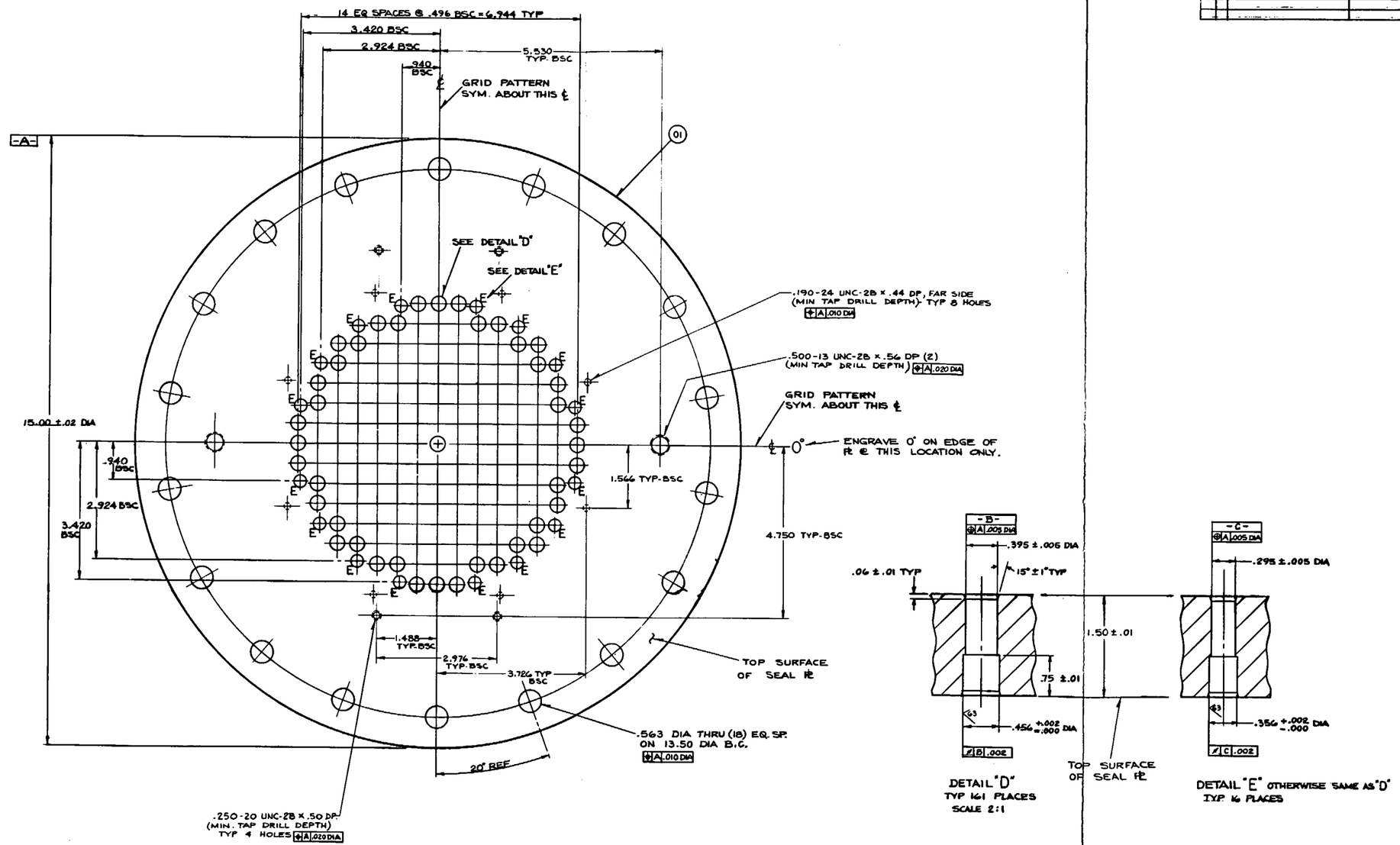

UNLESS OTHERWISE SPECIFIED THE FOLLOWING TOLERANCES APPLY

[illegible]

SEE PROCESS SPECIFICATION NO. CAP586128 FOR SUPPLEMENTARY MANUFACTURING INFORMATION.

Figure A-18. FLECHT SEASET Upper Seal Plate

BILL OF MATERIAL								
ITEM		PART NAME	PART NO.	MATERIAL	NO. PER GROUP			
					01	02	03	04
01		SEAL PLATE		ASTM 240 TYPE 405	1			

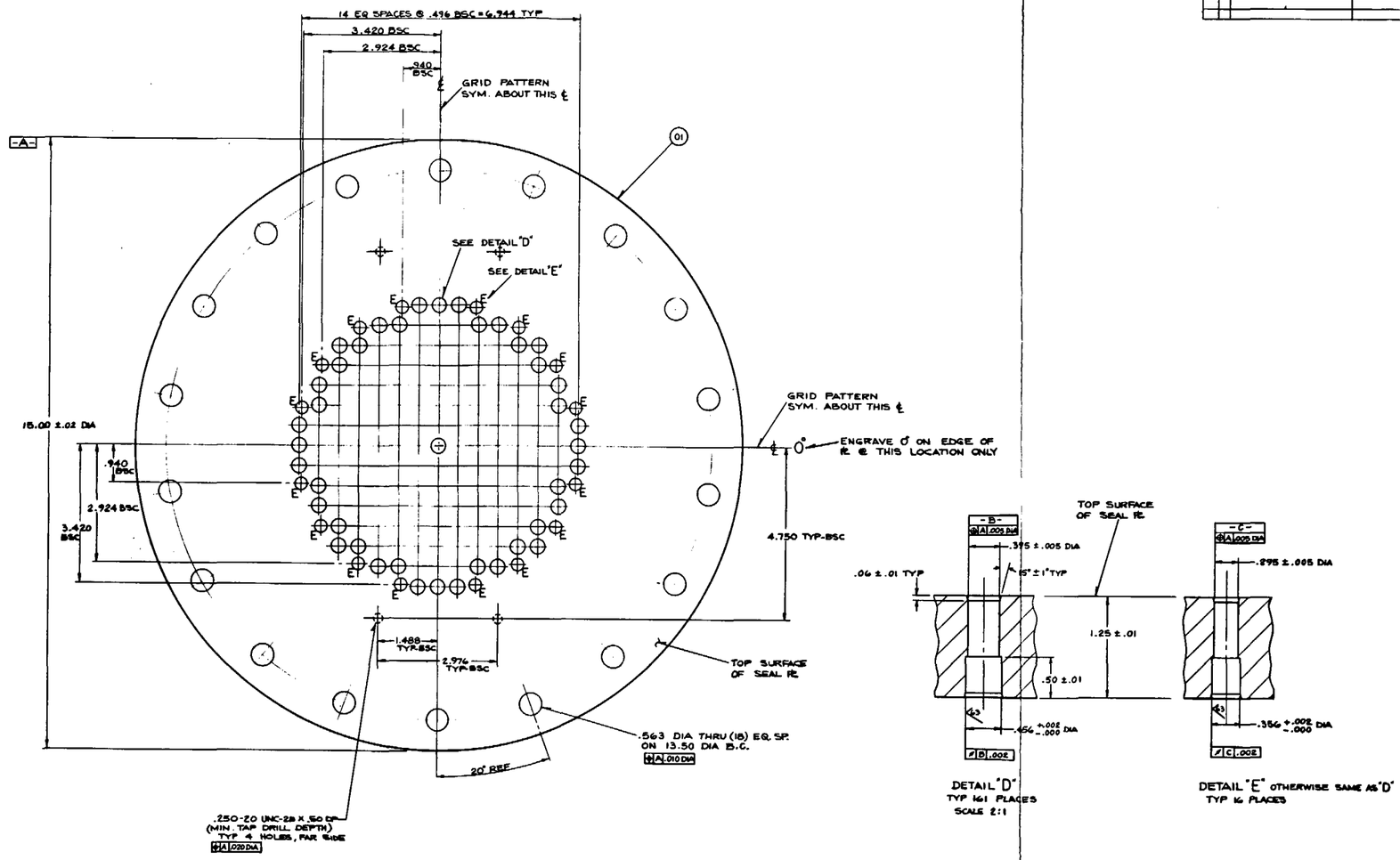

UNLESS OTHERWISE SPECIFIED THE FOLLOWING TOLERANCES APPLY

[illegible]

SEE PROCESS SPECIFICATION NO. CAP000126 FOR SUPPLEMENTARY MANUFACTURING INFORMATION.

Figure A-19. FLECHT SEASET Lower Seal Plate

BILL OF MATERIAL								
ITEM	NOTE	PART NAME	DRAWING & GR OR IT.	MATERIAL	REQ. PER GROUP			
					01	02	03	04
01	A	SLEEVE			1			
02	A	SLEEVE			1			
03	A	SLEEVE			1			

ITEM	B	C	D	E	F	G	H	J
01	.500	.975	.451	.410	.380	.435	.485	.100
02	.625	1.100	.451	.410	.380	.435	.485	.250
03	.625	1.100	.351	.310	.280	.335	.385	.100

A - MATERIAL - BERYLLIUM COPPER, BERYLCO 33-25, WILLIAMS & CO.

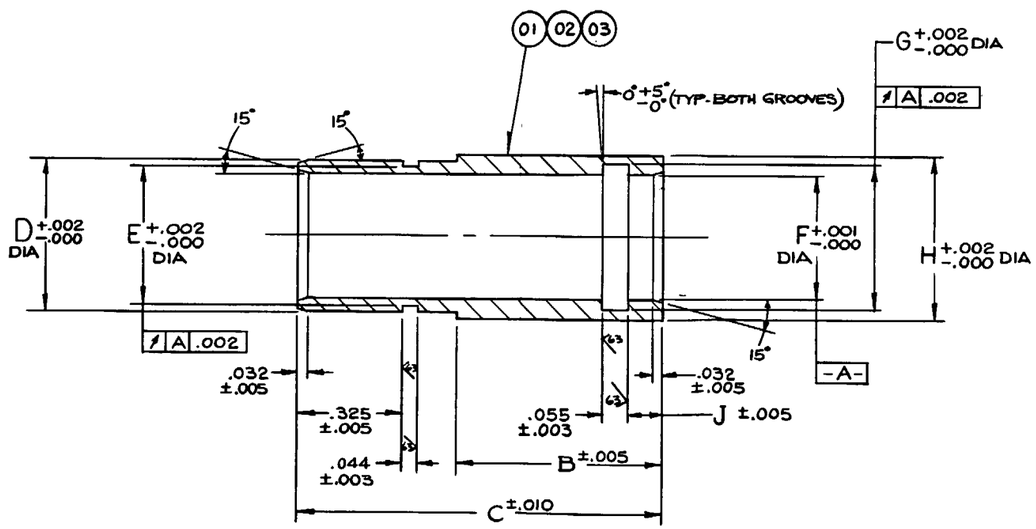

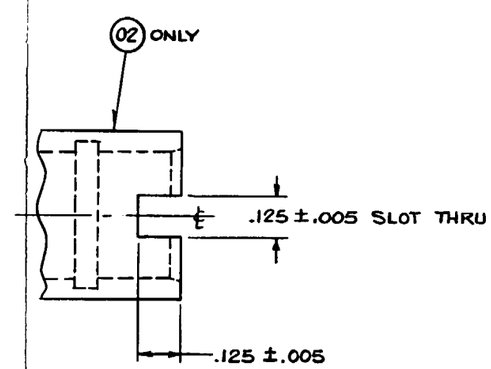

UNLESS OTHERWISE SPECIFIED THE FOLLOWING TOLERANCES APPLY

STRAIGHTNESS, FLATNESS, PERPENDICULARITY, ROUNDNESS, PARALLELISM, SYMMETRY AND ANGULARITY VARIATIONS FOR MACHINED SURFACES ARE PERMITTED WITHIN THE PROFILE ESTABLISHED BY THE LIMITS OF SIZE: VARIATIONS IN FORM FOR UNMACHINED FEATURES ARE PERMITTED WITHIN ESTABLISHED COMMERCIAL STANDARDS. CONCENTRICITY MUST BE WITHIN THE SUM OF THE TOLERANCES OF THE DIAMETERS BEING COMPARED. SURFACE ROUGHNESS ON HOLES: 250√ MAX. ALL EDGES OR CORNERS .005 - .020 (APPROXIMATE RADIUS OR CHAMFER) - ALL FILLETS .005 - .020 (APPROXIMATE RADIUS). SCREW THREADS PER ANSI B1.1 - PIPE THREADS PER ANSI B2.1 - WELD DIMENSIONS ARE MINIMUM - ALL DIMENSIONS CORRECTED TO 68°F ± 2°.

SEE PROCESS SPECIFICATION NO. CAP595128- FOR SUPPLEMENTARY MANUFACTURING INFORMATION.

Figure A-20. FLECHT SEASET O-Ring Sleeve

BILL OF MATERIAL								
ITEM	NOTE	PART NAME	DRAWING & GR OR IT.	MATERIAL	REQ. PER GROUP			
					01	02	03	04
01		RIM		304 SST	1			
02		TUBE		304 SST	1			

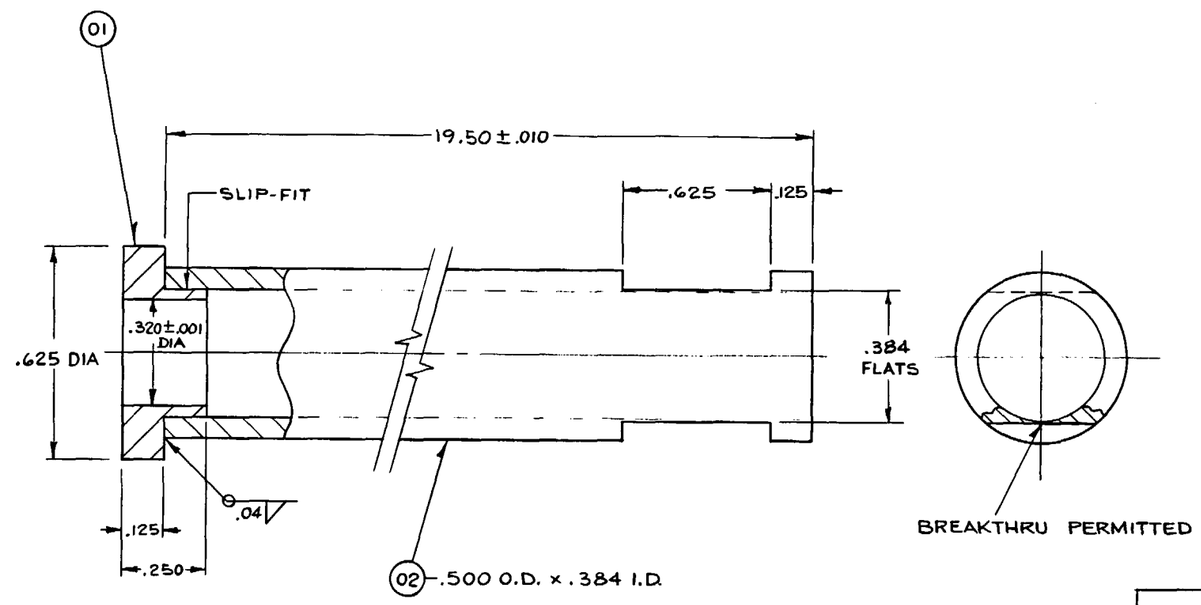

UNLESS OTHERWISE SPECIFIED THE FOLLOWING TOLERANCES APPLY
DIM. TOL. = ± .005

STRAIGHTNESS, FLATNESS, PERPENDICULARITY, ROUNDNESS, PARALLELISM, SYMMETRY AND ANGULARITY VARIATIONS FOR MACHINED SURFACES ARE PERMITTED WITHIN THE PROFILE ESTABLISHED BY THE LIMITS OF SIZE. VARIATIONS IN FORM FOR UNMACHINED FEATURES ARE PERMITTED WITHIN ESTABLISHED COMMERCIAL STANDARDS. CONCENTRICITY MUST BE WITHIN THE SUM OF THE TOLERANCES OF THE DIAMETERS BEING COMPARED. SURFACE ROUGHNESS ON HOLES - 250√ MAX. ALL EDGES OR CORNERS .005 - .020 (APPROXIMATE RADIUS OR CHAMFER). - ALL FILLETS .005 - .020 (APPROXIMATE RADIUS). SCREW THREADS PER ANSI B1.1 - PIPE THREADS PER ANSI B2.1 - WELD DIMENSIONS ARE MINIMUM - ALL DIMENSIONS CORRECTED TO 68°F ± 2°.

SEE PROCESS SPECIFICATION NO. CAP595128 FOR SUPPLEMENTARY MANUFACTURING INFORMATION.

Figure A-21. FLECHT SEASET Thimble Sleeve

BILL OF MATERIAL								
ITEM		PART NAME	PART NO.	MATERIAL	REQ. PER GROUP			
					01	02	03	04
01		FILLER STRIP		AISI 304 SST	1			
02		CLIP		AISI 304 SST	1			

NOTE:
1 - FINISHED PART MUST PASS THRU AN INSPECTION ENVELOPE EQUIV. TO END VIEW. MAX. AXIAL DEVIATION & TWIST OF .06 OVER ENTIRE LENGTH.

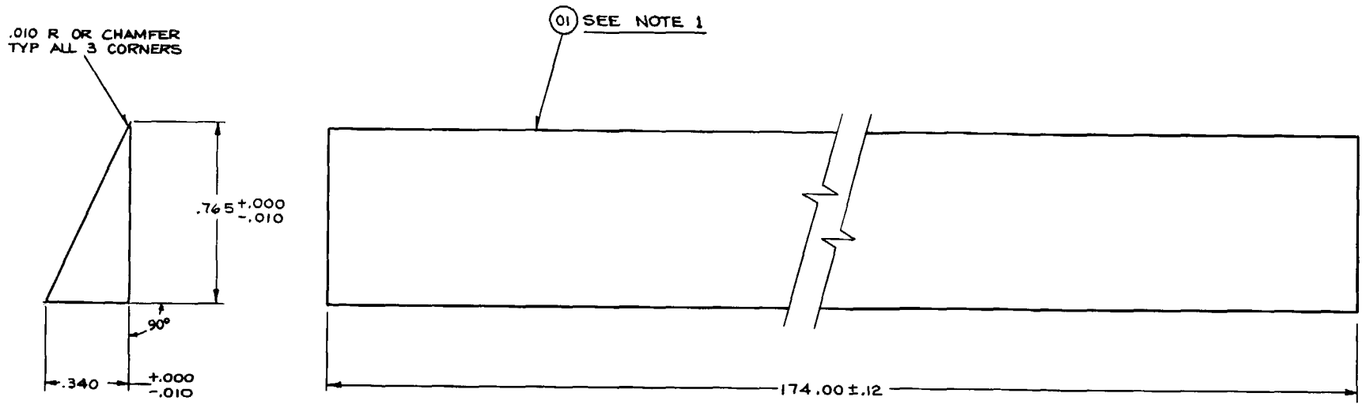

SCALE 4:1

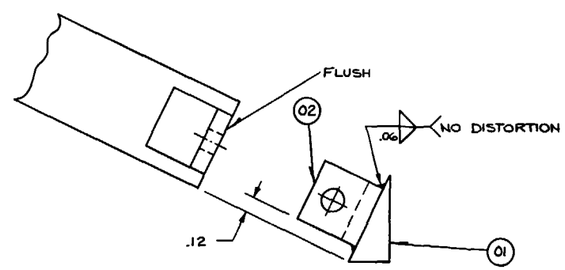

GROUP 1

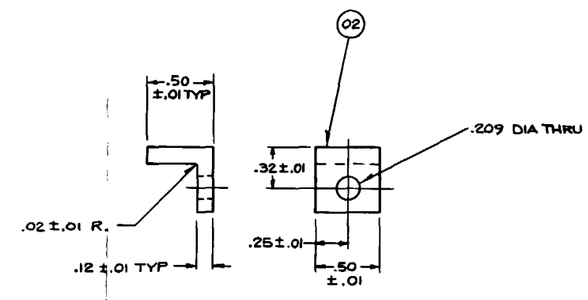

UNLESS OTHERWISE SPECIFIED THE FOLLOWING TOLERANCES APPLY

STRAIGHTNESS, FLATNESS, PERPENDICULARITY, ROUNDNESS, PARALLELISM, SYMMETRY, AND ANGULARITY VARIATIONS FOR MACHINED SURFACES ARE PERMITTED WITHIN THE PROFILE ESTABLISHED BY THE LIMITS OF SIZE. VARIATIONS IN FORM FOR UNMACHINED FEATURES ARE PERMITTED WITHIN ESTABLISHED COMMERCIAL STANDARDS. CONCENTRICITY MUST BE WITHIN THE SUM OF THE TOLERANCES OF THE DIAMETERS BEING COMPARED. SURFACE ROUGHNESS ON HOLES: 250 μ/RMS
ALL EDGES AND CORNERS .005 - .020 (APPROXIMATE RADIUS OR CHAMFER). - ALL FILLETS .005 - .020 (APPROXIMATE RADIUS). SCREW THREADS PER ANSIB1.1 - PIPE THREADS PER ANSIB2.1 - HELD DIMENSIONS ARE MINIMUM - ALL DIMENSIONS CORRECTED TO 68°F ± 2°.

SEE PROCESS SPECIFICATION NO. CAP595128 FOR SUPPLEMENTARY MANUFACTURING INFORMATION.

Figure A-22. FLECHT SEASET Filler Strip Detail

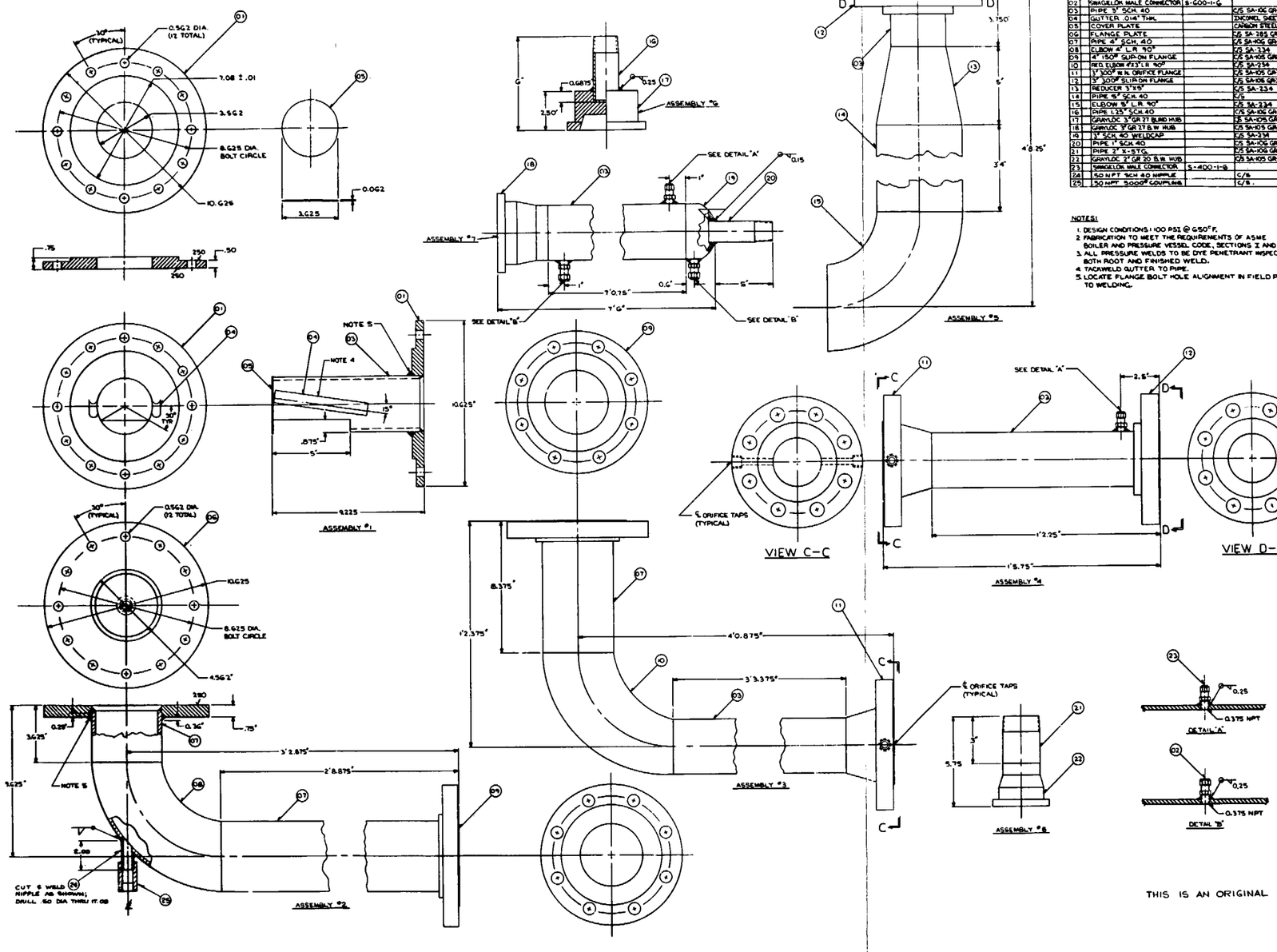

BILL OF MATERIAL

ITEM	PART NAME	PART NO.	MATERIAL	NO. PER GROUP #1	#2	#3	#4
01	FLANGE PLATE		C/S SA-285 GRC	1			
02	SWAGELOK MALE CONNECTOR	S-600-1-6		2			
03	PIPE 3" SCH. 40		C/S SA-106 GR B	AR			
04	GUTTER .014" THK.		INCONEL SHEET	2			
05	COVER PLATE		CARBON STEEL	1			
06	FLANGE PLATE		C/S SA-285 GRC	1			
07	PIPE 4" SCH. 40		C/S SA-106 GR B	AR			
08	ELBOW 4" L.R. 90°		C/S SA-234	1			
09	4" 150# SLIP-ON FLANGE		C/S SA-105 GR B	2			
10	RED. ELBOW 4"X3" L.R. 90°		C/S SA-234	1			
11	3" 300# R.F. ORIFICE FLANGE		C/S SA-105 GR B	2			
12	3" 300# SLIP-ON FLANGE		C/S SA-105 GR B	2			
13	REDUCER 3"X8"		C/S SA-234	1			
14	PIPE 8" SCH. 40		C/S	AR			
15	ELBOW 8" L.R. 90°		C/S SA-234	1			
16	PIPE 1.25" SCH. 40		C/S SA-106 GR B	AR			
17	GRAYLOC 3" GR 27 BLIND HUB		C/S SA-105 GR B	1			
18	GRAYLOC 3" GR 27 B.W. HUB		C/S SA-105 GR B	1			
19	3" SCH. 40 WELDCAP		C/S SA-234	1			
20	PIPE 1" SCH. 40		C/S SA-106 GR B	AR			
21	PIPE 2" X-STG.		C/S SA-106 GR B	AR			
22	GRAYLOC 2" GR 20 B.W. HUB		C/S SA-105 GR B	1			
23	SWAGELOK MALE CONNECTOR	S-400-1-6		2			
24	.50 NPT SCH 40 NIPPLE		C/S	1			
25	.50 NPT 3000# COUPLING		C/S	1			

NOTES:

1. DESIGN CONDITIONS: 100 PSI @ 650°F.
2. FABRICATION TO MEET THE REQUIREMENTS OF ASME BOILER AND PRESSURE VESSEL CODE, SECTIONS I AND IX.
3. ALL PRESSURE WELDS TO BE DYE PENETRANT INSPECTED, BOTH ROOT AND FINISHED WELD.
4. TACKWELD GUTTER TO PIPE.
5. LOCATE FLANGE BOLT HOLE ALIGNMENT IN FIELD PRIOR TO WELDING.

Figure A-23. Exhaust Line Details

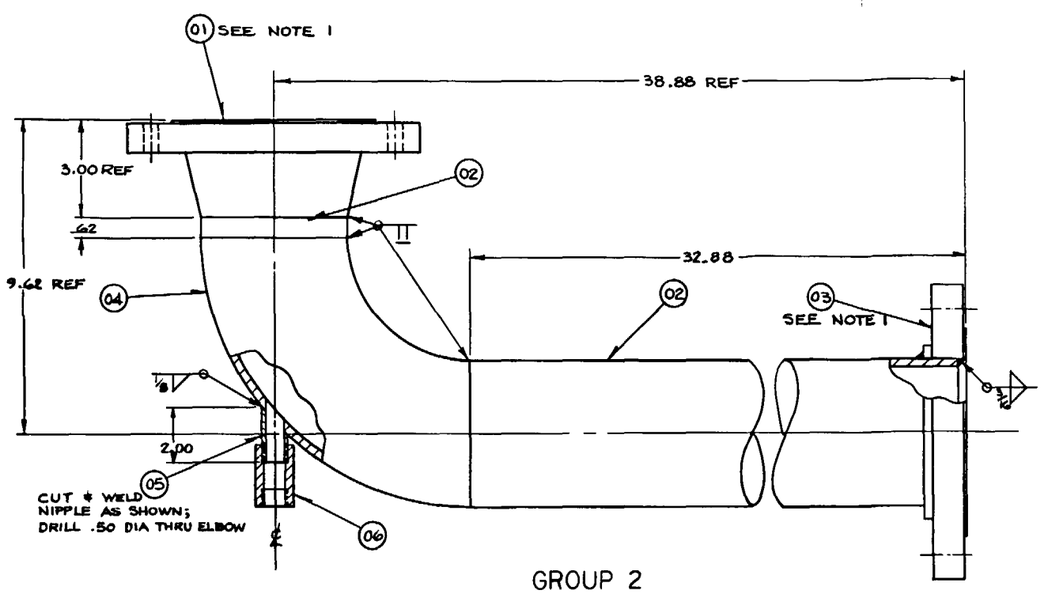

GROUP 2

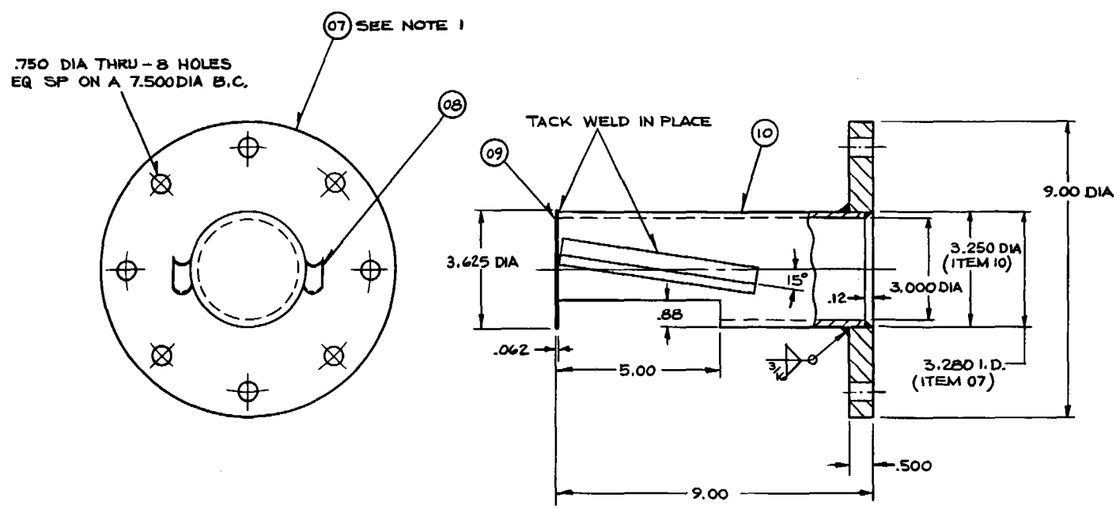

GROUP 1

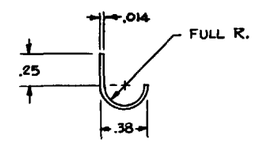

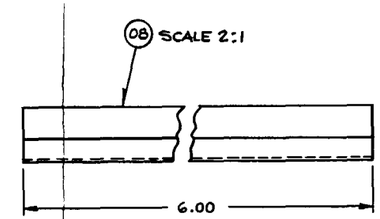

BILL OF MATERIAL								
ITEM	NOTE	PART NAME	DRAWING & GR OR IT.	MATERIAL	REQ. PER GROUP			
					01	02	03	04
01		4" 150 LB W/N FLANGE		SA-105 GR II		1		
02		4" SCH 40 PIPE		SA-106 GR B		AR		
03		4" 150 LB SLIP-ON FLANGE		SA-105 GR II		1		
04		4" 90° L.R. ELL		SA-234		1		
05		1/2 NPT SCH 40 NIPPLE		C. STL		1		
06		1/2 NPT 3000 LB COUPLING		C. STL		1		
07		FLANGE RE		SA-285-GRC	1			
08		GUTTER		INCONEL	2			
09		COVER RE		C. STL	1			
10		3" SCH 40 PIPE		SA-106 GR B	1			

NOTES:
1-ALIGN BOLT HOLES IN FIELD PRIOR TO WELDING.
2-DESIGN CONDITIONS: 100 PSI @ 650°F
3-FABRICATE PER ASME BOILER & PRESSURE VESSEL CODE, SECTIONS I & IX.
4-ALL PRESSURE WELDS TO BE DYE PENETRANT INSPECTED, BOTH ROOT & FINAL PASS.

UNLESS OTHERWISE SPECIFIED THE FOLLOWING TOLERANCES APPLY
TWO PLACE DECIMALS = ±.06, THREE PLACE DECIMALS = ±.010
STRAIGHTNESS, FLATNESS, PERPENDICULARITY, ROUNDNESS, PARALLELISM, SYMMETRY, AND ANGULARITY VARIATIONS FOR MACHINED SURFACES ARE PERMITTED WITHIN THE PROFILE ESTABLISHED BY THE LIMITS OF SIZE. VARIATIONS IN FORM FOR UNMACHINED FEATURES ARE PERMITTED WITHIN ESTABLISHED COMMERCIAL STANDARDS. CONCENTRICITY MUST BE WITHIN THE SUM OF THE TOLERANCES OF THE DIAMETERS BEING COMPARED. SURFACE ROUGHNESS ON HOLES: 250 μ (AA). ALL EDGES OR CORNERS .045 - .020 (APPROXIMATE RADIUS OR CHAMFER). - ALL FILLETS .005 - .020 (APPROXIMATE RADIUS). ALL THREADS PER ASME B1.1 - PIPE THREADS PER ASME B2.1 - WELD DIMENSIONS ARE MINIMUM - ALL DIMENSIONS CORRECTED TO 68°F ± 2°.

SEE PROCESS SPECIFICATION NO. CAP595128 FOR SUPPLEMENTARY MANUFACTURING INFORMATION.

Figure A-24. FLECHT SEASET Exhaust Line Details

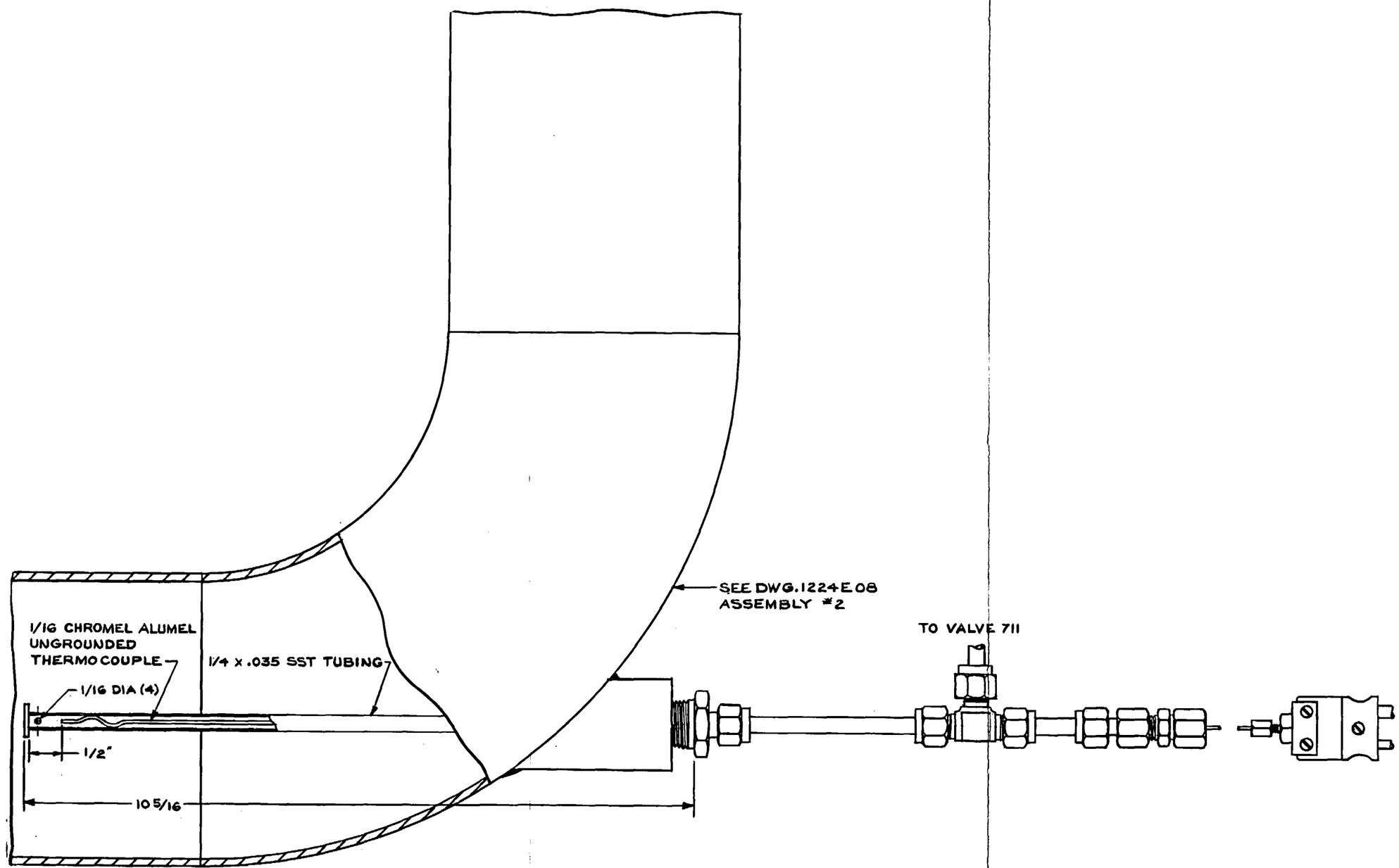

Figure A-25. Exhaust Line Steam Probe

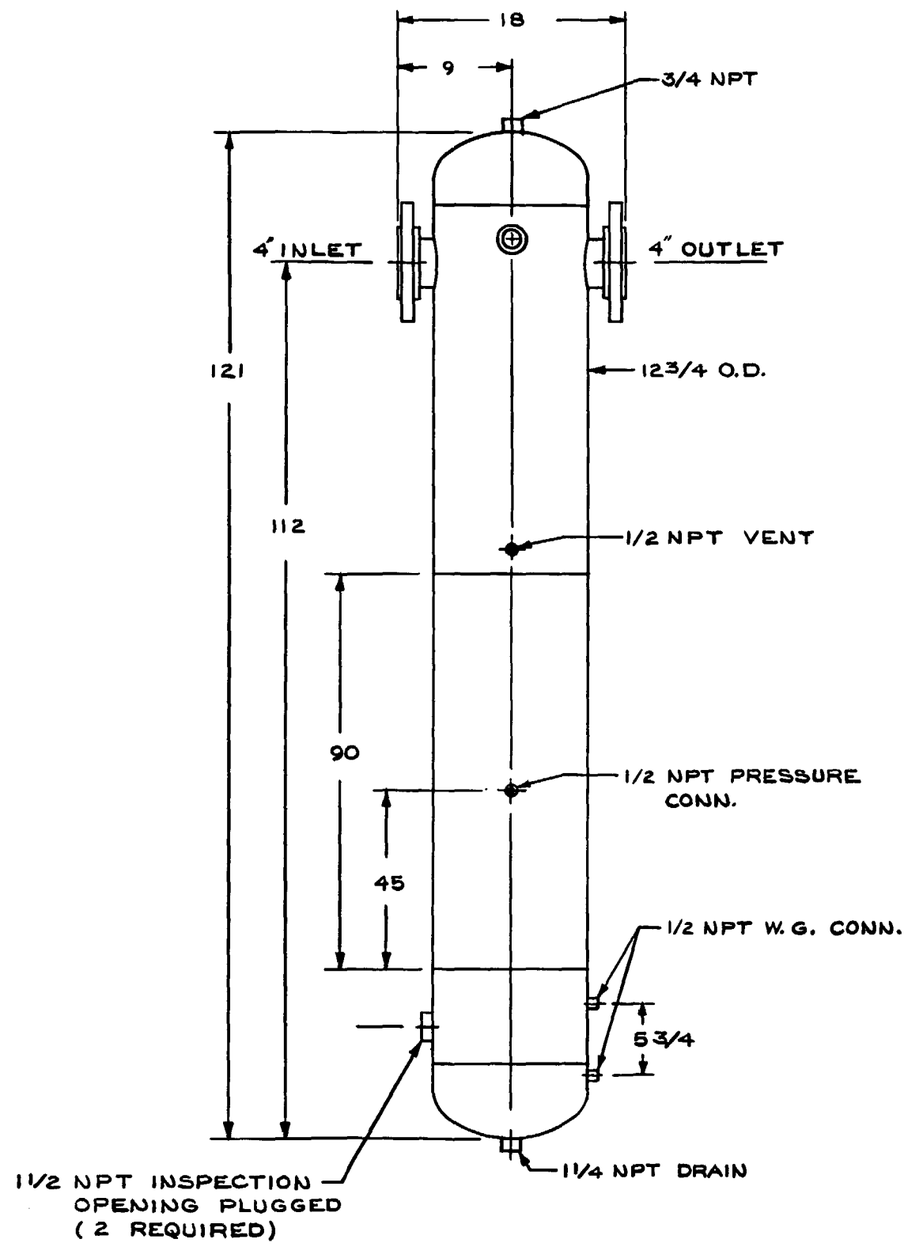

NOTE:

1. DESIGN: 180 PSIG @ 400°F
2. CONSTRUCTION, INSPECTION & STAMP PER ASME CODE, SECTION I "S" STAMP.
3. SEE WRIGHT-AUSTIN CO. DWG. 8578-17 FOR UNMODIFIED SEPARATOR.

Figure A-26. Steam Separator

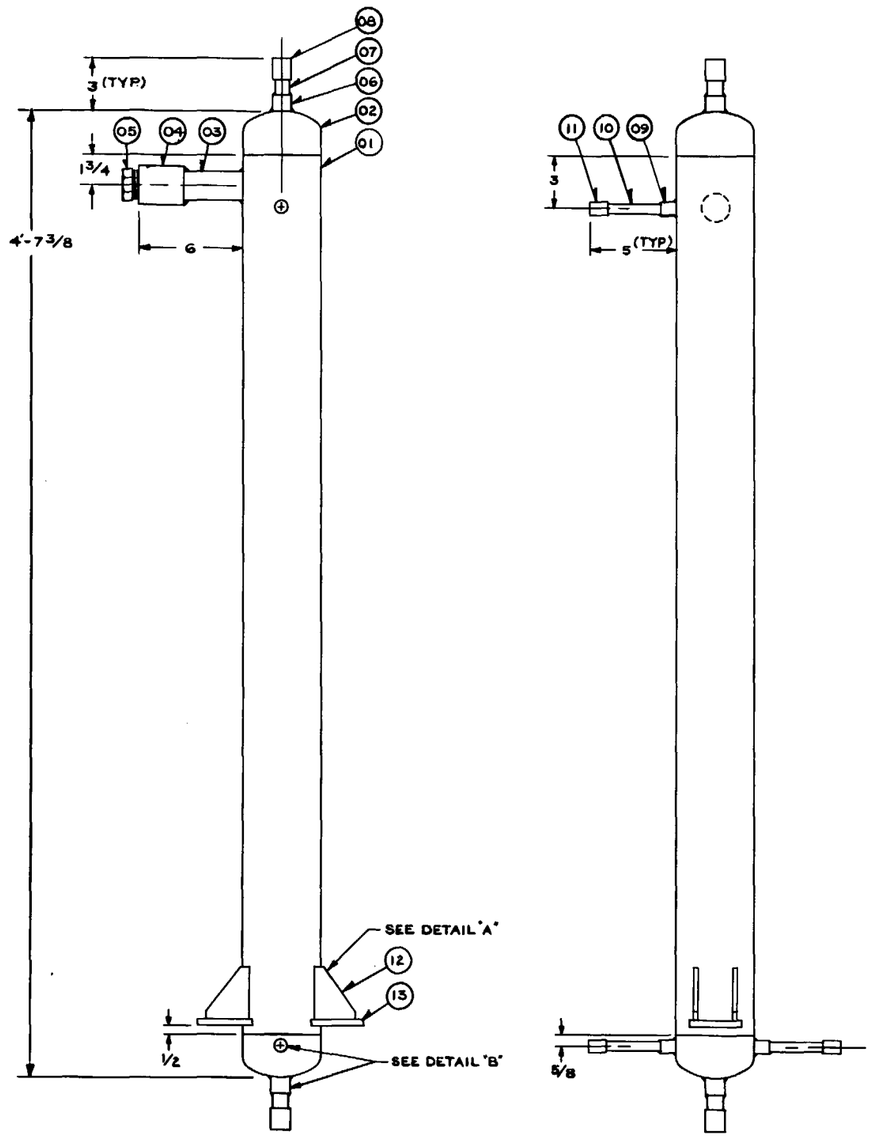

(SCALE 1/4-1)

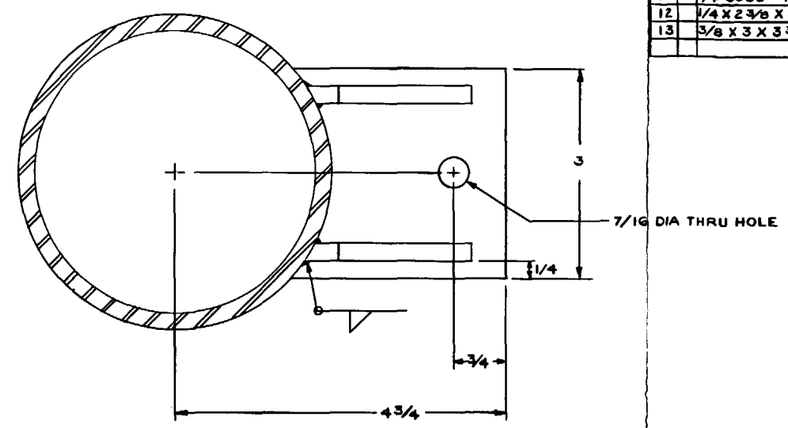

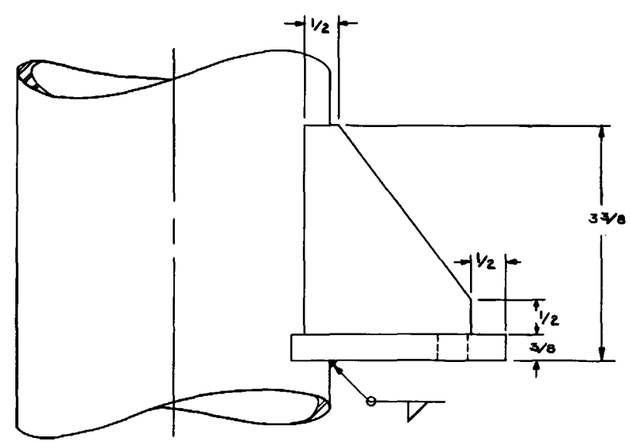

DETAIL "A"
(FULL SCALE)

BILL OF MATERIAL

ITEM	NOTE	PART NAME	DRAWING & GR OR IT.	MATERIAL	REQ. PER GROUP 01	02	03	04
01		4 STD. WT. PIPE (4-2 3/8 LG.)		SA-106 B	1			
02		4 STD. WT. B/W CAP		SA-234 B	2			
03		1 1/4 STD. WT. PIPE (6 LG.)		SA-106 B	1			
04		1 1/4 3000# THREADED CPLG.		SA-105	1			
05		1 1/4 THREADED PLUG		SA-105	1			
06		1/2 3000# S/W HALF CPLG.		SA-105	2			
07		1/2 X-STRONG PIPE (3 LG.)		SA-106B	2			
08		1/2 3000# THREADED CAP		SA-105	2			
09		1/4 3000# S/W HALF CPLG.		SA-105	3			
10		1/4 X-STRONG PIPE (5 LG.)		SA-106B	3			
11		1/4 3000# THREADED CAP		SA-105	3			
12		1/4 X 2 3/8 X 3 PLATE		SA-36	4			
13		3/8 X 3 X 3 3/32 PLATE		SA-36	2			

NOTES

1. THE ASSEMBLY IS TO BE FABRICATED, TESTED AND STAMPED IN ACCORDANCE WITH SECTION I OF THE ASME BOILER AND PRESSURE VESSEL CODE.
2. DESIGN PRESSURE - 100 PSI
   DESIGN TEMPERATURE - 650°F
3. TOLERANCE ON DIMENSIONS ± 1/8 UNLESS OTHERWISE SPECIFIED.

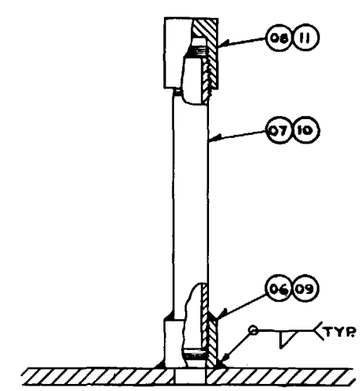

DETAIL "B"

Figure A-27. Separator Drain Tank

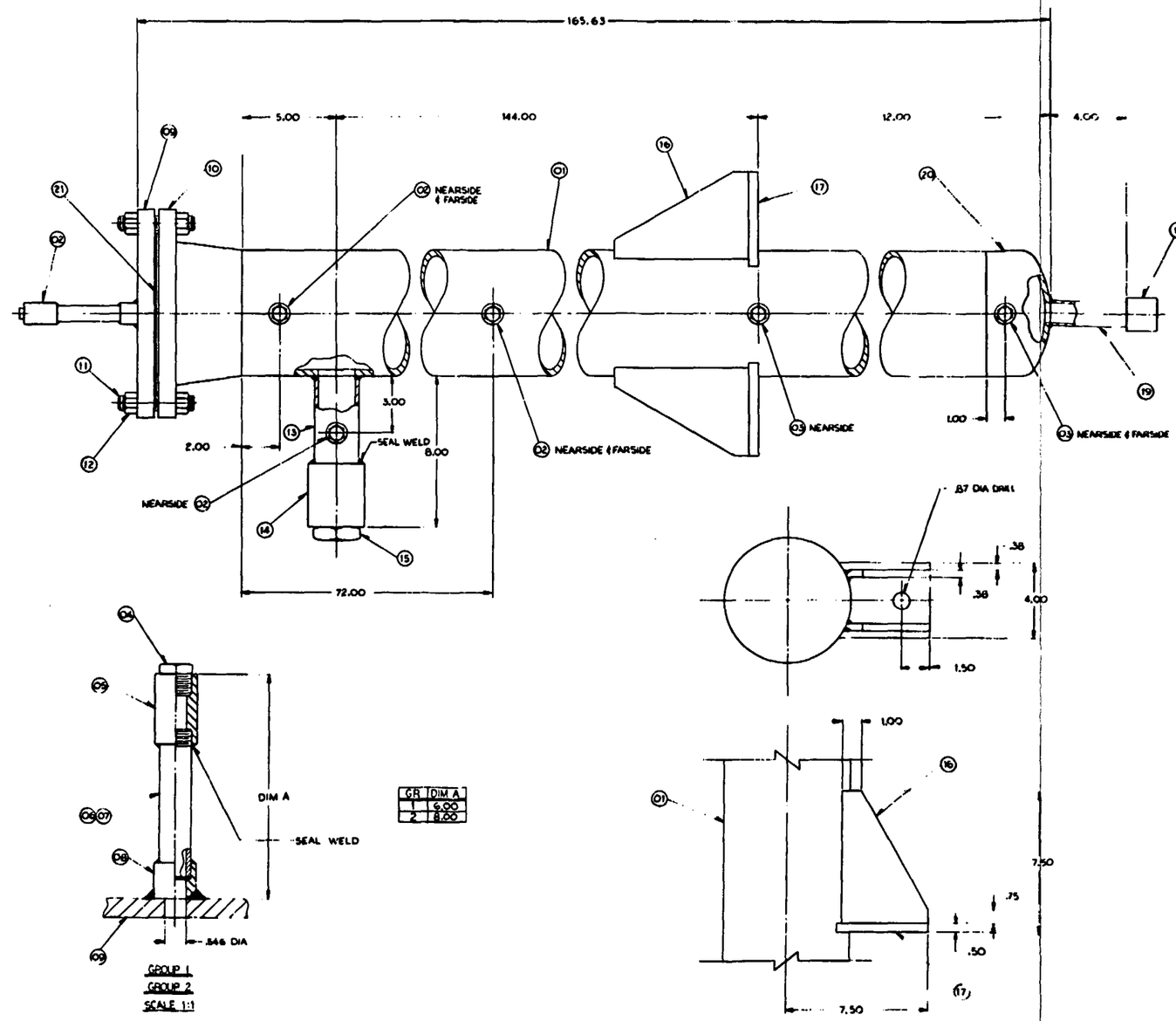

GR	DIM A
1	6.00
2	8.00

NOTES

1. THE ASSEMBLY IS TO BE FABRICATED TESTED, AND STAMPED IN ACCORDANCE WITH SECTION I OF THE ASME BOILER AND PRESSURE VESSEL CODE.
2. DESIGN PRESSURE 100 PSI
   DESIGN TEMPERATURE -850°F
3. SUPPORT LUGS TO SUSTAIN A STATIC VERTICAL LOAD OF 550 POUNDS.
4. TOLERANCE ON DIMENSIONS ± .125 UNLESS OTHERWISE SPECIFIED.

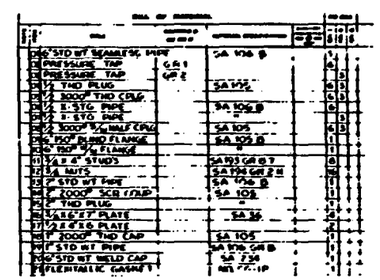

Figure A-28. Carryover Tank

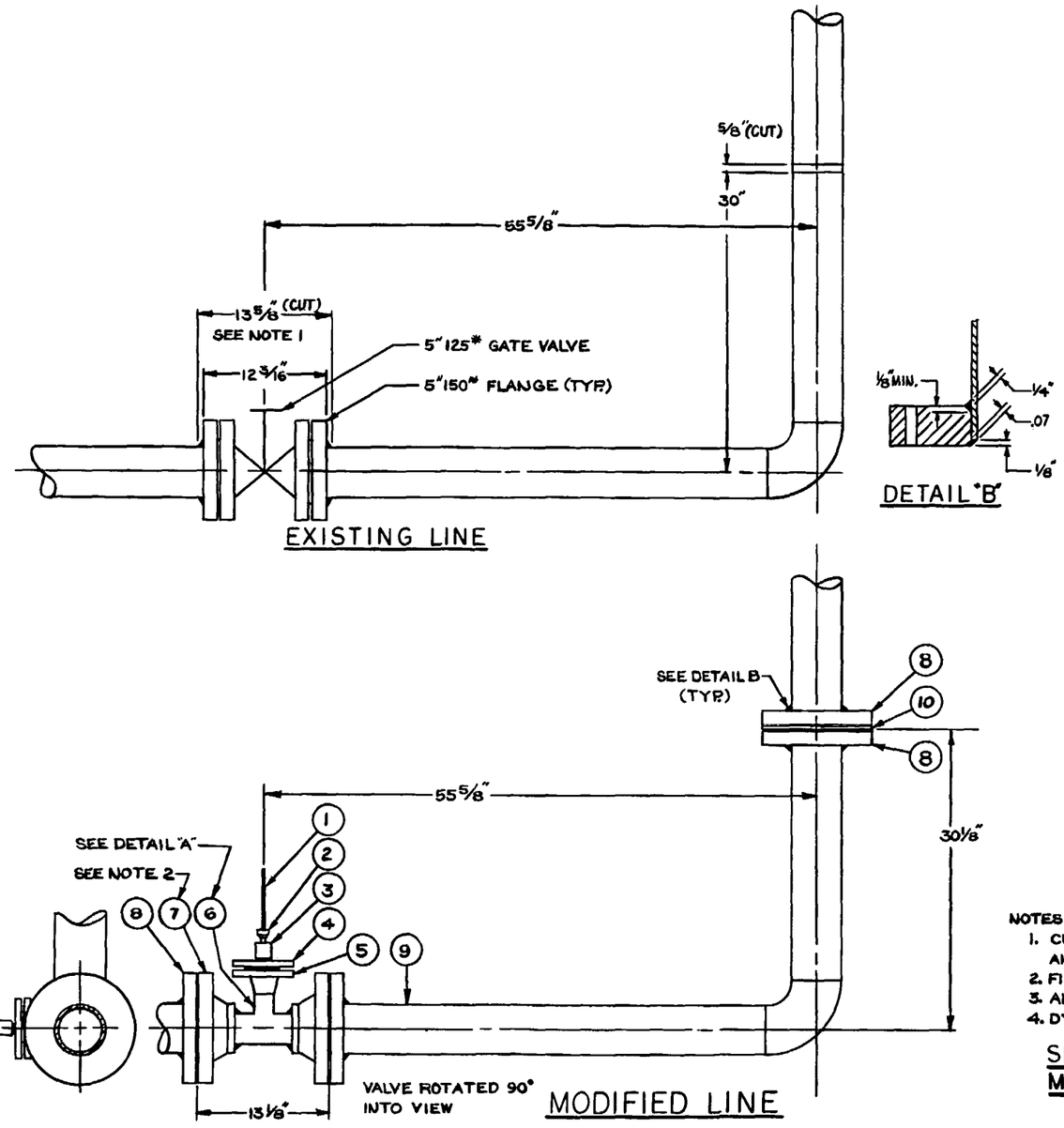

BILL OF MATERIAL					
NOTE	ITEM	TITLE	DRAWING & GR. OR IT.	MATERIAL SPECIFICATION	EQUIVALENT SPECIFICATIONS FOR (W) USE ONLY
	1	TURBOPROBE			
A	2	SWAGELOK MALE CONN.		TYPE 316 S.S.	
B	3	SPECIAL THREADED CPLG.		TYPE 316 S.S.	
C	4	2" 150# BLIND FLANGE		SA 105 GR. 1	
	5	2" 150# W/N FLANGE		SA 105 GR. 1	
D	6	3"x3"x2" STD. WT. TEE		SA 234 W.P.B.	
	7	5" 300# W/N FLANGE		SA 105 GR. 1	
E	8	5" 300# BLIND FLANGE		SA 105 GR. 1	
	9	5" O.D. x .12" WALL TUBING C.S.		SA 53 GR B	
	10	SPACER PLATE		316 S.S.	

A- 1210-1-12-BT
B- FURNISHED WITH TURBOPROBE
C- TAPPED TO FIT ITEM 3
D- SPECIAL BORE
E- BORED TO FIT 5" O.D. TUBING

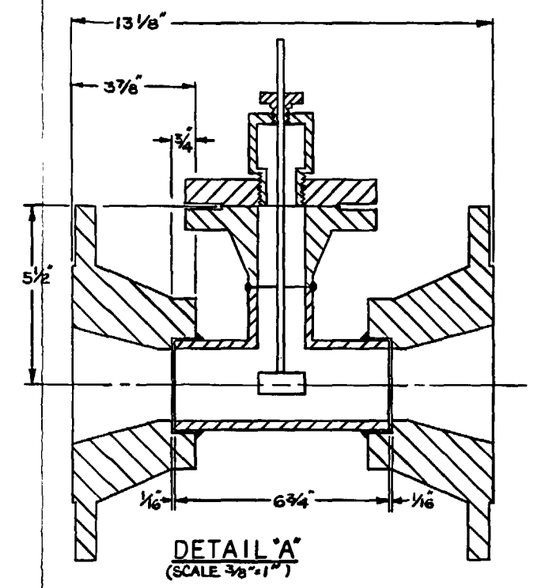

NOTES:
1. CUT AFTER TURBOPROBE SPOOL PIECE HAS BEEN FABRICATED AND DIMENSIONALLY CHECKED.
2. FIELD FIT TURBOPROBE SPOOL PIECE AFTER FABRICATION.
3. ALL WELDING PER (W) PROCESS SPEC. 82148, REV. 2.
4. DYE PENETRANT EXAMINATION OF ALL WELD REQUIRED.

SEE DWG. 501B615 FOR TURBOPROBE MODIFICATION

Figure A-29. Downcomer for Gravity Reflood Configuration

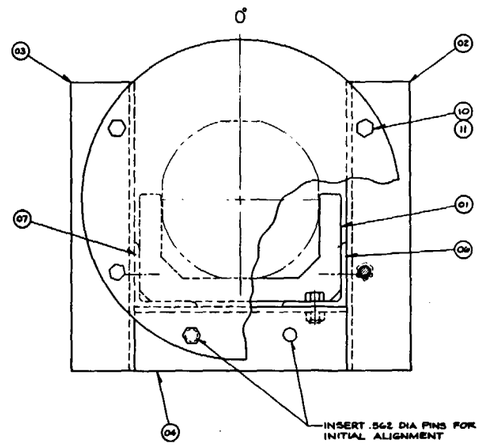

VIEW A-A
SCALE 1:2

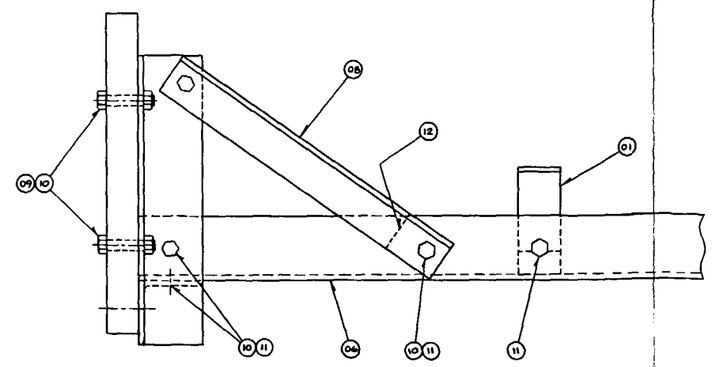

BILL OF MATERIAL

ITEM	SYM	PART NAME	DRAWING & GR OR N	MATERIAL	NO. PER GROUP 01	02	03	04
01		GRID SUPPORT		AL 6061-T6	6			
02		L 3×3×¼		ASTM A36	1			
03		L			1			
04		L			1			
05		L			2			
06		L			1			
07		L 3×3×¼			1			
08		L 2×2×¼		ASTM A36	2			
09		.50-13 UNC-2A×2.25 LG HEX HD BOLT		ALLOY STL	6			
10		.50-13 UNC-2B HEX NUT		ALLOY STL	24			
11		.50-13 UNC-2A×1.00 LG HEX HD BOLT		ALLOY STL	34			
12		SPACER		ASTM A36	2			

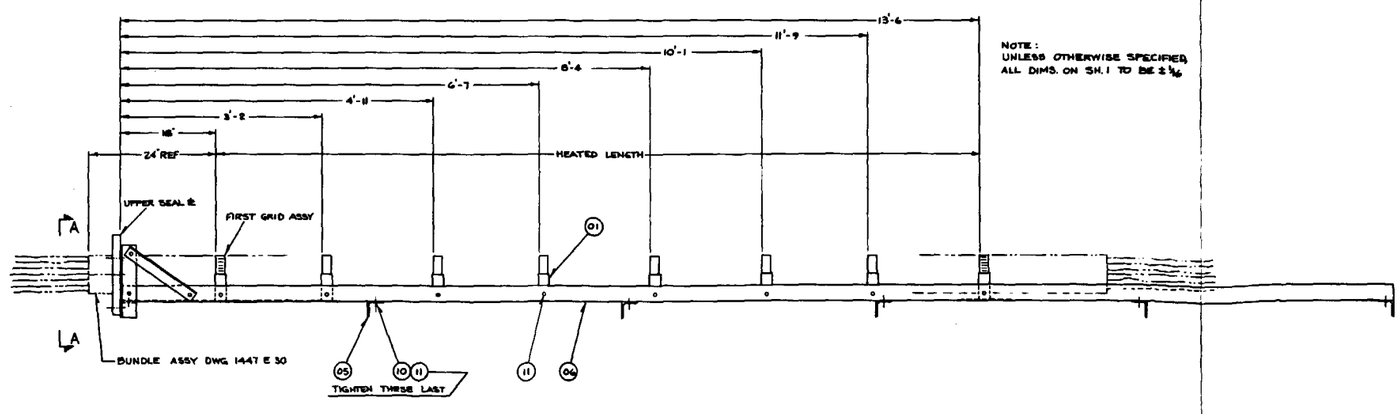

Figure A-30. Strong Back and Assembly Fixture (Sheet 1 of 2)

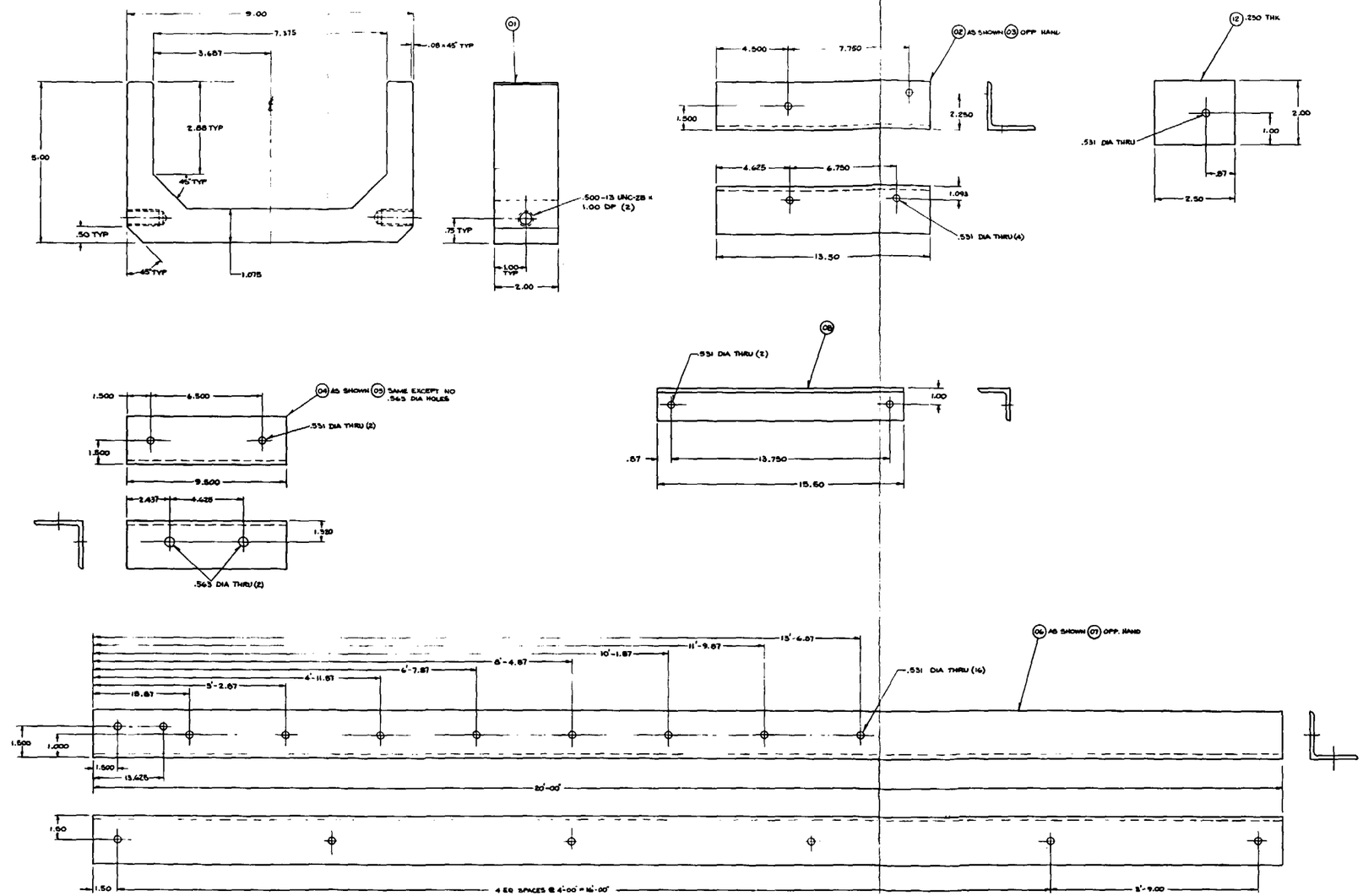

UNLESS OTHERWISE SPECIFIED THE FOLLOWING TOLERANCES APPLY
THREE PLACE DECIMALS = ± .010 TWO PLACE = ± .02

SEE PROCESS SPECIFICATION NO CAP586138 FOR SUPPLEMENTARY MANUFACTURING INFORMATION

Figure A-30. Strong Back and Assembly Fixture (Sheet 2 of 2)

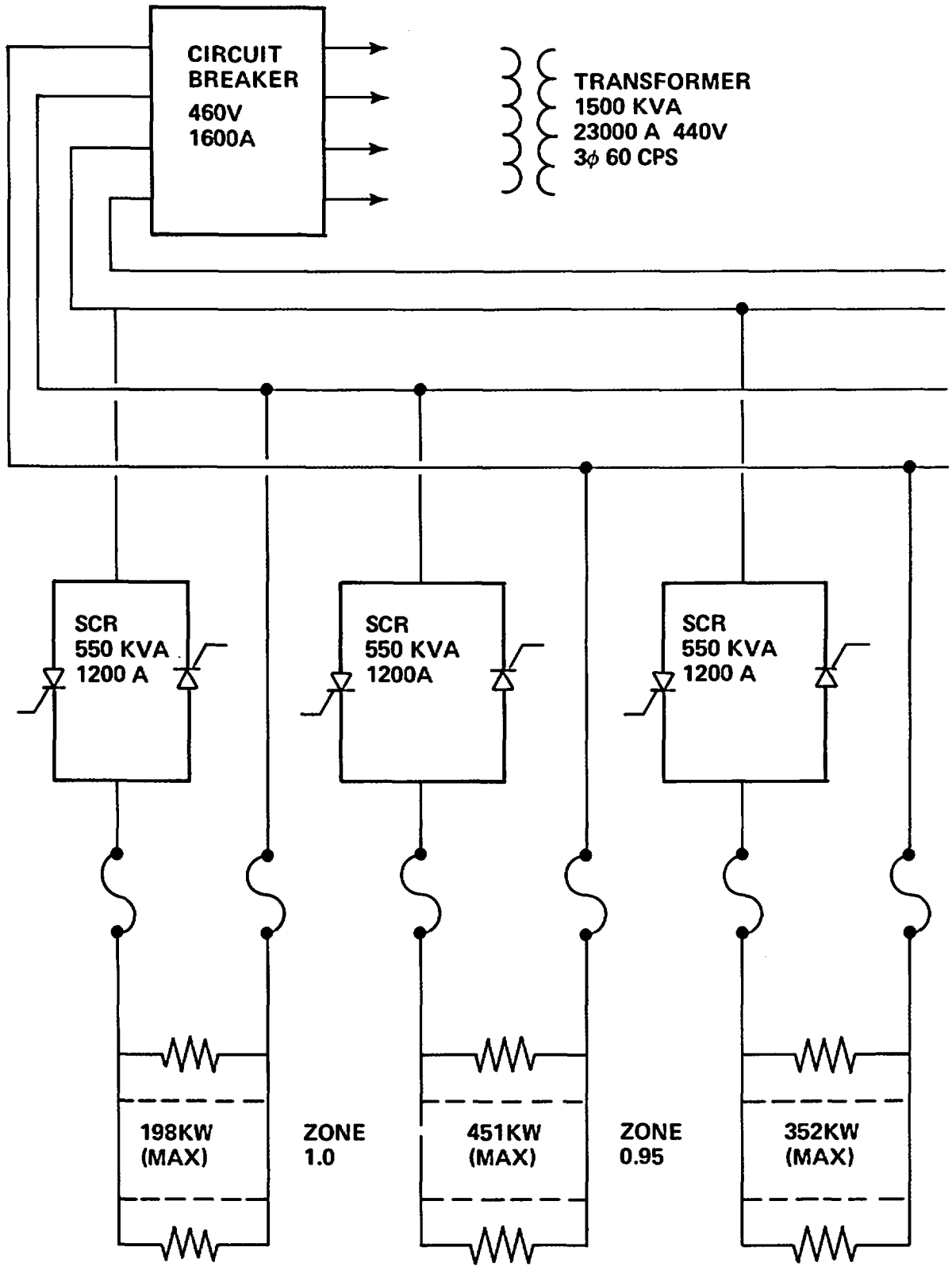

Figure A-31. Bundle Power

APPENDIX B
PHOTOGRAPHIC STUDIES

Black-and-white motion pictures at speeds from 400 to 2500 frames per second were taken through the housing windows for some of the test runs. These tests are listed in table B-1, along with the following information:

-- Initial test conditions
-- Window elevation
-- Film speed at which the movies were taken at each window
-- Time after flood when the first droplet was observed to pass by each window
-- Droplet size range
-- Droplet velocity range
-- Time in the test during which the movies were taken
-- Film quality with respect to lighting and focus

Movies at 50 frames per second were also taken through the upper plenum window for all photographed runs. Additional analyses of the movies will be performed for the data evaluation report, to be issued at a later date.

TABLE B-1

PHOTOGRAPHIC STUDY SUMMARY

Run No.	Initial Run Conditions	Window Elevation [m(in.)]	Film Speed (frames/sec)	Time of First Droplet (sec)	Droplet Size Range [mm(in.)]	Droplet Velocity Range [m/sec(in./sec)]	Time of Movie (sec)	Lighting	Focus	Remarks
31504	Reference run	0.91 (36)	2500	--	--	--	2-8	Good	Good	No droplets
		1.82 (72)	2500	--	--	--	0-6	Good	Good	No droplets
		1.82 (72)	2500	Before movie started	0.76-1.9 (0.030-0.075)	0.986-2.662 (38.8-104.8)	200-206	Good	Good	
		2.74 (108)	1000	Between 7 and 40 sec	0.53-1.1 (0.021-0.045)	3.559-5.855 (140.1-230.5)	0-7, 40-46 119-132, 180-182	Good	Good	
31701	152 mm/sec (6.0 in./sec) flooding rate	0.91 (36)	2500	Before movie started	0.45-1.83 (0.018-0.072)	0.83-1.43 (32.9-56.3)	2-9	Good	Good	
		2.74 (108)	2500	Before movie started	0.63-2.49 (0.025-0.098)	4.67-11.41 (183.9-449.2)	1-8	Good	Good	
31805	20 mm/sec (0.8 in./sec) flooding rate	0.91 (36)	2500	Before movie started	0.25-1.02 (0.010-0.040)	1.45-3.0 (57.4-118.1)	10-16	Good	Good	
		1.82 (72)	2500	Before movie started	0.76-1.52 (0.30-0.060)	3.71-4.06 (146.0-160.1)	10-16	Fair	Good	
		1.82 (72)	2500	Before movie started	Poor focus	4.95-5.94 (195.0-234.0)	110-116	Fair	Poor	
32235	Variable flooding rate: 152 mm/sec (6 in./sec) for 5 sec, 15.2 mm/sec (0.6 in./sec) onward; 0.14 MPa (20 psia) system pressure	0.91 (36)	2500	1.02	0.56-2.5 (0.022-0.097)	1.43-3.066 (56.3-120.7)	0-6	Fair	Fair	
		1.82 (72)	2500	--	--	--	1-7	Poor	Poor	Poor quality
		2.74 (108)	2500	0.61	0.89-1.5 (0.035-0.061)	7.699-10.34 (303.1-407.0)	0-10, 40-51	Fair	Fair	

TABLE B-1 (cont)

PHOTOGRAPHIC STUDY SUMMARY

Run No.	Initial Run Conditions	Window Elevation [m(in.)]	Film Speed (frames/sec)	Time of First Droplet (sec)	Droplet Size Range [mm(in.)]	Droplet Velocity Range [m/sec(in./sec)]	Time of Movie (sec)	Lighting	Focus	Remarks
32333	Variable flooding rate: 152 mm/sec (6 in./sec) for 5 sec, 20 mm/sec (0.8 in./sec) onward	0.91 (36)	2500	1.70	0.58-2.3 (0.023-0.091)	0.653-2.48 (25.7-97.7)	0-6	Good	Fair	
		1.82 (72)	2500	--	--	--	6-12	Poor	Poor	Poor quality
		2.74 (108)	2500	Before movie started	0.2-1.7 (0.008-0.065)	6.215-12.74 (244.7-501.6) Water fallback: (-2.14)-(-2.591) (-84.3)-(102.0)	10-20 50-61	Good	Good	
34524	3.2 kw/m (1.0 kw/ft) peak power	1.82 (72)	400	4.70	0.41-1.7 (0.016-0.065)	4.536-5.090 (178.6-200.4)	0-40	Good	Good	
		2.74 (108)	2000	8.56	0.58-2.3 0.023-0.090	4.069-6.998 (160.2-275.5)	0-24	Good	Good	
35212	10 mm/sec (0.4 in./sec) flooding rate;	1.82 (72)	400	1.10	0.38-2.5 (0.015-0.100)	1.34-1.91 (52.7-75.1)	0-40	Good	Good	
	0.14 MPa (20 psia) system pressure	2.74 (108)	2000	12.65	0.36-1.4 (0.014-0.056)	1.71-2.799 (67.5-110.2)	0-24	Good	Good	
34907	10 mm/sec (0.4 in./sec) flooding rate	1.82 (72)	400	--	--	--	0-40	Fair	Fair	No droplets
		2.74 (108)	2000	4.29	0.41-0.76 (0.016-0.030)	0.54-1.86 (21.2-73.3)	0-24	Good	Good	Very few droplets
32114	3°C (5°F) sub-cooling	0.91 (36)	2500	(a)	0.41-3.56 (0.016-0.140)	0.74-5.12 (29.2-201.6)	18-24	Good	Good	Good for droplet size and velocity
		1.82 (72)	2500	--	--	--	60-66	Poor	Fair	Poor quality
		2.74 (108)	2500	20.24	0.81-3.05 (0.032-0.120)	3.35-15.28 (132.1-601.7)	20-33	Good	Good	Good for droplet size and velocity
		2.74 (108)	2500	--	--	--	60-70	Fair	Fair	Poor quality

a. Before movie started

APPENDIX C
DATA TABLES AND PLOTS

Appendix C is furnished as a separate volume, Volume 2 of this report.

APPENDIX D
ERROR ANALYSIS

D-1. INSTRUMENTATION ERROR ANALYSIS

The instrumentation error associated with the data from the FLECHT SEASET unblocked bundle test series was derived either from equipment manufacturers' specifications or system calibration data. Component calibrations were performed to verify that the manufacturers' specifications were met, and these manufacturers' specifications were used to compute the error estimate for the data path. System calibrations were performed when component calibrations were not expedient or when an accuracy improvement could be accomplished with a system calibration. The system calibration data were used to compute an estimate of error for the system response, and calibration standard equipment specifications were used to compute the error of the calibration data points. The total system error from a system calibration is a function of both system response error and calibration data error.

In all cases of error estimate, the standard deviation has been computed and presented as the most probable error. The derivation of this error analysis is presented in paragraph D-7. The manufacturer-specified error is the maximum possible error. The standard deviation of the error is calculated from the maximum error by the following:[1]

$$\rho^2 = \sum_{i=1}^{n} \left(\frac{E_i^2}{3} \right)$$

where

ρ = data path standard deviation

E_i = component i maximum error

n = number of sources of error

1. Based on a uniform distribution over the error range

When a system calibration was performed, the standard deviation from the calibration data and that from the calibration equipment were combined by the following equation to produce the best estimate of error:

$$\rho = \sqrt{E_d^{\,2} + E_c^{\,2}}$$

where

E_d = calibration data standard deviation
E_c = calibration equipment standard deviation

The calibration data standard deviation is a measure of the error involved in fitting the calibration data. That is,

$$E_d = \left[\frac{\sum_{i=1}^{n} (Y_i - Y_f)^2}{n - 2} \right]^{1/2}$$

where

Y_i = calibration point
Y_f = predicted output from the calibration curve
n = number of calibration points

The calibration equipment standard deviation is a measure of the absolute error of the calibration point. This error can be computed using the method described in paragraph D-7. If the calibration point in the above equation is calculated from an equation of the form

$$Y = x_1 \cdot x_2 \cdot x_3$$

then

$$\left(\frac{\sigma_y}{y}\right)^2 = \sum_{i=1}^{n} \left(\frac{\sigma_{x_i}}{x_i}\right)^2$$

and

$$E_c = \sqrt{\sigma_y^2}$$

The standard deviation of best estimate of error is presented in table D-1 because it is statistically the most practical estimate of error. The standard deviations from all sources of error are combined in paragraph D-8 to get the confidence interval on the FLECHT SEASET heat transfer coefficient. The maximum possible error is also presented in table D-1. This is the sum of all the possible component errors and is the outer bound of error.

Table D-1 is a detailed listing of the errors by data channel and run number. To apply the information in table D-1 to the recorded data, an explanation of the analysis is necessary.

The data path has been broken down into three parts called sensor, conditioner, and readout. The sensor is the device whose electrical output is proportional to a physical quantity (temperature, pressure, flow, power). The conditioner is a device which matches the electrical output of the sensor to the input requirements of the readout device. The readout device measures and records the electrical value of the signal from the conditioner. This recorded electrical value is subsequently used to compute the physical quantity it represents. The errors due to the transmission wires between the elements were not included in this analysis; transmission wire errors are very small ($\pm$0.001 percent) in comparison to the element errors and are considered negligible.

The error values listed for sensor, conditioning, and readout are the manufacturers' specifications in engineering units. These numbers were used to compute the most probable and maximum error, as previously described. Where system calibrations were performed, the equipment calibration data list the standard deviation and maximum error as computed from the calibration data points in fitting the points to a first-order polynomial. The calibration point standard deviation was computed using the method described above. The calibration point maximum error was computed from the calibration equation by assuming that the maximum error occurs simultaneously in each component of the calibration equation.

The overall system standard deviation was calculated using the method described earlier for combining standard deviations.

Details of the instrumentation error analysis are given in the following paragraphs.

D-2. Temperature

Channels 1 through 221 were analyzed for temperature measurement error using type K thermocouples for sensing, a 65°C (150°F) reference junction for signal conditioning, and the computer for readout. The maximum values from the manufacturers' specifications are percentages of full-scale output of the unit. This gives a constant value of error which is independent of the magnitude of the data point recorded during a test run. The only exception to this rule in this analysis is type K thermocouples for temperatures from 277°C to 1316°C (530°F to 2400°F). In this range of temperatures, the error is a percentage of the magnitude of the temperature. Table D-1 has values for temperatures from -17.8°C to 277°C (0°F to 530°F). Table D-1 provides equations for computing the most probable error for values between 277°C and 1316°C (530°F and 2400°F). Additional steam probe errors are identified in paragraph D-10.

D-3. Power

Channels 222 through 227 provided bundle power readings. A system calibration was chosen for these channels to assess the system response under actual test conditions. Bundle power was phase-fired SCR controlled; this method produces a large amount of electrical noise that can affect the data path. A bench calibration will not account for the system interaction that a system calibration can provide. Three separate calibrations were performed on the power recording systems during the test series, and the combined data from all three were used to compute the equipment calibration data most probable and maximum errors. The calibration standard values were derived from the calibration equipment component errors using the same technique as for equipment data path errors. The system results were derived from the system calibration data and the calibration equipment error estimates.

TABLE D-1

INSTRUMENTATION ERRORS

Channel[a]	Run No.[b]	Sensor		Conditioner	Readout	Data Path Error		Equipment Response		Calibration Data		System Results	
		Type	Error	Error	Error	Most Probable	Maximum	Most Probable	Maximum	Most Probable	Maximum	Most Probable	Maximum
1-201	30123-37170	Heater rod and steam probe thermocouples	±1°C (±2°F) at -17.8°C-277°C (0°F-530°F) ±0.375% at 277°C-1316°C (530°F-2400°F)	±1.01°C(±1.82°F)	±2.03°C(±3.66°F)	±1.46°C(±2.63°F)	±4.16°C(±7.48°F)						
202-207	30123-37170	Thimble thermocouples	±1°C(±2°F) at -17.8°C-277°C (0°F-530°F) ±0.375% at 277°C-1316°C (530°F-2400°F)	±1.01°C(±1.82°F)	±2.03°C(±3.66°F)	±1.46°C(±2.63°F)	±4.16°C(±7.48°F)						
204	Out of service												
208-221	30123-37170	Loop thermocouple	±2°C(±4°F) at -17.8°C-277°C (0°F-530°F) 0.75% at 277°C-1316°C (530°F-2400°F) Use ±10°C(±18°F) maximum	±0.3°C(±0.5°F)	±2.03°C(±3.66°F)	±1.74°C(±3.14°F) ±5.89°C(±10.61°F)	4.53°C(8.16°F) ±12.3°C (±22.2°F)						

a. Refer to table 3-1 for identification of channels and functions.

b. All of these run numbers were applicable to these sensors, even though certain tests did not require certain transducers.

TABLE D-1 (cont)

INSTRUMENTATION ERRORS

Channel[a]	Run No.[b]	Sensor		Conditioner	Readout	Data Path Error		Equipment Response		Calibration Data		System Results	
		Type	Error	Error	Error	Most Probable	Maximum	Most Probable	Maximum	Most Probable	Maximum	Most Probable	Maximum
222	30123-37170	Power measurement						±1.12 kw	±2.43 kw	±2.13 kw	±3.9 kw	±2.41 kw	±6.30 kw
223	30123-37170	Power measurement						±0.15 kw	±0.25 kw	±2.13 kw	±3.9 kw	±2.14 kw	±4.15 kw
224	30123-37170	Power measurement						±2.48 kw	±4.58 kw	±2.13 kw	±3.9 kw	±3.27 kw	±8.57 kw
225	30123-37170	Power measurement						±0.29 kw	±1.11 kw	±2.13 kw	±3.9 kw	±2.15 kw	±5.10 kw
226	30123-37170	Power measurement						±2.19 kw	±3.96 kw	±2.13 kw	±3.9 kw	±3.05 kw	±7.92 kw
227	30123-37170	Power measurement						±0.7 kw	±3.7 kw	±2.13 kw	±3.9 kw	±2.24 kw	±7.66 kw
228	30123-32333	Turbine meter	±0.515x10^{-6} m^3/sec (±0.0817 gal/min)	±5.5x10^{-5} m^3/sec (±0.87 gal/min)	±5.4x10^{-6} m^3/sec (±0.086 gal/min)	±5.54x10^{-5} m^3/sec (±0.878 gal/min)	±6.549x10^{-5} m^3/sec (±1.038 gal/min)						
229	33544-36026	Low-flow rotameter						±5.2x10^{-6} m^3/sec (±0.082 gal/min)	±1.38x10^{-5} m^3/sec (±0.218 gal/min)	±2.0x10^{-6} m^3/sec (±0.031 gal/min)	±3.3x10^{-6} m^3/sec (0.053 gal/min)		
230	33338-33436	Medium-flow rotameter						±1.07x10^{-4} m^3/sec (±1.69 gal/min)	±1.23x10^{-4} m^3/sec (±1.95 gal/min)	3.05x10^{-5} m^3/sec (±0.484 gal/min)	±5.29x10^{-5} m^3/sec (0.838 gal/min)		
231		High-flow rotameter						±1.86x10^{-5} m^3/sec (±0.295 gal/min)	5.05x10^{-5} m^3/sec (±0.800 gal/min)	±4.0x10^{-6} m^3/sec (±0.063 gal/min)	±6.88x10^{-6} m^3/sec (±0.109 gal/min)		
232	33338-33436	Turbo-probe	±7.70x10^{-5} m^3/sec (±1.22 gal/min)	±1.63x10^{-4} m^3/sec (±2.58 gal/min)	±1.53x10^{-5} m^3/sec (±0.242 gal/min)	±1.34x10^{-4} m^3/sec (±2.12 gal/min)	±2.87x10^{-4} m^3/sec (±4.55 gal/min)						

TABLE D-1 (cont)

INSTRUMENTATION ERRORS

Channel[a]	Run No.[b]	Sensor		Conditioner	Readout	Data Path Error		Equipment Response		Calibration Data		System Results	
		Type	Error	Error	Error	Most Probable	Maximum	Most Probable	Maximum	Most Probable	Maximum	Most Probable	Maximum
233-244	30123-37170	D/P cell	±6.9 kPa (±1.0 psid)	±0.03 kPa (±0.005 psid)	±0.026 kPa (±0.0038 psid)	±0.047 kPa (±0.0068 psid)	±0.130 kPa (±0.0188 psid)						
245	30123-37170	D/P cell	±69.0 kPa (±10.0 psid)	±0.34 kPa (±0.05 psid)	±0.36 kPa (±0.053 psid)	±0.66 kPa (±0.096 psid)	±1.74 kPa (±0.253 psid)						
246	30123-37170	D/P cell	±6.9 kPa (±1.0 psid)	±0.03 kPa (±0.005 psid)	±0.026 kPa (±0.0068 psid)	±0.047 kPa (±0.0068 psid)	±0.130 kPa (±0.0188 psid)						
248	30123-37170	D/P cell	±69.0 kPa (±10.0 psid)	±0.34 kPa (±0.05 psid)	±0.36 kPa (±0.053 psid)	±0.66 kPa (±0.096 psid)	±1.74 kPa (±0.253 psid)						
249	30123-37170	D/P cell	±17 kPa (±2.5 psid)	±0.17 kPa (±0.025 psid)	±0.19 kPa (±0.027 psid)	±0.33 kPa (0.048 psid)	±0.876 kPa (±0.127 psid)						
250	30123-37170	D/P cell	±69.0 kPa (±10.0 psid)	±0.34 kPa (±0.05 psid)	±0.36 kPa (±0.053 psid)	±0.66 kPa (±0.096 psid)	±1.74 kPa (0.253 psid)						
251	30123-37170	D/P cell	±69.0/±34.5 kPa (±10.0/±5.0 psid)	±0.34/±0.17 kPa (±0.05/±0.025 psid)	±0.36/±0.19 kPa (±0.053/±0.027 psid)	±0.66/±0.33 kPa (±0.096/0.048 psid)	±1.74/±0.876 kPa (±0.253/±0.127 psid)						
252, 253	30123-37170	D/P cell	0.101-1.14 MPa (0-150 psig)	±2.59 kPa (±0.375 psid)	±2.70 kPa (±0.391 psid)	±2.63 kPa (±0.381 psid)	±7.874 kPa (±1.142 psid)						
254, 255	30123-37170	D/P cell	±69.0 kPa (±10.0 psid)	±0.34 kPa (±0.05 psid)	±0.36 kPa ±0.053 psid)	±0.66 kPa (±0.096 psid)	±1.74 kPa (±0.253 psid)						
256	30123-37170	D/P cell	±0.172 MPa (±25.0 psid)	±5.2 kPa (±0.75 psid)	±1.00 kPa (±0.145 psid)	±6.6 kPa (±0.96 psid)	±17 kPa (±2.5 psid)						

D-4. Flow

Channel 228 read data from the injection line turbine meter, whose components were calibrated separately by the manufacturer for most of the test runs. The error changed for different groups of tests because of component calibrations that changed the conversion from electrical to engineering units. Each time a different conversion factor was computed, the error associated with those conversion numbers changed the data path error. A system calibration was performed for a certain group of tests and the respective error was computed using the method for system calibration errors as previously explained (power channels 222 through 227).

Channels 229 through 231 read data from rotameters measuring injection line flow rate. A system calibration was performed and the error estimate made using the same technique as for power channels 222 through 227. Limited-range calibrations were performed for some tests to obtain more accurate data for tests that required specific flow rates. Because the rotameter for channel 230 was not linear over its entire range, a limited-range calibration was performed to minimize the impact of the nonlinearity on the data.

Channel 232 read data from the bidirectional turbo-probe used to measure the downcomer crossover flow rate for gravity reflood tests. The components were similar to those for the turbine meter, channel 228, and the error was estimated using the same technique as for that channel. The component calibrations were performed by the manufacturer, and the actual component calibration data were used to compute the standard deviation for the sensor and signal conditioner. These errors were then combined with the maximum error for the readout to produce the standard deviation for the entire system.

D-5. Pressure

Channels 233 through 256 were the loop pressure channels. The components were calibrated individually and the system error was estimated using the same technique as for thermocouples under 277°C (530°F).

D-6. HEAT TRANSFER COEFFICIENT ERROR ANALYSIS

The purpose of this error analysis was to estimate the confidence limits in the heat transfer coefficients calculated for heater rods in the FLECHT SEASET unblocked bundle test series. This error analysis closely followed the method used in the FLECHT low flooding rate skewed test series, reported in WCAP-9108.[1]

That error analysis used the FLECHT heat transfer coefficient calculated from test data, using DATARH. The sensitivity of the heat transfer coefficient to variations in the test data was also calculated by the code. This code solves an inverse heat conduction problem using a finite-difference technique.

The error analysis used standard statistical treatment of independent error components to establish 1σ and 2σ confidence intervals on the total error in the heat transfer coefficient. Individual error components were obtained from either heater rod inspection data, physical information, or professional experience and judgment. Each component of the total error was assumed to be independent, and of known variance.

The FLECHT SEASET unblocked bundle test series utilized stainless steel clad, boron nitride filled heater rods with coiled Kanthal wire heating elements (figure D-1). In the instrumented heater rods, thermocouples were located at several different axial locations on the inside wall of the cladding. The thermocouple output was used in the DATAR code to compute the heat transfer coefficient. The code input requires density, specific heat, and thermal conductivity for the heater rod materials and geometric details of the heater coil.

The heater rod geometric input included clad inside and outside diameters and thermocouple radial location. Code input from the FLECHT SEASET bundle test instruments included thermocouple temperature, bundle pressure, and SCR power output.

---

1. E. R. Rosal, et al., "FLECHT Low Flooding Rate Skewed Test Series Data Report," WCAP-9108, May 1977.

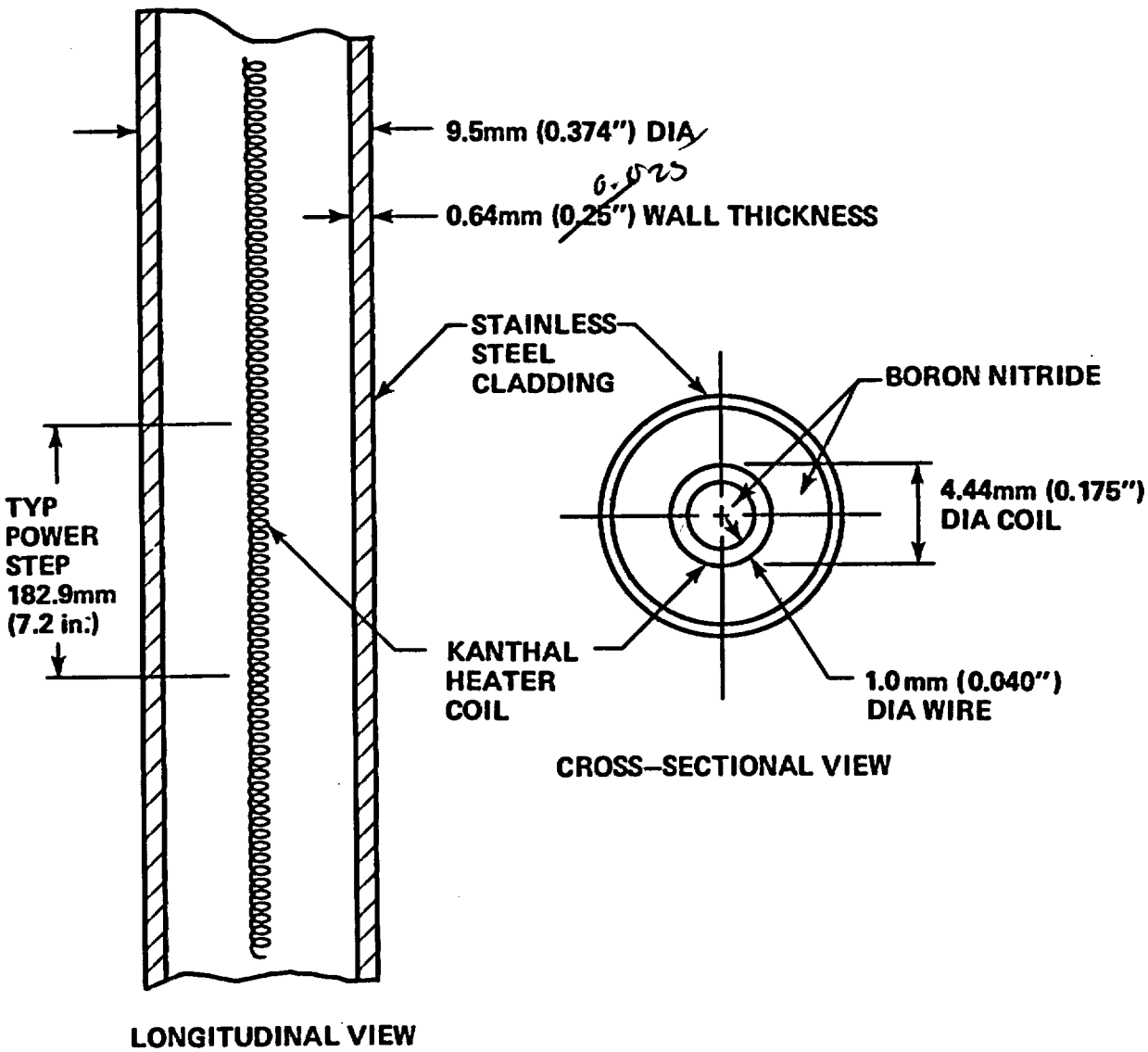

Figure D-1. FLECHT SEASET Heater Rod

D-7. Description of Error Calculation

The heat transfer coefficient may be expressed as

$$h = h\left[x_1, x_2, \ldots x_n\right]$$

where x_i ($i = 1, 2, \ldots n$) are the individual parameters that affect the heat transfer coefficient h. The statistical variation of calculated h about its expected value may be expressed by expanding the function $h\left[x_1, x_2, \ldots x_n\right]$ in a multivariable Taylor series.

Including only first-order terms, the result is

$$h\left[x_1, x_2, \ldots x_n\right] - E\left[h\right] = \sum_{i=1}^{n} \left(\frac{\partial h}{\partial x_i}\right)_{\bar{x}} \left\{x_i - E\left[x_i\right]\right\}$$

or

$$\Delta h = \sum_{i=1}^{n} \left(\frac{\partial h}{\partial x_i}\right)_{\bar{x}} \Delta x_i$$

where the derivatives are evaluated using the means of all the random variables x_i (denoted by $\bar{x}$). $E\left[h\right]$ is the expected or mean value of the function h, that is, h evaluated at the means of the random variables x_i. Each $(\partial h/\partial x_i)_{\bar{x}} \Delta x_i$ term also is a random variable with a mean of zero and a variance given by

$$\mathrm{var}\left(\frac{\partial h}{\partial x_i}\right)_{\bar{x}} \Delta x_i = \left(\frac{\partial h}{\partial x_i}\right)^2_{\bar{x}} \sigma^2_{x_i} = \sigma^2_{\Delta h_i}$$

where $(\partial h/\partial x_i)_{\bar{x}}$ is constant for given $\bar{x}$.

Assuming the $(\partial h/\partial x_i)_x \Delta x_i$ terms are independent, the mean of Δh becomes

$$E\left[\Delta h\right] = \sum_{i=1}^{n} \left(\frac{\partial h}{\partial x_i}\right)_{\bar{x}} \quad E\left[\Delta x_i\right] = 0$$

and the variance of Δh is

$$\sigma^2_{\Delta h} = \sum_{i=1}^{n} \sigma^2_{\Delta h_i} = \sum_{i=1}^{n} \left(\frac{\partial h}{\partial h_i}\right)^2_{\bar{x}} \sigma^2_{x_i}$$

Approximating the $(\partial h/\partial x_i)_x$ term by $(\Delta h_i/\Delta x_i)_x$, the variance becomes

$$\sigma^2_{\Delta h} = \sum_{i=1}^{n} \left(\frac{\Delta h_i}{\Delta x_i}\right)^2_{\bar{x}} \sigma^2_{x_i}$$

A consequence of the central limit theorem in statistics is that the distribution of the error calculated above approaches a normal distribution. With a known distribution function, the confidence interval of the error can be calculated from the variance. The 1σ (70-percent) and 2σ (95-percent) confidence intervals are reported in this evaluation.

These values were obtained by individually perturbing each parameter x_i from its expected value by its estimated standard deviation in numerous runs of the DATAR code. Each perturbation resulted in a new value of calculated h, from which the nominal or expected value was subtracted to provide a Δh_i. Since in these perturbations Δx_i was assumed to be equal to σ_{x_i}, the variance σ^2_h can be evaluated by simply summing the squares of the resultant Δh_i terms:

$$\sigma^2_{\Delta h} = \sum_{i=1}^{n} \Delta h_i^2$$

Positive and negative Δh_i terms (Δh_i^+, Δh_i^-) were obtained by perturbing each x_i both above and below its expected value. They are indicative of the heat transfer coefficient's sensitivity to uncertainty in each parameter, and were statistically combined to provide both upper and lower error bands on calculated h. Differences in the Δh_i^+ and Δh_i^- for each i are due to nonlinearities in the function $h\left[x_1, x_2, \ldots x_n\right]$.

D-8. Description of Parameters

Uncertainty in the heat transfer coefficient, h, calculated by the DATAR code stems from the following factors:

-- Uncertainty in the measured test parameters input to the program

-- Uncertainty due to manufacturing tolerances on heater rod dimensions and instrumentation location

-- Material property uncertainties

Measured test parameters that are input to DATAR are bundle power, pressure, and clad inside temperature.

The error in the measured parameters is combined with other sources of error by summing the variance of each error component. For the test instruments, the instrument error was assumed to be uniformly distributed over the error interval. The variance of a uniformly distributed random variable over the interval $-\alpha < x < \alpha$ is $\alpha^2/3$. The total instrument error consists of error in the sensor, in signal conditioning equipment, and in recording the signal. The variance of each of these components was calculated as described above and summed to get the total variance of the instrument error. Transducer uncertainty is normally dominant, and thus total error and transducer error will be very similar.

The standard deviation (that is, the positive square root of the variance) and maximum error for each data path are shown in table D-1. The maximum error was calculated by summing the maximum error of all contributors to the total instrument error.

Manufacturing tolerances on rod dimensions and instrumentation location also contribute to uncertainty in the calculated heat transfer coefficient h. Heater coil dimensions, clad inside and outside diameters, and thermocouple locations are incorporated in the DATAR geometric heater rod model, because they are possible contributors to uncertainty in h. Uncertainty in thermocouple radial location was estimated from X-ray inspection of actual heater rods. Clad outside diameter uncertainty was obtained from the rod inspection data. Uncertainty in clad inside diameter was estimated by combining the uncertainty in clad outside diameter with the uncertainty in clad thickness.

Axial power is also a factor. In FLECHT SEASET heater rods, the number of heater coil turns per inch (coil spacing) is variable (figure D-1); this changes the length of heater wire per unit length of heater rod. From the X-ray radiographs of the heater rods, the geometry of the axial power steps was determined.

The rod inspection data do not reflect any variation in the diameter of the Kanthal heater wire. The wire diameter was nominally 0.10 cm (0.040 in.), and small variations in diameter were beyond the resolution of the radiograph. To estimate the error due to wire diameter variation, the assumption was made that the local variation in wire resistance due to the wire cross-sectional area variation could be approximated from the variation in heater rod resistance between rods.

Uncertainty in the physical properties of the material in the heater rods was based largely on engineering judgment. The boron nitride density uncertainty was based on a sample of five measurements from sections of heater rods that were destructively analyzed.

The input parameters for power factor ($P_{local}/P_{average}$) determination are local step length, total heated length, local step length coil resistance, and total heated length coil resistance. An analysis identical to that discussed in paragraph D-7 was performed for this calculation, varying the input parameters by the estimated standard deviations. Estimated power factor parameter errors are shown in table D-2, and the power factor uncertainty analysis in table D-3.

TABLE D-2

ESTIMATED UNCERTAINTY OF POWER FACTOR CALCULATION

Parameter	Estimated Uncertainty[a]	Best-Estimated Value	Reference/ Comments
Step length	±0.06 in.	14..52 in.	Rod inspection data
Step resistance	±0.03%	3.595 Ω	Rod inspection data
Total length	±0.06 in.	144.48 in.	Rod inspection data
Total resistance	±0.03%	21.60 Ω	Rod inspection data

a. All uncertainties are listed at the 1 σ level.

TABLE D-3

THERMOCOUPLE POWER FACTOR UNCERTAINTY ANALYSIS

Parameter	Calculated P/P_{avg} (a)	$\Delta(P/P_{avg})^{+}$ (b)	$\Delta(P/P_{avg})^{-}$
Nominal case	1.6561		
Step length + 0.06 in.	1.6493		-0.0068
Step length - 0.06 in.	1.6630	0.0069	
Step resistance + 0.03%	1.6566	0.0005	
Step resistance - 0.03%	1.6556		-0.0005
Total length + 0.06 in.	1.6568	0.0007	
Total length - 0.06 in.	1.6554		-0.0007
Total resistance + 0.03%	1.6556		-0.0005
Total resistance - 0.03%	1.6566	0.0005	

Using values for $\Delta(P/P_{avg})^{+}$:

$$\sigma_{P/P_{avg}} = (0.0069^2 + 0.0005^2 + 0.0007^2 + 0.0005^2)^{1/2} = 0.0070 \text{ (absolute)}$$
$$= 0.42 \text{ (\%)}$$

Using values for $\Delta(P/P_{avg})^{-}$:

$$\sigma_{P/P_{avg}} = (0.0068^2 + 0.0005^2 + 0.0007^2 + 0.0005^2)^{1/2} = 0.0069 \text{ (absolute)}$$
$$= 0.42 \text{ (\%)}$$

a. $\frac{P}{P_{avg}} = \left(\frac{\text{step resistance}}{\text{step length}}\right) \left(\frac{\text{total length}}{\text{total resistance}}\right)$

b. $\Delta(P/P_{avg}) = P/P_{avg} - (P/P_{avg})_{nominal}$

Table D-4 summarizes the uncertainties of all the parameters used by DATAR to calculate the FLECHT SEASET heat transfer coefficient. These uncertainties were evaluated at the 1σ level. The uncertainties in table D-4 for the heater rod material properties are the same uncertainties used in the low flooding rate skewed test series data report (WCAP-9108); no better information is available.

Other sources of error that could lead to increased uncertainty in the value of h were reviewed; however, for the most part, they were of relatively minor importance and their absence in this analysis would not be significant. Those other factors were as follows:

- Induction and skin effects - These effects of high-frequency components of the chopped ac power were neglected.

- Wire effective length - Analytically, the effective length for a tightly coiled wire is less than the length based on the helix mean radius (which is used in DATAR). However, this source of error is the same for each wire and will cancel out in the relative power calculation. Therefore, such a correction was not required.

- Electrical resistivity variation with temperature at rod quench - Changes in rod temperature distribution will affect the local P/P_{avg}. For example, if half the rod is quenched, resistivity in the upper half could be as much as 4 percent greater than that in the lower half, and power would be redistributed within the rod. Since there was no method by which this could be accounted for proportionately, this effect was ignored.

- Kanthal heater helix position - The heater coil may be slightly off center in the rod. This effect was analyzed by varying the coil diameter; however, no coil displacement was examined.

- Thermocouple axial location - The thermocouples were located well within a given power step. Axial conduction in the heater rod in the vicinity of the thermocouples was assumed to be small and axial conduction effects were ignored.

TABLE D-4

ESTIMATED UNCERTAINTY OF PARAMETERS AFFECTING CALCULATED HEAT TRANSFER COEFFICIENT

Parameter	Estimated Uncertainty(σ)[a]	Reference/Comments
Measured power	$\pm$2.14 kw	Table D-1, channel 222
Measured temperature	At T < 277°C (530°F), $\pm$ 1.39°C ($\pm$ 2.51°F) At 277°C< T < 1316°C (530°F< T < 2400°F), $\pm [1.539 + (0.00217T)^2]^{1/2}$ °C $\{\pm [4.986 + (0.00217T)^2]^{1/2}$ °F$\}$	Table D-1 $\sigma^2_{temp} = 1/3\ (\sigma^2_{sensor} + \sigma^2_{cond} + \sigma^2_{readout}$
Measured pressure	$\pm$ 2.66 kPa ($\pm$ 0.386 psi)	Table D-1, channel 251
Thermocouple radial location	-0.05 mm (-0.002 in.)	X-ray inspection data. T/C location assumed at clad inside surface. Radial position can only be in boron nitride; thus there is only negative uncertainty.
Rod OD	$\pm$ 0.012 mm ($\pm$ 0.00049 in.)	Heater rod inspection data
Clad ID	$\pm$ 0.012 mm ($\pm$ 0.00049 in.)	Estimate based on rod OD and clad thickness inspection data

a. All errors or uncertainties are listed at the 1σ level.

TABLE D-4 (cont)

ESTIMATED UNCERTAINTY OF PARAMETERS AFFECTING CALCULATED HEAT TRANSFER COEFFICIENT

Parameter	Estimated Uncertainty(σ)[a]	Reference/Comments
Power step factor	$\pm$0.42%	Table D-3
Boron nitride properties		
Density	$\pm$3%	Heater rod inspection data
Thermal conductivity	$\pm$10%	Watlow Electric estimate
Specific heat	$\pm$5%	Touloukian,[b] engineering judgment
Kanthal properties		
Density	$\pm$2%	Engineering estimate
Thermal conductivity	$\pm$5%	Engineering estimate
Specific heat	$\pm$5%	Engineering estimate
Stainless steel 347 properties		
Density	$\pm$1%	Touloukian,[b] engineering judgment
Thermal conductivity	$\pm$3%	
Specific heat	$\pm$3%	

a. All errors or uncertainties are listed at the 1σ level.

b. Touloukian, Y. S., Thermophysical Properties of High Temperature Solid Materials, Macmillan, New York, 1967.

D-9. Results and Discussion

The error analysis was performed for test 31504 with the following nominal initial conditions:

-- Pressure	0.28 MPa (40 psia)
-- Initial clad temperature	871°C (1600°F)
-- Rod peak power	2.3 kw/m (0.7 kw/ft)
-- Flooding rate	25 mm/sec (1.0 in./sec)
-- ΔT subcooling	60°C (140°F)
-- Radial power distribution	Uniform
-- Housing temperature	T_{sat}

The analysis was performed on the heat transfer coefficient calculated for the hot rod 8K at the 1.98 m (78 in.) elevation. The calculated value of the heat transfer coefficient from rod 8K was obtained with the best-estimate values of all the parameters in table D-4. Both positive and negative values of Δh_i were obtained from subsequent DATAR calculations for which the parameters given in table D-4 were varied. The calculated positive and negative values of Δh_i are listed in table D-5 as a function of time. They are indicative of the heat transfer coefficient sensitivity for each parameter. The various values of Δh_i^+ and Δh_i^- are statistically combined in table D-6 and the resulting calculated h values with the estimated 95-percent confidence bands (2σ) are shown in table D-7.

Examination of the Δh_i values in table D-5 shows that the measured power, rod outside diameter, clad thickness, and power step factor had the largest effects on the calculated heat transfer coefficient. Other parameters such as the rod properties (except the boron nitride density), rod temperature, and system pressure clearly had second-order effects on the accuracy of the calculated heat transfer.

The method used in this analysis presupposes that the process is linear; higher-order terms in the Taylor series expansion [equation (D-1)] were neglected. If the method is linear, then the Δh_i values would be of equal magnitude but opposite sign. However, as the Δh_i values listed in table D-5 indicate, the inverse conduction scheme is not

TABLE D-5
PARAMETER SENSITIVITIES[a]

Time (sec)	Base Case	Measured Power ±2.14		Measured Temperature		Measured Pressure		Thermocouple Radial Location		Rod OD	
		Δh_1^+	Δh_1^-	Δh_2^+	Δh_2^-	Δh_3^+	Δh_3^-	Δh_4^+	Δh_4^-	Δh_5^+	Δh_5^-
0	1.3773	0.1603	-0.1602	0.0424	-0.0415	0.0007	-0.0006	0.0000	-0.0201	0.0594	-0.0592
1	0.9133	0.1585	-0.1584	0.0380	-0.0372	0.0004	-0.0004	0.0000	-0.0105	0.0585	-0.0584
2	1.0165	0.1568	-0.1568	0.0376	-0.0368	0.0005	-0.0005	0.0000	-0.0087	0.0575	-0.0574
3	1.1095	0.1553	-0.1553	0.0373	-0.0367	0.0005	-0.0006	0.0000	-0.0093	0.0567	-0.0567
4	1.2058	0.1538	-0.1537	0.0406	-0.0428	0.0006	-0.0005	0.0000	-0.0101	0.0561	-0.0559
5	1.1835	0.1523	-0.1522	0.0444	-0.0480	0.0006	-0.0005	0.0000	-0.0098	0.0554	-0.0552
10	1.3702	0.1450	-0.1450	0.0615	-0.0633	0.0006	-0.0006	0.0000	-0.0084	0.0516	-0.0515
20	3.5014	0.1340	-0.1339	0.0680	-0.0670	0.0014	-0.0013	0.0000	-0.0024	0.0413	-0.0412
30	4.7009	0.1276	-0.1268	0.0648	-0.0641	0.0017	-0.0018	0.0000	-0.0056	0.0354	-0.0353
40	7.1790	0.1219	-0.1219	0.0667	-0.0659	0.0026	-0.0025	0.0000	-0.0035	0.0278	-0.0277
50	7.1358	0.1183	-0.1182	0.0631	-0.0622	0.0025	-0.0024	0.0000	-0.0048	0.0258	-0.0257
60	8.0461	0.1157	-0.1154	0.0626	-0.0617	0.0028	-0.0026	0.0000	-0.0049	0.0225	-0.0222
70	7.9255	0.1133	-0.1133	0.0600	-0.0592	0.0026	-0.0026	0.0000	-0.0022	0.0209	-0.0209
80	8.0829	0.1116	-0.1115	0.0584	-0.0576	0.0027	-0.0026	0.0000	-0.0058	0.0198	-0.0196
90	8.2738	0.1100	-0.1100	0.0571	-0.0564	0.0027	-0.0027	0.0000	-0.0047	0.0180	-0.0180
100	9.0284	0.1091	-0.1089	0.0576	-0.0567	0.0030	-0.0028	0.0000	-0.0025	0.0156	-0.0154
120	9.9713	0.1085	-0.1084	0.0580	-0.0571	0.0032	-0.0031	0.0000	-0.0034	0.0126	-0.0124
140	10.9637	0.1091	-0.1088	0.0595	-0.0585	0.0036	-0.0034	0.0000	-0.0011	0.0097	-0.0094
160	11.8892	0.1116	-0.1116	0.0622	-0.0615	0.0039	-0.0039	0.0000	-0.0040	0.0080	-0.0080
180	15.2355	0.1165	-0.1164	0.0724	-0.0714	0.0052	-0.0052	0.0000	-0.0010	0.0020	-0.0018
200	15.5146	0.1235	-0.1233	0.0775	-0.0765	0.0057	-0.0055	0.0000	-0.0018	0.0029	-0.0026
220	17.2969	0.1318	-0.1317	0.0875	-0.0876	0.0067	-0.0039	0.0000	-0.0008	0.0009	-0.0008
240	18.8704	0.143	-0.1427	0.1001	-0.0985	0.0080	-0.0078	0.0000	-0.0033	0.0006	-0.0003
260	21.1816	0.1573	-0.1571	0.1400	-0.1378	0.0098	-0.0097	0.0000	-0.0029	0.0005	-0.0002
280	22.9392	0.1755	-0.1751	0.1558	-0.1577	0.0119	-0.0116	0.0006	0.0000	0.0011	-0.0006
300	28.0444	0.2007	-0.2005	0.1576	-0.1546	0.0164	-0.0164	0.0000	-0.0010	0.0038	-0.0036
320	49.1724	0.2500	-0.2500	0.3565	-0.3495	0.0364	-0.0366	0.1164	0.0000	0.0516	-0.0515
325	812.0703	2.3737	-2.3609	26.5086	-22.8027	7.4468	-7.2825	6.3471	0.0000	3.6697	-3.6360

a. $\Delta h_i = \left(\frac{\partial h}{\partial x_i}\right)_{\bar{x}} \sigma_{x_i}$

b. Values of h are given in Btu/hr-ft^2-^{o}F. To convert to w/m^2-^{o}C, multiply by 5.678.

TABLE D-5 (cont)

PARAMETER SENSITIVITIES[a]

Time (sec)	Clad ID		Power Step Factor Axial Power		Boron Nitride Density		Boron Nitride Specific Heat		Boron Nitride Thermal Conductivity		Kanthal Density	
	Δh_6^+	Δh_6^-	Δh_7^+	Δh_7^-	Δh_8^+	Δh_8^-	Δh_9^+	Δh_9^-	Δh_{10}^+	Δh_{10}^-	Δh_{11}^+	Δh_{11}^-
0	0.0138	-0.0137	0.0810	-0.0842	0.3231	-0.3228	0.5440	-0.5436	0.0128	-0.0112	0.0389	-0.0380
1	0.0127	-0.0126	0.0798	-0.0830	0.3359	-0.3295	0.5550	-0.5547	0.0064	-0.0052	0.0390	-0.0382
2	0.0122	-0.0122	0.0786	-0.0818	0.3240	-0.3239	0.5456	-0.5454	0.0048	-0.0039	0.0373	-0.0364
3	0.0121	-0.0122	0.0774	-0.0807	0.3182	-0.3182	0.5358	-0.5358	0.0050	-0.0042	0.0354	-0.0347
4	0.0121	-0.0120	0.0763	-0.0794	0.3123	-0.3122	0.5258	-0.5256	0.0051	-0.0041	0.0337	-0.0329
5	0.0120	-0.0119	0.0752	-0.0782	0.3084	-0.3083	0.5192	-0.5191	0.0044	-0.0036	0.0326	-0.0318
10	0.0111	-0.0111	0.0699	-0.0727	0.2840	-0.2840	0.4782	-0.4782	0.0017	-0.0013	0.0274	-0.0268
20	0.0079	-0.0078	0.0619	-0.0644	0.2114	-0.2114	0.3559	-0.3560	0.0033	-0.0040	0.0204	-0.0199
30	0.0066	-0.0067	0.0566	-0.0590	0.1647	-0.1648	0.2774	-0.2774	0.0009	-0.0007	0.0156	-0.0153
40	0.0040	-0.0040	0.0530	-0.0552	0.1044	-0.1044	0.1757	-0.1757	0.0007	-0.0008	0.0100	-0.0098
50	0.0038	-0.0037	0.0501	-0.0521	0.0918	-0.0918	0.1546	-0.1545	0.0006	-0.0004	0.0088	-0.0085
60	0.0029	-0.0027	0.0481	-0.0498	0.0657	-0.0654	0.1105	-0.1103	0.0018	-0.0012	0.0063	-0.0060
70	0.0022	-0.0022	0.0461	-0.0480	0.0602	-0.0602	0.1013	-0.1014	0.0007	-0.0007	0.0059	-0.0057
80	0.0023	-0.0022	0.0445	-0.0462	0.0491	-0.0490	0.0827	-0.0825	0.0029	-0.0023	0.0046	-0.0044
90	0.0017	-0.0017	0.0430	-0.0447	0.0395	-0.0395	0.0666	-0.0665	0.0017	-0.0014	0.0038	-0.0036
100	0.0007	-0.0005	0.0420	-0.0435	0.0217	-0.0215	0.0364	-0.0363	0.0002	0.0000	0.0022	-0.0020
120	0.0004	-0.0003	0.0404	-0.0419	0.0028	-0.0026	0.0046	-0.0045	0.0016	-0.0012	0.0003	-0.0001
140	0.0018	-0.0015	0.0395	-0.0408	0.0243	-0.0241	0.0408	-0.0406	0.0004	0.0000	0.0023	-0.0020
160	0.0020	-0.0020	0.0393	-0.0409	0.0418	-0.0418	0.0704	-0.0704	0.0030	-0.0026	0.0039	-0.0040
180	0.0049	-0.0048	0.0402	-0.0372	0.0982	-0.0981	0.1652	-0.1652	0.0013	-0.0011	0.0090	-0.0091
200	0.0047	-0.0044	0.0418	-0.0433	0.0973	-0.0971	0.1638	-0.1635	0.0038	-0.0028	0.0091	-0.0091
220	0.0056	-0.0055	0.0436	-0.0453	0.1210	-0.1209	0.2036	-0.2036	0.0017	-0.0014	0.0112	-0.0113
240	0.0059	-0.0056	0.0466	-0.0482	0.1382	-0.1379	0.2325	-0.2322	0.0051	-0.0040	0.0130	-0.0130
260	0.0066	-0.0065	0.0504	-0.0523	0.1618	-0.1616	0.2724	-0.2721	0.0044	-0.0035	0.0174	-0.0176
280	0.0074	-0.0070	0.0554	-0.0573	0.1660	-0.1656	0.2794	-0.2790	0.0025	-0.0017	0.0238	-0.0240
300	0.0095	-0.0094	0.0624	-0.0648	0.2317	-0.2315	0.3901	-0.3899	0.0142	-0.0116	0.0288	-0.0292
320	0.0457	-0.0457	0.0765	-0.0797	0.5322	-0.5330	0.8957	-0.8979	0.0619	-0.0694	0.0464	-0.0475
325	2.3341	-2.3172	0.7236	-0.7473	22.1188	-21.5054	37.6067	-35.8766	24.5470	-16.6868	2.7891	-2.8425

TABLE D-5 (cont)

PARAMETER SENSITIVITIES[a]

Time (sec)	Kanthal Thermal Conductivity		Kanthal Specific Heat		Stainless Steel Density		Stainless Steel Thermal Conductivity		Stainless Steel Specific Heat	
	Δh_{12}^{+}	Δh_{12}^{-}	Δh_{13}^{+}	Δh_{13}^{-}	Δh_{14}^{+}	Δh_{14}^{-}	Δh_{15}^{+}	Δh_{15}^{-}	Δh_{16}^{+}	Δh_{16}^{-}
0	0.0006	-0.0004	0.0975	-0.0974	0.0541	-0.0540	0.0006	-0.0006	0.1635	-0.1634
1	0.0004	-0.0003	0.0978	-0.0979	0.0541	-0.0541	0.0001	0.0000	0.1635	-0.1634
2	0.0004	-0.0003	0.0934	-0.0934	0.0530	-0.0530	0.0002	-0.0001	0.1602	-0.1602
3	0.0000	-0.0003	0.0887	-0.0888	0.0521	-0.0522	0.0001	-0.0001	0.1576	-0.1577
4	0.0004	-0.0003	0.0844	-0.0844	0.0514	-0.0513	0.0000	0.0000	0.1552	-0.1552
5	0.0003	-0.0002	0.0816	-0.0815	0.0508	-0.0507	0.0000	0.0000	0.1535	-0.1534
10	0.0002	-0.0001	0.0687	-0.0687	0.0470	-0.0469	0.0001	0.0000	0.1419	-0.1418
20	0.0001	0.0000	0.0510	-0.0510	0.0348	-0.0347	0.0003	-0.0003	0.1049	-0.1049
30	0.0000	-0.0001	0.0395	-0.0393	0.0276	-0.0276	0.0002	-0.0001	0.0834	-0.0834
40	0.0000	0.0000	0.0251	-0.0251	0.0174	-0.0174	0.0003	-0.0002	0.0526	-0.0525
50	0.0001	0.0000	0.0219	-0.0219	0.0156	-0.0155	0.0002	-0.0001	0.0469	-0.0469
60	0.0002	0.0000	0.0157	-0.0155	0.0113	-0.0111	0.0002	-0.0001	0.0339	-0.0337
70	0.0000	0.0000	0.0146	-0.0146	0.0100	-0.0100	0.0003	-0.0003	0.0302	-0.0302
80	0.0002	0.0000	0.0116	-0.0114	0.0086	-0.0085	0.0002	0.0000	0.0259	-0.0258
90	0.0001	0.0000	0.0094	-0.0094	0.0068	-0.0068	0.0002	-0.0001	0.0206	-0.0206
100	0.0001	0.0000	0.0055	-0.0052	0.0036	-0.0034	0.0003	-0.0002	0.0108	-0.0105
120	0.0001	0.0000	0.0006	-0.0005	0.0006	-0.0005	0.0003	-0.0002	0.0017	-0.0015
140	0.0002	0.0000	0.0056	-0.0053	0.0046	-0.0043	0.0005	-0.0003	0.0136	-0.0133
160	0.0001	-0.0001	0.0100	-0.0100	0.0071	-0.0071	0.0003	-0.0002	0.0215	-0.0215
180	0.0001	0.0000	0.0231	-0.0230	0.0170	-0.0169	0.0007	-0.0005	0.0512	-0.0511
200	0.0002	0.0000	0.0232	-0.0229	0.0166	-0.0164	0.0007	-0.0006	0.0499	-0.0497
220	0.0001	0.0000	0.0285	-0.0284	0.0205	-0.0204	0.0009	-0.0007	0.0618	-0.0617
240	0.0002	0.0000	0.0332	-0.0329	0.0229	-0.0226	0.0009	-0.0006	0.0688	-0.0686
260	0.0001	0.0000	0.0444	-0.0442	0.0264	-0.0262	0.0012	-0.0010	0.0796	-0.0814
280	0.0003	0.0000	0.0608	-0.0604	0.0274	-0.0270	0.0018	-0.0014	0.0824	-0.0820
300	0.0005	-0.0003	0.0736	-0.0734	0.0377	-0.0375	0.0027	-0.0025	0.1136	-0.1135
320	0.0022	-0.0023	0.1188	-0.1191	0.1024	-0.1024	0.0260	-0.0244	0.3095	-0.3093
325	0.3265	-0.3061	7.1965	-7.0988	2.1869	-2.1797	8.3582	-7.6746	6.6077	-6.5858

TABLE D-6

UPPER, LOWER, AND AVERAGE STANDARD DEVIATIONS ON CALCULATED HEAT TRANSFER COEFFICIENTS[a]

Time (sec)	σ_h^+	$2\sigma_h^+$	σ_h	$2\sigma_h^-$	$(\sigma_h)_{avg}$
0	0.6921	1.3842	0.6921	1.3842	0.6921
1	0.7034	1.4068	0.7029	1.4058	0.7031
2	0.6906	1.3812	0.6907	1.3814	0.6906
3	0.6781	1.3562	0.6845	1.3690	0.6813
4	0.6659	1.3318	0.6662	1.3324	0.6660
5	0.6577	1.3154	0.6581	1.3162	0.6579
10	0.6080	1.2160	0.6085	1.2170	0.6082
20	0.4634	0.9268	0.4637	0.9274	0.4635
30	0.3720	0.1384	0.3723	0.1393	0.3721
40	0.2617	0.5234	0.2619	0.5238	0.2618
50	0.2377	0.4754	0.2378	0.4756	0.2377
60	0.1955	0.3910	0.1952	0.3904	0.1953
70	0.1848	0.3696	0.1851	0.3702	0.1849
80	0.1685	0.3370	0.1686	0.3372	0.1685
90	0.1553	0.3106	0.1555	0.3110	0.1554
100	0.1386	0.2772	0.1384	0.2768	0.1385
120	0.1303	0.2606	0.1303	0.2606	0.1303
140	0.1400	0.2800	0.1396	0.2796	0.1398
160	0.1590	0.3180	0.1592	0.3184	0.1591
180	0.2469	0.4938	0.2460	0.4920	0.2464
200	0.2505	0.5010	0.2499	0.4998	0.2502
220	0.2971	0.5942	0.2969	0.5938	0.2970
240	0.3353	0.6706	0.3346	0.6692	0.3349
260	0.3959	0.7918	0.3954	0.7908	0.3956
280	0.4193	0.8386	0.4195	0.8390	0.4194
300	0.5441	1.0882	0.5431	1.0862	0.5436
320	1.2007	2.4014	1.1897	2.3794	1.1952
325	58.0459	116.0198	52.8334	105.6668	55.439

a. $\sigma_h^+ = [\sum_i (\Delta h_i^+)^2]^{1/2}$

$\sigma_h^+ = [\sum_i (\Delta h_i^-)^2]^{1/2}$

$(\sigma_h)_{avg} = \dfrac{\sigma_h^+ + \sigma_h^-}{2}$

TABLE D-7

CALCULATED h AND 95-PERCENT CONFIDENCE LIMITS VERSUS TIME

Time (Sec)	Calculated $h^{(a)}$	Upper 95% Confidence Limit[a] Absolute $(h + 2\sigma_h^+)$	Upper 95% Confidence Limit[a] Percent Error $\left(\frac{2\sigma_h^+}{h} \times 100\right)$	Lower 95% Confident Limit Absolute $(h - 2\sigma_h^-)$	Lower 95% Confident Limit Percent Error $\left(\frac{2\sigma_h^-}{h} \times 100\right)$
0	1.3773	2.7615	100.50	-0.0069	100.50
1	0.9133	2.3201	154.03	-0.4925	153.93
2	1.0165	2.3977	135.88	-0.3649	135.90
3	1.1095	2.4657	122.24	-0.2595	123.39
4	1.2058	2.5376	110.45	-0.1260	110.50
5	1.1835	2.3670	111.14	-0.1309	111.21
10	1.3702	2.5862	88.75	0.1532	88.82
20	3.5014	4.4282	26.47	2.5740	26.49
30	4.7009	4.8393	2.94	4.5616	2.96
40	7.1790	7.7024	7.29	6.6552	7.29
50	7.1358	7.6112	6.50	6.6602	6.66
60	8.0461	8.4371	4.86	7.6557	4.85
70	7.9255	8.2951	4.66	7.5553	4.67
80	8.0829	8.4199	4.17	7.7457	4.17
90	8.2738	8.5844	3.75	7.9628	3.75
100	9.0284	9.3056	3.07	8.7516	3.06
120	9.9713	10.2319	2.61	9.7107	2.61
140	10.9637	11.2437	2.55	10.6841	2.55
160	11.8892	12.2072	2.67	11.5708	2.68
180	15.2355	15.7293	3.24	14.7435	3.23
200	15.5146	16.0156	3.23	15.0148	3.22
220	17.2969	17.8911	3.44	16.7031	3.43
240	18.8704	19.5410	3.55	18.2012	3.54
260	21.1816	21.9734	3.74	20.3908	3.73
280	22.9392	23.7778	3.66	22.1002	3.66
300	28.0440	29.1322	3.88	26.9578	3.87
320	49.1724	51.5738	4.88	46.7930	4.84
325	812.0703	928.0901	14.29	706.4035	13.01

a. Values of h are given in Btu/hr-ft^2-^{o}F. To convert to w/m^2-^{o}C, multiply by 5.678.

a linear equation and Δh_i values can have different magnitudes if the deviation is taken in either the positive or negative direction from the normal value. Therefore, when the upper and lower bands are calculated as in table D-6, these bands will not have the same magnitude. One method of compensating for the effect of nonlinearity is to simply average each deviation, both positive and negative values, and obtain an averaged deviation at each time step. This will result in a centered confidence band about the estimated heat transfer coefficient data. The calculations for this approach are given in table D-8.

Figure D-2, which shows the calculated heat transfer coefficient (h) with the 95-percent confidence limits, indicates that the largest uncertainty in h is early in the transient, particularly at the beginning of reflood. Figure D-3 shows the relative error for the upper 95-percent confidence band as plotted from table D-6; it indicates that the relative error quickly decreased to approximately 10 percent by 30 seconds for this test.

D-10. STEAM PROBE TEMPERATURE MEASUREMENT ERROR ANALYSIS

D-11. Analytical Investigation

As previously discussed (paragraph 3-9), the steam probes utilized in the unblocked bundle employed a design in which two steam temperature measurements were obtained for each thimble tube. To place two steam probes in one thimble, one probe aspirated through the top of the bundle and the other probe aspirated through the bottom of the bundle. The probe design which aspirated through the top of the bundle was used in the cosine test series[1] and the skewed test series.[2] An analysis was performed on the probe design which aspirated through the top of the bundle to determine its sensitivity to flow and temperature conditions. The effect of heat transfer between the vapor and the thimble wall and between the vapor and the shield, as the vapor aspirated into the steam probe, was investigated. If significant heat transfer occurred, then the resulting vapor temperature measurement would not be a true indication of the nonequilibrium vapor temperature in the rod bundle.

1. Rosal, E. R., et al., "FLECHT Low Flooding Rate Cosine Test Series Data Report," WCAP-8651, December 1975.

2. Rosal, E. R., et al., "FLECHT Low Flooding Rate Skewed Test Series Data Report," WCAP-9108, May 1977.

TABLE D-8

CALCULATED h AND 95-PERCENT CONFIDENCE LIMITS VERSUS TIME

USING $(\sigma_h)_{avg}$ VALUES

Time (sec)	Calculated $h^{(a)}$	$(\sigma_h)_{avg}$	$2(\sigma_h)_{avg}$	Upper 95% Confidence Limit $h + 2(\sigma_h)_{avg}$	Lower 95% Confidence Limit $h - 2(\sigma_h)_{avg}$	Percent Error $\frac{2(\sigma_h)_{avg}}{h} \times 100$
0	1.3773	0.6921	1.3842	2.7615	-0.0069	100.5009
1	0.9133	1.4063	2.8126	3.7259	-1.8993	307.9601
2	1.0165	1.3813	2.7626	3.7791	-1.7461	271.7757
3	1.1095	1.3626	2.7252	3.8347	-1.6157	245.6241
4	1.2058	1.3321	2.6642	3.8700	-1.4584	220.9487
5	1.1835	1.3158	2.6316	3.8151	-1.4481	222.3574
10	1.3702	1.2165	2.4330	3.8032	-1.0628	177.5653
20	3.5014	0.9271	1.8542	5.3556	1.6490	52.9560
30	4.7009	0.1389	0.2778	4.9787	4.4231	5.9095
40	7.1790	0.5236	1.0472	8.2262	6.1318	14.5870
50	7.1358	0.4755	0.9510	8.0868	6.1848	13.3271
60	8.0461	0.3907	0.7814	8.8275	7.2647	9.7115
70	7.9255	0.3699	0.7398	8.6653	7.1867	9.3344
80	8.0829	0.3371	0.6742	8.7571	7.4087	8.3410
90	8.2738	0.3108	0.6216	8.8954	7.6522	7.5129
100	9.0284	0.2770	0.5540	9.5824	8.4744	6.1362
120	9.9713	0.2606	0.5212	10.4925	9.4501	5.2270
140	10.9637	0.2798	0.5596	11.5233	10.4041	5.1041
160	11.8892	0.3182	0.6364	12.5256	11.2528	5.3528
180	15.2355	0.4929	0.9858	16.2213	14.2497	6.4704
200	15.5146	0.5004	1.0008	16.5154	14.5138	6.4507
220	17.2969	0.5940	1.1880	18.4849	16.1089	6.8683
240	18.8704	0.6699	1.3398	20.2102	17.5306	7.1000
260	21.1816	0.7913	1.5826	22.7642	19.5990	7.4716
280	22.9392	0.8388	1.6776	24.6168	21.2616	7.3132
300	28.0440	1.0872	2.1744	30.2184	25.8696	7.7535
320	49.1724	2.3904	4.7808	53.9532	44.3916	9.7225
325	812.0703	110.8433	221.6866	1033.7569	590.3837	27.2989

a. Values of h are given in Btu/hr-ft^2-^{o}F. To convert to w/m^2-^{o}C, multiply by 5.678.

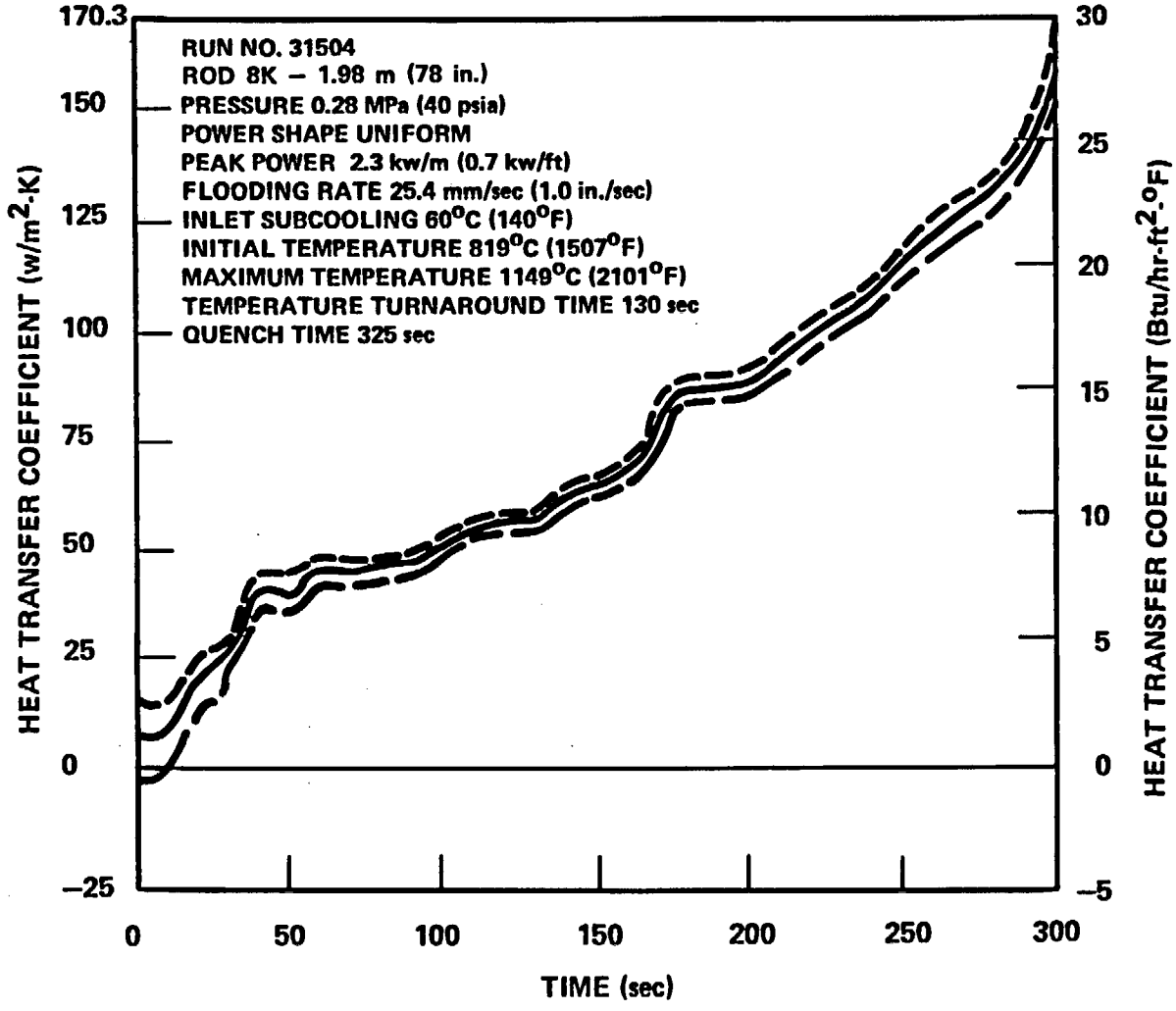

Figure D-2. Rod Heat Transfer Coefficient as a Function of Time (95% Confidence Limits)

16539-38

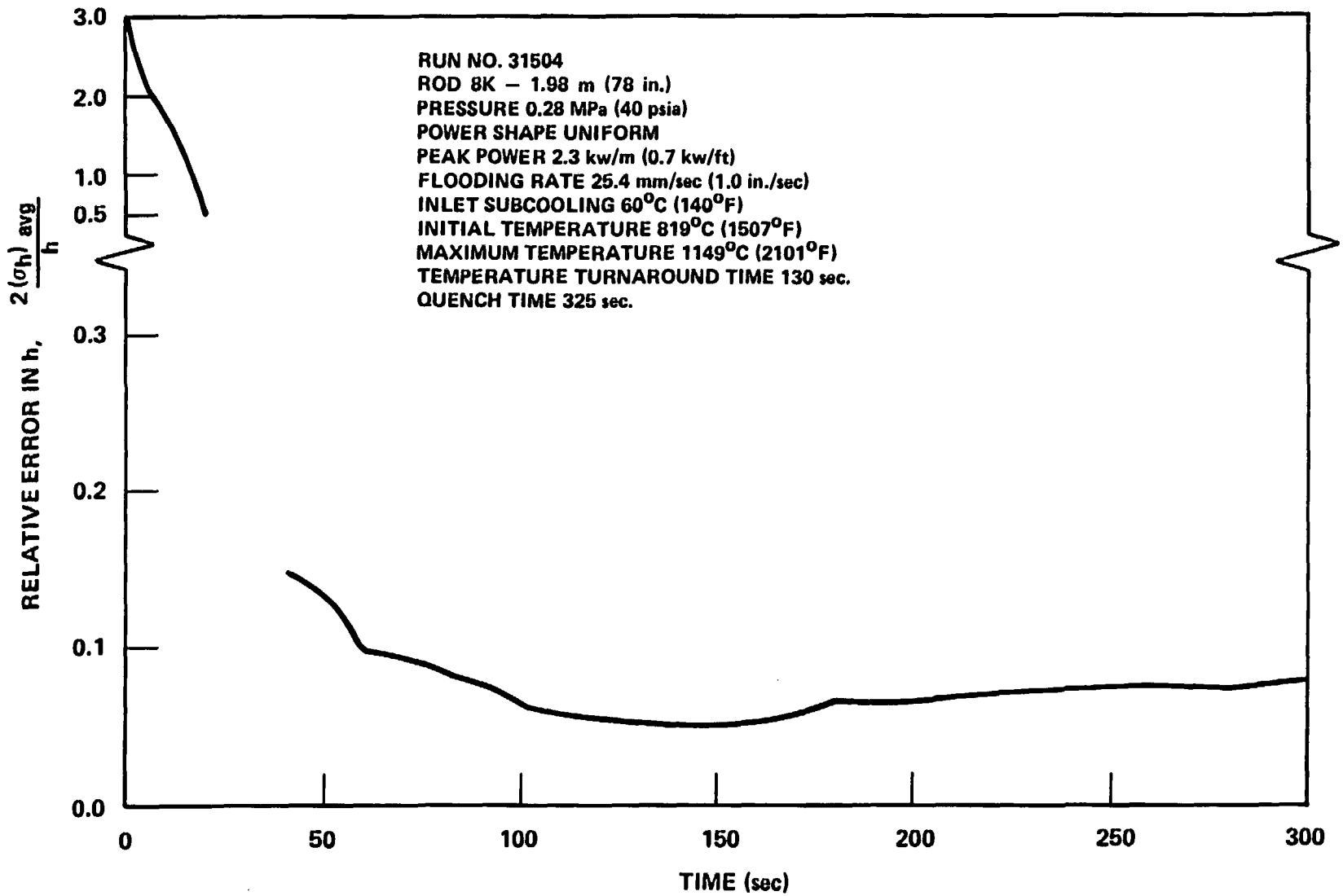

Figure D-3. Relative Error in Heat Transfer Coefficient as a Function of Time

A combined radiation and convection heat transfer model of the top steam probe was developed (figure D-4). A steady-state energy balance was performed on the shield and on the thermocouple. A steady-state calculation was performed, since the low flooding rate FLECHT SEASET tests are essentially quasi-steady-state. The thermocouple temperature, obtained by solving the energy balance equations simultaneously, was compared with the bundle steam temperature. The sensitivity of the convective heat transfer coefficients was also examined in this analysis. The heat transfer utilized for the thimble and shield are presented in table D-10. The results of this analysis are presented in figure D-5. Figure D-5a shows that, for the reference film coefficients, the thermocouple measured an increase of approximately 1 percent in the vapor temperature as the vapor flowed through the probe, based on a 28°C (50°F) temperature difference between the thimble and the steam. The sensitivity of the steam temperature measurement to the film coefficient between the vapor and the thermocouple is shown in figure D-5b to be very small. However, the steam temperature measurement is shown in figure D-5c to be very sensitive to the film coefficient between the thimble wall and vapor.

D-12. Experimental Investigation

The steam probe which aspirated through the bottom of the bundle was of a different design from that of the top steam probe. To provide separation for the water droplets which may be entrained in the steam which flows into the thimble, an additional shield was incorporated within the thimble. A schematic diagram of the top and bottom steam probes is shown in figure D-6, with the corresponding steam flow paths. This figure shows that the flow paths for the two probes are significantly different. It is believed that the more torturous flow path in the bottom probe caused significant steam desuperheating.

A comparison of the steam temperatures in figures D-7, D-8, D-9, and D-10 for runs 31203, 31504, 31805, and 34103, respectively, measured by a top steam probe and a bottom steam probe at approximately the same elevations, 1.83 m (72 in.) and 1.70 m (67 in.), respectively, shows this steam desuperheating effect. The two steam probes measured approximately the same steam temperature in the early part of the test. Also shown is the upper plenum fluid temperature, which indicates that at the time

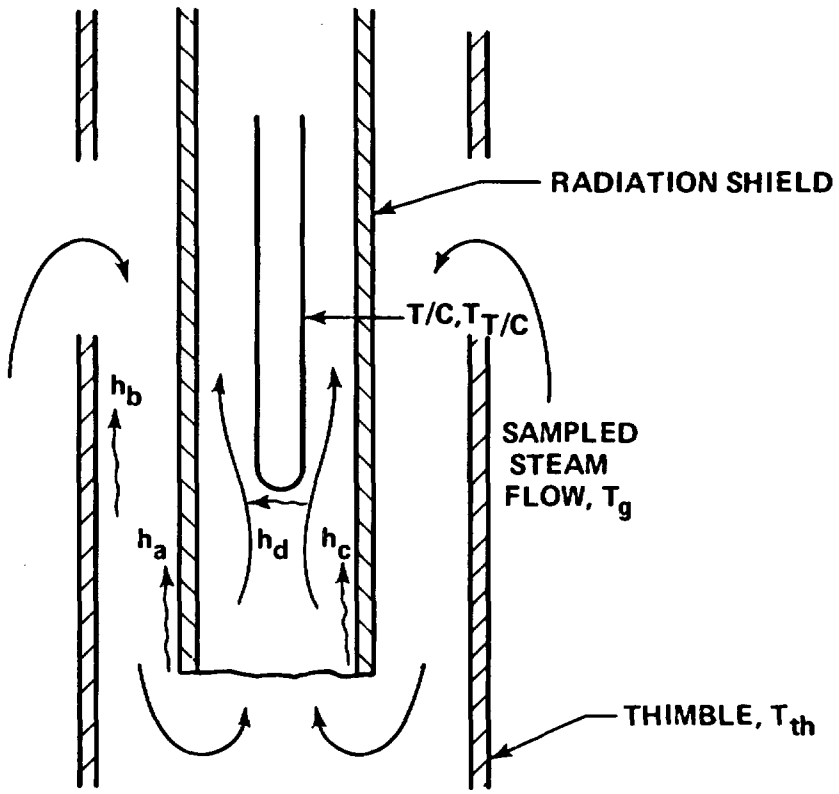

STEAM PROBE DESIGN

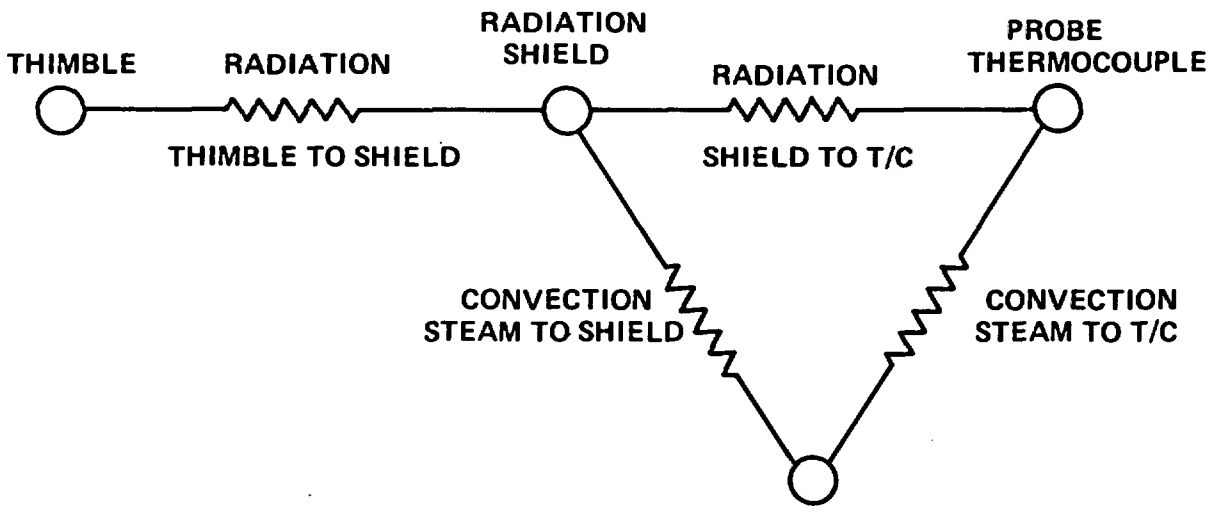

STEAM TEMPERATURE

Figure D-4. Steam Probe Radiation/Convection Network

TABLE D-10

HEAT TRANSFER COEFFICIENT CORRELATIONS

Coefficient	Correlation[a]	Comments	Reference
h_a	$h = \frac{K}{D}(1.86)\left[(Re)\ (Pr)\left(\frac{D}{L}\right)\right]^{\frac{1}{3}}$	Laminar pipe flow approximation	Equation 8.11[b]
h_b	$h = \frac{K}{D}(0.664)\ (Re)^{\frac{1}{2}}\ (Pr)^{\frac{1}{3}}$	Laminar flat plate flow approximation	Equation 8.3[b]
h_c	$h = \frac{K}{D}(0.036)\ (Re)^{0.8}(Pr)^{\frac{1}{3}}\left(\frac{D}{L}\right)^{\frac{1}{18}}$	Turbulent pipe flow approximation	Equation 8.17[b]
h_d	$h = \frac{K}{D}\left[2 + 0.03\ (Pr)^{0.33}\ (Re)^{0.54} + 0.35\ (Pr)^{0.356}(Re)^{0.58}\right]$	Cross flow to sphere approximation	Equation 11.87[c]

a. All properties were evaluated at bulk fluid temperature.

b. Chapman, A. J., Heat Transfer, 3rd edition, MacMillan, New York, 1974.

c. Kutateladze, S. S., Fundamentals of Heat Transfer, 2nd edition, Academic Press, New York, 1963.

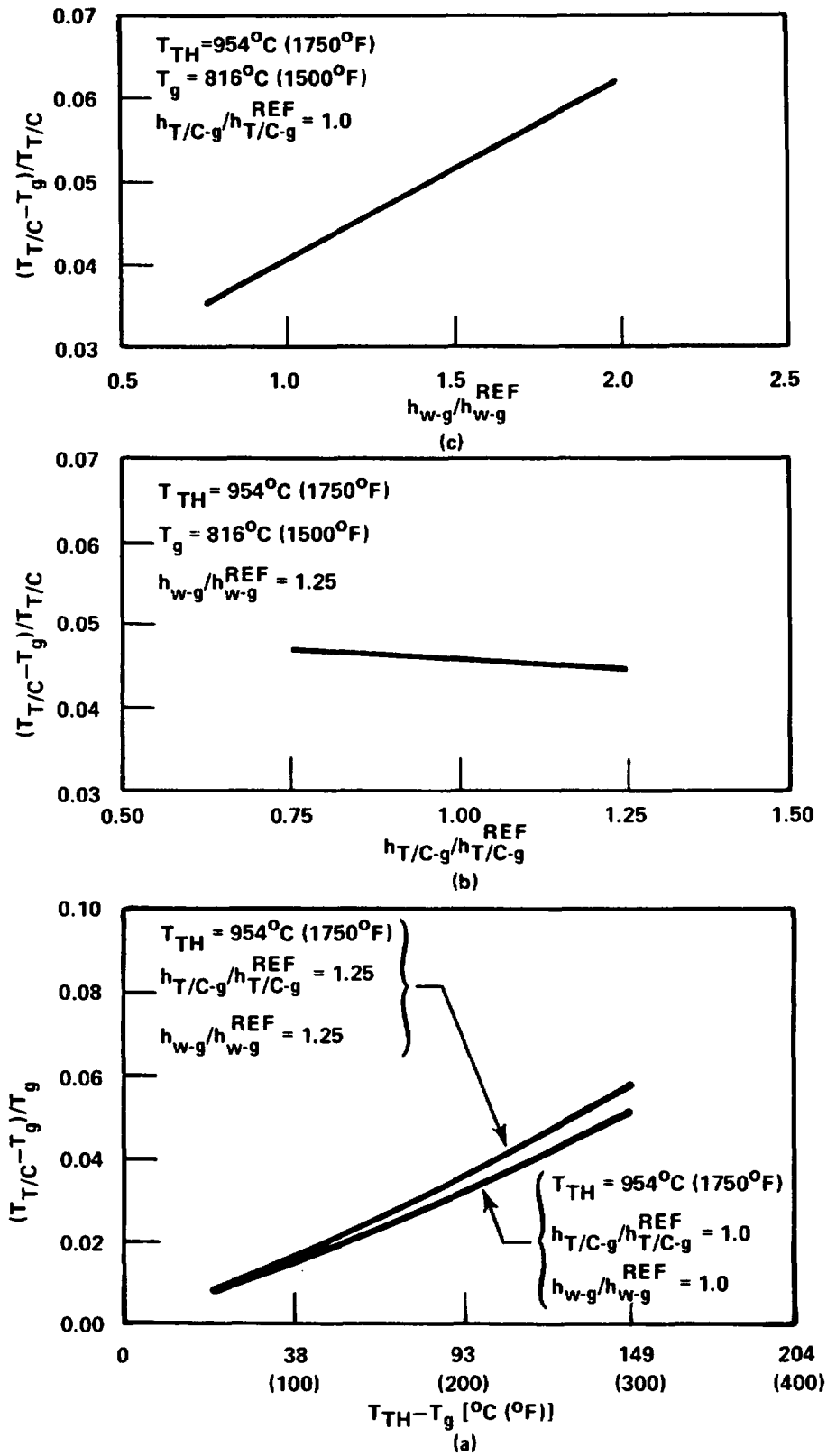

NOTES:

T_{TH} = THIMBLE TEMPERATURE

$T_{T/C}$ = THERMOCOUPLE TEMPERATURE

T_g = INLET VAPOR TEMPERATURE

h^{REF}_{w-g} = REFERENCE CALCULATED FILM COEFFICIENT BETWEEN WALL AND VAPOR

h_{w-g} = FILM COEFFICIENT BETWEEN WALL AND VAPOR USED TO CALCULATE $T_{T/C}$

$h^{REF}_{T/C-g}$ = REFERENCE CALCULATED FILM COEFFICIENT BETWEEN THERMOCOUPLE AND VAPOR

$h_{T/C-g}$ = FILM COEFFICIENT BETWEEN THERMOCOUPLE AND VAPOR USED TO CALCULATE $T_{T/C}$

Figure D-5. Steam Probe Sensitivity

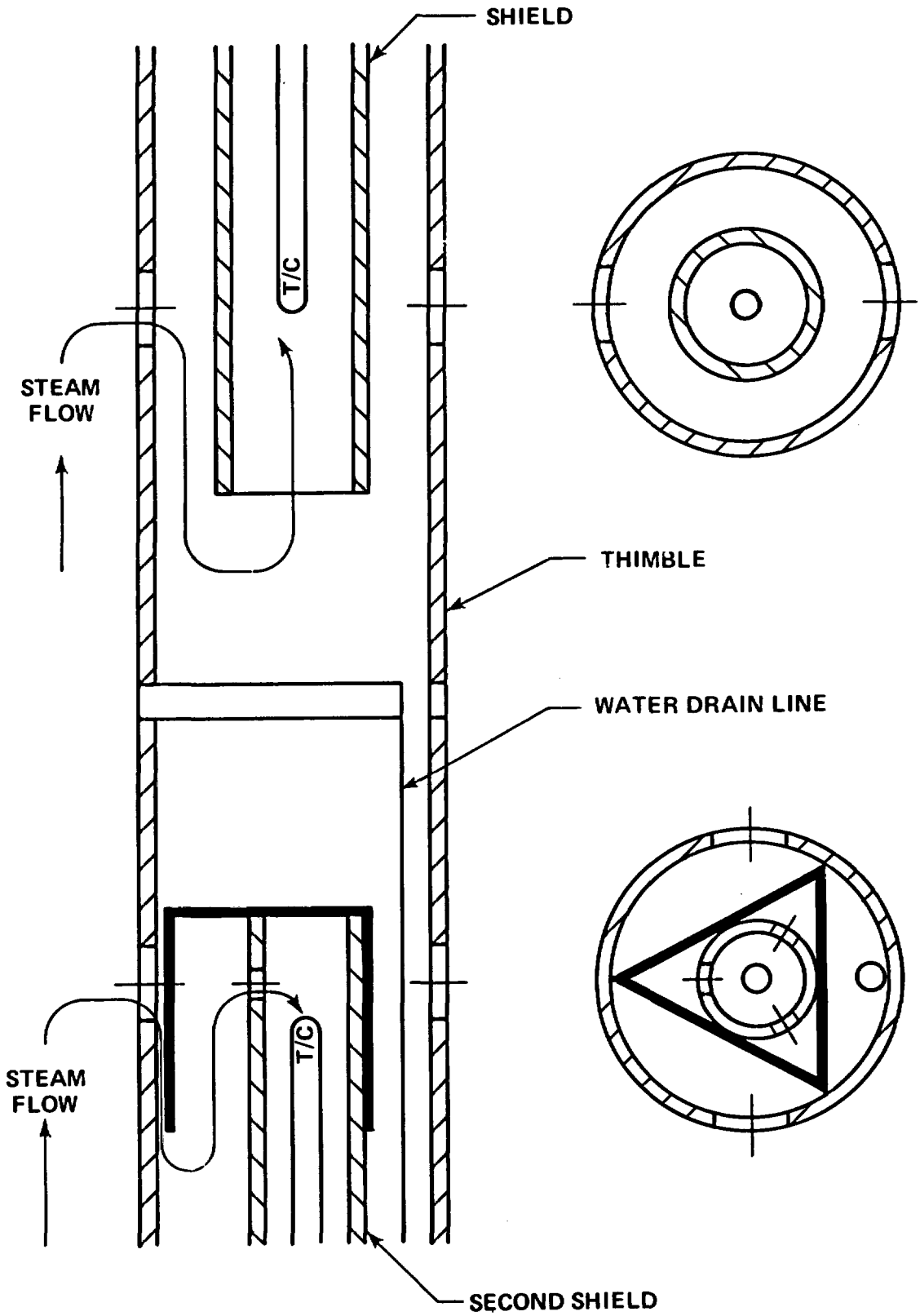

Figure D-6. Steam Probe Design

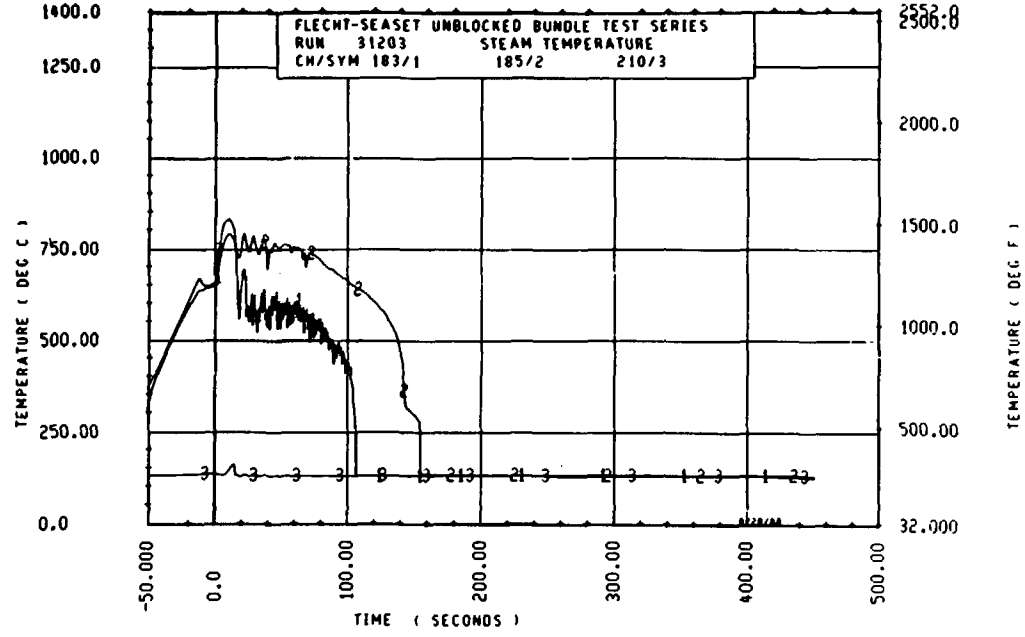

Figure D-7. Steam Temperature Versus Time, Run 31203

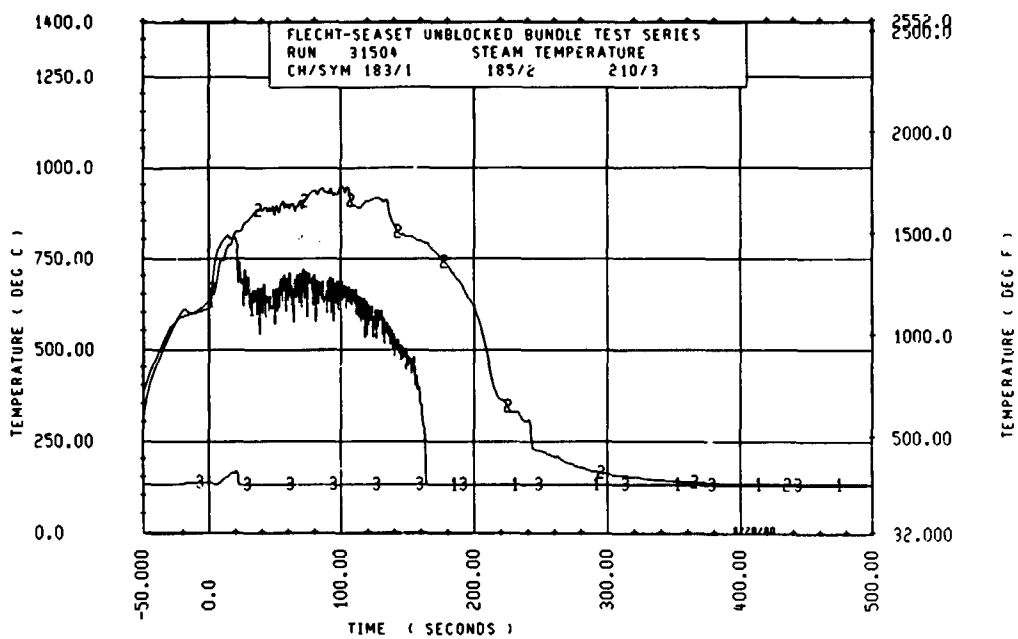

Figure D-8. Steam Temperature Versus Time, Run 31504

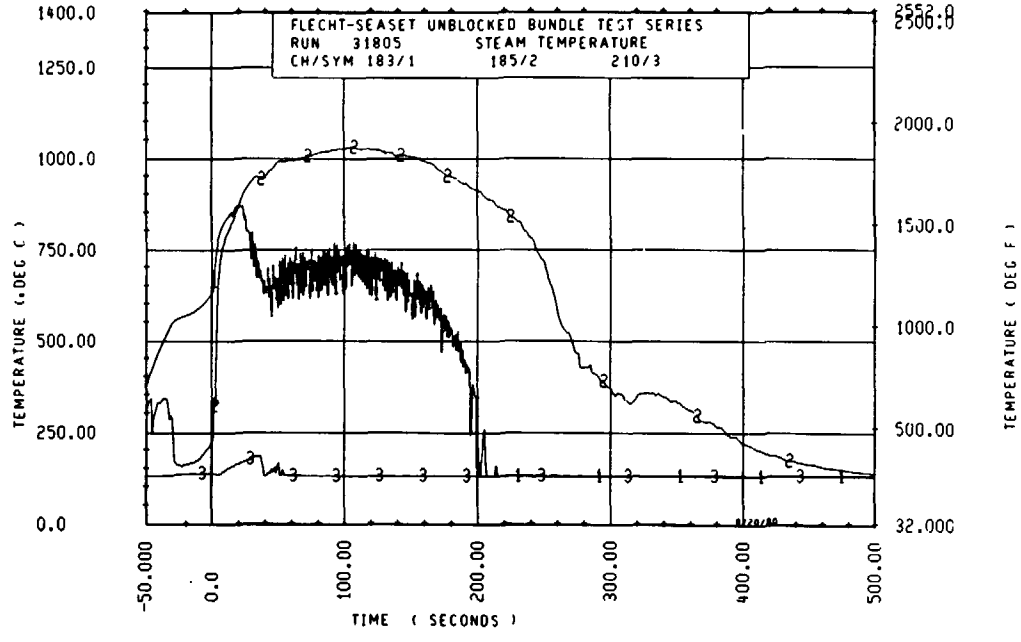

Figure D-9. Steam Temperature Versus Time, Run 31805

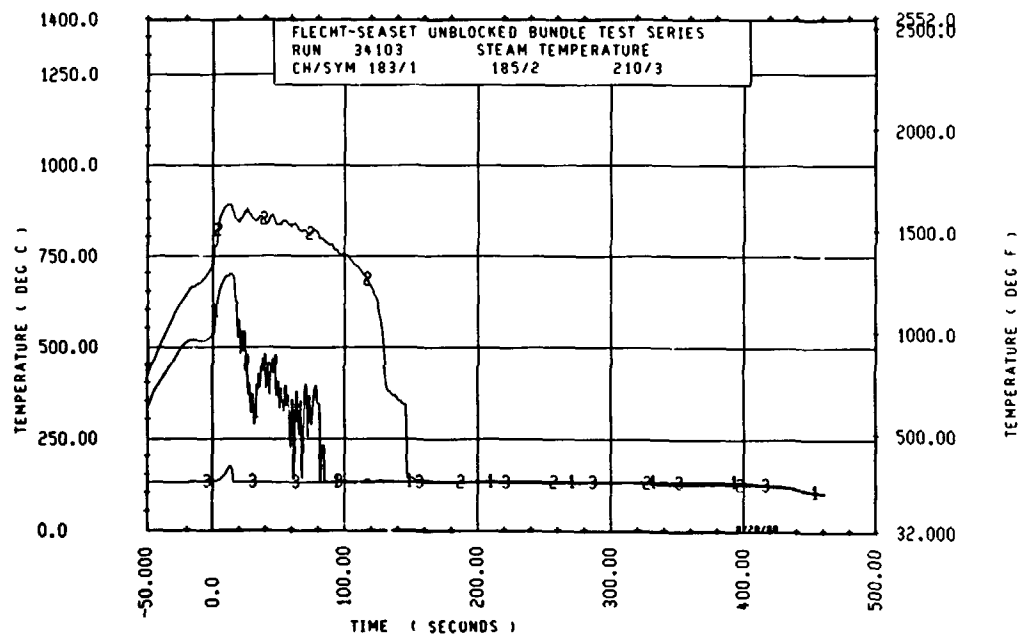

Figure D-10. Steam Temperature Versus Time, Run 34103

the upper plenum fluid thermocouple quenched, the bottom steam probe measured a much lower steam temperature. This is a good indication that the bottom steam probe is quite sensitive to the presence of water in the steam flow. All the steam probes which aspirated through the bottom of the bundle behaved similarly through the entire test program.

The steam probes which aspirated through the bottom of the bundle include the following:

Elevation [m (in.)]	Radial Location	Channel No.
0.991 (39)	10F	179
1.22 (48)	7I	180
1.52 (60)	5K	181
1.70 (67)	7F	182
	10I	183
1.83 (72)	4F	184
	10L	186
1.98 (78)	10C	187
	13F	188
2.13 (84)	7C	189
	13I	190

The data from these probes are not presented in the data package summaries (appendix C) for the forced and gravity reflood tests.

It is recommended that the lower steam probe design not be utilized in future reflood testing.

The steam probe test data were examined to determine whether the steam temperature was affected by the rod radiation heat transfer. The radial locations of the thimble, steam probe, and heater rod are shown in figure D-11. The thimble, steam, and rod temperatures at the 1.83 m (72 in.) elevation for the 38, 25, and 20 mm/sec (1.5, 1.0,

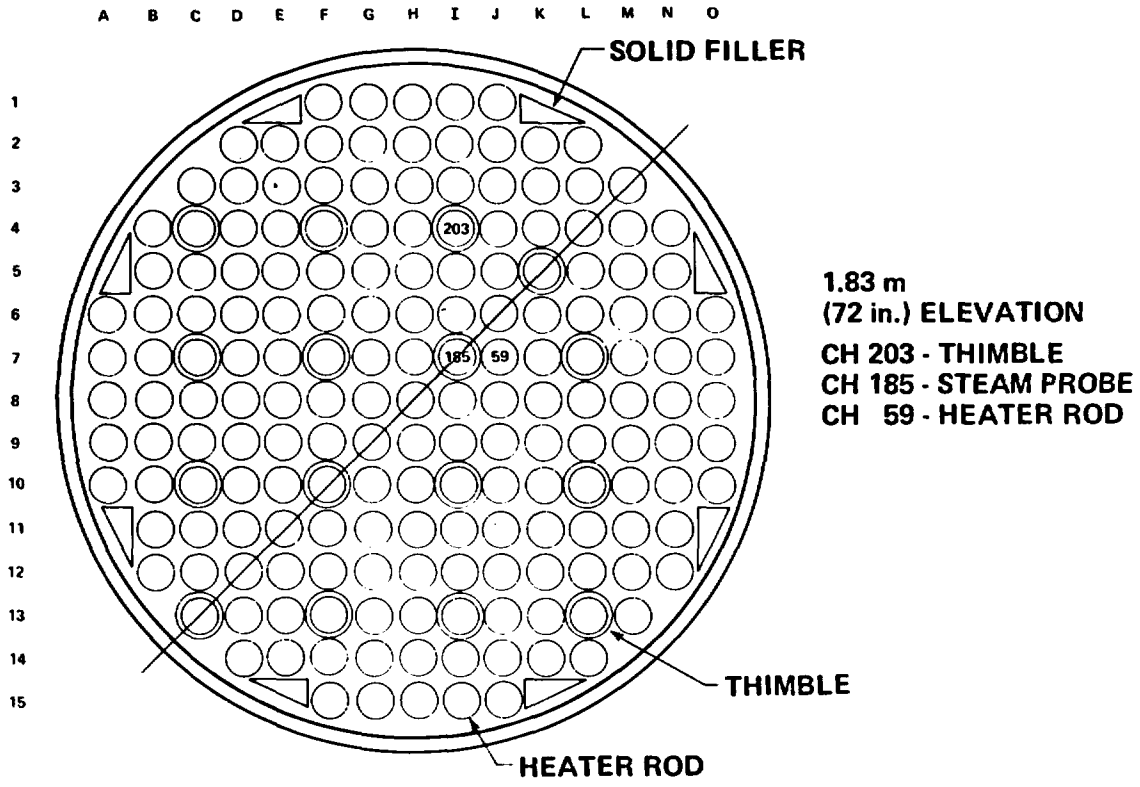

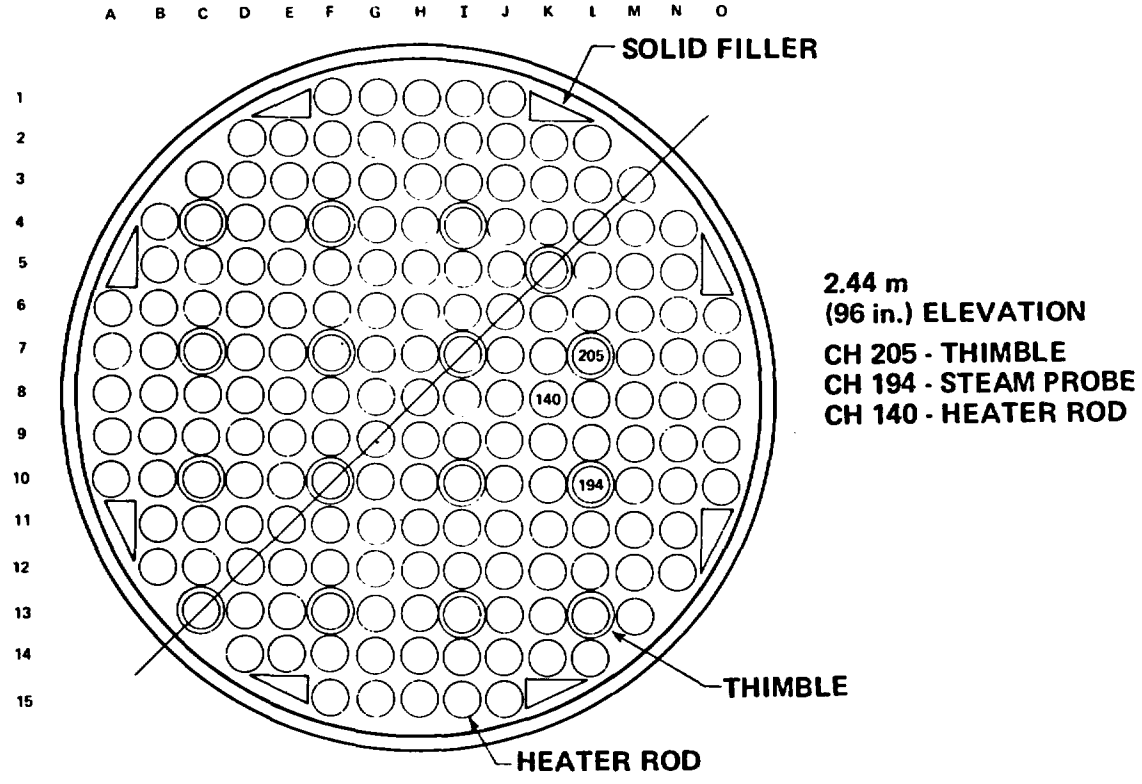

Figure D-11. Bundle Cross Section

and 0.8 in./sec) flooding rate tests are shown in figures D-12, D-13, and D-14, respectively. The thimble, steam, and rod temperatures at the 2.44 m (96 in.) elevation for the 38 and 25 mm/sec (1.5 and 1.0 in./sec) flooding rate tests are shown in figures D-15 and D-16, respectively.

These figures indicate that the steam probe generally measured a temperature lower than that of the thimble as would be expected, since the steam probe was shielded from the rod radiation heat transfer. The steam temperature also oscillated more than the thimble temperature as would also be expected, since the thimble thermocouple was attached to the "massive" thimble and therefore did not respond as quickly to temperature changes as the 0.10 cm (0.040 in.) diameter steam probe thermocouple.

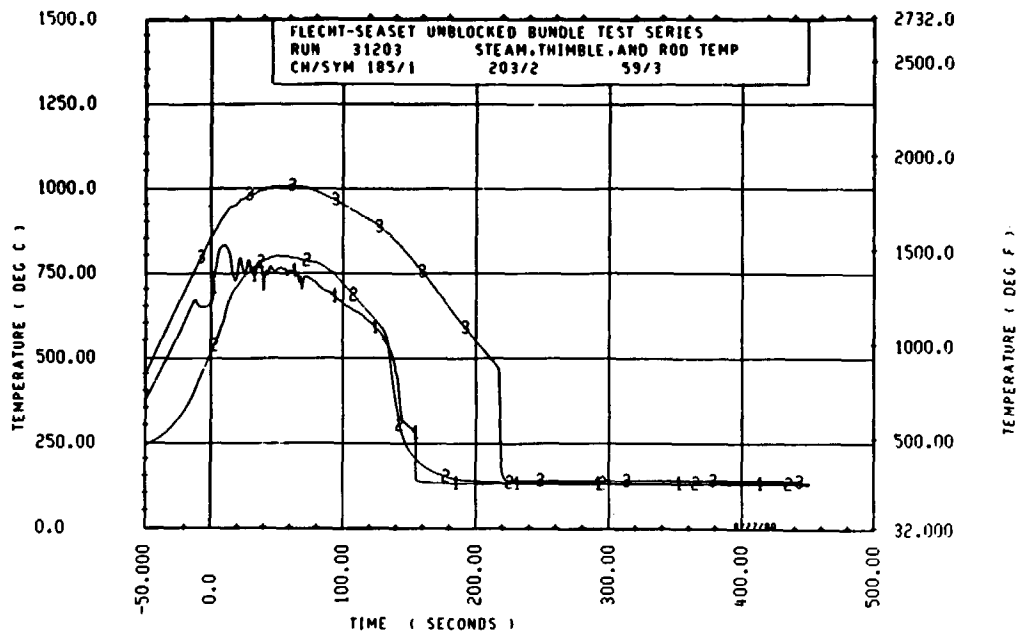

Figure D-12. Steam, Thimble, and Rod Temperatures Versus Time, Run 31203 [38 mm/sec (1.5 in./sec) Flooding Rate, 1.83 m (72 in.) Elevation]

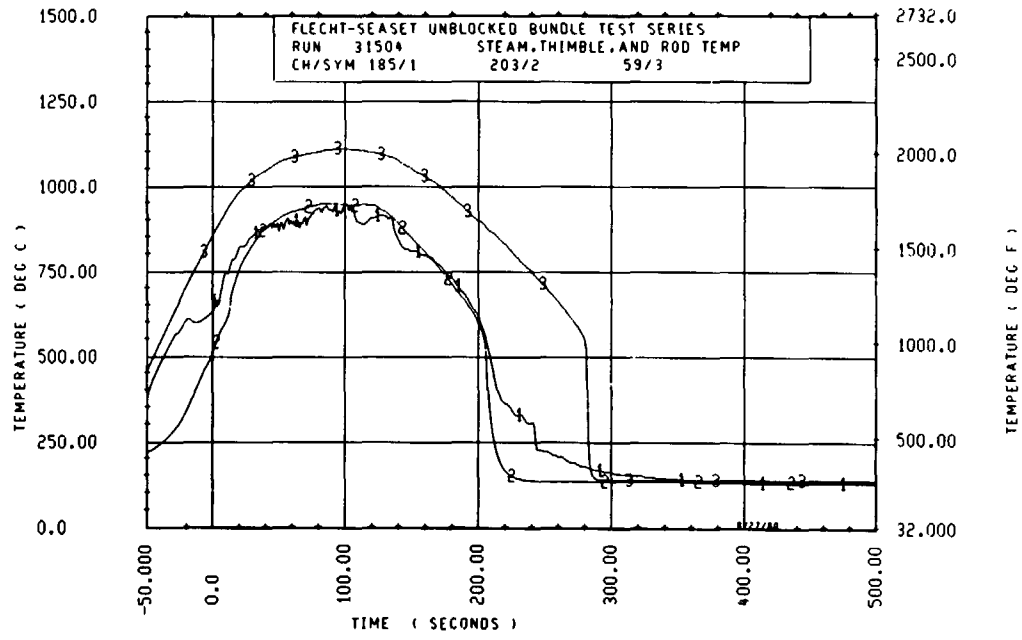

Figure D-13. Steam, Thimble, and Rod Temperatures Versus Time, Run 31504 [25 mm/sec (1.0 in./sec) Flooding Rate, 1.83 m (72 in.) Elevation]

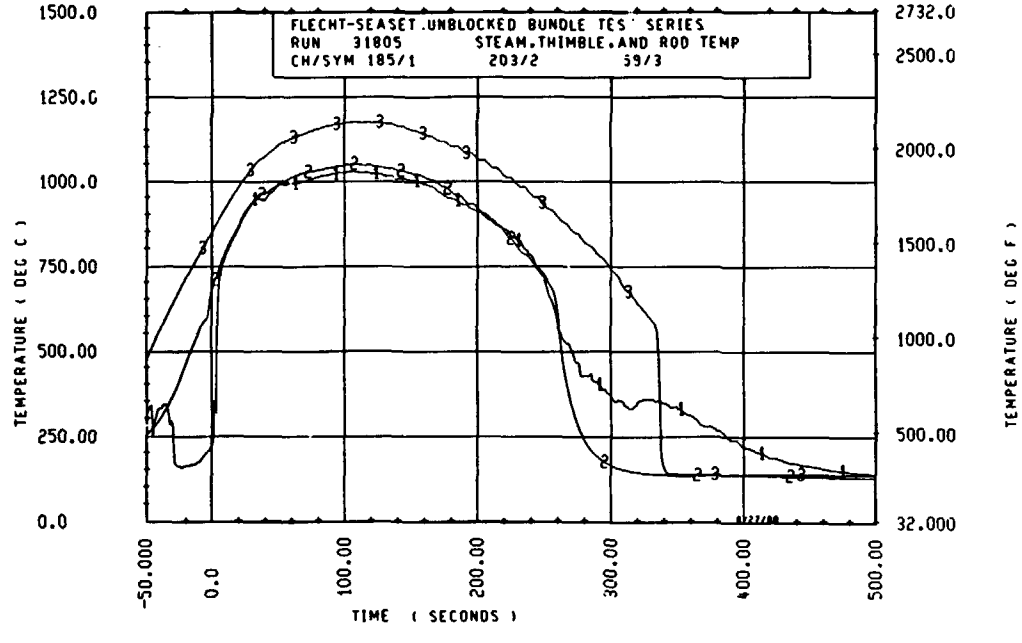

Figure D-14. Steam, Thimble, and Rod Temperatures Versus Time, Run 31805 [20 mm/sec (0.8 in./sec) Flooding Rate, 1.83 m (72 in.) Elevation]

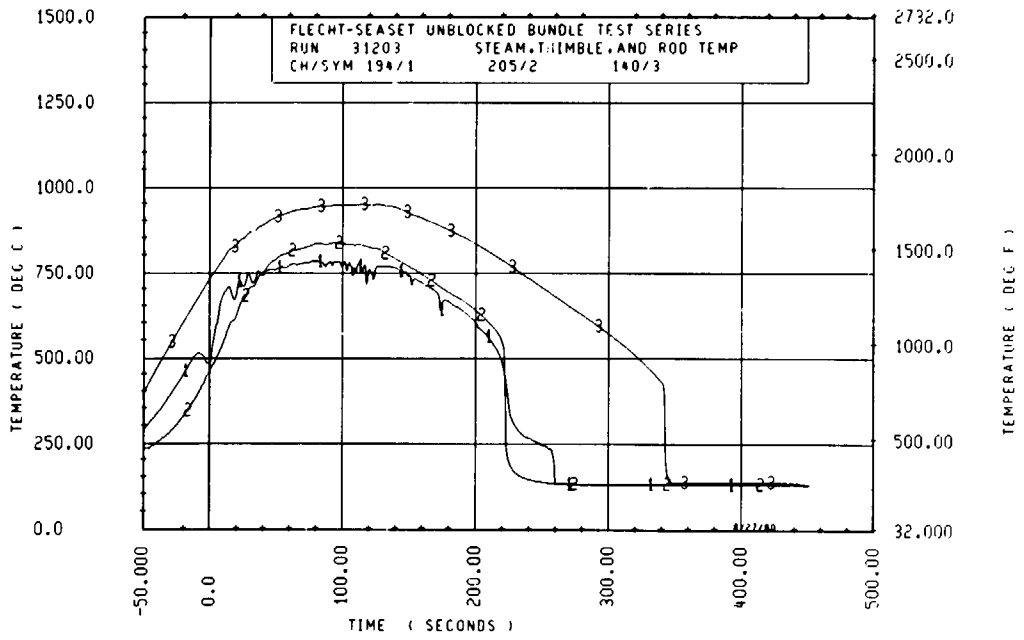

Figure D-15. Steam, Thimble, and Rod Temperatures Versus Time, Run 31203 [38 mm/sec (1.5 in./sec) Flooding Rate, 2.44 m (96 in.) Elevation]

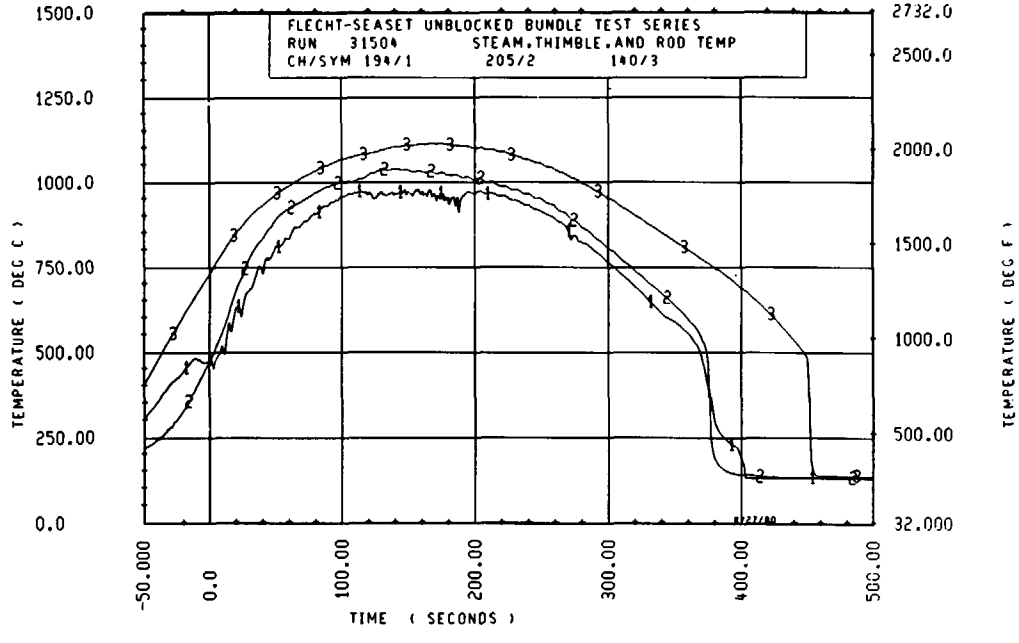

Figure D-16. Steam, Thimble, and Rod Temperatures Versus Time, Run 31504 [25 mm/sec (1.0 in./sec) Flooding Rate, 2.44 m (96 in.) Elevation]

APPENDIX E
CALCULATION TECHNIQUES

E-1. DATAR PROGRAM

The purpose of the DATAR model is to calculate the heat transfer coefficient for heater rods in the experimental facility. It accomplishes this by using available experimental data (as read from data tapes) and as-built heater rod dimensions, coupled with a mathematical model (paragraph E-2).

The DATAR code consists of 13 overlays, to reduce the computer field length required for code execution. These overlays consist of the following:

- The main program overlay, together with those subroutines necessary to calculate film coefficients
- The overlay which controls the reading and checking of input data, from both cards and tape
- The overlay which checks for restart and, if present, properly positions input and output files and sets internal values
- The overlay which reads input information from the main data tape header and calculates several internal values based on this information
- The overlay which checks card input consistency and echoes the information to printed output
- The overlay which echoes data tape header information to printed output
- The overlay which reads input from cards and performs miscellaneous operations on the data

The program provides its own dynamic field length management, resulting in minimum operating expense.

The main program generally controls the flow of most input and output data read and generated by the program. A typical run is conducted using the following steps:

(1) Radial node positions are calculated based on built-in radii and interval information. It should be noted that the code performs its calculations in the radial direction only. Axial conduction is ignored.

(2) The appropriate time values are calculated for each data point produced.

(3) Header information (run number, number of data scans, and the like) is written to the output tape, data tapes are read and correctly positioned, and the bundle power is calculated. The sink temperature is assumed to be the saturation temperature corresponding to the specified pressure for the test.

(4) The temperature data for a rod thermocouple are read from the main data tape; miscellaneous information for that thermocouple, such as bundle position and axial and radial power factors, is read from a secondary data tape.

(5) The thermocouple is considered good if the channel is not included in the bad channel list and the first temperature is greater than 66°C (150°F). If these two criteria are not met, a short entry is made on the output tape and data from the next channel are read.

(6) Rod temperature profiles, surface heat flux, and heat transfer coefficients are calculated by successively calling subroutines containing the model described in paragraph E-2.

(7) The data and results of calculations performed in step (6) are written to output.

(8) Steps (4) through (7) are repeated for all bundle thermocouple channels; the run is then terminated.

DATAR uses three principal subroutines. Their functions are as follows:

-- To calculate the coefficient matrix

-- To calculate the temperatures and surface heat flux given the coefficient matrix

-- To invert the tridiagonal coefficient matrix

Several other subroutines perform miscellaneous calculations, such as material property evaluation and data interpolation.

E-2. Calculation Method

A heat conduction problem is termed an "inverse heat conduction problem" if at least one spatial condition is specified at an interior point of a heat-conducting body. Because of this unorthodox condition, the solution to an inverse problem is very complicated. Even if the governing equations are linear, classical methods such as Fourier analysis and Laplace transformation fail to yield a solution. For the Fourier method, the eigenvalues are not readily obtainable from the resulting Strum-Louisvalle system of equations; hence, a Fourier series representation of the solution cannot be determined. Transformation techniques lead to a solution in Laplace variable space, which defies an inverse transform into the real time space. Although the numerical method is not without difficulty, meaningful results can be obtained if due care is exercised.

The mathematical formulations and methods used in DATAR to solve the inverse heat conduction problem are described in the following paragraphs. The governing partial differential equation and the associated difference approximation are outlined below. The key assumption used in the development of the approximation is that the nonlinear coefficients are slowly varying functions of the temperature of the system and may therefore be treated as constants. The validity of this assumption is addressed in paragraph E-10. When the difference approximation has been obtained, the solution method is described in considerable detail.

E-3. Basic Equations and Geometry

Let T(r,t) denote the temperature at position r and time t in the ranges $0 \leq r \leq b$, $t \geq 0$. The applicable partial differential equation is

$$\frac{\partial}{\partial r}\left(k\frac{\partial T}{\partial r}\right) + \frac{k}{r}\frac{\partial T}{\partial r} + q''' = \rho c\left(\frac{\partial T}{\partial r}\right) \qquad \text{(E-1)}$$

where k and c depend on T and are thermal conductivity and specific heat, respectively, and ρ is density. Axial heat conduction is neglected, since calculations have shown an insignificant effect unless within approximately 25.4mm (1 in.) of the quench front.

The following boundary and initial conditions are given:

$$\frac{\partial T(0,t)}{\partial r} = 0 \qquad \text{(E-2)}$$

$$T(a,t) = T_D(t) \qquad 0 < a < b \qquad \text{(E-3)}$$

$$\frac{\partial T(b,t)}{\partial r} = -\phi/k \qquad \text{(E-4)}$$

T(r,0) the initial temperature distribution, is also given.

Equation (E-2) assures symmetry at r = 0. Equation (E-3) represents the measured temperature at an internal point a. Equation (E-4) introduces another unknown, ϕ, the flux to be determined.

Since the measured temperature is given at discrete times, the partial differential equation may be viewed as a system of ordinary differential equations, one equation for each temperature measurement. The factor ϕ could then be computed at each time step so that the measured temperature is obtained; this approach is not used in DATAR. There are two primary reasons for considering the transient behavior of the system: first, the experimental error in the data, and second, the propagation time effects in the system. As shown below, if ϕ is computed at each time step using only the measured temperature at that time step, then the flux and external temperature

will behave erratically. The second reason, the propagation effect, occurs because the flux ϕ reflects the behavior of the rod at the boundary, and the temperature is measured at an internal point of the rod. The temperature propagation time of the rod must be accounted for, since the measured temperature reflects changes in the boundary temperature that have occurred earlier. If the propagation time is greater than 0.5 second, then this transport effect must be allowed for by adjusting ϕ at one time step, given the temperature measurements at future times. A representative propagation time is not known, but rough estimates indicate that it is greater than 0.5 second. A detailed analysis of this phenomenon should prove useful in any future modifications of DATAR.

The spatial aspects of the problem are now considered. The physical region under consideration ($0 \leq r \leq b$) is composed of n radial regions, each with potentially different physical properties. The result is a set of n partial differential equations, one equation for each region. At the interface points of the regions, temperature and heat transfer are required to be continuous. Let d be an interface point between regions R_{i-1} and R_i; then,

$$\lim_{\substack{r \in R_{i-1} \\ r \to d}} T(r,t) = \lim_{\substack{r \in R_i \\ r \to d}} T(r,t) \tag{E-5}$$

$$\lim_{\substack{r \in R_{i-1} \\ r \to d}} \frac{\partial T(r,t)}{\partial r} \quad k(T) = \lim_{\substack{r \in R_i \\ r \to d}} \frac{\partial T(r,t)}{\partial r} \quad k(T) \tag{E-6}$$

Given equations (E-1) through (E-6), the appropriate difference equation is first derived for each region separately using equation (E-1); then the regions are coupled by imposing equations (E-5) and (E-6). Equations (E-2) and (E-4) supply the boundary values, and equation (E-3) and the initial temperature distribution are used to develop the solution for $t \geq 0$.

E-4. Difference Equations

The following approximations are used for the partial derivatives in equation (E-1):

$$\frac{\partial}{\partial r} \quad k \frac{\partial T}{\partial r} \quad \simeq \quad \frac{k}{(\Delta r)^2} \left[T(r + \Delta r, t) - 2T(r,t) + T(r - \Delta r, t) \right] \tag{E-7}$$

$$\frac{k}{r} \quad \frac{\partial T}{\partial r} \simeq \frac{k}{r} \left[\frac{T(r + \Delta r, t) \quad - \quad T(r - \Delta r, t)}{2\Delta r} \right] \tag{E-8}$$

$$\rho c \quad \frac{\partial T}{\partial t} \quad \simeq \quad \rho c \left[\frac{T(r,t) \quad - \quad T(r,t - \Delta t)}{\Delta t} \right] \tag{E-9}$$

The approximation of equation (E-7) neglects the term $(\partial k/\partial r)(\partial T/\partial r)$. The justification for this omission follows from the fact that $(\partial k/\partial r)(\partial T/\partial r)$ is much smaller than $k/r\,(\partial T/\partial r)$ the term in equation (E-8).

Since $\frac{\partial k}{\partial r} = \frac{\partial k}{\partial T} \frac{\partial T}{\partial r}$,

$$\frac{\frac{\partial k}{\partial r} \frac{\partial T}{\partial r}}{\frac{k}{r} \frac{\partial T}{\partial r}}$$

may be written as

$$\frac{r}{k} \frac{\partial k}{\partial r} \frac{\partial T}{\partial r}$$

Now r is small, less than 0.1. It is shown in paragraph E-10 that, for each material, $(1/k)(\partial k/\partial r)$ is less than 0.01. In fact, it is less than 0.001 for almost all materials. Finally, $\partial T/\partial r$ is a well-behaved function of r. Therefore the term omitted from equation (E-7) is less than 0.1 percent of the term in equation (E-8).

The approximations of equations (E-7), (E-8), and (E-9) also make use of the fact that k and c are slowly varying functions of T. In paragraph E-10, these assumptions are justified by showing that $\partial k/\partial T$ and $\partial c/\partial T$ are small.

Other approximations that could be used instead of equation (E-7) have been tested; no appreciable difference can be seen between the schemes which keep k constant and those which do not.

Note that k and c are evaluated at $T(r, t - \Delta t)$. Here the assumption is made that T is given at time $t - \Delta t$, and the procedure is advancing to time t. Since t is given at time $t = 0$, the required initial condition is supplied.

Equations (E-7), (E-8), and (E-9) are only used inside each region; the interface between regions is covered in paragraph E-5.

The approximations in equations (E-7), (E-8), and (E-9) are substituted into equation (E-1). Letting $r_1, \ldots, r_k$ denote the points in a region R and letting $\Delta r_i = r_{i+1} - r_i$ and $T_i = T(r_i,t)$, equation (E-1) may be rewritten as follows:

$$B_i T_{i-1} + A_i T_i + C_i T_{i+1} = D_i \qquad \text{(E-10)}$$

where the coefficients are given by

$$B_i = 1 - (\Delta r)_i/2(r_i) \qquad \text{(E-11)}$$

$$A_i = -2 - (\rho_i c_i/k_i)(\Delta r_i)^2/\Delta t \qquad \text{(E-12)}$$

$$C_i = 1 + (\Delta r)_i/(2r_i) \qquad \text{(E-13)}$$

$$D_i = -q'''_i - (\rho_i c_i / k_i)(\Delta r_i)^2 T_i^{old} / \Delta t \qquad \text{(E-14)}$$

In equations (E-11) through (E-14), ρ_i, c_i, k_i, and q_i denote the value at the point r_i, and T_i^{old} is given by $T(r_i, t - \Delta t)$. Note that c_i and k_i are evaluated using the previous temperature T_i^{old}. This assumption is related to the assumption used in deriving equations (E-7), (E-8), and (E-9).

In equations (E-10) through (E-14), the two points r_o and r_{k+1} were used; these points reside at a distance Δr from the region r. The use of interface and boundary conditions eliminates these fictitious points.

E-5. Interface Conditions

Equations (E-10) through (E-14) hold for each region. The interface conditions in equations (E-5) and (E-6) are now applied and the redundant temperatures are eliminated. Ignoring for a moment the left-hand boundary of region 1 (the origin) and the right-hand boundary of region n (the external surface), equation (E-10) can be written for each of the internal interface points.

For region R_i, the equation for the right-hand boundary may be written

$$B_k T_{k-1} + A_k T_k + C_k T_{k+1} = D_k \qquad \text{(E-15)}$$

Here k denotes the right-hand end point of R_i.

For region R_{i+1}, the equation for the left-hand boundary may be written

$$B'_1 T'_0 + A'_1 T'_1 + C'_1 T'_2 = D'_1 \qquad \text{(E-16)}$$

Here 1 denotes the left-hand end point of R_{i+1}, and primes are used on the coefficients and temperatures.

Because of the overlap of the regions, the temperatures T_{k-1}, T_k, and T_{k+1} refer to the same spatial points as do T'_0, T'_1, and T'_2, respectively.

The interface conditions, equations (E-5) and (E-6), then lead to the following equations:

$$T_k = T_1' \tag{E-17}$$

$$k_i \left[\frac{T_{k+1} - T_{k-1}}{2(\Delta r)_i} \right] = k_{i+1} \left[\frac{T_2 - T_0}{2(\Delta r)_{i+1}} \right] \tag{E-18}$$

Equation (E-17) requires that the temperatures are in agreement at the interface point. Equation (E-18) is a difference approximation to equation (E-6), which requires that the heat transfer out of region R_1 is the same as the heat transfer into region R_{i+1}.

Equations (E-15) through (E-18) are a set of four equations in six unknowns that may be reduced to one equation in three unknowns: the temperatures at the interface and at the adjacent points on either side. Using T_{k-1}, T_k, and T_{k+1} for these temperatures, and letting

$$\sigma = \frac{k_{i+1} \quad (\Delta r)_i}{k_i \quad (\Delta r)_{i+1}}$$

equations (E-8) through (E-15) may be combined to obtain

$$B_k' T_{k-1} + A_k' T_k + C_k' T_{k+1} = D_k' \tag{E-19}$$

where the primed coefficients are given by

$$B_k' = B_1'(B_k + C_k) \tag{E-20}$$

$$A_k' = B_1' A_k + \sigma A_1' C_k \tag{E-21}$$

$$C_k' = \sigma C_k (B_1' + C_1') \tag{E-22}$$

$$D_k' = B_1' D_k + \sigma D_1' C_k \tag{E-23}$$

Equations (E-10) and (E-19) now provide a tridiagonal system for the temperatures internal to the total region under consideration, $0 \leq r \leq b$. For a point internal to a region R_i, equation (E-10) is used, and for interface points, equation (E-19) is used.

E-6. Boundary Conditions

Derivation of boundary condition equations is given in the following paragraphs.

E-7. External Surface Boundary -- Letting T_N represent the temperature at the external boundary, equation (E-10) may be written

$$B_N T_{N-1} + A_N T_N + C_N T_{N+1} = D_N \tag{E-24}$$

Further, equation (E-4) may be written in difference form as

$$\frac{T_{N+1} - T_{N-1}}{2\Delta r_{N-1}} = -\frac{\phi}{k_N} \tag{E-25}$$

Combining these two equations yields

$$(B_N + C_N)\, T_{N-1} + A_N T_N = D_N + \frac{2C_N \Delta r_{N-1}}{k_N}\, \phi \tag{E-26}$$

E-8. Internal Boundary -- For $r = 0$, equation (E-1) and the condition in equation (E-2) may be used to derive the appropriate equation for T_0. Rewriting equation (E-1) yields

$$\frac{\partial k}{\partial r}\frac{\partial T}{\partial r} + k\frac{\partial^2 T}{\partial r^2} + \frac{k}{r}\frac{\partial T}{\partial r} = \rho c \frac{\partial T}{\partial t} - q''' \tag{E-27}$$

At $r = 0$, $\partial T/\partial r = 0$; moreover the term $(1/r)(\partial T/\partial r)$ may be replaced by $\partial^2 T/\partial r^2$ at $r = 0$, by using L'Hospital's rule, since $\partial T/\partial r = 0$. Using these expressions, equation (E-27) may be rewritten as

$$2 \frac{\partial^2 T}{\partial r^2} = \frac{\rho c}{k} \frac{\partial T}{\partial t} - \frac{q'''}{k} \tag{E-28}$$

The term $\partial^2 T/\partial r^2$ in equation (E-28) is approximated using $(2T_1 - 2T_0)/(\Delta r_0)^2$. This expression is the standard three-point difference approximation to the second derivative with the symmetry condition $T_{-1} = T_1$ being used, since $\partial T/\partial r = 0$.

The difference equation may be written

$$A_0 T_0 + C_0 T_1 = D_0 \tag{E-29}$$

where the coefficients are given by

$$A_0 = -4 - \frac{\rho_0 c_0}{k_0} \frac{(\Delta r_0)^2}{\Delta t} \tag{E-30}$$

$$C_0 = 4 \tag{E-31}$$

$$D_0 = \frac{-\rho_0 c_0}{k_0} \frac{(\Delta r_0)^2}{(\Delta t)} T(0, t - \Delta t) - q_0''' \frac{(\Delta r_0)^2}{k_0 (\Delta t)} \tag{E-32}$$

Equations (E-10), (E-19), (E-26), and (E-29) form a linear tridiagonal set of N+1 equations in the N+1 unknowns $T_0, \ldots, T_N$. However, equation (E-26) introduced another unknown, ϕ, but equation (E-3) leads to one of the T's. As a result, there remain N+1 equations in N+1 unknowns. Let T_M denote the given internal temperature. Since k and c depend on the temperature at time $t - \Delta t$, ϕ is not brought over to the left-hand side of the equations nor is T_M moved to the right-hand side. Instead, ϕ is estimated using the values of T_M at future times. T_M is treated as an unknown, thus keeping the tridiagonal structure of the equations.

E-9. Method of Solution

Let $\underline{T}^t = (T_0, \ldots, T_N)$; T_i is at time t. $\underline{T}^{t-1}$ is a similar vector at time t - Δt. Now let A be the tridiagonal matrix:

$$\begin{bmatrix} A_0 & C_0 & & & & \\ B_1 & A_1 & C_1 & & & \\ & B_2 & A_2 & C_2 & & \\ & & \ddots & \ddots & \ddots & \\ & & & B_{N-1} & A_{N-1} & C_{N-1} \\ & & & & B_N & A_N \end{bmatrix}$$

Let S be a diagonal matrix with the i-th element given by

$$\frac{\rho_i c_i}{k_i} \quad \frac{(\Delta r_i)^2}{\Delta t}$$

Here c_i and k_i are evaluated at $T_i^{t-\Delta t}$.

Let $\underline{q}$ be the vector with the i-th component given by

$$- q'''_i \quad \frac{(\Delta r_i)^2}{k_i(\Delta t)}$$

Finally, let $\underline{\delta}$ be a vector with $\delta_i = 0$; i = 0, ..., N-1; and $\delta_N = \Delta r_{N-1}/C_N k_N$.

Equations (E-10), (E-19), (E-26), and (E-29) may be abbreviated as

$$A\underline{T}^i = D\underline{T}^i = \underline{q} + \phi^i \underline{\delta} \qquad \text{(E-33)}$$

Again, ϕ^i is unknown, but T_M^i is known.

For simplicity, assume $i = 1$; that is, the initial data for time = 0 are given, and the calculation is proceeding to time Δt.

Let $\underline{P}^k$ denote a particular solution of the following equation:

$$A\underline{P}^k = D\underline{P}^{k-1} + \underline{q} \tag{E-34}$$

with $\underline{P}^{k-1}$ given. Similarly, let $\underline{H}^k$ denote a homogeneous solution of the following:

$$A\underline{H}^k = D\underline{H}^{k-1} \tag{E-35}$$

with $\underline{H}^{k-1}$ given. Begin these sequences as follows:

$$\underline{P}^0 = \underline{T}^0 \tag{E-36}$$

and

$$A\underline{H}^1 = \underline{\delta} \tag{E-37}$$

Define $\underline{T}^1$ by $\underline{T}^1 = \underline{P}^1 + \phi^1\underline{H}^1$; then $\underline{T}^1$ satisfies equation (E-33) in the form

$$A\underline{T}^1 = D\underline{T}^0 + \underline{q} + \phi^1\underline{\delta}$$

This may be proved as follows. Multiplying the equation defining $\underline{T}^1$ by A yields

$$\begin{aligned} A\underline{T}^1 &= A(\underline{P}^1 + \phi^1 H^1) \\ &= A\underline{P}^1 + \phi^1 A\underline{H}^1 \\ &= D\underline{P}^0 + \underline{q} + \phi^1\delta \end{aligned}$$

using equations (E-34) and (E-37).

Notice, however, that $\underline{P}^0 = T^0$ from equation (E-36); the proof is complete.

Moreover, if

$$\underline{T}^k = \underline{P}^k + \phi^k \underline{H}^1 + \phi^{k-1} \underline{H}^2 + \ldots + \phi^1 \underline{H}^k \tag{E-38}$$

then $\underline{T}^k$ satisfies equation (E-33) for all $\phi^1, \phi^2, \ldots, \phi^k$. The proof of this result is easily given by induction.

Therefore, given $\underline{T}^0$, future temperatures may be approximated by $\underline{T}^1, \underline{T}^2, \ldots, \underline{T}^k$, as far as necessary.

Note that the computation of $\underline{P}^i$ and $\underline{H}^i$ requires only the solving of a tridiagonal system with the same matrix A (see equations (E-34), (E-35), and (E-37)).

Given that $T^1, T^2, \ldots, T^k$ have been computed, the values of ϕ^i are chosen so that T^i_m agrees with T^i_{data}. Since there are k conditions and k unknowns, the values of ϕ may be obtained exactly. However, the experimental error in T_{data} causes ϕ to behave erratically if this procedure is followed.

It is more reasonable to derive a relationship between the ϕ^i values, and then to obtain k equations in the one unknown, ϕ^i. In other implementations it is assumed that either ϕ is constant (that is, $\phi^i = \phi^2 = \ldots = \phi^k$) or that ϕ^{i+1} is a prescribed linear or quadratic function of ϕ^i.

The approach in this study was to use the measured temperature profile to derive a relationship between ϕ^i and ϕ^{i+1}. First, the heat balance for the whole rod may be written as follows:

$$q'''V - \phi A = \frac{\partial T}{\partial t} \times \text{constant} \tag{E-39}$$

where

V = volume of heated region

A = rod surface area

The $\partial T/\partial t$ term in equation (E-39) cannot be computed before ϕ is calculated; however, it may be estimated by

$$\left(\frac{\partial T}{\partial t}\right)^i \simeq \frac{T_D^i - T_D^{i-1}}{\Delta t}$$

Here T_D^i is the measured temperature T_{data}. Therefore equation (E-39) may be approximated, yielding

$$q'''V - \phi^i A = \frac{T_D^i - T_D^{i-1}}{\Delta t^i} \times \text{constant} \qquad \text{(E-40)}$$

Assuming that the constant is independent of time, and writing equation (E-40) for both i and i+1, the constant may be eliminated. Solve for ϕ^{i+1} in terms of ϕ^i to obtain

$$\phi^{i+1} = E^{i+1}\,\phi^i + F^{i+1} \qquad \text{(E-41)}$$

where E^{i+1} and F^{i+1} are given by

$$E^{i+1} = \frac{(T_D^{i+1} - T_D^i)/(\Delta t)^{i+1}}{(T_D^i - T_D^{i-1})/(\Delta t)^i}$$

$$F^{i+1} = \left[(q''')^{i+1} \times V - E^{i+1} \times (q''')^i \times V\right]/A$$

This relationship predicts the future behavior of ϕ^i more accurately than any of the aforementioned methods.

Moreover, a similar relationship may be derived for ϕ^{i+2}, ϕ^{i+3}, ... in terms of ϕ^i. If these expressions for future ϕ values are substituted into equation (E-38), there results the following expression for $\underline{T}^k$ in terms of $\underline{H}^1$, $\underline{H}^2$, ... $\underline{H}^k$, $\underline{P}^k$ and ϕ^1:

$$\underline{T}^k = \underline{\alpha}^k + \phi^1 \beta^k$$

where α^k and β^k are given by

$$\underline{\alpha}^k = \underline{P}^k + \sum_{j=1}^{k-1} F^{k+1-j} \underline{H}^j$$

$$\underline{\beta}^k = \underline{H}^k + \sum_{j=1}^{i-1} E^{k+1-j} \underline{H}^j$$

Now choose ϕ^1 by the standard least-squares procedure so that T^1_m, ..., T^k_m best fits T^1_{data}, ..., T^k_{data}. Thus,

$$\phi^1 = \frac{\sum_{i=1}^{k} (T^i_{data} - \alpha^i_m) \times \beta^i_m}{\sum_{i=1}^{k} (\beta^i_m \times \beta^i_m)}$$

where α^i_m and β^i_m represent the m-th components of the temperature vectors $\underline{\alpha}^i$ and $\underline{\beta}^i$. Therefore ϕ^1 is chosen so that the computed temperatures for the next k time steps best fit the measured temperatures for those k time steps.

Experience with this method suggests that k = 3 is an appropriate number of time steps.

E-10. Variation of k and c With Respect to T

In deriving the difference approximations for equations (E-1) and (E-4), it has been assumed that k and c are constants and that they may be evaluated using the

temperature of the previous time step. Moreover, it has been assumed that (1/k dk/dT) is less than 0.01. These assumptions are justified by considering the following expressions. For each material, dk/dT, (1/k dk/dT), and dc/dT are listed. The expressions are obtained from the formulas in paragraph E-11. For materials in which c(T) is a linear interpolate of a table, dc/dT has been estimated by computing the maximum $\Delta c/\Delta T$ value, as follows:[1]

-- Boron nitride

$$\frac{dk}{dT} = -8.8889 \times 10^{-4} \text{ Btu/hr-ft-}^{o}\text{F}^{2}$$

$$\frac{1}{k}\frac{dk}{dT} = \frac{-8.8889 \times 10^{-4}}{14.778 - 8.8889 \times 10^{-4} T} \; {}^{o}\text{F}^{-1}$$

$$\frac{dc}{dT} = (0.333492)\; 1.3611 \times 10^{-3} e^{-(1.3611 \times 10^{-3} T)} \text{ Btu/lbm-}^{o}\text{F}^{2}$$

-- Kanthal

$$\frac{dk}{dT} = 4.3 \times 10^{-3} \text{ Btu/hr-ft-}^{o}\text{F}^{2}$$

$$\frac{1}{k}\frac{dk}{dT} = \frac{4.3 \times 10^{-3}}{9.7 + 4.3 \times 10^{-3} T} \; {}^{o}\text{F}^{-1}$$

$$\frac{dc}{dT} = 0.0003 \text{ Btu/lbm-}^{o}\text{F}^{2}$$

-- Magnesium oxide

$$\frac{dk}{dT} = (121.814) \left[0.010722 \quad e^{-0.010722T}\right] - \frac{2\,(7015.835)}{T^{2}} \text{ Btu/hr-ft-}^{o}\text{F}^{2}$$

1. The results of these computations are given in English engineering units, the form in which the data are analyzed by the code.

$$\frac{1}{k}\frac{dk}{dT} = \frac{(121.814)\left[0.010722\ e^{-0.010722T}\right] - \frac{2\ (7015.835)}{T^2}}{0.2529 - 121.814\ e^{-0.010722T} + \frac{7015.835}{T}}\ {}^{o}F^{-1}$$

$$\frac{dc}{dT} = (0.111256)\left[1.33715 \times 10^{-3}\ e^{(-1.33715 \times 10^{-3}\ T)}\right] \text{Btu/lbm-}{}^{o}F^{2}$$

-- Nichrome V

$$\frac{dk}{dT} = 5.75 \times 10^{-3}\ \text{Btu/hr-ft-}{}^{o}F^{2}$$

$$\frac{1}{k}\frac{dk}{dT} = \frac{5.75 \times 10^{-3}}{5.2 + 5.75 \times 10^{-3}\ T}\ {}^{o}F^{-1}$$

$$\frac{dc}{dT} = 0.0002\ \text{Btu/lbm-}{}^{o}F^{2}$$

-- Stainless steel 304

$$\frac{dk}{dT} = 4.2 \times 10^{-3}\ \text{Btu/hr-ft-}{}^{o}F^{2}$$

$$\frac{1}{k}\frac{dk}{dT} = \frac{4.2 \times 10^{-3}}{8.4 + 4.2 \times 10^{-3}\ T}\ {}^{o}F^{-1}$$

$$\frac{dc}{dT} = 0.001\ \text{Btu/lbm-}{}^{o}F^{2}$$

-- Stainless steel 316

$$\frac{dk}{dT} = 4.3 \times 10^{-3}\ \text{Btu/hr-ft-}{}^{o}F^{2}$$

$$\frac{1}{k}\frac{dk}{dT} = \frac{4.3 \times 10^{-3}}{7.5 + 4.3 \times 10^{-3}\ T}\ {}^{o}F^{-1}$$

$$\frac{dc}{dT} = 0.001\ \text{Btu/lbm-}{}^{o}F^{2}$$

-- Stainless steel 347

$$\frac{dk}{dT} = 4.2 \times 10^{-3} \text{Btu/hr-ft-}^{o}\text{F}^{2}$$

$$\frac{1}{k}\frac{dk}{dT} = \frac{4.2 \times 10^{-3}}{8.3 + 4.2 \times 10^{-3}\,T}\ {}^{o}\text{F}^{-1}$$

$$\frac{dc}{dT} = 2.8 \times 10^{-5}\ \text{Btu/lbm-}^{o}\text{F}^{2}$$

For each material excluding dk/dT and (1/k dk/dT) for magnesium oxide it is clear that temperature derivatives and the (1/k) (dk/dT) term are appropriately small. Because of the special form of k(T) for magnesium oxide, the analysis of dk/dT and (1/k) (dk/dT) is more complicated. The interaction of the negative exponential term and the 1/T term makes precise estimates difficult. An alternative approach is to consider the original data. The k(T) functions fits the following table:

T (^{o}F)	k (Btu/hr-ft-^{o}F)
212	20.8
392	16.33
752	9.53
1112	6.65
1472	4.91
1832	4.04
2192	3.53

The maximum $\Delta k/\Delta T$ for this table is 0.02 in the interval between 212°F and 392°F. The corresponding (1/k) ($\Delta k/\Delta T$) value is 0.001, as required.

E-11. Material Properties

DATAR contains a built-in library of pertinent material properties which are unalterable by the user, to avoid potential errors and inconsistencies. Thermal conductivity and specific heat versus temperature curves are built in for each of the materials shown in table E-1. A constant density is built in for each of the materials, with the exception of magnesium oxide and boron nitride. In these two cases, the user must supply the

TABLE E-1

MATERIAL PROPERTY DATA SOURCES

Material	Property	Source of Data
Boron nitride	K	(a)
	Cp	Touloukian[b]
	ρ	Supplied by user
Kanthal	K	(c)
	Cp	(c)
	ρ	Supplier[d]
Magnesium oxide	K	Kingery, et al.[e]
	Cp	Touloukian[b]
	ρ	Supplied by user
Nichrome V	K	Touloukian[b]
	Cp	Touloukian[b]
	ρ	Touloukian[b]
Stainless steel 304	K	WCAP-2808[f]
	Cp	Touloukian[b]
	ρ	Touloukian[b]
Stainless steel 316	K	WCAP-2808[f]
	Cp	Touloukian[b]
	ρ	Touloukian[b]
Stainless steel 347	K	WCAP-2808[f]
	CP	Touloukian[b]
	ρ	Touloukian[b]
Air	K	Baumeister[g]
	Cp	Baumeister[g]
	ρ	Baumeister[g]

a. The thermal conductivity of powdered boron nitride is dependent on several factors. The formula used for this quantity reflects an engineering judgment which considers those factors pertinent to the Westinghouse use of this material.

b. Touloukian, Y. S., Thermophysical Properties of High Temperature Solid Materials, Macmillan, New York, 1967.

c. This quantity has been derived as a function of temperature from data obtained on materials of similar composition.

d. "Physical Properties of Kanthal Alloys," G-45-07, The Kanthal Corporation, Bethel, CT.

e. Kingery, W. D., et al., "Thermal Conductivity X. Data for Pure Oxide Materials Corrected to Zero Porosity," J. Am. Ceram. Soc. 37, 107-110 (1954).

f. Marti Balaguer, L., "MPD Materials Design Manual," WCAP-2808, July 1966.

g. Baumeister, T., Mechanical Engineers Handbook, 6th edition, McGraw-Hill, New York, 1958.

density for the appropriate material. The thermal conductivity and specific heat of boron nitride are not a function of the density, since the heater rods are highly swaged, which provides for approximately 95-percent theoretical density. Note that the thermal conductivity of magnesium oxide depends on the density.

Each thermal conductivity or specific heat is calculated by either a least-squares fit to available data or a linear interpolation from a table of available data. Table E-1 gives the source of the data for each material. A summary of the methods used for each material follows:

-- Boron nitride

$$k = 25.571 - 0.00276T \text{ w/m-}^{o}\text{C}$$
$$(14.778 - 8.8889 \times 10^{-4}\ T \text{ Btu/hr-ft-}^{o}\text{F})$$

$$Cp = 2017.74 - 1396.26e^{-0.00295T} \text{ J/kg-}^{o}\text{C}$$
$$(0.48193 - 0.333492e^{-1.3611 \times 10^{-3} T} \text{ Btu/lb-}^{o}\text{F})$$

$$\rho = \text{input quantity}[\text{kg/m}^3\ (\text{lb/ft}^3)]$$

-- Kanthal

$$k = 16.789 + 0.0134T \text{ w/m-}^{o}\text{C}$$
$$(9.7 + 4.3 \times 10^{-3}\ T \text{ Btu-hr-ft-}^{o}\text{F})$$

Cp = linear interpolation from the following:

T[°C (°F)]		Cp[J/kg-°C (Btu/lb-°F)]	
-32	(0)	456.4	(0.109)
648	(1200)	753.6	(0.180)
760	(1400)	1172.3	(0.280)
871	(1600)	745.2	(0.178)
1204	(2200)	779.6	(0.185)

$$\rho = 7144.2 \text{ kg/m}^3\ (446.0 \text{ lb/ft}^3)$$

-- Magnesium oxide

$$k = \rho_{MgO}\,(0.0273 - 13.15e^{-0.0192T} + 420.9/T)/223 \text{ w/m-}^{o}\text{C}$$
$$[\rho_{MgO}\,(0.2529 - 121.814e^{-0.010722T} + 7015.835/T)/223 \text{ Btu/hr-ft-}^{o}\text{F}]$$

$$Cp = 1377.353 - 465.805e^{-0.002406T} \text{ J/kg-}^{o}\text{C}$$
$$(0.328976 - 0.111256e^{-1.33715\times10^{-3}T} \text{ Btu/lb-}^{o}\text{F})$$

ρ = input quantity[kg/m^3 (lb/ft^3)]

-- Nichrome V

$$k = 8.997 + 0.0179T \text{ w/m-}^{o}\text{C } (5.2 + 5.75 \times 10^{-3}T \text{ Btu/hr-ft-}^{o}\text{F})$$

Cp = linear interpolation from the following:

T[^{o}C (^{o}F)]		Cp[J/Kg-^{o}C (Btu/lb-^{o}F)]	
-32	(0)	427.1	(0.102)
260	(500)	502.4	(0.120)
482	(900)	535.9	(0.128)
593	(1100)	577.8	(0.138)
704	(1300)	623.8	(0.149)
816	(1500)	653.1	(0.156)
871	(1600)	661.5	(0.158)
982	(1800)	653.1	(0.156)

ρ = 8361.63 kg/m^3 (522.0 lb/ft^3)

-- Stainless steel 304

$$k = 14.535 + 0.01308T \text{ w/m-}^{o}\text{C } (8.4 + 4.2 \times 10^{-3}\,T \text{ Btu/hr-ft-}^{o}\text{F})$$

Cp = linear interpolation from the following:

T [°C (°F)]		Cp [J/kg-°C (Btu/lb-°F)]	
-32	0	372.6	(0.089)
149	(300)	372.6	(0.089)
260	(500)	378.9	(0.0905)
371	(700)	389.4	(0.093)
482	(900)	404.0	(0.0965)
593	(1100)	420.8	(0.1005)
816	(1500)	458.4	(0.1095)
926	(1700)	475.2	(0.1135)
1038	(1900)	483.6	(0.1155)
1093	(2000)	485.7	(0.116)

ρ = 8025.2 kg/m^3 (501.3 lb/ft^3)

-- Stainless steel 316

k = 12.978 + 0.01339T w/m-°C (7.5 + 4.3 x 10^{-3} T Btu/hr-ft-°F)]

Cp = linear interpolation from the following:

T [°C (°F)]		[Cp J/kg-°C (Btu/lb-°F)]	
-32	(0)	439.6	(0.105)
204	(400)	510.8	(0.122)
315	(600)	540.1	(0.129)
427	(800)	561.0	(0.134)
871	(1600)	619.6	(0.148)
1038	(1900)	659.4	(0.1575)
1204	(2200)	703.4	(0.168)

ρ = 7949.96 kg/m^3 (496.3 lb/ft^3)

-- Stainless steel 347

k = 13.064 + 0.0143T w/m-°C (7.55 + 4.58 x 10^{-3} T Btu/hr-ft-°F)

$$Cp = 447.99 + 0.211T \text{ J/kg-}^{o}\text{C } (0.107 + 2.8 \times 10^{-5} \text{ T Btu/lb-}^{o}\text{F})$$

$$\rho = 7905.1 \text{ kg/m}^3 \ (493.5 \text{ lb/ft}^3)$$

-- Air

$$k = 20.91 \times 10^{-5} (T + 273)^{0.846} \text{ w/m-}^{o}\text{C}$$
$$[7.35 \times 10^{-5} (T + 460)^{0.846} \text{ Btu/hr-ft-}^{o}\text{F}]$$

$$Cp = 1009.02 \text{ J/kg-}^{o}\text{C } (0.241 \text{ Btu/lb-}^{o}\text{F})$$

$$\rho = 1.201 \text{ kg/m}^3 \ (0.075 \text{ lb/ft}^3)$$

Although the option is generally only used in the heater region, DATAR permits a mixture of any two materials to exist in any radial region. In this instance, the properties at each node in the region must be adjusted to account for the effect of the mixture. This is accomplished as follows:

Let

x	= volume fraction of material A
ρ_A, K_A, C_A	= properties of material A
ρ_B, K_B, C_B	= properties of material B
$\bar{\rho}, \bar{K}, \bar{C}$	= mixture properties

Then

$$\rho = x\rho_A + (1 - x)\rho_B$$

$$K = xK_A + (1 - x)K_B$$

$$\bar{C} = \frac{x\rho_A C_A}{\bar{\rho}} + \frac{(1 - x)\rho_B C_B}{\bar{\rho}}$$

This formulation provides an exact accounting of the mixture heat capacity and a parallel conduction path approximation for the effective thermal conductivity. The approximation to the mixture thermal conductivity is not expected to introduce any significant error, however, since the only mixed region for a normal case is the second radial region, which conducts less heat than any of the more exterior regions.

E-12. QUENCH PROGRAM

The QUENCH program was utilized for reduction of heater rod thermocouple data. This program was designed to determine the following quantities:

-- Initial temperature

-- Maximum temperature

-- Turnaround time

-- Quench time

-- Quench temperature

The initial temperature or temperature at flood time was determined by interpolating between the temperature recorded at the last negative time (preflood) and the temperature recorded at the first positive time (postreflood). The maximum temperature was determined by simply searching for that temperature and the turnaround time was the time at which the maximum temperature occurred.

To determine the quench time and temperature, the following method was used.

The program advances sequentially through all the data for each thermocouple channel, looking at five points at a time [T(t) at 1 through 1 + 4, figure E-1, sheet 1]. The first criterion applied is that the temperature, T(t), must be greater than 149°C (300°F) to qualify as a potential quench condition. If it is not, the remaining criteria are skipped.

The second criterion checks whether the slope of the temperature-time curve between the third and fourth points is greater than 28°C (50°F) per second, that is, whether

$$\frac{T(1+3) - T(1+2)}{t(1+3) - t(1+2)} < -50^{\circ}F/sec$$

The decision whether a quench exists or not is made on this basis. If not, the remaining criteria are skipped and the program advances to the next data point.

The third criterion checks whether the absolute value of the slope between the third and fourth points is two times greater than the absolute value of the slope between the first and second points, that is, whether $S_2 > 2S_1$. If so, a quench condition exists. If not, the program skips out of the search and advances to the next set of data points.

Finally, the program checks the absolute value of the slope between the fourth and fifth data points (S'_2) and compares it to the absolute value of the slope between the third and fourth points (S_2).

If $S'_2 > S_2$, then the quench time and temperature is defined to be the intersection of L'_1 and L'_2 (figure E-1, sheet 2).

E-13. FFLOWS PROGRAM

The FFLOWS program was utilized to calculate mass balance and void fraction.

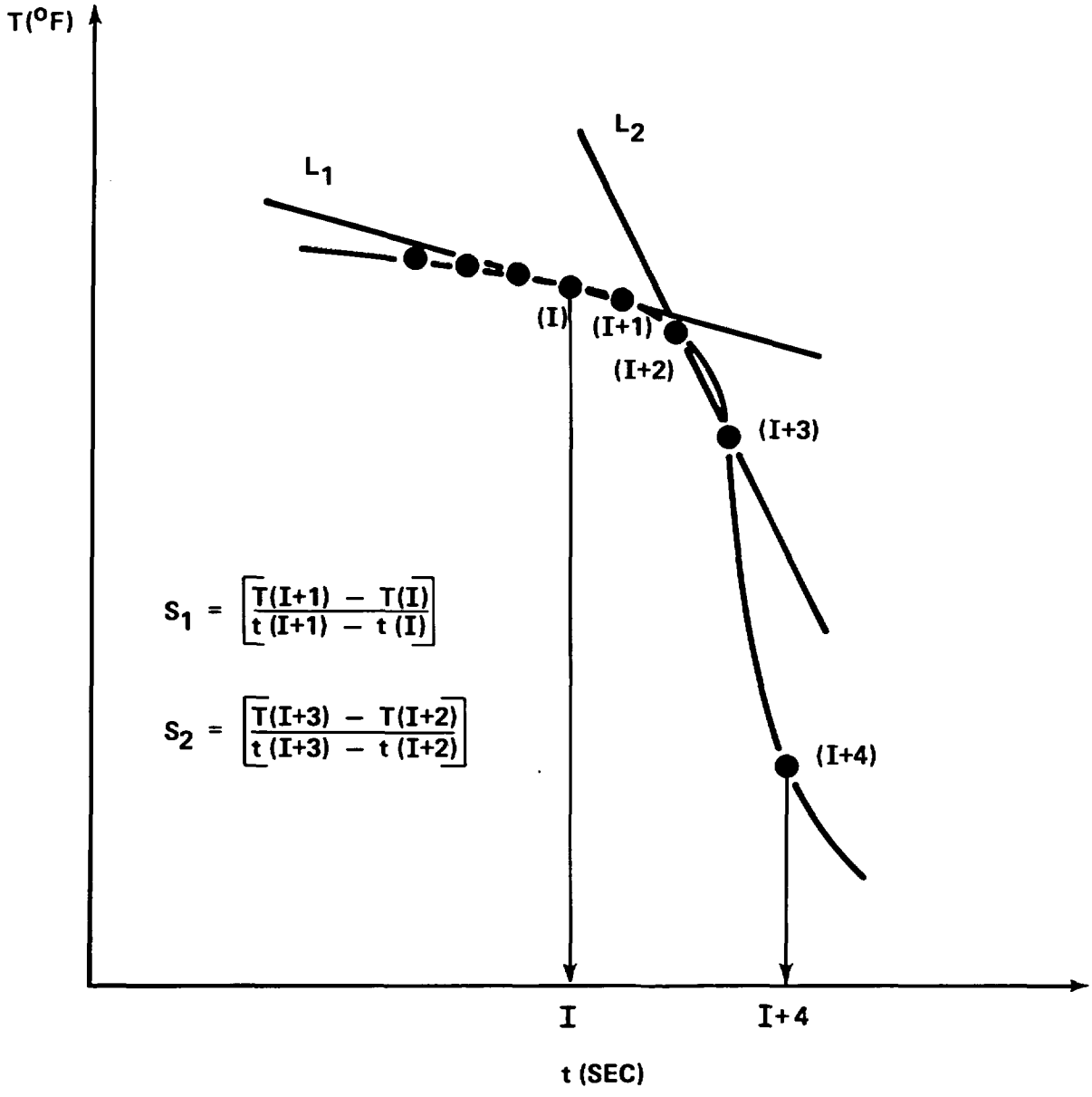

Figure E-1. Determination of Quench Time and Temperature (sheet 1 of 2)

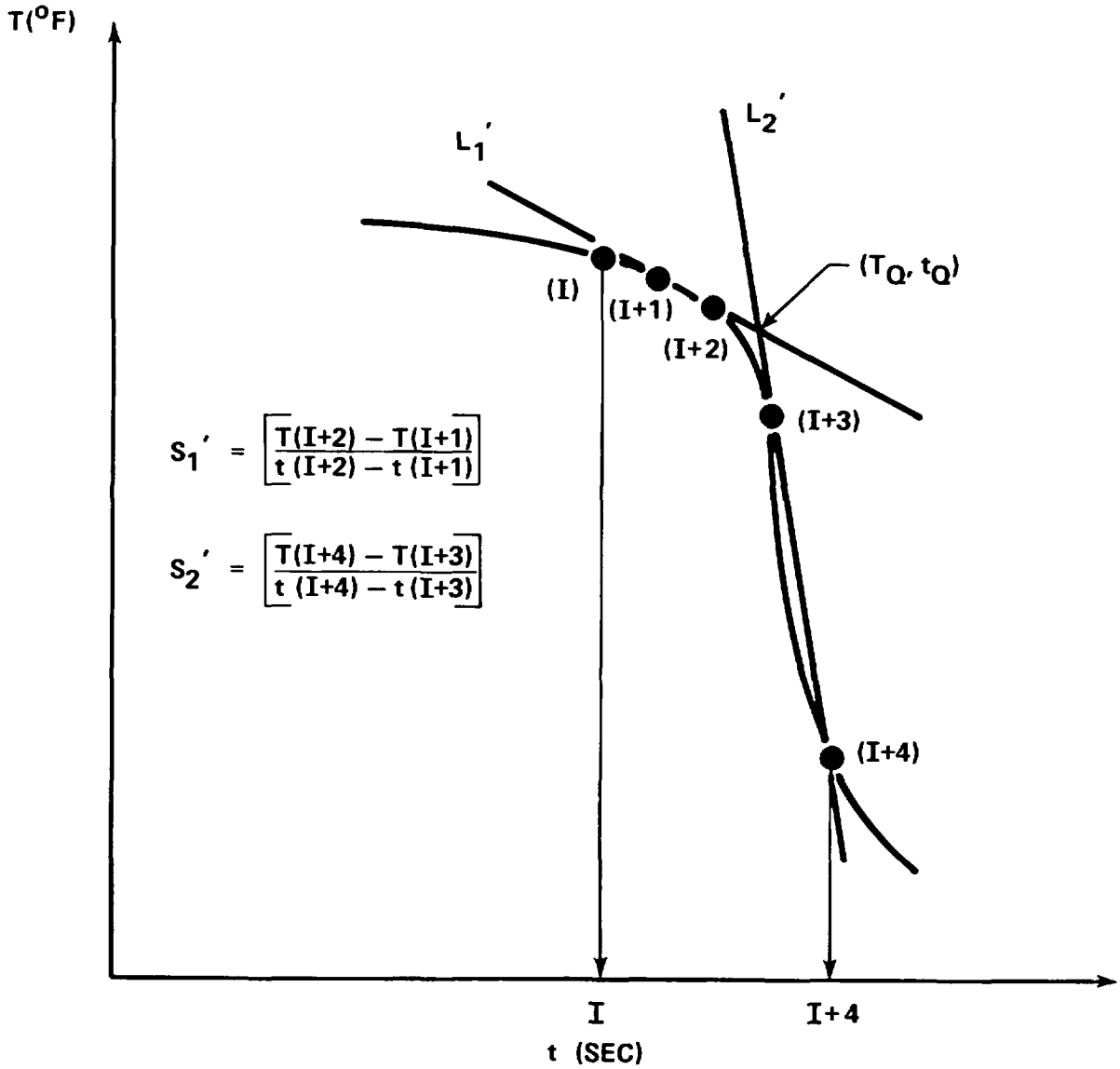

Figure E-1. Determination of Quench Time and Temperature (sheet 2 of 2)

A mass balance was calculated for each test using the FFLOWS program, which calculated the flow rates, mass storage, frictional pressure drop, and bundle void fraction distribution. This program is a modification of the mass balance program used in the FLECHT skewed test series.

The following steps were carried out:

-- The injected mass was calculated from the inlet turbine meter.

-- The liquid collected was calculated from the differential pressure cells on the carryover tank, upper plenum, and steam separator tanks, assuming all differential pressure was elevation head with water at the saturation temperature.

-- The steam flow was calculated from the orifice differential pressure cell using the measured steam temperature and local pressure to obtain the steam density.

-- The mass storage in the test bundle was calculated using the 0 to 3.66 m (0 to 144 in.) differential pressure cell reading (corrected for frictional pressure drop).

There was between 0.9 and 5.9 kg (2 and 13 lb) of water collected in the steam probe collection tanks during a reflood test. This mass represents approximately 0.7 to 5 percent of the injected mass; however the average for 41 reflood tests was 1.4 percent (figure E-2). When this mass was added to the total mass flow out of the system and the mass collection in the test system, the test mass balance was usually within 10 percent, with an average of 5.3 percent. The mass balance results for all reflood tests are shown in appendix C.

In addition to calculation of the mass flows through the test system, the space-averaged void fraction was calculated from the measured pressure drop over each of the 0.30 m (12 in.) sections of the bundle. The measured pressure drop consists of three effects: elevation head, frictional pressure drop, and acceleration pressure drop due to liquid vaporization:

$$\Delta P_{measured} = \Delta P_{elevation} + \Delta P_{acceleration} + \Delta P_{friction}$$

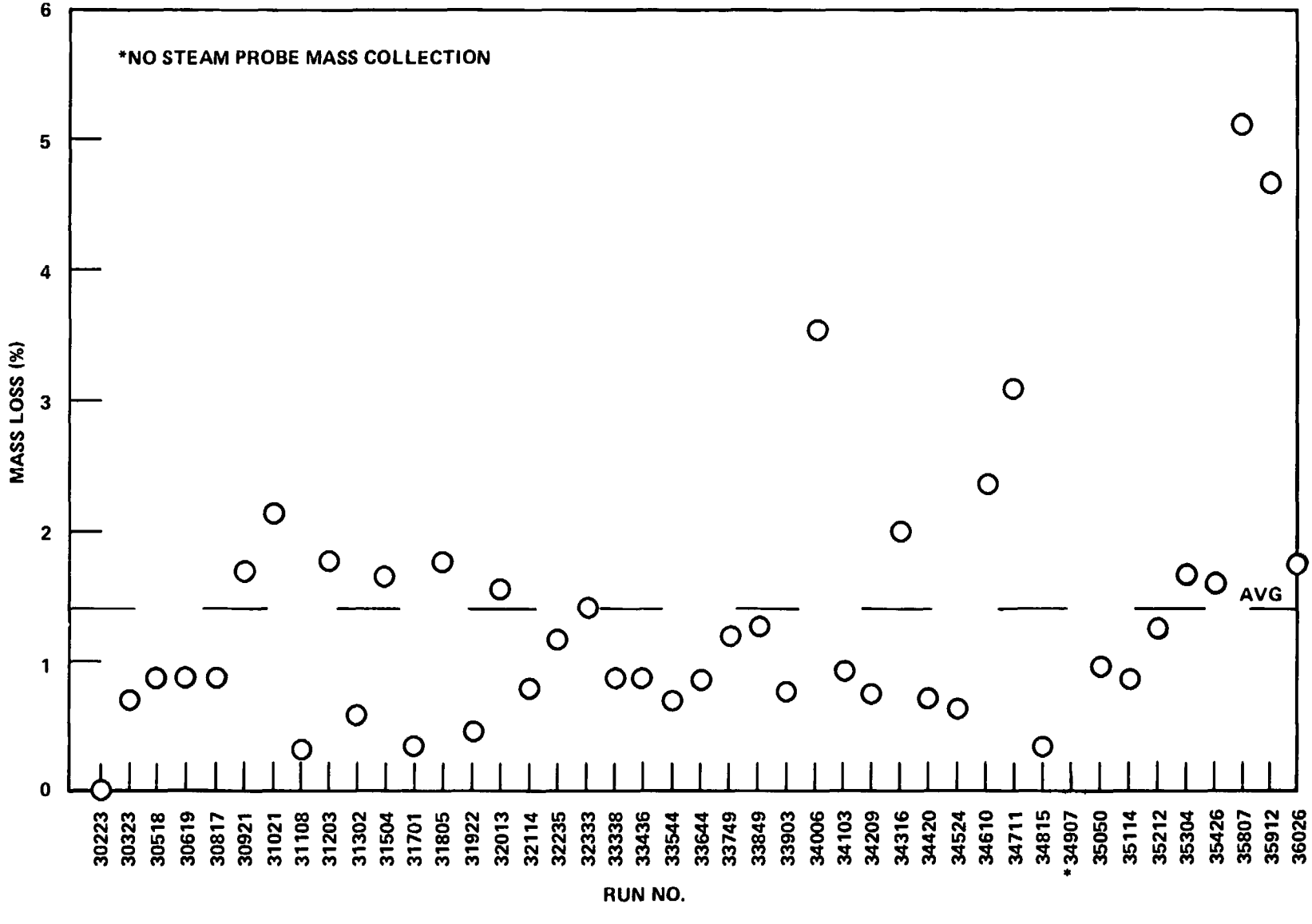

Figure E-2. Mass Loss Through Aspirating Steam Probes

The relative magnitude of each of these components has been examined in the FLECHT-SET Phase A report.[1] It was concluded that the vapor elevation head and the acceleration pressure drop were completely negligible and that the frictional pressure drop was a second-order effect compared to the liquid elevation head. The small frictional pressure drop for a gravity reflooding situation is attributed to the high injection rate, which quickly absorbs the bundle energy. Therefore, the steam generation rate is small during the transient. It was felt that forced low flooding rate tests would result in such substantial evaporation of the injected flow that frictional pressure drop could be important during the transient. Because the 12 axial differential pressure cells on the test bundle were $\pm$ 0.0069 MPa ($\pm$ 1.0 psid) pressure cells, the frictional pressure drop could be measured in the tests and accurately accounted for. In this fashion, if the frictional pressure drop was calculated for a test, this value could be subtracted from the measured pressure drop to obtain the liquid elevation head, and therefore, the space-averaged void fraction.

The frictional pressure drop was calculated as

$$\Delta P_{friction} = \left(\frac{fL}{D_e} + K_g\right)\frac{\rho_b V_b^2}{2g_c}$$

where

L = length = 0.30m (12 in.)

K_g = $C_V E^2$ [2]

C_V = 6.5 for Re > 30,000 = 196 $Re^{-0.33}$

E = A_G/A_B

A_G = cross-sectional area of grid

A_B = cross-sectional area of bundle

1. Blaisdel, J. A., et al., "PWR FLECHT-SET Phase A Report," WCAP-8238, December 1973.
2. Rehme, K., "Pressure Drop Correlation for Fuel Element Spacers," Nucl. Technol. 17, 15-23 (1973).

ρ_b = bundle steam density evaluated from the average of the 22 bundle steam probe readings at respective elevations and test section pressure

D_e = bundle hydraulic diameter = 4 (flow area)/wetted perimeter = 0.960 cm (0.378 in.)

V_b = bundle steam velocity obtained from the mass flow rate through the exhaust orifice = $M/(\rho_b \times \text{bundle flow area})$

The housing was assumed to be hydraulically smooth and the heater rod roughness was taken as that for drawn tubing $(\theta/D_e = 3.0 \times 10^{-4}$ cm $(1.2 \times 10^{-4}$ in.)).

Therefore, the friction factor for Re > 2000, which is a curve fit to data presented in Crane,[1] is

$$f = 5.5 \times 10^{-3} \left[1.0 + \left(20000 \frac{\theta}{D_e} + \frac{10^6}{R_c}\right)^{1/3}\right]$$

For Re < 2000,

$$f = 64/Re$$

In calculating the frictional pressure drop, the criterion used to determine when the frictional pressure drop was important relative to the elevation head within a 0.30 m (12 in.) span was that if the measured axial differential pressure for that span was 0.014 MPa (0.21 psid) or greater ($\alpha \sim 50$ percent), the span was considered to be full of water or two-phase mixture. In this case, no frictional pressure drop was calculated for that span. It should be noted that the pressure drop across a totally full 0.30 m (12 in.) span is 0.0029 MPa (0.42 psid) for saturated water at 0.28 MPa (40 psia). If the measured differential pressure was less than 0.0014 MPa (0.21 psid) for a given span, then the frictional pressure drop was calculated for the entire span and its value was subtracted from the measured pressure drop to obtain the elevation pressure drop component. The calculated elevation pressure drop was then used to calculate the mass storage and the void fraction within the 0.30 m (12 in.) span.

1. Flow of Fluids Through Valves, Fittings, and Pipe, Crane Co., New York, 1979.

That is,

$$\alpha = 1 - \frac{(\Delta P_{measured} \quad \Delta P_{friction})}{\rho_{sat\ liquid} \quad gL}$$

where L = the distance between differential pressure cells 0.30 m (12 in.).

Examples of the calculated frictional pressure drop for the entire bundle for three tests are shown in figures E-3 through E-5. These frictional pressure drop values represent the summation of all the individual 0.30 m (12 in.) span frictional pressure drops for the bundle in which the measured pressure drop was less than 0.0014 MPa (0.21 psid) in each span.

As these figures show, the calculated frictional pressure drop was quite small for tests 31504 and 31922, averaging approximately 0.000069 to 0.00017 MPa (0.01 to 0.025 psid) for each 0.30 m (12 in.) span. The calculated frictional pressure drop followed the steam flow history in the rod bundle and decreased with time.

The oscillations in the calculated frictional pressure drop were due to steam flow oscillations caused by the pressure control valve variations during the test. The maximum calculated frictional pressure drop per 0.30 m (12 in.) span was only 10 percent of the elevation pressure drop for a 50-percent void fraction mixture in that span, and was normally a small correction to the measured pressure drop.

When variable flooding rate tests (run 32333) were conducted, another trend was observed in the frictional pressure drop. Initially, the calculated frictional pressure drop was large, because of the large burst of steam flow generated by the variable flooding rate. The steam flow stayed higher for the additional 5 seconds after the high flow period ended. The large steam flow was due to the boiloff of the high flow injected mass. Once this mass had been boiled and entrained out of the bundle, the steam flow and resulting frictional pressure drop decreased sharply, and was quite small to the end of the test. Therefore, the void fractions calculated at early time in variable flooding rate tests must be evaluated carefully, since the frictional pressure drop is large.

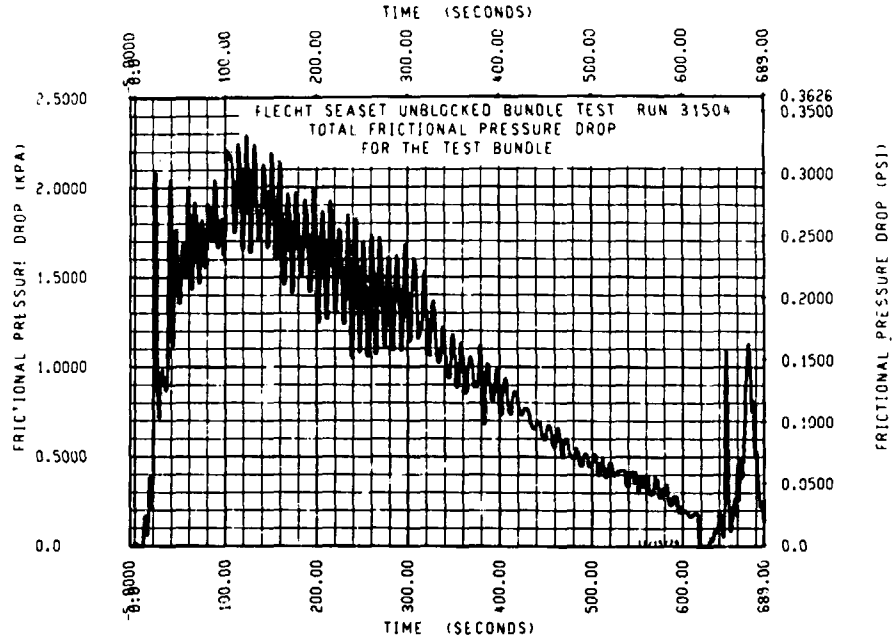

Figure E-3. Frictional Pressure Drop Versus Time, Run 31504

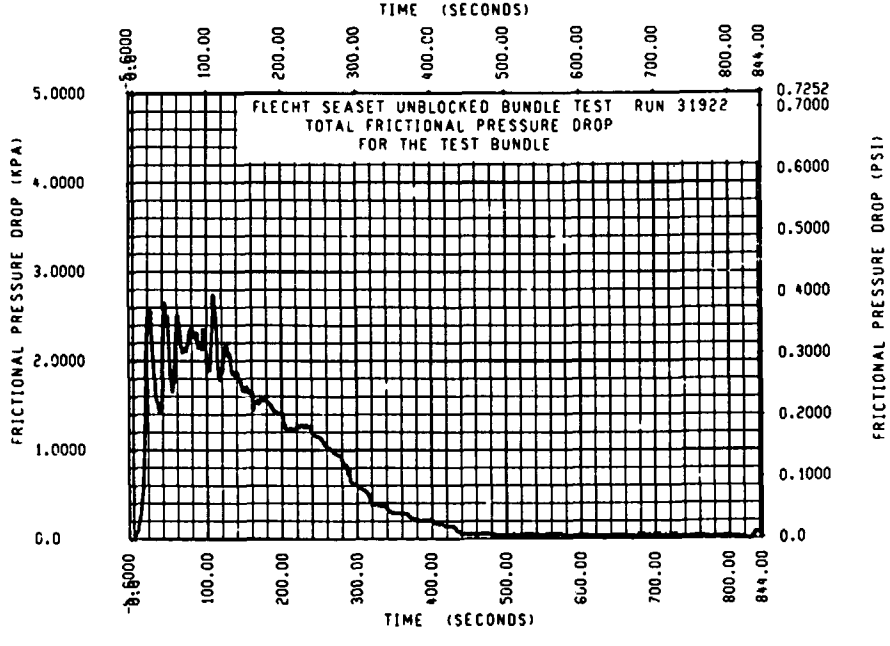

Figure E-4. Frictional Pressure Drop Versus Time, Run 31922

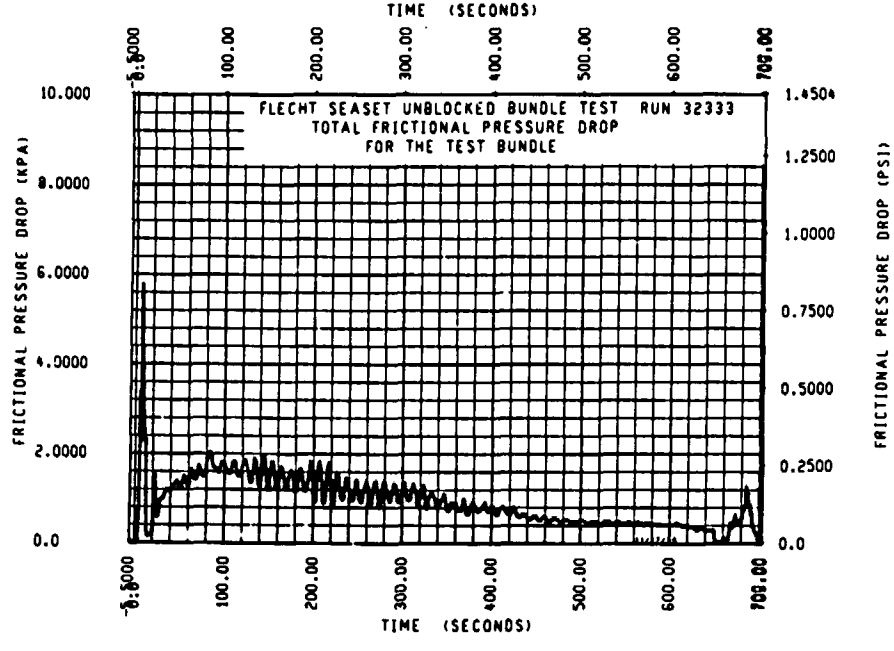

Figure E-5. Frictional Pressure Drop Versus Time, Run 32333

In general, it can be concluded that the frictional pressure drop is small relative to the water elevation head and can be accounted for by the method outlined above. The only case in which the frictional pressure drop becomes large compared to elevation head pressure drop is during forced variable injection tests, in which a large amount of boiloff occurs.

For 11 test runs, the carryover tank had to be drained prior to completion of the test, because of its limited capacity. The carryover tank was originally sized for and used in the FLECHT skewed test series, whose injected water mass was only about 60 percent of that of the unblocked bundle test series. The water which was drained from the carryover tank during the test was collected and subsequently weighed, and the overall mass balance was corrected. This correction is shown by the vertical line at the end of the total mass inventory line in figure E-6 for run 31203. The 11 tests in which the carryover tank was drained during testing were runs 30619, 30817, 31108, 31203, 31302, 31701, 33903, 34103, 34209, 34524, and 34815.

For these tests, an overall mass balance based on the collection tank differential pressure measurements could not be performed. However, an overall mass balance based on the posttest collected water weights could be performed. A comparison of the two methods of calculating an overall mass balance was made for 28 reflood tests in which the carryover tank did not have to be drained during the test run. This comparison, shown in figure E-7, indicates that the two methods of calculating the overall mass balance are in good agreement. The average difference between the two methods was 4.2 percent, with a standard deviation of 2.1 percent.

In the 152 mm/sec (6 in./sec) flooding rate test (run 31701), the upper plenum filled prior to filling of the carryover tank; this was attributed not only to the relatively small drain size between the upper plenum and the carryover tank but also to the rate of carryover. With the upper plenum full, water ran down the exhaust line to the steam separator. The separator drain tank quickly filled and the separator began to fill. An unknown quantity of water exited through the exhaust line orifice during the test, which resulted in a poor overall mass balance (28 percent). However, the mass balance was satisfactory (8 percent) through the time of bundle quench, as shown in figure E-8.

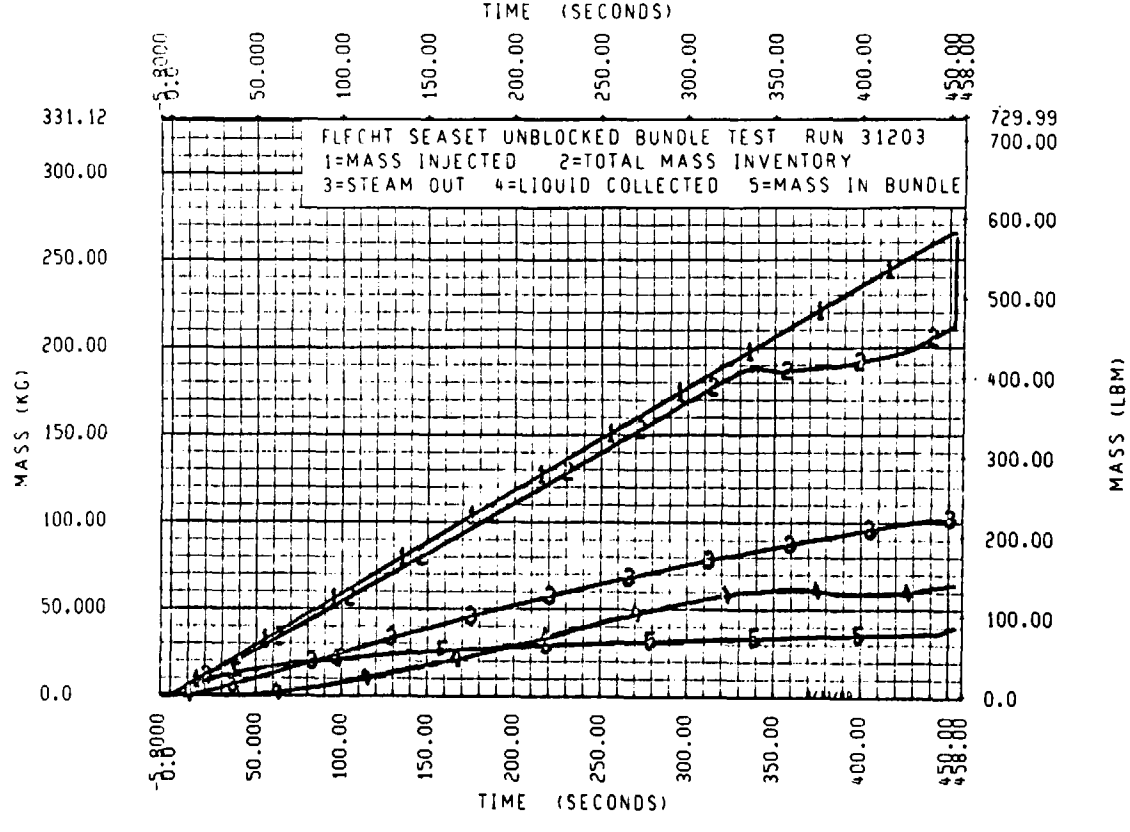

Figure E-6. Mass Injected Versus Total Mass Inventory, Run 31203

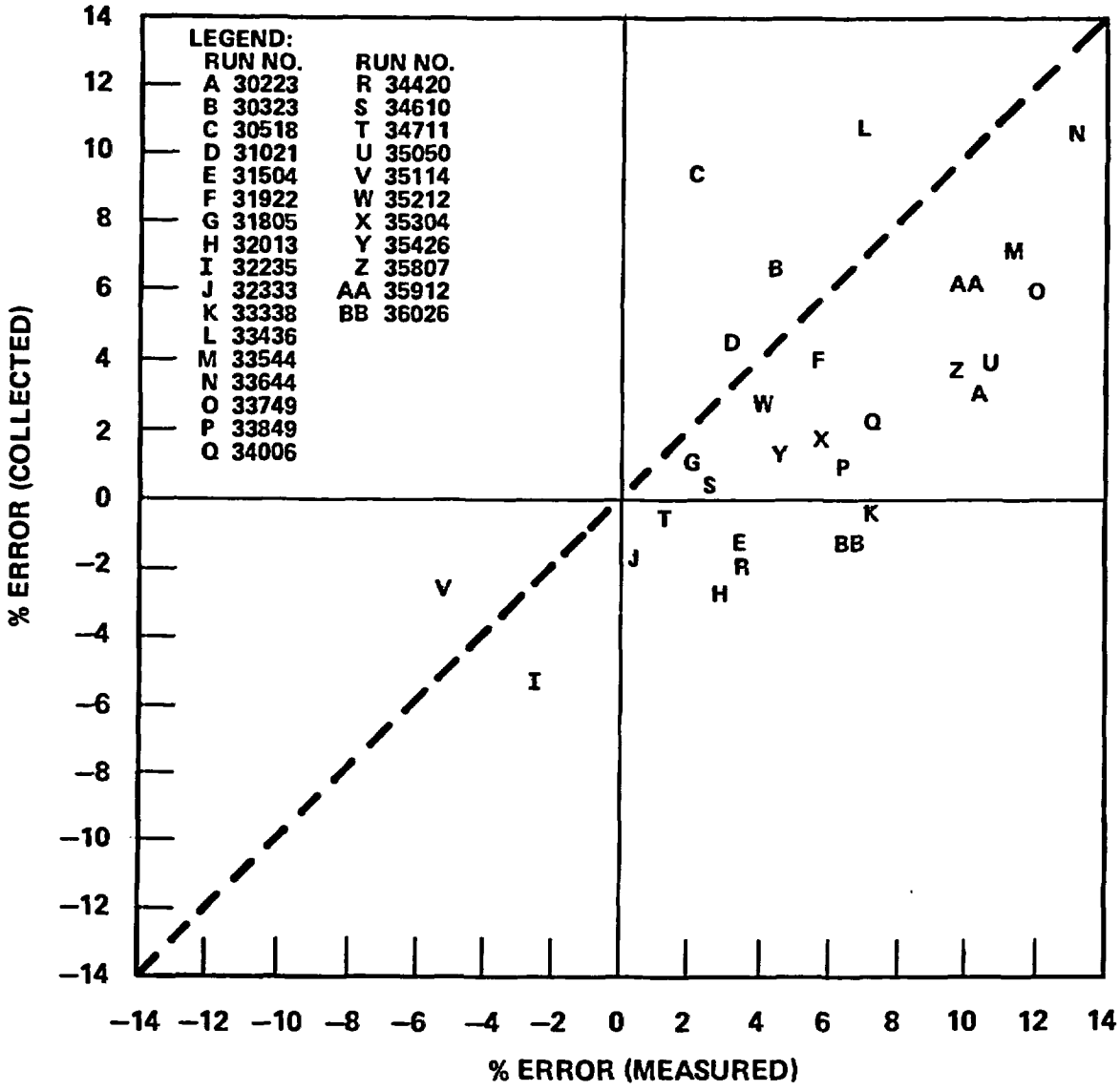

Figure E-7. Mass Balance Comparison

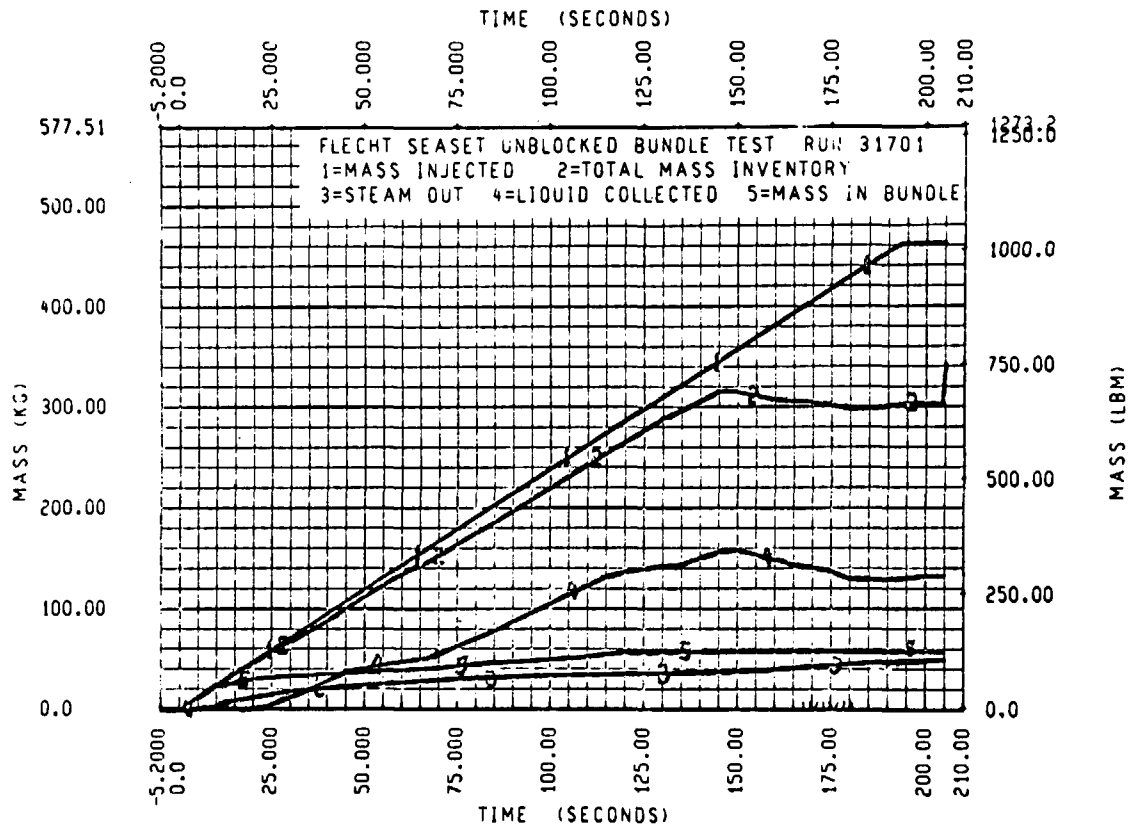

Figure E-8. Mass Injected Versus Total Mass Inventory, Run 31701

In the 25 mm/sec (1 in./sec) flooding rate test at 0.14 MPa (20 psia) system pressure (run 31922), the carryover tank filled and the upper plenum subsequently filled. The water then ran down the exhaust line to the steam separator, which filled to less than half its capacity. It is believed that no water, or at least very little water, was lost through the exhaust orifice since the mass balance as calculated from the collection tank differential pressure cells was satisfactory (6 percent), as shown in figure E-9. This mass balance agreed fairly well with the drained water weights obtained at the conclusion of the test (4 percent). The carryover tank and upper plenum filled after the bundle had quenched. A rod thermocouple which failed during the test provided a signal to the CDAS that the bundle had not quenched. Therefore, injection flow was maintained for approximately 500 seconds until terminated by the loop operators.

In the gravity reflooding tests, a mass balance calculation was performed around the downcomer, as in the FLECHT skewed testing program. The flooding rate into the bundle was calculated using the following equation:

$$M_{input} = \int_0^t \dot{m}_{input}\, dt = \int_0^t \dot{m}_{inj}\, dt - M_D(t)$$

where

M_{input} = mass of water in the bundle kg (lb)

m_{input} = mass flooding rate into the bundle kg/sec (lb/sec)

$\dot{m}_{inj}$ = mass injection rate into the downcomer kg/sec (lb/sec)

M_D = mass stored in the downcomer kg (lb)

The flooding rate into the bundle, m_{input}, was obtained from the time rate of change of mass put into the test section, M_{input}. The injection rate into the downcomer was measured by the turbine meter. The mass stored in the downcomer was calculated

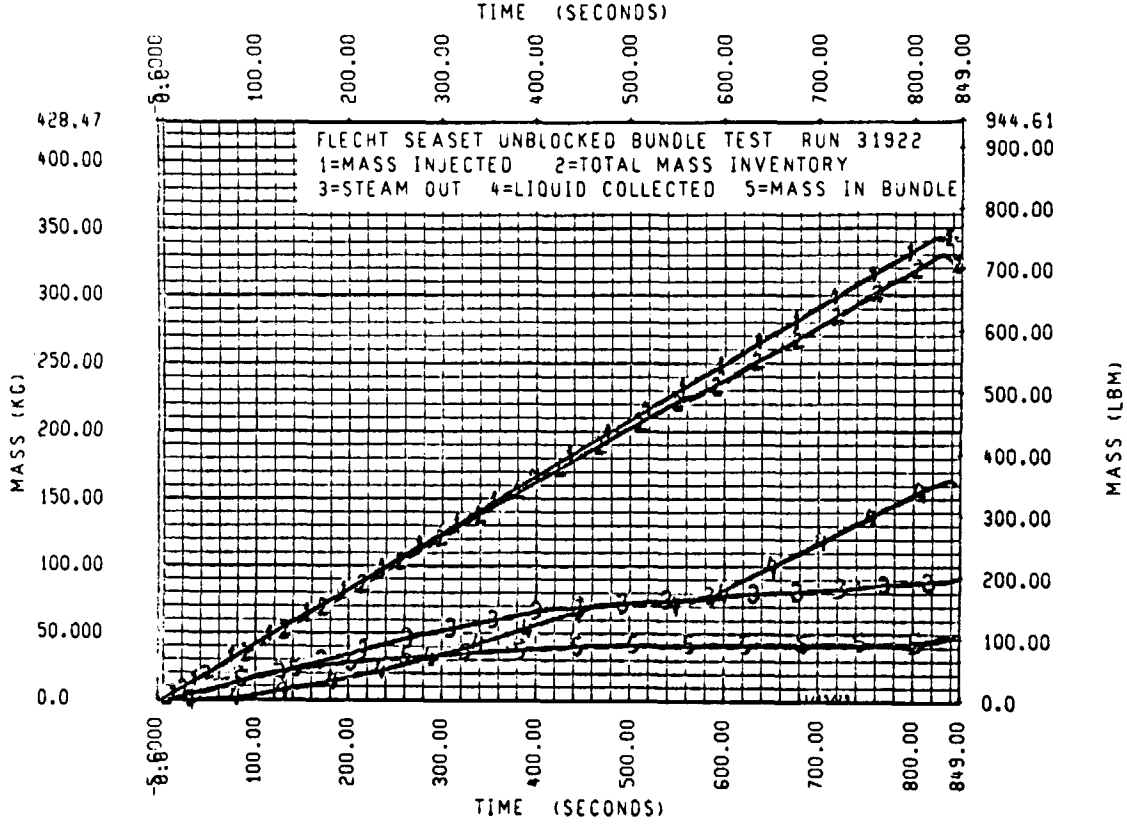

Figure E-9. Mass Injected Versus Total Mass Inventory, Run 31922

using the output of the differential pressure transducer which measured the liquid level in the downcomer. Bundle flooding rates calculated with this technique were compared to the flooding rates measured by the bidirectional turbo-probe installed in the crossover pipe.

E-14. DATA AVERAGING

A simple averaging technique was used for reducing much of the data presented in this report. This was done to clarify graphic presentation of results and to obtain average values of oscillating quantities where use of the instantaneous values could result in large errors. The technique used consisted of replacing each data point with the mean value of the original data point and a specified number of points before and after the time of interest. This process is defined by the following equation:

$$x(i) \equiv \frac{1}{t(i + \Delta - 1) - t(i - \Delta)} \sum_{n=i\Delta}^{n=i + \Delta-1} \frac{x(n) + x(n + 1)}{2}$$

where

$x(n) = f(t)$

Δt = interval between data points

$\Delta = n \times \Delta t$

n = integer

APPENDIX F
FAILED ROD ANALYSIS

F-1. INTRODUCTION

Shortly after the FLECHT SEASET unblocked bundle test series began, in run 30418, rod 4G failed when the heater coil shorted to ground. An adjacent heater rod, 5G, failed in an attempt to dry out the boron nitride insulation after run 30418. To prevent any additional damage to these rods or other rods within the bundle, these two rods remained unpowered for the remainder of the test series. Approximately midway through the test series in run 33849, rod 12J failed when the heater coil shorted to ground. The adjacent heater rods, 11I, 11J, 11K, 12I, 12K, 13J, and 13K, were found to have low isolation resistance. These rods also remained unpowered for the remainder of the test series. The unpowered rods in the test bundle constituted a possible heat sink for hotter rods in the bundle which would otherwise not be present. Therefore, an analysis was undertaken to determine what effect unpowered rods had on the data from the powered rods.

F-2. METHOD OF ANALYSIS

The following two methods were utilized to assess the effect of failed rods on the adjacent heater rods:

-- Examination of the heat transfer behavior of heater rods which would not be influenced by the failed rods

-- A MOXY calculation of the unblocked bundle rod array with and without the initial pair of failed rods

F-3. HEAT TRANSFER COMPARISONS

The initial pair of failed rods in the FLECHT SEASET unblocked bundle, rods 4G and 5G, are shown in figure F-1. The effect of the failed rods on the bundle heat transfer was examined by comparing heat transfer coefficients for rods one, two, and more rows

away from the failed rods. Several of these rods were in symmetrical positions with respect to the failed rods. Because of the large number of thermocouple failures in the early part of the test program, it was not possible to provide a complete set of comparisons at one elevation. Therefore several elevations were compared to achieve the objective of this analysis. The instrumented heater rods and the two failed rods are shown in figures F-2 through F-9 for the 1.83 through 1.98 m (72 through 78 in.) elevations.

The tests chosen for this analysis were runs 31504 and 31805. These tests provided the greatest number of instrumented rods of the initial low flooding rate tests conducted. The low flooding rate provided for high rod temperatures and therefore maximized the radiation heat transfer effect between failed rods and adjacent powered rods. The nominal initial conditions for runs 31504 and 31805 were as follows:

-- 871°C (1600°F) initial clad temperature
-- 2.3 kw/m (0.7 kw/ft) peak linear power
-- 78°C (140°F) inlet subcooling
-- 0.28 MPa (40 psia) system pressure
-- 25 mm/sec (1 in./sec) flooding rate for run 31504
-- 20 mm/sec (0.8 in./sec) flooding rate for run 31805

Figures F-2 through F-9 show the heat transfer for heater rods one, two, and more rows away from the failed rods. These figures indicate that the radiation heat transfer effect between the failed rods and the adjacent powered rods was very localized.

F-4. ROD POWER ANALYSIS

The two-phase flow behavior is primarily dependent on the total amount of energy which must be removed by the coolant. Since the FLECHT SEASET unblocked bundle represents a total energy input from 161 rods, the loss of two rods is only a 1.24 percent decrease in the total power into the bundle. This small power decrease had a negligible

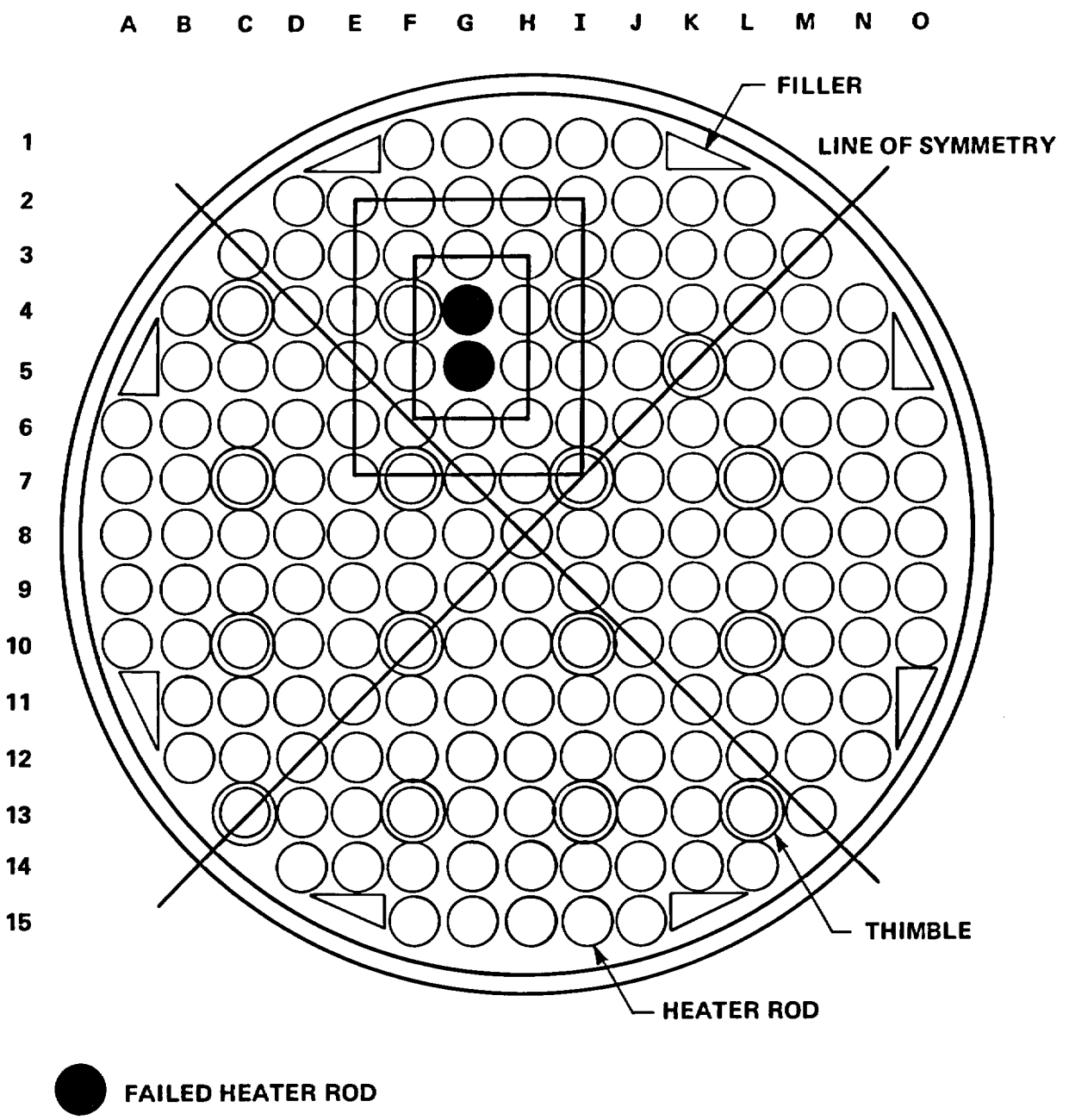

Figure F-1. Bundle Cross Section

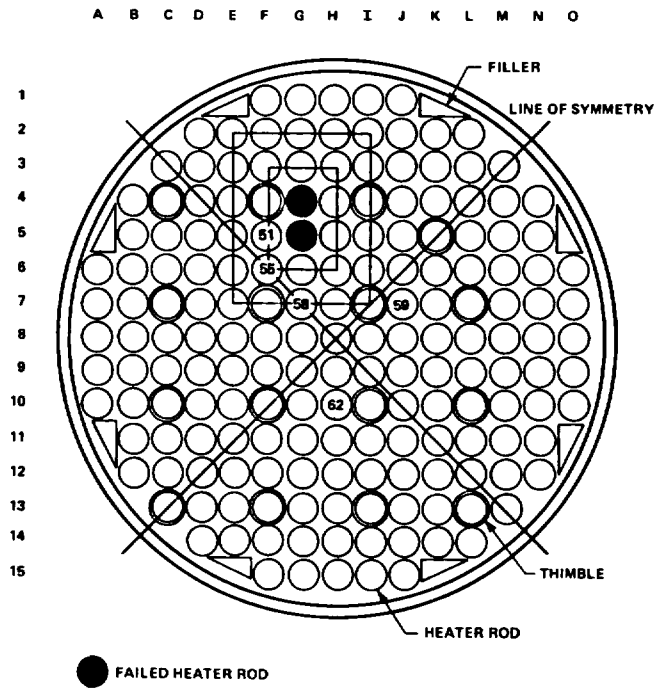

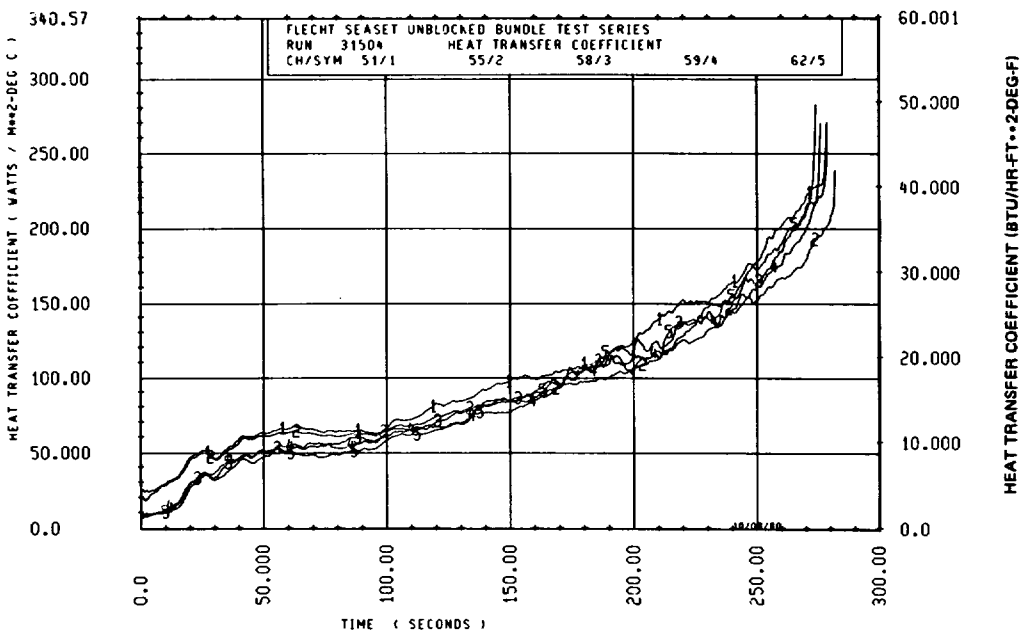

Figure F-2. Bundle Cross Section and Instrumentation, and Heat Transfer Results, at 1.83 m (72 in.) for Run 31504 (sheet 1 of 2)

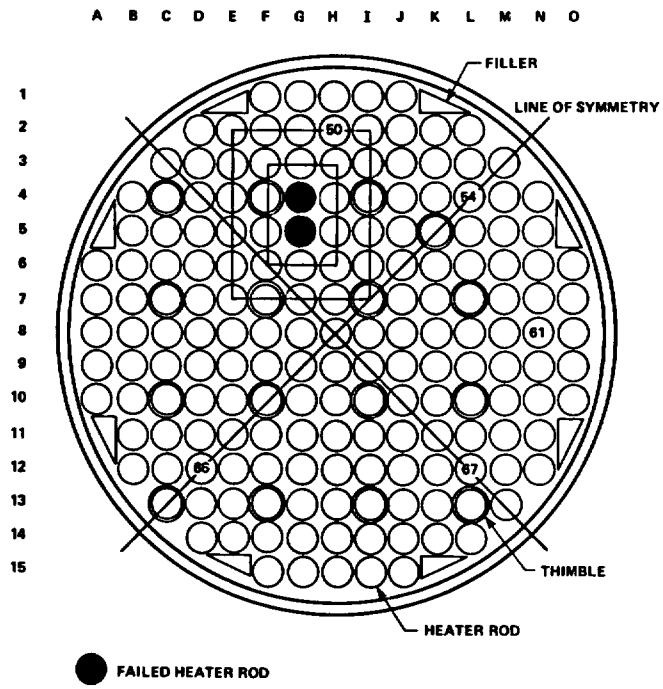

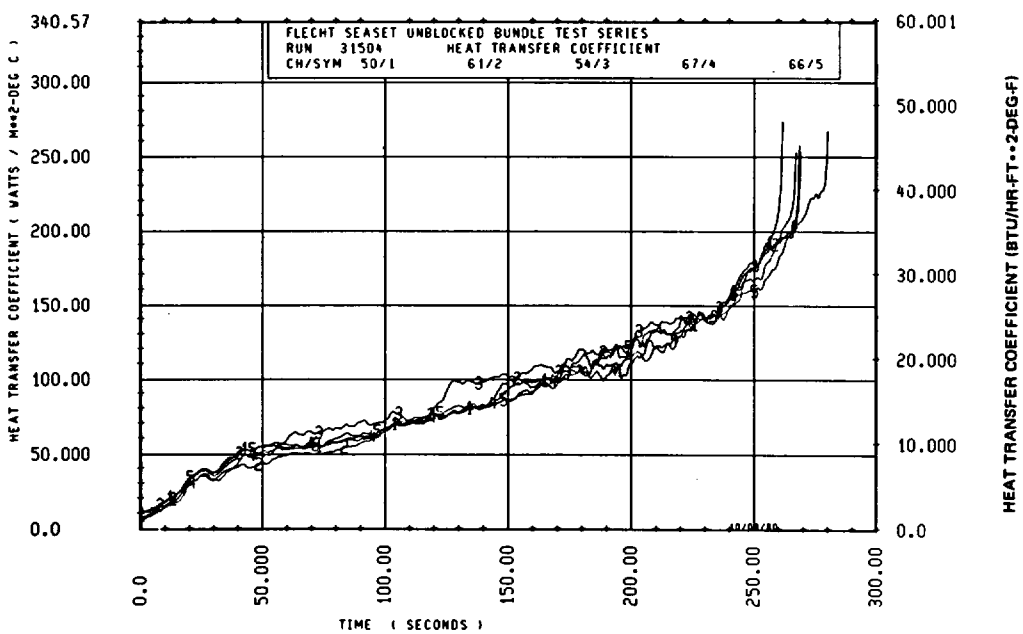

Figure F-2. Bundle Cross Section and Instrumentation, and Heat Transfer Results, at 1.83 m (72 in.) for Run 31504 (sheet 2 of 2)

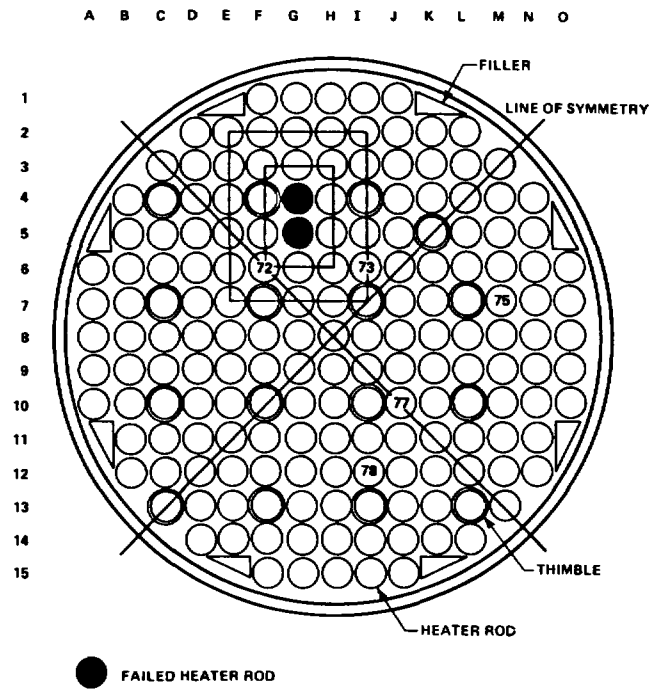

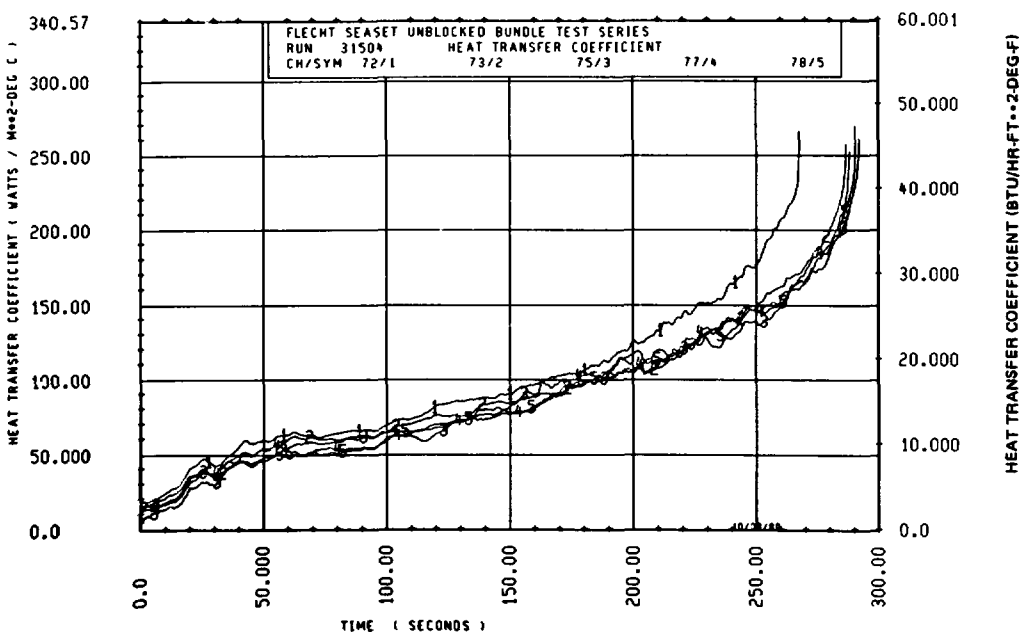

Figure F-3. Bundle Cross Section and Instrumentation, and Heat Transfer Results, at 1.88 m (74 in.) for Run 31504 (sheet 1 of 2)

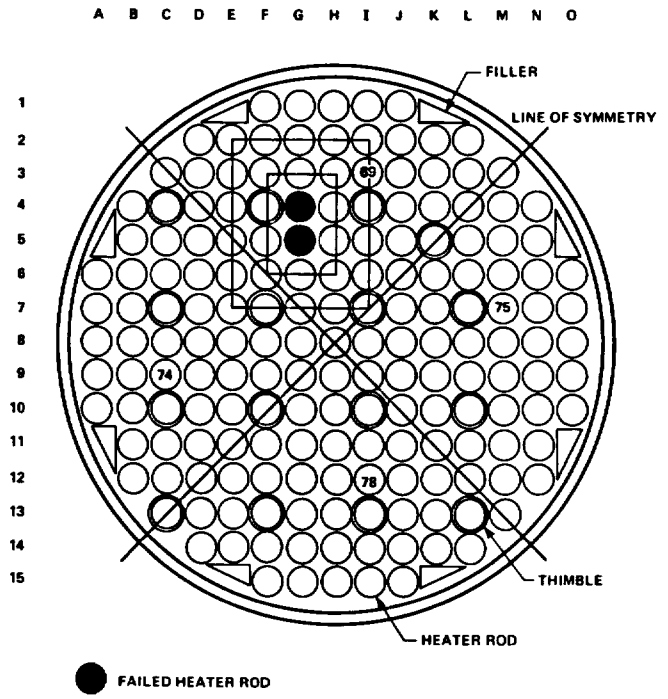

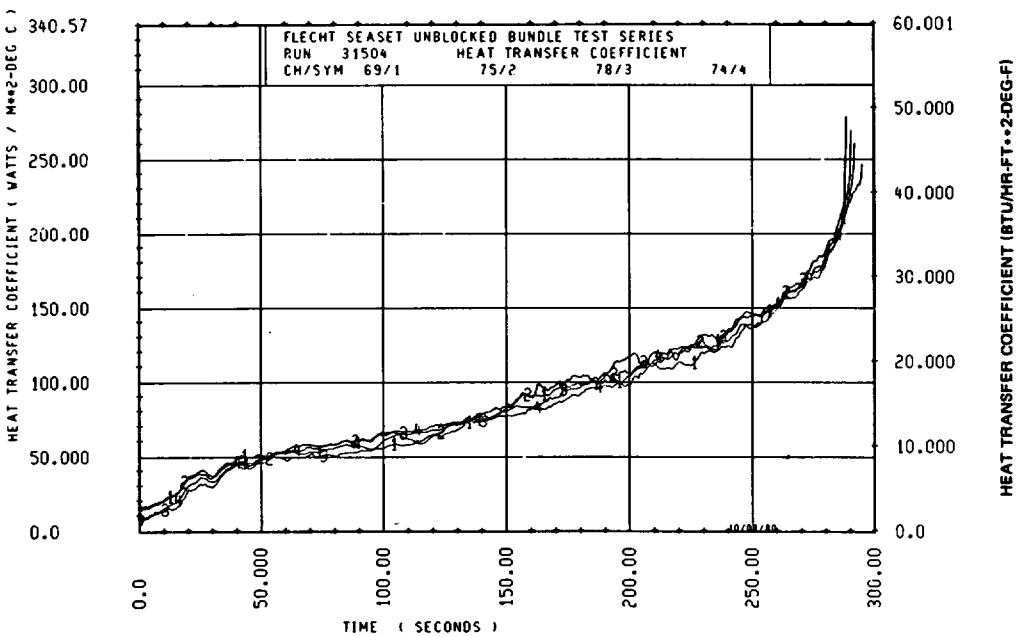

Figure F-3. Bundle Cross Section and Instrumentation, and Heat Transfer Results, at 1.88 m (74 in.) for Run 31504 (sheet 2 of 2)

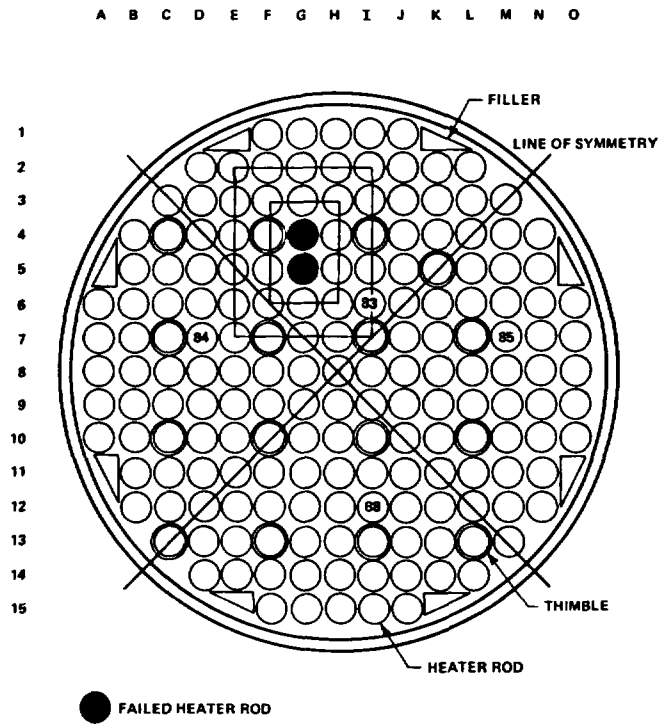

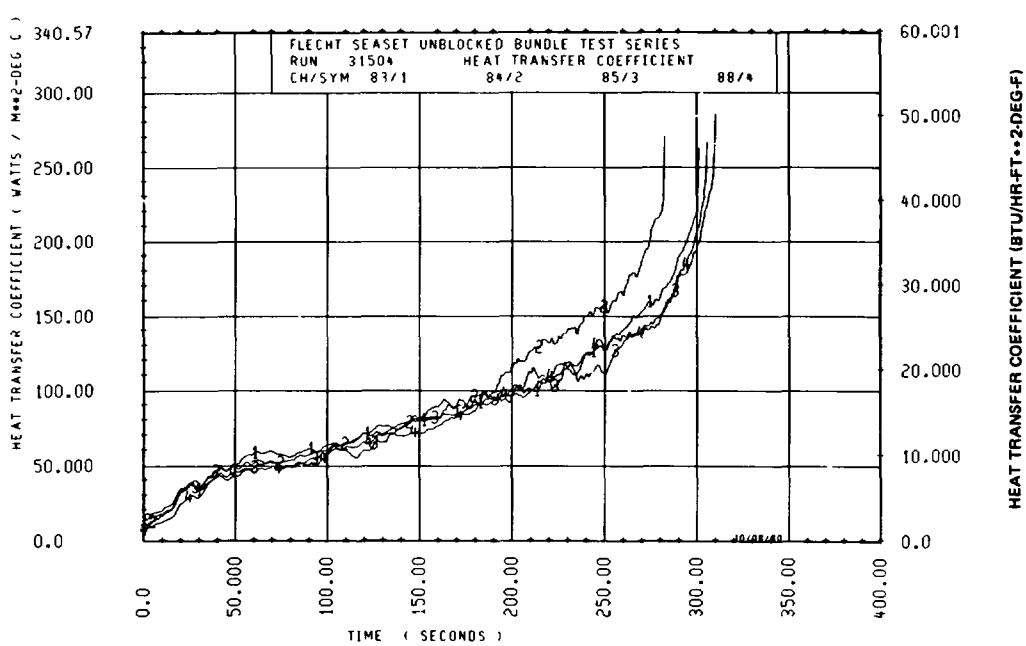

Figure F-4. Bundle Cross Section and Instrumentation, and Heat Transfer Results, at 1.93 m (76 in.) for Run 31504

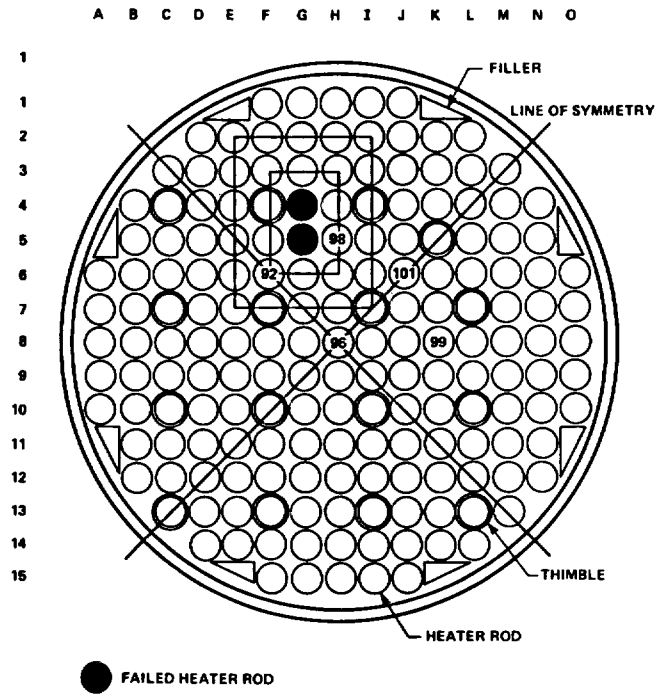

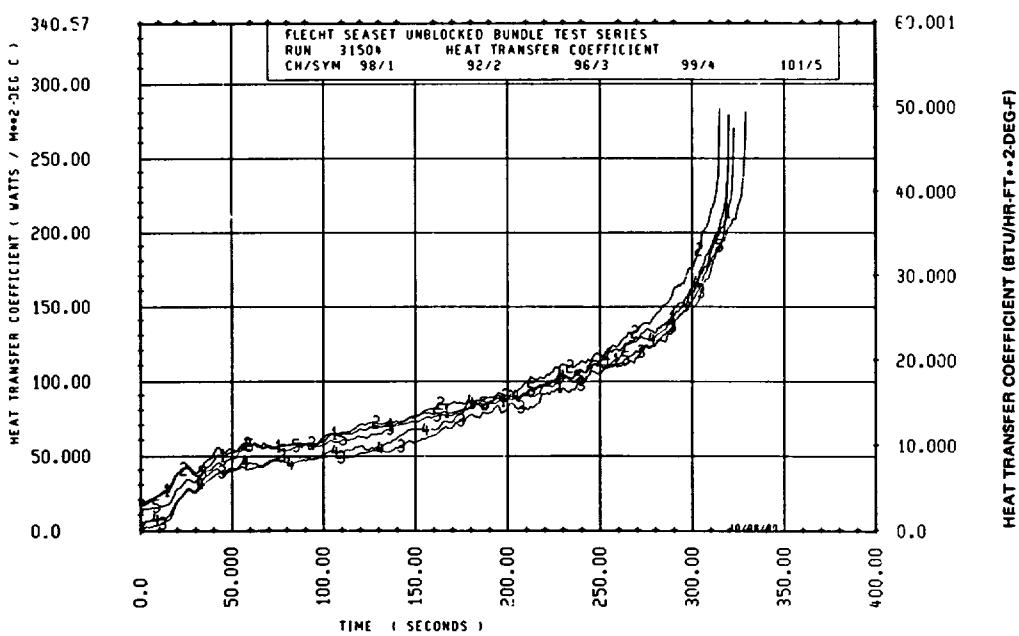

Figure F-5. Bundle Cross Section and Instrumentation, and Heat Transfer Results, at 1.98 m (78 in.) for Run 31504

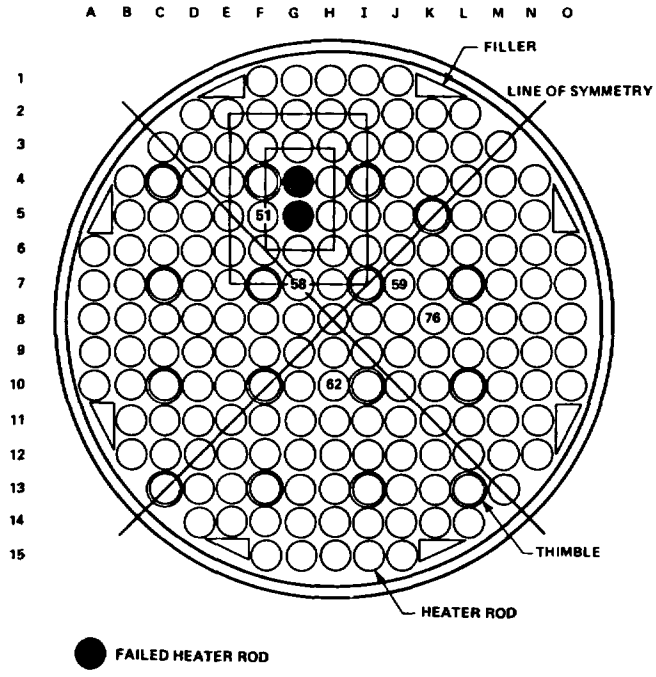

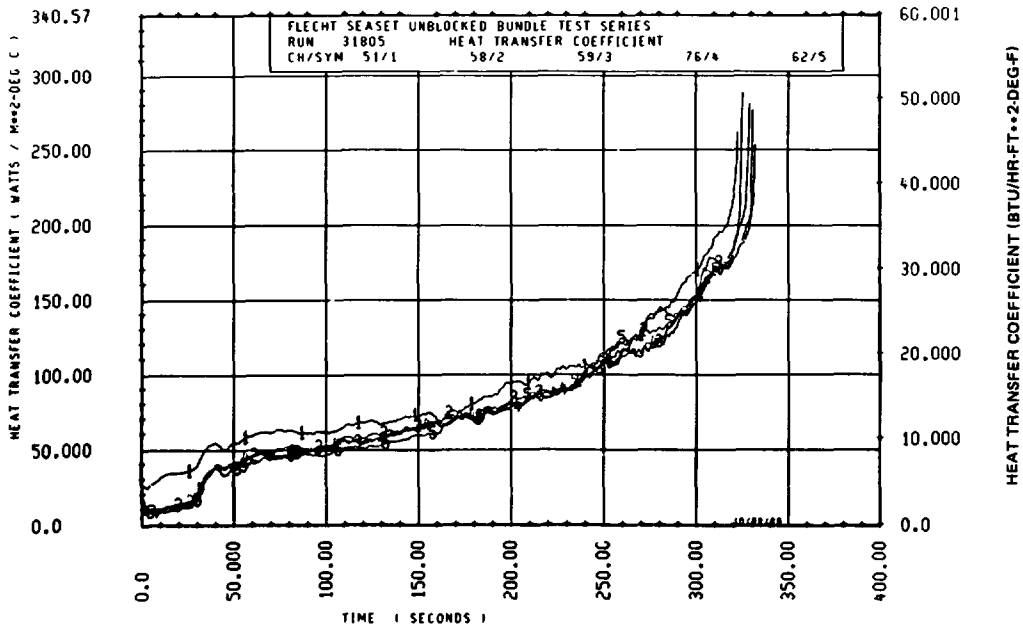

Figure F-6. Bundle Cross Section and Instrumentation, and Heat Transfer Results, at 1.83 m (72 in.) for Run 31805 (sheet 1 of 2)

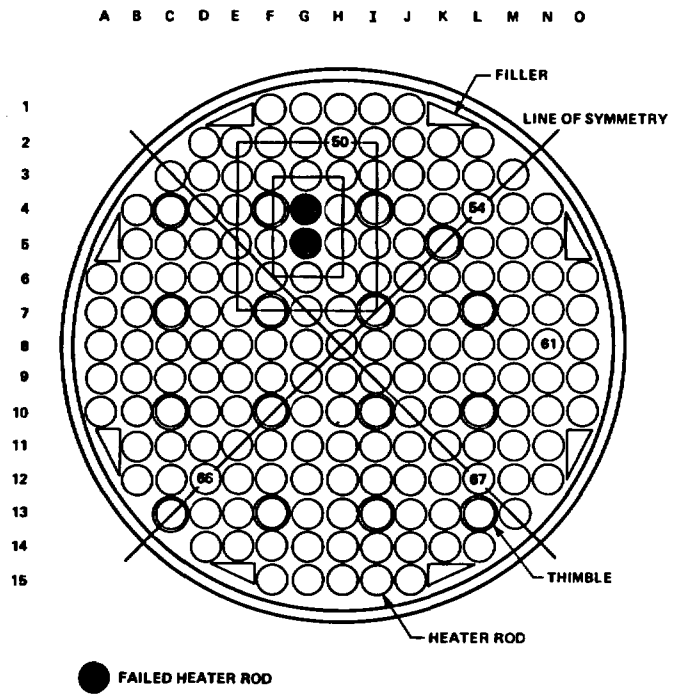

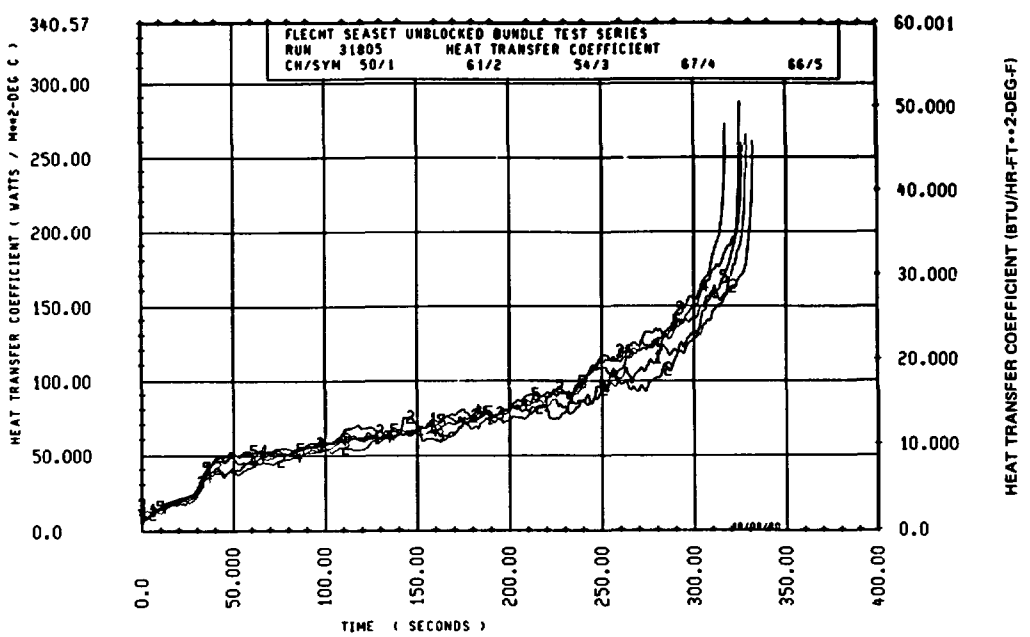

Figure F-6. Bundle Cross Section and Instrumentation, and Heat Transfer Results, at 1.83 m (72 in.) for Run 31805 (sheet 2 of 2)

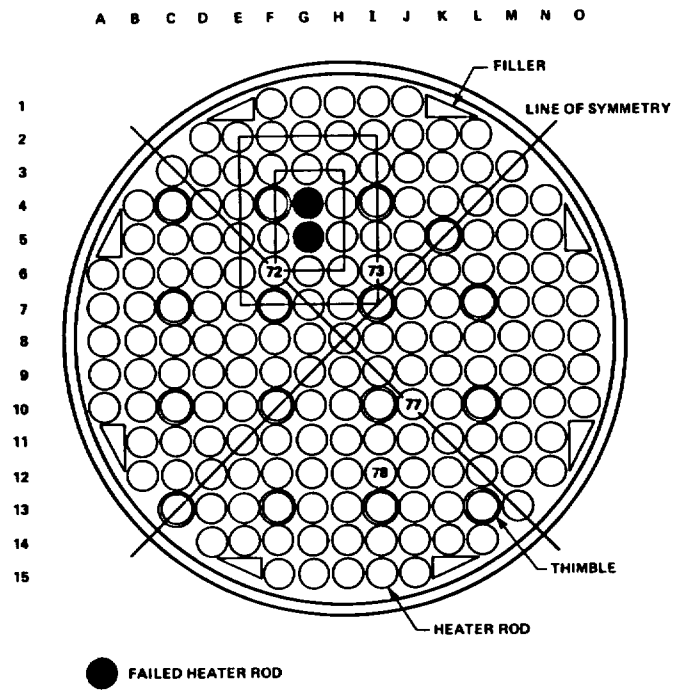

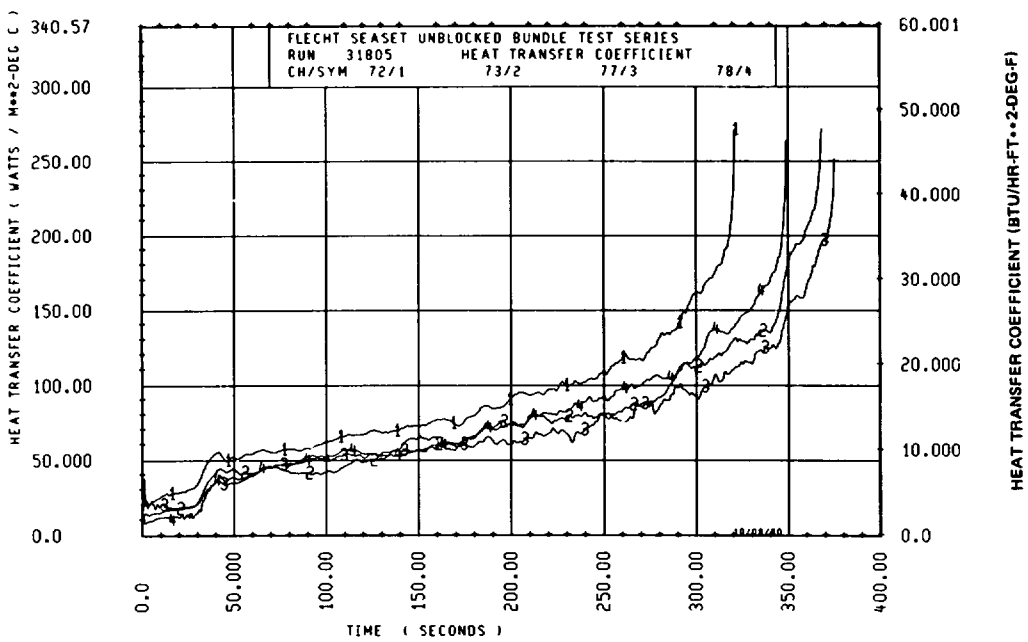

Figure F-7. Bundle Cross Section and Instrumentation, and Heat Transfer Results, at 1.88 m (74 in.) for Run 31805

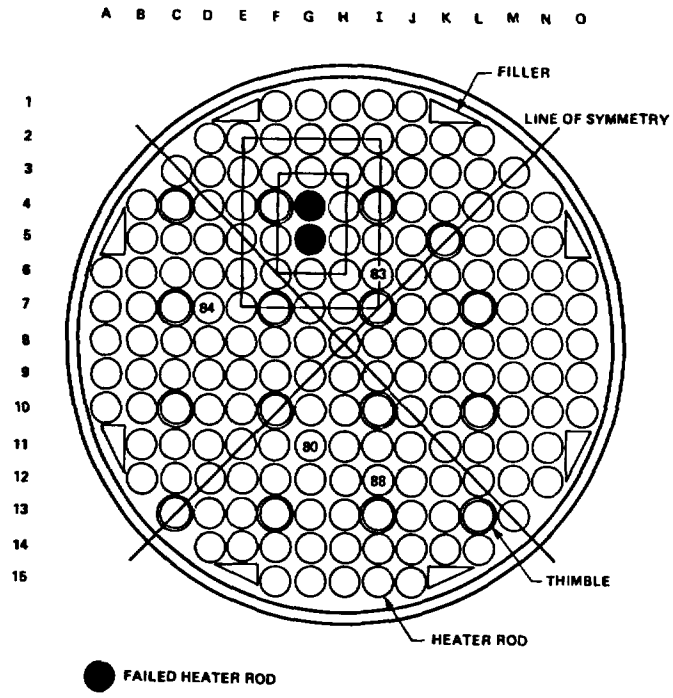

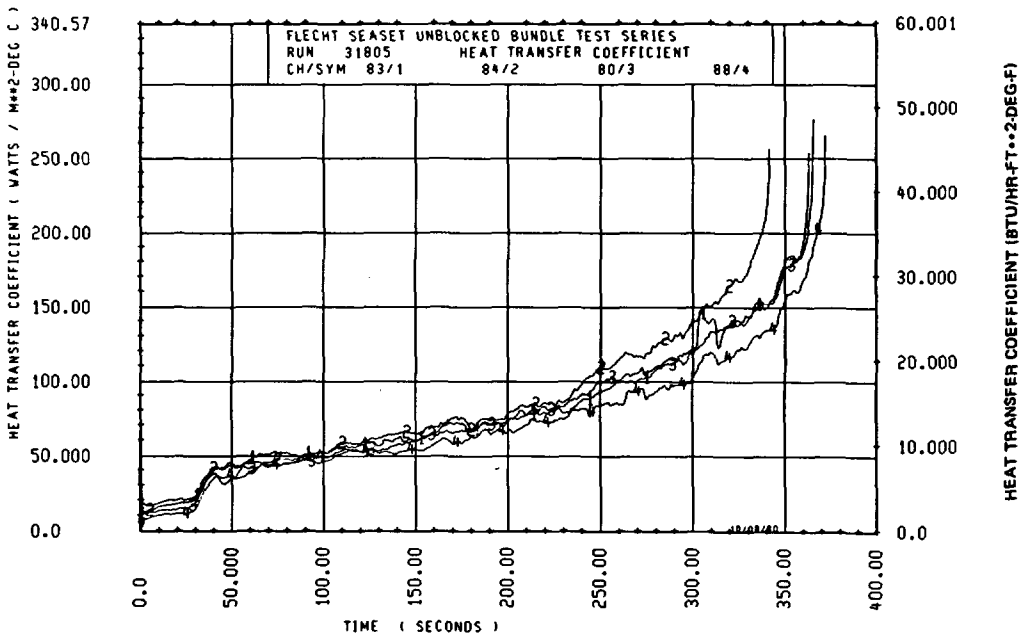

Figure F-8. Bundle Cross Section and Instrumentation, and Heat Transfer Results, at 1.93 m (76 in.) for Run 31805

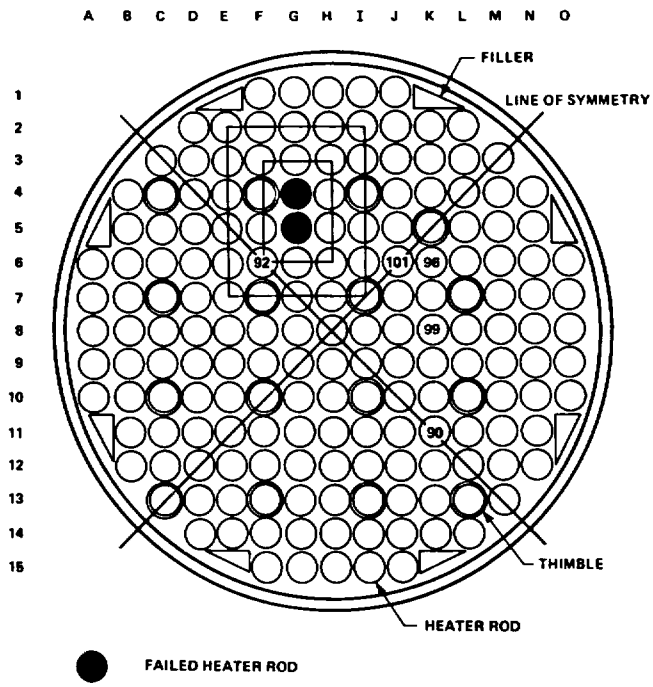

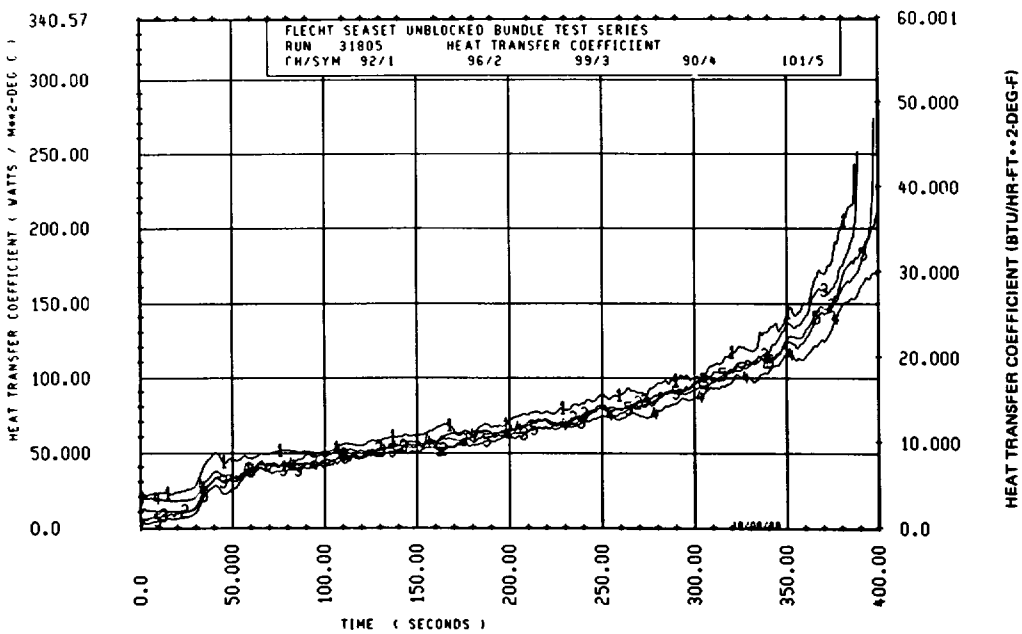

Figure F-9. Bundle Cross Section and Instrumentation, and Heat Transfer Results, at 1.98 m (78 in.) for Run 31805

effect on the resulting two-phase flow structure within the bundle. However, the loss of eight additional rods approximately midway through the test program resulted in a 6.2 percent decrease in the total power into the bundle. To counteract this effect, the bundle power was increased to a level prior to the loss of the eight heater rods, since most of the tests were conducted with the original pair of failed rods, rods 4G and 5G. The rod power was subsequently increased to the ratio of 159 to 151, or by 5.3 percent.

To evaluate the impact of increasing the rod power by 5.3 percent, two tests were conducted with 10 unpowered rods with (run 34103) and without (run 33903) the 5.3-percent increased rod power. These two tests were subsequently compared to a test (run 31203) conducted earlier in the test program at nominal rod power with only two unpowered rods. The nominal test conditions for all three tests were as follows:

-- 871°C (1600°F) initial clad temperature
-- 0.28 MPa (40 psia) system pressure
-- 78°C (140°F) inlet subcooling
-- 38 mm/sec (1.5 in./sec) flooding rate
-- Uniform radial power distribution

Heat transfer coefficient comparisons were made for several rod thermocouples away from the eight failed rods which were not common to all three tests between the 1.70 m (67 in.) and 3.05 m (120 in.) elevations. These thermocouples (as shown in figure F-10) represented the locations which were recorded for all three tests. (See table C-2 for exact elevations.) Figure F-11 indicates that the heat transfer for run 34103, with increased rod power and 10 failed rods, compares much better than does run 33903, with nominal rod power and 10 failed rods, with run 31203, with nominal rod power and two failed rods. The quench times for all rod thermocouples are shown in figures F-12 and F-13 for tests 31203, 33903, and 34103. As shown in the figures, the quench front for test 31203 was simulated better by run 34103 than by run 33903. Therefore, the effect of failed rods on the bundle two-phase flow structure was minimized by the appropriate increase in the rod power. The increased rod power was utilized for all subsequent tests.

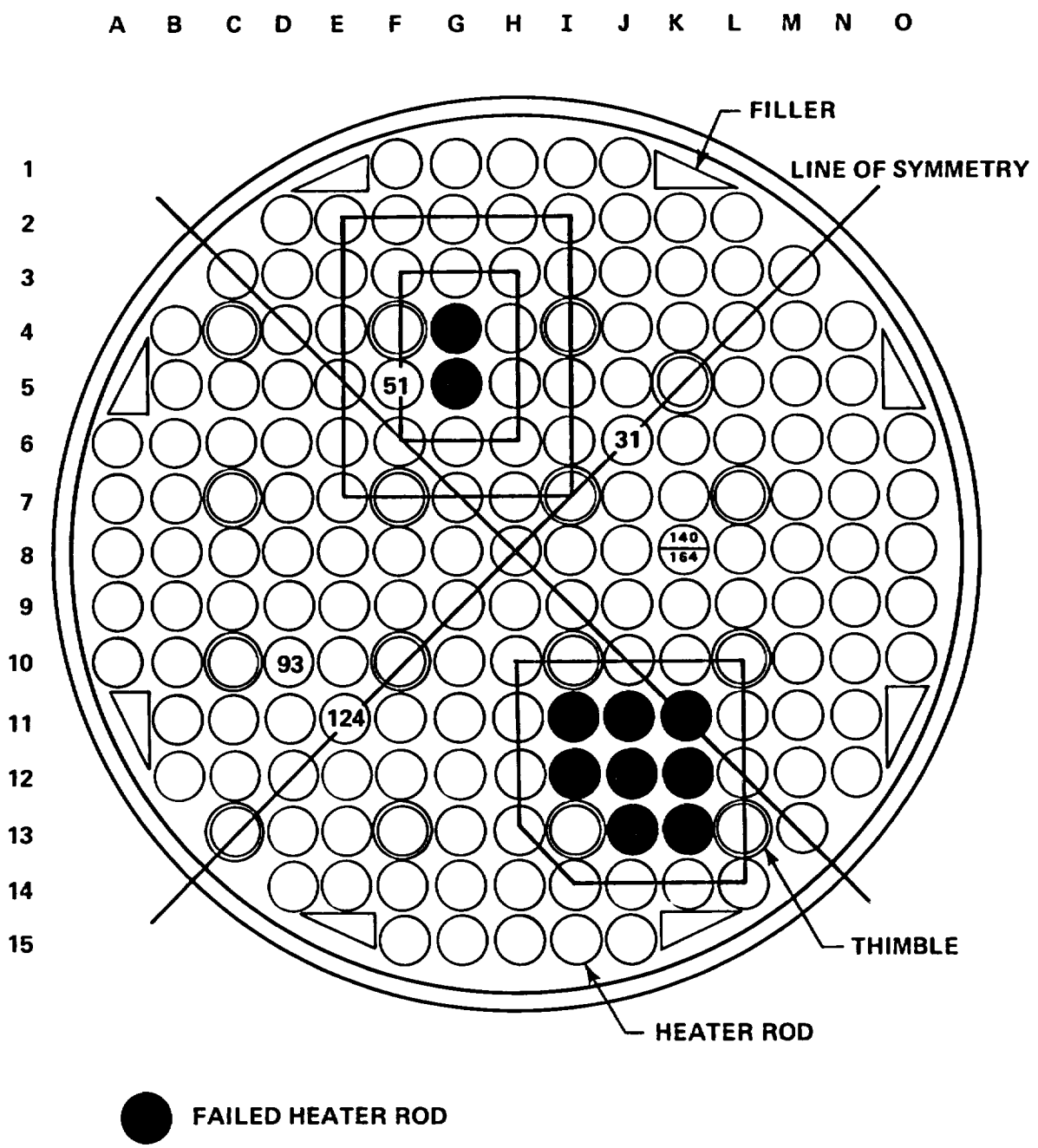

Figure F-10. Bundle Cross Section and Rod Thermocouple Locations

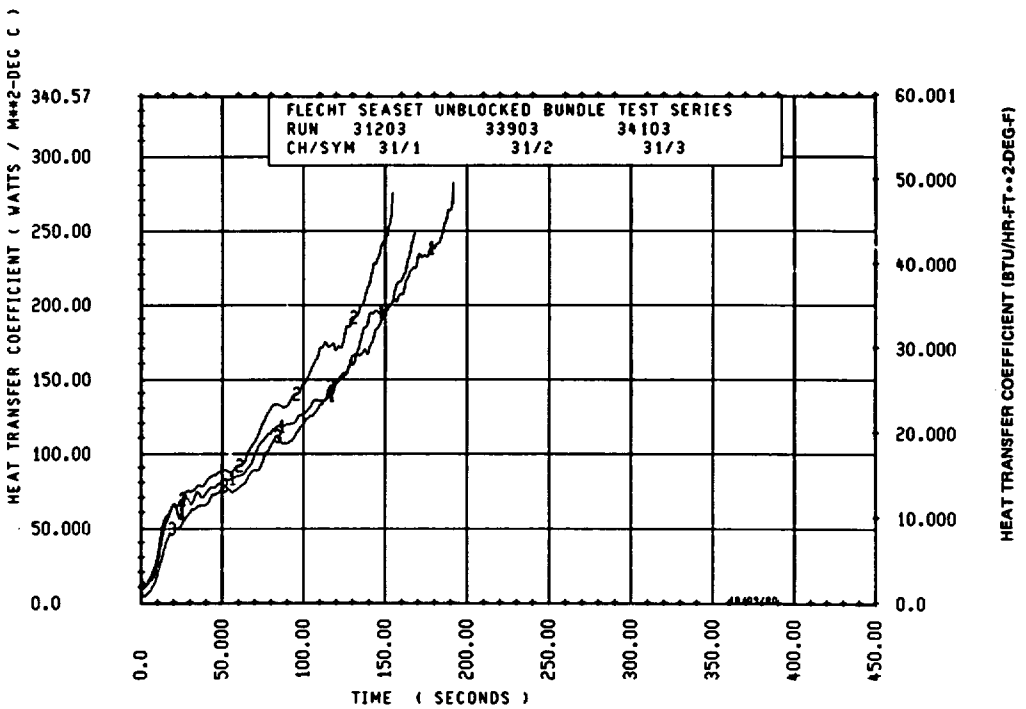

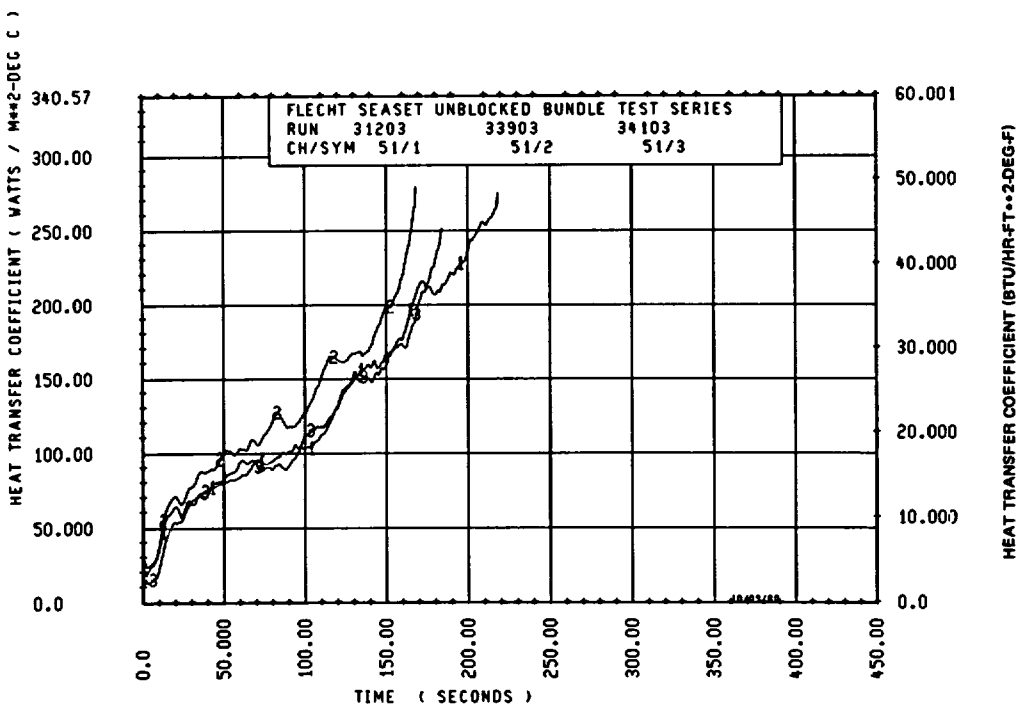

Figure F-11. Heat Transfer Coefficient Comparison for Runs 31203, 33903, and 34103 (sheet 1 of 3)

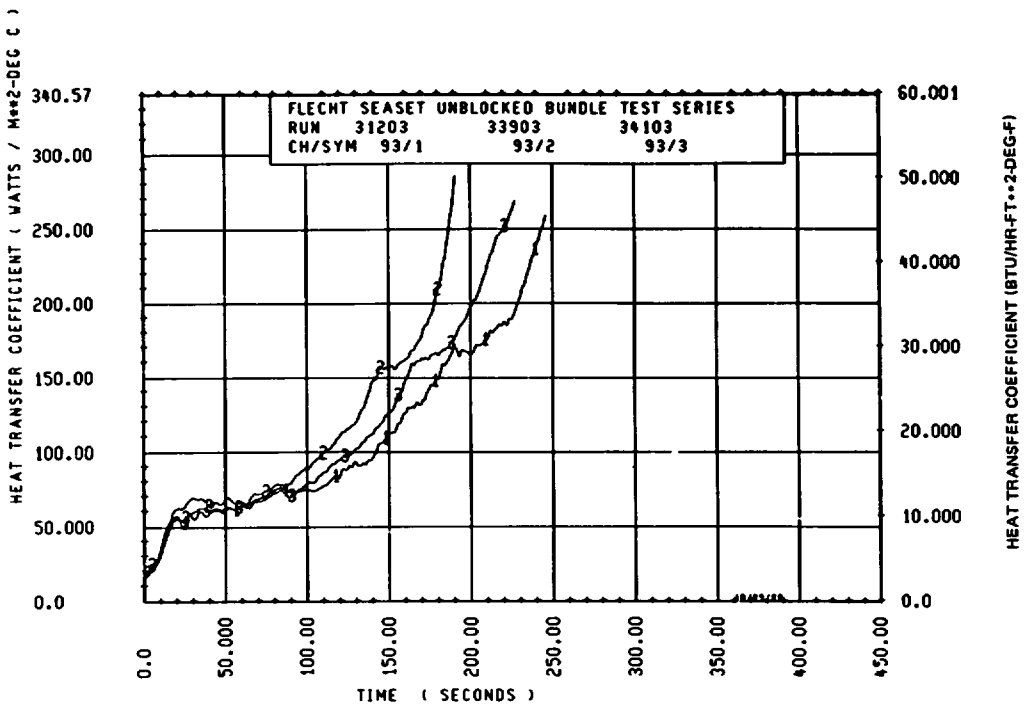

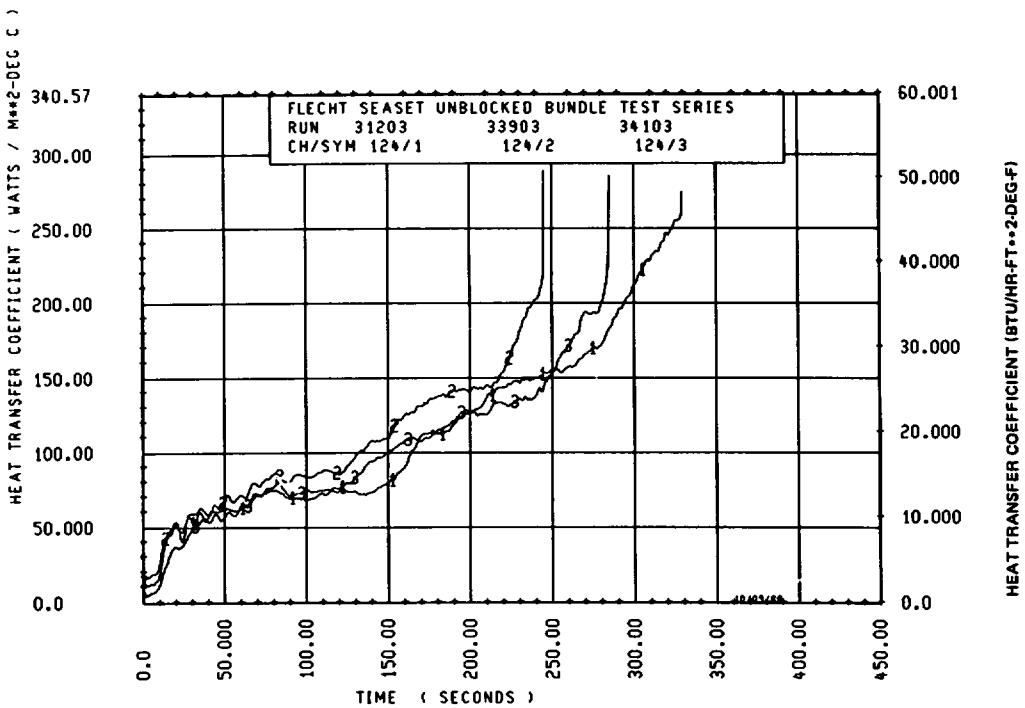

Figure F-11. Heat Transfer Coefficient Comparison for Runs 31203, 33903, and 34103 (sheet 2 of 3)

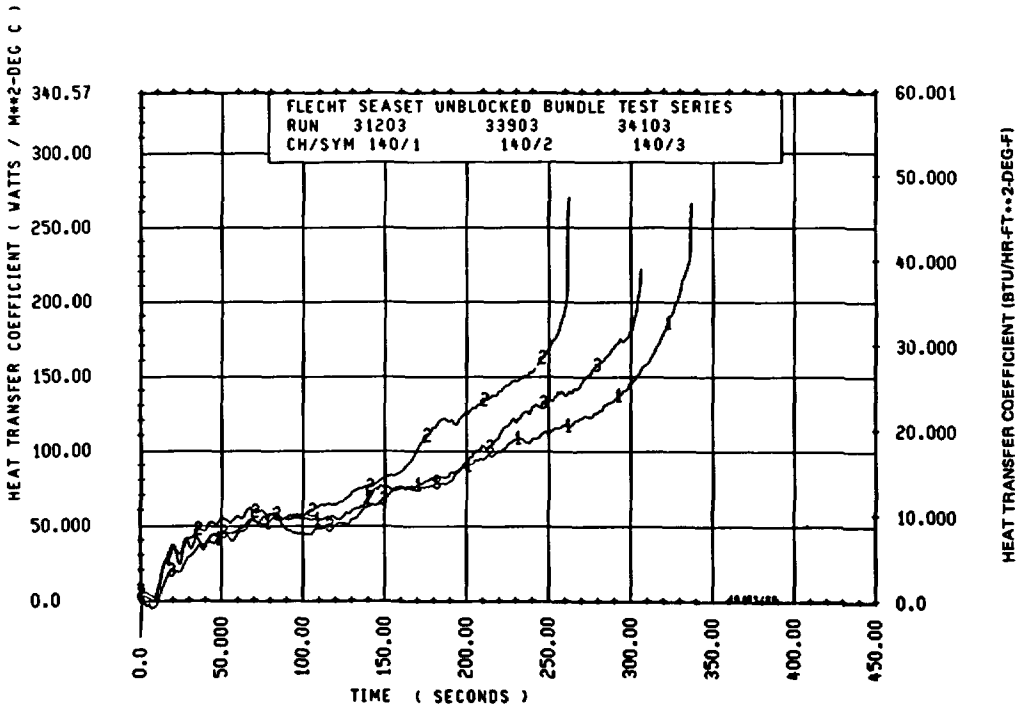

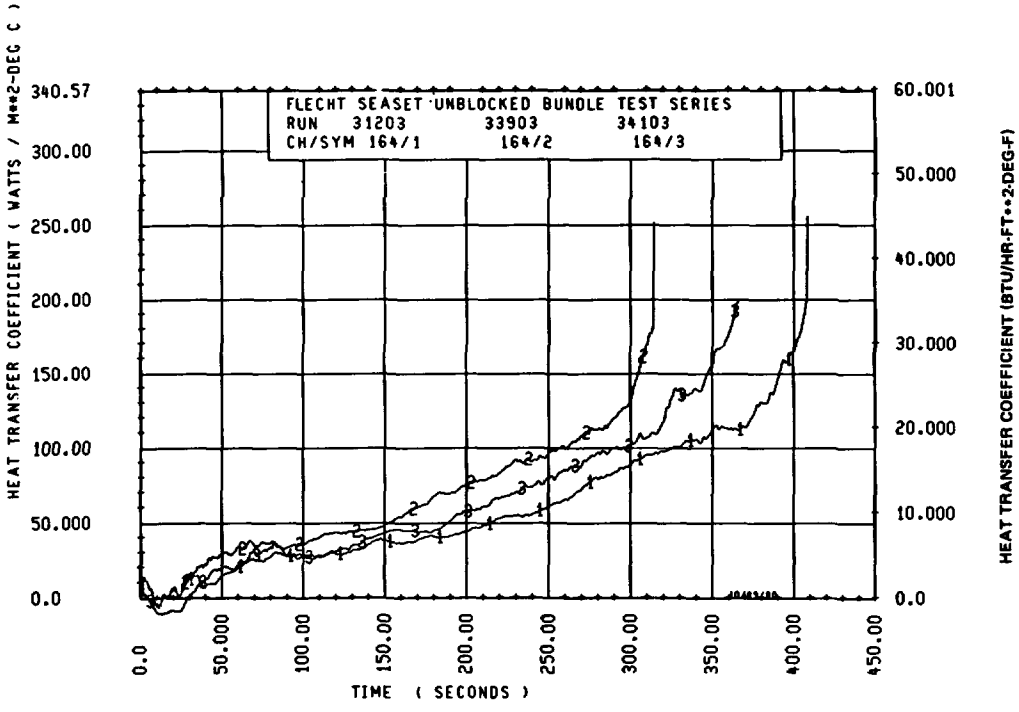

Figure F-11. Heat Transfer Coefficient Comparison for Runs 31203, 33903, and 34103 (sheet 3 of 3)

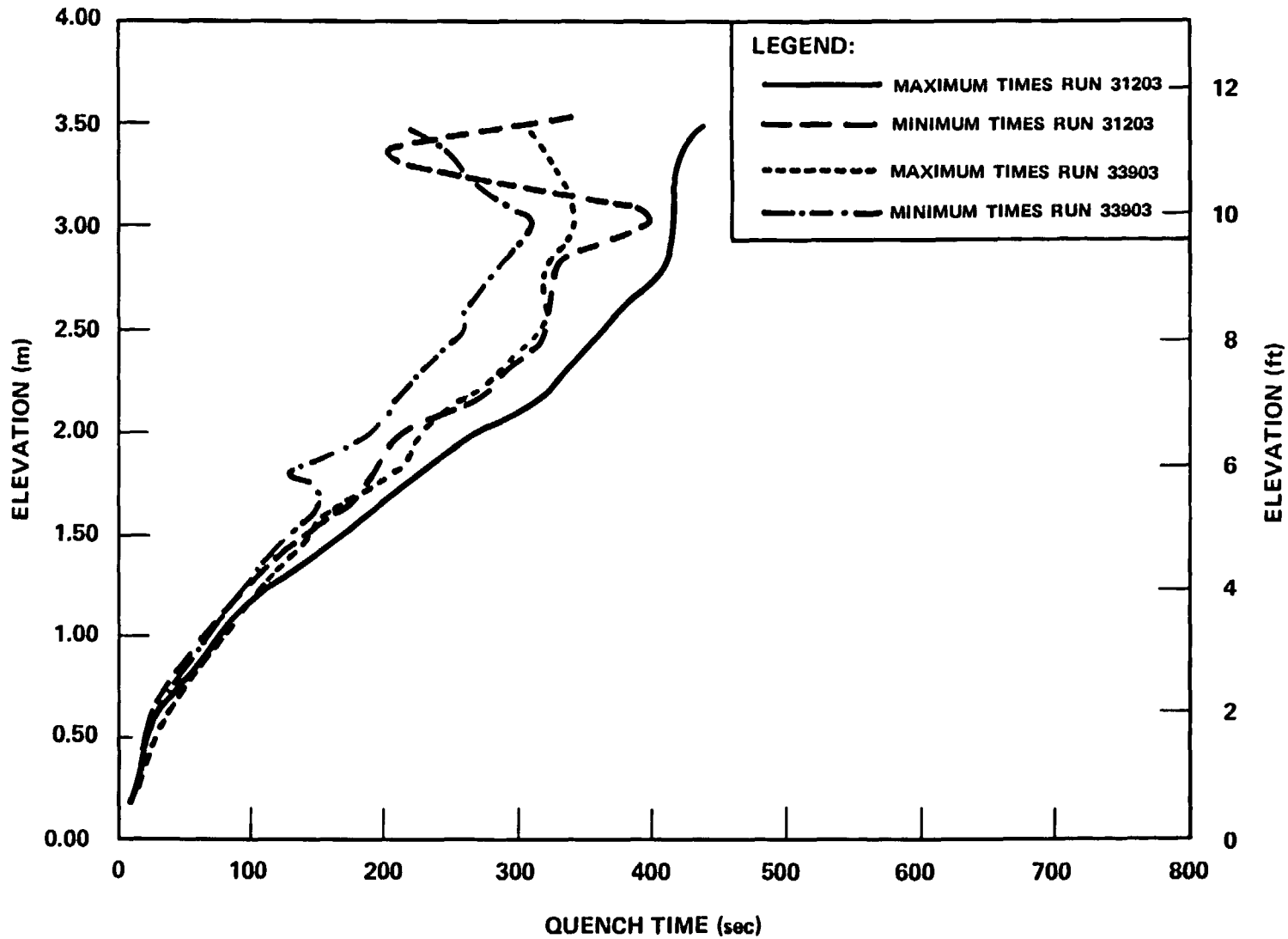

Figure F-12. Quench Time Comparison for Runs 31203 and 33903

16539-64

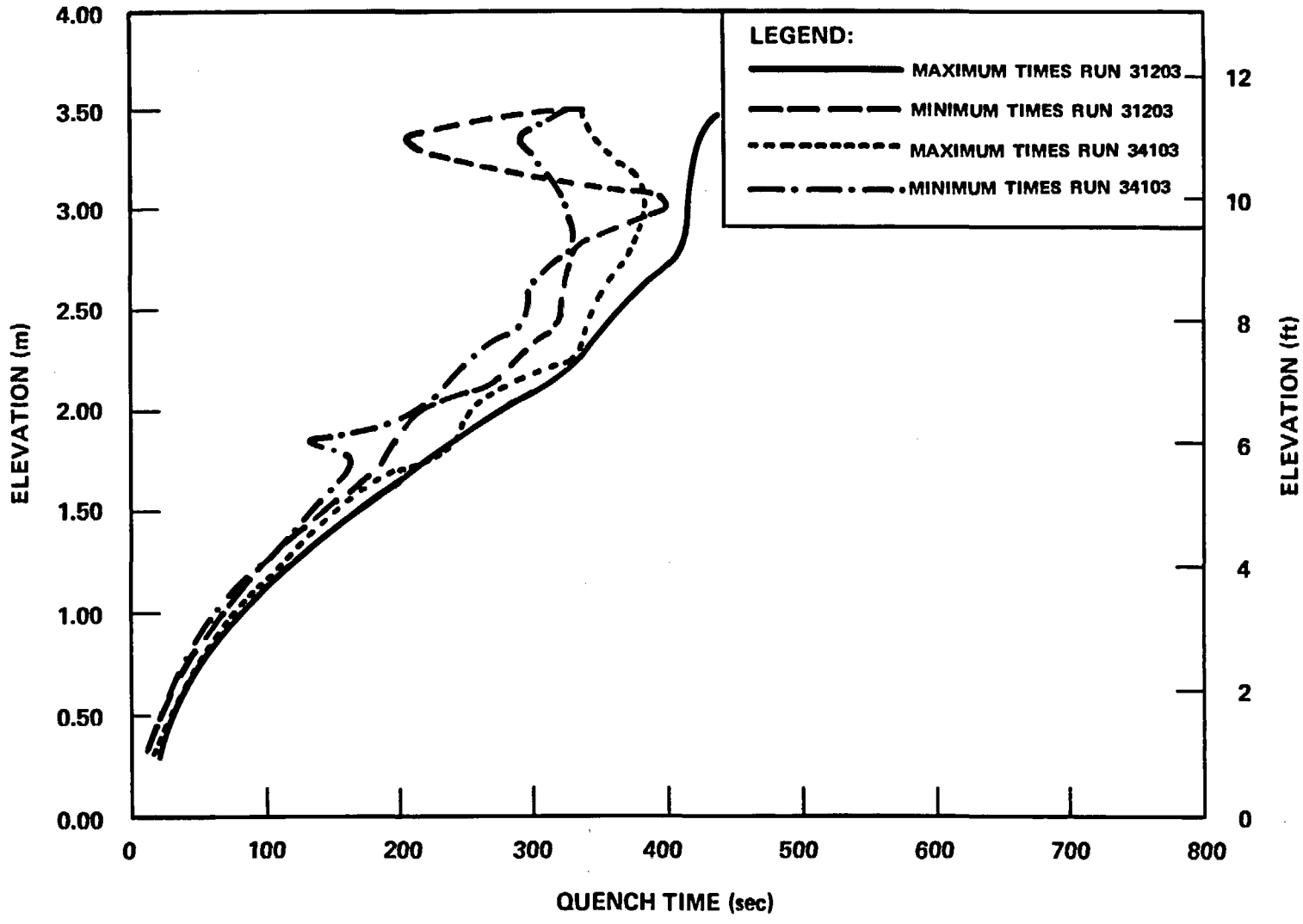

Figure F-13. Quench Time Comparison for Runs 31203 and 34103

16539-65

F-5. MOXY CODE ANALYSIS OF FAILED ROD EFFECTS

To further define the effect of failed rods on the heat transfer of the adjacent rods, a MOXY code[1] analysis of the FLECHT SEASET unblocked bundle was performed.

This analysis was performed by having the initial pair of failed rods, rods 4G and 5G, powered and subsequently unpowered. The MOXY code representation of the FLECHT SEASET unblocked bundle is shown in figure F-14. Since the MOXY code can accommodate only up to a 12 x 12 square array, the housing surface area and thickness had to be scaled to obtain the proper radiation heat transfer area and stored energy effect. The convective heat transfer coefficient was calculated from a proprietary 17 x 17 reflood heat transfer program.[2] The housing, thimbles, and failed rods had the same convective heat transfer coefficient as the powered heater rods. The convective component of the total heat transfer was estimated by subtracting the heat transfer coefficient at flood time and assuming this initial value to be due to radiation only. The convective heat transfer coefficient is shown in figure F-15. Therefore, only the estimated convective portion of the total heat transfer was input into MOXY, and MOXY was allowed to calculate the radiation heat transfer on a rod-to-rod basis. The radiation between the two failed rods, nodes 39 and 40, and the surrounding powered rods and thimbles is shown in figure F-16. It can be seen that the effect of radiation due to the failed rods does not extend beyond the second row to any significant degree. Therefore it was not necessary to consider the region of eight unpowered rods, since there would not be any radiation heat transfer interaction between the two regions of unpowered rods, which were approximately four rows apart.

1. Evans, D. R., et al., "The MOXY Core Heat Transfer Code: Model Description and User's Guide," PG-R-76-003, December 1976. (EG+G Idaho, Inc.)

2. "Westinghouse ECCS Evaluation Model, October 1975 Version," WCAP-8622, November 1975.

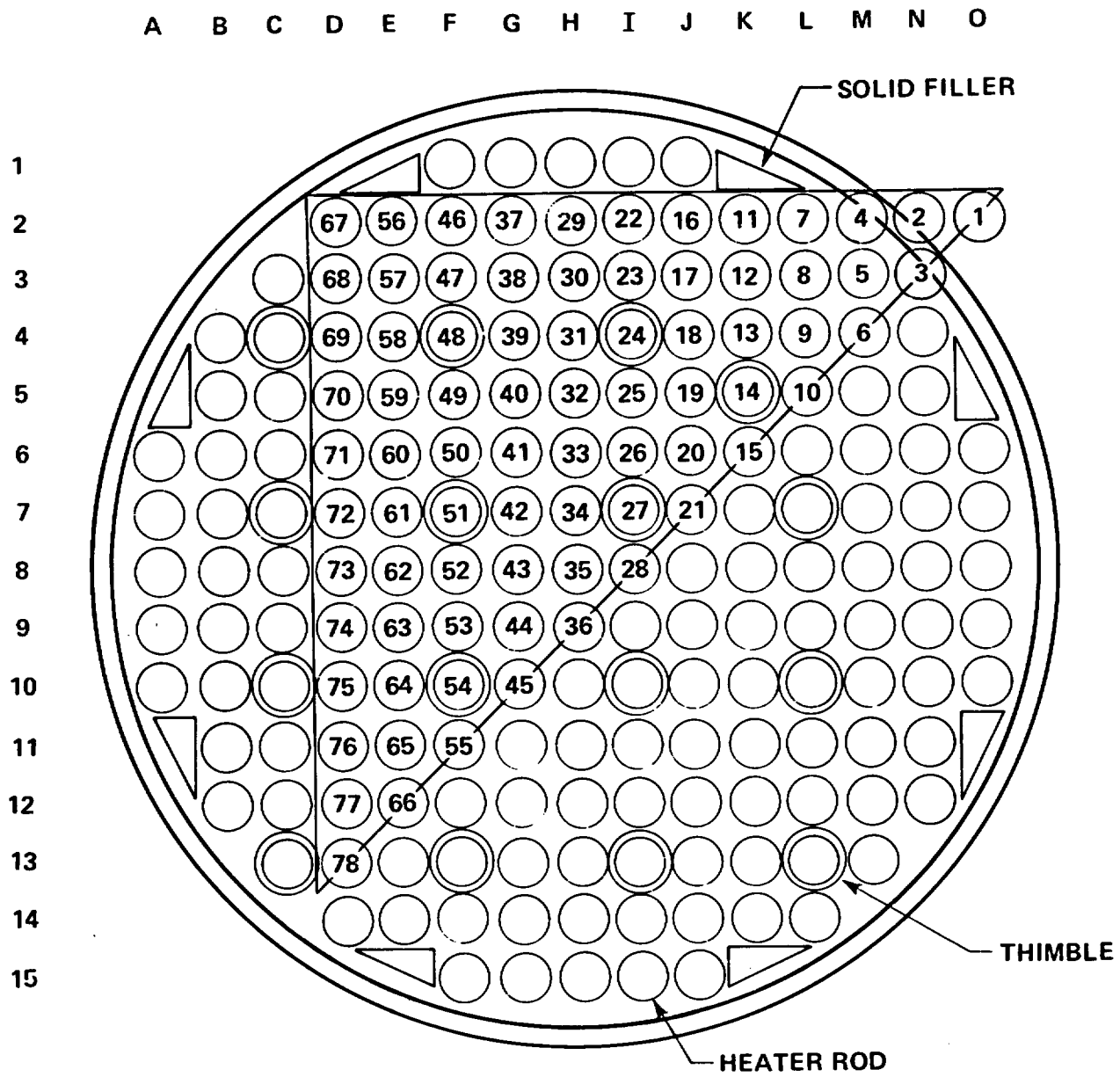

Figure F-14. MOXY Code Representation of FLECHT SEASET Unblocked Bundle

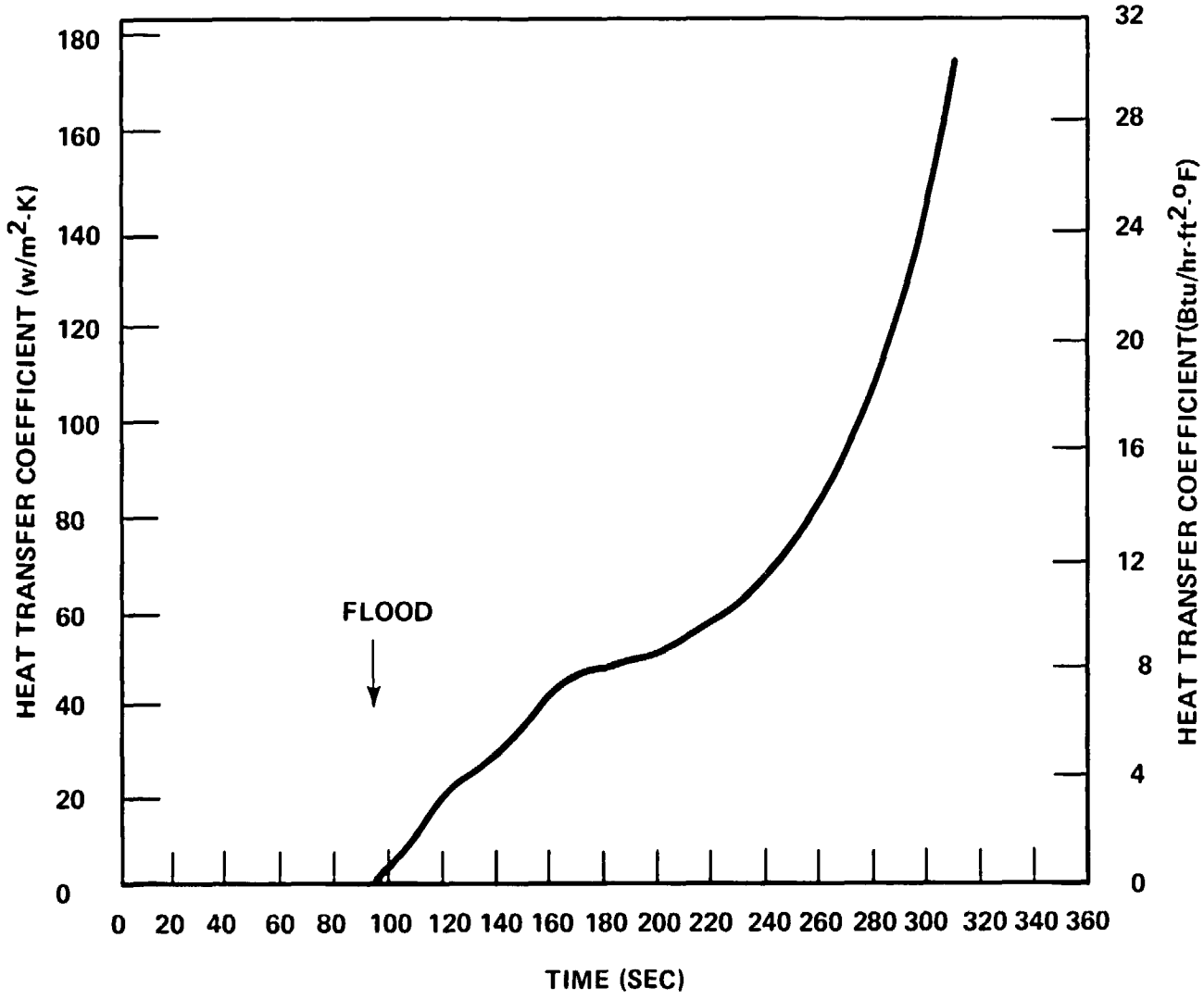

Figure F-15. Convective Heat Transfer Coefficient - All Nodes

16539-22

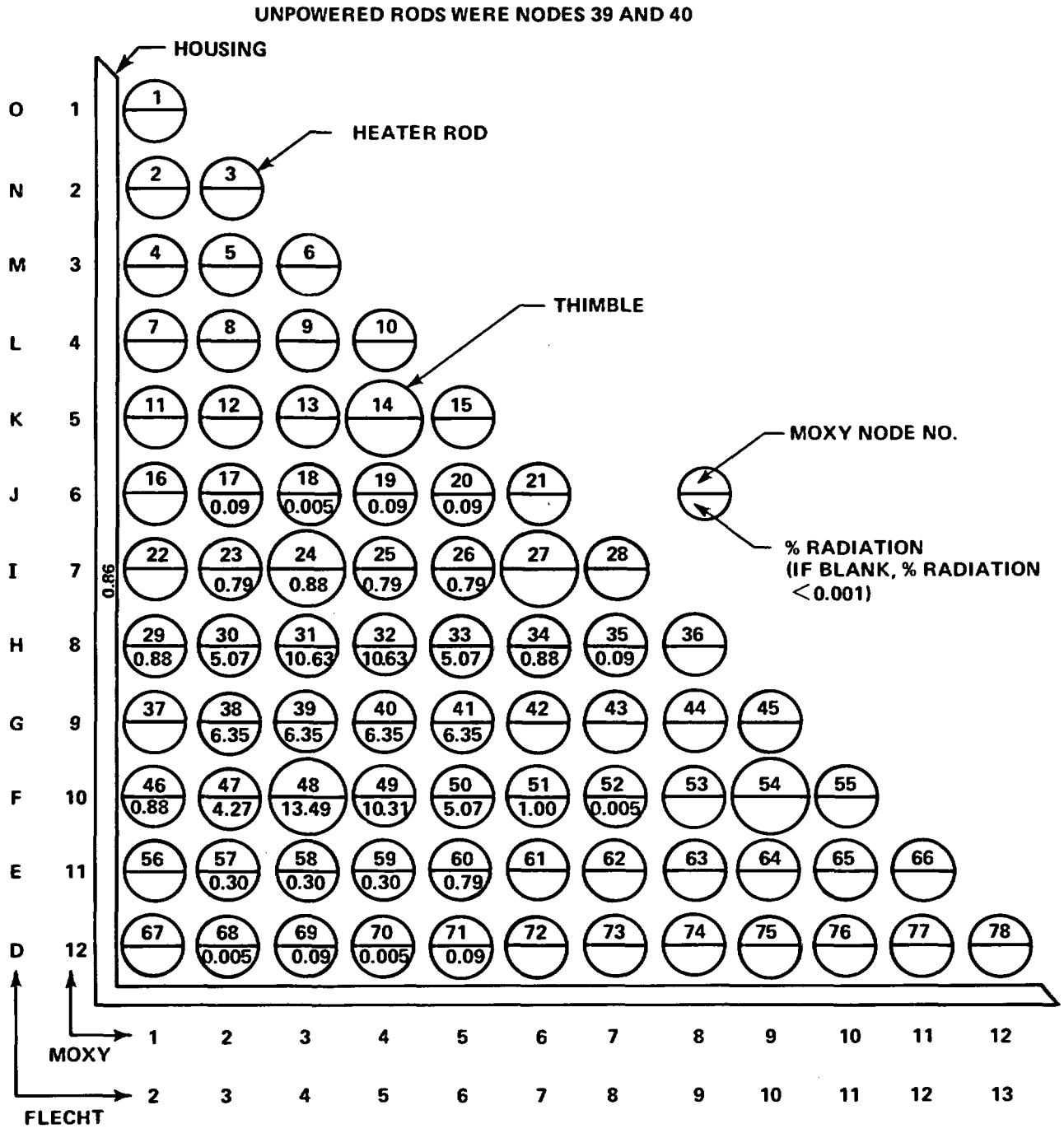

Figure F-16. Percentage of Radiation From Unpowered Rods to Surrounding Rods

The general results from an analysis performed for the FLECHT cosine test series[1] indicate that the MOXY code will predict the same transient heater rod performance as observed in reflood tests. Therefore, the effects of the failed rods on the adjacent rods in the unblocked bundle were determined by comparing the rod temperature transients with and without the failed rods. The MOXY code predictions for rods adjacent to, diagonal to, and one row away from the failed rod, with and without the failed rods, are shown in figures F-17 through F-19. These plots indicate that a maximum temperature difference occurred at approximately 200 seconds. The temperature differences at 200 seconds for rods within two rows and one row are tabulated in tables F-1 and F-2, respectively. The results show approximately a 2.6-percent decrease in temperature two rows away and a 5.4-percent decrease in temperature one row away from the failed rods. The radiation and convective heat transfer coefficients for a rod adjacent to and two rows away from the failed rods are shown in figures F-20 and F-21. These figures show that the effect of radiation heat transfer for a rod adjacent to the unpowered rods was significant early in the transient, approximately 20 percent greater at 140 seconds. However, as the transient progressed, this effect became much less, approximately 3.8 percent greater at 200 seconds. For a rod two rows away from the unpowered rods, the radiation heat transfer effect was 8.6 percent greater at 140 seconds and 3.4 percent greater at 200 seconds. Therefore, only the rods directly adjacent to the unpowered rods were significantly affected by the radiation heat transfer to these "cold" rods.

F-6. CONCLUSION

Both methods of analysis have shown that the effect of failed rods in the FLECHT SEASET unblocked bundle was local and only significantly affected those rods which were immediately adjacent. Therefore, it is recommended that data from those rods directly adjacent to the unpowered rods not be utilized in development of a hot rod heat transfer correlation.

1. Rosal, E. R., et al., "FLECHT Low Flooding Rate Cosine Test Series Data Report," WCAP-8651, December 1975.

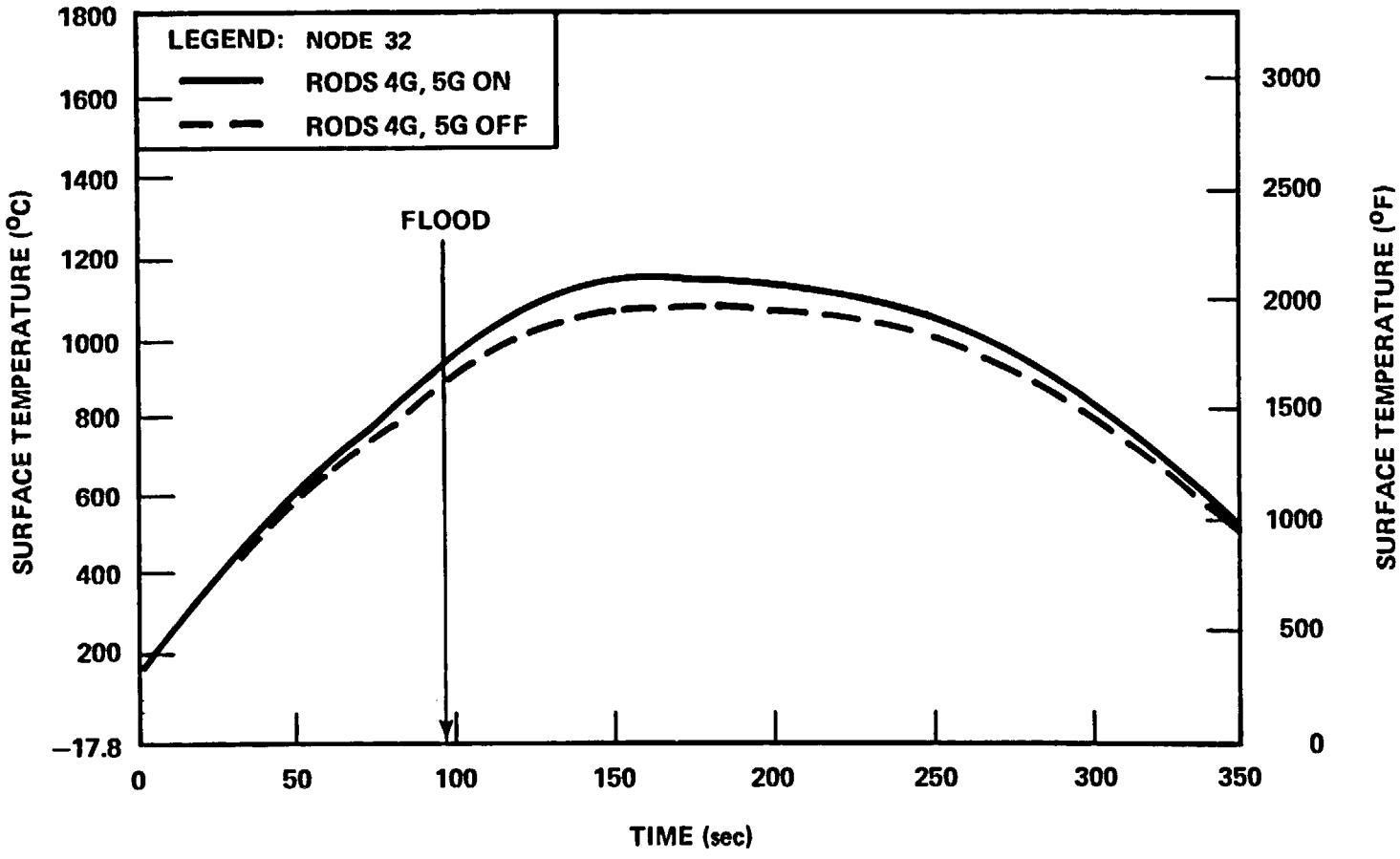

Figure F-17. MOXY Code Prediction for Rods Adjacent to Failed Rods (4G and 5G)

16539-62

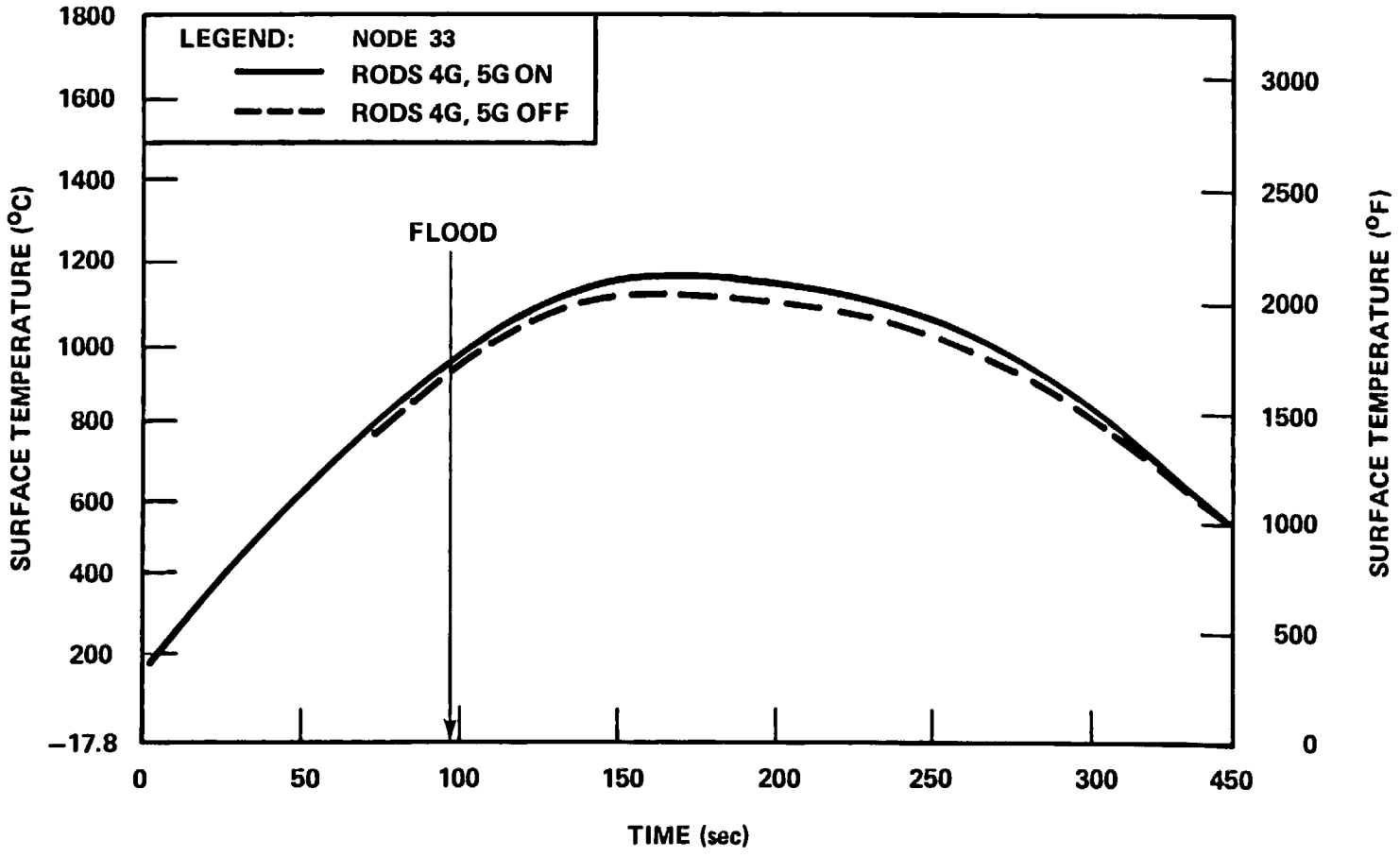

Figure F-18. MOXY Code Prediction for Rods Diagonal to Failed Rods (4G and 5G)

16539-61

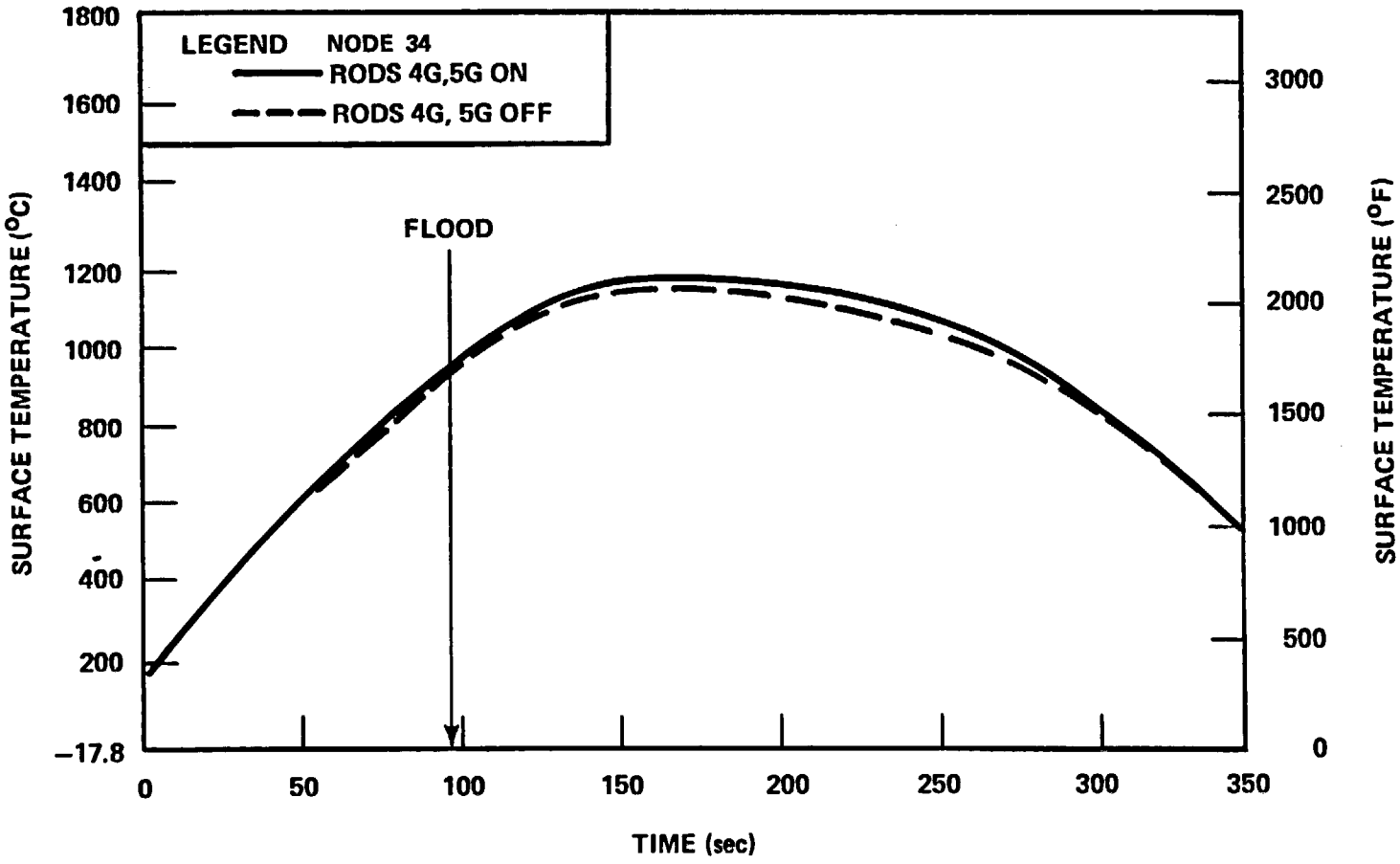

Figure F-19. MOXY Code Prediction for Rods One Row Away From Failed Rods (4G and 5G)

16539-60

TABLE F-1

TEMPERATURE DIFFERENCE AT 200 SECONDS FOR RODS TWO ROWS AWAY FROM UNPOWERED RODS

Node	Temperature Difference[a] [°C (°F)]	Percent Change[b]
22	17 (31)	1.6
23	27 (48)	2.4
24	44 (80)	4.7
25	34 (61)	2.9
26	29 (52)	2.5
27	29 (52)	3.0
29	26 (47)	2.5
34	32 (58)	2.8
37	27 (48)	2.5
42	26 (47)	2.3
46	26 (46)	2.5
51[c]	32 (58)	3.3
56	17 (30)	1.6
57	25 (45)	2.3
58	32 (57)	2.9
59	32 (58)	2.9
60	27 (49)	2.5
61	17 (30)	1.5

a. Temperature difference = temperature with 4G and 5G powered minus temperature with 4G and 5G unpowered

b. Percent change = Temperature difference divided by temperature with 4G and 5G powered

c. Thimbles had a tendency to show a higher effect, since they were totally heated by surrounding rods.

TABLE F-2

TEMPERATURE DIFFERENCE AT 200 SECONDS FOR RODS ONE ROW AWAY FROM THE UNPOWERED RODS

Node	Temperature Difference[a] [°C (°F)]	Percent Change[b]
30	48 (87)	4.4
31	69 (125)	6.1
32	68 (123)	5.9
33	47 (85)	4.1
38	57 (102)	5.1
41	54 (98)	4.7
47	46 (83)	4.2
48[c]	89 (161)	9.6
49	68 (122)	6.0
50	47 (84)	4.1

a. Temperature difference = temperature with 4G and 5G powered minus temperature with 4G and 5G unpowered

b. Percent change = temperature difference divided by temperature with 4G and 5G powered

c. Thimbles had a tendency to show a higher effect since they were totally heated by surrounding rods.

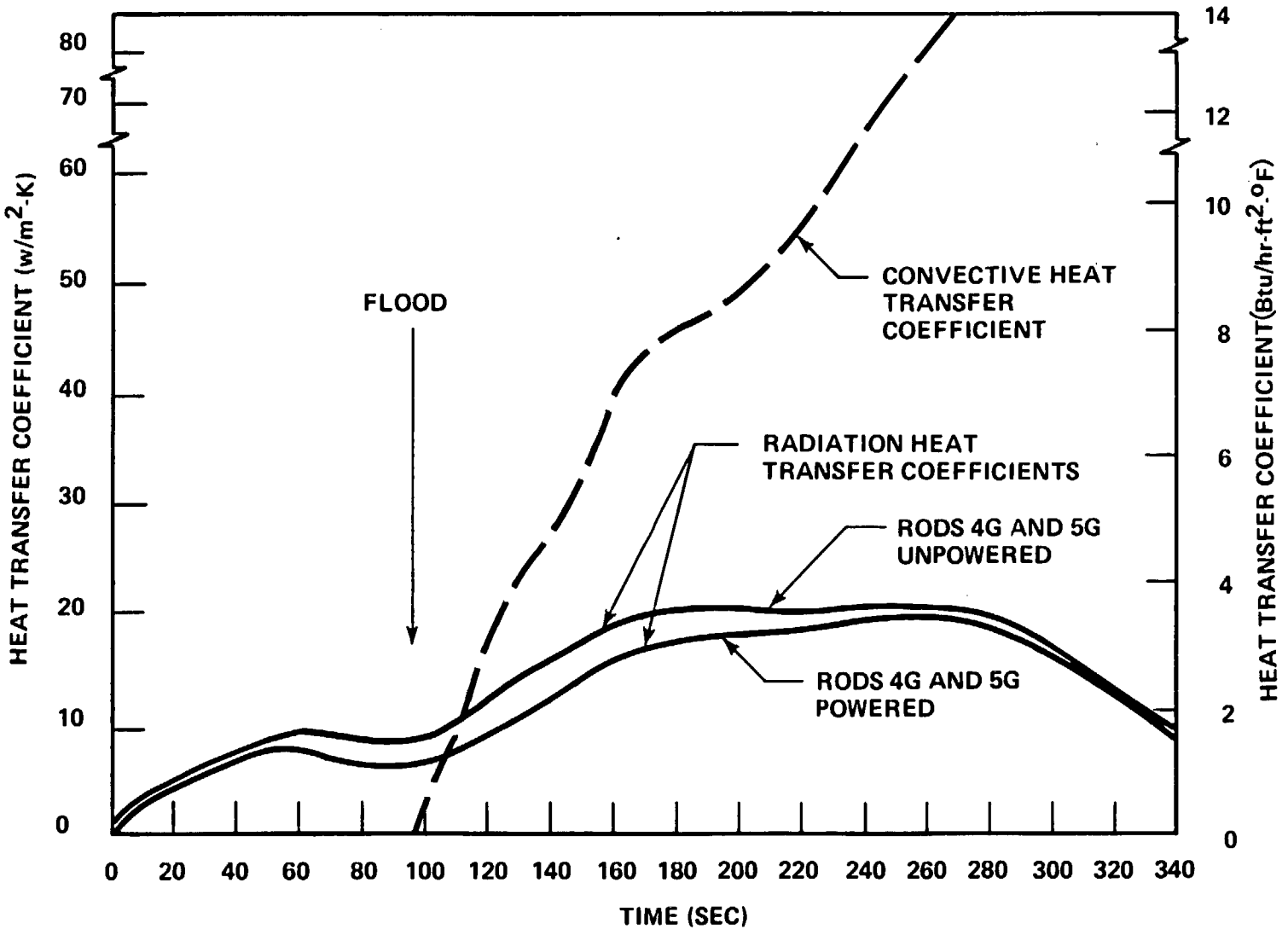

Figure F-20. Node 34 Heat Transfer Coefficients Used in MOXY Code

16539-23

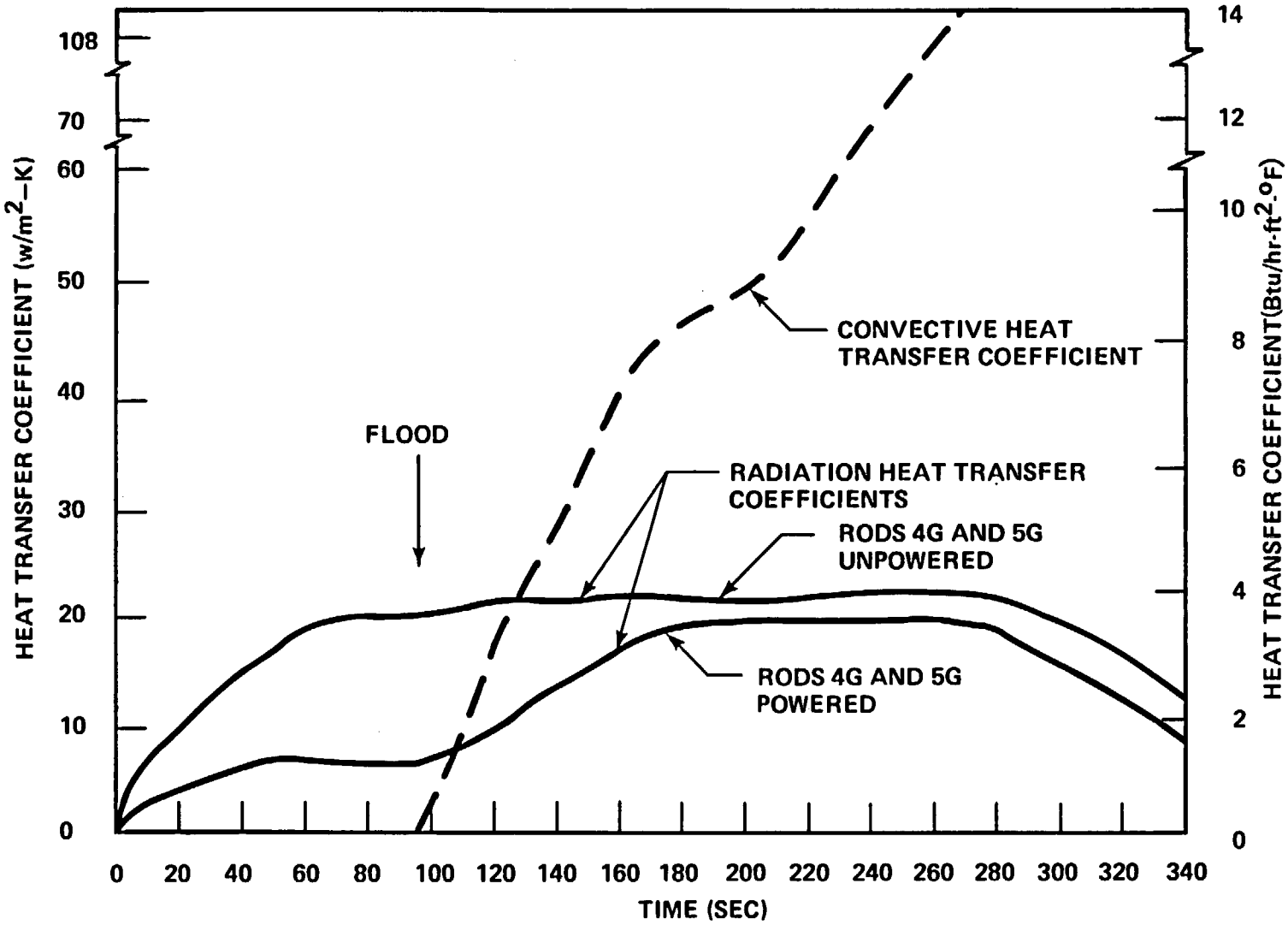

Figure F-21. Node 32 Heat Transfer Coefficients Used in MOXY Code

16539-21

APPENDIX G
ROD BUNDLE DISTORTION

G-1. INTRODUCTION

This appendix is devoted to the study of the effects on the heat transfer measurements due to the bundle geometric distortion observed in the FLECHT SEASET 161-rod unblocked bundle. The heater rods of the unblocked bundle were initially placed in the bundle straight and properly spaced by the FLECHT egg-crate grids. The eight triangular filler supports were welded to each grid to maintain proper grid spacing and to minimize excess flow area. The heater rods and thimble guide tubes carried only their own weight; they were not support members.

During the unblocked bundle reflood test series, repeated thermal cycling up to heater rod temperatures of 1232°C (2250°F), as shown in table G-1, caused bowing of the fillers, which in turn caused bowing of the heater rods and thimbles. The filler bowing, believed to have first taken place near the housing, was observed through the housing windows during the testing. As the high-temperature testing continued, the filler bowing became more severe and caused both thimbles and heater rods to bow. After the unblocked tests were complete, the bundle was disassembled and photographs were taken. It was then discovered that between the 1.52 and 2.44 m (60 and 96 in.) elevations, rod bowing had spread across the entire bundle. The severe bundle distortion observed across the central bundle near the midplane was thought to be partly due to interaction between the rods and spacer grids. Near the midplane of the cosine-shaped power bundle, the heater rod temperature was high and thermal expansion of the rods caused contact with the spacer grids. The contact resistance between the rods and the spacer grids, and the bow caused by the filler supports, prevented the rods from expanding freely in the axial direction, and thus caused severe rod bowing near the midplane.

It must be determined when the bundle distortion occurred, and more important, at which run the distortion was of sufficient severity that data taken from the unblocked bundle were no longer reliable and should not be utilized for heat transfer model and correlation development for undistorted rod bundle geometries.

TABLE G-1
MAXIMUM ROD TEMPERATURES FOR REFLOOD
AND STEAM COOLING TESTS

Run	Temperature [°C(°F)]	Run	Temperature [°C(°F)]
30223	455(852)	33749	1017(1861)
30323	459(859)	33849	1025(1878)
30518	653(1208)	33903	1048(1919)
30619	727(1340)	34006	1163(2126)
30817	832(1530)	34103	1089(1992)
30921	949(1740)	34209	1161(2121)
31021	941(1726)	34316	1207(2206)
31108	938(1720)	34420	1207(2205)
31203	1092(1998)	34524	1204(2199)
31302	932(1710)	34610	1052(1926)
31504	1150(2101)	34711	1119(2045)
31615	1220(2228)	34815	1178(2152)
31701	923(1694)	34907	1232(2250)
31805	1232(2250)	35050	958(1758)
31922	975(1787)	35114	1192(2178)
32013	1171(2139)	35212	1231(2247)
32114	1189(2172)	35304	1230(2246)
32235	1146(2096)	35426	1229(2243)
32333	1148(2099)	35557	1093(2000)
32452-32955	<204(<400)	35658	1093(2000
33056	827(1520)	35759	1093(2000)
33338	925(1697)	35807	1182(2160)
33436	910(1670)	35912	1128(2062)
33544	908(1668)	36026	1174(2145)
33644	930(1705)	36160-37170	<204(<400)

This appendix describes the methods used to study the unblocked bundle distortion, and resolves the above-stated question. It is hypothesized that bundle distortion would increase the rod-to-rod variation of heat transfer data. The method adopted is basically a statistical analysis of rod-to-rod variation of data or data-based heat transfer parameters taken from heater rods at the same elevation. The results and conclusions of the statistical analysis are supplemented by visual observations through the housing windows, and also by knowledge of the test cycle at which heater rods could be removed from the test section and replaced.

In the following paragraphs, the observed bundle distortion is described in detail. The statistical analysis is then described and the results and their interpretations are presented. It is shown that the bundle distortion affected data taken from the first two heater rod rows from the housing relatively early in the reflood test series, but data from the central bundle (more than two rod rows from the housing) were not affected by the distortion until near the end of the reflood test cycles.

Filler bowing was also observed in the FLECHT skewed test series,[1] but it affected only the outer row of rods in the bundle and did not affect the center rods. The skewed test series were generally lower-temperature tests with fewer high-temperature [> 1093°C (2000°F)] cycles. Also, the skewed bundle rods were 10.7 mm (0.422 in.) in diameter compared to the 9.5 mm (0.374 in.) diameter of the unblocked bundle rods; thus the skewed bundle rods were more resistant to bowing.

G-2. VISUAL OBSERVATIONS OF THE UNBLOCKED BUNDLE DISTORTION

Observations of the bundle distortion through the housing windows are summarized in table G-2. These data show that at the 1.83 m (72 in.) elevation, filler and rod bowing occurred relatively early near the housing. Distortion was also observed at the 2.75 m (108 in.) elevation, but did not occur as early and was not as severe as at the 1.83 m (72 in.) elevation. No apparent distortion was observed through the 0.91 m (36 in.) elevation windows. Visual observations of the bundle subchannels through the housing windows

1. Rosal, E. R., et al., "FLECHT Low Flooding Rate Skewed Test Series Data Report," WCAP-9108, May 1977.

TABLE G-2

OBSERVATIONS OF BUNDLE DISTORTION

Run	Window Elevation [m (in.)]	Observations
31615	1.83(72)	Rod distortion occurred in one subchannel at the outer row of rods.
31805	1.83(72)	Rod distortion occurred in all subchannels; backlighting for movies could not penetrate the bundle during most of the test.
31922	2.75(108)	Four out of six subchannels were blocked.
32013	1.83(72)	Filler distortion was observed.
32235	1.83(72)	Backlighting for movies could not penetrate.
32235	2.75(108)	Backlighting for movies could not penetrate three of the six subchannels.
32333	2.75(108)	Backlighting for movies could not penetrate four of the six subchannels.
All runs	0.92(36)	No apparent distortion was observed.
33056	--	Pulled and replaced 15 heater rods at central bundle
33849	--	Attempted to pull rod 12J and surrounding rods but failed

revealed at which test cycle rod bowing started to occur near the housing. The visual field through the housing windows was about two rows deep; once the subchannels near the housing had been blocked by bowed rods, visual observations were no longer possible. Therefore, observations through the windows could not furnish information regarding distortion in the center of the bundle.

Photographs of the center row of the disassembled bundle are shown in figures G-1 through G-8. The photographs show that between the 1.52 and 2.44 m (60 and 96 in.) elevations, the bundle distortion was not limited to near the housing, but also extended across the entire bundle cross section. The distortion was most severe near the 1.83 m (72 in.) elevation, and was less severe between the 2.13 and 2.44 m (84 and 96 in.) elevations. The disassembled bundle revealed the degree of severity of the bundle distortion at different elevations and locations at the conclusion of the test cycles, but gave no indication of when the distortion occurred.

As noted in paragraph 4-6, heater rod failures occurred during the tests. After run 33056, it was possible to pull and replace 15 heater rods, all in the central bundle region (at least two rod rows away from the housing). This indicated that the central bundle geometry was still intact. After run 33849, more heater rod failures occurred. An attempt to pull and replace heater rod 12J and the surrounding heater rods was not successful. Because of the closely-packed structure of the unblocked rod bundle, only minor rod bowing or distortion is required to prevent the heater rods from being pulled out. The fact that the rods could not be pulled indicated that at least some degree of bundle distortion existed in the center region after run 33849.

It is not possible to conclude from the above observations how the distortion affected the heat transfer data. The effect of the bundle distortion on the reflood data was analyzed by statistical methods, as described in paragraph G-4.

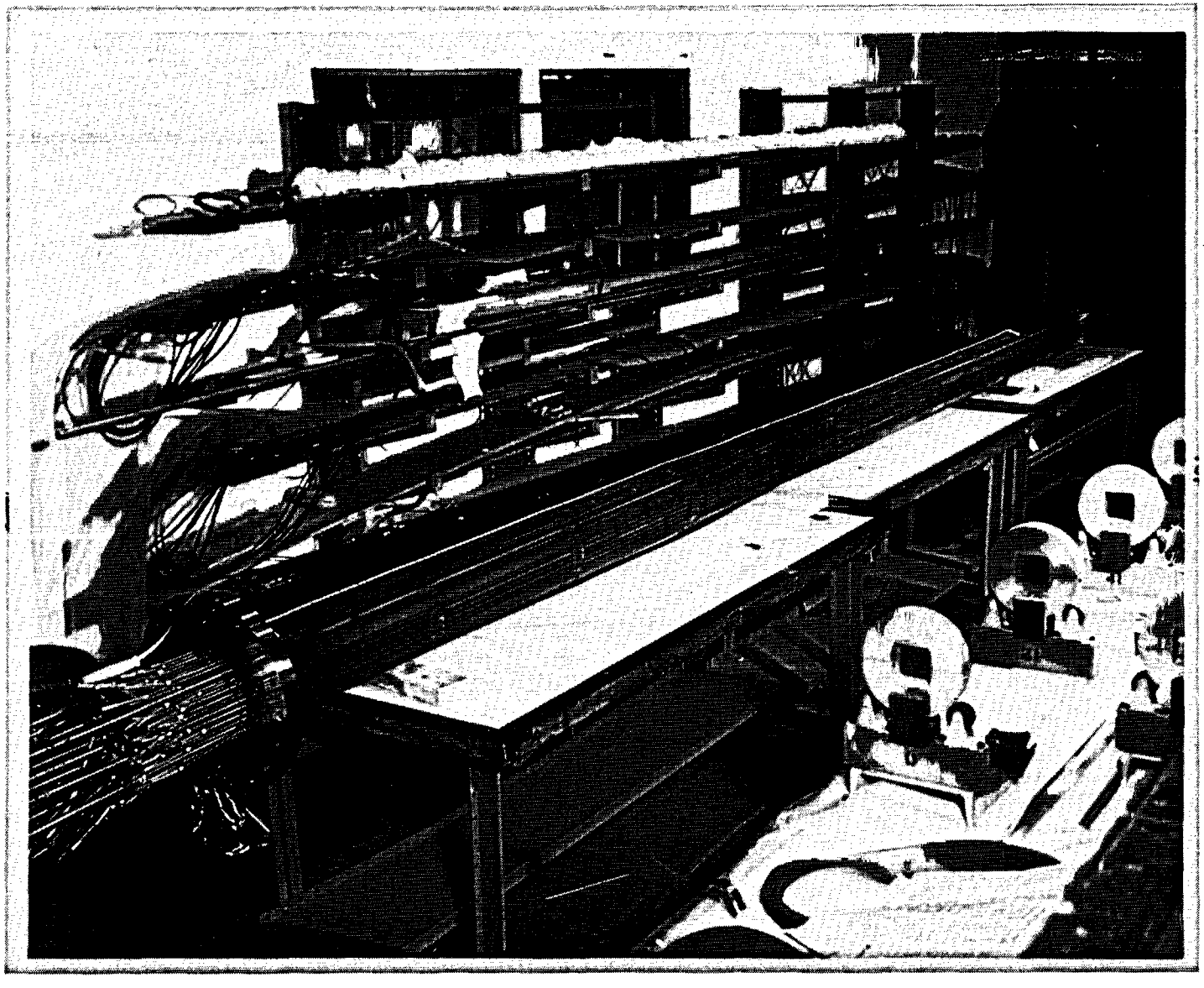

Figure G-1. Overall Bundle, Posttest

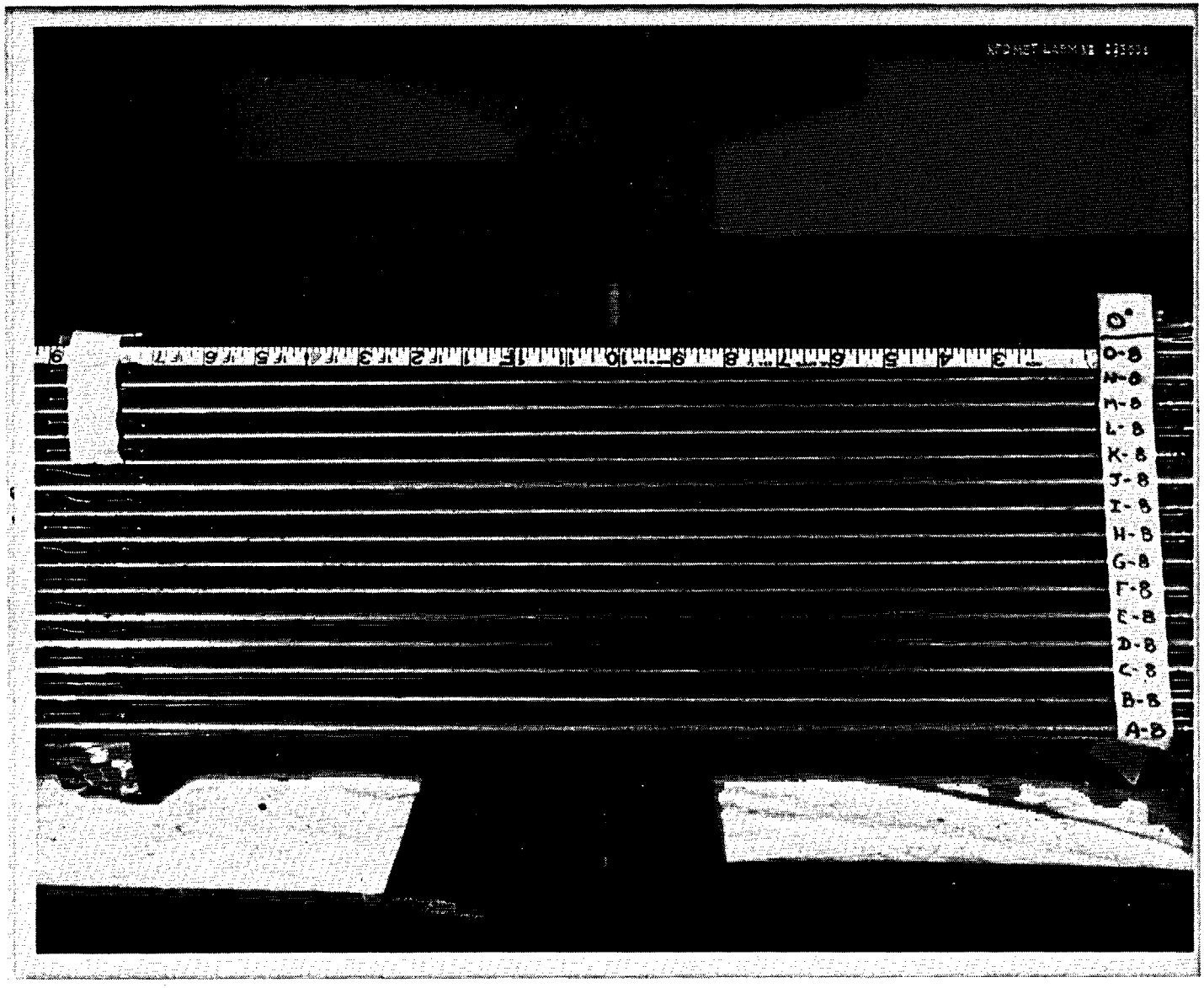

Figure G-2. Bundle, Posttest 0-0.53 m (0-21 in.)

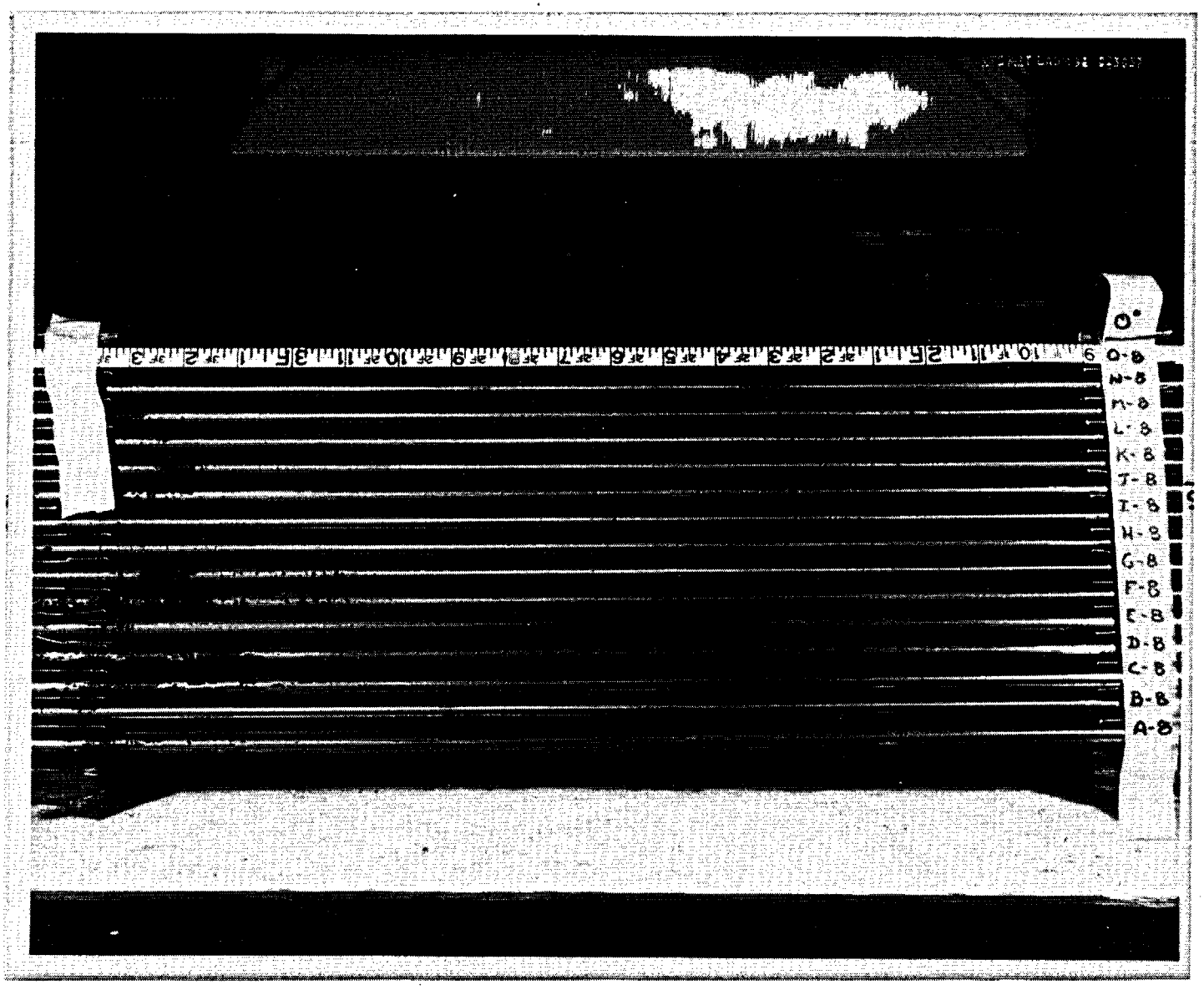

Figure G-3. Bundle, Posttest 0.53-1.04 m (21-41 in.)

Figure G-4. Bundle, Posttest 1.04-1.57 m (41-62 in.)

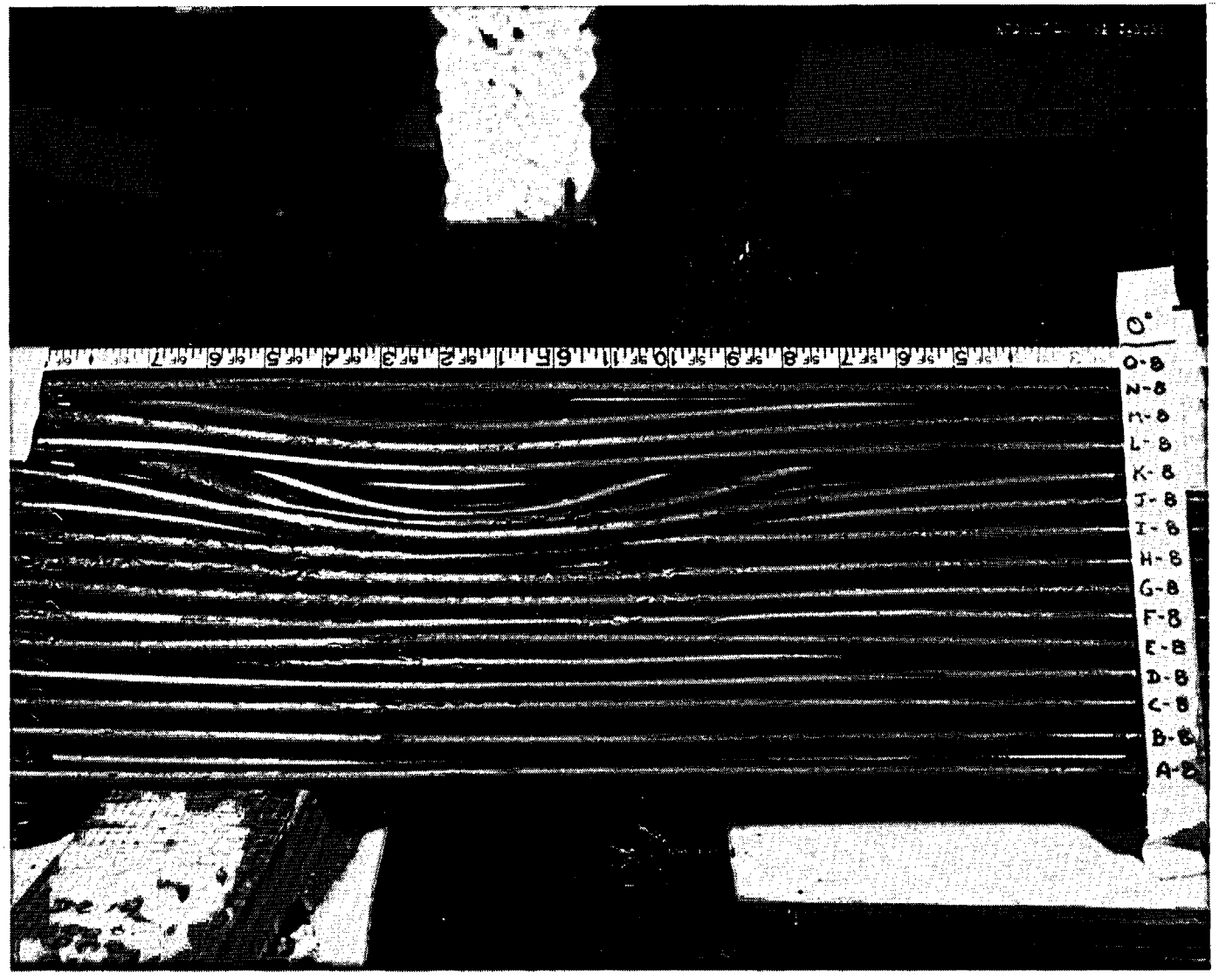

Figure G-5. Bundle, Posttest 1.57-2.11 m (62-83 in.)

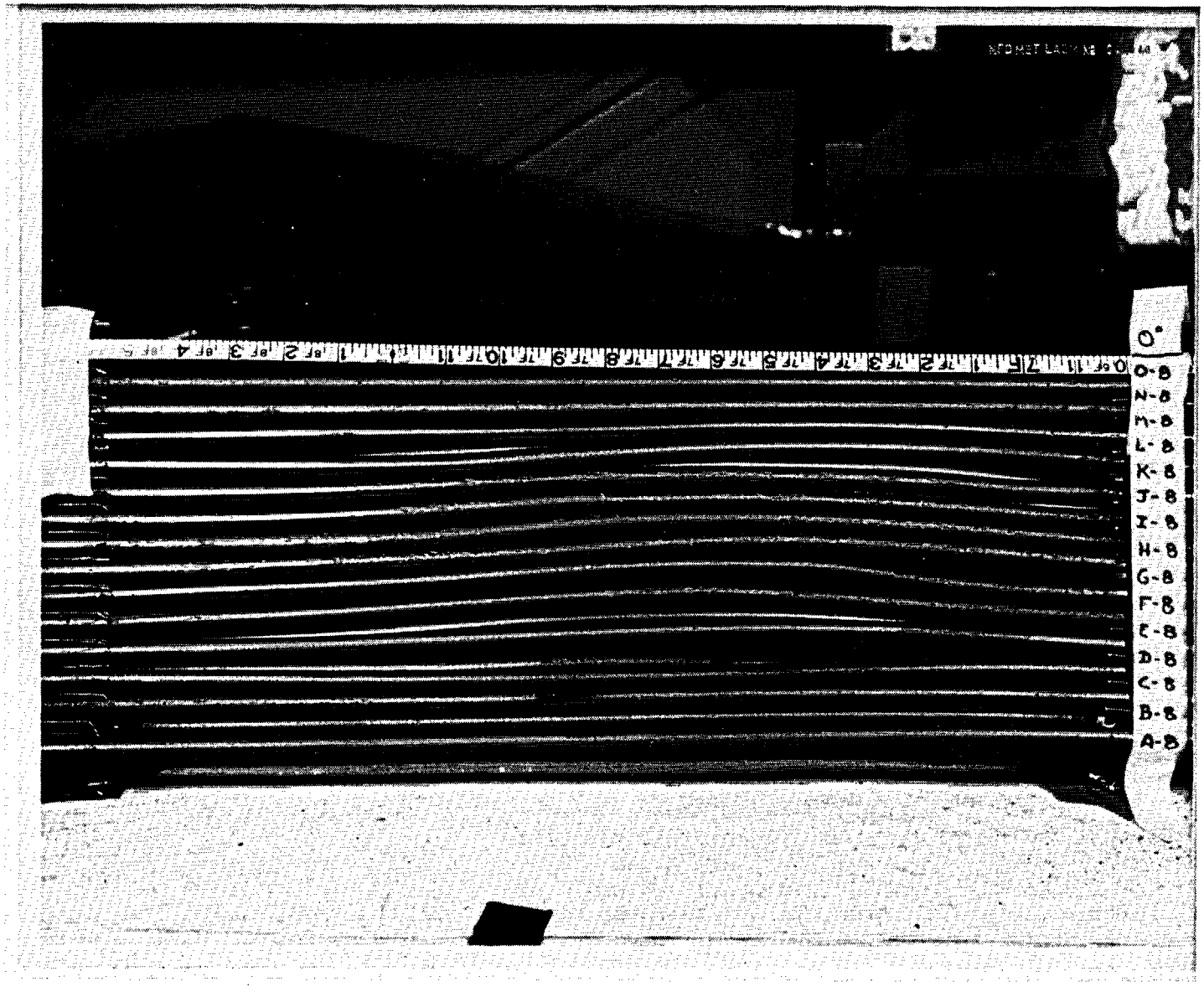

Figure G-6. Bundle, Posttest 2.11-2.62 m (83-103 in.)

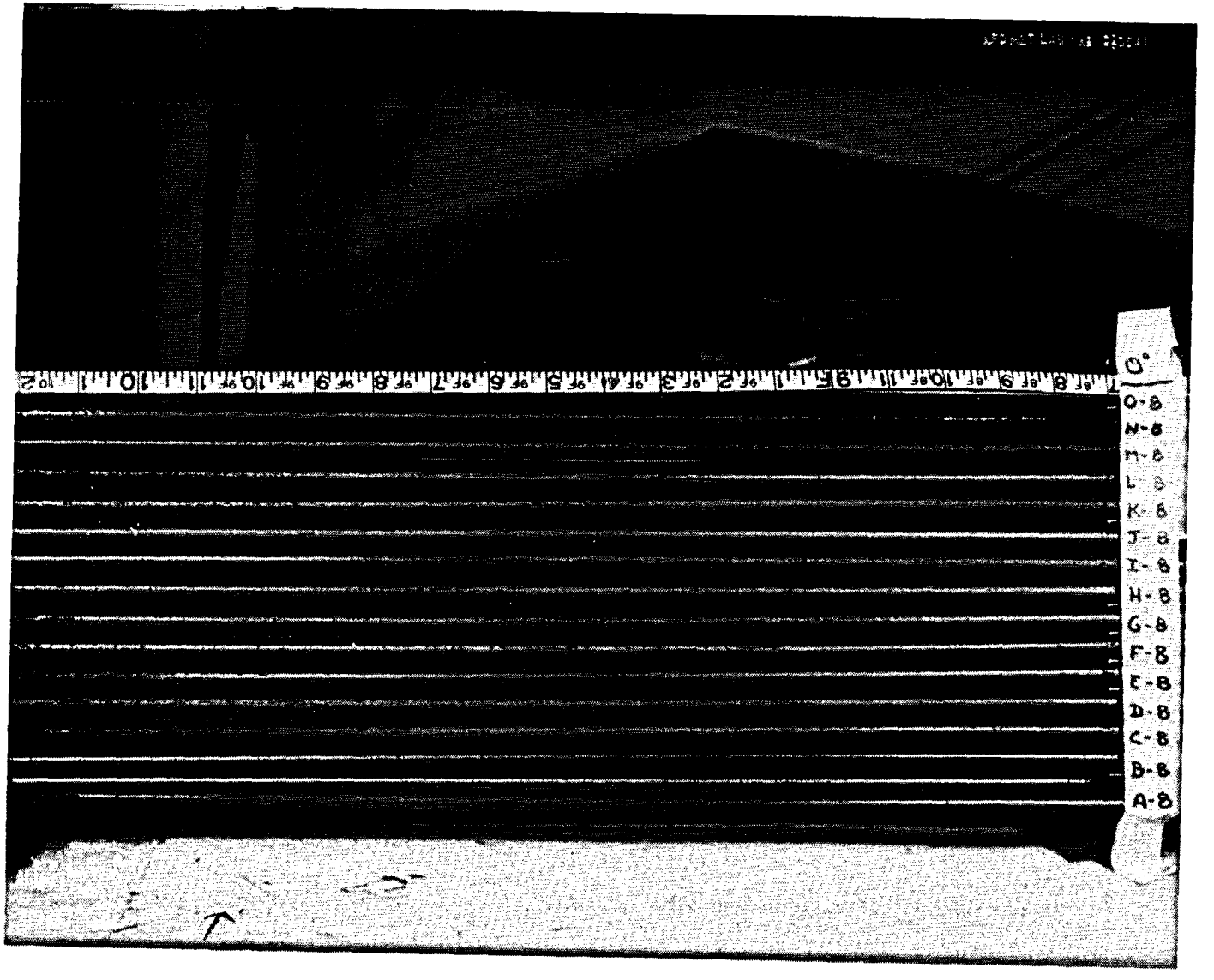

Figure G-7. Bundle, Posttest 2.62-3.15 m (103-124 in.)

Figure G-8. Bundle, Posttest 3.15-3.66 m (124-144 in.)

G-3. REPEATABILITY DATA

A comparison of data from the repeat tests conducted at periodic intervals in the testing was performed. This comparison included quench front data for the heater rods connected to each of three power supplies. Figure G-9 shows which heater rods were connected to the three power supplies. Comparison of data from run 34103 with data from run 31203, and comparison of data from run 35304 with data from run 31504 shows that the quench fronts (figures G-10 through G-15) do not compare as well for runs 31504 and 35304 as those for runs 31203 and 34103. The heat transfer coefficients for rods located away from the failed rods, as shown in figure G-16, also do not compare as well for runs 31504 and 35304 as those for runs 31203 and 34103 (figures G-17 through G-26). Thus it is concluded from the repeat tests that bundle distortion occurred in the center of the bundle between runs 34103 and 35304.

G-4. STATISTICAL ANALYSIS OF BUNDLE DISTORTION

Data and data-based heat transfer parameters from different heater rods at the same elevation of the unblocked bundle are not exactly the same. Numerous factors contribute to the rod-to-rod variation of heat transfer parameters; some of the factors are the finite size of the rod bundle, cross-sectional variation of local flow conditions, presence of the relatively cold thimbles, fillers and housing, individual heater rod manufacturing differences, and subchannel flow area differences. If rod bowing occurred across the bundle cross section, the geometric distortion would be expected to increase the rod-to-rod variation of heat transfer data. If the rod bowing is severe, the effect of geometric distortion will dominate, and a persistent and large increase of rod-to-rod variation will be observed. However, if rod bowing is not severe, the effect of the distortion will not dominate and the increase of rod-to-rod variation will not be readily observable nor persistent. In this case, the effect of geometric distortion on the data is expected to be of the same order of mangitude as the other parameters given above, and it will not affect model and correlation development for an intact bundle geometry.

In the following paragraphs, the rod-to-rod variation is described by calculating the standard deviations of various heat transfer parameters taken from different heater rods at the same elevation. The parameters chosen for the statistical study are the heat transfer coefficient, the heater rod turnaround temperature, the initial temperature

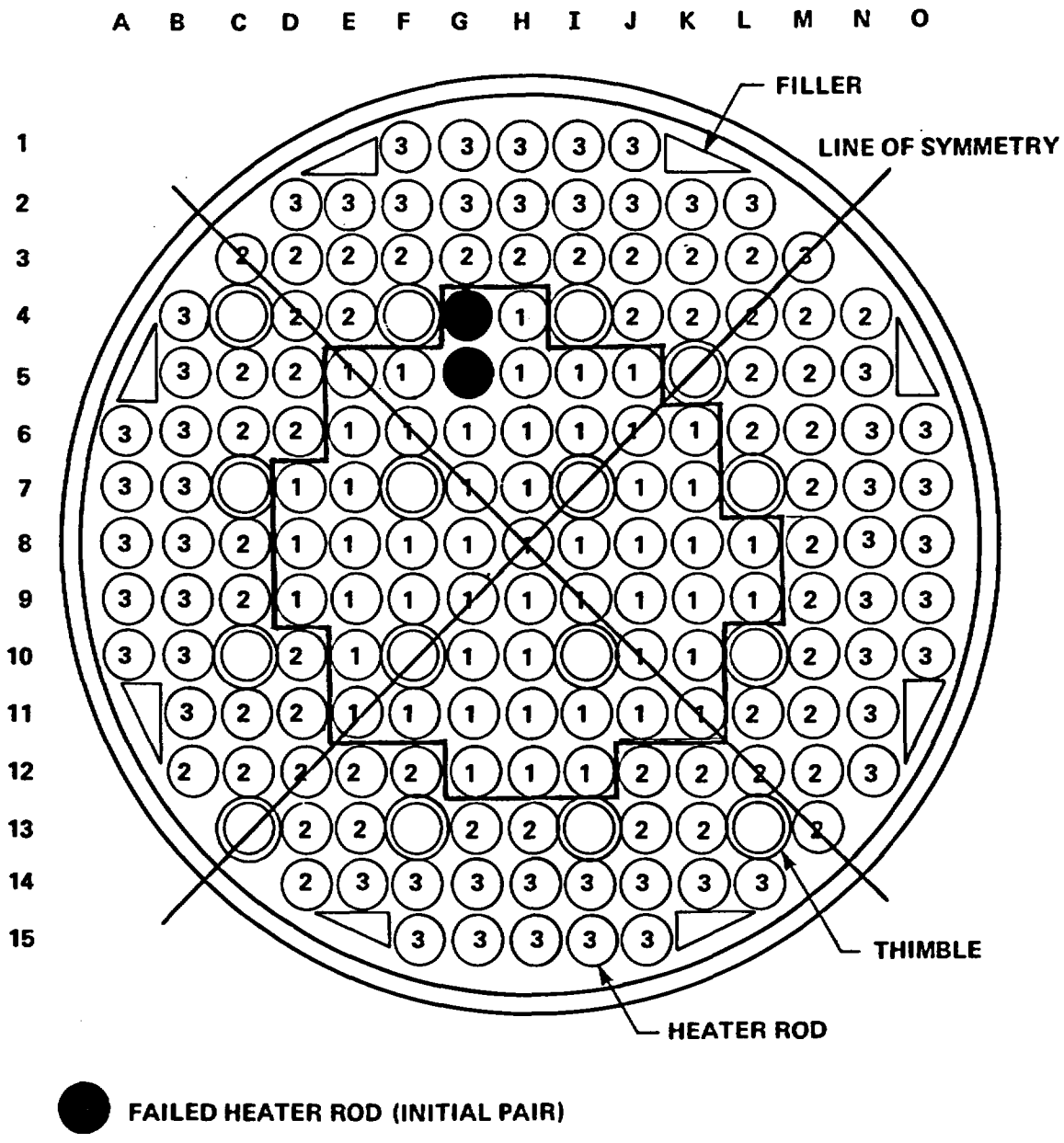

Figure G-9. Heater Rod Power Groups

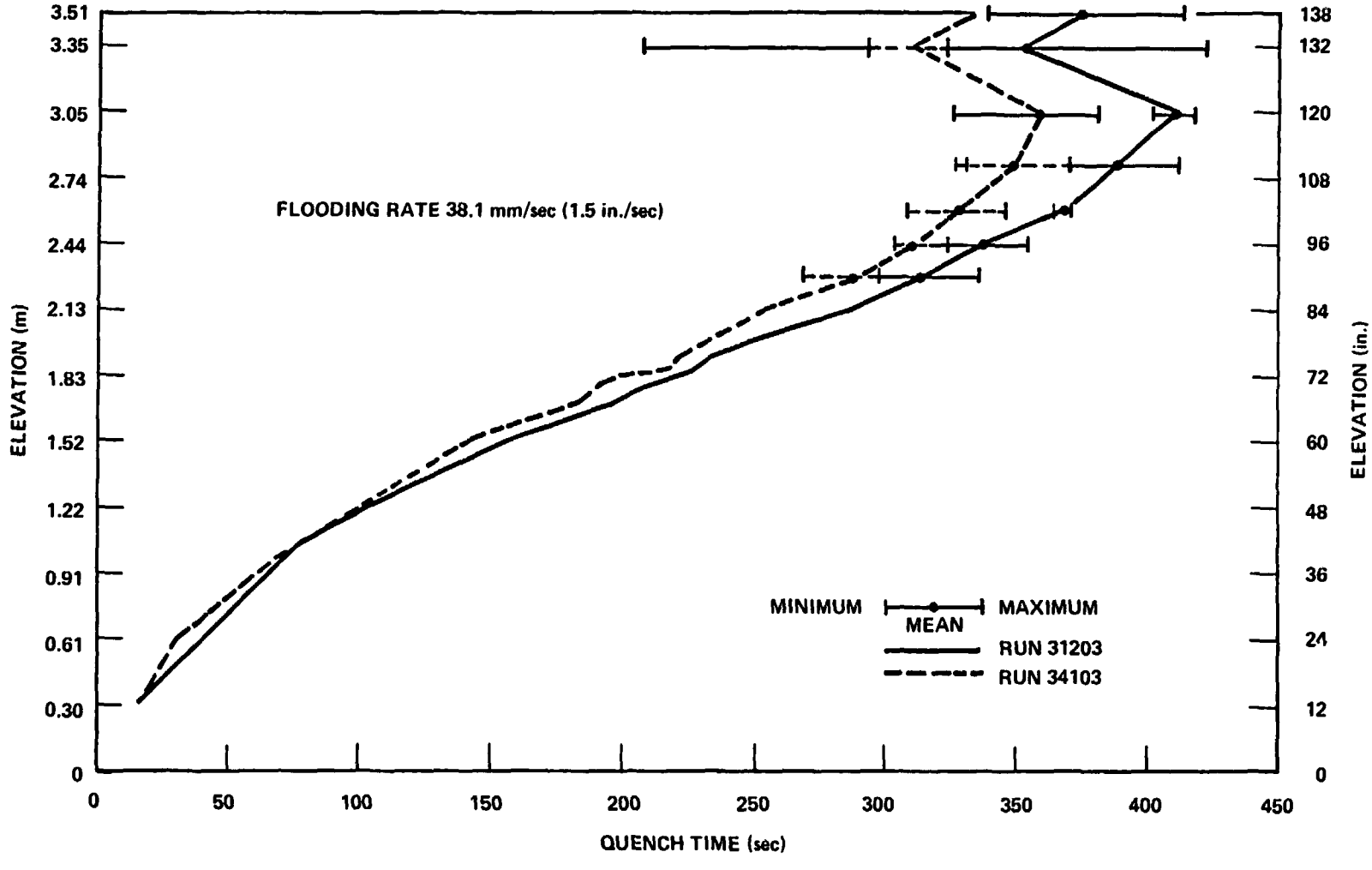

Figure G-10. Quench Curves for Group 1 Heater Rods, Runs 31203 and 34103

16539

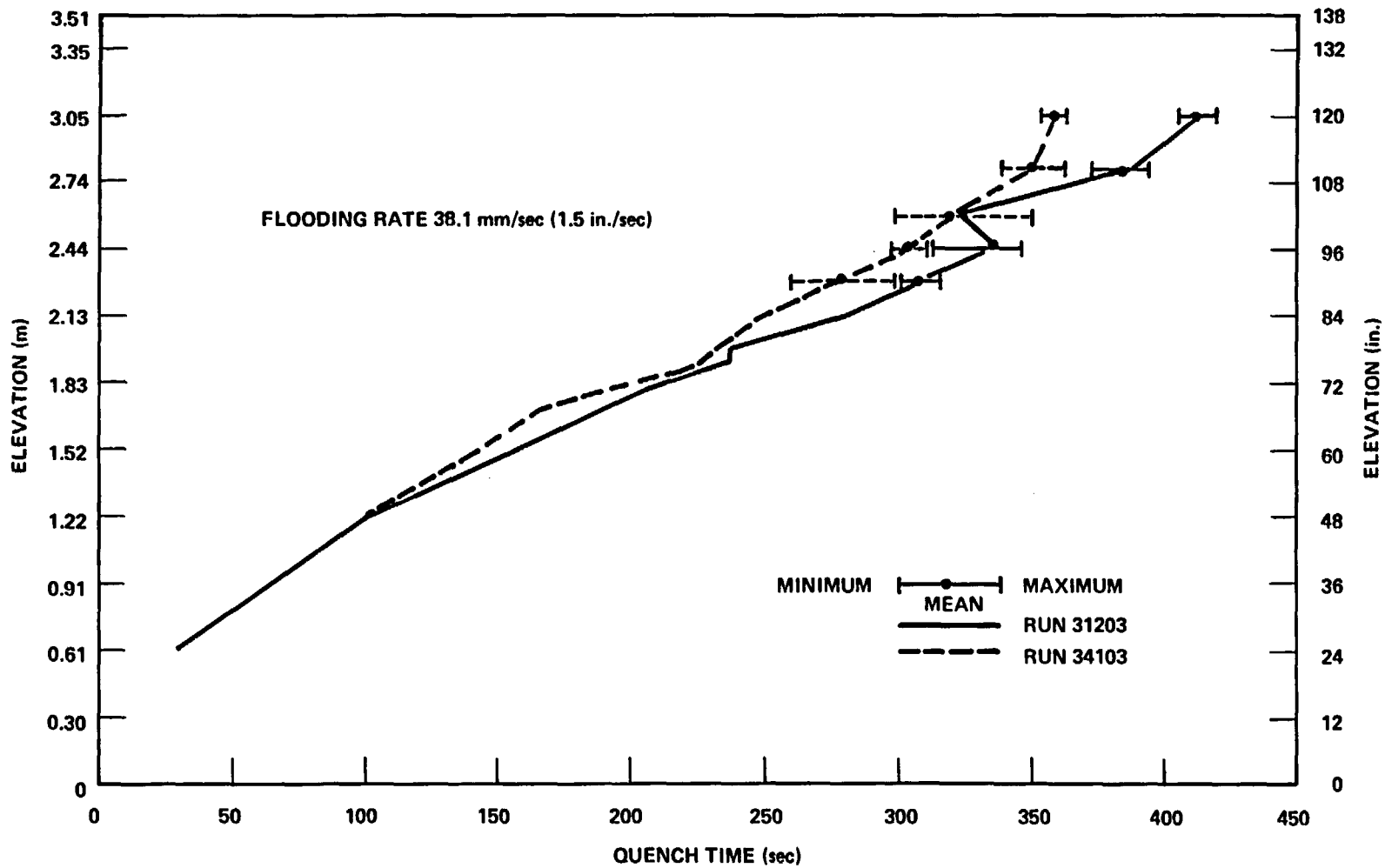

Figure G-11. Quench Curves for Group 2 Heater Rods, Runs 31203 and 34103

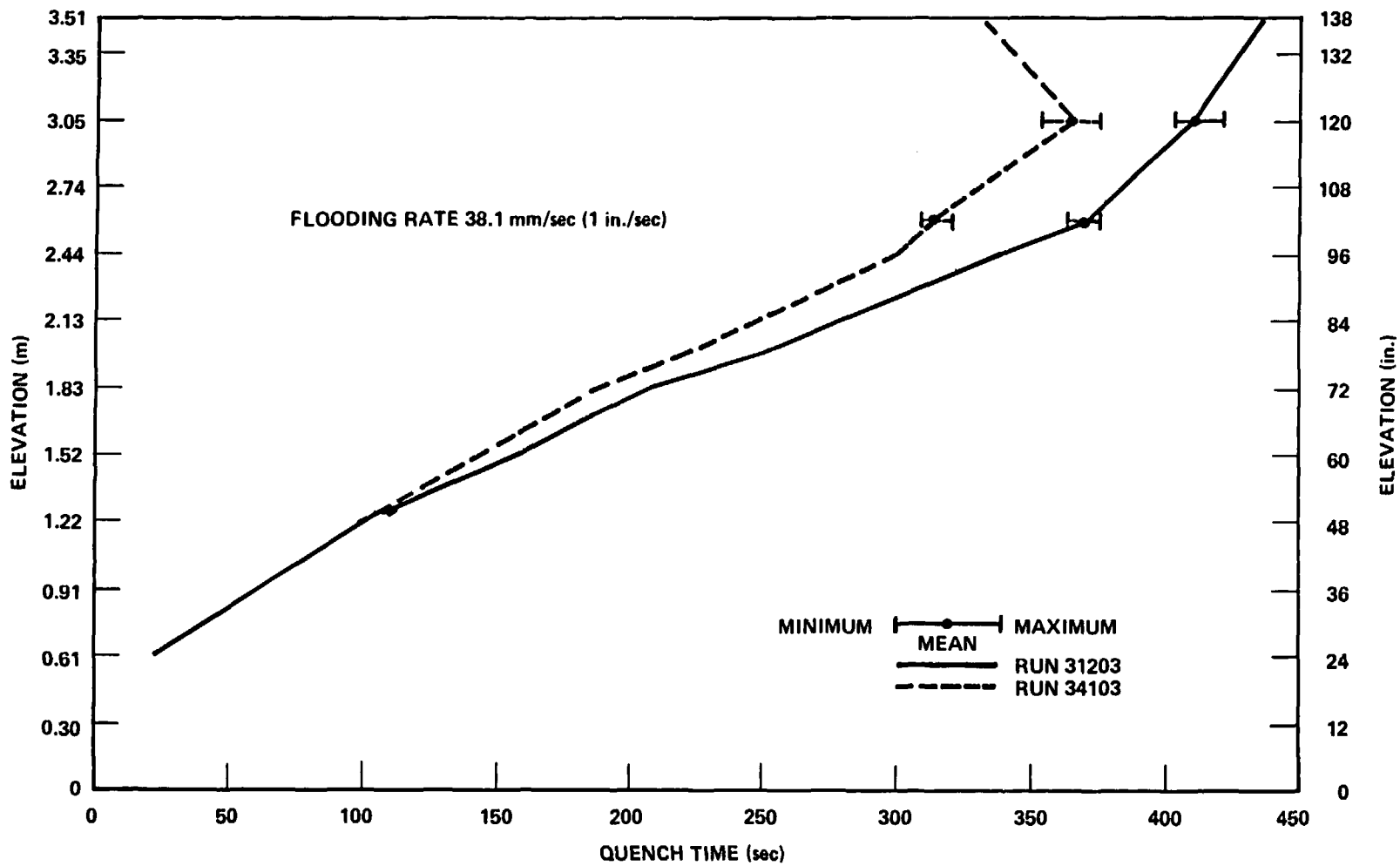

Figure G-12. Quench Curves for Group 3 Heater Rods, Runs 31203 and 34103

16539

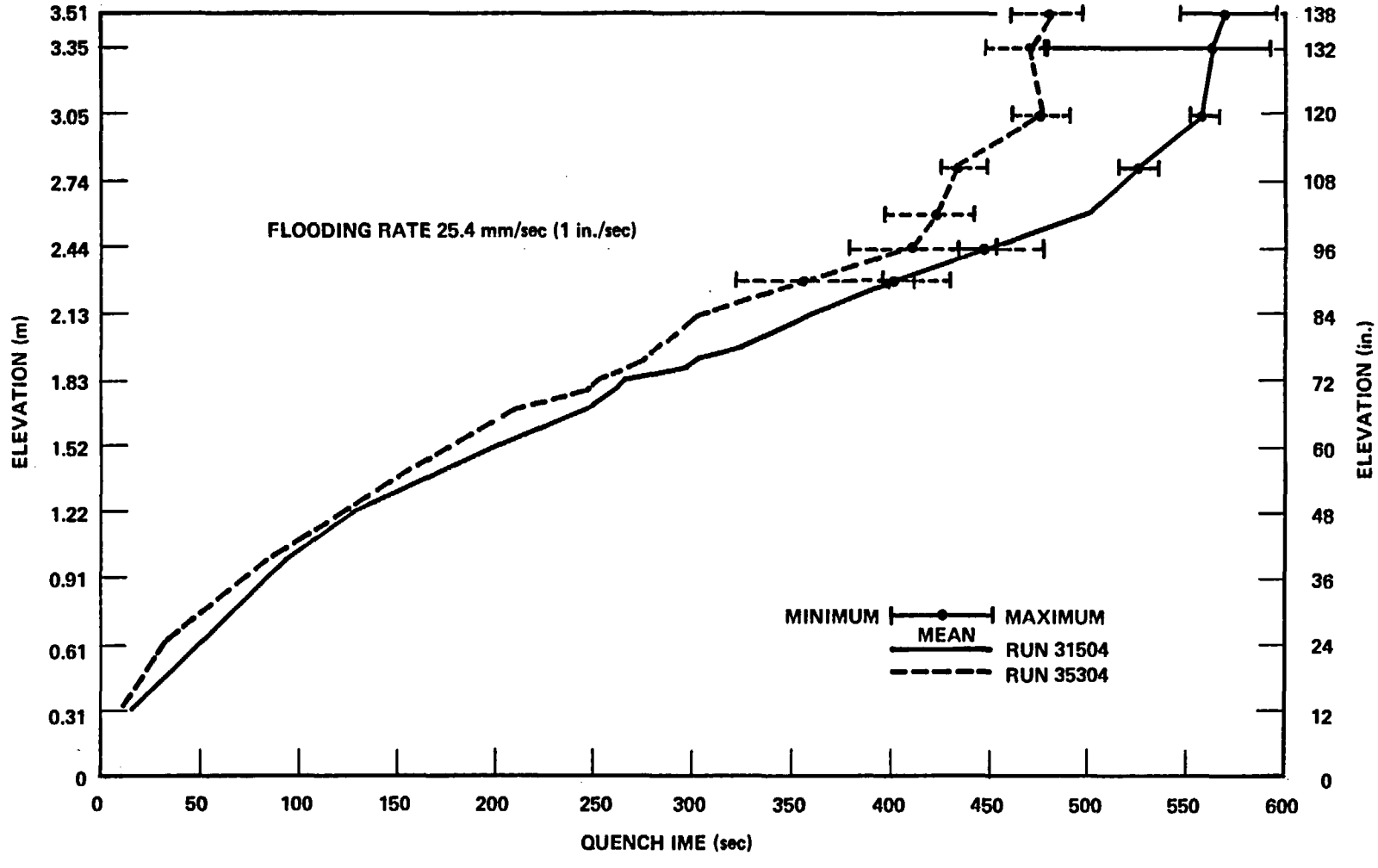

Figure G-13. Quench Curves for Group 1 Heater Rods, Runs 31504 and 35304

16539

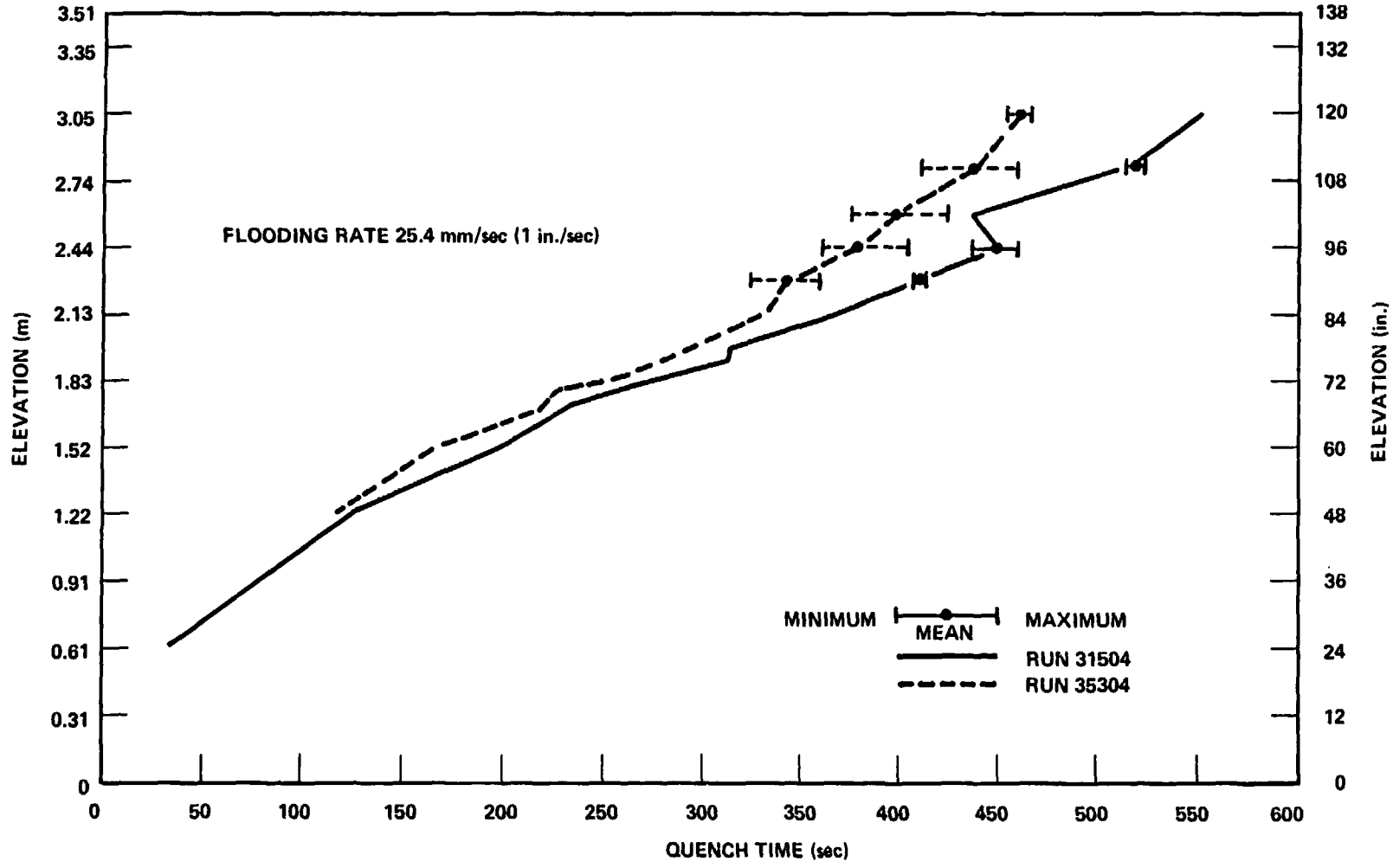

Figure G-14. Quench Curves for Group 2 Heater Rods, Runs 31504 and 35304

16539

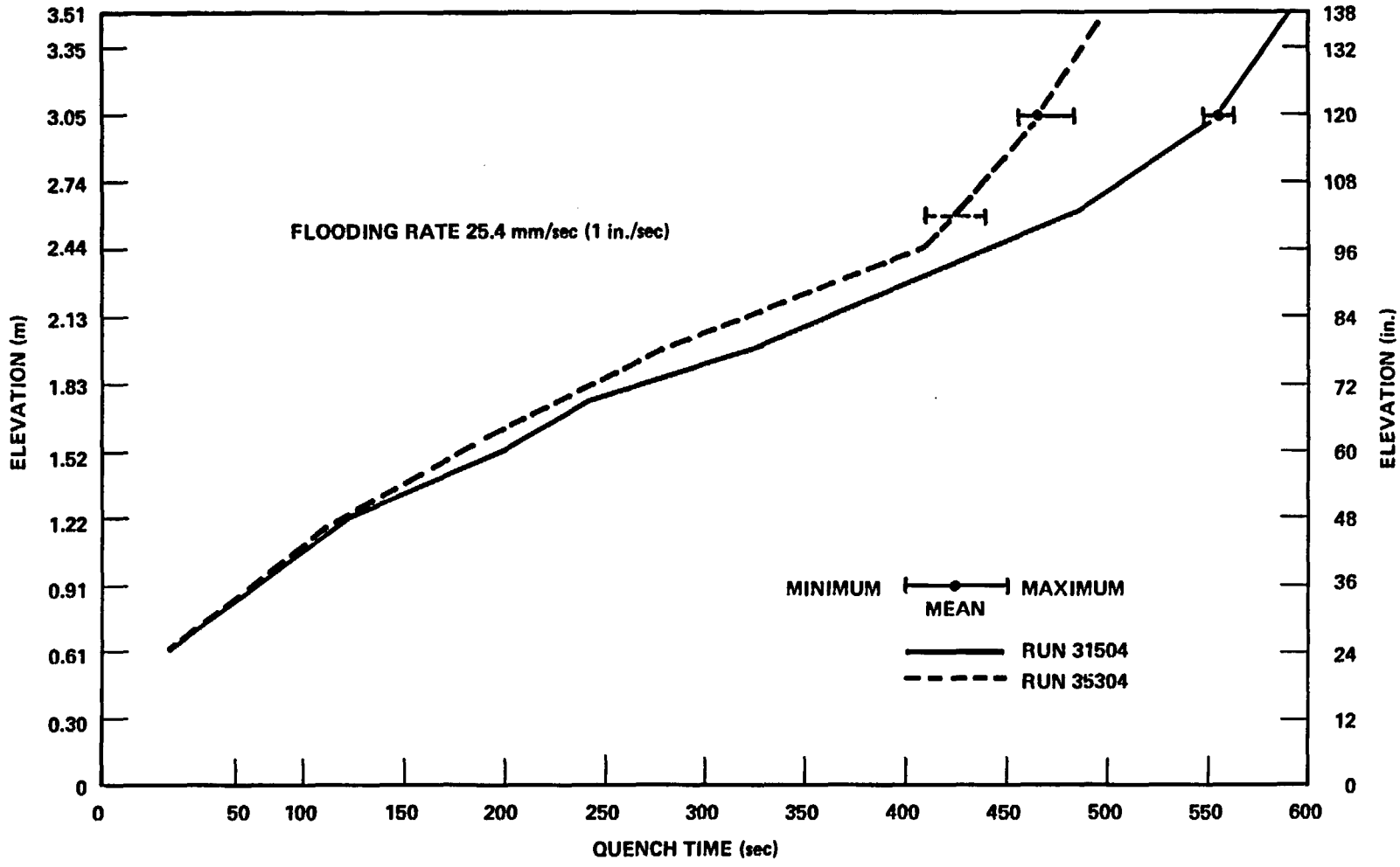

Figure G-15. Quench Curves for Group 3 Heater Rods, Runs 31504 and 35304

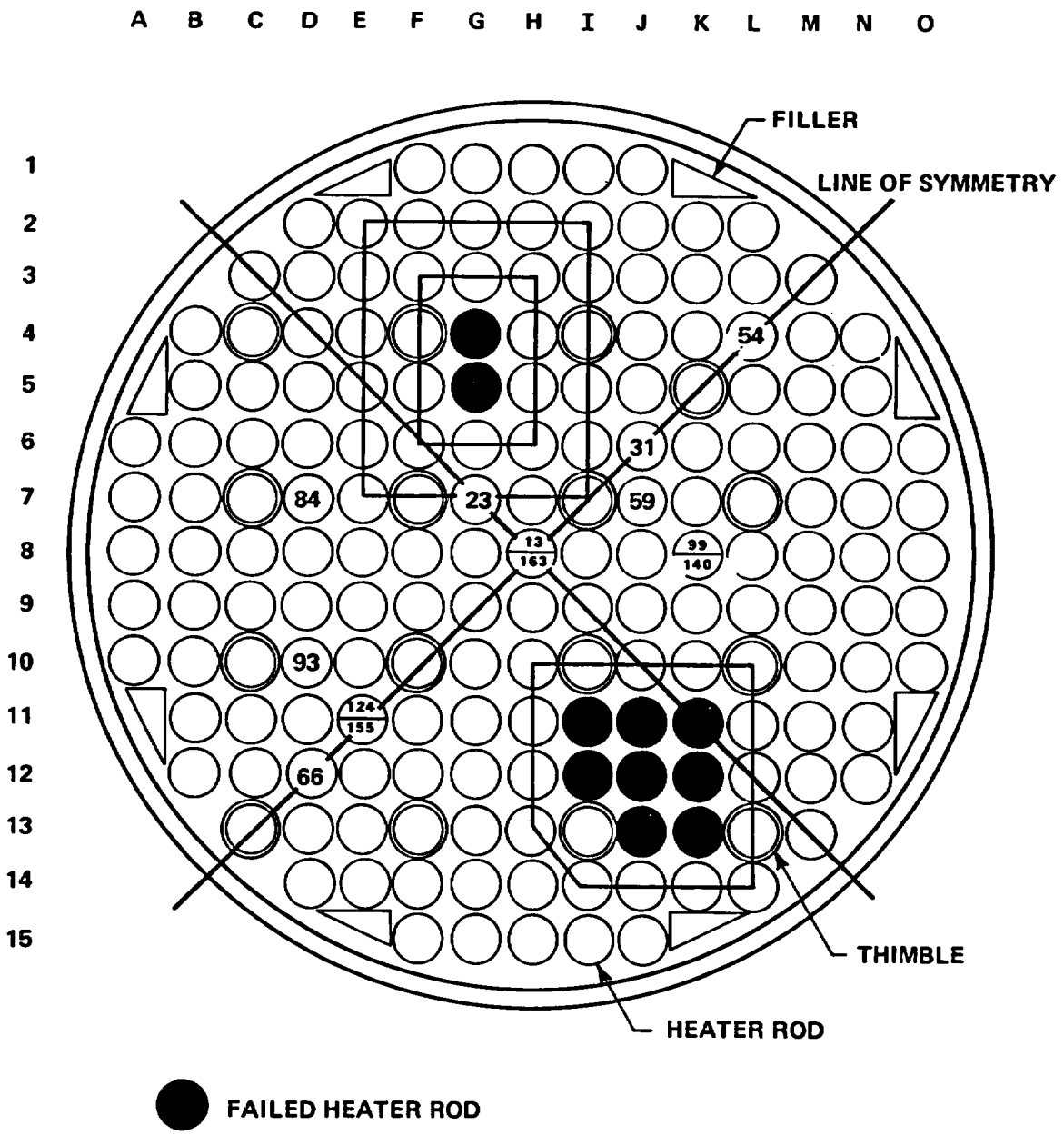

Figure G-16. Bundle Cross Section

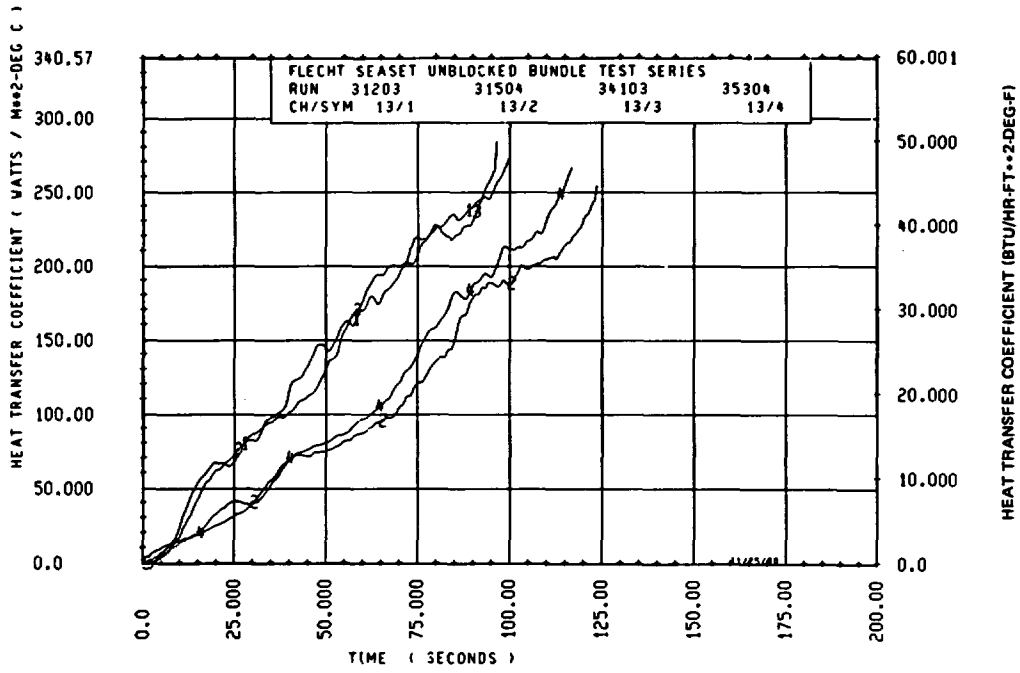

Figure G-17. Heat Transfer Coefficient Curves, Location 8H, 1.22 m (48 in.)

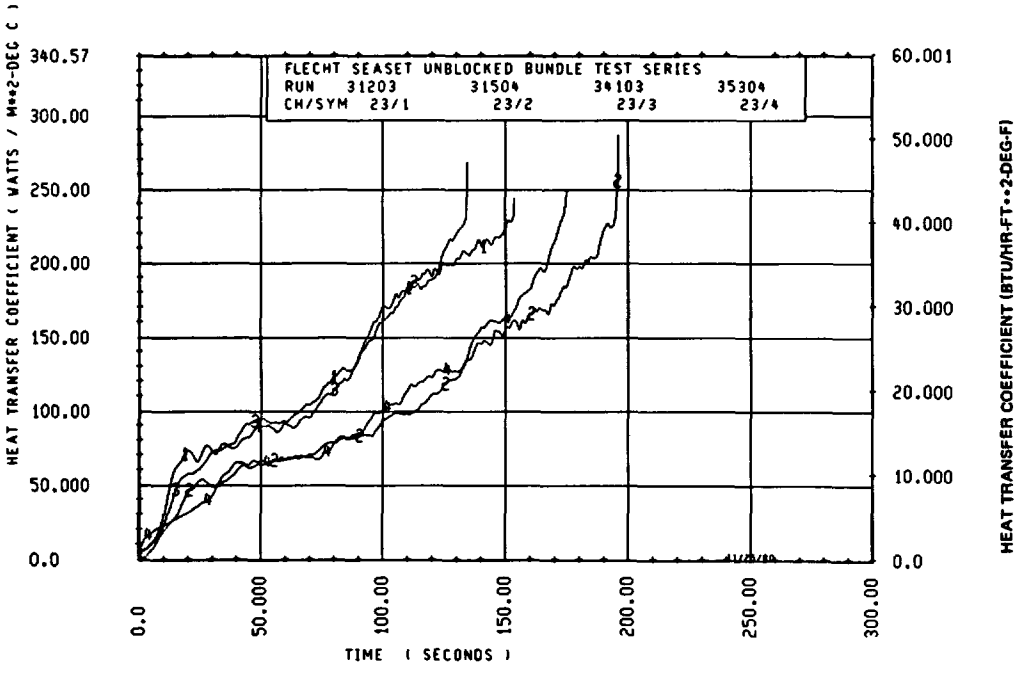

Figure G-18. Heat Transfer Coefficient Curves, Location 7G, 1.52 m (60 in.)

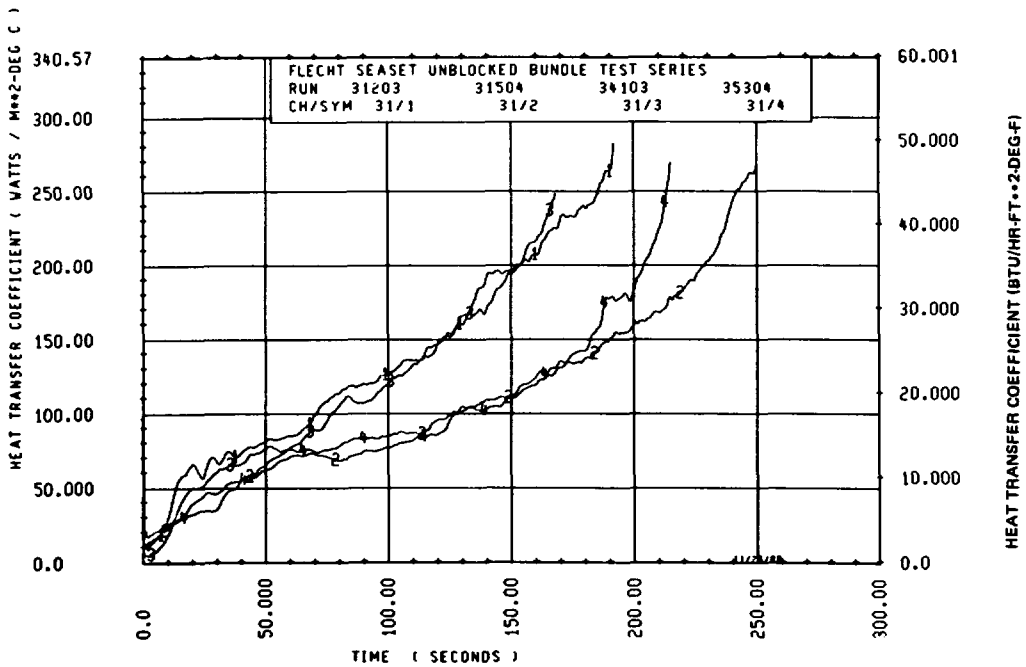

Figure G-19. Heat Transfer Coefficient Curves, Location 6J, 1.70 m (67 in.)

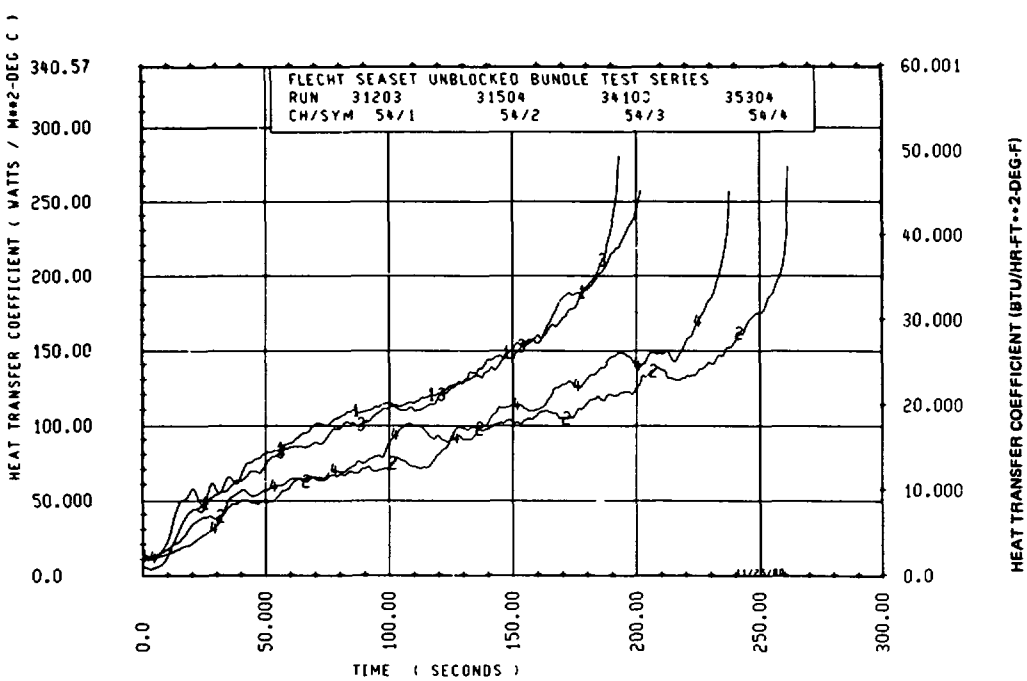

Figure G-20. Heat Transfer Coefficient Curves, Location 4L, 1.83 m (72 in.)

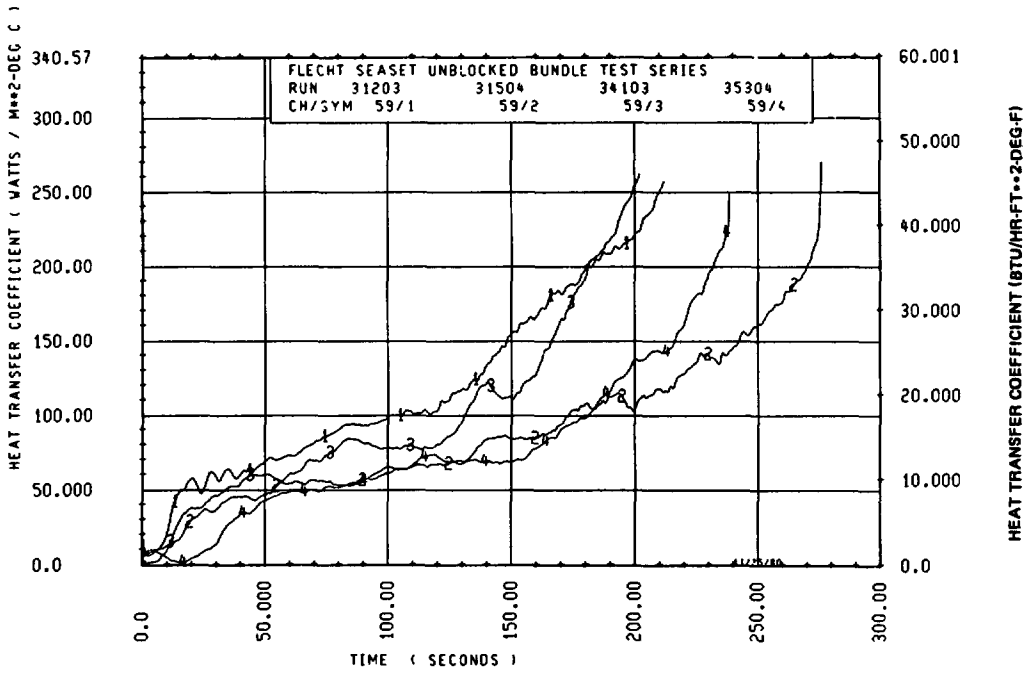

Figure G-21. Heat Transfer Coefficient Curves, Location 7J, 1.83 m (72 in.)

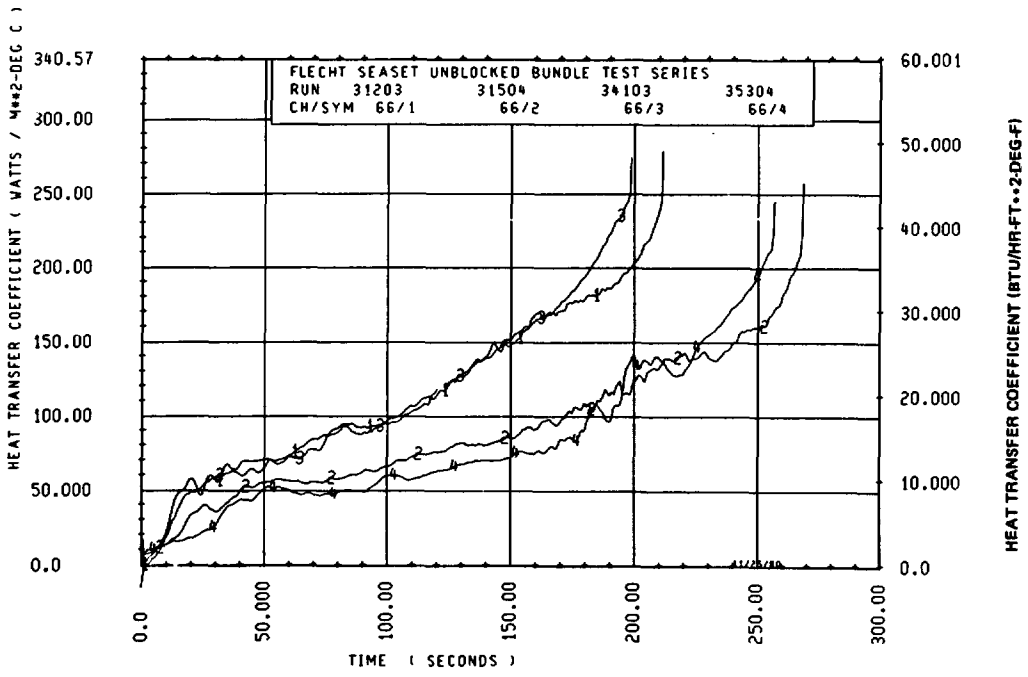

Figure G-22. Heat Transfer Coefficient Curves, Location 12D, 1.83 m (72 in.)

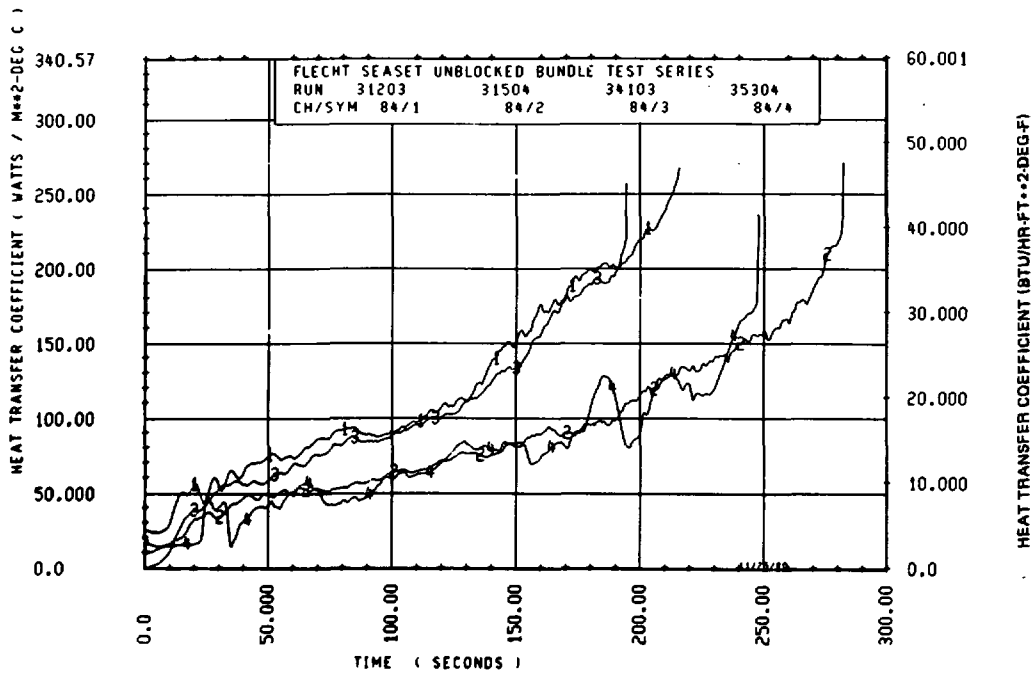

Figure G-23. Heat Transfer Coefficient Curves, Location 7D, 1.93 m (76 in.)

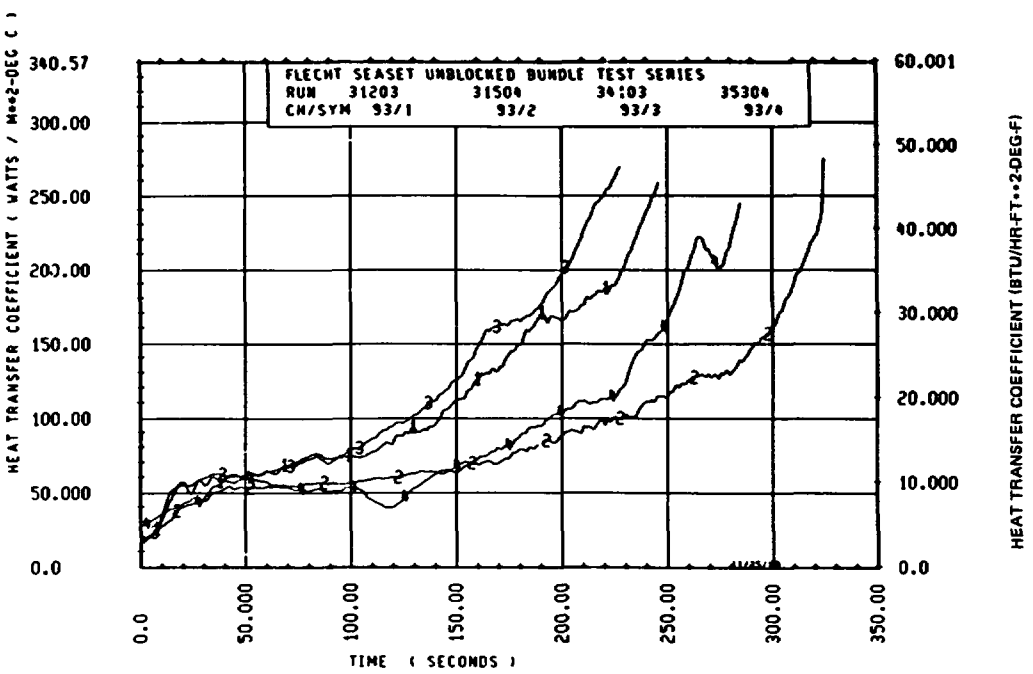

Figure G-24. Heat Transfer Coefficient Curves, Location 10D, 1.98 m (78 in.)

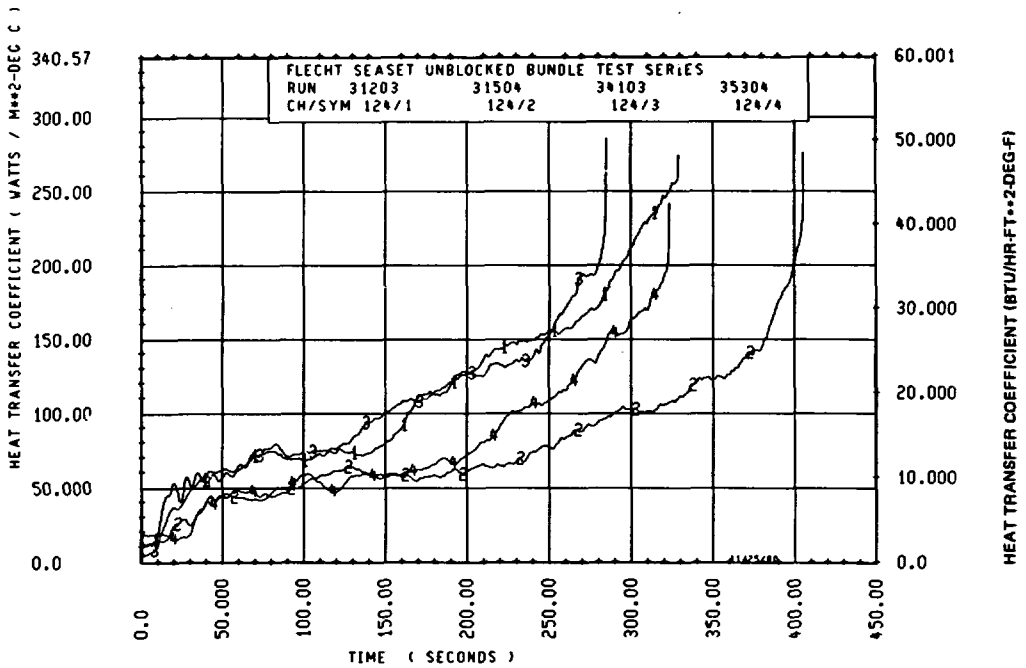

Figure G-25. Heat Transfer Coefficient Curves, Location 11E, 2.29 m (90 in.)

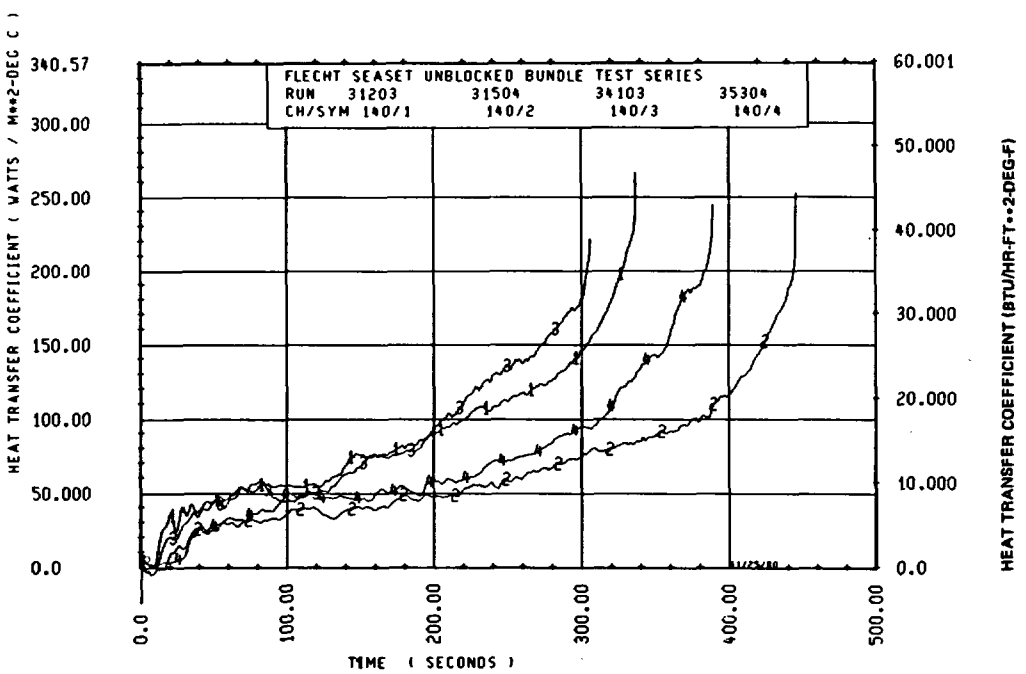

Figure G-26. Heat Transfer Coefficient Curves, Location 8K, 2.44 m (96 in.)

(temperature at beginning of flooding), and the heater rod temperature rise (turnaround temperature minus initial temperature). The basic equations are presented in the paragraphs below; the results and their interpretations are presented in paragraphs G-10 through G-14.

G-5. Basic Equations for Statistical Analysis

Let P be the heat transfer parameter chosen for the statistical study. Let $P_i^{(j)}(z,t)$ be the value of P measured during the j-th reflood test cycle from the i-th heater rod at elevation z and time t. The mean value of P is then given by

$$\bar{P}^{(j)}(z,t) = \frac{1}{N} \sum_{i=1}^{N} P_i^{(j)}(z,t) \qquad \text{(G-1)}$$

where N is the number of measurements or instrumentation locations available at z. The standard deviation of P is then given by

$$\sigma^{(j)}(z,t) = \sqrt{\frac{\sum_{i=1}^{N} [P_i^{(j)}(z,t) - \bar{P}^{(j)}(z,t)]^2}{N-1}} \qquad \text{(G-2)}$$

G-6. Statistical Analysis of Heat Transfer Coefficient

The local heat transfer coefficients, based on vapor saturation temperature, have been calculated by the DATAR inverse conduction code. Using the heat transfer coefficient for the statistical test, the standard deviations were calculated for 31 forced reflood runs at two different elevations and at six different times. The 31 reflood runs, together with their test conditions, are shown in table G-2. The standard deviations were calculated at the 1.83 m (72 in.) and 1.52 m (60 in.) elevations. As mentioned before, severe bundle distortion across the 1.83 m (72 in.) cross section was observed from the disassembled bundle; hence it is most important to study the effect of bundle distortion at the 1.83 m (72 in.) elevation and determine at which run data taken from this elevation were no longer reliable. Except for the rods adjacent to the housing, the rod bundle at the 1.52 m (60 in.) elevation remained

intact at the conclusion of the test series. Results from the 1.53 m (60 in.) elevation can be compared with those from the 1.83 m (72 in.) elevation, as a check for the statistical test. Since the heat transfer coefficient is also time dependent, and the time scales for different reflood tests and at different elevations are different, it is necessary to compare the results at some appropriate reference times. The turnaround time and the quench time seem to be appropriate references. The average turnaround time, $t_T^{(j)}(z)$, and quench time, $t_q^{(j)}(z)$, at elevation z for the j-th reflood test cycle were first calculated:

$$\bar{t}_T^{(j)}(z) = \frac{1}{N} \sum_{i=1}^{N} t_{T_i}^{(j)}(z) \qquad \text{(G-3)}$$

$$\bar{t}_q^{(j)}(z) = \frac{1}{N} \sum_{i=1}^{N} t_q^{(j)}(z) \qquad \text{(G-4)}$$

The mean heat transfer coefficients, h, and standard deviations, σ_h, for the j-th reflood test cycle at elevation z were then calculated at six different times during reflood:

$$\bar{h}^{(j)}(z,t_k) = \frac{1}{N} \sum_{i=1}^{N} h_i^{(j)}(z,t_k) \qquad \text{(G-5)}$$

$$\sigma_h^{(j)}(z,t_k) = \sqrt{\frac{\sum_{i=1}^{N} [h_i^{(j)}(z,t_k) - \bar{h}^{(j)}(z,t_k)]^2}{N-1}} \quad ; k = 1,2...6 \qquad \text{(G-6)}$$

where t_1 is the average turnaround time, and t_2, t_3 ..., t_6 are 3/10, 4/10, ... 7/10 of the quench time respectively:

$$t_1 = \bar{t}_T^{(j)}(z) \tag{G-7}$$

$$t_k = \frac{(k+1)\ \bar{t}_q^{(j)}(z)}{10}, \quad k = 2,3,\ldots 6 \tag{G-8}$$

Since the magnitudes of the heat transfer coefficients were different for different test cycles and at different elevations and times, it is more meaningful to compare the standard deviation normalized with respect to the mean heat transfer coefficient:

$$\sigma_h'^{(j)}(z,t_k) = \frac{\sigma_h^{(j)}(z,t_k)}{\bar{h}^{(j)}(z,t_k)} \tag{G-9}$$

Results of the statistical analysis of the heat transfer coefficient are presented in paragraph G-10.

G-7. Statistical Analysis of Measured Heater Rod Temperature

Using the heater rod turnaround temperature, the initial temperature, or the temperature rise for the statistical study, equations (G-1) and (G-2) become

$$\bar{T}^{(j)}(z) = \frac{1}{N} \sum_{i=1}^{N} T_i^{(j)}(z) \tag{G-10}$$

$$\sigma_T^{(j)}(z) = \sqrt{\frac{\sum_{i=1}^{N} [T_i^{(j)}(z) - \bar{T}^{(j)}(z)]^2}{N-1}} \tag{G-11}$$

where T stands for the turnaround temperature, the initial temperature, or the temperature rise, respectively.

As with the heat transfer coefficient, it is more meaningful to consider the temperature standard deviations normalized with respect to the mean temperatures:

$$\sigma_T'^{(j)}(z) = \frac{\sigma_T^{(j)}(z)}{\bar{T}^{(j)}(z)} \qquad \text{(G-12)}$$

The temperature standard deviations were calculated for the same 31 reflood tests as the heat transfer coefficients. Besides the 1.52 m (60 in.) and 1.83 m (72 in.) elevations, the temperature standard deviations were also calculated at the 2.29 m (90 in.) elevation. The results and interpretation are given in paragraphs G-11 through G-14.

G-8. EFFECT OF HOUSING AND DISONNECTED RODS ON ROD-TO-ROD VARIATION

It is important to distinguish the effect of bundle distortion on the rod-to-rod variation from the effects of other factors. An obvious factor affecting the rod-to-rod variation is the relatively cold region near the housing and the disconnected rods. To distinguish the effect of the bundle distortion in the central bundle from that near the housing and the disconnected rods, two different cases were considered.

First, when calculating the standard deviation at a given elevation z, not all available data at z were used; data taken from heater rods one rod row away from the housing and disconnected rods were not used. Second, the calculation was repeated by eliminating an additional heater rod row from the housing and disconnected rods. That is, data taken from the first two heater rod rows from the housing and disconnected rods were not used. The disconnected rods, the first and second heater

rod rows from the housing, and the disconnected rods are shown in figure G-27. It will be noted that two heater rods were disconnected after run 30418 and eight more were disconnected after run 33849. In the calculation of the standard deviations, however, data from all heaters rods near the 10 rods which were disconnected after run 33849 were discarded for all 31 reflood test runs, even though at the beginning of the test, none or only two heater rods were disconnected in the bundle. By discarding data from the same heater rods for all runs, the results are more meaningful for comparison.

It is shown in paragraphs G-9 through G-14 that bundle distortion near the housing and disconnected rods had an apparent effect on the rod-to-rod variation, and the distortion near the housing and disconnected rods affected the heat transfer data earlier than the distortion at the central bundle. In the development of heat transfer correlations, data from the central bundle are of primary interest. The fact that data at the central bundle were not affected by the bundle distortion until late at the reflood test cycles means that more data and a wider range of reflood conditions are available for correlation development. Hence it is important to distinguish the bundle distortion near the housing and disconnected rods from that at the central bundle.

G-9. RESULTS OF STATISTICAL ANALYSIS AND INTERPRETATION

In the following paragraphs, discarding one or two heater rod rows means discarding data from the first, or the first and second, heater rod rows from the housing and disconnected rods, as shown in figure G-27; the central bundle refers to rods which are more than two rod rows away from the housing and disconnected rods.

The calculated standard deviations were plotted as a function of test runs, so that any change in rod-to-rod variation during the reflood series could be observed. The run sequence (or j) in the abscissa in figures G-28 through G-50 corresponds to the reflood test runs, as shown in table G-3. In the runs below point 14 on this scale (indicated by arrow A), 15 rods in the central bundle were pulled and replaced. In the runs above point 16 (indicated by arrow B), rod 12J and the surrounding rods could not be pulled. The ordinate is the scale of the normalized standard deviations calculated from equations (G-9) and (G-12).

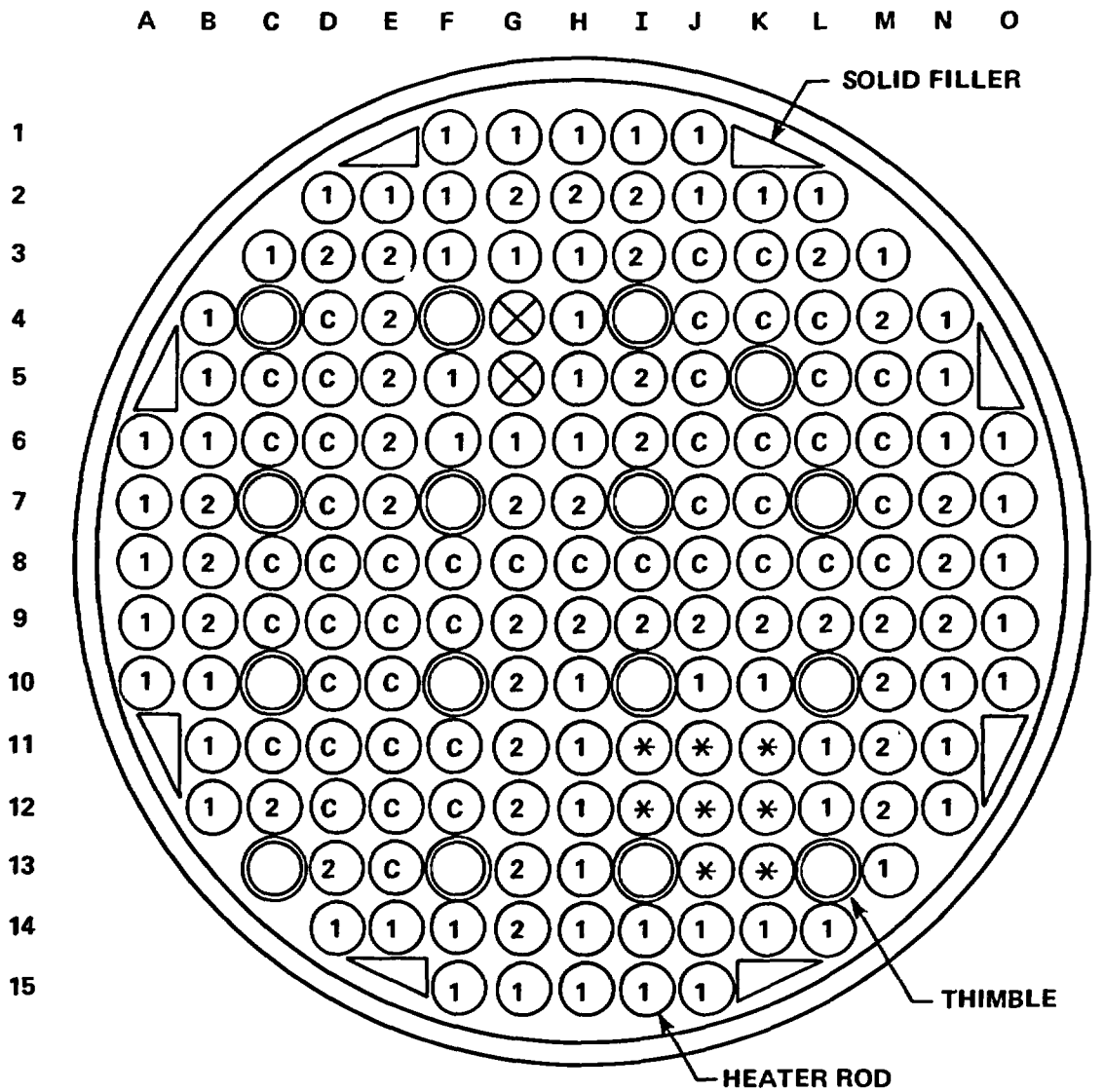

⊗ HEATER RODS DISCONNECTED AFTER RUN 30418

(*) ADDITIONAL HEATER RODS DISCONNECTED AFTER RUN 33849

(1) HEATER RODS 1 ROD ROW FROM HOUSING OR DISCONNECTED ROD ZONE

(2) HEATER RODS 2 ROD ROWS FROM HOUSING OR DISCONNECTED ROD ZONE

(C) HEATER RODS AT CENTRAL BUNDLE

Figure G-27. Disconnected Rods, Housing Rods, and Rods at Central Bundle

TABLE G-3

FORCED REFLOOD TESTS USED IN STATISTICAL ANALYSIS

Run Sequence No.	Run	Test Conditions Different From Reference Run
1	30323	3.8 cm/sec, 1.3 kw/m, 257°C (1.5 in./sec, 0.4 kw/ft, 500°F)
2	30518	3.8 cm/sec, 257°C (1.5 in./sec, 500°F)
3	30619	3.8 cm/sec, 0.13 MPa, 257°C (1.5 in./sec, 20 psia 500°F)
4	30817	3.8 cm/sec, 538°C (1.5 in./sec, 1000°F)
5	31021	3.8 cm/sec, 1.3 kw/m, (1.5 in./sec, 0.4 kw/ft)
6	31108	7.6 cm/sec, 0.13 MPa (3 in./sec, 20 psia)
7	31203	3.8 cm/sec (1.5 in./sec)
8	31302	7.6 cm/sec (3 in./sec)
9	31504	Reference run
10	31805	2.0 cm/sec (0.8 in./sec)
11	31922	1.3 kw/m, 1.3 MPa (0.4 kw/ft, 20 psia)
12	32013	0.41 MPa (60 psia)
13	32235	Stepped flow: 15 cm/sec (6 in./sec) for 5 sec, 2.5 cm/sec (1 in./sec) for 200 sec, 1.5 cm/sec (0.6 in./sec) onward; 0.13 MPa (20 psia)

TABLE G-3 (cont)

FORCED REFLOOD TESTS USED IN STATISTICAL ANALYSIS

Run Sequence No.	Run	Test Conditions Different From Reference Run
14	32333	Stepped flow: 15 cm/sec (6 in./sec) for 5 sec, 2.0 cm/sec (0.8 in./sec) onward
15	33749	1.9 kw/m, 732°C, 67°C subcooling (0.57 kw/ft, 1350°F, 120°F subcooling)
16	33849	1.9 kw/m, 732°C, 67°C subcooling (0.57 kw/ft, 1350°F, 120°F subcooling)
17	33903	3.8 cm/sec (1.5 in./sec) -- repeat test (10 unpowered rods at nominal power)
18	34006	1.5 cm/sec, 1.3 kw/m (0.6 in.sec, 0.4 kw/ft)
19	34103	3.8 cm/sec (1.5 in./sec) -- repeat test (10 unpowered rods at 159/151 x nominal power)
20	34209	0.13 MPa (20 psia)
21	34316	Variable subcooling: 78°C - 3°C (140°F - 5°F) linear (500 sec)
22	34420	3.8 cm/sec, 1093°C (1.5 in./sec, 2000°F)
23	34524	3.8 cm/sec, 3.3 kw/m (1.5 in./sec, 1.0 kw/ft)
24	34610	2.0 cm/sec, 1.3 kw/m, 0.13 MPa (0.8 in./sec, 0.4 kw/ft, 20 psia)

TABLE G-3 (cont)

FORCED REFLOOD TESTS USED IN STATISTICAL ANALYSIS

Run Sequence No.	Run	Test Conditions Different From Reference Run
25	34711	1.5 cm/sec, 1.3 kw/m, 0.13 MPa (0.6 in./sec, 0.4 kw/ft, 20 psia)
26	34815	0.13 Mpa, 3°C subcooling (20 psia, 5°F subcooling)
27	35050	1.5 kw/m, 732°C (0.46 kw/ft, 1350°F)
28	35114	3°C (5°F) subcooling
29	35304	Reference run -- repeat test
30	35807	1.0 cm/sec, 0.89 kw/m (0.4 in./sec, 0.27 kw/ft)
31	35912	1.0 cm/sec, 0.89 kw/m, 0.13 MPa (0.4 in./sec, 0.27 kw/ft, 20 psia)

The following points are essential to meaningful interpretation of the statistical results:

- Random fluctuations exist in the statistical results even without bundle distortion. To determine the effect of bundle distortion, one must look for a persistent trend of increase in magnitude or fluctuation of the calculated standard deviations, and must examine all time periods.

- For more confidence in interpreting the statistical results, one can compare the effects of bundle distortion with results from an intact geometry. Two such references can be used: first, the results at the 1.52 m (60 in.) elevation where geometry is known to be intact from the disassembled bundle, and second, all results before run 33056 (since 15 heater rods were pulled and replaced after this run, before which the bundle geometry was still intact).

G-10. Statistical Analysis of Heat Transfer Coefficient

Figures G-28 through G-33 show the calculated standard deviations of the heat transfer coefficient at the 1.52 m (60 in.) elevation with the data from one heater rod row deleted at the six time steps, as defined in equations (G-7) and (G-8). The results at the 1.52 m (60 in.) elevation show the results one would expect from an intact geometry. Note that even for an intact geometry, the fluctuations of the standard deviations could be quite large, and vary with both time and run sequence. The important point to note is that there is no persistent trend such that the magnitude or the fluctuation of the standard deviations tends to increase.

Figures G-34 through G-39 show the results at the 1.83 m (72 in.) elevation with the data from two heater rod rows discarded. The figures indicate a slight increase in the magnitude of the standard deviations from run sequence number 16 (run 33849) to run sequence number 24 (run 34610). It will be recalled that after run 33849, an unsuccessful attempt was made to pull rod 12J and the surrounding rods. The increase in the standard deviations and the unsuccessful attempt to pull rods seem to indicate

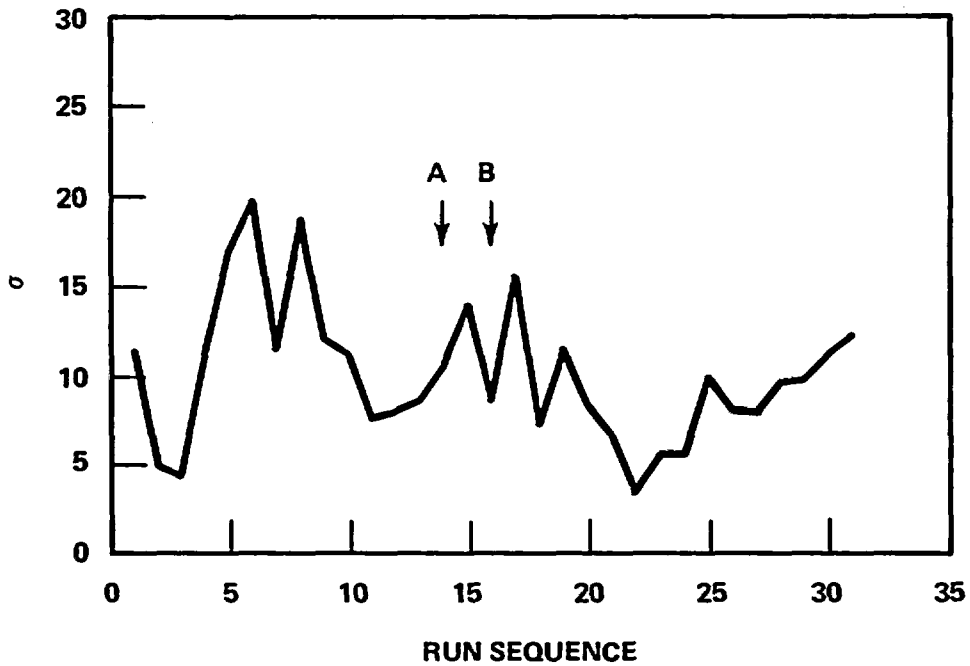

Figure G-28. Normalized Standard Deviation of Heat Transfer Coefficient at 1.52 m (60 in.), Turnaround Time, One Heater Rod Row Discarded

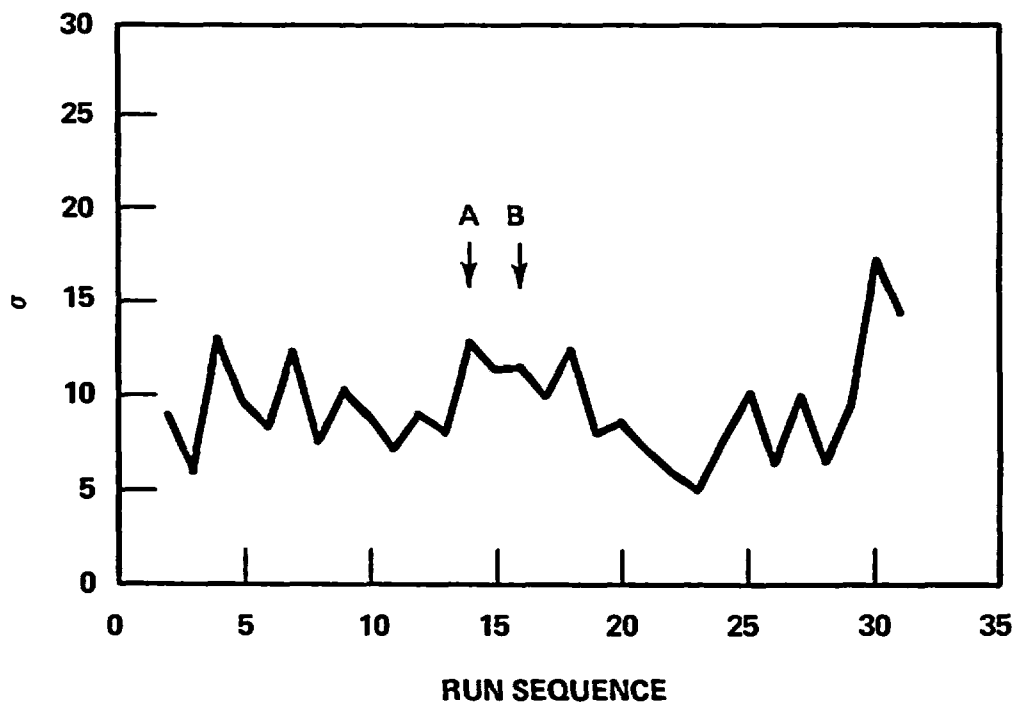

Figure G-29 Normalized Standard Deviation of Heat Transfer Coefficient at 1.52 m (60 in.), 0.3 x Quench Time, One Heater Rod Row Discarded

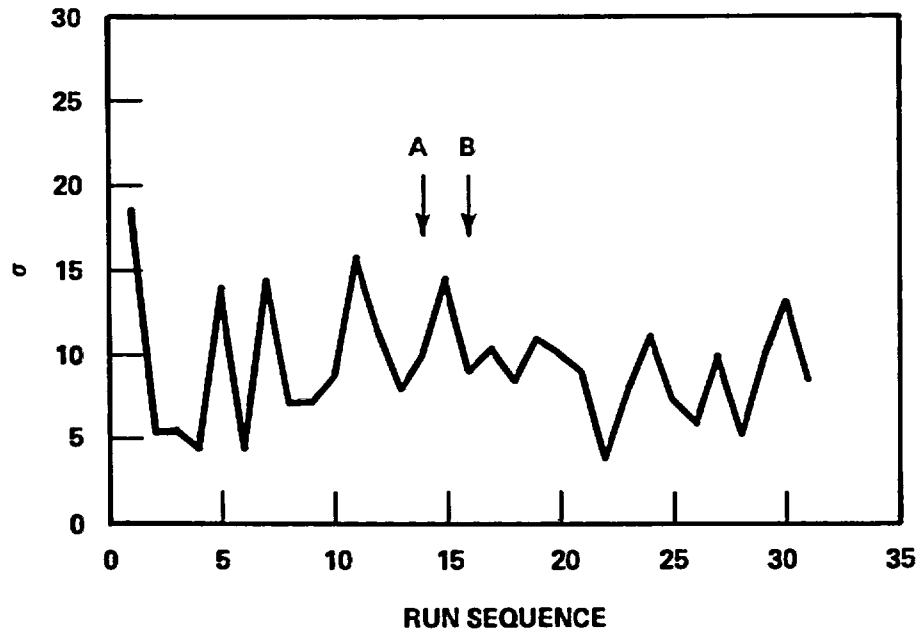

Figure G-30. Normalized Standard Deviation of Heat Transfer Coefficient at 1.52 m (60 in.), 0.4 x Quench Time, One Heater Rod Row Discarded

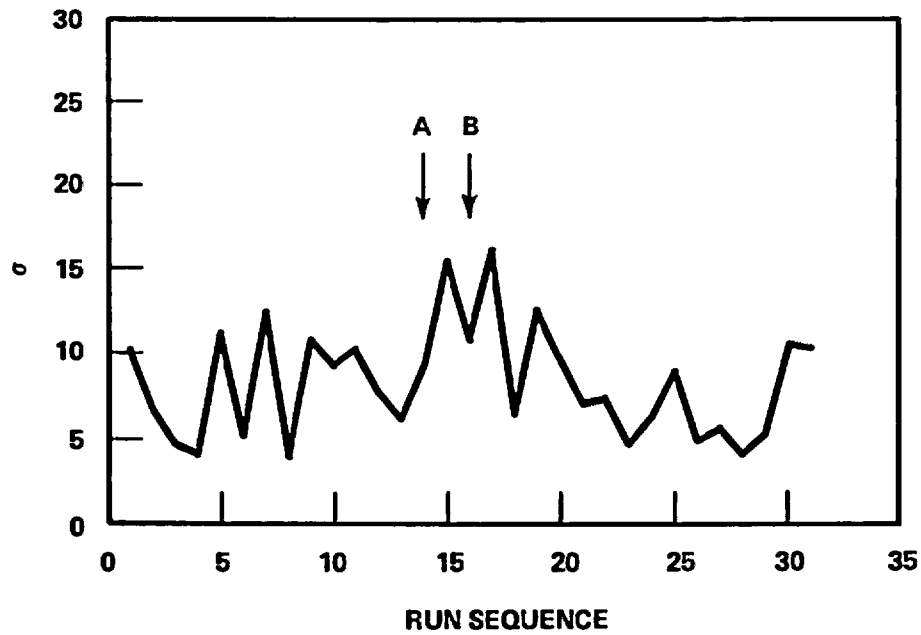

Figure G-31. Normalized Standard Deviation of Heat Transfer Coefficient at 1.52 m (60 in.), 0.5 x Quench Time, One Heater Rod Row Discarded

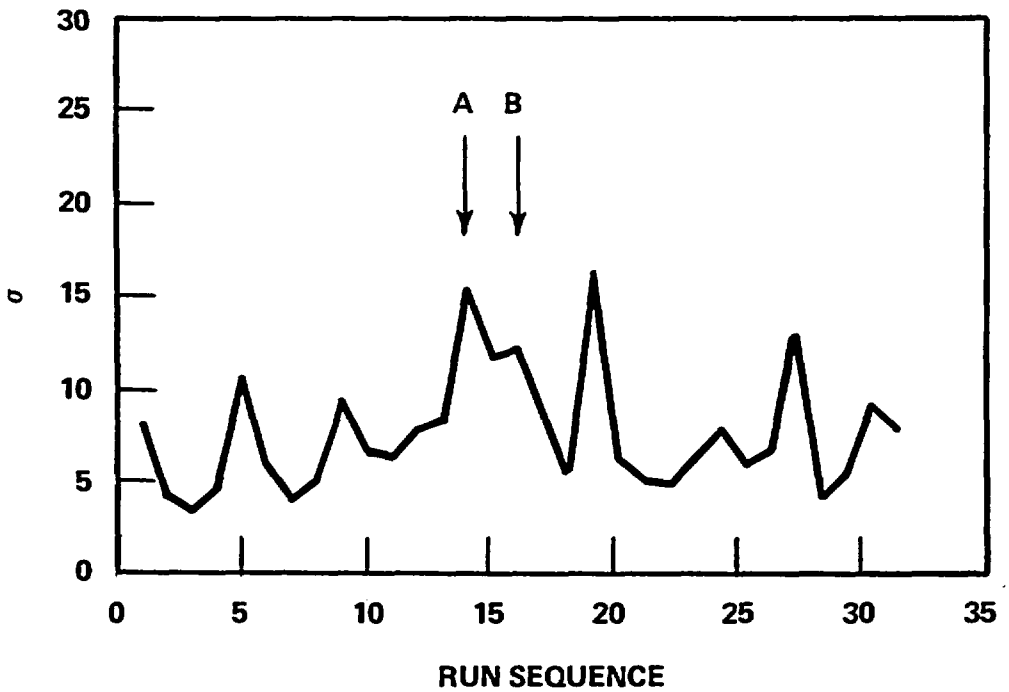

Figure G-32. Normalized Standard Deviation of Heat Transfer Coefficient at 1.52 m (60 in.), 0.6 x Quench Time, One Heater Rod Row Discarded

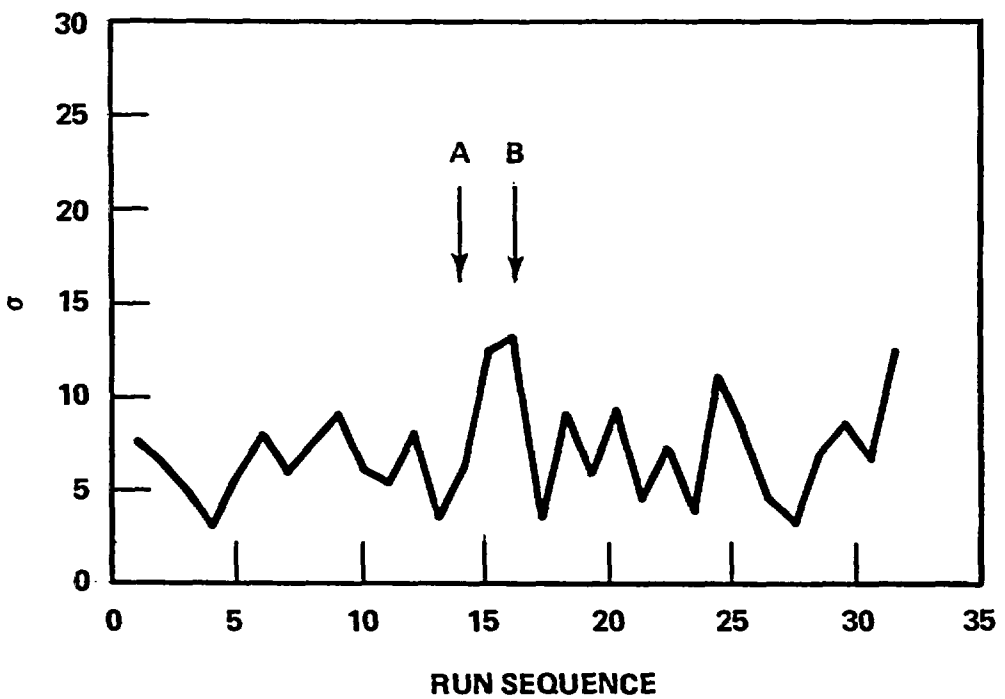

Figure G-33. Normalized Standard Deviation of Heat Transfer Coefficient at 1.52 (60 in.), 0.7 x Quench Time, One Heater Rod Row Discarded

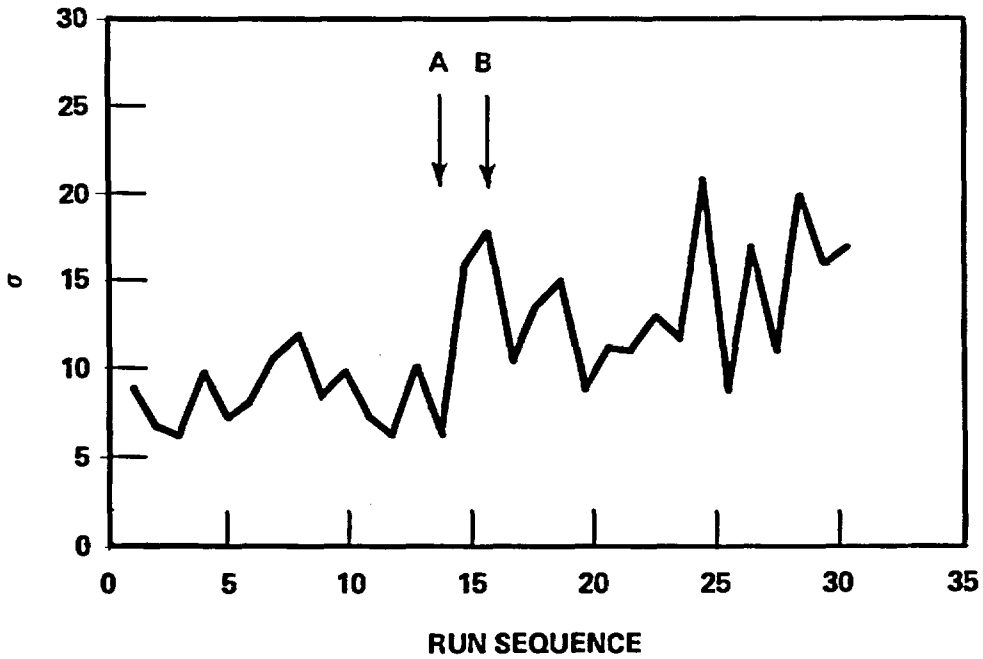

Figure G-34. Normalized Standard Deviation of Heat Transfer Coefficient at 1.83 m (72 in.), Turnaround Time, Two Heater Rod Rows Discarded

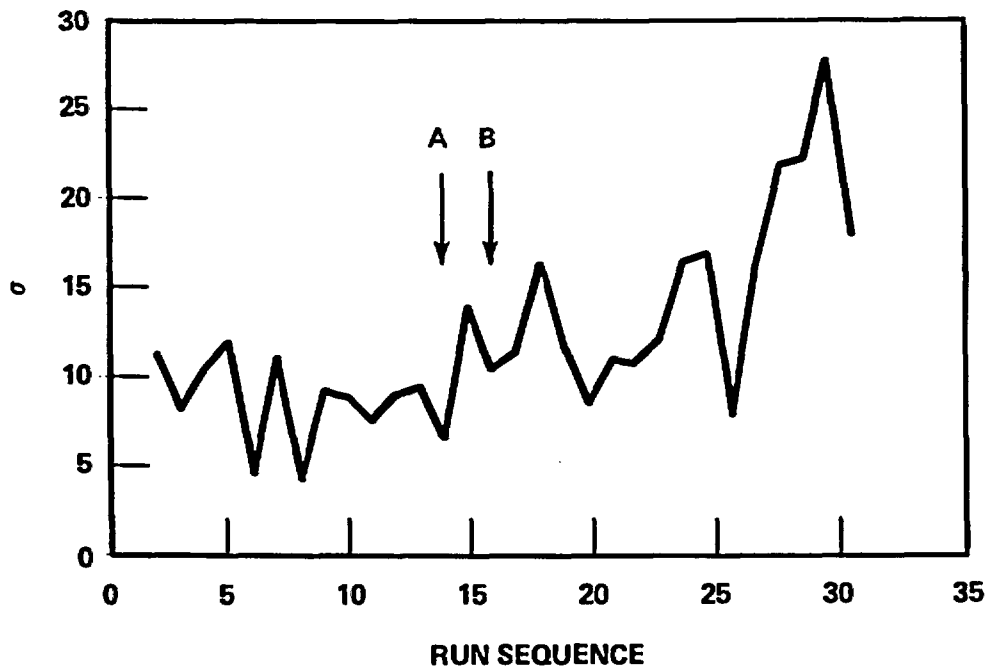

Figure G-35. Normalized Standard Deviation of Heat Transfer Coefficient at 1.83 m (72 in.), 0.3 x Quench Time, Two Heater Rod Rows Discarded

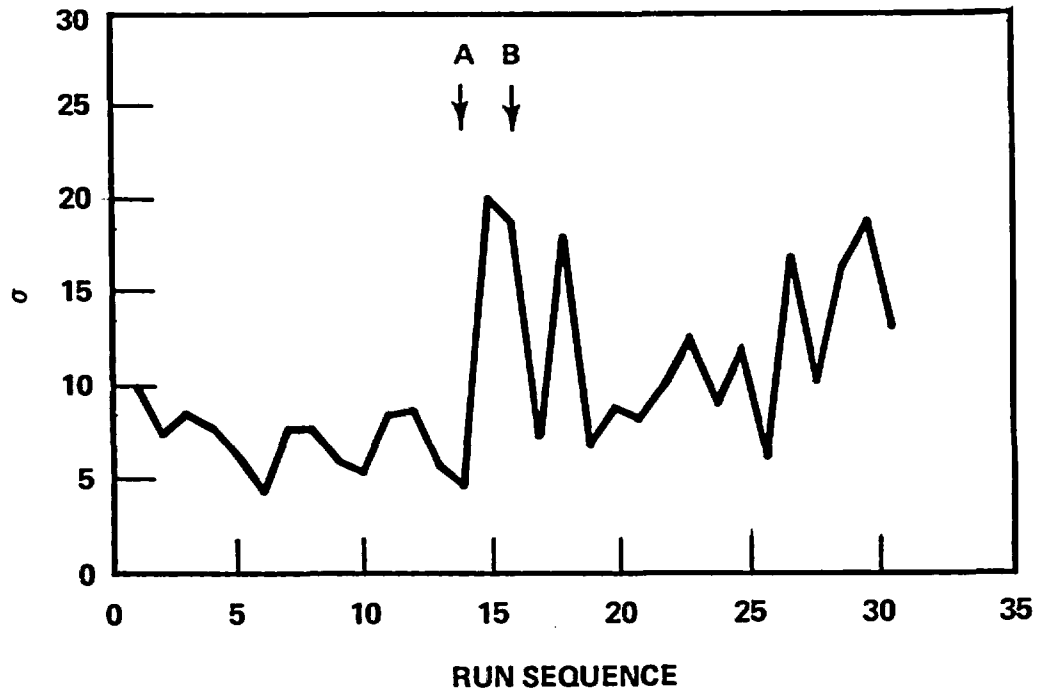

Figure G-36. Normalized Standard Deviation of Heat Transfer Coefficient at 1.83 m (72 in.), 0.4 x Quench Time, Two Heater Rod Rows Discarded

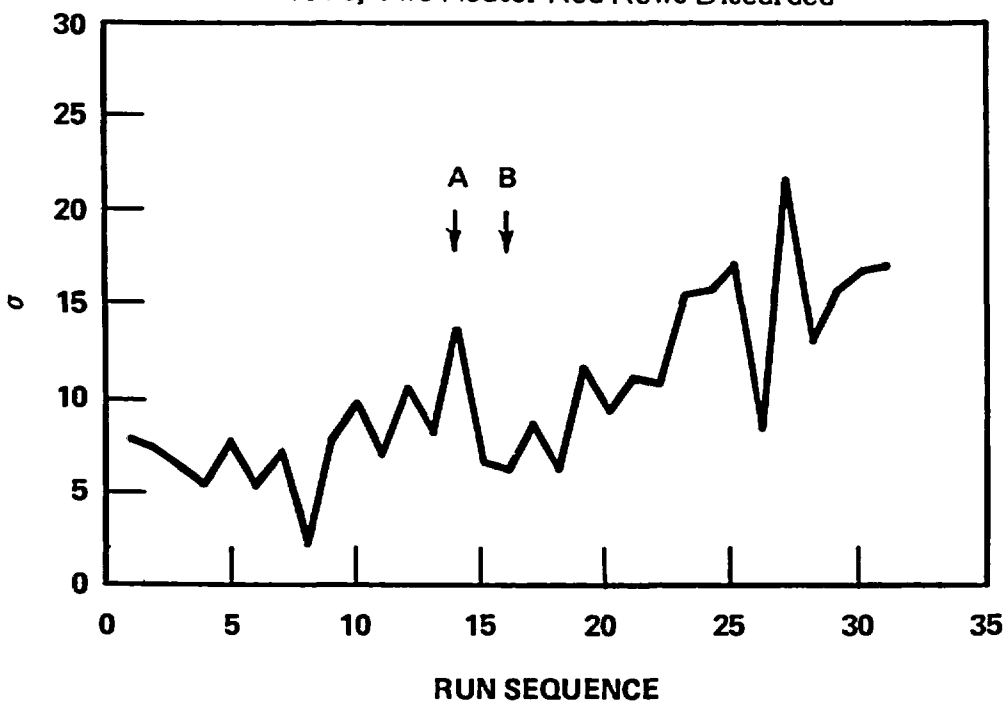

Figure G-37. Normalized Standard Deviation of Heat Transfer Coefficient at 1.83 m (72 in.), 0.5 x Quench Time, Two Heater Rod Rows Discarded

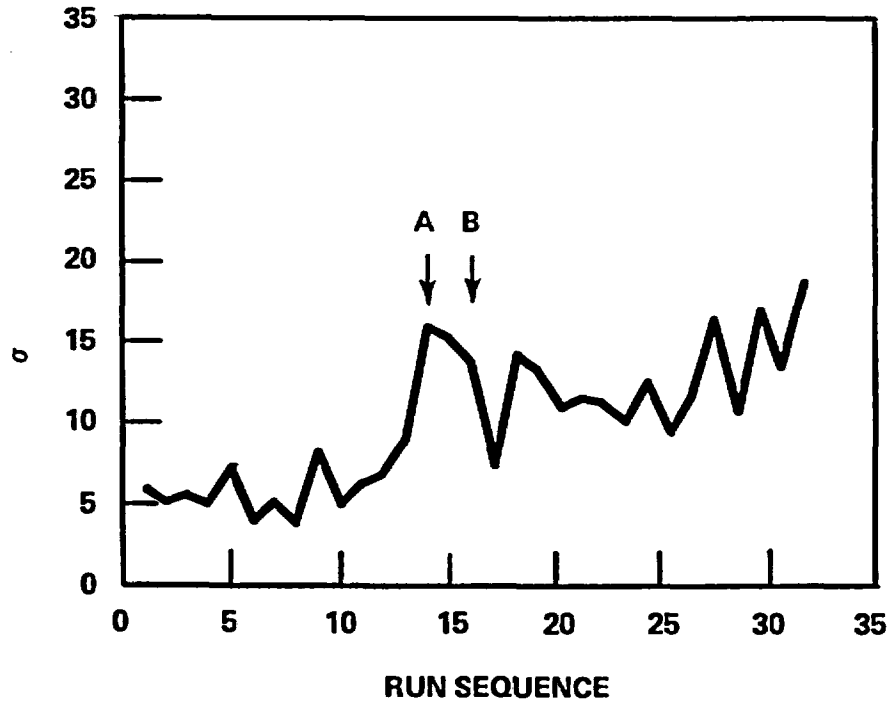

Figure G-38. Normalized Standard Deviation of Heat Transfer Coefficient at 1.83 m (72 in.), 0.6 x Quench Time, Two Heater Rod Rows Discarded

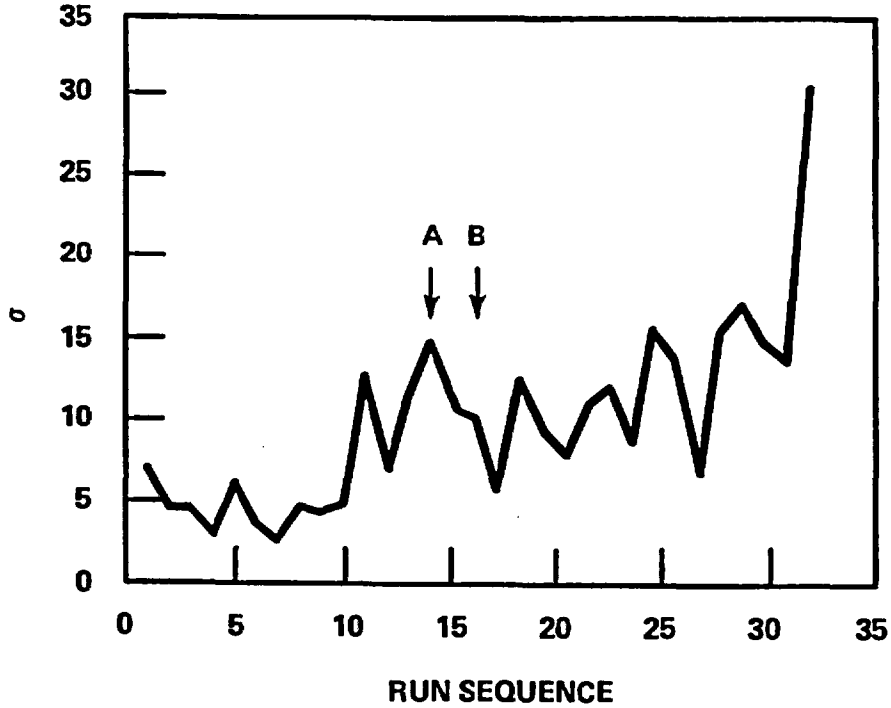

Figure G-39. Normalized Standard Deviation of Heat Transfer Coefficient at 1.83 m (72 in.), 0.7 x Quench Time, Two Heater Rod Rows Discarded

some degree of geometry distortion in the central bundle and a resultant increase in the rod-to-rod variation of the heat transfer coefficient. The increase, however, is only slight, and the magnitudes of the standard deviations at the "minimums" of the fluctuations fall well within the range of the magnitudes of the standard deviations when the geometry of the central bundle was still intact (before run 33056 when rods could be pulled and replaced). The effects of bundle distortion between runs 33849 and 34610, therefore, could not have been significant nor dominating; they could at most be of the same order of magnitude as other parameters affecting the local values of the heat transfer coefficient (for instance, local variation of flow conditions or rod-to-rod manufacturing differences). After run sequence number 24 (run 34610), both the magnitude and fluctuation of the standard deviations seem to undergo a bigger increase, indicating a more significant and dominating effect of the bundle distortion. After run 34610, the bundle geometry distortion started to have a more pronounced effect on the measured heat transfer coefficient. At this point, the heat transfer coefficient data can no longer be used confidently, without first addressing the effect of geometry.

Figures G-40 through G-45 show the results at the 1.83 m (72 in.) elevation, but with data from only one heater rod row discarded. Four important observations can be made from these figures. First, the magnitudes of the standard deviations are considerably greater than those with data from two heater rod rows discarded, showing the significance of the effects of the housing and disconnected rods.

Second, the calculated standard deviations show an apparent increase in magnitude after run sequence number 10 (run 31805). It will be recalled that at runs 31615 and 31805, row bowing was observed through the 1.52 m (72 in.) housing windows (table G-2). The geometric distortion near the housing (and possible near the relatively cold unpowered rods) caused the rod-to-rod variation of the heat transfer coefficient to increase, thus the increase in the calculated standard deviations.

Third, from run sequence number 10 to number 24 (runs 31805 to 34610), the standard deviations for the same time step remain similar in magnitude[1] and pattern of

1. The peak at run sequence number 18 (run 34006) was thought to be partly due to the pressure oscillation that occurred through the entire run, and partly due to the relatively small magnitude of the heat transfer coefficient for this test cycle.

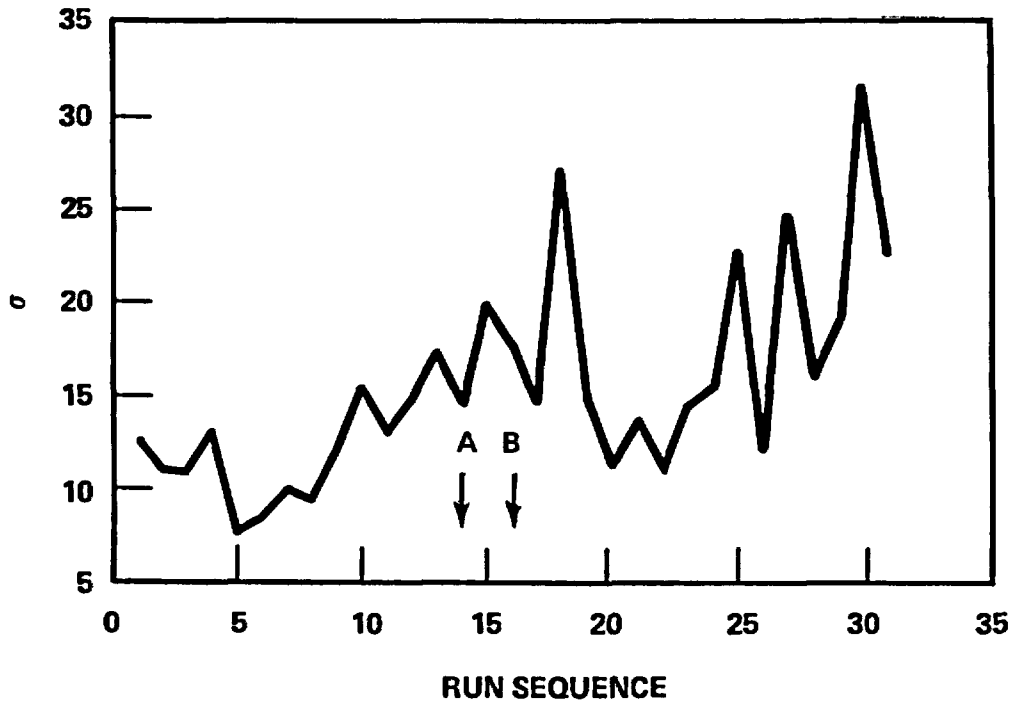

Figure G-40. Normalized Standard Deviation of Heat Transfer Coefficient at 1.83 m (72 in.), Turnaround Time, One Heater Rod Row Discarded

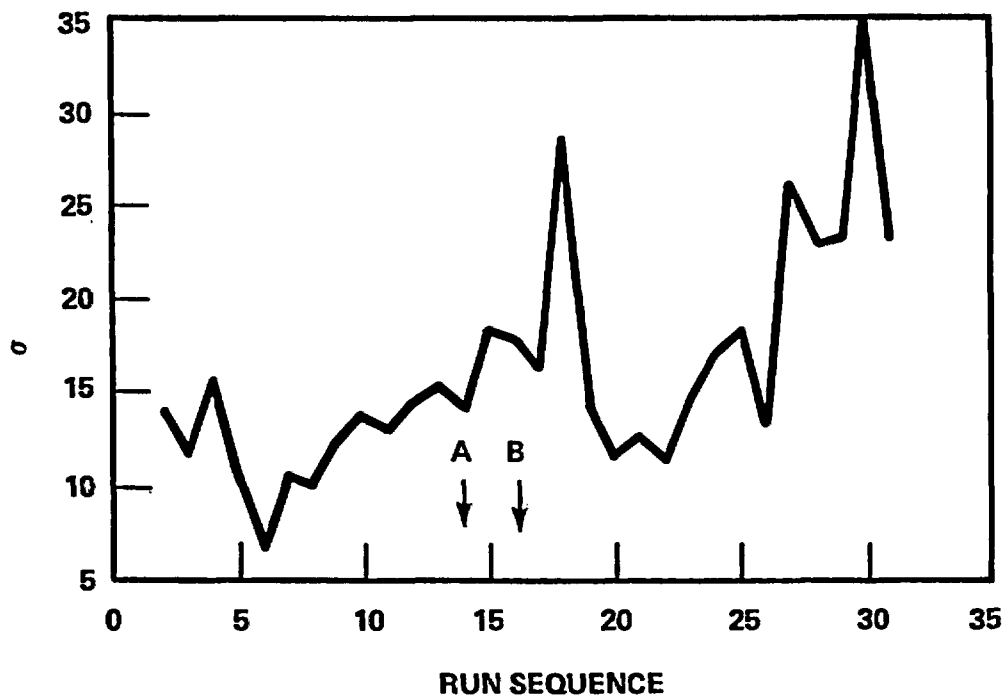

Figure G-41. Normalized Standard Deviation of Heat Transfer Coefficient at 1.83 m (72 in.), 0.3 x Quench Time, One Heater Rod Row Discarded

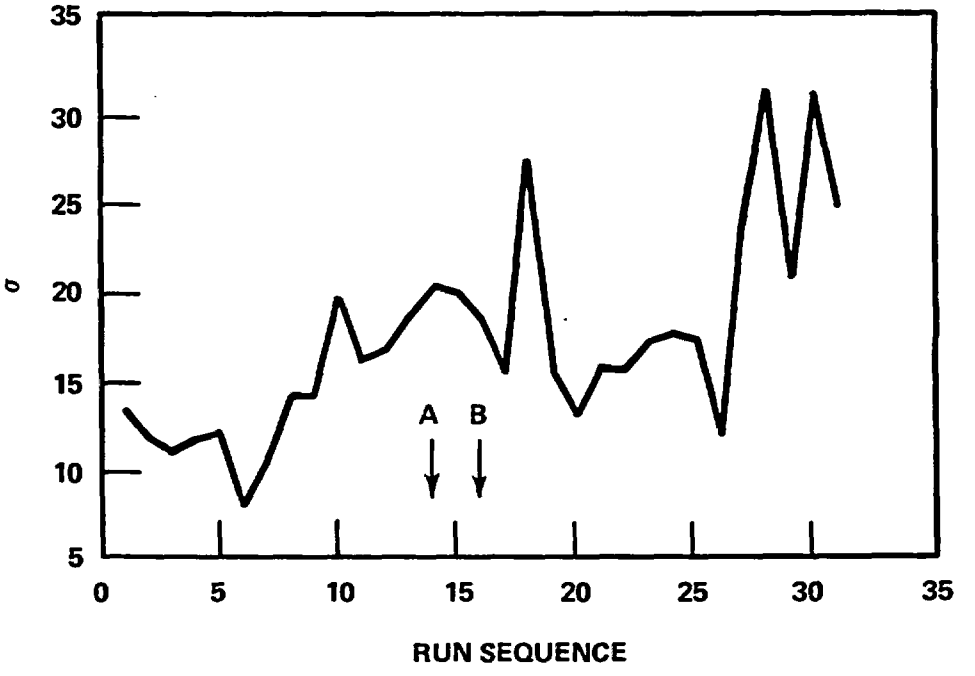

Figure G-42. Normalized Standard Deviation of Heat Transfer Coefficient at 1.83 m (72 in.), 0.4 x Quench Time, One Heater Rod Row Discarded

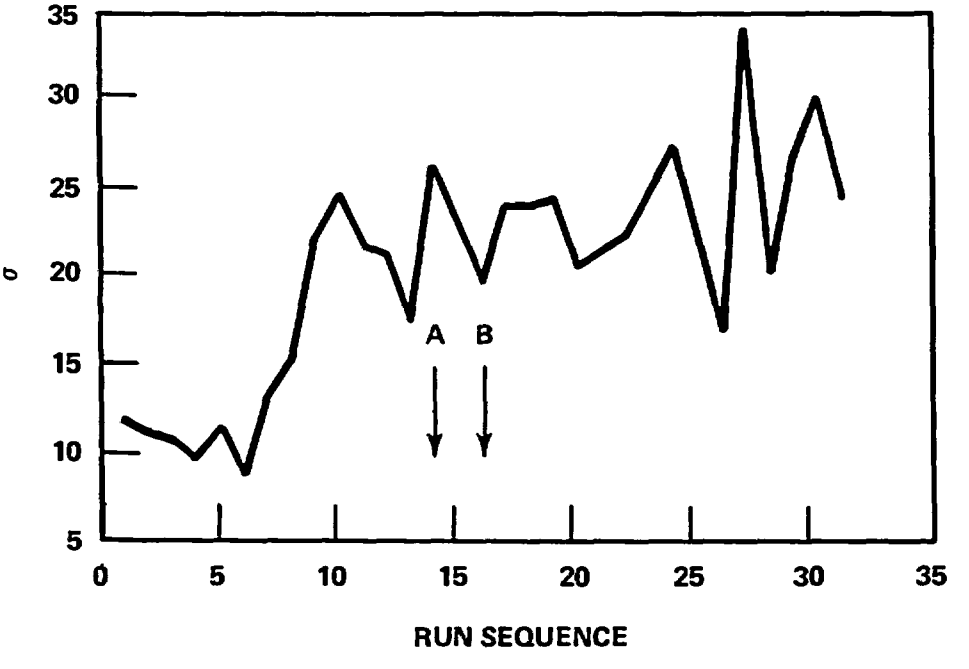

Figure G-43. Normalized Standard Deviation of Heat Transfer Coefficient at 1.83 m (72 in.), 0.5 x Quench Time, One Heater Rod Row Discarded

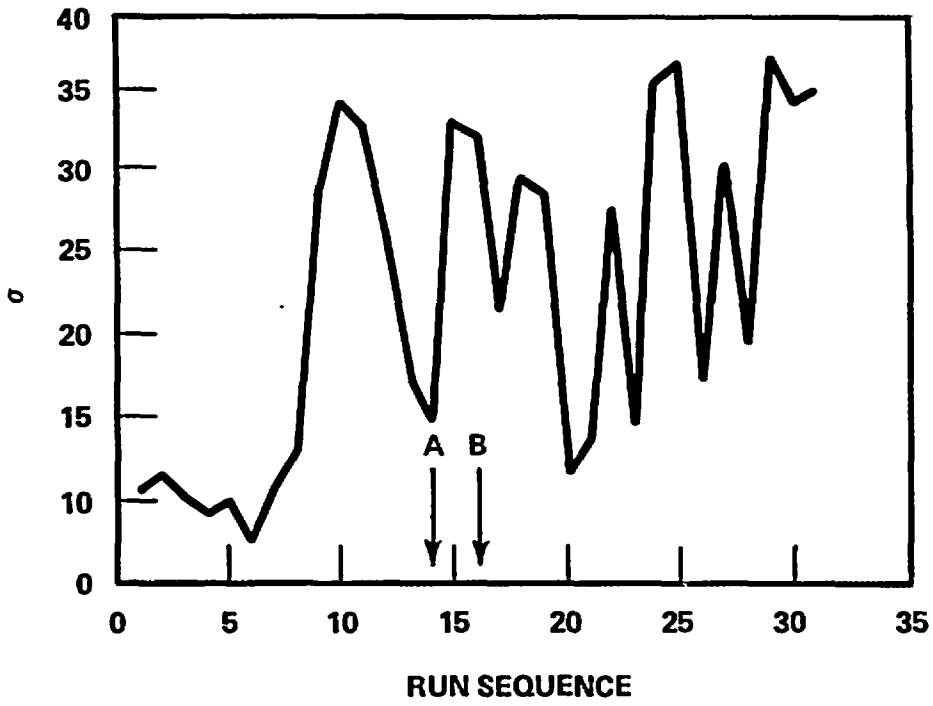

Figure G-44. Normalized Standard Deviation of Heat Transfer Coefficient at 1.83 m (72 in.), 0.6 x Quench Time, One Heater Rod Row Discarded

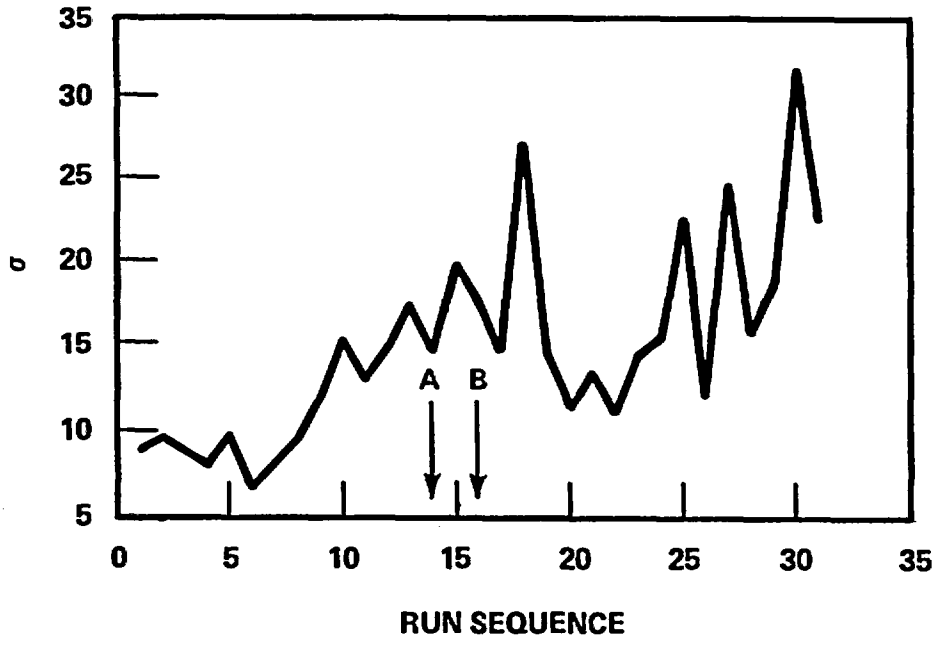

Figure G-45. Normalized Standard Deviation of Heat Transfer Coefficient at 1.83 m (72 in.), 0.7 x Quench Time, One Heater Rod Row Discarded

fluctuation. An increase in the standard deviations was also noted after run sequence number 16 (run 33849) in figures G-34 through G-39, and the increase was attributed to geometric distortion in the central bundle.

These observations can be interpreted together as follows: rod bowing that occurred near the housing and unpowered rods caused the standard deviations to increase after run sequence number 10 (run 31805). The effect of the housing and unpowered rods remained the dominating factor through run sequence number 24 (run 34610), and so the standard deviations remained similar between these runs. Only minor distortion occurred in the central bundle and the effect was of second order; hence a slight increase in the standard deviations (after run 33849) was observed in figures G-34 through G-39, when data from two heater rod rows from the housing and unpowered rods were discarded, but when data from rods near the housing and unpowered rods were included, the effect of the central bundle was negligible and cannot be observed in figures G-40 through G-45.

Fourth, after run sequence number 24 (run 34610), both the magnitude and fluctuation of the standard deviations show an apparent increase. The same observation has been made in figures G-34 through G-39, showing that the increase was due to distortion in the central bundle. After run 34610, the effect in the central bundle became comparable to that due to the housing and unpowered rods, and bundle distortion had apparently spread across the entire bundle at the 1.52 m (72 in.) elevation after run sequence number 24 (run 34610).

G-11. Statistical Analysis of Heater Rod Temperature

The statistical analysis of rod-to-rod variation was repeated with the heater rod initial temperature (temperature at beginning of flooding), turnaround temperature, and temperature rise (turnaround minus initial). The various heater rod temperatures and the heat transfer coefficients showed varying degrees of sensitivity to rod-to-rod variation, but their results were consistent. The results of the temperature statistics and their interpretations are given in the following paragraphs.

G-12. Heater Rod Turnaround Temperature -- The standard deviations of the turnaround temperature were calculated at the 1.52, 1.83, and 2.29 m (60, 72, and 90 in.)

elevations according to equations (G-11) and (G-12); the results are shown in figures G-46 and G-47. In figure G-46, the temperature standard deviations at the 1.83 m (72 in.) elevation show a trend similar to those of the heat transfer coefficients (figures G-34 through G-39): the magnitudes of the temperature standard deviations were slightly increased after run sequence number 16 (run 33849), and the increase was more apparent for the last several runs. The trend for the results at the 2.29 m (90 in.) elevation was less apparent, and was consistent with the observation from the disassembled bundle that the bundle geometry at the 2.29 m (90 in.) elevation was less severly distorted than at the 1.83 m (72 in.) elevation. In figure G-47, the temperature standard deviations were again consistent with the heat transfer coefficient results (figures G-40 through G-45). The standard deviations at the 1.83 m (60 in.) elevation generally had a larger magnitude (compared to those in figure G-46) and showed an early trend to increase at run sequence number 10 (run 31805), showing the significance of the housing effect. The results at the 2.29 m (90 in.) elevation showed that, except for the last three runs, bundle distortion was not significant and the results were consistent with observation of the disassembled bundle. The results at the 1.52 m (60 in.) elevation showed no apparent persistent trends, verifying that the bundle geometry there was intact.

G-13. Heater Rod Initial Temperature -- The results of the heater rod initial temperature analysis are shown in figures G-48 and G-49. The peaks that occurred at run sequence number 10 (run 31805) in figure G-48 and at run sequences numbers 10, 29, 30, and 31 (runs 31805, 35304, 35807, and 35912, respectively) in figure G-49 were due to an exceptionally low measured initial temperature for one of the heater rods in these runs; these rods were rod 9C in run 31805, rod 7H in run 35304, and rod 9J in runs 35807 and 35912. Excluding these rods in the calculations gave results that were consistent with the rest of the test cycles, as shown by the asterisk in the figures. With the possible exception of the last few runs at the 1.83 m (72 in.) elevation in figure G-49, both the magnitude and pattern of fluctuation of the standard deviations were quite similar for all runs at all elevations, suggesting that the rod initial temperatures were relatively insensitive to bundle distortion and rod-to-rod variation. Although no concrete conclusions can be drawn becaue of the insensitivity of the rod initial temperature to geometry, the results of the initial temperature analysis do not contradict those of the turnaround temperature and heat transfer coefficient analyses.

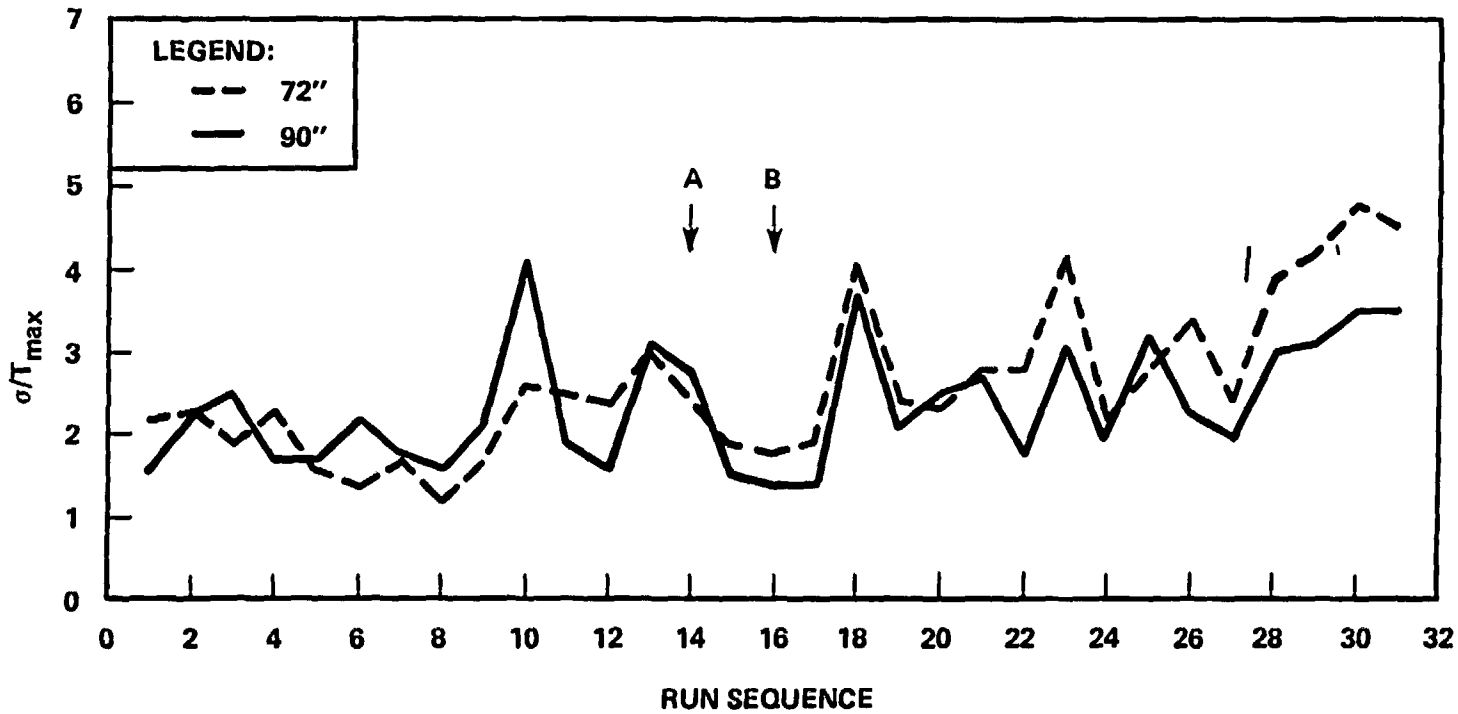

Figure G-46. Normalized Standard Deviation of T_{max} With Two Heater Rod Rows Discarded

16539-86

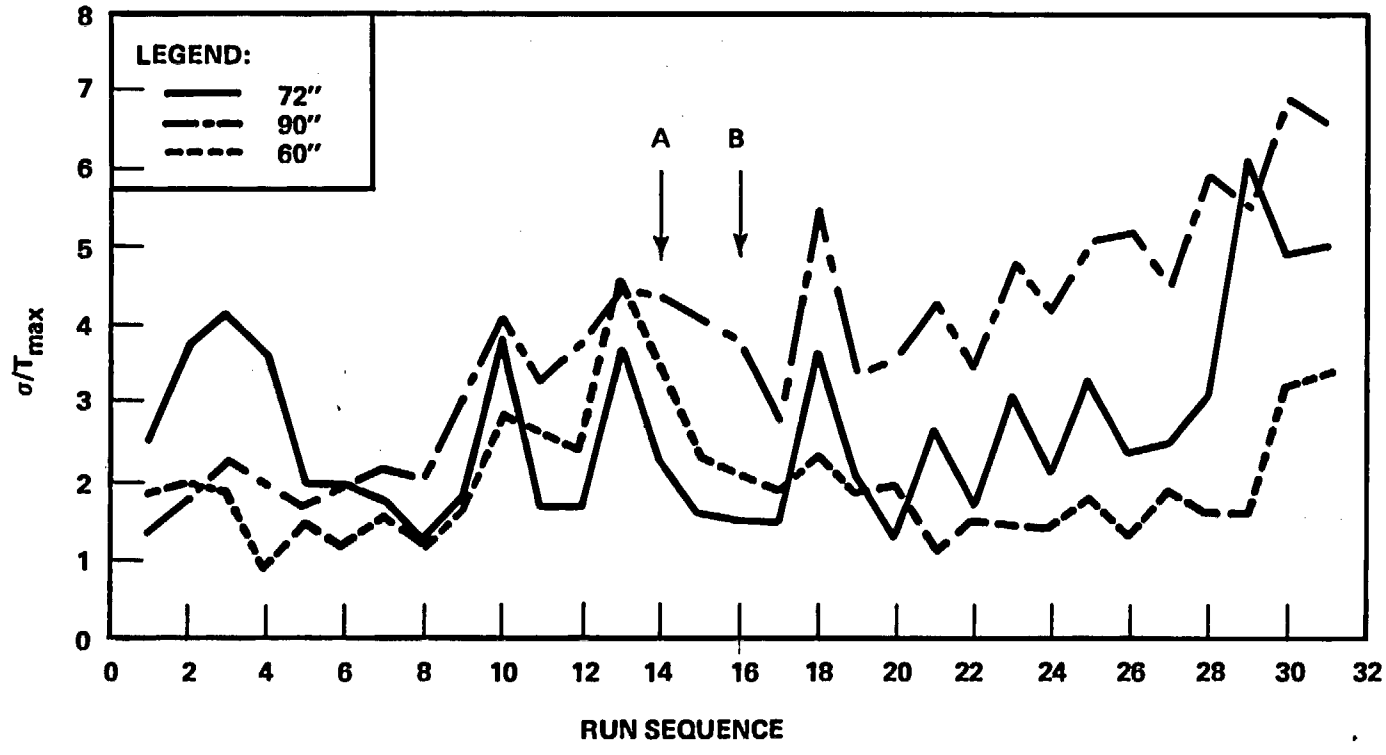

Figure G-47. Normalized Standard Deviation of T_{max} With One Heater Rod Row Discarded

16539-87

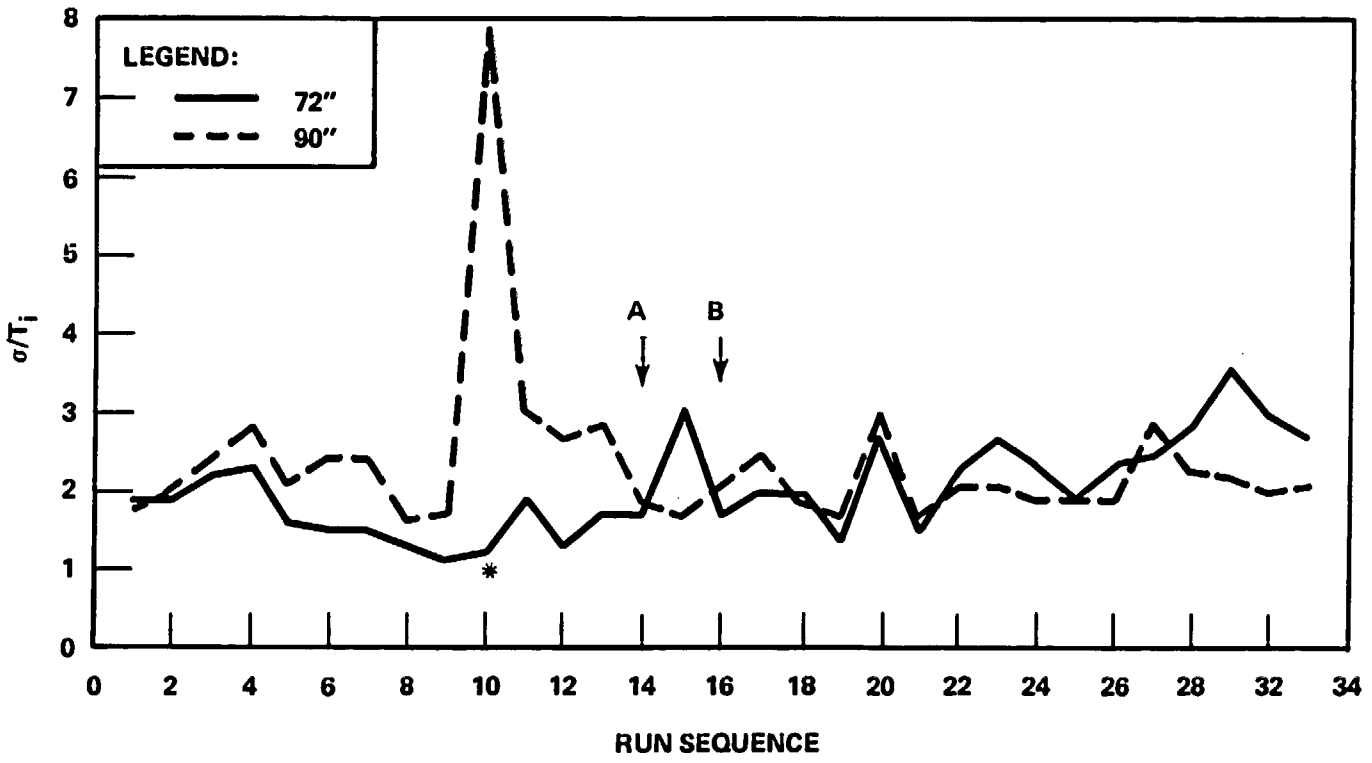

Figure G-48. Normalized Standard Deviation of T_i With Two Heater Rod Rows Discarded

16539-88

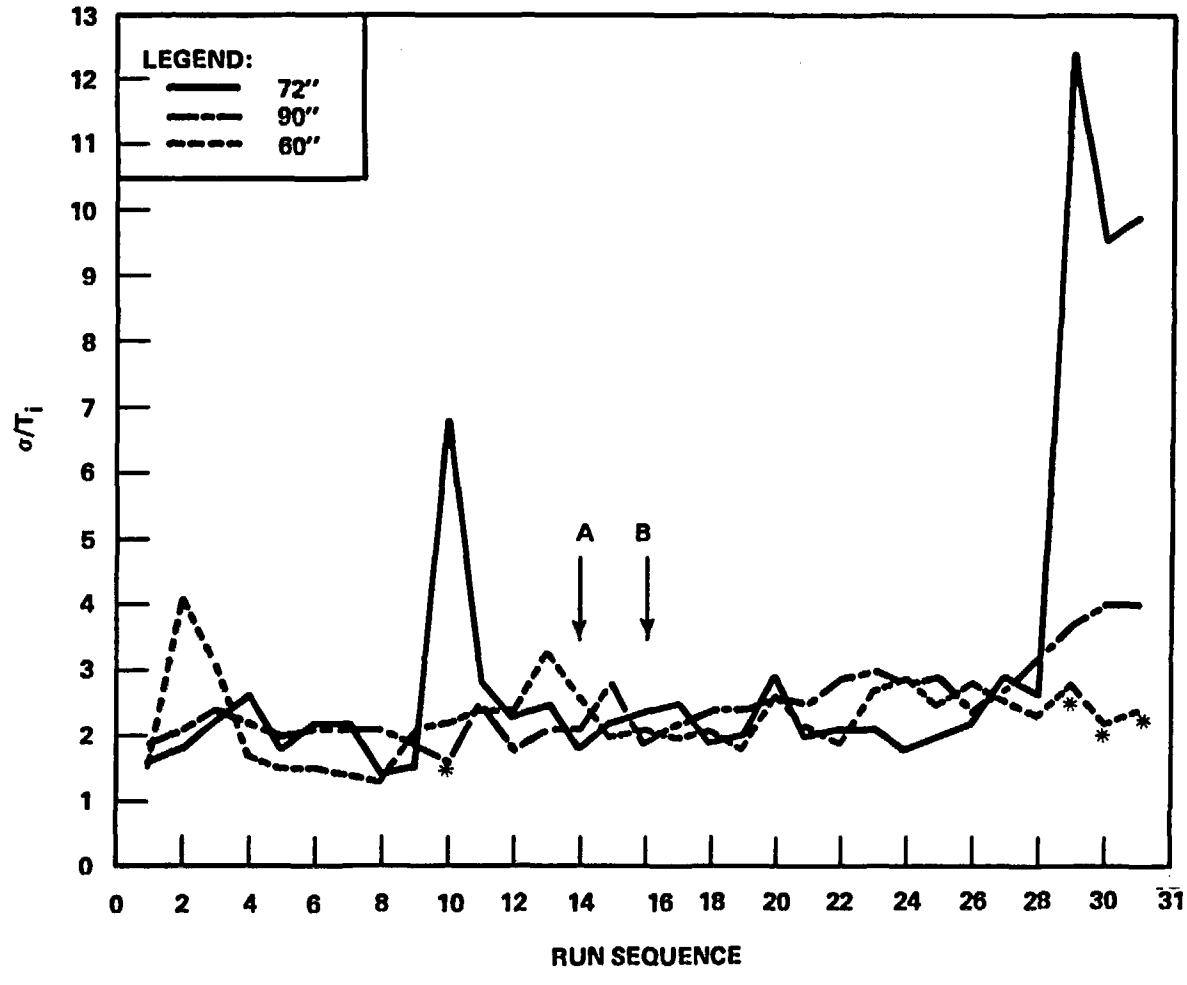

Figure G-49. Normalized Standard Deviation of T_i With One Heater Rod Row Discarded

G-14. Heater Rod Temperature Rise -- The results of the calculated standard deviation analysis for the heater rod temperature rise (turnaround minus initial temperature) are shown in figures G-50 and G-51. The large fluctuations of the standard deviations in these figures indicate large rod-to-rod variations of the heater rod temperature rise. Figure G-51 shows that the fluctuations of the standard deviations at all three elevations are similar; figure G-50 shows that the standard deviations at the 1.83 m (72 in.) elevation after run sequence number 16 (run 33849) are similar to that from run sequence numbers 8 to 16 (runs 31302 to 33849). Since the geometry at the 1.52 m (60 in.) elevation and at all elevations before run sequence number 14 (run 32333) was known to be intact, the results suggest that the large fluctuations of the standard deviation are not due to the bundle geometry distortion. Bundle geometry is apparently a second-order effect in the rod-to-rod variation of the heater rod temperature rise; thus no quantitative conclusions can be drawn from the results.

G-15. CONCLUSIONS

The effects of bundle geometry on the rod-to-rod variation of the heat transfer coefficient, heater rod turnaround temperature, initial temperature, and temperature rise have been presented above. These results show that the rod-to-rod variation of the heat transfer coefficient and the heater rod turnaround temperature were most sensitive to bundle geometry, but the effects of bundle geometry on heater rod initial temperature and temperature rise were only of second order.

It can be concluded from these analyses that geometric distortion near the 1.83 m (72 in.) elevation was most severe and occurred earliest. Heat transfer data near the housing and disconnected rods were affected as early as run 31805. The geometry of the central bundle remained intact through run 32333. From run 32333 to run 34610, heat transfer data in the central bundle were affected by geometric distortion, but the effect of distortion was neither significant nor dominating, and was of the same order of magnitude as that of other parameters affecting the local heat transfer data. After run 34610, the bundle geometry became more severely distorted and the geometry affected the heat transfer data more significantly. One can use the FLECHT SEASET 161-rod heat transfer data with confidence through run 34610 for model and heat transfer correlation development for an intact bundle; beyond run 34610, one should not use the heat transfer data without first addressing the effect of geometry distortion.

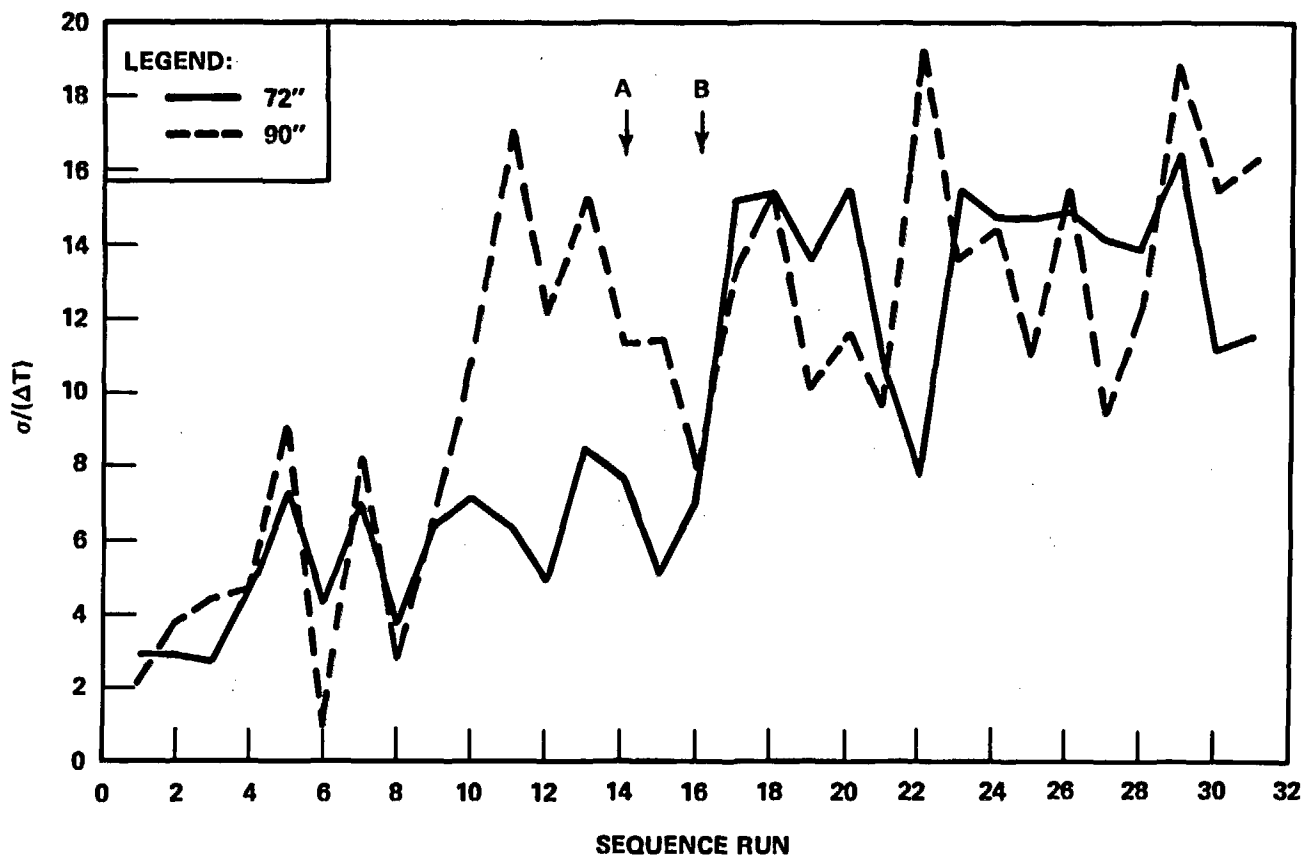

Figure G-50. Normalized Standard Deviation of $\Delta T(T_{max} - T_i)$ With Two Heater Rod Rows Discarded

16539-90

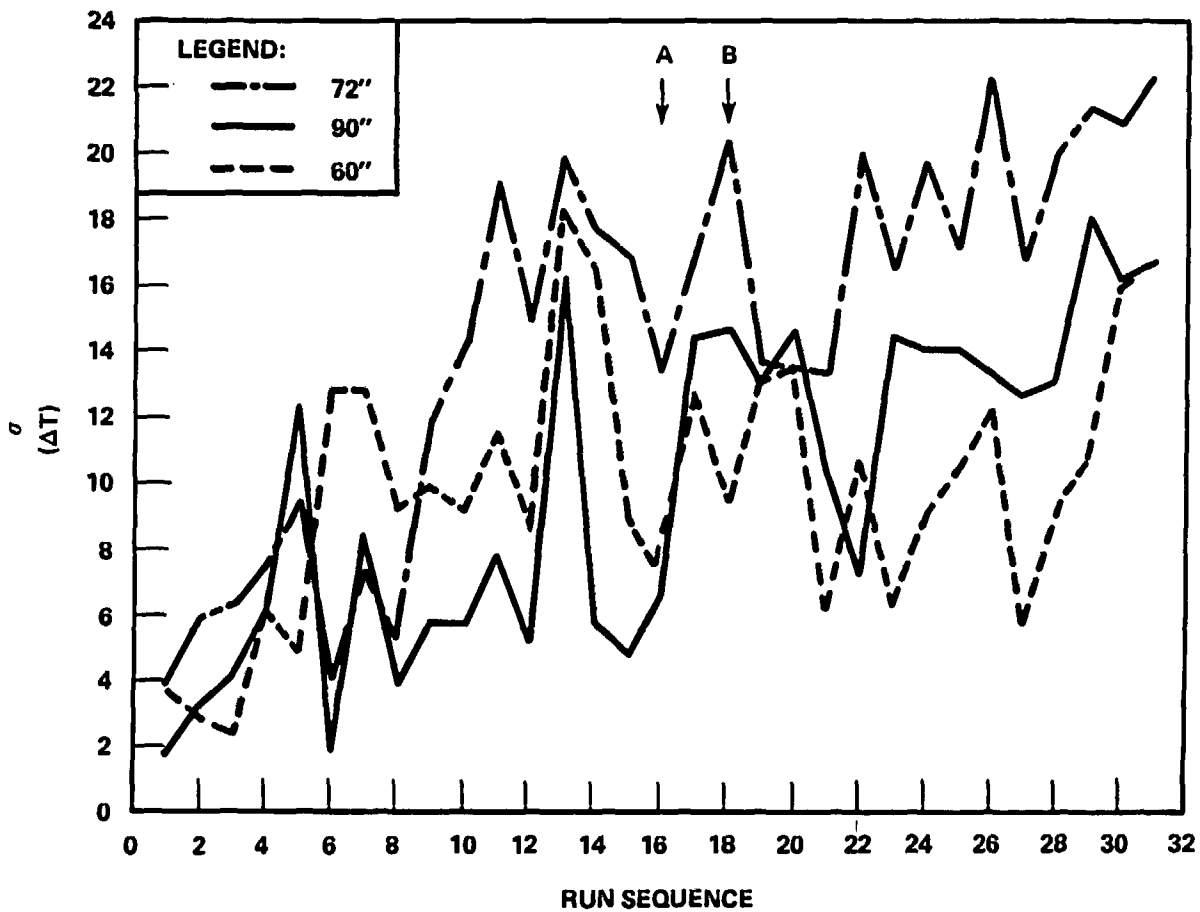

Figure G-51. Normalized Standard Deviation of $\Delta T(T_{max} - T_i)$ With One Heater Rod Row Discarded

16539-91

NRC/EPRI/WESTINGHOUSE REPORT NO. 7
EXTERNAL DISTRIBUTION

Dr. L. S. Tong, Assistant Director
Water Reactor Safety Research
Division of Reactor Safety Research
U.S. Nuclear Regulatory Commission
Washington, DC 20555

Dr. H. Sullivan
Division of Reactor Safety Research
U. S. Nuclear Regulatory Commission
Washington, DC 20555

A. L. M. Hon
Separate Effects Research Branch
U. S. Nuclear Regulatory Commission
Washington, DC 20555

K. V. Morton, Chief
Research Contracts Branch
Division of Contracts
U. S. Nuclear Regulatory Commission
Washington, DC 20555

D. E. Solberg
U. S. Nuclear Regulatory Commission
Washington, DC 20555

Mr. Wayne Hodges
U. S. Nuclear Regulatory Commission
DSS
Washington, DC 20555

Mr. L. Phillips
NRR
U. S. Nuclear Regulatory Commission
Washington, DC 20555

Mr. Harry Balukjan
NRR
U. S. Nuclear Regulatory Commission
Washington, DC 20555

Dr. D. Ross
NRR
U. S. Nuclear Regulatory Commission
Washington, DC 20555

Dr. W. Johnston
Core Performance Branch
U. S. Nuclear Regulatory Commission
Washington, DC 20555

Dr. B. Bingham
Babcock & Wilcox Company
P. O. Box 1206
Lynchburg, VA 24505

Mr. N. H. Shah
Babcock & Wilcox Co. (NPGD)
P.O. Box 1260
Lynchburg, VA 24505

Mr. W. Kayser
Exxon Nuclear
2101 Horn Rapids Road
Richland, WA 99352

J. A. Dearien
EG&G Idaho, Inc.
P. O. Box 1625
Idaho Falls, ID 83401

P. North
EG&G Idaho, Inc.
P. O. Box 1625
Idaho Falls, ID 83401

Mr. G. Sozzi
General Electric Co.
175 Curtner Avenue
San Jose, CA 95125

Dr. P. Griffith
Dept. of Mechanical Engineering
MIT
Cambridge, MA 02139

Dr. P. A. Lottes
Argonne National Laboratory
9700 South Cass Avenue
Argonne, IL 60439

Mr. G. Ofey
Sandia National Laboratory
P.O. Box 5800
Albuquerque, NM 87185

Dr. F. Mynatt
Engineering Technology Division
Oak Ridge National Laboratory
Box 7
Oak Ridge, TN 37830

Mr. R. Jensen
Intermountain Technology
Box 1604
Idaho Falls, ID 83401

Mr. F. D. Lang
Energy Incorporated
P. O. Box 763
Idaho Falls, ID 83401

Dr. J. Chen
Lehigh University
Dept. of Mechanical Engineering
Bethlehem, PA 18015

Dr. K. H. Sun (5 copies)
Nuclear Power Division
Electric Power Research Institute
P. O. Box 10412
Palo Alto, CA 94303

Dr. J. J. Cudlin
Power Generation Group
Babcock & Wilcox
P. O. Box 1260
Lynchburg, VA 24505

Mr. J. Longo, Jr.
Combustion Engineering
P. O. Box 500
Windsor, CT 06095

Mr. J. Blaisdell
Combustion Engineering
P.O. Box 500
Windsor, CT 06095

Mr. Ken Moore
Energy, Inc.
P. O. Box 736
Idaho Falls, ID 83401

Dr. K. P. Galbraith
Nuclear Safety Engineering
Exxon Nuclear Company
2101 Horn Rapids Road
Richland, WA 99352

Dr. J. A. Block
Creare Inc.
Hanover, NH 03755

Dr. W. Hancox
Whiteshell Nuclear Laboratory
Atomic Energy of Canada
Pinawa, Manitoba
Canada ROE 1LO

Professor T. Theofanous
Department of Nuclear Energy
Purdue University
West Lafayette, IN 47907

Professor I. Catton
Dept. of Chemical, Nuclear, and
Thermal Engineering
University of California
Los Angeles, CA 90024

Dr. Max W. Carbon
Nuclear Engineering Department
The University of Wisconsin
Madison, WI 53706

Professor R. A. Seban
Dept. of Mechanical Engineering
University of California
Berkeley, CA 94720

Professor W. Y. Chon
Dept. of Engineering Science,
Aerospace Engineering, and
Nuclear Engineering
State University of New York
Buffalo, NY 14214

Dr. R. R. Gay
Nuclear Engineering Department
Rensselaer Polytechnic Institute
Troy, NY 12181

Dr. Owen Jones
Brookhaven National Laboratory
Building 820
Upton, NY 11973

Professor E. V. McAssey, Jr.
Dept. of Mechanical Engineering
Villanova University
Villanova, PA 19085

Professor S. C. Yao
Dept. of Mechanical Engineering
Carnegie-Mellon University
Pittsburgh, PA 15213

Dr. S. J. Board
CEGB
Berkeley Nuclear Laboratory
Berkeley
Gloucestershire, England

Prof. T. Wu
California Institute of Technology
Pasadena, CA 91109

Dr. S. Levy
S. Levy, Inc.
1901 S. Bascom Ave. Suite 275
Campbell, CA 95008

Professor A. Tapucu
Ecole Polytechnique,
Universite de Montreal
Institut de Genie Nucleaire
Casier Postale 6079
Succursal "A,"
Montreal, Quebec H3C 3A7

Mr. Marv Thurgood
Battelle P.N.L.
P.O. Box 999
Richland, WA 99352

Mr. Cleon Dodge
Box 81
Springtown, PA 18081

Mr. Don Ogden
EG&G Idaho, Inc.
P.O. Box 1625
Idaho Falls, ID 83401

Mr. Peter Davis
Inter-Mountain Technology
P.O. Box 1604
Idaho Falls, ID 83401

Distribution Services Branch (360 copies)
Nuclear Regulatory Commission
7920 Norfolk Avenue
Bethesda, MD 20555

Ms. Nora Schofield
EG&G Idaho, Inc.
P. O. Box 1625
Idaho Falls, ID 83401